REMOVAL OF FORMALDEHYDE AND BTEX IN INDOOR AIR USING ACTIVATED CARBON PRODUCED FROM HORSE CHESTNUT (*Aesculus hippocastanum* L.) SHELL

AT KESTANESİ (*Aesculus hippocastanum* L.) KABUĞUNDAN ÜRETİLMİŞ AKTİF KARBON İLE İÇ ORTAM HAVASINDAN FORMALDEHİT VE BTEX GİDERİMİ

KAAN IŞINKARALAR

PROF. DR. GÜLEN GÜLLÜ

Supervisor

Submitted to
Graduate School of Science and Engineering of Hacettepe University
as a Partial Fulfillment to the Requirements
for the Award of the Degree of **Doctor of Philosophy**
in Environmental Engineering

2020

Being a Family is the most intense and beautiful feeling of the world …

…To My Parents and sincerely appreciate My Grandmother,

My Little Daughter and My Wife.

ETHICS

In this thesis study, prepared in accordance with the spelling rules of Institute of Graduate School of Science and Engineering of Hacettepe University,

I declare that

- all the information and documents have been obtained in the base of the academic rules,
- all audio-visual and written information and results have been presented according to the rules of scientific ethics,
- in the case of using other works, related studies have been cited in accordance with the scientific standards,
- all cited studies have been fully referenced,
- I did not do any distortion in the data set,
- and any part of this thesis has not been presented as another thesis study at this or any other university.

24/11/2020

KAAN IŞINKARALAR

YAYINLANMA FİKRİ MÜLKİYET HAKKLARI BEYANI

Enstitü tarafından onaylanan lisansüstü tezimin/raporumun tamamını veya herhangi bir kısmını, basılı (kağıt) ve elektronik formatta arşivleme ve aşağıda verilen koşullarla kullanıma açma iznini Hacettepe üniversitesine verdiğimi bildiririm. Bu izinle Üniversiteye verilen kullanım hakları dışındaki tüm fikri mülkiyet haklarım bende kalacak, tezimin tamamının ya da bir bölümünün gelecekteki çalışmalarda (makale, kitap, lisans ve patent vb.) kullanım hakları bana ait olacaktır.

Tezin kendi orijinal çalışmam olduğunu, başkalarının haklarını ihlal etmediğimi ve tezimin tek yetkili sahibi olduğumu beyan ve taahhüt ederim. Tezimde yer alan telif hakkı bulunan ve sahiplerinden yazılı izin alınarak kullanması zorunlu metinlerin yazılı izin alarak kullandığımı ve istenildiğinde suretlerini Üniversiteye teslim etmeyi taahhüt ederim.

Yükseköğretim Kurulu tarafından yayınlanan "***Lisansüstü Tezlerin Elektronik Ortamda Toplanması, Düzenlenmesi ve Erişime Açılmasına İlişkin Yönerge***" kapsamında tezim aşağıda belirtilen koşullar haricince YÖK Ulusal Tez Merkezi/H. Ü. Kütüphaneleri Açık Erişim Sisteminde erişime açılır.

□ Enstitü/Fakülte yönetim kurulu kararı ile tezimin erişime açılması mezuniyet tarihimden itibaren 2 yıl ertelenmiştir.

□ Enstitü/Fakülte yönetim kurulu gerekçeli kararı ile tezimin erişime açılması mezuniyet tarihimden itibaren .... ay ertelenmiştir.

□ Tezim ile ilgili gizlilik kararı verilmiştir.

24/11/2020

KAAN IŞINKARALAR

ABSTRACT

REMOVAL OF FORMALDEHYDE AND BTEX IN INDOOR AIR USING ACTIVATED CARBON PRODUCED FROM HORSE CHESTNUT (*Aesculus hippocastanum* L.) SHELL

Kaan IŞINKARALAR

Doctor of Philosophy, Department of Environmental Engineering

Supervisor: Prof. Dr. Gülen GÜLLÜ

November 2020, 298 pages

Activated carbon can be used in the adsorption of volatile organic compounds in abundant quantity in indoor air. This study aims to produce a material to be used for cleaning the indoor air.using activated carbon transformed from horse chestnut (*Aesculus hippocastanum* L.) shell, which is a kind of organic lignocellulosic waste and easily found in nature. The scope of the research consists of activated carbon production, characterization processes, hydrogen storage capacity measurements, formaldehyde and BTEX (benzene, toluene, ethylbenzene, m, p-xylene, o-xylene) adsorption experiments and cost-benefit analysis.

Activated carbon was produced by chemical activation method using carbonization process at different temperatures (400, 500, 550, 600, 700, 800 and 900°C) and at different concentrations (1 M, 3 M and 5 M) of $ZnCl_2$ in order to determine the most efficient production conditions of activated carbon. As a result of the characterization tests, optimum conditions were determined as the carbonization process at 600°C and the use of $ZnCl_2$ at 3 M concentration. The characteristic properties of activated carbon were revealed by conducting BET, SEM/EDX, XRD, FTIR-ATR, DTA/TG analyzes of the activated carbon samples and measuring the hydrogen storage capacity. Hydrogen storage capacities were tested using $ZnCl_2$ at 25°C and -196°C. The highest capacity was found in the use of 3 M $ZnCl_2$ and at -196°C temperature. Accordingly, capacity was measured as 3.18 wt% under 43907.27 mbar pressure.

A batch reactor with a volume of 0.002 m^3 was produced by using glass material for adsorption experiments. In the experiments, commercial activated carbon removal efficiencies purchased from the market were compared with the efficiency of activated carbon produced within the scope of the thesis. Considering the limit values for formaldehyde and BTEX gases values with low concentrations for formaldehyde of 170±14.92, 260±23.76, 720±47, 1040±68.47, 1220±72.14, 1900±83.37, 3290±95.44 and 7650±111.18 $\mu g/m^3$. Highly concentrated formaldehyde values were studied as 30,000±207,44, 50,000±338,61, 60,000±376,89 and 110,000±497,21 $\mu g/m^3$. Initial concentrations were determined as 2.4±0.45, 5.5±1.09, 54±10.73 and 322±47.80 $\mu g/m^3$ for benzene, 3.7±0.58, 9±2.62, 86±15.83 and 414±47.26 $\mu g/m^3$ for toluene, 9±0.66, 9.2±1.59, 90±15.55 and 430±46.64 $\mu g/m^3$ for ethylbenzene, 3.4±0.72, 8.5±1.32, 83±12.95 and 397±82.10 $\mu g/m^3$ for m, p-xylene, 5.2±0.82, 10±2.49, 100±24.38 and 483±102.67 $\mu g/m^3$ for o-xylene, 18.5±1.89, 42±4.97, 412±48.74 and 2045±203.37 $\mu g/m^3$ for BTEX. Isotherm parameters for commercial activated carbon and activated carbon produced within the scope of the thesis are presented by comparing. The data were applied to Dubinin-Radushkevich, Langmuir and Freundlich isotherms, and it was observed that the isotherms favorable to the equilibrium data. It was determined that the findings are more suitable for the Freundlich isotherm among these isotherms.

The best performing values in terms of efficiency were found at low concentrations. In the formaldehyde removal test conducted at a concentration of 170±14.92 μg/m^3, the efficiency of commercial activated carbon was 47.83%, while the efficiency of the produced activated carbon reached 73.37%, and the highest concentration value was 110,000±497.21 μg/m^3. While the values were 26.39% for commercial activated carbon, it was 32.89% for activated carbon produced within the scope of the thesis. Commercial activated carbon was 65.23%, while the activated carbon produced was 73.86% at benzene removal experiment. Commercial activated carbon was 43.44%, while the activated carbon produced was 63.31% at toluene removal experiment. Commercial activated carbon was 50.08%, while the activated carbon produced was 65.96% at ethylbenzene removal experiment. Commercial activated carbon was 42.04%, while the activated carbon produced was 60.28% at m, p-xylene removal experiment. Commercial activated carbon was 78.99%, while the activated carbon produced was 88.07% at o-xylene removal experiment. Commercial activated carbon was 52.43%, while the activated carbon produced was 71.7% at BTEX removal experiment.

The efficiency values obtained with the activated carbon produced within the scope of the thesis were found to be higher than commercial activated carbon for formaldehyde and BTEX concentrations. It was determined that horse chestnut shell is a raw material with a high potential due to its pore structure, high surface area and adsorption capacity in activated carbon production. It was found efficient for the removal of formaldehyde and BTEX from indoor air using decorative products containing activated carbon.

Keywords: Adsorption, Activated Carbon, BTEX, Formaldehyde, Hydrogen Storage, Indoor Air Pollution.

ÖZET

AT KESTANESİ (*Aesculus hippocastanum* L.) KABUĞUNDAN ÜRETİLMİŞ AKTİF KARBON İLE İÇ ORTAM HAVASINDAN FORMALDEHİT VE BTEX GİDERİMİ

Kaan IŞINKARALAR

Doktora, Çevre Mühendisliği Anabilim Dalı

Tez Danışmanı: Prof. Dr. Gülen GÜLLÜ

Kasım 2020, 298 sayfa

İç ortam havasında bol miktarda bulunan uçucu organik bileşiklerin adsorpsiyonunda aktif karbonlar kullanılabilmektedir. Çalışmada, lignoselülozik yapıda organik bir atık olan ve doğada kendi halinde rahatlıkla bulunabilen at kestanesi (*Aesculus hippocastanum* L.) kabuğundan aktif karbon üretilip iç ortam havasından Formaldehit ve BTEX gideriminde kullanılacak bir malzeme elde edilmesi amaçlanmıştır. Araştırma kapsamını, aktif karbon üretimi, karakterizasyon işlemleri, hidrojen depolama kapasitesi ölçümleri, formaldehit ve BTEX (benzene, toluen, etilbenzen, m, p-ksilen, o-ksilen) adsorpsiyon deneyleri ve fayda-maliyet analizi oluşturmaktadır.

Aktif karbonun en verimli üretim koşullarını belirlemek amacıyla farklı sıcaklıklarda (400, 500, 550, 600, 700, 800 ve 900°C) karbonizasyon işlemi ve farklı konsantrasyonlarda (1 M, 3 M ve 5 M) $ZnCl_2$ kullanılarak kimyasal aktivasyon yöntemiyle aktif karbon üretilmiştir. Karakterizasyon testleri sonucunda optimum koşullar 600°C' de karbonizasyon işlemi ve 3 M konsantrasyonunda $ZnCl_2$ kullanımı olarak tespit edilmiştir. Aktif karbon numunelerinin BET, SEM/EDX, XRD, FTIR-ATR, DTA/TG analizleri yapılarak ve hidrojen depolama kapasitesi ölçülerek aktif karbonun karakteristik özellikleri ortaya konmuştur. Hidrojen depolama kapasiteleri farklı konsantrasyonlarda $ZnCl_2$ kullanılarak 25°C ve -169°C' de test edilmiştir. En yüksek kapasite 3 M $ZnCl_2$ kullanımında ve -169°C' de bulunmuştur. Buna göre, depolama kapasitesi 43.907,27 mbar basınç altında ağırlıkça %3,18 olarak ölçülmüştür.

Adsorpsiyon deneyleri için cam malzeme kullanılarak 0,002 m^3 hacimli sızdırmaz kesikli reaktör üretilmiştir. Deney düzeneği ve ölçüm cihazları kullanılarak yapılan deneylerde, giderim verimleri piyasadan satın alınan ticari aktif karbonu referans alınarak karşılaştırılmıştır. Formaldehit ve BTEX gazları için limit değerleri göz önünde bulundurularak sırasıyla formaldehit için düşük konsantrasyona sahip değerler 170±14.92, 260±23.76, 720±47.61, 1040±68.47, 1220±72.14, 1900±83.37, 3290±95.44 ve 7650±111.18 μg/m^3 ve yüksek konsantrasyona sahip değerler 30.000±207,44, 50.000±338,61, 60.000±376,89 ve 110.000±497,21 μg/m^3 olarak çalışılmıştır. Benzen için; 2,4±0,45, 5,51,09±, 54±10.73 ve 322±47.80 μg/m^3, toluen için; 3,7±0,58, 9±2,62, 86±15.83, 414±47.26 μg/m^3, etilbenzen için; 3,9±0,66, 9,2±1,59, 90±15.55, 430±46.64 μg/m^3 , m, p-ksilen için; 3,4±0,72, 8,5±1,32, 83±12.95, 397±82.10 μg/m^3, o-ksilen için 5,2±0,82, 10±2.49, 100±24.38, 483±102.67 μg/m^3, BTEX için 18,3±1,89, 42±4.97, 412±48.74 ve 2045±203.37 μg/m^3 olmak üzere farklı başlangıç konsantrasyonları belirlenmiştir. Ticari aktif karbon ve tez kapsamında üretilen aktif karbon için izoterm parametreleri karşılaştırılarak sunulmuştur. Deneyler sonucunda elde edilen veriler Dubinin-Radushkevich, Langmuir ve Freundlich izotermlerine uygulanmış, izotermlerin denge verilerini iyi bir şekilde temsil ettiği gözlenmiştir. Bu izotermler arasında bulguların Freundlich izotermine daha uygun olduğu belirlenmiştir.

Verim açısından en iyi performans gösteren değerler, düşük konsantrasyonlar olarak bulunmuştur. 170±14.92 μg/m^3 konsantrasyonda yapılan formaldehit giderim deneyinde ticari aktif karbonun verimi %47,83 iken üretilen aktif karbonda verim %73,37'e değerine ulaşmıştır. 7650±111.18 μg/m^3 başlangıç konsantrasyonunda bu değerler ticari aktif karbonda %35,99, tez kapsamında üretilen aktif karbonda %47,58'e düşmüştür. Benzen giderim deneyinde, ticari aktif karbon %65,23 iken üretilen aktif karbon %73,86'dir. Toluen deneyinde ticari aktif karbon %43,44 iken üretilen aktif karbonda %63,31'dir. Etilbenzen deneyinde ticari aktif karbon %50,08 iken üretilen aktif karbon %65,96'dır. M, p-ksilen deneyinde ticari aktif karbon %42,04, üretilen aktif karbon %60,28'dir. O-ksilen deneyinde ticari aktif karbon %78,99 iken üretilen aktif karbon %88,07'dir. BTEX deneyinde ise 18,5 μg/m^3 konsantrasyonda ticari aktif karbon %52,43, üretilen aktif karbon %71,7 verim sağlamıştır.

Tez kapsamında üretilen aktif karbon ile elde edilen verim değerleri formaldehit ve BTEX konsantrasyonları için ticari aktif karbona kıyasla daha yüksek bulunmuştur. Gözenek yapısı, yüksek yüzey alanı ve adsorplama kapasitesine sahip olmasına bağlı olarak at kestanesi kabuğunun aktif karbon üretiminde potansiyeli yüksek bir hammadde olduğu tespit edilmiştir. Aktif karbon içeren dekoratif ürünler ile iç ortam havasından formaldehit ve BTEX giderimi için verimli bulunmuştur.

Keywords: Adsorpsiyon, Aktif Karbon, BTEX, Formaldehit, Hidrojen Depolama, İç Ortam Hava Kirliliği.

ACKNOWLEDGMENTS

First of all, I am thrilled to come to the end of my Ph.D. career, a long, tiring and difficult process. I am grateful for support, guidance and encouragement during my Ph.D. education to my supervisor Prof. Dr. Gülen GÜLLÜ, whom I owe a dept gratitude and who I took a role model for me. The end of this hard process gives me happiness. Despite the long hours of frustration, fatigue and anxiety during the work, I complete this difficult process.

I appreciate Asst. Prof. Dr. Aydın Türkyılmaz, Prof. Dr. Savaş Canbulat, Assoc. Prof. Dr. Hakan Şevik, Assoc. Prof. Dr. Nejdet Gültepe, Asst. Prof. Dr. Kutalmış Gökkuş for their help with ideas that brighten up my life and invaluable suggestions and comments. I am also thankful to Assoc. Prof. Dr. Selim Latif Sanin, Asst. Prof. Dr. Yusuf Çağatay Erşan and Prof. Dr. Rukiye Tıpırdamaz. Moreover, I want to thank Res. Asst. Dr. Yeşer Aslanoğlu and Ph.D. student Parisa Babaei.

My words are not enough to describe my love for my dear wife and little baby, and I am grateful to them. They were always there for me and shared my apprehension.

I have to express that I will always remember the support of my most precious friends who never left me alone, my parents; my father, mother, sister and dear grandmother.

Thank you all…

Kaan IŞINKARALAR

November 2020, Ankara

TABLE OF CONTENTS

LIST OF FIGURES

LIST OF TABLES

SYMBOLS AND ABBREVIATIONS

Symbols

$(CH_3)_2S$	Dimethyl sulfide
Å	Ångström
Ar	Argon
CFC-11	Trichlorofluoromethane
CFC-H	Chlorofluorocarbon gases
CH_3OH	Metanol
CH_3SH	Methanethiol
CH_4	Methane
CO	Carbon monoxide
CO_2	Carbon dioxide
CS_2	Carbon disulfide
F-gases	Fluorinated gases
H_2O_2	Hydrogen peroxide
H_2S	Hydrogen sulphur
HCHO	Formaldehyde
HCOOH	Formic acid
HCs	Hydrocarbons
He	Helium
HNO_3	Nitric acid
HO_2	Hydroperoxyl
Kr	Krypton
N_2	Nitrogen
Ne	Neon

NH_3	Ammonia
NO_x	Nitrogen oxides
O_2	Oxygen
O_3	Ozone
OH	Hydroxide
SO_2	Sulphur dioxide
Xe	Xenon

Abbreviations

AC	Activated Carbon
AE	Arrhenius Equation
APC	Air Pollution Control
BET	Brunner Emmett Teller
BVOCs	Biogenic VOCs
CBA	Cost-Benefit Analysis
D-R	Dubinin-Radushkevich
DTA	Diffrential Thermal Analysis
EMRA	Energy Market Regulatory Authority
EU	Europe Union
FTIR	Fourier Transform Infrared Spectroscopy
GA	Gas Adsorption
GEMS	Global Environment Monitoring System
GHG	Greenhouse Gases
HAP	Hazardous Air Pollutant
IAQ	Indoor Air Quality

IAP	Indoor Air Pollutant
LDF	Linear Driving force
LOD	Diagnostic Limit
LOQ	Lower Limit of Determination
MDF	Medium-Density Fibreboard
MIR	Maximum Incremental Reactivity
NHMRC	National Health and Medical Research Council
OVOCs	Oxygenated VOCs
PCBs	Polychlorinated Biphenyls
PM	Particulate Matter
POCP	Photochemical Ozone Creation Potential
SEM	Scanning Electron Microscope
TDS	Thermal Desorption Spectroscopy
TG	Thermogravimetry
TSP	Total Suspended Particulate Matter
UNEP	United Nations Environment Programme
USEPA	United States Environmental Protection Agency
VOCs	Volatile Organic Compounds
WHO	World Health Organization

1. INTRODUCTION

The natural resources are damaged day by day because of various reasons. One of these sources is the air, and the quality of it is getting worse every day. The main reasons for this situation are the development of industrial and rapid urbanization. Air pollution started with coal use, which emerged with industrial activities and accelerated with increasing autonomy and urban sprawl in the 18th century [1, 2].

Developments such as the use of newly discovered heavy weapons among warriors after World War II and the development of industrial revolutions such as furniture one after another paved the way for pollution. Different chemicals have entered our homes like adhesive resin. Scientists are faced with a new type of air pollution after these events. This problem showed up that it was not an ordinary smoke and smog. It was a photochemical smog. It was reputed to be oil and gasoline refineries and some chemical storage facilities. So, people tried to control them. After that, they found out what the main problem. It was the engine that internal combustion. It appears that photochemical oxidations are observed like haze at the top of the atmosphere. This brown, slight haze is a blend of some pollutants that occur from particulate matter (PM), sulfur oxides (SO_x), nitrogen oxides (NO_x), volatile organic compounds (VOCs) and other many pollutants in the atmosphere [3, 4].

Today's world is called to emerge from various technologies regarding self-reliance products given the problem's progress and established. Investigating different issues based on this analysis goes to reconstruct in terms of separation and recycling resources. These products are widely used in all areas, which are frequently used for every place such as doors, glass, wood joinery, paving stones. Many other materials can be included in this area. These companies proudly present the latest technology by using high-tech products. However, the studies' results clearly show the negative effects of new and firsthand indoor air quality products. In this way, people who care about their own lives and who read and adopt these works have started to pay attention to regulate their internal environment as they are gradually impeller and away from technology. In the surveys on

remarkable health, some people have realized this awareness and have used wood products for their health and used only wood products for installation. In particular, they have taken measures against indoor air pollutants (IAP) [5, 6].

Many states and governments have issued some new air pollution decisions because of the adverse effects of air pollutants in the developing world. Some communities like World Health Organizations (WHO) and the United States Environmental Protection Agency (USEPA) have been created about people and the environment healthy. Increasing urbanization and industry processes cause irreversibly destroying resources in the air, water and soil. Leading organizations, all the adverse effects of pollutants on the environment and human beings have been investigated and listed in IAP [7, 8].

In particular, with recent studies, it is emphasized that unlike water, the air is not only a regional problem, it is also a global problem that the world needs to be handled together in the Earth. Humanity is exposed to abundant amounts of air pollutants both inside and outside of the air by breathing. Volatile Organic Compounds (VOCs) are ubiquitous in our life. These compounds are found in indoor air and composed of various reagent substances. Although they have different properties and different chemical structures, they critically affect the environment and human health [9, 10].

1.1. Framework

Air pollution control (APC) actions of human beings date back to at least the thirteenth century despite most of the world's significant endeavors since 1945. Until this time, humanity had problems with other issues. However, the awareness increased with black air and thick fumes, where the factories released air rapidly in the 1930s and 1940s. Until 1945, it was tried to control these fumes and mists on site. This uncontrollable situation broke out between 1945 and 1969, and awareness of those residents increased. A new trend started to emerge in the 1980s. In this current, it concluded that air pollution began to cause problems both locally and globally. The increase in awareness and the expansion of the studies on air quality, a detailed introduction, was made not only to the outdoor air

but also to the indoor air. The awareness of air pollution, which emerges as humans spend more time indoors, has become more conscious.

The studies have shown that 89% of people living in the United States and 80% of the people living in developing countries spend their time in indoor environments [11]. Therefore, people face a variety of indoor pollutants. The VOCs are liquids or solids that involve organic carbon, which significantly evaporated in the background. They are possibly the second-most prevalent and assorted class of emissions after particulates. Therefore, one of the increasingly popular topics about indoor pollution. They are emitted by specific sources, either interior or outdoor, as if they are a ventilator. The impact of pollutants in indoor air; depends on the building's features, the material used in its construction like a heating system, ventilation situation, and the behavior of the people living in it (such as smoking). The most important pollutants that threaten IAQ are generally below the level that can be perceived by smell [12]. VOCs' sources in buildings are very diverse in construction materials (paints, varnishes, adhesives and construction materials), printers and copiers used in school and office environments and outdoor traffic. Another source of them is cigarettes and their derivatives are widely consumed in the world. The pollutants mentioned have many bad influences or many adverse effects on metabolism and the human body.

Based on modern science because of new inventions and technology, the framework is still being developed a wide variety of ways to eliminate VOCs' negative features. This problem addressed a study performed in cooperation of produced in our facility activated carbon in the context. The study's focus is to analyze how and its dissimilarity is removing this generated activated carbon (AC).

1.2. The Aim and Scope of the Thesis

The thesis's primary purpose is to investigate adsorption potential of AC produced from horse chestnut. This study's hypothesis is defined as "the activated carbons produced from horse chestnut have more efficient adsorption capacity than commercial activated

carbons." In this context consists of eight sections in total. Also, the purpose and scope of this study can be summarized as follows:

In Chapter 1, the main lines, frame, objective, content and originality of the thesis are explained.

In Chapter 2, the general characteristics of the formaldehyde and BTEX gases commonly found in the indoor environment, the production and available parts of the activated carbon, the hydrogen storage capacity and data of the activated carbon produced and the adsorption isotherm of the removal parameters identification in this part.

In Chapter 3, powder activated carbon production is lignocellulosic biomass. It can be collected easily from nature, with a high surface area produced with the help of zinc chloride ($ZnCl_2$) in horse chestnut compared to commercial activated carbons. The activated carbons are capable of storing hydrogen. Analyzes have been made to reveal some characteristic features and hydrogen storage capacity of the produced activated carbon. Drawing graphics by adapting formaldehyde and BTEX removal data to the adsorption isotherms, hydrogen storage tests of activated carbon.

In Chapter 4, separate investigation of the formaldehyde removal efficiencies and it is the adaptation of the data obtained after the formaldehyde removal study in the batch reactor to the Freundlich, Langmuir, Dubinin-Radushkevich isotherm. Transformation of the data obtained for formaldehyde and individually evaluated as benzene, toluene, ethylbenzene, m, p-xylene, o-xylene adapted to to the adsorption parameters are suitable for Freundlich isotherm.

In Chapter 5, this thesis's overall outcome was discussed and described the results of applying an approach to VOCs with activated carbon. The removal of formaldehyde and BTEX gases shows that a useful model and this removal method used is the conclusion that explains that it is quite successful. Lignocellulosic wastes transformed the activated

carbon, with which we were obtained successful results into final products. They are mainly used in homes and offices and decorative products for passive air purifiers.

1.3. Novelty of the Thesis

Studies have been conducted in different research centers worldwide to eliminate volatile organic compounds in the air. However, successful studies on VOC removal with activated carbons have not been presented in the literature. The removal techniques and methods are quite different, but they cannot focus entirely outdoor and indoor on removing VOCs in the air. Compared to other studies in this thesis multiple gas removal is aimed with the help of activated carbon.

The main features of these experimental studies can be summarized as follows. The raw material of the activated carbon produced within the scope of the study constitutes the original value of the thesis. The production of activated carbon from *Aesculus hippocastanum* L. (horse chestnut) shell which to our knowledge has never been investigated before for such a purpose. The characterization studies of this activated carbon first, then the ability to store hydrogen and then remove formaldehyde and BTEX gases at the internal environment level. It has also been aimed to obtain higher efficiency from produced activated carbon than commercial activated carbons called high-efficiency adsorbents, which are imported at exorbitant prices, especially from abroad. However, there are a limited number of experimental studies about removing VOCs from the air by using activated carbon.

2. THEORETICAL BACKGROUND

Air pollution control system is difficult from other pollutant controls, air pollution control (APC), which had become a significant problem of the present day. However, its intervention is also essential, together with being very difficult for APC. The various materials and methods have been developed against APC. The first of the pollutants mentioned above are carbon dioxide (CO_2), carbon monoxide (CO), sulfur dioxide (SO_2), methane (CH_4), nitrogen oxides (NO_x), chlorofluorocarbon gases (CFC-H), hydrocarbons (H_xC_x), particulate matter (PM), ozone (O_3), water vapor and VOCs. These pollutant gases are so active that they react with each other in the troposphere and turn into different pollutants. The concentrations of gases and retention times in the ambient air were givenin Table 2.1 [13, 14].

These gases are usually divided into two categories as primary and secondary pollutants. The primary contaminants (PM, CO_x, NO_x, SO_2 and C_xH_y) are harmful chemicals entering the atmosphere. The other pollutants (O_3, SO_3, etc.) are detrimental chemicals that form in the atmosphere where react with standby gases. The more commonly found and ample pollutants (PM, NO_x, SO_2, VOCs, CO and O_3) are located in the troposphere. According to the formed shape, NO_x ($NO+NO_2$) is produced from atmospheric N_2 and O_2, which are as generate with chemical and physical transformations NO_x gases are the primary substance of NO, NO_2 and N_2O [15].

$NO+O_3 \rightarrow NO_2+ O_2$		rxn1
$NO_2+ O_3 \rightarrow NO_3+ O_2$		rxn2
$NO_3+ h\nu \rightarrow NO+ O_2$	(~10%)	rxn3
$NO_3+ h\nu \rightarrow NO_2+ O(^3P)$	(~90%)	rxn4

It can occur similarly as in some reactions between SO_x, S_2 and O_2. It first occurs chemically; then, it becomes SO_3, a second gas in which SO_2 reacts with O_2. The situation of CO_x increases with domestic and non-domestic fossil fuel usage, which is consumable

residential heating, cooling, transporting and other manufacture of goods. CO_2 is a gas that can be formed by humans during natural processes such as the decay of plants. The O_3 is another pollutant that can produce both natural and approach in the troposphere, mainly in the stratosphere [16-20].

$O_2 + h\nu\ (\lambda < 240\ nm) \rightarrow O + O$ rxn5

$O + O_2 \rightarrow \cdot O_3$ rxn6

It is a secondary pollutant in the troposphere when the NO_x react with VOCs under solar light. This thesis focuses on VOCs, a pollutant in indoor and outdoor environments. They are released due to fossil fuel, petroleum refineries, chemical producing plants, power plants, preparation of solvents, building and commercial paints and some combustion of solids [21, 22].

$CH_2O + h\nu\ (\lambda < 340\ nm) + 2O_2 \rightarrow HO_2 + HO_2 + CO$ rxn7

$H_2O_2 + h\nu\ (\lambda < 350\ nm) \rightarrow \cdot OH + \cdot OH$ rxn8

$HONO + h\nu\ (\lambda < 395\ nm) \rightarrow OH + NO$ rxn9

Table 2.1. Components of atmospheric air [23].

	Species	Average concentration (ppm)	Approximate residence time
Major species	N_2	780,840	10^{-6} yr
	O_2	209,460	10 yr
	H_2O	Variable	
Inert gases	Ar	9,340	
	Ne	18	
	He	5.2	

	Kr	1.1	
	Xe	0.09	
Trace species	CO_2	350	15 yr
	CH_4	1.72	10 yr
	H_2	0.58	10 yr
	N_2O	0.33	150 yr
	CO	0.05-0.2	65 days
	NH_3	0.01	20 days
	NO/NO_2		
	Remote regions	< 0.00004	1 day
	Rural continental	0.0002-0.0005	1 day
	U.S. Urban	0.001	1 day
	O_3 (troposphere)	0.02-0.05	< 1 yr
	H_2O_2	0.001	
	HNO_3	0.001-0.0001	1 day
	HCs	0.001-0.050	
	HCHO	< 0.0005-0.00075	
	HCOOH	> 0.02	
	CH_3OH	0.04-0.06	
	CFC11	0.003	65 yr
Sulfur compounds	SO_2	0.0002	40 days
	COS	0.0005	> 0.3 x 10^5 h
	CS_2	0.00001-0.0002	> 1.8 x 10^5 h
	CH_3SH		3-13 h
	$(CH_3)_2S$		31 h

	H_2S		53 h
Free radicals	·OH	1-10 x 106 molecules/cm^3	
	·HO_2	1 x 109 molecules/cm^3	

The PM is the other important pollutant with specific dimensions compared to others and it is a mixture of different sizes of solid and liquid particles in the atmosphere. It has a different concentration and chemical composition and is emitted from anthropogenic activities. It can move within NO_3^- and SO_4^{-2} a different type of organic chemicals (organic carbon, black carbon and biogenic emissions), sea salt, metals and soil or dust particles. These particles can release into the air from sources or forms. If the smaller sizes (≤PM2.5) than the others (some are too small) are inhaled, they generally pass through the nose before entering the lungs. Then they have negative impacts of human organs like the heart and lungs. The relatively larger particles (≥PM10) have bigger than 10 μm diameter. These dangerous matters are produced by fossil fuel combustion, renewal for collapsed buildings and structures, some urbanization problems such as the closure of air corridors resulting from distorted urbanization, etc. [24-27].

These pollutants mentioned that air pollutants' diffusion and dispersion increase with transport with windy, dry and wet precipitation. Also, air masses transported from the pollution point source region have almost like the air cleaner is disposed of the PM. The air pollution is reduced by the environmental laws and regulations, which target to prevent all these pollutants. The environmental policy has been developing by many countries to decrease the harm to air and control the air pollutants level by improving monitoring and modeling systems [28].

2.1. Air Pollution

Air pollution is generally known as an indoor and outdoor environment in the language of society or among the public. Air pollution that human beings should focus on, also soil and water sources all over the world. Greenhouse gases (GHG), CO_2, CH_4, N_2O and F-gases contribute significantly to global warming. Increasing human activities and low

urbanization cause gas emissions to accelerate with their release. The various gases, liquids, or small invisible solids that cause air pollution are mixed within the atmosphere by different natural phenomena, human activities and the reaction of high levels of gases [27, 29, 30].

Nowadays, with the rising standards of life brought some problems are discussed more often in the World. At the beginning of this matter, there is air pollution that the increasing urban form. The industrial revolution within the last 100 years has become a popular topic and the research about this topic has become widespread, with many research institutes and centers. For example, WHO's data shows that 1.5 billion people died every year, depending on breathing due to exceeding the specified air pollution limits [31]. The weather conditions are noticeably high and visibly impaired when the population is crowded. CO_2 is one important air pollution parameter representing other pollutants and is regularly measured at Mauna Loa Observatory, Hawaii. Since the 1900s, a steady increase of CO_2 has been seen according to the values measured. it has increased rapidly since the 1960s in Figure 2.1. This value of it in recent years is 406.82 ppm at the date of January 2018. According to the Earth System Research Laboratory Global Monitoring System's official website, it was 411.75 ppm in February 2019, while this value reached 414.11 ppm in February 2020 [32-37].

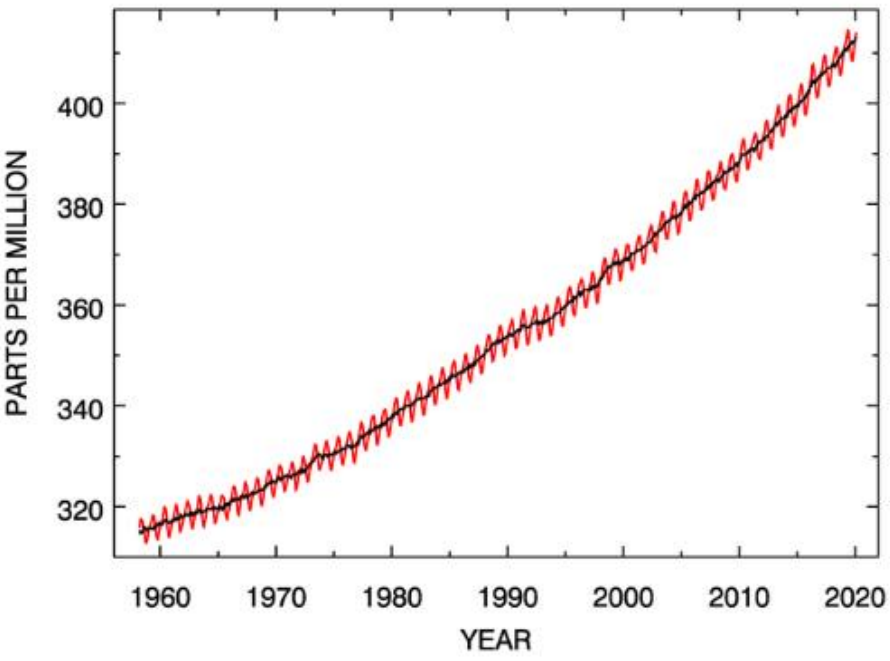

Figure 2.1. The carbon dioxide changes by years Mauna Loa constitute [38, 39].

Depending on this, air quality is getting worse, likely environment quality, which contributes to greenhouse gas emissions. Mobile pollutants, which use fossil fuel like cars, buses, trucks, planes and ships are increasing and the most fantastic examples of emission sources. As a growing population and tree massacres, we indirectly affect and call anthropogenic (human related). If generalized to do air pollution is an anthropogenic source or natural source. The other natural source that the specks of dust carried by the Sahara region's winds and a similar source is volcanic eruption [40].

On the other hand, the particulate matter arises from nuclear power plants and other heavy machine industries, which is an important role an import and export. They produce an adverse effect to i.e., nature, human, fish, plant, crops, bird, etc. that is to all ecosystems. The respiratory system, which is an impact to humans adverse with chronic lung disease and cardiovascular problems. The productivity of crops is decreasing due to acid precipitation [24, 41-43].

2.1.1. Concept of Air Pollution

United Nations Conference on Human and Environment adhered to eliminating all environmental pollution in Stockholm in 1972. The United Nations Environment Programme (UNEP) and the WHO commenced as co-occurring to explain urban air pollution problems. Some striking examples give like the 1952 London Fog in which over 3000 people gone to meet one's maker [44-46].

In 1974, UNEP and WHO consisted of the Global Environment Monitoring System (GEMS) about the urban air pollution monitoring network (GEMS/Air). However, it has obtained many air quality data in surplus 50 cities in 35 countries from top to bottom in the World. At the beginning of sulfur dioxide (SO), particulate matter (PM) with the high-volume sampler method and lead (Pb) analyses of the TSP (Total suspended particulate matter) filters were identified in the developing countries. The WHO and UNEP created some reports and shared them with the World in 1976, 1977, 1980, 1989, 1991 and 1992. In 1992, Agenda-21 was apparent that our future problem is urban air pollution and if

people are not prepared, a public health and environmental problem of crisis proportion occurs [47-49].

The cities with excessive pollutant load this so-called super city to face global atmospheric pollution like greenhouse gases. WHO and UNEP studied air quality in 20 of the 24 megacities of the World. Suppose summarized these studies about the air pollution situation show that megacities have faced increasing problems and their difficulties in finding solutions. After people pollute, cleaning it will be more expensive [50, 51].

2.1.2. Principal of Air Pollutants

The numerous institutes defined that biogenic and anthropogenic sources give lots of information about the air pollutants in Table 2.2. Air pollutants are separated as dust and gaseous pollutants. Particularly photochemical smog, aerosols, acid rain, dioxins, Polychlorinated biphenyls (PCBs), polycyclic aromatic hydrocarbons (PAHs), particulate organic compounds (POCs) and volatile organic compounds (VOCs) [52, 53, 54].

A tremendous amount of CO produced from incomplete combustion in fossil fuel uses. However, the amount of CO has not risen for many years because CO_2 has been growing up. The four nitrogen forms show in Table 2.2 and they reduced formation as NH_3, N_2O, NO, NO_2. The N_2O is inert gas as anesthetics and laughing gas. The NO and NO_2 are produced from the oxidation of the N_2, which at high combustion temperature and congruently lightning. Generally, nitrogen compounds are consisting of the combustion of fossil fuels. Although NO is the ruler NO_x compound emitted by most resources, NO_2 fractions from sources differ slightly depending on the source type. Ozone (O_3) is reformed by photochemical reactions easily recognized and located in from the stratosphere to the troposphere [57-60].

The reactive hydrocarbons sources are generally olefins and aromatics, both backgrounds of natural and anthropogenic. Although nonreactive hydrocarbons, mostly methane (CH_4) and saturated hydrocarbons, are relatively inert and not considered a vital pollutant or

contributor to pollution. A significant source of airborne organic compounds are the emissions from motor vehicles that consist of unburned fuel [61, 62].

Table 2.2 summarises species classified as air pollutants. In general, the focus point in terms of air pollution in this table is on the primary compounds from combustion, such as the oxides of nitrogen, sulfur dioxide, carbon monoxide, unburned hydrocarbons and particulate matter. In addition to these, heavy metal oscillations are also available, but bioindicators are also used in their control. This list of most prevalent pollutants identified in ambient air and potentially toxic atmospheric organic species [63-66].

Table 2.2. Sources of air pollutants [67, 68].

Air Pollutants	Anthropogenic	Natural
SO_2	Combustion of coal and usage oil	Atmospheric oxidation of organic sulfides, volcanoes
H_2S	Chemical processes and sewage treatment	Volcanoes and biological decay
N_2O	None	Biological decay
NO	Combustion	Bacterial, action in soil, photo-dissociation of N_2O and NO_2
NO_2	Combustion	Bacterial, action in soil, oxidation of NO
NH_3	Coal burning, fertilizer and waste treatment	Biological decay
CO	Auto exhaust and other combustion processes	Oxidation of methane, photo dissociation of CO_2, forest fires and oceans
O_3	No primary source, formed as a secondary pollutant from atmospheric reactions involving hydrocarbons and oxides of nitrogen	Tropospheric reactions and transport from stratosphere
Reactive hydrocarbons	Auto exhaust and combustion of oil	Biological processes in forests
Nonreactive hydrocarbons	Auto exhaust and combustion of oil	Biological processes in swamps, ruminant emissions

2.2. Volatile Organic Compounds (VOCs)

VOCs are defined as a hydrocarbon. They contain at least one carbon and hydrogen atom in its structure, defined as in aliphatic and aromatic structure solvents or directly involved in chemical reactions in chemical, pharmaceutical and hydrocarbon industries. According to USEPA, a total of 188 air pollutants as dangerous air pollutants and 149 were VOCs. They are separated into three parts; volatile, semi-volatile, VOCs and very persistent with chlorinated and brominated compounds, which have pressure higher than 10^{-1} torr at 25 °C and 760 mmHg [69-71].

According to The European Union (EU), VOCs are organic compounds which are observed as boiling point less than or equal to 260 °C at a standard pressure of 101.3 kPa. The countries that are members of the EU has been checked based on Directive 2004/42/EC of the European Parliament and of the Council of 21 April 2004 on the limitation of emissions of VOCs due to the use of organic solvents in different products Directive 1999/13/EC. These countries make a decision to reduce the hydrocarbon emissions about 30% also for lower the ozone formation potential need to stop nitrogen oxides emission [62, 72].

Many international protocols have been made to control carbon dioxide (CO_2) and nitrogen oxides (NO_x). They found a solution with the Montreal Protocol on Protection of Ozone Layer in 1987, London Revisions to do Protocol in 1990 and Copenhagen's Protocol in 1992. Also, the Kyoto Protocol's reduction of methane carbon dioxide and nitrous oxide aimed in 1997 [61, 73, 74].

2.2.1. The Physical and Chemical Properties of VOCs

The VOCs have been included in hazardous air pollutant (HAP) due to chemical properties and various health problems. They release into the atmosphere, also cause their elimination from the atmosphere because oxygenated with a photochemical process. Generally, numerous reactions begin with the hydroxyl radical ($^{\cdot}OH$) and O_3, NO_3, Cl, Br, which has different atmospheric lifetime depending on their severity of solar radiation, chemical structure and radical concentration. NO is changing to NO_2 while

photolysis and contributes to tropospheric ozone formation due to VOCs diminished in contaminated air masses at night time [75].

Nontrivial ·OH radicals are the most crucial interacting substance and there are approximately 1.1×106 radicals/cm^3 in the degradation of VOCs. Another radical is Cl, which has not been certainly checked as a global scale. Even though its reactions have been identified in some cities. The situation for alkanes that can seriously pollute when it reacts with O_3 and NO_3 [9, 76, 77].

The physical and chemical behavior of the troposphere affects to VOCs in many ways. For example, the most significant contribution to air pollution is the photochemical ozone formation. The VOCs are based on the temporal and spatial type of emission, molecular-dependent potential to produce ozone and the photochemical reaction rates. The use of VOCs' scale, which are their ozone production skill under atmospheric conditions, are the photochemical ozone creation potential (POCP) and maximum incremental reactivity (MIR). POCP tells the quantity of O_3 while calculating of its contour models under real-world conditions in Eq. (1). When comparing VOCs' ozone potential, it is calibrated by rating its values with these other VOCs (i.e., benzene) as follows [78-83].

$$POCP_{\alpha} = \frac{\text{Simulated extra amount of ozone based on VOC}\alpha}{\text{Simulated extra amount of ozone based on Benzene} \times 100} \quad \text{Eq. (1)}$$

Carter et al. evaluated ozone formation along with the range of up to a day with optimum VOC/NOx situations in urban areas in the United States by the other scale that MIR specified from irradiation of a more simple model of photochemical systems [84, 85].

Most of the VOCs given in Table 2.3 are emitted from motor vehicle emissions in various solvent production, dry cleaning and usually reach higher concentration values in winter. These VOCs vary depending on different situations. They are like the limit values determined by NHMRC. Concentrations computed at specific temperature and 101.3 kPa

compared with the NHMRC indoor air (1-h) target, set at 500 μg/m^3 for TVOC and 250 μg/m^3 for any VOCs [86, 87].

Table 2.3. The properties of some VOCs [88].

Compound	Formula	C_p (J/mol °C)	B.P. (°C)	ΔG_f (kJ/mol)	ΔH_f (kJ/mol)	ΔH_c (kJ/mol) at 25°C
Toluene	C_7H_8	166.0	110.6	114.09	12.0	-3909.8
Propane	$C3H_8$	73.8	-42	23.4	-103.8	-2220.0
Benzene	C_6H_6	136.1	80.1	124.5	49.0	-3267.6
Ethylbenzene	C_8H_{10}	185.9	136	120.0	-12.5	-4564.7
O-Xylene	C_8H_{10}	188.8	144	110.8	-24.4	-4552.8
Acetylene	C_2H_2	44.1	-84	209.2	226.7	-1299.6
Acetone	C_3H_6O	125.0	56	155.3	-248.1	-1789.9
Formaldehyde	CH_2O	35.4	-19	109.9	-115.9	-563.4
n-Hexane	C_6H_{14}	195.0	68	4.0	-198.8	-4163.1
Dicholoromethane	$C_2H_2Cl_2$	50.8	39.6	68.9	-95.5	-583.8
Tricholoromethane	$CHCl_3$	65.8	61.2	68.5	-101.3	-435.2
Tetracholoromethane	CCl_4	133.9	76.72	62.5	-132.8	-260.7
Tricholoroethylene	C_2HCl_3	80.02	87.2	6.7	-19.1	-910.8
Tetracholoroethylene	C_2Cl_4	95.6	121.1	20.6	-14.2	-772.8
Acetaldehyde	C_2H_4O	53.7	20.2	-133.2	-166.4	-1192.3
Ethylene	C_2H_4	42.9	-103.7	68.4	52.5	-1411.1

2.2.2. Sources of VOCs

People have basic needs, such as eating and drinking, shelter and transportation, which release invisible dangerous gases. These activities humankind do in our daily life cause some pollutants like VOCs. According to the National Air Quality and Emissions Trends Report; the estimate of fuel combustion emissions, industrial processes, transportation and miscellaneous. Almost 100 TgC/year is surmised to be exuded from technology

brought by technology besides the 150 TgC/year from all human-made sources, including biomass burning. Coal production, which is the energy source of industry and residences, causes significant methane causes emission and minor emissions of ethane and propane. Also, liquid fossil fuel production, storage and distribution result a wider variety of organic gas emissions to the outside [89-91].

The production platforms of crude oil are healthy point sources of hydrocarbons, for instance, methane, ethane, propane, butanes, pentanes, hexanes, heptanes, octanes and cycloparaffins. The primary sources from processing liquid fossil fuels are catalytic cracking (0.25–0.63 kg/m^3 of feed), coking (about 0.4 kg/m^3 of meal) and asphalt blowing (about 27 kg of VOC/m^3 of asphalt). Moreover, supposedly leakage emissions can come true from leaks and evaporation from all equipment and installations. However, not many volatile emissions are estimated to be 2.9 kg/t of fuel at petrol and service stations where have filled a car with gasoline or gasoline. Substantially petrochemical products involve in a limited number of compound classes such as acyclic alkanes, cyclic alkanes, monoaromatics and diaromatics. Each of many (tens of thousands) individual homologs and isomers consist of them. This report reflects that on-road vehicles, solvent utilization, non-road engines and cars are the highest sources of VOCs in the United States in Table 2.4. This Table also reveals a wide variety of other manufacturing processes. The total emissions have shown almost 0.32% of the US's unlimited electric utilization usage [92-94].

Table 2.4. National emissions estimate of VOCs for 1999 [90].

Manufacturing areas	Sources	Thousands of tons/yr	Percent of total
Fuel Combustion	Electric utilization	56	0.32
	Industrial	178	1.01
	Residential wood	608	3.45
Industrial Processes	Chemical and Allied Products	395	2.24

	Metal Processing	77	0.44
	Petroleum and Related Industries	424	2.40
	Solvent Utilization	4825	27.36
	Storage and Transport	1240	7.03
	Waste Disposal and Recycling	586	3.32
Transportation	On- road vehicles	5297	30.04
	Non-road engines and vehicles	3232	18.33
Miscellaneous		716	4.06
Total		17634	100

There are many sources available for direct and indirect release VOCs. At the beginning of indirect sources are photolysis and oxidation. The natural sources are biomass burning, anthropogenic activities and vegetation. The largest VOCs' direct source is vegetation and total emissions estimated at 770-1400 Tg/yr, although isoprene (C_5H_8) has been attributed to as 500-750 Tg/yr ratio [95-97].

This release is also known as biogenic VOCs (BVOCs). Table 2.5 shows that isoprene, terpenes, terpenoids, alcohols, aldehydes, organic acids and esters emitted with potentially many compounds. BVOCs have profoundly temporarily and geographically variables such as plant species, solar volume, warming and phenological events and other parameters excluding CO_2 that is not certain whether increases or not. The BVOCs also increase ozone production and the atmospheric lifetime of methane, enhancing the greenhouse effect in Figure 2.2 [98-100].

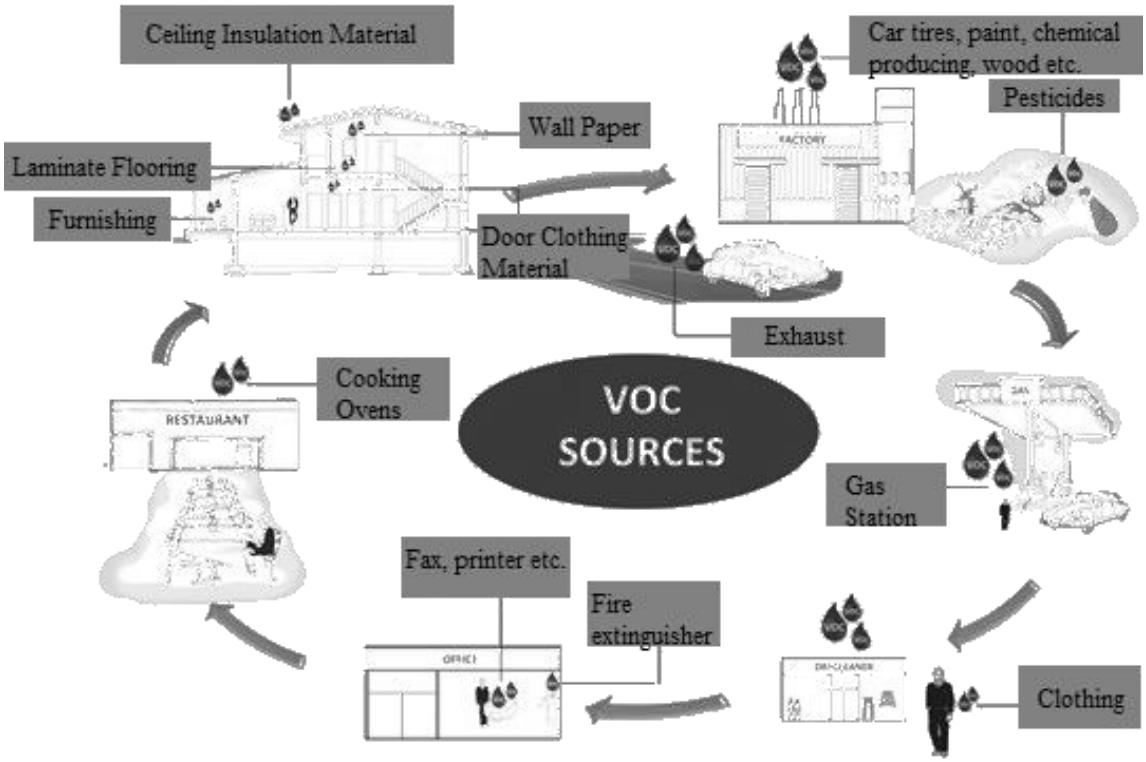

Figure 2.2. Common VOC resources adopted from [3, 101-103].

VOCs' second size of emission is biomass burning and fires, which emissions are more significant than 400 Tg/yr. Alkanes, alkenes, alcohols, aldehydes, ketones and organic acids, as well as nitrogen and sulfur-containing species such as nitric oxide (NO), nitrogen dioxide (NO_2), nitrous oxide (N_2O), ammonia (NH_3), hydrogen cyanide (HCN), acetonitrile (CH_3CN), sulfur dioxide (SO_2) and carbonyl sulfide (OCS) are release from sources [104, 105].

The other considerable factors are anthropogenic sources, which emissions were approximately 160 Tg for the year 2008 by the Emission Database for Global Atmospheric Research. This rate depends on population, transportation, agriculture, cooking, painting, smog, etc. [106, 107].

2.2.3. Effects of VOCs

People spend most of their time in houses, works, hospitals, universities, sports halls, restaurants, cafes and entertainment places such as indoor environments and the

remaining time is spent outside that both of them cause released VOCs from used materials by there. This situation is getting worse because recent epidemiologic studies indicate that lung problems can be linked to health problems and even death. Another serious problem is growing asthma and allergic cases. The tropospheric ozone problem is another issue, which can irritate airways. It can allow us to predict and to evaluate the efficiency of emissions between VOCs and NO_x. The reaction of O_3 to changes in VOCs and NO_x emissions, although gases, reveal a complex dependence on the levels and ratio of VOCs to NO_x emissions. To the constant level of VOCs emissions peak, O_3 increases as NO_x emissions increase until the critical ratio of VOC to NO_x is reached and then as a reverse proportion, O_3 decreases and NO_x emissions [108-110].

$O_3+h\nu \rightarrow O^1D$ $O^1D+H_2O \rightarrow 2OH$	rxn10
$HCHO+h\nu \rightarrow 2HO_2$	rxn11
$Alkene+O_3 \rightarrow$ radicals	rxn12
$OH+VOC_i \rightarrow a\ HO_2+b\ RO_2+CO_3$	rxn13
$HO_2+NO \rightarrow NO_2+OH$	rxn14
$RO_2+NO \rightarrow$ d ($NO \rightarrow NO_2$ + conversions) + HC oxidation products	rxn15
$RCO_3 + NO \rightarrow$ e($NO \rightarrow NO_2$ conversions) + HC oxidation products	rxn16
$NO_2 + h\nu \rightarrow NO+O$ $O+O_2 \rightarrow O_3$	rxn17

Starting with rxn10 and rxn11, which reaction chain results consist of photochemical O_3 (rxn17) by free radicals. This chain continues with ·OH oxidizes VOCs (rxn13), forming peroxy radicals as photolyzed (rxn17) O_3 that turn into NO to NO_2 (rxn14- rxn16) and rxn15- rxn16 sections are the conversions of NO_2. Then loop of reactions is being completed for another cycle by remodeling both OH in rxn14 and NO in rxn17. In rxn13 part, it could be CO, hydrocarbon, or HCHO instead of VOCs that enters the reaction [111, 112].

The VOCs that contain gases such as chlorine, fluorine, bromine, or iodine break down ozone in the stratosphere. Contrary to the troposphere's ozone, VOCs' adverse effects on the ozone layer protect people against harmful ultraviolet (UV) rays in the stratosphere. Chlorine, fluorine, bromine or iodine reaching the stratosphere with solar, then they are separated from this structure by the effect of light and become free. In this case, these substances are very reactive in their free form, attacking the O_3, which tends to react and disintegrate it. Until these substances disappeared in the stratosphere, they repeatedly turn into other states and break down hundreds and thousands of molecules of ozone [113, 114].

In ornamental and agricultural plants, catalyze many airborne and absorbed VOCs then transport them from leaves to roots. Plants' activities sometimes deteriorate due to accumulating within the plate, in vacuoles or cell walls in terms of secondary pollution, possibly toxic, effects on herbivorous animals in Figure 2.3 [119, 120].

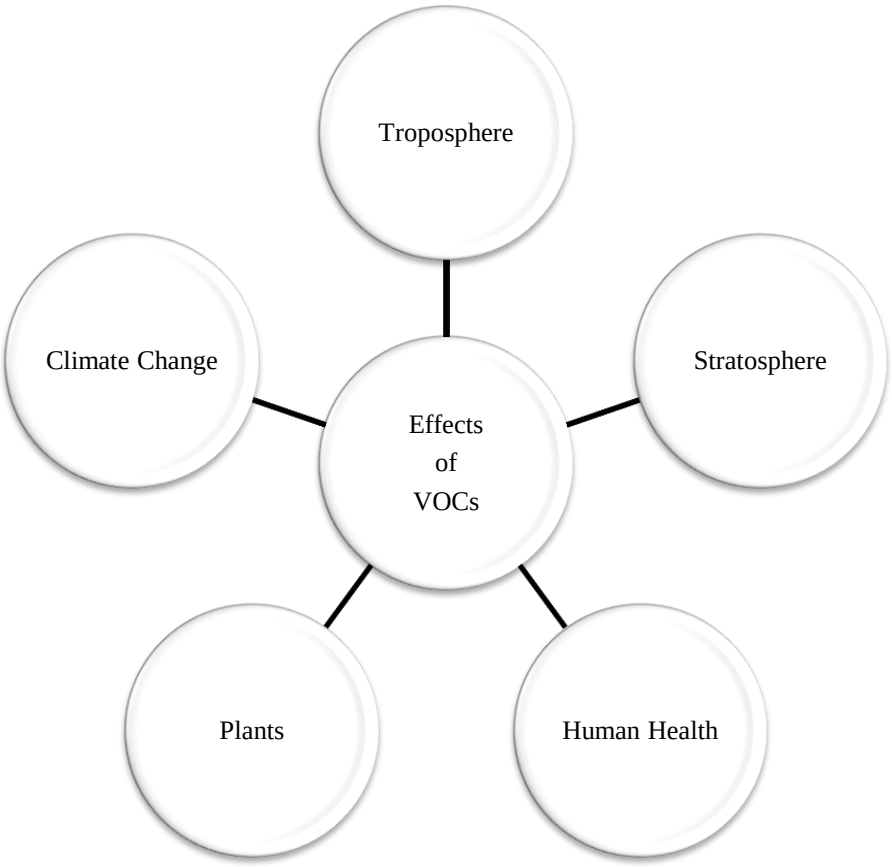

Figure 2.3. Effects of VOCs [115-118].

Climate diversity occurs due to various air pollutants that the leading source of harmful gases released into the air from multiple sources. Here is transformed into more dangerous chemicals that can absorb them and increase the air's ozone concentration. Consequently, these gases may be entering with some reactions, sunlight and water vapor converted into other reactive gases. Nevertheless, don't have the direct effect of VOCs on climate change [121, 122].

2.2.4. Control and Removal Techniques

VOCs have commercial importance that are valuable fuels or solvent if we can recover them in the pure or nearly pure form we can reuse or sell to obtain a profit. These sectors, such as oil, gas, paint and various chemical production, cause adverse effects on the nervous system and aspiring ways in humankind's health. Developed and developing countries decided to reduce and even prevent harmful gases. Certainly, VOC containing gas streams must be more often economical but not often for small streams. VOCs' removal by condensation, adsorption, absorption, combustion and biological oxidation in Table 2.5 [123, 124].

Table 2.5. Control methods of VOCs.

Methods	Advantages	Disadvantages	Ref.
Absorption (Scrubbing)	-VOCs concentration ranges from 500 to 5000 ppm and it can achieve VOC removal efficiencies of 90-98% -Safe, fast, reasonable and economically	-Residence time of liquid and vapor is short (1-10s) -It is not suitable for continuous operation	[125]
Adsorption	-The use of activated carbon is quite common and successful -It can be used repeatedly with desorption	-It is expensive to treat a very low VOC concentration in exhaust air -However, activated carbon, which is not chosen correctly, is easily blocked due to its low porous structure	[126]
Condensation	-It is effective in contaminants with a concentration of 5000 ppm and higher and with a boiling point above 100°F	-The water obtained after operation needs to be given to the wastewater treatment plant or to the package treatment plant	[124]
Thermal Oxidation	-Technology can reach up to 95–99% VOC removal efficiency and there is a prospect for recovery of Energy -Temperatures range from 1300 to 1800°F	-Require additional treatment	[124]
Membrane Separation	-The efficiency varies according to the selectivity and pressure of the membrane	-High initial investment cost -There may be additional refinement depending on the situation	[127]

	-It can easily recycle of compounds		
Catalytic Oxidation	-Systems operate at lower temperatures, typically 700–900°F	-Require additional treatment	[124]
Biofiltration	-A popular choice for treating odorous streams and come out CO_2 and H_2O -95% yield is obtained in solvent such as toluene and ethanol -It does not need too much chemicals during the operation phase	-Biofilter beds cannot absorb large amounts of VOC at a time -It does not be effective for highly halogenated compounds such as trichloroethylene (TCE) and trichloroethane (TCA) due to their biodegrade ability	[128]

Each of these methods has different advantages and disadvantages. The gases used for the removal of VOCs may contain enough various. Some are cheap, lower price for investment costs, have a long life span and high recovery, while others are expensive, short-term and low on productivity.

Although some systems' implementation is difficult and limited, the system cannot respond with sudden loads, but nowadays, it is not the only way to go. Still, two successive ways are being tried like biofiltration as a post-treatment to adsorption [27, 129].

2.2.5. Glossary of VOCs

The VOCs are grouped into five groups; aliphatic, aromatics, chlorinated hydrocarbons, aldehydes and ketones in Table 2.6. Also, it has a vital role in ozone formation [130, 131].

Table 2.6. Classification of VOCs sources.

Sources of VOCs by classes	Features of the class	Ref.
Alkanes	-Low reactivity in the atmosphere. -The primary sources are emissions from biomass burning and exploitation and distribution of natural gas. -Ethane (C_2H_6) is the most abundant and Propane (C_3H_8) is the next higher alkane in the atmosphere. -C_4-C_5 alkanes are primarily emitted from the evaporation of fossil fuel and C_6 alkanes are released from solvents and fossil fuel evaporation.	[132]
Alkenes	-Alkenes mainly caused by vehicle exhaust, biofuel combustion and biomass combustion. -Ethene (C_2H_4) and Propene (C_3H_6) are the most abundant species in air. -High reactivity in the atmosphere. -Alkadienes (C_nH_{2n-2}) that it spreads as a by-product of incomplete combustion processes.	[13, 133]
Alkynes	-Ethyne (acetylene) (C_2H_2) is the dominant alkyne in the atmosphere. -It is emitted from unburned fossil fuel in urban areas, whereas emissions from biomass burning and biofuel combustion in other regions.	[134]
Aromatics	-The most common aromatic VOCs are benzene, toluene, ethylbenzene, xylenes, styrene and trimethyl benzenes.	[135]
Oxygenated VOCs (OVOCs)	-Primary sources are anthropogenic and biogenic and produced from photochemical reactions. -The highest additives from vehicle sources are formaldehyde, acetaldehyde, oxygen aromatics and acetone.	[136]

In the research scope, firstly, formaldehyde and then adsorption studies were carried out for BTEX gases.

2.2.5.1. Formaldehyde

In the first part of our study, formaldehyde (CH_2O) gas, which has thermodynamic properties in Table 2.3, also features given in Table 2.7. It is a colorless, reactive, flammable, pungent odorous gas at room temperature with a molecular weight of 30.03 g/mol and is commercially available as a 37% solution. In other words, formalin or formol is also frequently used in methanal, methylene oxide, oxymethylene, methyl aldehyde, oxomethane solutions.

Although synthesized by Russian chemist Aleksandr Butlerov in 1859, August Wilhelm von Hofmann successfully carried out the synthesis by passing methanol and air over the heated platinum spiral in 1867. Although other forms of formaldehyde can be obtained, this form of production is still in use today. The combustion temperature is 4.47 kcal/g of formaldehyde gas, which is easily soluble in water, alcohols and other polar solvents but has low solubility in apolar liquids.

Formaldehyde is a hazardous substance for living organisms and is present in water as a hydrate and tends to polymerize. It also is polymerized in concentrated formaldehyde solutions, forms a substance called paraformaldehyde. The usage area of formaldehyde and its derivatives with its rapidly growing population and developing industry has a broad place. However, it degrades by giving menthol and carbon monoxide while slowly degrading at high temperatures [118, 137-140].

It is a field of medicine in an area where formaldehyde is widely used. It is commonly used in this area because of fungicide, germicide, disinfectant and protective properties in hospitals' pathology laboratories to fix tissues and cells. Formaldehyde is also used to preserve grain and seeds in agriculture, skin layering, wood preservation and preservation of tissue samples in hospitals and laboratories [141].

Table 2.7. The physical and chemical properties of formaldehyde [92, 93, 101, 142].

Chemical Formula	CH_2O, HCHO	
CAS Registry Numbers	50-00-0	
Synonyms	Formalin, methanal, oxoymethane, oxomethylene, methylene oxide, formic aldehyde, methyl aldehyde	
Mole weight	30.03 g/mol	
Melting point	-118°C	
Boiling point	-19.2°C	
Density (at 20 °C, 1 atm)	0.815 g/L	
Relative density (air =1)	1.04	
Solubility	Soluble in water, ethanol, ether and acetone	
Resolution	High resolution (55%) (in Freshwater) and 400,000 – 550,000 mg/L	
Henry's Law Constant	$3.27x10^{-7}$ atm.m^3/mol and $2.2x10^{-2}$ – $3.4x10^{-2}$ Pa.m^3/mol	
Steam Pressure	516.000 Pa; >3.883 mm Hg	
Ignition Temperature	300°C	
Photolysis	Half-life (in sunlight) 1.6 - 19 hours H_2 and CO or H^+ and HCO^-	
Conversion factors	at 760 mmHg at 20°C 1 ppm = 1.249 mg/m^3 1 mg/m^3 = 0.801 ppm	at 760 mmHg at 25°C 1 ppm = 1.228 mg/m^3 1 mg/m^3 = 0.814 ppm

It is effortless for people to be exposed to formaldehyde in industrialization. However, it can occur naturally in the atmosphere and it can also be released to air, lakes, rivers and seas. Gravimetric, spectrophotometric, spectrofluorometric and chromatographic methods have been developed to determine formaldehyde. Each of these methods have different degrees of sensitivity in Table 2.5. This material is used in many other places and areas, from animal feed to accessory products [143].

The amount of formaldehyde present in the indoor environment is relatively high compared to the external environment. If we look at the reasons for these main reasons, smoking, followed by cooking in homes or restaurants at located incineration processes, is the most common in Table 2.8. Apart from the previously mentioned sources, some materials emit formaldehyde. In particular, the newly produced materials have also been exacerbated even more when moisture and room temperature are exceeded. The most significant danger coming from the modern furniture used today is the formaldehyde pollution in the houses. The particleboard, Medium-Density Fibreboard (MDF) products are produced with urea-formaldehyde glue and formaldehyde can spread for a long time from MDF products. Two factors are the release of formaldehyde increases the humidity and temperature [144].

Table 2.8. Oscillating places of formaldehyde [145-148].

Oscillating places				
Medium Density Fiber Board	Non-natural Varnishes	Insulation Materials	Synthetic Lacquers	Paints and Adhesives
Nail Varnishes	Cleaning Products	Computers	Electronic Materials	Filler Foam
Particleboard	Carpets	Hardeners	Photocopy	Synthetic Resins
Wood Materials	Textile Products	Plywood	Insecticides	Lostra Halls

The formaldehyde is generally used and potential may be in oscillation places. Secondary formaldehyde formation is sometimes present. For example, it can occur by internal chemical reactions between ozone and terpenes [149, 150].

Depending on the samples' age taken with the various studies conducted in the literature, they found that the interior space was a significant determinant of air quality density due to many chipboard slabs at home. In the bedrooms (besides separating smokers and non-smokers), people made measurements on the complaints in children's rooms and the

kitchens. As a result of the samples, formaldehyde was determined in products. In another study, it is seen that the pressed wood products are among the primary sources contributing as a source of formaldehyde if inhaled at home. In another study, it has been shown that formaldehyde release is intense in newly painted rooms or ceiling coverings of the house. Formaldehyde concentrations were negatively correlated with ambient ventilation. Depending on the building's age, indoor levels, wall or floor coverings, especially in new buildings (less than one year of age) and cigarettes' use due to increased formaldehyde. In homes with new wood or melamine furniture and newly purchased paintings or new-varnished flats, significantly higher results were found in negative effect. In a similar study, formaldehyde was determined by looking at the state of paint and ventilation in schools [151-154].

In recent years, synthetic resins are a leading main product and a cheap starting material. The main ones are urea-formaldehyde (UF), melamine-formaldehyde (MF) and phenol-formaldehyde (PF) adhesives, respectively. These resins in the plates' production process are modified according to their application areas [155, 156].

Table 2.9. Properties of resins made from urea, phenol and melamine formaldehyde [157, 158].

UF	PF	MF
Most common species, Low price	The second most common species	Condensation product
Depending on the variable factors (ph value, molar level, humidity)	Usually used in furniture production (MDF etc.)	Resistant to water
Short drying time after hot press	Occurs from condensation reaction of formaldehyde with phenol	
Vulnerable to outside weather conditions	1.1 - 2 mole of formaldehyde with 1 mole of phenol in the alkaline	
Negative effect on human health (if where ventilation is low)	Resistant to various fungal, insect, water and some organic solvents	

Table 2.9 shows in the formaldehyde varieties; an unmodified particleboard UF resin, the above-mentioned F/U molar ratio, was approximately 1.6 at the end of the 1970s. It is now in the range 1.02 to 1.08, but the board performance requirements, as given in the relevant quality standards, are still the same [159].

The formaldehyde is classified as carcinogenic to humans in Group 1A by International Agency for Research on Cancer (IARC). Mucous membrane irritation, contact dermatitis, teratogenicity and carcinogenicity. The irritant effects of formaldehyde exposure are increased concentration. Depending on the dose and the impact of side effects due to and are depicted within categorization in Figure 2.4 [160].

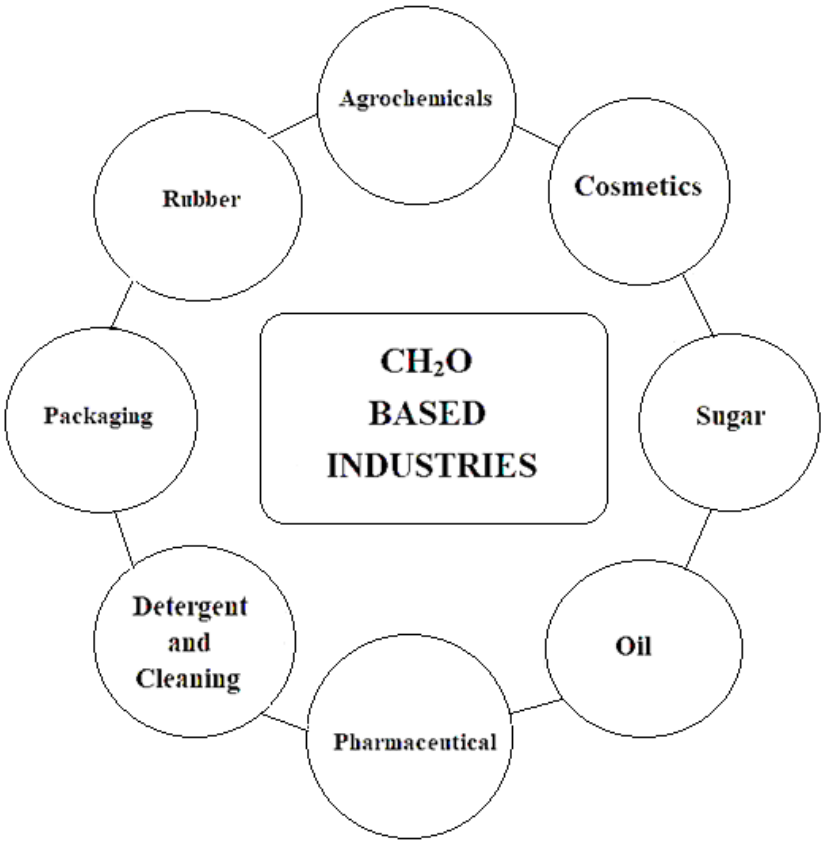

Figure 2.4. Industries that use of formaldehyde [108, 161].

Formaldehyde is a large-area common pollutant with an annual emission of 52 million tonnes in 2017. However, the range of formaldehyde in outdoor air are generally below 0.001 mg/m^3 in rural areas and 0.02 mg/m^3 in urban areas. It may occur at a rate of 0.003-0.2 kg/ton according to the chemical industry's used processes at the chimney filter and emitted 40 mg/m^3 formaldehyde from the wood industry's flue gases combustion event is not fully realized in fossil fuel vehicles [162, 163].

Since they are used in various amounts such as in the production of pesticides and insecticides against insects and pests, as a preservative in the packaging phase of some fruit juices, in the rubber industry, in pulp making, in automotive production, in the metal industry, in various amounts such as air, water, soil and nature, perhaps the most significant problem brought about by all of this industrialization given in industries. However, in the food industry, which is probably one of the most critical sectors, formaldehyde amounts can contaminate different foods. Due to the lack of controls in the

food sector, poor infrastructure for transport, saving and cooling and increased consumer claim for fresh products have led to increased fraud applications to enrich food products' lives. Although formaldehyde is naturally present at varying concentrations in foods, its qualitative detection is not conclusive evidence of adulteration. Primarily, free formaldehyde is of toxicological interest and it is the compound measured as a potential adulterant with some studies available in Table 2.10 [164, 165].

Table 2.10. Formaldehyde content in food products [75, 166, 167].

Drinks (mg/kg)		Dairy products (mg/kg)		Meat and sea products (mg/kg)		Fruits and vegeTables (mg/kg)	
Potable water	0.1	Goat's milk	1	Pig	5.8-20	Pear	38.7-60
Soft drink	7.4-8.7	Cow's milk	<3.3	Poultry meat	5.7	Apple	17.3
Coffee	3.4-4.5	Fresh milk	0.027	Processed meat products	< 20.7	Banane	16.3
Instant coffee	10-16.3	Commercial milk	0.164	Liver paste	< 11.9	Cabbage, Cauliflower	4.7
Syrup	<1 – 1.54	Cheese	<3.3	Fresh Water fish	8.8	Carrot	6.7-10
Alcoholic beverage	0.02-3.8			Frozen cod	20	Shiitake mushroom	100-320
				Shrimp	0.39-1.44	Green onion	13.3
				Crustaceans	1-60	Spinach	3.3
				Dried squid	35.3	Tomato	5.7
						White radish	3.7

The reference dose for formaldehyde determined 0.2 mg/kg body weight per day (mg/kg/d) based on a decrease in body weight gain by the USEPA. According to WHO, 0.15 mg/kg body weight per day was determined in daily formaldehyde intake [168, 169].

Shiitake mushroom has the highest concentration of formaldehyde, although fresh milk has a low concentration. The results of various analyzes in foods show that the amounts of formaldehyde are present in general. When we look at the internal and external parts of formaldehyde, controlled or uncontrolled, the test was conducted concerning various conditions in Table 2.11 [170].

Table 2.11. Average amounts of exposure to formaldehyde [139].

Internal areas	Amounts of formaldehyde (μg/m^3)
0-5 years of in new built houses [170]	0.17-1.28
Over 10 years old in homes [171]	~ 0.25
Woodmaking workshops [172]	340-4270
Business environment [173]	100-890
Different brands of cigarettes [138]	~100-1000
Pathology Lab. [174]	90–3610

The formaldehyde is one of the intermediate substances needed for all cells as well as essential substances. It is transformed into formaldehyde with dehydrogenase enzyme at the first contact site according to the exposure site. The carbon atom formed by the oxidation of formaldehyde to the form is oxidized to carbon dioxide or thymidine, purine and amino acid are used in the biosynthesis pathways [175, 176].

Exogenous, although the skin's absorption is minimal, formaldehyde can be easily absorbed by the respiratory and gastrointestinal tract. The NHMRC set 130 μg/m^3 as the upper limit for indoor air [40, 177-179].

Formaldehyde is quickly metabolized in the body and its storage is not counted as a toxicity factor. The gastrointestinal tract and inhalation cannot be detected in exposed human blood because it is rapidly induced by inhalation. Besides, exposure to formaldehyde may be by inhalation, mouth or skin contact in Table 2.12 [180].

Table 2.12. Dose-dependent side effects of formaldehyde [115, 181].

Concentration (μg/m^3)	Side effect
>111.15	Asthma in children [182]
61.75-1235	Bad smell [183]
617.5-3705	Eye irritation, neuropsychological effect [184]
308.75-3705	Nose, throat irritation [139]
605.15-3705	Dermatitis and burning on skin [62]
6175-24,700	Tear, dyspnea, cough, nose, eye and light burning [184]
+24,700	Pulmonary edema, pneumonia [172]
+123,500	Death [185]

Exposure of formaldehyde by inhalation; irritant effect in eyes, nose and throat, redness of eyes, burn-in eyes, runny nose, coughing, sneezing, itching, decreased pulmonary function, chest pain, hypothermic breathing, shortness of breath was determined in syndromes in Table 2.13 [185].

Table 2.13. Exposure of formaldehyde by according to the shape ingestion [139, 149, 181].

Inhalation	Mouth	Skin Contact	Cerebrally
Muscle and joint stiffness in musculoskeletal system	Respiratory system apnea, decreased respiratory rate and acute respiratory stress	Allergic reactions	Distractibility
Renal failure in renal system	Reduction of blood pressure in the cardiovascular system, hypotension.	Contact dermatitis	Mood swings

Distractions, mood changes and Reduction in coordination, decrease in learning capacity	Gastrointestinal pain, dysphagia, oropharyngeal ulcer	Eye irritation	Distortion in coordination
Short-term memory deterioration, memory loss	Acidosis and hyperlactation in the metabolic system	Small skin ulcers	Decreased learning capacity
Genotoxic chromosomal fractures and DNA repair reduction in a mechanism	Anuria and renal failure in renal system	Hyperplasia in the epidermis	Short-term memory impairment
To decrease sperm morphology and number in reproductive system	Hepatomegaly in hepatic system, icter and hepatic parenchyma bleeding	Vapor or solutions may cause skin irritation and burns	Stroke and loss of consciousness
Cancer causes nasopharynx; nasal and lung cancer	In the neurological system, laterji, paralysis and loss of consciousness		Memory loss, laterji and distortion in coordination

The formaldehyde reaction time was determined as approximately 4 hours in the atmosphere under sunlight [13, 133].

It is the relationship between formaldehyde and O_3 in summer with a photochemical reaction, which is an important one that increases the amount of ozone (O_3) in the atmosphere. This relationship is strongly correlated with temperature. Another contributing process is photo-oxidation, which is essential in determining the atmosphere's oxidation capacity in Table 2.14 [186, 187].

Table 2.14. Removal of formaldehyde from atmosphere by photolysis and hydroxyl radicals [102].

Photolysis	·OH· Radical
$HCHO + h\nu \longrightarrow H\cdot + HCO\cdot$ $\lambda<320$ nm	$HCHO + OH\cdot \longrightarrow HCO\cdot + H_2O$
$HCHO + h\nu \longrightarrow H_2 + CO\cdot$ $\lambda>320$ nm	$HCO\cdot + O_2 \longrightarrow HO_2\cdot + CO$
Released CH_2O undergoes physical and chemical transformations.	$HCHO + h\nu \longrightarrow 2HO_2 + CO$
With the help of rain and snow particles away from the atmosphere	$HCHO + h\nu \longrightarrow H_2 + CO$
	$HCHO + OH\cdot \longrightarrow H_2O + HCO$(in a laboratory experiment)
$CH_2(OH)_2 + HO\cdot \longrightarrow CH(OH)_2 + H_2O$	
$CH(OH)_2 + O_2 \longrightarrow HCOOH + HO_2\cdot$	
$HO_2\cdot + HO_2\cdot \longrightarrow H_2O_2 + O_2\cdot$	
The hydroxyl radical (·OH) reacts with formaldehyde and combines with molecular oxygen to convert to hydrogen peroxide	
·OH radicals form droplets of formic acid, a component of acid rain in clouds	

The limit values of such a widely available pollutant that could be exposed internally have been determined and stated in developed countries' regulations. The EC and the WHO set the value of 0.1 ppm (0.124 mg/m^3) to some countries that have established their limit values in Table 2.15 [93,188].

Table 2.15. Effects of formaldehyde on non-human organisms.

Microorganisms	Aquatic Organisms	Plants and Soils
Mutagenic effects in prokaryotic and low eukaryotic test systems, their ability to form adenine dimers	Precipitate mortality in fi sh with gill disease, due to the formaldehyde treatment like in Chinook salmon	Some plants are able to remove to formaldehyde. Formaldehyde-free control sample mixed with the silane peanut plant proteins

through methylene bridge [161, 162].	(*Oncorhynchus tshawytscha*) [189].	did not cause a big change in pH change and there was a big decrease in ammonia concentration and protected against protein nitrogen degradation effect [190].
Some microorganism populations with 50 μg/mL formaldehyde interfering changes in non-ribosomal RNA [191].	Algae and some invertebrate marine organisms are more sensitive to formaldehyde than some unicellular organisms (acute lethal concentrations ranging from 0.3 to 22 mg/L) [192].	Spider plant (*Chlorophytum comosum* L.) is the best example [193].
Pure spores of *Aspergillus*, *Scopulariopsis* and *Penicillium crustosum* were exposed to 2.4 mg/m^3 formaldehyde for 24 hours and all spores were destroyed [185].		It has been proved that formaldehyde as a cen-tral intermediate of photosynthetic carbon dioxide fixation ingreen plants can be removed by forming S-formylglutathione [118].

2.2.5.2. BTEX

The most common ones are benzene, toluene, ethylbenzene, m, p-xylene, o-xylene. The chemical structure and Chemical Abstracts Service (CAS) number of which were given in Figure 2.5. Some gases arise from the incomplete combustion of fossil fuels [194, 195].

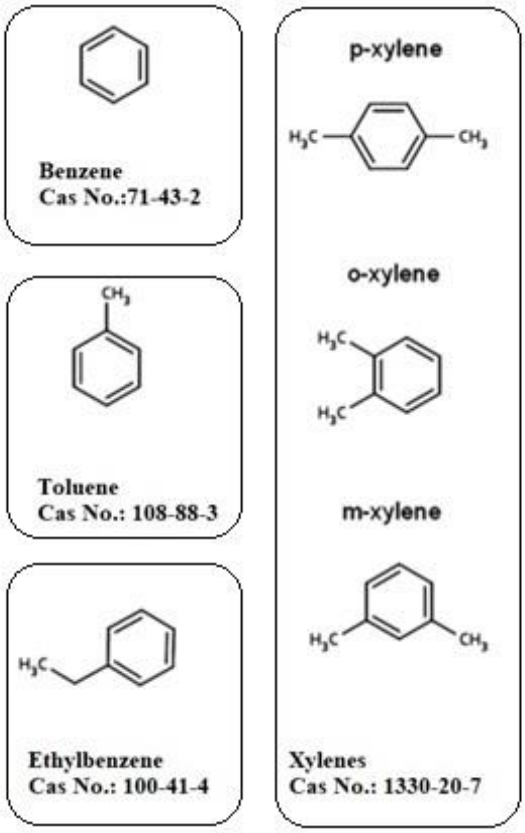

Figure 2.5. Structures and CAS registry numbers of BTEX [196].

The widespread use of BTEX's adverse effects is given as the common areas of service in various sizes. In sectors containing benzene; iron and steel industry, coal-based industries contain the use of fossil fuels. Although the ethylene gasoline is less in emissions, the amount increases if discharged from the exhaust without full combustion. Parallel to this, it can reach higher amounts of oscillation in diesel-powered machines and vehicles than gasoline. Toluene is also more common in solvent production and dyestuffs used in industries. The xylene is widely used in petrochemical plants. BTEX also plays a vital role in the synthesis of thousands of organic compounds [17, 197-200].

These gases, commonly referred to as BTEX, are found in benzene, toluene, ethylbenzene, meta-xylene, para-xylene, ortho-xylene in some places and atmospheres, which may contain more than 60% anthropogenic non-methane organic compounds. They are monocyclic, more volatile and similar to each other in other physical and chemical features. In particular, these are the essential compounds of the furniture industry, paint and the oil industry. As for atmospheric chemistry, BTEX can produce

secondary pollutants such as ozone and secondary aerosol through photochemical reactions of pollutants, gas-particle conversion processes [98, 111, 201].

The effects of these gases on human health have been demonstrated in many studies. Starting with the 1950s, the most toxic chemical in the BTEX family, benzene, was a different cleaning product and adhesive (>1000 $\mu g/m^2h$) classified as carcinogenic. Ethylbenzene is classified as carcinogenic risk, toluene and xylene are group D. Direct exposure to BTEX gas causes various acute and chronic health effects. Acute and chronic respiratory effects, neurological toxicity, cancers (especially lungs), damage to the eye and nose canals, headache and dizziness, nausea and vomiting, drowsiness and neurological disorders may cause some. Also, cardiovascular, respiratory and endocrine systems have been associated with adverse health outcomes, even at levels below the inhalation reference concentrations set by the USEPA in Figure 2.6 [142, 161, 174, 202, 203].

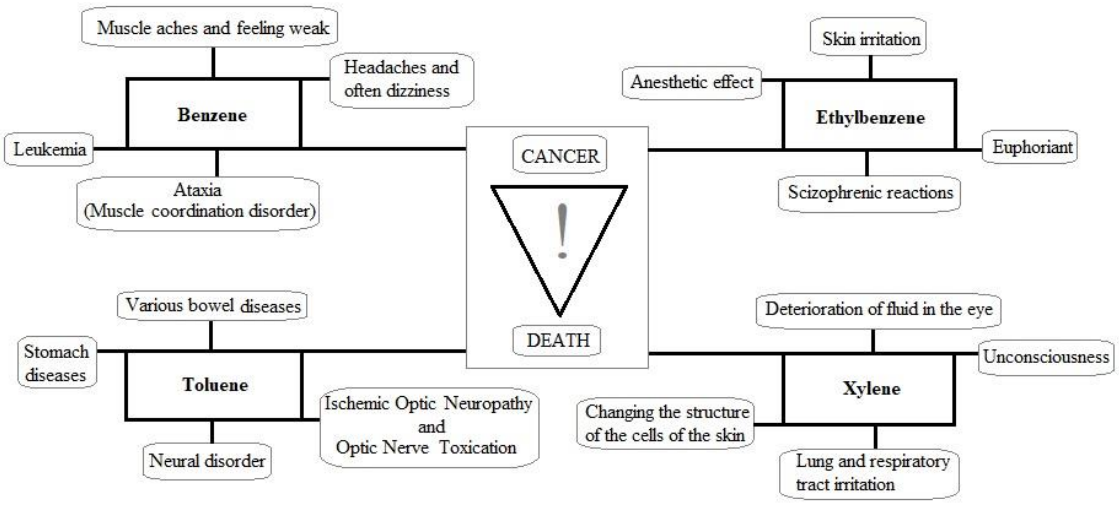

Figure 2.6. Some adverse effects of BTEX [194, 204-207].

Benzene-toluene (B/T) ratio, which is considered in the evaluations made according to the measured BTEX results, generally determines BTEX compounds' emission sources. A rate exceeding 0.5 indicates that the benzene source is related to traffic and other

sources. T ratios suggest that transport is the dominant source of BTEX. Xylenes/Benzene (X/B) and Ethylbenzene/Benzene (Ebz/B) ratios are generally photochemical reactivity indices. In addition to if BTEX>1 (average indoor/outdoor concentration ratio) indicates the presence of indoor sources for these compounds along with the infiltration of outdoor air [208-211].

BTEX's long-term monitoring in the subject of study in a large number of VOCs and low-cost analysis is required. The most detailed air pollution studies need time-weighted average concentration data for each VOCs, which may vary in wind direction, the cycle of activity of neighboring industries and the timing of peak traffic periods. Because of all these reasons can cause the toxicity of BTEX.

The EU and the USEPA have announced that the annual average standards of ambient air for benzene are 5 $\mu g/m^3$ and 10 $\mu g/m^3$, respectively. The rules for this toluene, ethylbenzene and xylene are 0.92 ppm, 0.106 ppm and 0.22 ppm, respectively [212, 213].

The average values of indoor and outdoor air, the ventilation of the rooms, garage and hobby rooms and building materials used in buildings in some studies BTEX formation is increasing about IAQ. However, the phrase is not found in the overall relationship between building materials. According to BTEX contamination, it is usually higher than inside, possibly due to an imbalance between the outflow of pollutants in Table 2.16 [79, 114].

Table 2.16. Benzene values of indoor and outdoor in different cities.

Examples of different seasons and places in different cities	Indoor Concentration μg/m^3	Outdoor Concentration μg/m^3	Ref.
Boston, USA	2.6	0.88	[214]
New York City, USA	3.64	1.82	[215]
Los Angeles, USA	3.87	3.32	[215]
Minnesota, USA	3.9	3.3	[2]
Melbourne, Australia	1-81	<1–14	[40]
Southeast Michigan, USA	2	0.4	[25]
Hannover, Germany	2.06-3.87	-	[216]
Hannover, Germany	3.3	9.6	[217]
Erfurt, Germany	2.5	1.9	[217]
Hamburg, Germany	2.3	1.3	[217]
Some European towns	1.5–47	-	[79]
Amsterdam, Holland	5.7-7.7	3-5.7	[103]
Mumbai, India	43.9-166.4	21.1-47.7	[218]
Fuji, Japan	0.694-6.89	0.779-6.04	[219]
Kocaeli, Turkey	7.5-19.77	4.77-16.61	[220]

In another saying, the house itself can act as a flywheel created by adsorbent surfaces on walls, floors and furniture. This idea is supported by experimental studies in which various efforts are made to reduce the benzene values due to benzene is an IARC Category 1 carcinogen. Some country has no guidelines like Australia for indoor air benzene concentrations. Still, an annual urban air objective recommended by the UK Ministry of Environment, Transport and Regions is 16 μg/m^3 (current) and wants to reduce until 3.2 μg/m^3. The countries that care about the environment's outdoor air benzene

concentrations are trying to reduce it gradually. Therefore, the studies conducted in this direction [40, 221, 222].

2.3. Adsorption of VOCs

Gas adsorption (GA) is used for different industrial activities. One of them is odor control that the treatment of some gases includes benzene, ethylbenzene, xylene, toluene and freon. Generally, many of the studies that have been done focus on fixed bed, batch reactor and fluidized bed systems. The elimination of low or medium concentration gases and vapors from the outing stream by holding these materials to the surface of porous solid and outline performance or its efficiency may vary depending on some conditions like adsorbent and contact time [41].

The adsorption is a process that permits the contaminants on the surface of adsorbents in the granular or powder zone to move with Knudsen, Surface and Molecular diffusion ways. Three lines define these diffusion ways of gas molecules. Also, these models deficiency its boundaries between these mechanisms cannot be seen strongly. The process's effect shows the variability between the size of molecules and an adsorbent's pore size. There are three types of diffusions appears that during the adsorption process at the same time. After the adsorption of the pollutants occurs, if possible, it is made ready for use again with the necessary operations. The repulsion force and weak force draw between the adsorbent's surface and the VOC molecule. Potential energy molecules from the atomic attraction force distribute the adsorbent through its pores. Also, it has a higher surface area because it recovers the VOC molecules at the high concentration required for kinetic energy, which then allows the VOC molecules to fly out of the adsorbent bed [223, 224].

The adsorption mechanism hinges on several parameters, such as the system's pressure and temperature, adsorbate concentration and type. Usually, it needs to remove each pollutant for trace elements, generally up to 1 percent of mass fraction in the gas stream, which is a known process of purification. The other definement is the purification and bulk separation purification process. Removal of adsorbate is present to a higher level

than 1 percent of the mass flow fraction percent in gas flow. The pressure and temperature are higher concentration (> than 1%) of the inlet gas and the pressure range varies roughly between 2 and 25 bars and temperature adsorption for attention shows the variability of the adsorbate ranging from 1 to 100 g/m^3 of the inlet gas flow with 100-250°C [206, 225].

The two types of removal methods of adsorption systems have physical adsorption (Van der Waals) and chemical adsorption (chemisorption). The physical adsorption has a weak bonding of gas molecules to the solids. In liquid, the term is called binding energy similar to the attraction forces between molecules. The adsorption process is emitted heat and is usually higher than vaporization heat in the adsorbed material. The holding power of gas molecules to the solid are readily elimination with not only the application of heat but also the reduction of pressure also similarly this method uses to regenerate in the adsorbent. This situation may change in the chemisorption. The moment it enters the reaction occurs that chemical bonding by adsorbate in a solid. Almost heats of chemisorption are the same size as heats of reaction and chemisorption, which makes deterioration like it will not get old. The AC with alumina usually acts as catalysts of response with several gaseous mixtures when designed to control and recover. It may not be necessary to reuse the adsorbent when chemically attached to the solids [48].

Isotherm of adsorption improves to associate with equilibrium data temper to adsorbent goods and advanced process design for its properties. Various isotherm shows up: Smith, Harkins-Jura, BET, Freundlich, Langmuir, Dubinin-Raduskevich. The adsorption system depends on the gas adsorbed and it is linked with pressure, temperature, solid adsorbent and removal required gas. These isotherms have been derived from Gibbs isotherm, which is the base equation in adsorption models [226]. Differentiation is made according to shapes and how they look in Figure 2.7 [227].

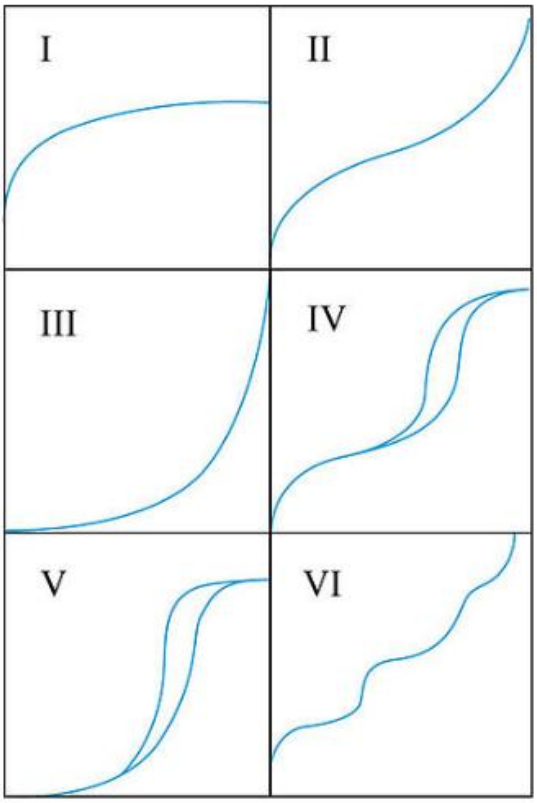

Figure 2.7. Adsorption isotherm types [226, 228].

The graph types obtained are used as six types of isotherm in both liquid and gas phases based on the different experimental results. I.'s type of graphics is more suitable for Langmuir and adsorbents with small pores, II. Adsorption with solids in pores more significant than 20 nm shown in III. Isotherm is not very common, IV. Type isotherm adsorption in solids containing micro and mesopores, the same isotherm in V. isotherm. As in the rare, VI. Isotherm is a rare condition involving micro and mesopores [226].

2.3.1. Langmuir Isotherm

There are some issues to consider when setting up these models. These are the main enthalpy of adsorption, the pore size of adsorbent, condensation of adsorbate in pore size and adsorbate effect on the thickness of the adsorption layer. These properties are experimentally tested several times and the efficiencies are determined because of the synthesis in a proportional manner. The most commonly used of these is the Langmuir model in Eq. (2). It depends on the constituted of a monolayer of adsorbed molecules. The surface of adsorbent is homogenized in terms of energy but not a relationship in

molecules. The adsorption site has embodied only one molecule that is a perfect phase. It can be said that Van't Hoff's law emphasizes affinity coefficient, adsorption enthalpy and temperature as a function [164, 229].

$$\frac{Ce}{Qe} = \frac{1}{K_L Q_m} + \frac{Ce}{Q_m} \qquad \text{Eq. (2)}$$

Where:

Ce : concentration of substance remaining in solution after adsorption (mg/L)

Qe : the amount of material adsorbed on the unit adsorbent (mg/g)

K_L : constant due to adsorption energy (L/mg)

Q_m : single layer adsorption capacity (mg/g)

Ce is the experimental concentration at the thermodynamic equilibrium (mol/m^3) and Qe is the adsorbed amount (mol/kg). Langmuir adsorption model, according to $1/Ce$, which are obtained from slope of the plot of $1/Qe$. In the Langmuir, K_L is constant, the degree of surface adsorption demonstrate a positive relationship with the extent of adsorbate also adsorbed amount increases as constant K_L increase [230, 231].

Where b and C_0 values were acquired from Langmuir isotherm in Eq. (3). Decreases in rising temperatures clearly indicate that the ongoing adsorption process is very suitable for after 40°C. The parameters indicate the shape of isotherm accordingly [232, 233].

$$R_L = \frac{1}{1 + bC_0} \qquad \text{Eq. (3)}$$

where:

b: (L/mg) Langmuir constant

R_L: Dimensionless separation factor constant of model

C_0: Initial concentration of substance to be removed (mg/L)

Table 2.17. Significations versus R_L [161].

R_L value	Signification
$R_L > 1$	Unfavourable
$R_L = 1$	Linear
$0 < R_L < 1$	Favourable
$R_L = 0$	Irreversible

2.3.2. Freundlich Isotherm

In the Freundlich isotherm, k is constant, defines a positive link with adsorption capacity. Despite this the adsorption capacity is demoted when 1/n is larger than 2. Then k and 1/n values are determined by plotting the adsorbed amount with respect to the adsorbate [104].

$$Qe = K_F Ce^{1/n} \quad \text{Eq. (4)}$$

$$lnQe = lnK_F + \frac{1}{n} lnCe \quad \text{Eq. (5)}$$

where:

Ce : concentration of substance remaining in solution after adsorption (mg/L)

Qe : the amount of material adsorbed on the unit adsorbent (mg/g)

K_F : adsorption capacity

n : adsorption intensity

The graph in which log Qe is plotted against log Ce indicates a line which this slope of the graph is 1/n, the cut-off point is log k. This equation is both physical and chemical adsorption [234, 235].

2.3.3. Dubinin-Radushkevich Isotherm

Dubinin-Radushkevich, D-R, isotherm that occurs in the same type of porous structures and calculates adsorption energy. Most of the constants obtained from different isotherm do not give information about adsorption's physical and chemical properties. However, the average free energy of adsorption calculated from the D-R isotherm provides information about adsorption's physical and chemical properties.

Freundlich is an alternative to adsorption isotherm to D-R, which is not based on a homogeneous surface and a constant adsorption potential in Eq. (6) and Eq. (7). The D-R isotherm is more general than Langmuir isotherm. It is used analogously with Langmuir isotherm because it does not accept homogeneous surface presence or constant adsorption potential. Polanyi first proposed it that an empirical equation was developed by the D-R, which was compatible with adsorption potential [236, 237].

The Dubinin–Radushkevich isotherm equation is expressed as:

$$q_e = q_m exp\left(-K\left[RTln\left(1+\frac{1}{C_e}\right)\right]^2\right) \quad \text{Eq. (6)}$$

$$q_e = q_m exp(-K\varepsilon^2) \quad \text{Eq. (7)}$$

Its linear form can be represented as:

$$lnq_e = lnq_m - K\varepsilon^2 \quad \text{Eq. (8)}$$

where:

ε: Polanyi potential

K: Dubinin–Radushkevich constant related to mean free energy of adsorption

A plot ln q_e versus ε^2 gives a straight line from which K and q_m (mg/g) can be evaluated from the slope and intercept. The mean free energy of sorption can be computed using the following relationship (kJ/mol):

$$E_s = \frac{1}{\sqrt{2K}}$$ Eq. (9)

E_s is calculated to obtain information about the physical and chemical properties of the adsorption process. If size of E_s between 8 and 16 kJ/mol, the process proceeds via ion exchange adsorption or chemisorption. On the other hand, if the value of E_s less than, the adsorption process is physical [238].

2.4. Activated Carbon

Activated carbon can be defined as a carbonaceous material with a very high pore and surface area, which cannot be characterized by structural formulas or chemical analysis. Generally, activated carbon is produced in two different ways that physical and chemical methods. Physical operations consist of two steps; carbonization of the raw material, controlled gasification using oxidizers such as steam, CO_2 and air. The expanded surface area, porous structure and high adsorption capacity of activated carbon makes it a unique removal agent. The pore volume of activated carbons is generally greater than 0.2 mL/g and the internal surface area is greater than 400 m^2/g (surface area measured by BET method using nitrogen gas) [224, 239].

The pore diameter varies between 3 Å and several thousand angstroms. The organic-based activated carbon; the composition may contain 87 to 97% carbon, while the remainder may contain hydrogen, oxygen, sulfur and nitrogen. It may also contain different elements depending on the raw material used and the content of other chemicals involved in the process [240].

The activated carbon is an excellent adsorbent and has a wide range of applications in the industry. The search for a suitable method for producing activated carbon and improving the pore structure and surface area is continuing at present [241].

No matter how widespread it is used today, it is high in the past. So the carbon has been used from ancient times to the present. The various areas of carbon used have been reached in the mysterious pages of history. According to the sources found in an Egyptian papyrus in the BC 3750-1500s, it was used in medical fields for therapeutic purposes in the Egyptians and Sumerians [141]. In addition to its use for medical purposes, coke coal and filte applications were found in wells for drinking water in India and Japan. In the 17th century, they successfully carried out gold's adsorption from the chloride solution in Australia after finding that the removal of color with activated carbon, bleaching and gas adsorption can be done successfully in various liquids in the 18th century [197, 242, 243-245].

In chronological order of activated carbon, the first commercial powder activated carbon was prepared with wood (ebonite) in 1909. Then it produced activated carbon used in the sugar industry in the Netherlands (norit) in 1911. During World War I, the Germans employed chlorine gas as a weapon in 1915. This gas prevented people from breathing and drowned. Both sides did not know how to protect against this wind-dispersed gas. This sometimes caused German soldiers to die in severe and difficult situations. The Germans started using gas masks containing activated carbon to protect against this gas brought the first use of activated carbon to defense [55, 246].

2.4.1. Area of Utilization

The most important application area of activated carbon is removing taste, odor, coloring and unwanted organic impurities from water. Many pharmaceutical and chemical products are used as gas-phase applications in purification. In recent years, the applications of activated carbon in the recovery of gold, silver and molybdenum in the field of hydrometallurgy are gradually increasing in recovery technologies. Today, activated carbons have become an indispensable part of our daily lives, whether directly or indirectly. The use of started carbon environmental applications and water cleaning areas is 300 million kg/yr, with 7% per year in the World's [247].

Suppose the activated carbon has a surface area of 800-3000 m^2/g and more resistant than activated carbons used. Higher density granular or different shapes are used in gas phase applications. They used recovery of precious solvents, ventilation of dangerous industrial emissions, adsorption of various organic vapors, filter units and removal of heavy metals from flue gases [24, 248].

The uses of activated carbon are gradually increasing and especially MDF, which is one of the leading sectors of formaldehyde, has started new searches in MDF production and different adhesives are used in furniture production, especially MDF production. Formaldehyde is somehow present in these adhesives, which MDFs with activated carbon additions are produced for VOCs, which may even occur in MDF production and MDFs are modified by adding 5% by volume of AC and MDFs are made with less emission. AC usage has started to increase in newly produced home decoration products and will be widely used in the future [249].

The recovery of the solvents is effective and fast by using activated carbon and it is achieved with an efficiency of 85-95%. The activated carbons' structure for valuable solvent recovery is mostly microporous which provides strong adsorption properties to capture small vapor molecules, such as acetone. The more mesoporous activated carbons have been used to recover benzene and cyclohexanone [250].

Protective filters used as gas masks, thin or fibers in activated carbon-containing protective clothing, are used in the military field.; Activated carbon filters are used to remove air pollutants in the industrial airfield. Also, the activated carbon saturated with iodine compounds is used to remove radioactive iodine compounds in the nuclear field atmosphere. Gas purification is another method that many processes such as the production of pure gases, protection against toxic gases, ventilation systems, removal of compressor oils from compressed air and purification of polluted air. The unwanted steam or gas is adsorbed onto the activated carbon [251, 252].

Technology is used to improve air quality as in all other areas. Carbon nanotubes (CNTs) have been developed to capture CO_2 and compete with CO_2 gases in the low-temperature range (20-100 ^oC) for active adsorption zones and improve adsorption performance in the presence of moisture [253]. Also, purification and the emission control of the desired gas can play an active role that activated carbon used in gas emission control must have high hardness, working capacity under steam and a high degree of saturation in gas emission control. Activated carbon filters are used to prevent gases from motor vehicles from polluting the environment [163, 254].

The retention of gases to avoid emissions depends on the chemical properties of the activated carbon or impregnated substances in control by chemical reaction. Gas storage with activated carbon is defined as a pressure reducing medium to store compressed gases that cannot be strongly adsorbed. Natural gas stored in passenger transport vehicles operating with natural gas is used in commercially available cylindrical tubes [255, 256].

The catalysts are substances that increase the rate of progressive reactions under the present activation conditions and are not on the product's side in any way due to the response. The activated carbon's wide internal surface area and surface activity also allows it to be used as a catalyst and catalyst promoter. In liquid phase applications, powder or shaped activated carbons having a higher density in particulate form are used in desired operations [257].

Powdered activated carbons are smaller than 0.18 mm, particle size or shaped activated carbons have particle sizes between 0.2 mm and 5 mm. 60% of the activated carbons produced for use in liquid phase applications are in powder form. Particulate and shaped activated carbons are generally used in continuous systems where a liquid is passed through a fixed bed. It is mostly used in mixing tanks. In these systems, carbon is separated from the scenario by filtration or precipitation. The wastewater purification mechanism is the best example for liquid phase applications. Also, it can be used 24% of activated carbon in drinking water processes. In these processes, particulate activated carbon filters remove toxic and other organic substances and remove foul odors [258, 259].

In addition to surface waters, it has increased activated carbon in groundwater improvement by 4%. Two methods are used in the removal of pollutants. One of these is the direct adsorption of pollutants by activated carbon in powdered granular or shaped form. Another technique is stripping the water's volatiles with the air's help and then separating the air from the volatiles as it passes through the carbon bed. It is also widely used in color removal processes and purification that 21% of liquid phase activated carbons is used for sugar, corn syrup, white sugar, sugar cane and sugar beet juice. The color removal is successfully done with activated carbon or ion exchange resin in the obtained solution [260].

The use of activated carbon is 8% of the total in chemical processes. For a high-quality product, impurities are removed with the help of activated carbon. Examples of this are removing organic compounds during the production of alum, soda ash and potassium hydroxide in solution. Food, beverage and cooking oil have 6% of the activated carbons used in liquid phase applications widely used in the food industry. Animal fats are refined from organic and inorganic compounds using activated carbon. With activated carbon, only impurities are removed, other values of the product are not damaged to other things. The alcoholic beverage groups have used to removal of unwanted tastes and odors in drinks. Phenol and trihalomethanes are removed in the structure of alcohol. Among the most important of these sectors is the health industry where used in many chemical and pharmaceutical production processes. They used liquid and gas phase applications that provide the advantage of low cost and easy storage [261, 262].

2.4.2. Chemical Structure of Activated Carbon

Since activated carbon has elements chemically bonded with oxygen and hydrogen, free electrons, particularly polar or polarizable substances, affect the activated carbon's adsorption capacity. These elements can result from raw material or carbonization, which cannot be idealized, forming a chemical bond with the surface during the activation process [263].

The primary purpose of oxidizing the carbon surface is to have a hydrophilic surface containing more oxygen. The formation of surface functional groups occurs due to the activator's direct contact or some of the impurities present in the environment with the raw material during the carbonization and activation processes [264].

The use of carbonaceous compounds as adsorbents is quite common science and industry. Besides the importance of pore structures and surface areas, their surfaces' chemistry plays a vital role in adsorbing various substances. The surface chemistry of carbon is related to the carbon surface's heteroatoms and is determined by acidic or basic surface functional groups. However, so far, the essential character of the carbon surface has not been fully understood in the scientific community. Carbon-oxygen surface compounds can be determined using water adsorption, temperature-programmed desorption or the Boehm method [265].

2.4.3. Surface Area

The most important physical property of activated carbon is its surface area. The surface area of the activated carbon is determined by the BET (Brunauer-Emmet-Teller) method. In this method, nitrogen or helium gases are generally used as adsorbed material. The BET is a method that provides information about the surface area of gases by using the physical adsorption characteristic of solid materials to surfaces. It takes the principle of single layer physical adsorption of gas on a solid surface [266, 267].

The result is the amount of gas mixture adsorbed to the solid sample surface at different pressures. Detailed information about the pore volume, porosity and active surface area of the sample can be obtained from the BET device. Typical commercial products have a surface area in the range of 500-2000 m^2/g. although synthetic origin activated carbons are used for special purposes because of their high adsorption capacity, almost 3500-5000 m^2/g surface area. The internal surface area of the activated carbon particles used in water treatment should be at least 1000 m^2/g since the pollutants are retained on the activated carbon surface, that is a highly effective factor in removing impurities. In principle, the

larger surface area, the greater the number of adsorption centers are considered in the process [268, 269].

2.4.4. Activated Carbon Production

The raw material to be selected for activated carbon production is also required to low inorganic components, high carbon content and low cost. As a result of the carbonization and activation processes applied during activated carbon production, the product's mineral content may vary according to the selected raw material. The density and volatile content of the raw material is essential. High density increases the structural strength of carbon. That is, it increases the resistance of the particles against comminution during use. Charcoal types are the most commonly used activated carbon raw materials because they are easy to find and cheap. However, activated carbon can also be produced from some renewable sources. The most commonly sought qualifications for activated carbons were givenin Table 2.18 [270, 271].

Table 2.18. Criteria to consider when selecting raw materials for ACs.

Raw materials for ACs	
Extremely low inorganic component content	Easy accessibility to raw materials
Abundant quantity available from anywhere	Storage life of raw materia
Workability of raw materials	High content potential

The properties of the activated carbon show differences content and the density of the raw material significantly affect the properties of the obtained activated carbon. If necessary, the raw material is washed with acid solution, solvents or pure water only to remove impurities that may affect the activation process. After washing, drying is done to remove moisture on the raw material. One of the steps of raw material before activation is sizing material. This process is necessary to produce activated carbon of the desired size and pore structure. The raw material's particle size affects essential properties such as surface area, micropore volume of produced activated carbon [272, 273].

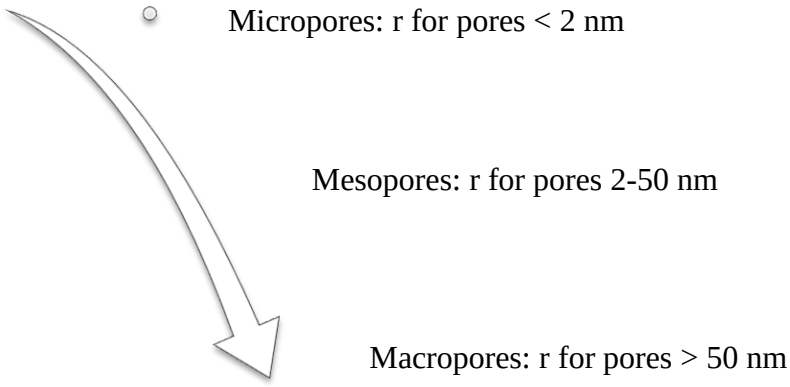

Figure 2.8. Micropores, mesopores, macropores and their dimensions [274].

The pore volume of the activated carbon typically varies found in the range of 0.20-0.60 cm^3/g. However, in some cases, it has also been found to be about 1 cm^3/g. The most important properties of activated carbon are its high surface area and porous structure. In general, the surface area of the activated carbons produced by different methods from different sources varies between 400-1500 m^2/g. However, activated carbon samples with a surface area of more than 3000 m^2/g are found in the literature. Surface areas often contain micropores with pore diameters less than 2 nm. These superior properties make activated carbon a popular adsorbent for many applications in Table 2.19 [21, 189, 275-278].

Table 2.19. The types of ACs [279, 280].

Powder AC	Granular AC	Pellet AC
The ground powder into small sizes.	Larger particle than powder activated carbon.	It consists of large granular granules that resemble a cylindrical shape.
Dimensions in the range of < 0.2 mm.	Dimensions in the range of 0.2-5 mm.	Dimensions in the range of 0.8-6 mm.
Has a large surface area and small diffusion distance.	Larger particle than powder activated carbon size and smaller outer surface area.	It has low pressure, high mechanical strength and low dust content.

Mainly used in liquid phase applications and flue gas treatment.	Liquid and gas phase applications.	Mainly used in gas phase applications.

The commercially activated carbons (COM-ACs) are available in granular, pellet and powder form in sold. There may be differences in the dimensions and usage areas of these forms. However, the graphs were drawn due to the isotherm used in calculating the removal efficiencies.

2.5. Hydrogen Storage

Hydrogen is a renewable energy source that can surpass the fossil fuel-based fuel systems used in energy production and consumption. The fact that the waste produced as a result of combustion is only water and does not contain carbon shows how much this substance is advantageous in the future. Despite having three times more gravimetric energy density than hydrogen fossil fuels, the energy content by volume is lower due to the low density of the gaseous state of fossil fuels [255, 281].

The hydrogen is a synthetic product formed by various forms of formation. These paths can be sorted by heat from biomass from fossil fuels, photosynthesis from bacteria and algae, by breaking water with electricity or sunlight. Today, most of the hydrogen production is made from fossil raw materials. Percentages hydrogen produced 48% of the World's hydrogen production from natural gas, 30% from refinery products, 18% from coal and the remaining 4% by electrolysis of water, respectively. In the name of science, new studies are underway to contribute to hydrogen storage methods that have gained momentum since the 1980s [282, 283].

The hydrogen can be stored in many different forms, which are troublesome of storage as renewable energy sources. Canada and New Zealand are top countries in the World that attach great importance to renewable energy resources, which have plenty of hydroelectric energy resources, have started programs in this direction. These countries store excess energy produced from hydroelectric power plants and unused by converting

them into hydrogen by electrolysis of water and then exporting them to different European countries. Renewable energy sources and hydrogen energy storage are great importance due to the limited and decreasing energy sources in the growing energy economy [284, 285].

A definite solution must first be found for storage and transport to promote hydrogen, which is the fuel with the highest calorie. It remains the most important obstacle in the transition to hydrogen energy. In today's technology, storing, transport, or using hydrogen in the gas or liquid phase despite storage or use in the gas phase requires vast volumes. Similar structures to large-scale tanks for hydrogen storage is much and it is as a liquid causes very high pressure and high cost, which involves great risk in terms of usage as the safest and cheapest storage method, the storage and transportation of hydrogen in solid materials eliminates all these drawbacks and eliminates the danger of hydrogen explosion in hazardous situations such as fire and accident [286, 287].

Hydrogen metal hydrides can be stored in solid materials such as organo-metal compounds, zeolites, carbon derivatives. There are several metal hydrides available for commercial use and it has a weighty material compared to stored hydrogen. The synthesis of suitable materials for hydrogen storage has recently been the main objective of the research and development focal point. It has been found that a high proportion of hydrogen can be stored in carbon-structured materials, significantly activated carbon [288, 289]. The most common hydrogen storage methods occupy a lot of space in pressure tanks. It is known that 1 gram of hydrogen gas occupies a volume of 11 liters at atmospheric pressure and therefore requires tanks with high storage volumes. Thus, they are stored in 50 L cylindrical tanks, which are resistant to 200-250 atm pressure. Due to the high pressure, these tanks are quite heavy. This creates significant problems during the transport and storage of hydrogen. This problem can be solved by using composite materials as tank materials. While hydrogen can be stored between 1-7% by weight depending on the tank's mass and type, this ratio can reach 11.3% in tanks using composite material. In the filling station, 20% of the fuel's energy content is used to compression hydrogen gas [290-292].

One of the methods used to increase the relatively low volumetric density in gaseous storage is to store the gas at lower temperatures (-253ºC) and in liquid form in insulated tanks. Storage as a liquid poses a significant risk in terms of use as it causes both very high pressure and high costs. Because it is necessary to cool the hydrogen to -252ºC to make it liquid, in this case, the cost of this system is 3-4 times higher than the price of gasoline. More importantly, even when the vehicle is not running, liquid hydrogen must be cooled and boiled. Liquid hydrogen is widely used in space technology and high-energy nuclear physics applications [293, 294]. In this technique, hydrogen is stored in a well-insulated tank at atmospheric pressure (at -253.15ºC). Since the liquefaction process occurs at -252.9ºC, the liquid tanks' thermal insulation comes to the forefront. Also, hydrogen requires a very long time and energy to cool to this temperature and hydrogen can be stored up to 16% of the total weight (including tank and insulation) Liquefying fuel, 40% of the energy content is spent. Therefore, new storage technologies are being developed which can store large amounts of hydrogen in small volumes [295-297].

3. MATERIALS AND METHODS

ACs are solid, porous, black carbon coal dust-like material. It can be prepared from many substances, such as coconut shell, rice husk, wood waste, coffee waste and cellulose residues. Any untreated carbon substances can be easily converted into activated carbon by some methods. During the carbonization of the raw material, most non-carbon elements emerge as pyrolytic gases. In these, the porous structure is mainly known as the distinguishing feature. The higher surface area, the more contaminants can be attached to the surface. Besides, it has been possible to increase the attachment some process.

Horse chestnut (*Aesculus hippocastanum* L.) was used as a raw material in this study. The homeland of it is the Balkan Peninsula but spreads throughout the northern hemisphere. The height of the tree, which shed its leaves in winter, reaches 25 meters. It is generally used as a boulevard and park tree in Turkey because of its magnificence [298]. Horse chestnut, which has many usage areas, forms the basis of activated carbon production.

3.1. Preparation of Activated Carbon

Chemical processes were preferred in the study, the only difference from the physical production was carried out in one step and zinc chloride ($ZnCl_2$) was used as a chemical agent. The production flow diagram of the activated carbon was given in Figure 3.1.

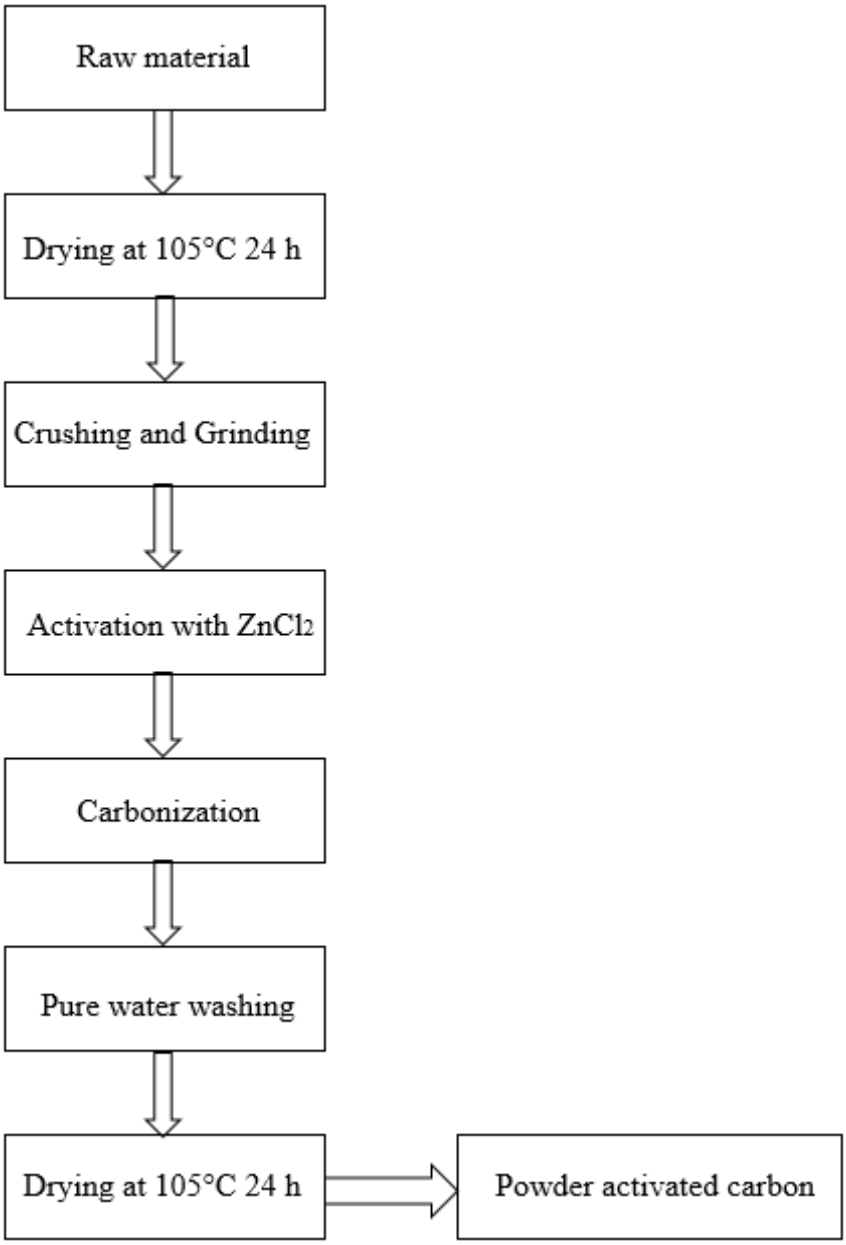

Figure 3.1. Protocol used to produce activated carbon.

The raw material used in the production of activated carbon, namely horse chestnut shell, was first washed with plenty of pure water, then kept at 105°C for 24 hours and the moisture was removed from the spirit. The dried sample was milled in a Retsch PM 100 ball mill. After grinding, the piece was passed through a 500 µm sieve using a Vibrating Sieve Shaker AS 200 basic sieve. After the grinding process, horse chestnut shell samples were subjected to carbonization and activation processes to produce activated carbon in Figure 3.2.

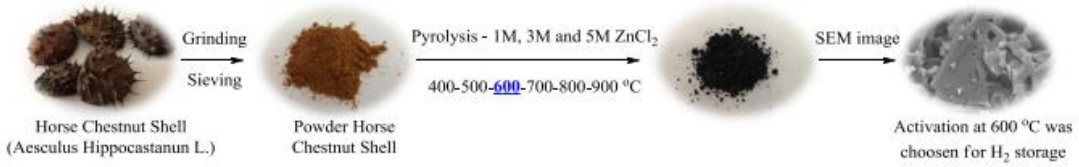

Figure 3.2. The KN-ACs production of the experimental process.

The $ZnCl_2$ was selected as the activating chemical in the chemical activation process and it was tested at different concentrations (1 M-3 M-5 M) to find the optimum ratio. This ratio of chemical agent/raw material ratio was formed in solution. The AC production was carried out using $ZnCl_2$ at a heating rate of 10°C/min and 400-900°C in a nitrogen gas (N_2) medium at 150 mL/min for 3 hours' stainless steel reactor in oven. In this study, the highest surface area value of the samples produced at 600°C was 1858 m^2/g, which is observed to have a much higher micropore structure and higher surface area than other temperatures.

3.1.1. BET Surface Properties

The BET surface area results of the activated carbons synthesized with $ZnCl_2$ used in the study were given in the Table 4.1. As can be seen from the results, BET surface areas of the activated carbons were increased with increasing concentration of the activating agent. Activated carbon samples were degas at 250°C for 24 hours before analysis. Surface area measurements of degassed samples were carried out Quantachrome Nova 2200e brand. Also using pure nitrogen gas as adsorbate in a liquid nitrogen environment (-169°C).

3.1.2. XRD Analysis

XRD patterns of the ACs were obtained using an Analytical Philips X'Pert-Pro X-Ray diffractometer. Include in a back monochromator running at 40 kV and copper cathode as the X-Ray source as a wave length was 1.54 Å.

3.1.3. FTIR-ATR Analysis

FTIR-ATR spectra analysis of the samples were done between 600 and 4000 cm^{-1} wavelengths with the PerkinElmer 100.

3.1.4. DTA/TG Analysis

The DTA/TG (Differential Thermal Analysis) thermograms of HCS and KN-ACs carried out using the Perkin Elmer Brand Diamond.

3.1.5. SEM-EDX Analysis

The surface activated morphology of the $ZnCl_2$ activating agent was analyzed by using the chemical activation method and the activated charcoal samples, commercial activated carbon and feedstock Horse Chestnut (*Aesculus hippocastanum* L.) shells (HCS) surface morphology was examined using FEI Quanta FEG 250 SEM (Scanning Electron Microscope).

3.1.5. Hydrogen Storage Analysis

Hydrogen storage capacities of synthesized activated carbon samples from HCS were measured at low and high pressures at room (25°C) and cryogenic temperatures (-169°C). Hydrogen gas adsorption measurements of the samples were carried out using Hiden brand IMI PSI. Experiments should be performed at low temperatures to increase the Van der Waals interactions between adsorbent and hydrogen. Therefore, the samples were first placed in an airtight measuring cell and then immersed in a Dewar container filled with liquid nitrogen under vacuum. To store high amounts of hydrogen, weak interactions that hold hydrogen molecules become more critical at cryogenic temperatures (-169°C) and high pressures. According to the ideal gas law, the amount of adsorbed hydrogen can be calculated from the pressure difference. The adsorbent's hydrogen storage capacity can be found from gravimetric removal, expressed as weight% hydrogen holding degrees according to different pressure values of activated carbon produced by using 1 M $ZnCl_2$, 3 M $ZnCl_2$ and 5 M $ZnCl_2$ in the thesis. Hydrogen storage capacity increases with increasing pressure in all molarity.

The storage capacities of KN-ACs (1 M $ZnCl_2$, 3 M $ZnCl_2$ and 5 M $ZnCl_2$) were obtained from the study at room and cryogenic temperatures using Hiden brand IMI PSI device. The hydrogen storage capacities of KN-AC were measured at room temperature and -169°C in the low and high-pressure range. According to the ideal gas law, the amount of adsorbed hydrogen can be calculated from the pressure difference. Hydrogen storage capacity can be found in gravimetric removal (expressed as weight %).

$$\%\, Weight = \frac{m_{H_2}}{m_{H_2} + m_s} \times 100 \qquad \text{Eq. (10)}$$

where;

$m_{s:}$ a mass of adsorbent

$m_{H2:}$ a mass of adsorbed hydrogen

3.2. Adsorption Experiment Methods

This section describes the material and method of hydrogen storage and adsorption processes. Hydrogen storage capacity was investigated room temperature and cryogenic temperature values then compared. Although gases' solubility was inversely proportional to temperature, experimental temperatures have not been studied with different temperatures in the adsorption study. The reason for this was that this study, which was led by the improvement of IAQ, was studied at 25°C to comply with room temperature conditions.

3.2.1. Formaldehyde Removal

For forrmaldehyde removal the Hach brand DR 3800 model Benchtop Spectrophotometer, which was used to obtain the results of removal with activated carbons, has been acquired by reading the abs values at different concentration values (0, 0.05, 0.1, 0.15, 0.25, 0.35, 0.5, 0.75 ppm) for calibration purposes before starting the experiments. Correlation coefficient (R^2) scanning with the EPA 323 method 412 nm

wavelength using. The total of 5 mL amber vials prepared acetylacetone reagent (2 mL each viale) and ultra-pure water.

All of the chemicals used in preparing the Acetylacetone reagent used as a coloring agent were all Merck branded. Mix 15.4 g of Ammonium Acetate and 50 mL of pure water for 2 minutes and add 0.20 mL of Acetyl acetone and 0.30 mL of Glacial Acetic acid to 100 mL of ultrapure water. Then, for the intermediate stock solutions, firstly, 2.7 mL of formaldehyde solution of 7 mL was put into a 1000 mL flask with the help of 1-10 mL adjustable automatic pipette brand and completed to 1000 mL with pure water. This solution was pulled through a 1 mL automatic pipette up to 100 mL with distilled water.

The samples were stored on ice (-20°C) if they were to be read. Then injected 2 mL of absorbance and 2 mL of acetylacetone reagent in vials. Vortex (Gilson Mini Vortex Mixer) process was applied for one minute to mix amber bottles with a total volume of 4 mL. We put the bottles in the water bath (Elmasonic Brand P Ultrasonic Bath) and allow it to react with the reagent at 60°C for 10 minutes. After reaching room temperature, the spectrophotometer read at 412 nm wavelength and the average of abs values were recorded for calculation [299]. All these experimental steps were carried out three times in Figure 3.3.

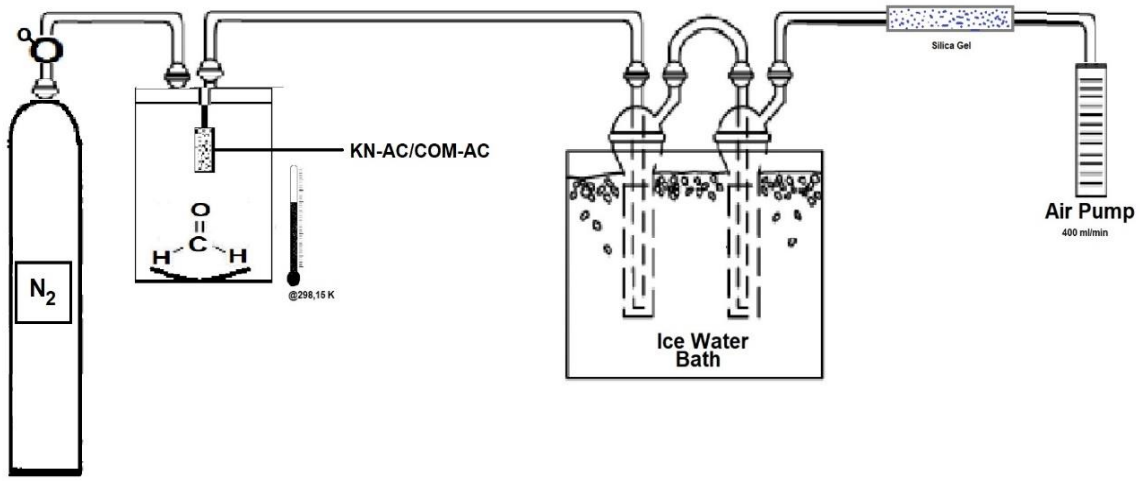

Figure 3.3. Experimental setup-batch reactor.

Before starting the experiment, the indoor temperature and relative humidity, start and end time of the investigation were recorded until stable in the batch reactor. The batch reactor made of glass, which was checked to have a sealed volume of 0.002 m^3, was specially designed where formaldehyde was injected at different concentrations (170±14.92, 260±23.76, 720±14.92, 1040±68.47, 1220±72.14, 1900±83.37, 3290±95.44, 7650±111.18 $\mu g/m^3$ in as a low concentration and 30,000, 50,000, 60,000, 110,000 $\mu g/m^3$ in as a high concentration). The test system was established using the EPA 323 Method.

The experiments were carried out under three different conditions, without activated carbon, using commercial activated carbon and activated carbon-produced in the study. Each experiment consisted of three replicates and the mean values of the findings were used in the experiment. First, the temperature and relative humidity were recorded before sampling. After the injection of formaldehyde, it was allowed to evaporate spontaneously at 25°C.

In the experiments using activated carbon, a high-quality thin stainless steel wire mesh cylinder produced in the laboratory. It designed to insert the activated carbon into the reactor. The ACs used in the study were placed in the reactor to be suspended to 0.5 g. Silica gel was connected to the outlet of the pump to remove moisture from the system. 40 mL of ultrapure water was charged to 2 gas flasks and the connection with silica gel was completed. Gas washing bottles were placed in ice water bath.

The adjustable pump was operated at a flow rate of 400 mL/min. In each repetition, the gas flasks were filled into 2 mL volatile organic analysis flasks (VOA) with three samples and 2 mL acetylacetone reagent was added and the vortex was mixed for 1 minute. It was then placed in a 60°C water bath for 10 minutes and allowed to cool to room temperature. The concentration of formaldehyde in the batch reactor was determined using the EPA 323 method with the acetylacetone reagent defined in the international standard. This method's principle was based on formaldehyde reaction with acetylacetone compound determined using a spectrophotometer (at 412 nm).

3.2.2. BTEX Removal

To monitor BTEX and other VOCs and determine their value, which has been broad, the passivated stainless steel drums or inert bags were used to collect VOCs air samples in the environment. This was a critical issue; many early sorbent tube monitoring studies suffered from excessive artifact formation and erroneous results principally because the sorbent selected was too weak to retain the analyte of interest quantitatively. 500 mg Tenax TA sorbent in tubes were used in this study [300].

The experimental samples used the analysis method in tube/thermal desorption/gas chromatographic-based monitoring method in Table 3.1. It is US-EPA (Environmental Protection Agency) Method TO-17 "Determination of VOCs in Ambient Air Using Active Sampling onto Sorbent Tubes" for VOCs in ambient air at 0.5 to 25 parts per billion (ppbv) concentration levels.

Table 3.1. Parameters of oparating conditions for GC-MS and UNITY-2.

TD Markes Unity		GC Agilent 6890N				MS Agilent 5975C			
Operating Conditions									
Oven temp °C	200	Injection	TD split ratio		Splitless	MS Source	230ºC		
Trap temp °C	35	Total flow	45 mL/min			MS Quad	150ºC		
Transfer line temp °C	200	Oven				SIM Mode Settings			
		Oven Step	°C/min	Final temp	Stay Time (min)	Ion	Obs time	CAS no	Boiling point °C
Humidity control system line temp °C	200	Starting	0	65	0	benzene	4.6	71-43-2	80.1
Trap desorp temp °C	300	1.Step	5	170	0	toluene	6.55	108-88-3	110.6
Tube firing temp °C	250	Last Step	10	220	5	ethylbenzene	8.73	100-41-4	136
	250	Carrier (He)	7 mL/min			m-xylene	8.96	108-38-3	138-139

Trap firing temp °C				p- xylene		106-42-3	
Humidity control system firing temp °C	300	Heater	300 °C	o- xylene	9.61	95-47-6	144
Carrier gas (He) flow mL/min	40	Used Column					
Carrier gas (He) pressure psi	20	Agilent JandW	DB-1 and 1 µm injection				
VOC Method		Microbore					
Tube desorp time min	3	ID (mm)	0.05-0.10				
Tube desorp temp **°C**	225	Length (m)	10-40				
Tube desorp time min	1	Film (µm)	0.05-0.40				
Trap firing time min	15	Temperature Limits (°C)	-60-325/350°C				
Tube cleaning method		Capillary					
Pre-cleaning time min	5	ID (mm)	0.15-0.32				
Tube desorb time min	1	Length (m)	10-150				
Tube desorb temp °C	320	Film (µm)	0.10-5.00				
Trap desorb time min	1	Temperature Limits (°C)	-60-325/350°C -60-300/320°C (1.50 µm) -60-280/300°C (2, 3, 5 µm)				
Trap firing time min	45	Megabore					
		ID (mm)	0.45-0.53				
		Length (m)	5-105				

	Film (μm)	0.15-5.00
	Temperature Limits (°C)	-60-260/280°C (2.55, 2.65, 3.00, 5.00 μm) -60-300/320°C (0.50, 1.00, 1.50 μm) -60-320/340°C (0.25 μm) -60-320/350°C (1.50, 2.65 μm) -60-325/350°C (1.27, 2.65, 5.00 μm) -60-340/360°C (0.10, 0.15 μm)

When calibrating the system, 200 μg/mL was used to achieve known concentrations of BTEX standard solution (Ultra Scientific brand Aromatic Hydrocarbons Mixture DWM-550-1) in TD-GC-MS system. The calibration of the is based on the seven standards given above which were prepared as 10 ng/μL, 20 ng/μL, 40 ng/μL, 60 ng/μL, 80 ng/μL, 100 ng/μL and 200 ng/μL. The method was loaded with 1 μL of each concentration that was studied in 4 replicates.

Laboratory blind samples were collected in order to determine whether the thermally cleaned tubes used for the VOC sampling were exposed to contamination from the laboratory environment. Cleaning the tubes to be used in sampling was a sensitive step. The most important thing to consider was to make sure they were clean for this reason. The contamination that may arise from the laboratory environment has been tried to be determined in advance. Sampling tubes have been checked for cleanness in TD-GC-MS. If they are not clean, they are conditioned by a program in the TD and analyzed by GC-MS Selective Detector to ensure that the tubes are cleaned according to US EPA Method-TO 17. The clean tubes were wrapped in aluminum foil by tightly closing the Teflon caps until the sampling order was reached and placed in an airtight glass container containing silica-gel and stored in a deep-freezer free of the organic matter until taken to the sampling time.

The experimental apparatus of Figure 3.3 similar to Figure 3.4. Before starting the experiment, the indoor temperature and relative humidity, start and end time of the

investigation were recorded in that time. Our batch reactor's features have made of 0.002 m^3 as glass and given in the formaldehyde removal section.

The pump (SKC The AirChek XR5000) flow rate used 100 mL/min before each sampling period was calibrated with a rotameter. The experiments were carried out under three different conditions, free-AC, COM-AC and KN-AC in a high-quality ultra-thin stainless steel wire mesh cylinder to insert into the reactor. The activated carbons used in the study were placed in the reactor to be suspended as a 0.1 g. COM-AC after KN-AC, respectively. Specially designed batch reactor where BTEX was injected at four concentrations. The initial concentrations for benzene was 2.4±0.45, 5.5±1.09, 54±10.73 and 322±47.80 μg/m^3; toluene was 3.7±0.58, 9±2.62, 86±15.83 and 414±47.26 μg/m^3, ethylbenzene was 3.9±0.66, 9.2±1.59, 90±15.55 and 430±46.64 μg/m^3, m, p-xylene was 3.4±0.72, 8.5, 83±12.95 and 397±82.10 μg/m^3, o-xylene was 5.2±0.82, 10, 100±24.38 and 483 μg/m^3, BTEX 18.5±1.89, 42±4.97, 412±48.74 and 2045±203.37 μg/m^3, respectively. Ultra Scientific brand Aromatic Hydrocarbons Mixture DWM-550-1 (200 μg/mL in Methanol) was purchased and used as the VOC sampling.

The sampling time was 15 minutes. A sample was made to receive a total of one hour. The sample type and quantity of BTEX were determined by operating GC-MS unit in SIM mode. The calibrations of the devices were made before starting the work. Agilent 6890N Network Gas Chromatograph and Agilent 5975 Series also Markes Unity-2 TD was used in experimental apparatus. Before beginning the experiments, GC-MS and Thermal Desorber were run as empty for one day. All these operating conditions have been appropriately operated and data acquisition has been started. The data obtained were calculated with EUR 17675EN and ISO 16000-6 in BTEX's calculation [301, 302].

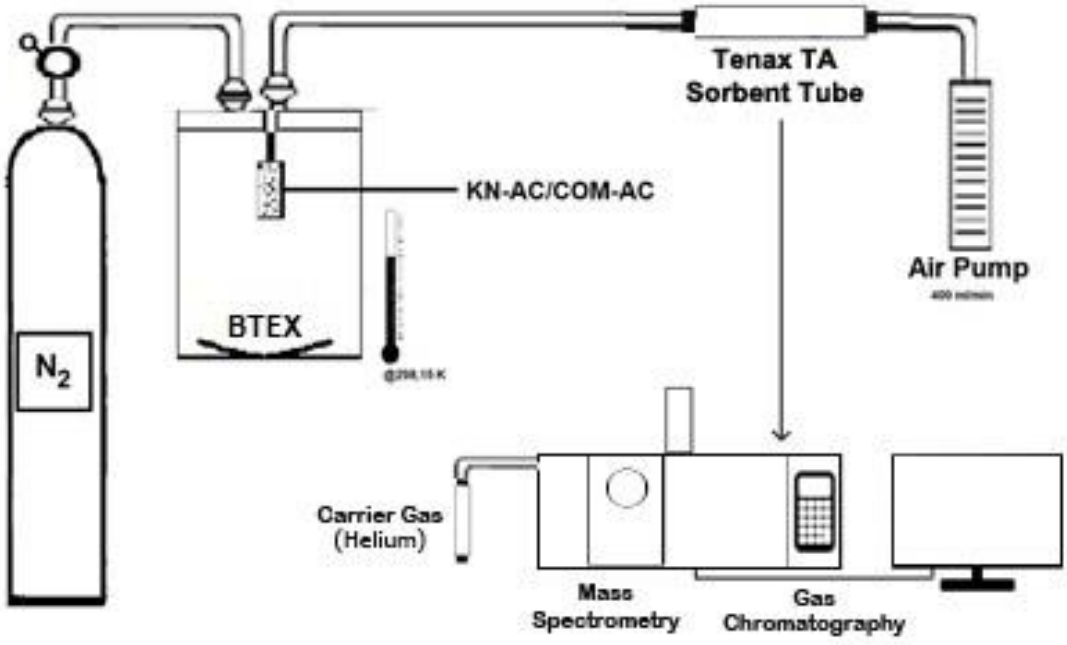

Figure 3.4. The experimental setup of BTEX gases via batch reactor.

Tenax TA is a sorbent tube, which can be used for general purpose. It helps quality inspection of various health sectors and food. Despite having a heat-resistant porous structure, the error rate is reduced at low temperatures. The structural error rate is too low (<1 ng), ideal for inert and sensitive products because it is hydrophobic. The tubes' lifetime is approximately 100 thermal cycles and its efficient desorption results in sharp GC peaks.

When the maximum temperature is exceeded, the structure of the sorbent is deteriorating and may disappear. Before starting the experimental studies, the tubes were cleaned with a program prepared in Thermal Desorber (TD) to ensure that they must be cleaned and then analyzed by Gas Chromatography-Mass Selector Detector (GC-MS) for ensuring according to US EPA Method-TO 17. The sorbent tubes permit the desired volatile and semi-volatile compounds to be captured and re-released by TD. It can be analyzed at any time by closing the caps or tubes can be stored as a witness sample [303].

The sorbent tubes' features vary according to the type of piece and the purpose of the analysis. They have been checked for cleanness and enveloped with aluminum foil by

tightly closing the teflon caps that were placed in an airtight glass container containing silica-gel and dehumidifier with adsorbent kept until use. The flow rate of the pump used before each sampling period was calibrated with rotameter [303].

The TD has been a very successful sample entry system for gas chromatography (GC) since 1980. It is generally used, but not necessarily, by GC-Mass Spectrometry (GC-MS). TD is the addition of gas chromatography, which provides desorption of organic volatiles and semi-volatiles retained in samples or sorbents heated by an inert carrier gas stream and injection or transfer to a carrier with GC. As in GC, the key parameters are temperature, flow rate, desorption time and sorbent material.

UNITY 2 TD unit is a new generation of thermal desorption created with Markes technical equipment which is an upgrade of the old system with cryogenic tube desorption and sudden desorption in the trap. As a TD device, UNITY 2 traps organic compounds in the gas phase in a trapping environment and provides sampling and sends them to GC for analysis. It can be divided into three main sections: tube desorption furnace, cold trap and GC transfer line. When the amount of sample is inadequate, the backup unit (split) empty sorbent tube can be installed by backing up the sample.

Agilent 6890N Network Gas Chromatograph describes all chromatographic methods in which the mobile phase is a gas. It is based on the analyte's distribution between the gaseous mobile phase and the stationary liquid phase attached to the surface of a solid. The evaporated sample is injected into the chromatographic column inlet and eluted with an inert mobile gas phase in GC. Unlike other chromatographic methods, the gas phase does not interact with the analyte; The only function of the gas is to carry the analyte through the column. There are two types of gas chromatography: gas-solid chromatography (G-SC), gas-liquid chromatography (G-LC). Since gas-liquid chromatography is widely used in many fields, the name is often abbreviated and the term gas chromatography is used in experimental results. Gas-liquid chromatography was first developed in 1941 by Martin and Synge. Its experimental application took more than a decade and the first gas chromatography device was introduced "vapor-phase" in 1954, also homemade gas chromatography used in 1955 [137].

The chromatography is a method of separating the components of a sample in a two-phase system that is not mixed with one stationary and one mobile phase. The role of the mobile phase in GC that is to carry only substances. There is no interaction between the importance to be separated and the mobile phase. The mass spectrometer evaporates, ionizes and separates the ions formed according to their mass/charge (m/e or m/z) values. The mass spectrometer aims to plot the mass of the + particles formed by electron bombardment according to the relative abundances of the mass/charge (m/e) value to include the Mass Spectrum. Mass Spectrum is the graph of relative lot of m/e values of peaks of + charged ions (cations and radical cations) formed by the bombardment of matter with electrons. The GC-MS system uses a mass spectral database to interrogate for the naming of compounds detected by electron ionization [304].

4. RESULTS AND DISCUSSION

4.1. Characteristic of Adsorbent

The studies were mentioned as grouped under four main headings. These were AC production and characterization, hydrogen storage capacity of ACs produced, the efficiency of this activated carbon in formaldehyde removal and finally performance of BTEX gases removal with Langmuir, Freundlich and Dubinin-Radushkevich isotherm, respectively. Characterization of KN-AC samples obtained from $ZnCl_2$ by chemical activation. It was performed qualitative analysis of functional groups such as BET (Brunauer-Emmett-Teller) for surface area, SEM-EDX (Scanning Electron Microscope) for morphological characterization, DTA/TG (Differential Thermal Analysis-Thermogravimetry) for thermal characterization, XRD (X-ray diffractometer) for microstructure analysis and FTIR-ATR spectrophotometer for chemical structure characterization. For the best make up the surface chemical structure and hydrogen storage devices.

4.1.1. BET Surface Properties

The BET surface area firstly increased due to an increase in agent concentration and then decreased in Figure 4.1. The increase in agent concentration caused activated carbon samples' morphology to change in parallel with SEM images. The surface areas for 1 M $ZnCl_2$, 3 M $ZnCl_2$ and 5 M $ZnCl_2$ were measured at different temperatures and the highest surface area was calculated at 600°C. BET surface areas of the activated carbons synthesized at 1 M $ZnCl_2$, 3 M $ZnCl_2$ and 5 M $ZnCl_2$ concentrations were determined as 795, 1858 and 1600 m^2/g at 600°C carbonization temperature, respectively. Total pore volumes (V_{Total}) relative pressure can be last measured. When calculating with value data, micropore volumes (V_{micro}) were calculated using the D-R equation. The mesopore volume was calculated by the difference between the total pore volume and the micropore volume. Again, micro, meso and total pore size results of activated carbons were 0.47, 0.14 and 0.33 cm^3/g; 0.49, 0.24 and 0.73 cm^3/g and 0.34, 0.07 and 0.41 cm^3/g, respectively

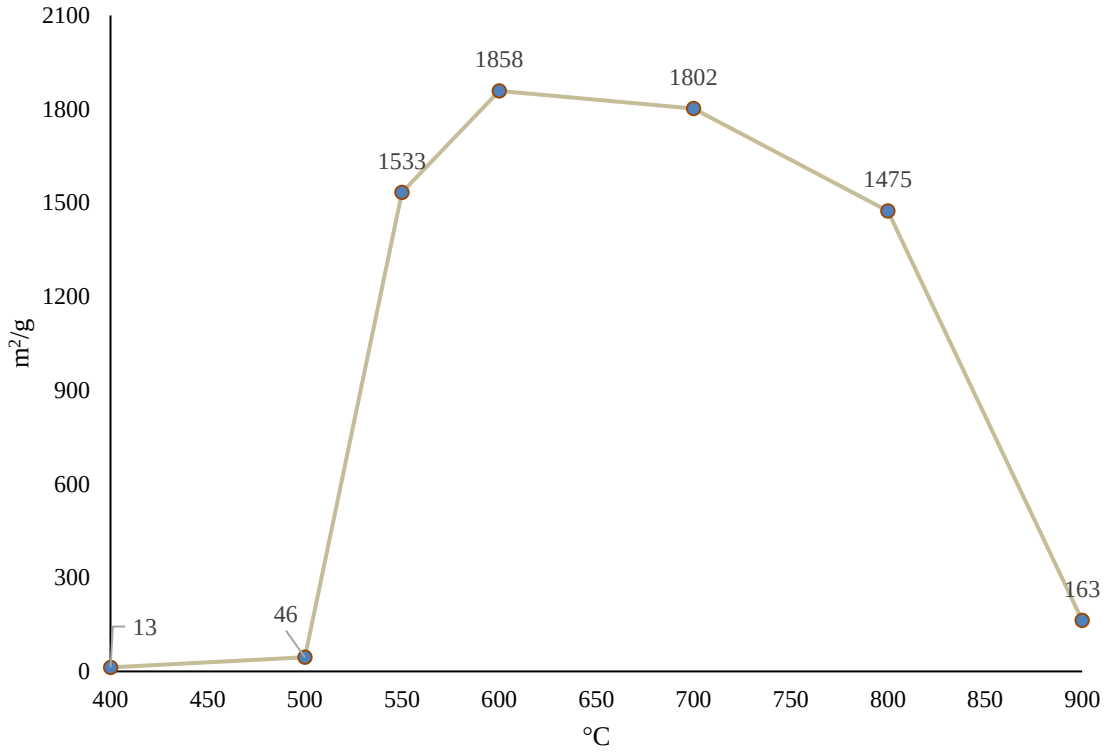

Figure 4.1. Surface area of activated carbon depend on tempreture.

The data related to surface area analysis (BET) were givenin Table 4.1. The effect of different temperature values on the surface area in the range of 400 - 900°C was investigated and maximum surface area was tried to be obtained. When the findings were evaluated, ACs were produced as KN-AC with 3 M $ZnCl_2$ at 600°C.

Table 4.1. BET results of KN-ACs.

Chemical agent	Thermal Activation Temperature °C	Chemical activation agent concentration	BET Surface Area (m^2/g)	R^2	V_{Total} (cm^3/g)	V_{Meso} (cm^3/g)	V_{Micro} (cm^3/g)
$ZnCl_2$	600	1 M	795	0.999	0.47	0.14	0.33
	400	3 M	13	0.969			
	500		46	0.959			

	550		1533	0.998			
	600		1858	0.999	0.73	0.24	0.49
	700		1802	0.999			
	800		1475	0.999			
	900		163	0.992			
	600	5 M	1600	0.999	0.41	0.07	0.34

The pore volume diagram obtained for the KN-ACs and COM-AC in the thesis was given in Figure 4.2. Accordingly, pore volume values were distributed under 40,000 Å.

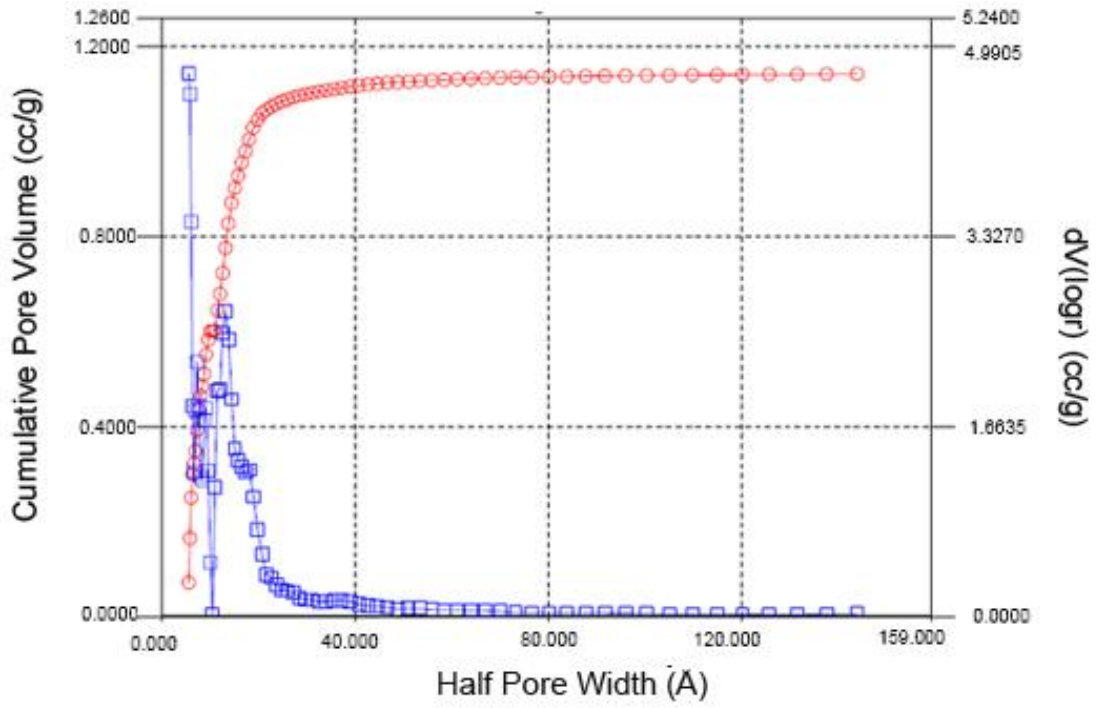

Figure 4.2. The pore size of KN-AC.

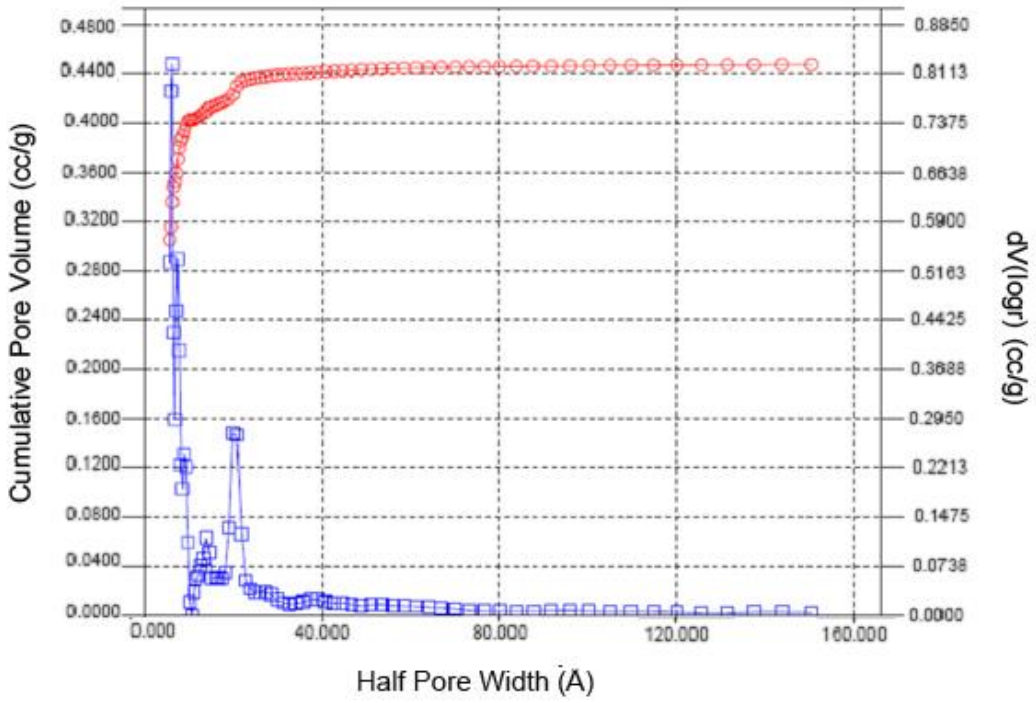

Figure 4.3. The pore size of COM-AC.

4.1.2. XRD Analysis

Figure 4.4 shows XRD (X-Ray Diffraction Method) patterns of activated carbon samples synthesized from horse chestnut shells. No diffraction peaks of any crystalline or semi-crystalline structure were observed. However, the weak peaks at 2θ =21.4º and 2θ =24.2º indicate graphite crystals in constructing the activated carbon. After carbonization at 600°C, the broad peak at 21.4˚ disappeared [305].

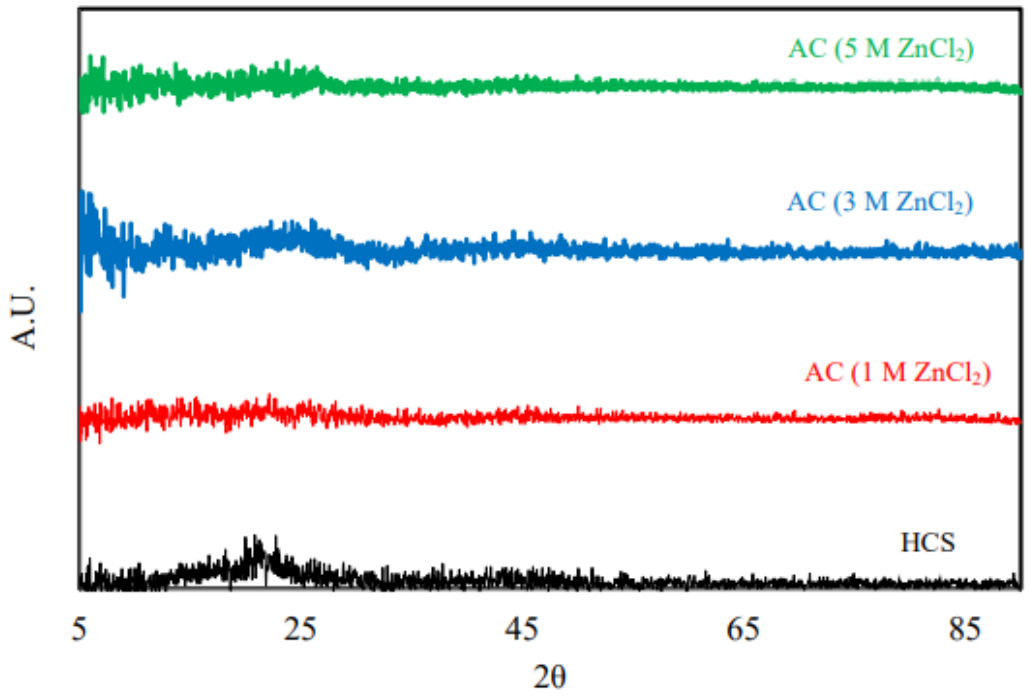

Figure 4.4. XRD pattern of HCS and KN-ACs.

4.1.3. FTIR-ATR Analysis

Horse chestnut shell contains lignin and cellulose in its structure. Figure 4.5 shows FTIR-ATR (Fourier Transform Infrared) spectra of activated carbons synthesized with $ZnCl_2$ activation and horse chestnut shell showing characteristic bands of lignin and cellulose. In the case of horse chestnut shell, the band at 3285 cm^{-1} can be attributed to -OH stretching vibration, band at 2850-2918 cm^{-1} aliphatic CH symmetrical and asymmetric stretching vibrations, band at 1730 cm^{-1} C=O vibration, band at 1603 cm^{-1} C=C stretching vibration and band at 1045 cm^{-1} intense C-O vibration. In the FTIR-ATR spectrum of activated carbons, the ·OH band's beating at 3285 cm^{-1} and aliphatic –CH vibrations at 2918 cm^{-1} disappeared. The C=C vibrating at 1603 cm^{-1} decreased and shifted to 1559 cm^{-1}. Most importantly, the intensity of CO vibration at 1045 cm^{-1} was greatly reduced. These spectral data have supported the formation of activated carbons [88].

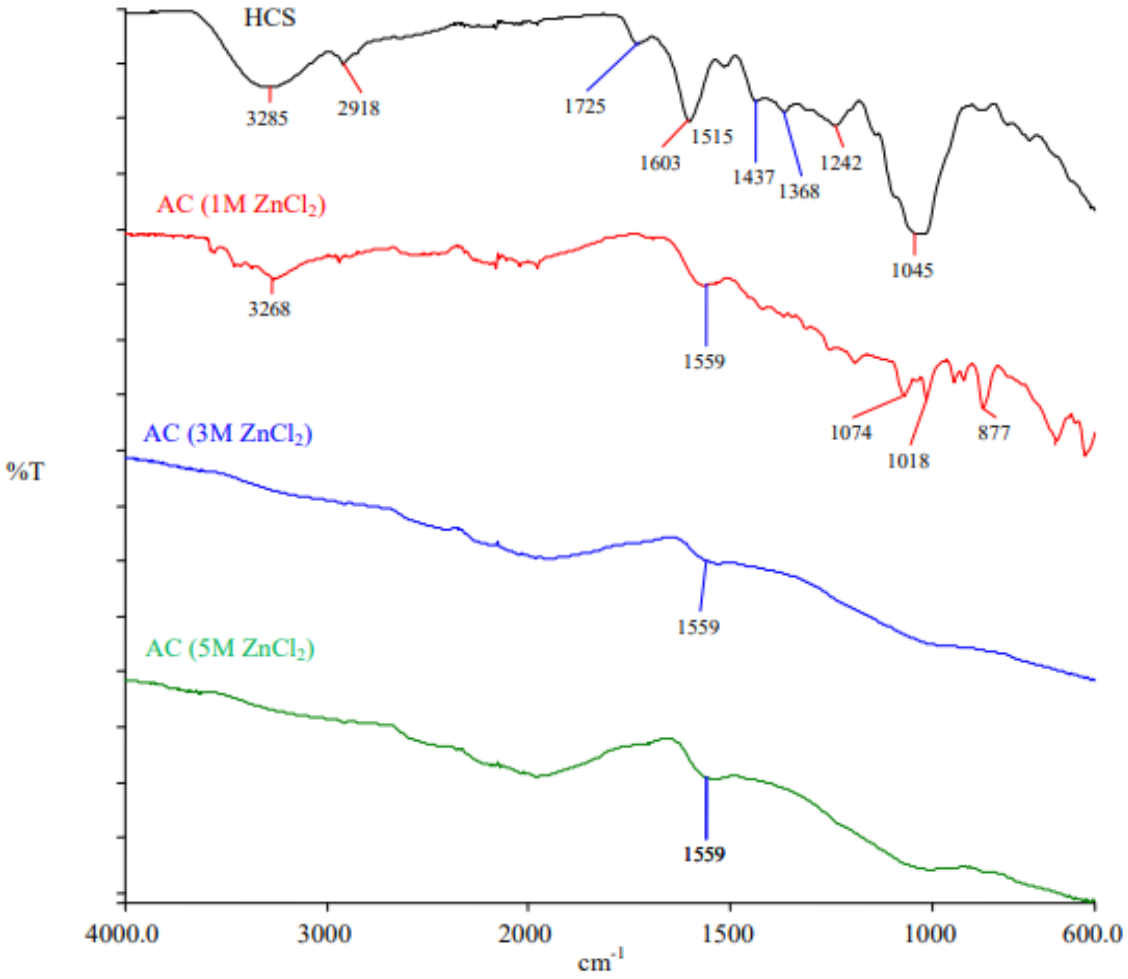

Figure 4.5. FTIR-ATR spectra of HCS and KN-ACs.

4.1.4. DTA/TG Analysis

The d[TG] thermogram of HCS shows an extreme minimum at 79 and 322°C. At the end of the analysis, the residue amount was 26.8 wt% at 1200°C. The TG and d[TG] thermograms of HCS indicate that a vital mass loss and another decomposition stage do not occur at above temperatures of 600°C in Table 4.2. Therefore, the production of activated carbon from HCS was realized at 600°C. This result was agreement with BET surface area results obtained at different carbonization temperatures. The highest surface area for activated carbon samples was found for the models carbonized at 600°C. The thermogram of KN-ACs has shown four decomposition stages. Thermograms offer a minimum at 53°C and it was dedicated to the release of adsorbed water in micropores, which show high hydrophilicity of the activated carbon surface. The second stage was

related to the organic carbon structure's thermal decomposition and comes off in a wide temperature range from 300°C to 600°C. The second maximum decomposition temperature, T_{max2}, was 539.2°C. The third stage of decomposition was the secondary degassing, manifested on the TG curve as a band at 958.43°C. The last step corresponds to the corruption of surface functional groups of low stability generated upon activation [26].

Table 4.2. The data obtained from TG and d[TG] thermograms.

	Samples of KN-ACs				
	HCS	1 M $ZnCl_2$	3 M $ZnCl_2$	5 M $ZnCl_2$	Stage
Onset (°C)	62.3	40	45	29.9	1st
Endset (°C)	102.8	60	66.9	73.2	
T_{max1} (°C)	78.7	42.61	53	44.3	
ΔY %	5.7	2.1	4.2	5.2	
Onset (°C)	259.2	173.4	508.7	264.3	2nd
Endset (°C)	361.4	182.30	620.1	414	
T_{max1} (°C)	321.7	176.52	539.1	340	
ΔY %	49.4	0.91	13.4	2.24	
Onset (°C)	-	556.24	939.3	507	3rd
Endset (°C)	-	675.6	972.6	810.8	
T_{max1} (°C)	-	634.7	958.4	619.5	
ΔY %	-	19.78	3	9.71	
Onset (°C)	-	884	1099	1190	4th
Endset (°C)	-	1057	1133.6	1275	
T_{max1} (°C)	-	935.4	1118.6	1036	
ΔY %	-	20.2	2.5	3.55	
Residue 1200°C	26.8	57.6	68.4	79.9	

The d[TG] thermogram of activated carbon samples also shows a slight loss of about 1118.60°C, which can belong to the decomposition of functional groups and partial gasification of the least thermally steady piece carbon structure. The mass loss at this stage was 2.50 wt% [187, 305-307].

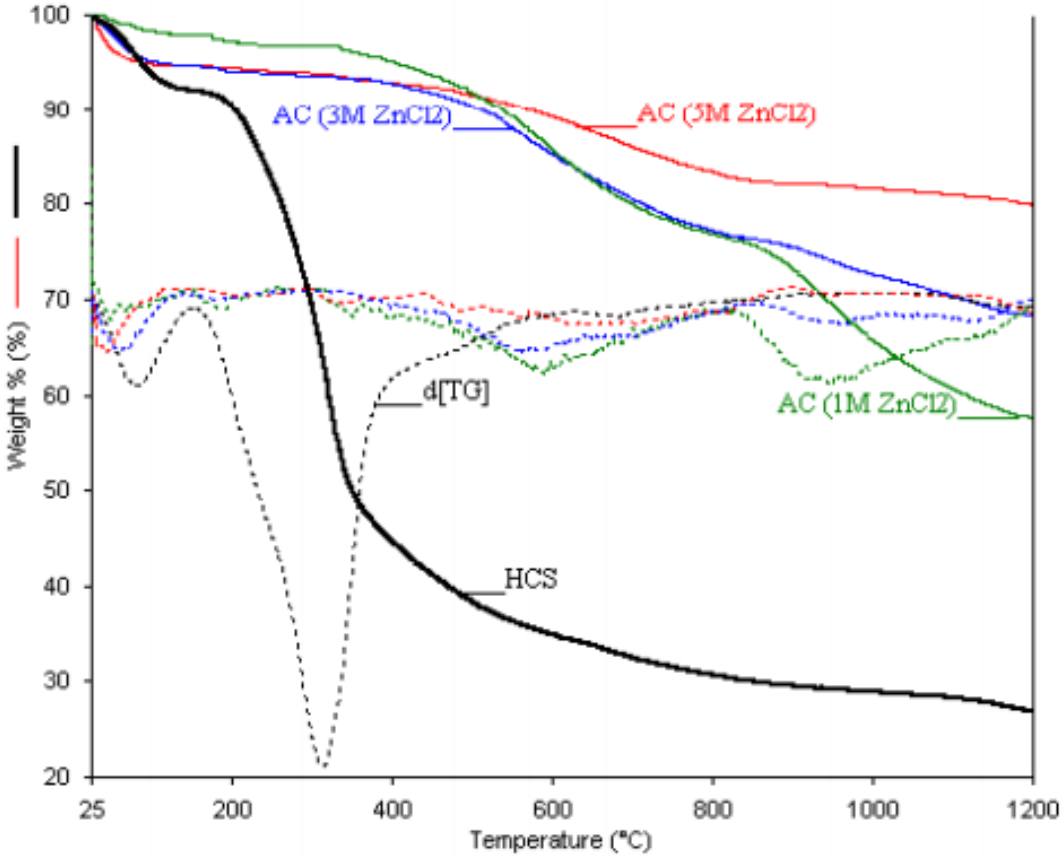

Figure 4.6. The TG and d[TG] thermograms of HCS and KN-ACs.

According to the data presented in Figure 4.6, HCS and KN-ACs exhibit different thermal stabilities. HCS was less thermally stable than activated carbon as its total residue was 26.83 wt%. The deposition of AC (3 M $ZnCl_2$) was 68.38 wt%.

4.1.5. SEM-EDX Analysis

The images obtained from the SEM device were sequenced from a coarse image to fine print with magnifications of 100 nm, 40 nm, 20 nm, 10 nm, respectively. The SEM images given in the raw state of HCS was collected from Figure 4.7 to Figure 4.10. Commercial

activated carbon (COM-AC) purchased from Merck brand from based-coal and produced activated carbon with $ZnCl_2$ from Horse Chestnut (*Aesculus hippocastanum* L.) Shells (KN-AC). According to these Figures, the magnitude of the SEM image enlarged at 100 nm in the coarsest state belongs to Horse Chestnut (*Aesculus hippocastanum* L.) Shells to obtain a clearer picture. After descending to a size of 10 nm, the structure was not homogeneous but scattered and irregular.

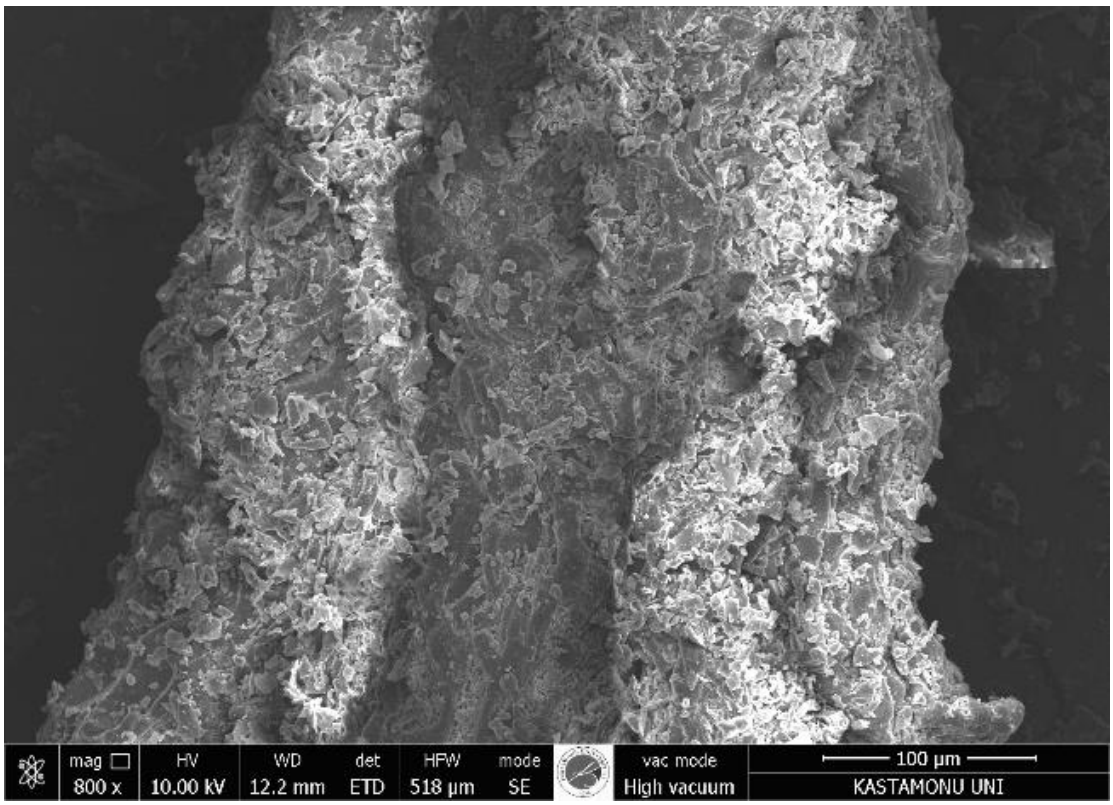

Figure 4.7. SEM image of feedstock HCS at 100 nm.

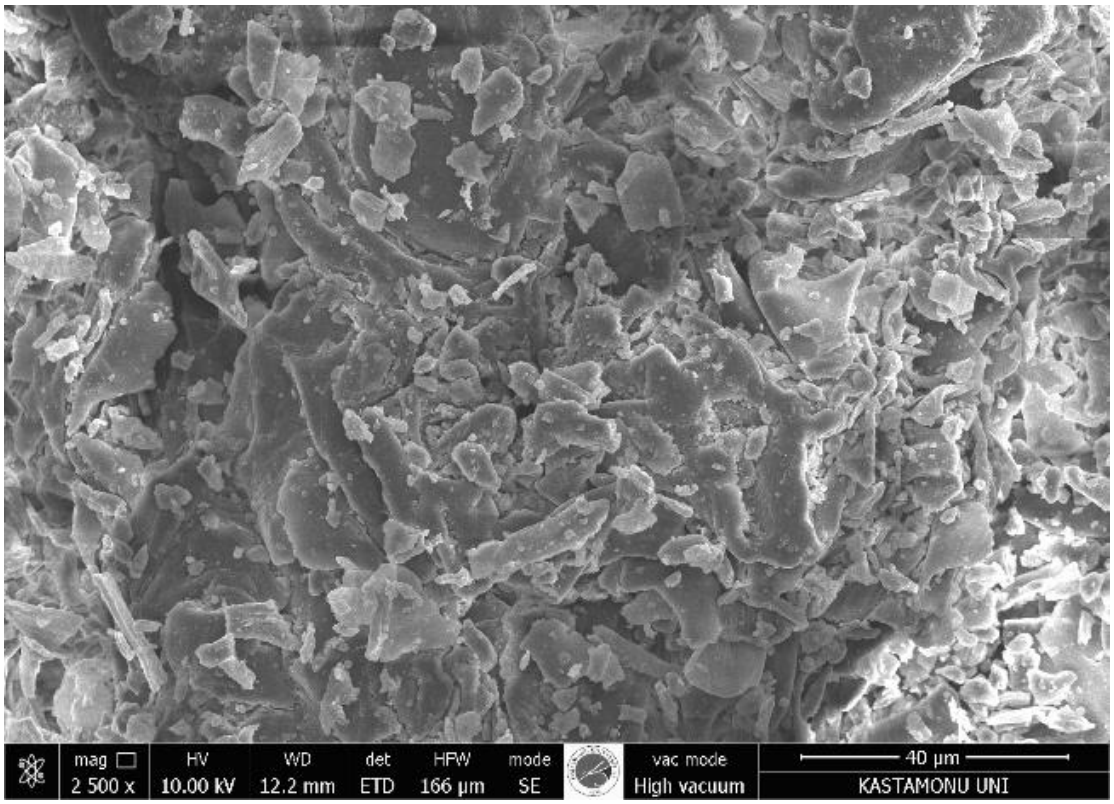

Figure 4.8. SEM image of feedstock HCS at 40 nm.

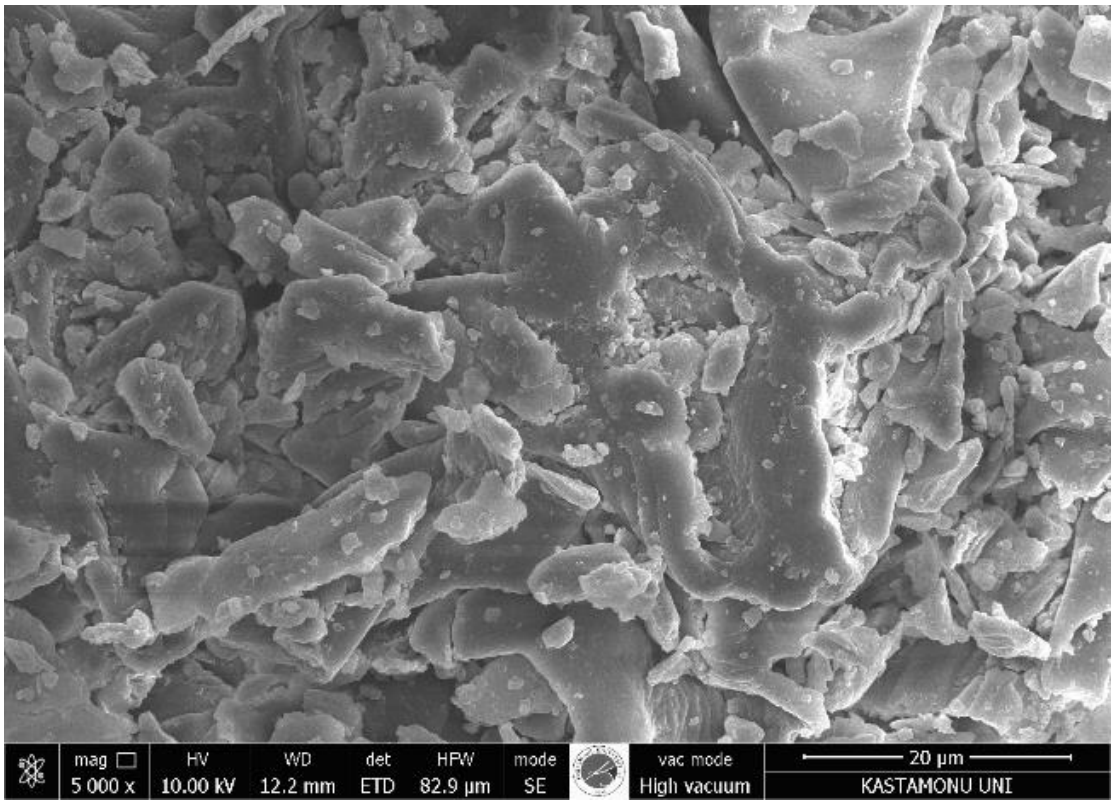

Figure 4.9. SEM image of feedstock HCS at 20 nm.

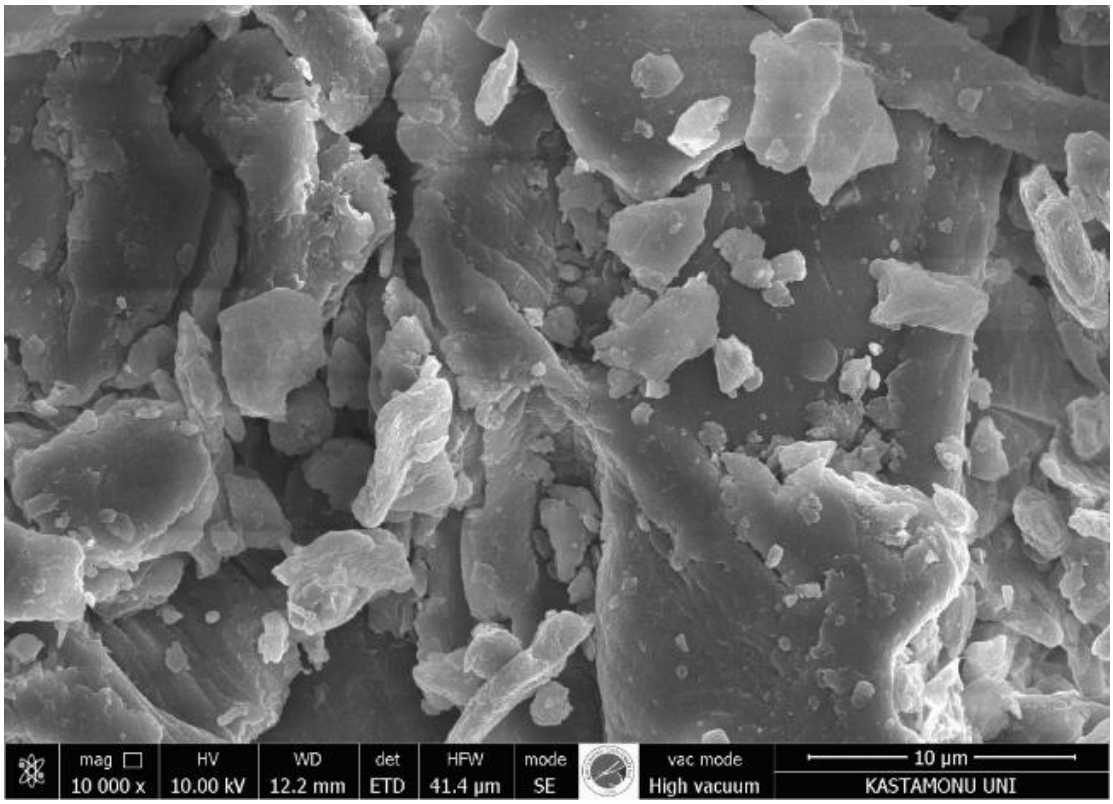

Figure 4.10. SEM image of feedstock HCS at 10 nm.

As shown in Figure 4.11, the magnification of the 500 nm given in the commercial activated carbon taken from the commercial products by looking at the detailed image of the SEM view. The most regular groups of the image in 10 nm, it was clear that the purchased AC has a more uniform structure and homogeneous distribution compared to organic materials in Figure 4.14.

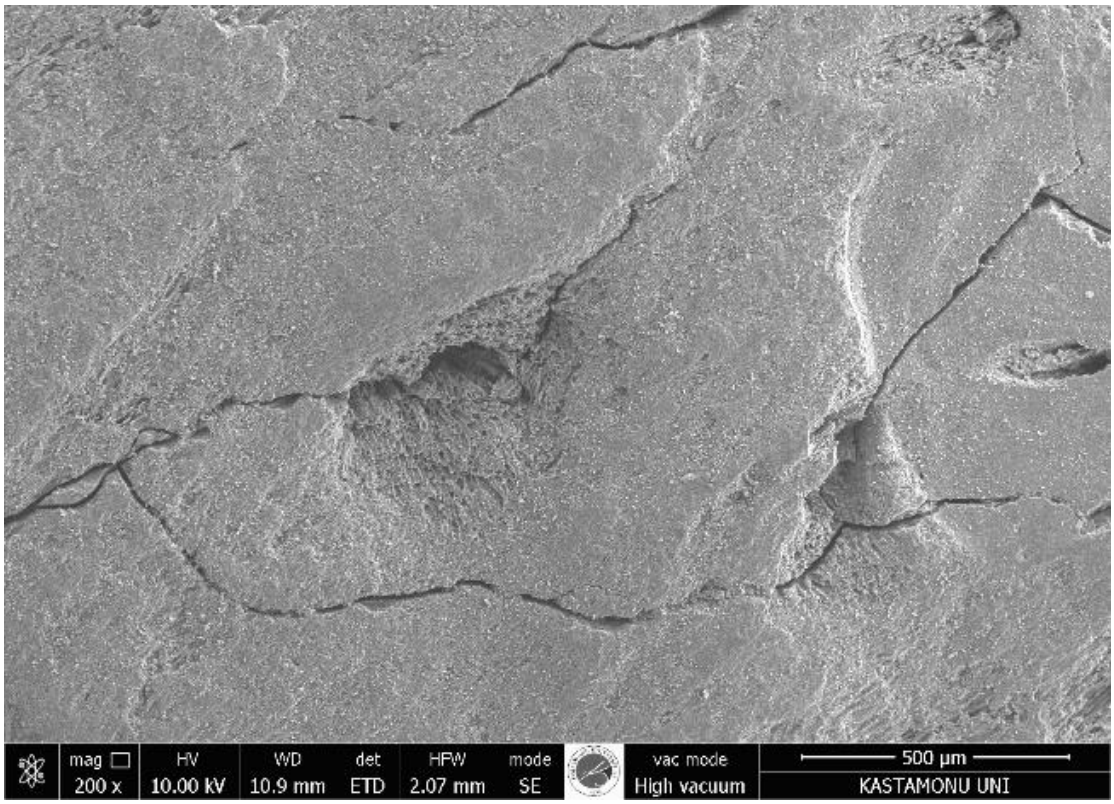

Figure 4.11. SEM image of COM-AC at 500 nm.

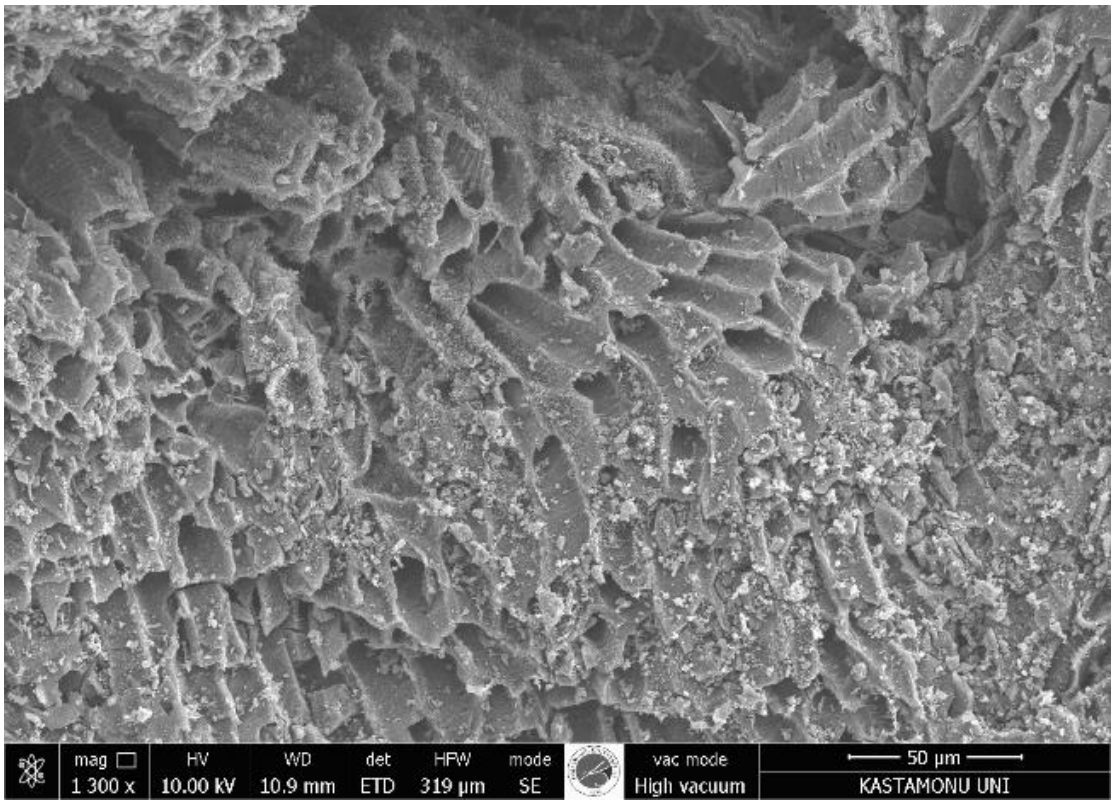

Figure 4.12. SEM image of COM-AC at 50 nm.

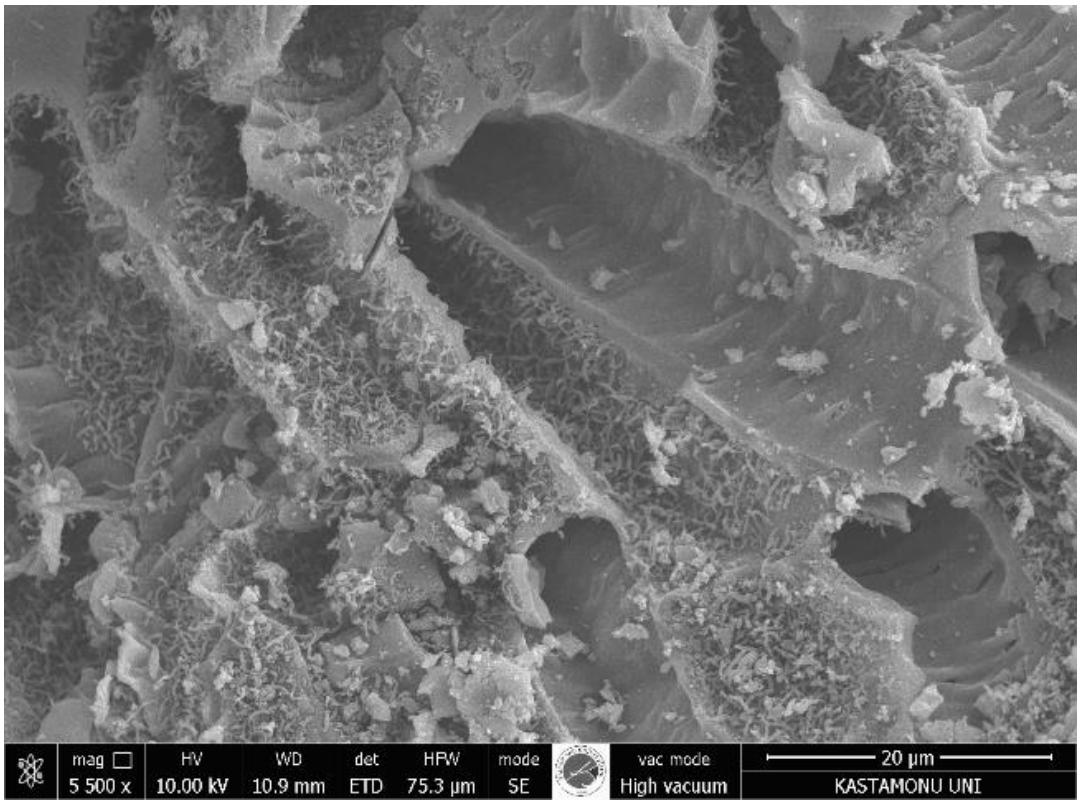

Figure 4.13. SEM image of COM-AC at 20 nm.

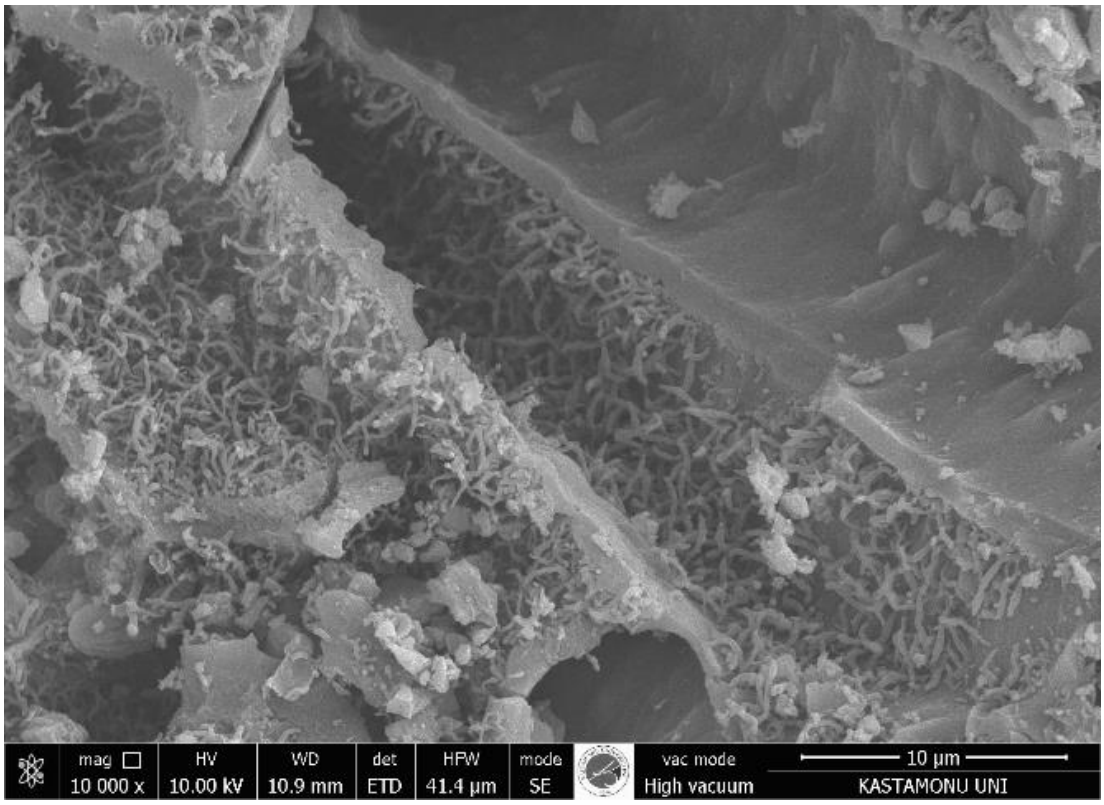

Figure 4.14. SEM image of COM-AC at 10 nm.

When the SEM image of 500 nm given in Figure 4.15 was examined, it is seen that $ZnCl_2$ activates the substance. Accordingly, it does not have a structure as in Figure 4.3 and it is seen that the pores' inner surface develops more. It is seen from the SEM images that the activated carbons were transformed into a more porous structure. It is seen range from Figure 4.15 to Figure 4.18 that it does not have a homogenized structure due to its content of lignocellulosic-based activated carbon.

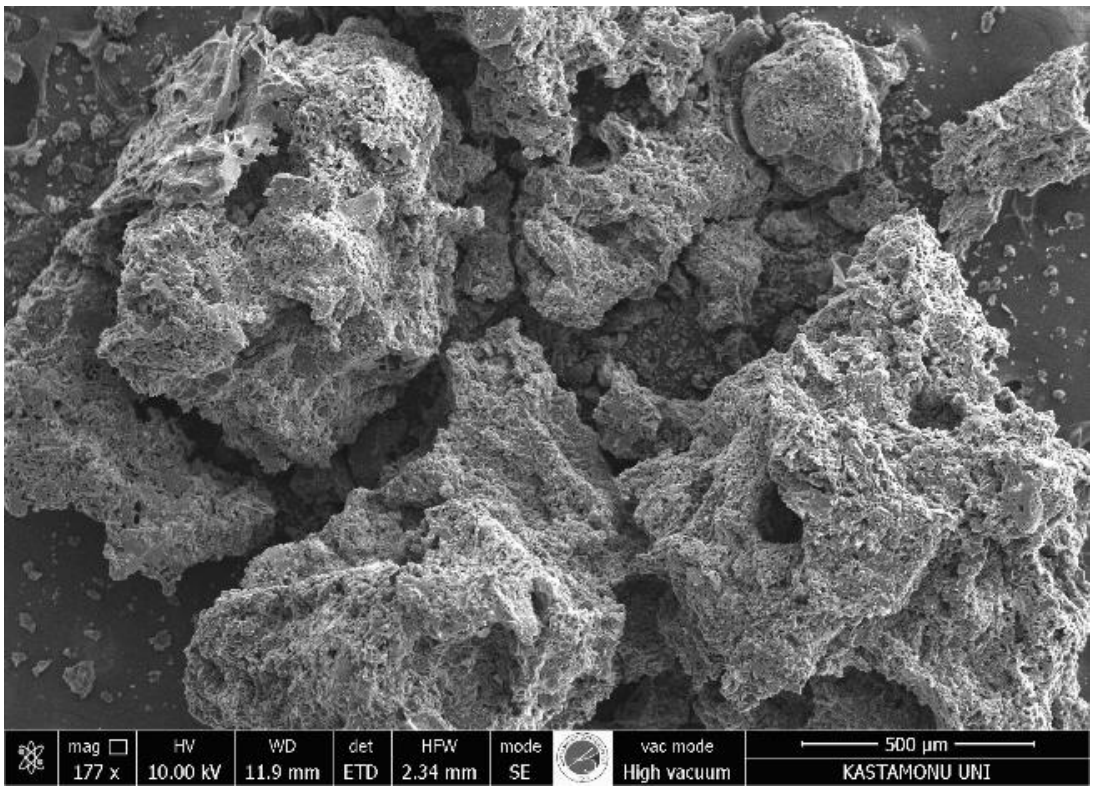

Figure 4.15. SEM image of KN-AC at 500 nm.

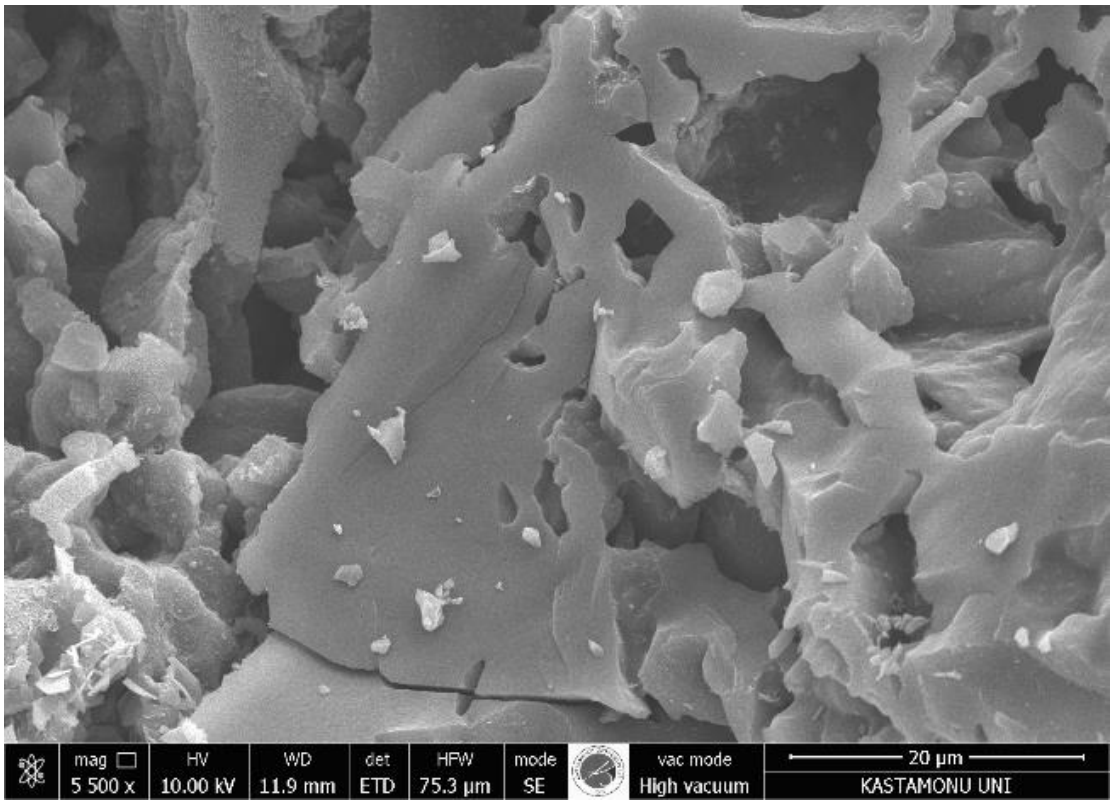

Figure 4.16. SEM image of KN-AC at 20 nm.

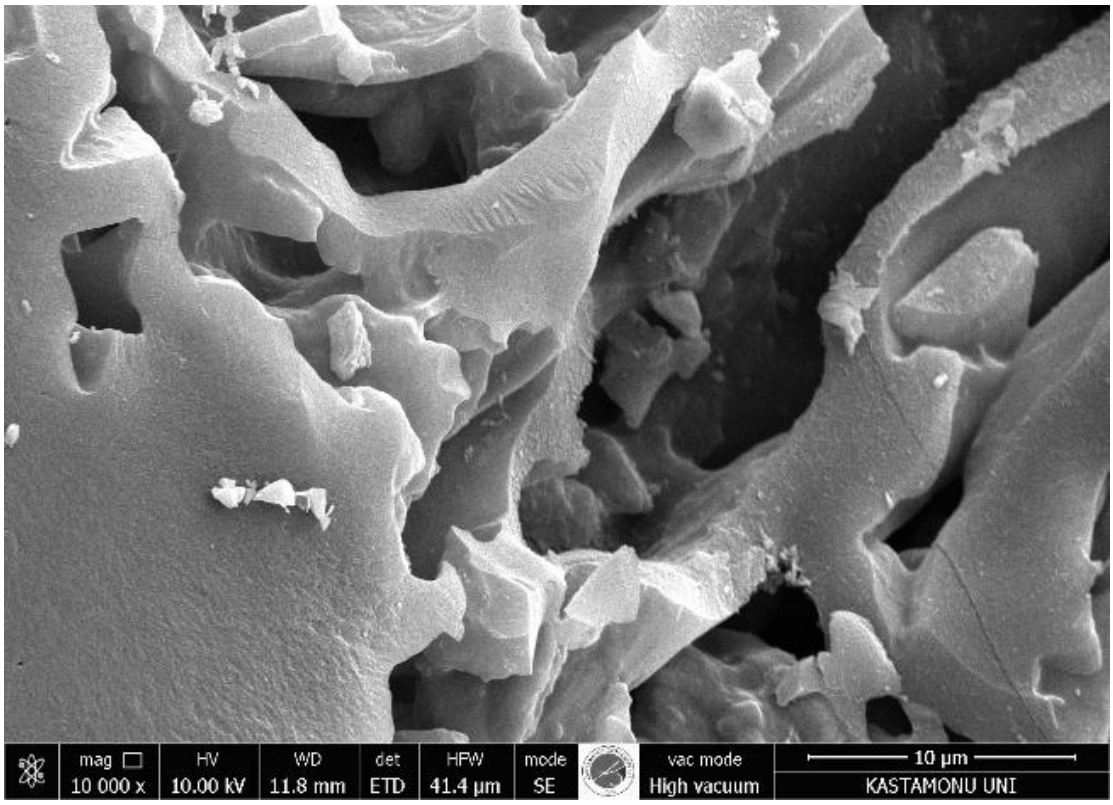

Figure 4.17. SEM image of KN-AC at 10 nm part a.

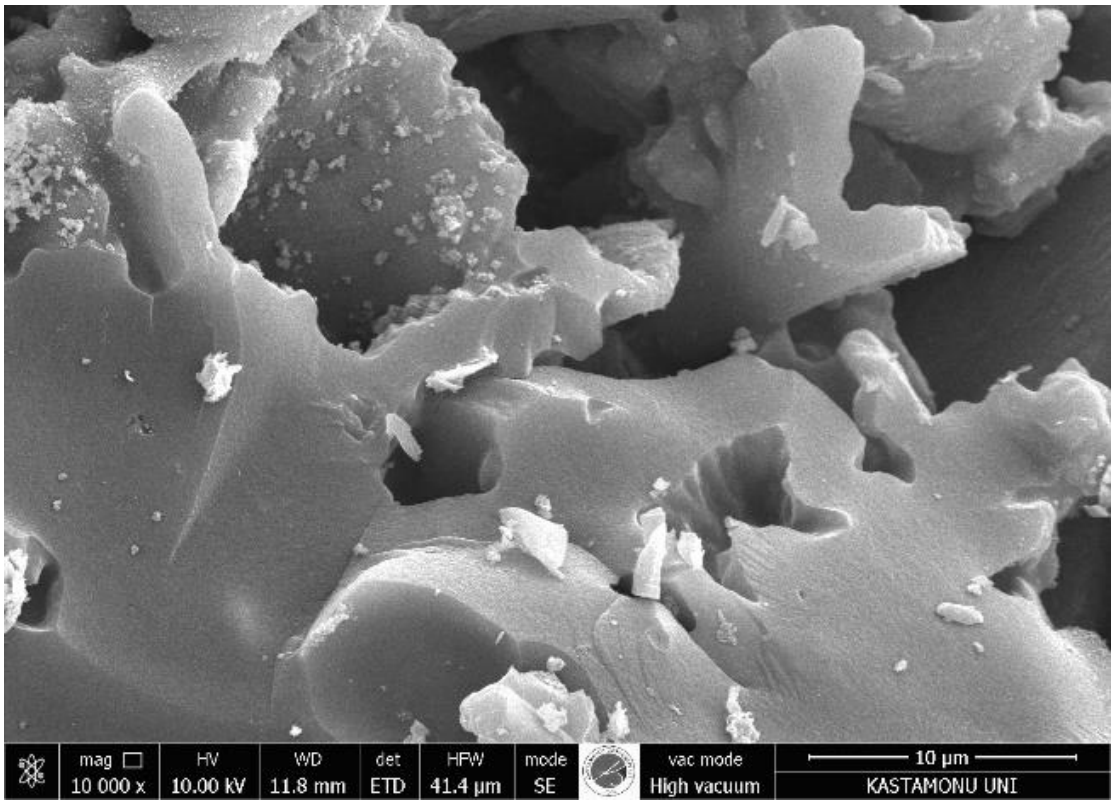

Figure 4.18. SEM image of KN-AC at 10 nm part b.

The SEM-EDX images of HCS and KN-ACs and the percent elemental contents determined from these patterns in Table 4.3. While SEM measurement were made with gold plated as homogeneously. It can be said that ACs have a porous structure due to the degradation of lignin and cellulose in HCS's form with the $ZnCl_2$ activation agent [308].

Table 4.3. Elemental analysis of HCS and KN-ACs.

Samples	C (wt%)	O (wt%)	Zn wt%)	Cl (wt%)	Si (wt%)	K (wt%)	Ca (wt%)
HCS	55.16	40.79	-	-	0.13	3.16	0.77
KN-AC (1 M $ZnCl_2$)	66.46	10.17	19.87	3.32	0.16	-	-
KN-AC (3 M $ZnCl_2$)	87.81	8.83	0.51	1.35	1.43	-	-
KN-AC (5 M $ZnCl_2$)	69.08	25.09	1.86	0.65	0.23	-	-

Following the above explanation, activated carbon samples were transformed into a porous structure. In EDX analysis, the carbon and oxygen contents of HCS were 55.16 and 40.79 wt%, respectively. The carbon and oxygen contents of activated carbon samples synthesized using 1 M $ZnCl_2$, 3 M $ZnCl_2$ and 5 M $ZnCl_2$ activation agents were 66.46 and 10.17 wt%; 87.81 and 8.83 wt% and 69.08 and 25.09 wt%, respectively. During the synthesis of activated carbon from HCS, the carbon contents (wt%) of activated carbons increased while the oxygen contents decreased. This indicates significant changes in the structure of HCS with the $ZnCl_2$ activation agent in parallel with the results of both BET and SEM analysis. The reduction of the amount of oxygen in the design by the synthesis of activated carbon results from the removal of hydroxyl functional groups in the cellulose structure. FTIR-ATR analysis results confirmed this. It was determined from BET analysis that the activated carbon having the highest surface area was the sample synthesized with 3 M $ZnCl_2$ at 600°C carbonization temperature.

The SEM images supported this with changes in surface morphology. When the carbon and oxygen contents of the synthesized activated carbon samples were compared, it can be said that the activated carbon synthesized with 3 M $ZnCl_2$ has higher carbon and lower oxygen content. This shows that the activated carbon synthesized under these conditions was better activated. This result is in good agreement with FTIR-ATR, BET and SEM analysis in Figure 4.19.

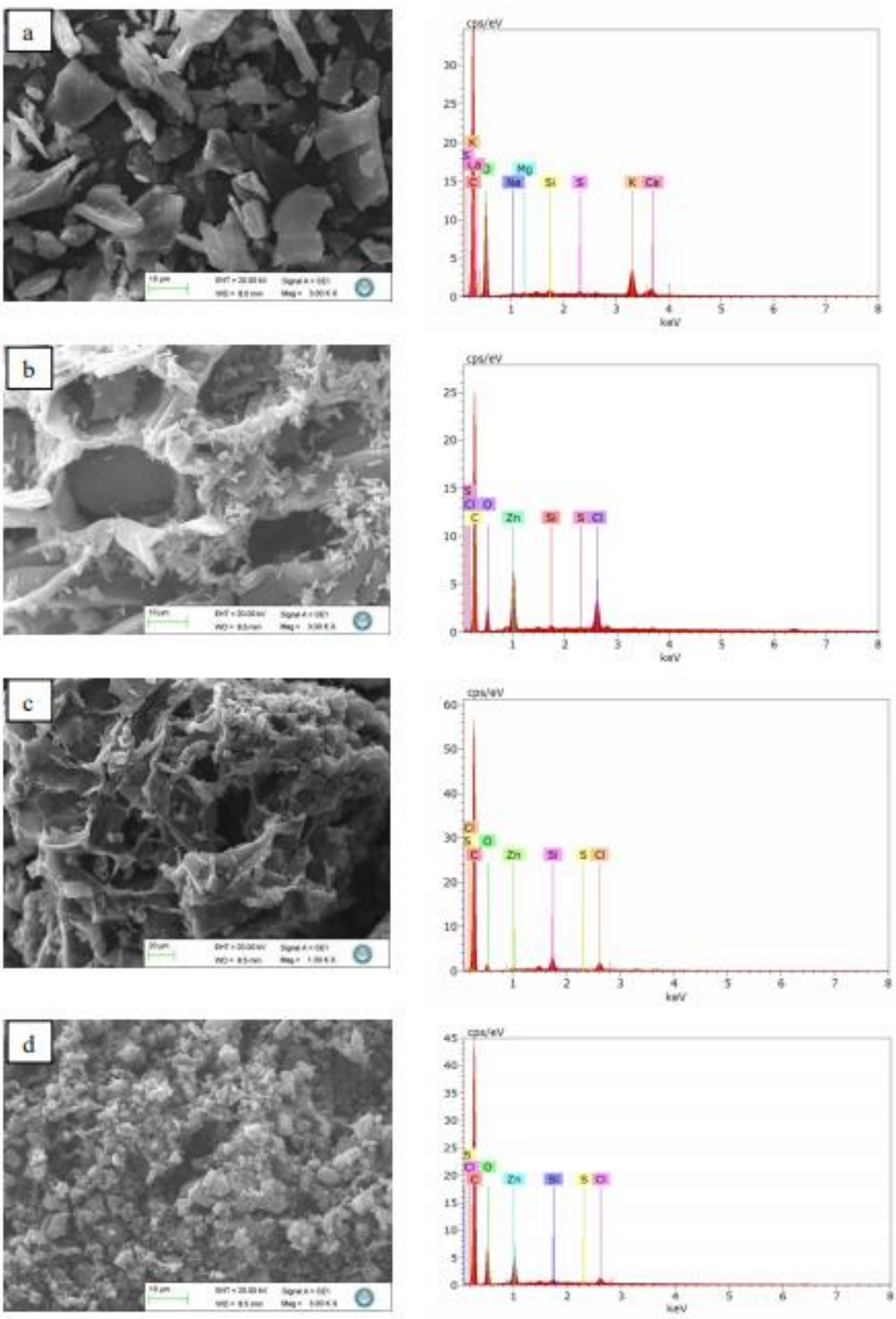

Figure 4.19. SEM images and EDX pattern of a. HCS, b. KN-AC (1 M $ZnCl_2$) c. KN-AC (3 M $ZnCl_2$) and d. KN-AC (5 M $ZnCl_2$)

4.1.6. Evaluation of Hydrogen Storage Capacity

The hydrogen storage capacities were givenin Table 4.4 at cryogenic temperatures. When 1 M $ZnCl_2$, 3 M $ZnCl_2$ and 5 M $ZnCl_2$ were used, the highest hydrogen storage capacities obtained 2.20 wt%, 3.18 wt% 1.94 wt% respectively at max mbar. Storage capacity increases with pressure in both molarities.

Table 4.4. Hydrogen storage data from KN-ACs at -169°C.

1 M $ZnCl_2$		3 M $ZnCl_2$		5 M $ZnCl_2$	
Pressure (mbar)	H_2 uptake (wt%)	Pressure (mbar)	H_2 uptake (wt%)	Pressure (mbar)	H_2 uptake (wt%)
2.33	0.12	0.24	0.08	113.32	0.15
7.70	0.12	2.52	0.14	329.80	0.30
119.03	0.63	50.84	0.49	639.84	0.45
413.34	0.97	215.64	0.88	1030.09	0.59
836.37	1.20	541.65	1.22	1470.46	0.71
1334.43	1.35	1001.44	1.49	1949.37	0.82
1860.21	1.46	1536.22	1.69	2445.99	0.91
2394.80	1.55	2108.94	1.84	2950.92	0.98
2923.90	1.61	2687.30	1.96	3465.57	1.05
3447.18	1.67	3259.60	2.06	4131.95	1.12
4119.99	1.73	3969.62	2.16	4906.61	1.20
4901.86	1.78	4779.77	2.25	5758.96	1.28
5762.46	1.83	5663.96	2.34	6665.53	1.34
6664.07	1.87	6587.02	2.42	7607.45	1.41
7604.16	1.91	7545.68	2.49	8566.06	1.46
8564.38	1.93	8521.92	2.56	9548.23	1.51
9537.16	1.96	9509.17	2.62	10534.88	1.56
10520.30	1.98	10505.68	2.67	11530.72	1.60
11507.08	1.99	11506.53	2.71	12525.63	1.64
12497.09	2.04	12503.09	2.76	13520.66	1.67
13490.75	2.10	13505.33	2.80	14834.64	1.71

14803.54	2.18	14823.97	2.85	16375.66	1.75
16333.62	**2.20**	16360.88	2.89	19017.45	1.81
18954.85	2.10	19006.62	2.96	22404.78	1.87
22318.82	1.98	22394.72	3.03	26299.55	1.91
26178.93	1.93	26297.90	3.08	30545.02	1.93
30388.56	1.85	30542.77	3.12	36601.41	1.94
36381.48	1.73	36602.73	3.16	43899.27	**1.94**
43600.50	1.58	43907.27	**3.18**	-	-

Accordingly, when using 3 M $ZnCl_2$, hydrogen storage capacity was higher in all pressure values than 1 M $ZnCl_2$ and 5 M $ZnCl_2$ at -169ºC, although the hydrogen storage capacity increases with increasing pressure at 25°C in KN-ACs.

The hydrogen storage capacity of KN-AC samples produced at 1 M $ZnCl_2$, 3 M $ZnCl_2$ and 5 M $ZnCl_2$ concentrations at room temperature was given in Table 4.5. Hydrogen storage capacity increases with increasing pressure at 1 M, 3 M and 5 M molarity in Figure 4.20.

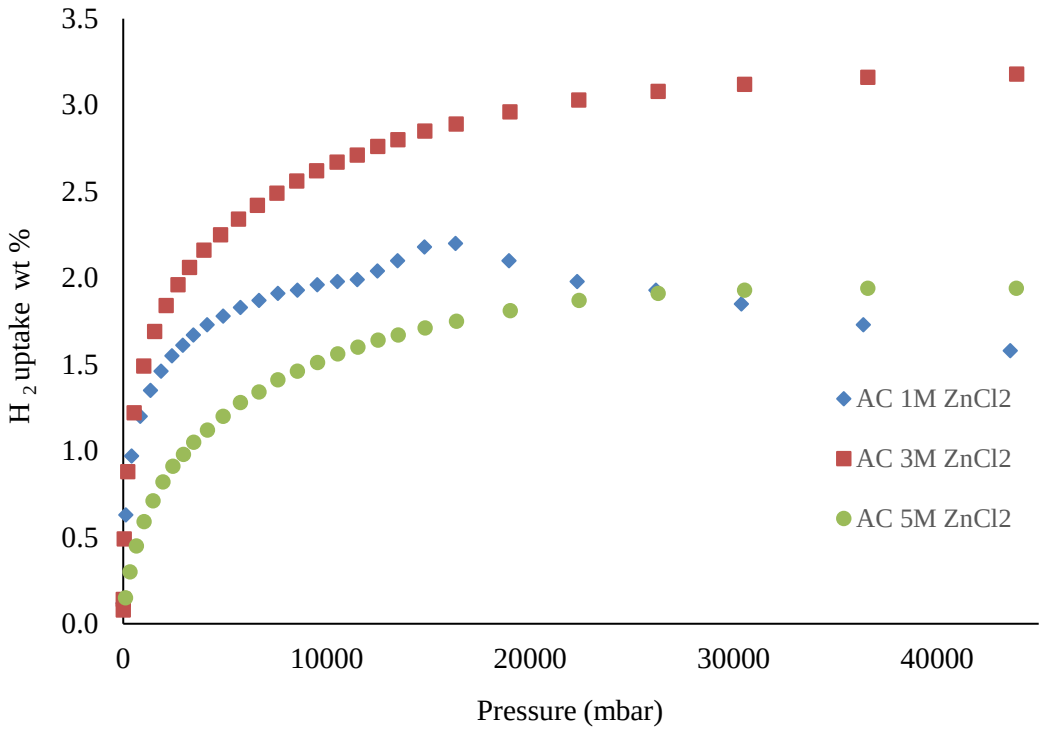

Figure 4.20. Excess and total gravimetric hydrogen uptake of KN-ACs at -169ºC.

When Table 4.4 and Table 4.5 compared it found that the hydrogen storage capacities were relatively low, given in Table 4.5. Because these values were analyzed at room temperature (25 ºC). When these values were examined, the highest hydrogen storage capacities obtained when using 1 M $ZnCl_2$ were 0.26 wt%, 3 M $ZnCl_2$ was 0.3 wt%, and 5 M $ZnCl_2$ got as 0.21 wt% at max mbar.

Table 4.5. Hydrogen storage data from KN-ACs at 25ºC.

1 M $ZnCl_2$		3 M $ZnCl_2$		5 M $ZnCl_2$	
Pressure (mbar)	H_2 uptake (wt%)	Pressure (mbar)	H_2 uptake (wt%)	Pressure (mbar)	H_2 uptake (wt%)
1249.07	0.01	0.16	0	-2.11	0
1747.34	0.01	64.55	0.01	52.67	0.01
2232.93	0.02	97.06	0.01	92.27	0.01
2738.49	0.02	366.82	0.02	375.85	0.01
3231.88	0.02	792.13	0.02	792.29	0.01
3731.03	0.03	1247.40	0.03	1253	0.01
4234.41	0.03	1735.13	0.03	1738.42	0.02
4996.12	0.04	2223.29	0.04	2236.26	0.02
5879.63	0.05	2710.66	0.04	2722.15	0.02
6819.15	0.05	3216.91	0.05	3222.02	0.03
7802.30	0.06	3715.78	0.06	3717.62	0.03
8787.64	0.07	4219.45	0.06	4207.22	0.03
9782.45	0.08	4975.50	0.06	4974.37	0.03
10785.99	0.10	5863.86	0.06	5866.31	0.04
11782.28	0.11	6812.39	0.06	6822.90	0.05
12776.91	0.12	7786.45	0.07	7806.78	0.05
13776.84	0.13	8771.68	0.08	8784.30	0.06
14765.14	0.14	9770.83	0.08	9778.84	0.07
16284.71	0.16	10776.54	0.08	10784.87	0.07
18051.48	0.17	11768.71	0.15	11772.64	0.07
21751.10	0.21	12768.90	0.20	12771.40	0.09

25912.33	0.24	13775.58	0.26	13782.63	0.15
30510.71	0.26	14767.67	0.30	14783.21	0.21

Experiments should be performed at low temperatures to increase the Van der Waals interactions between adsorbent and hydrogen. Therefore, the experiments were carried out by placing the samples into an airtight measuring cell and immersing them in a vacuum filled Dewar container under liquid nitrogen.

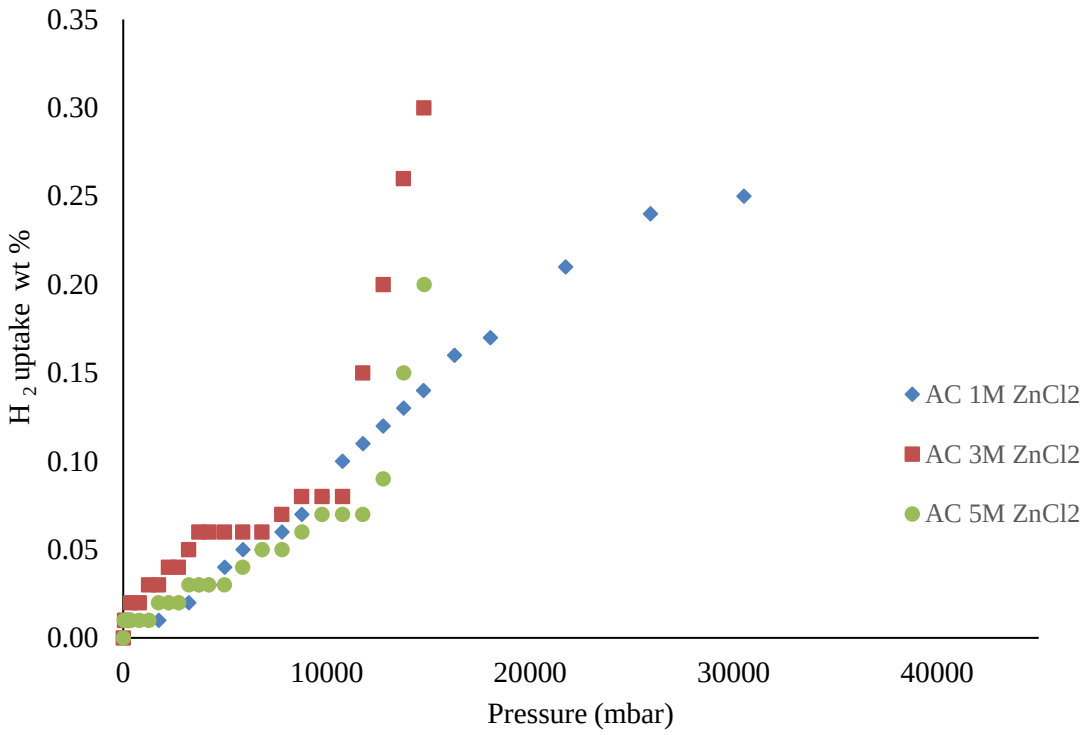

Figure 4.21. Excess and total gravimetric hydrogen uptake of KN-ACs at 25ºC.

The weak interactions that hold the hydrogen molecules together become more important at -169ºC and at elevated pressures for large amounts of hydrogen to be stored. Increased hydrogen storage capacity by decreasing the temperature value hydrogen can be explained by desorbing with increasing temperature. The hydrogen adsorption capacity on a material depends on the specific surface area of the material. As a result, the same material's hydrogen storage capacity under the same conditions decreases with increasing temperature.

The hydrogen storage capacities of activated carbon samples calculated from these curves were given in Table 4.6. The hydrogen storage capacities of KN-AC (1 M $ZnCl_2$), KN-AC (3 M $ZnCl_2$) and KN-AC (5 M $ZnCl_2$) samples were determined as 0.25, 0.26 and 0.20 wt% at room temperature, and as 2.20, 3.18 and 1.94 wt% at cryogenic temperature, respectively. Hydrogen storage capacities also increased with increasing pressure. When the hydrogen storage capacities of the samples were compared, it can be said that the activated carbon synthesized with 3 M $ZnCl_2$ has a higher hydrogen storage capacity.

Table 4.6. H_2 uptake of the various ACs in literature.

ACs	H_2 uptake (wt%)	Ref.
Ch1000/700/3	3.62 at -169ºC	[309]
AC6	2.58 at -169ºC	[306]
AC	1.06 at 25°C	[310]
AC-K3	2.23 at -169ºC	[311]
KN-AC-(1 M $ZnCl_2$)	2.20 at -169ºC	In this study
KN-AC-(1 M $ZnCl_2$)	0.25 at 25ºC	In this study
KN-AC-(3 M $ZnCl_2$)	3.18 at -169ºC	In this study
KN-AC-(3 M $ZnCl_2$)	0.26 at 25ºC	In this study
KN-AC-(5 M $ZnCl_2$)	1.94 at -169 ºC	In this study
KN-AC-(5 M $ZnCl_2$)	0.20 at 25 ºC	In this study

As can be seen from Table 4.1, both the BET surface area and the micropore volume of this sample were higher than those of activated carbons synthesized with 1 M and 5 M $ZnCl_2$. In this case, it can be stated that hydrogen was adsorbed on the surface and pores of the activated carbon. Again, when hydrogen storage capacities of the activated carbons were compared at room and cryogenic temperatures, more hydrogen was adsorbed on activated carbon's surface and pores. Due to increased Van der Waals forces between hydrogen molecules and activated carbons at cryogenic temperatures. The decrease in hydrogen storage capacity of the activated carbons with increasing temperature may be

due to the desorption of the hydrogen molecules held together by Van der Waals interactions on the surfaces and pores of the activated carbons at room temperatures. The hydrogen adsorption capacity on a material depends on the material's specific surface area and pore size volume. As a result, the same material's hydrogen storage capacity under the same conditions decreases with increasing temperature.

The hydrogen storage capacities of some activated carbon samples synthesized from different sources were given in Table 4.6. The hydrogen storage capacities of these activated carbons have varied in the range of 1.06-3.62 wt%, depending on the temperature. When these values were compared with the hydrogen storage capacities of the activated carbons synthesized in this study, it can be said that especially KN-AC (3 M $ZnCl_2$) can be used for hydrogen storage purposes.

4.2. Removal of Formaldehyde

The calibration graph was plotted as $R^2 = 0.9989$ in Figure 4.22.

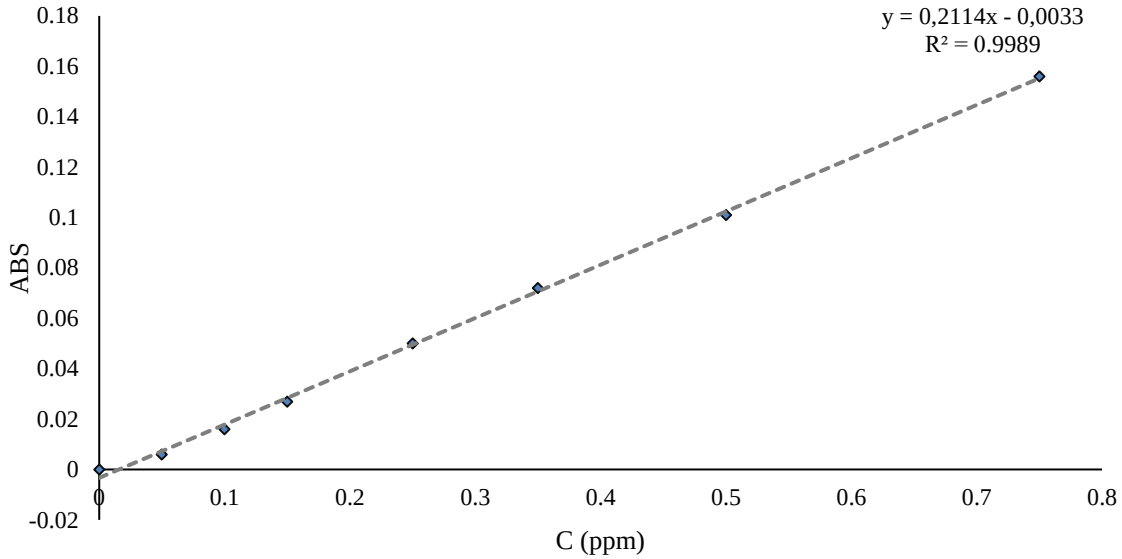

Figure 4.22. Calibration graph for formaldehyde adsorption.

4.2.1. Sorption Equilibrium Modeling of Formaldehyde

When Freundlich, Langmuir and Dubinin-Radushkevich isotherms were adapted, the linearized isotherm graphs for COM-AC and KN-AC. Thus the difference of KN-AC has emerged that linearized graphics more suitable for formaldehyde removal. The linearity of kinetic models is essential for deciding the model's suitability for the adsorption system [278].

4.2.1.1. Freundlich Isotherm Modelling of Formaldehyde

Firstly, COM-AC and KN-AC were tested using the Freundlich isotherm model. A graph of log qe was plotted against log Ce were plotted to test the compatibility of equilibrium data to the multilayer adsorption system in the adsorption processes to CH_2O. The linear function of Freundlich isotherm used for testing was used with Eq. (5), then R^2, n and K_F were calculated by the isotherm constants from the slope and shear values in Table 4.7

for COM-AC, in Table 4.8 for KN-AC. The lines drawn range from Figure 4.23 to Figure 4.36 for COM-AC and range from Figure 4.37 to Figure 4.50 for KN-AC.

The CH_2O removal studies were performed in a batch system, room temperature conditions with constant temperature and reactor having a volume of 0.002 m^3. Before starting the analysis, 0.5 g COM-AC and KN-AC were weighed separately on the precision balance. In all experiments, it was aimed to keep the environment under constant conditions by operating the activated carbonless system to adjust the desired concentration.

Graphics of the Freundlich isotherm model depending on different concentrations were drawn as linearized. It was removed from low concentration to high, respectively. In Figure 4.31, where the formaldehyde removal studies with low COM-AC concentrations were carried out, the graph of the removal studies with KN-AC was given in Figure 4.45.

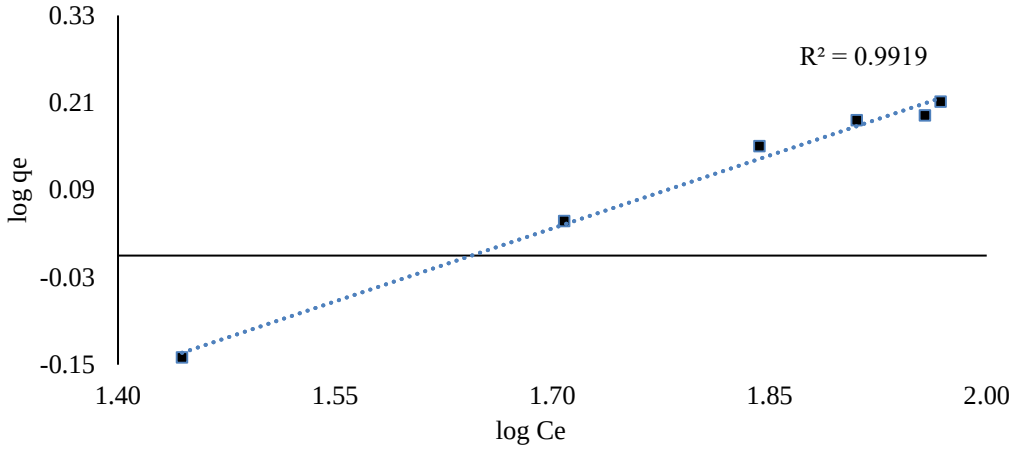

Figure 4.23. Freundlich isotherm graph of COM-AC for formaldehyde at 170 µg/m³.

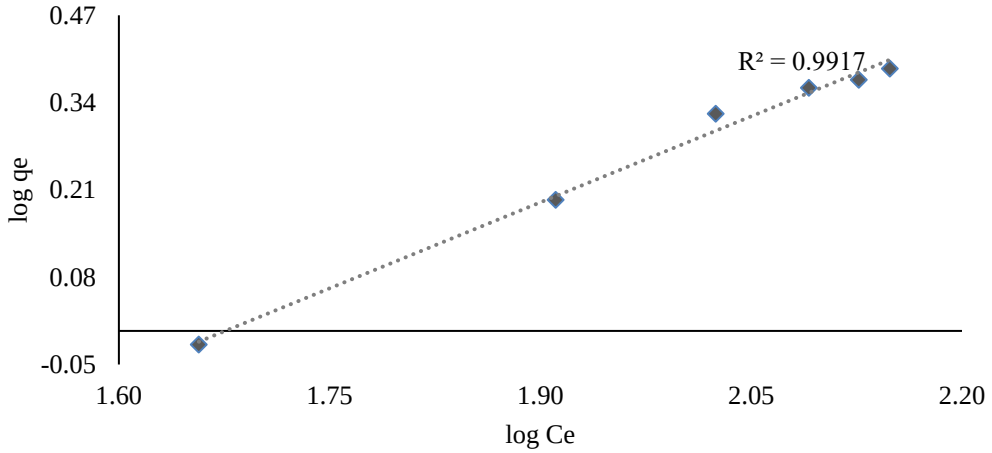

Figure 4.24. Freundlich isotherm graph of COM-AC for formaldehyde at 260 µg/m³.

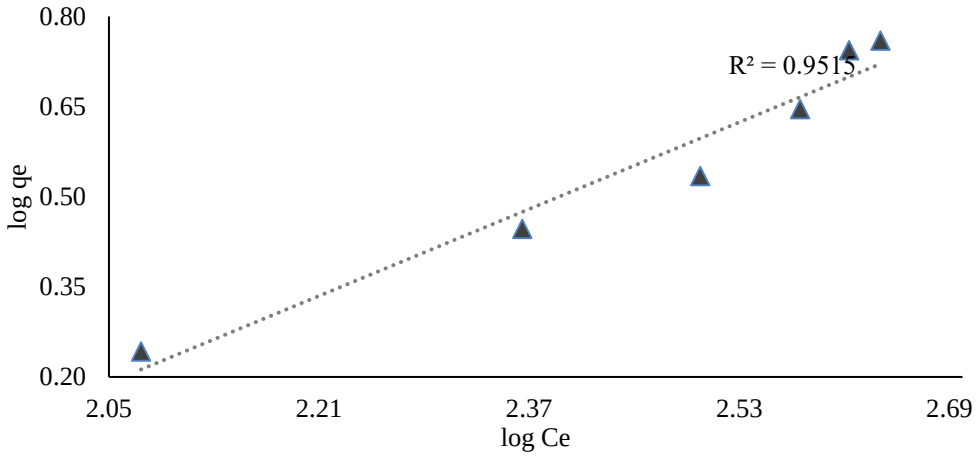

Figure 4.25. Freundlich isotherm graph of COM-AC for formaldehyde at 720 µg/m³.

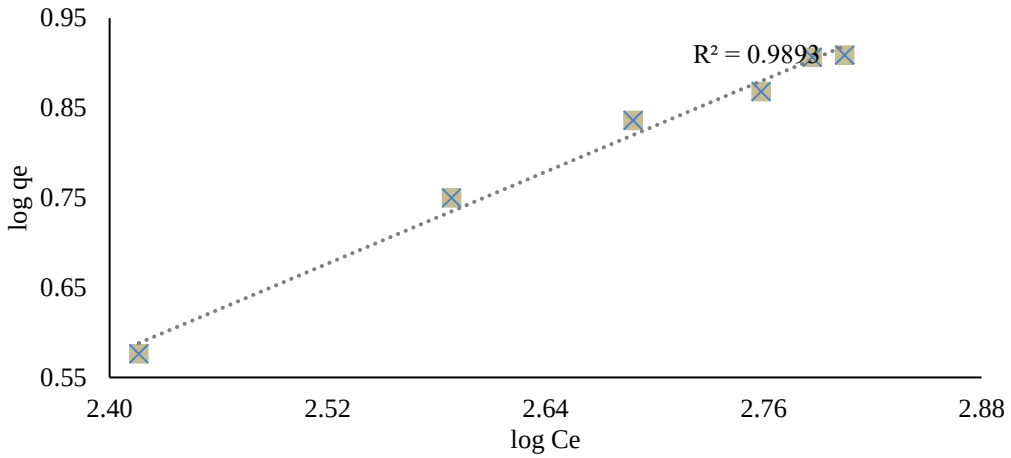

Figure 4.26. Freundlich isotherm graph of COM-AC for formaldehyde at 1040 µg/m³.

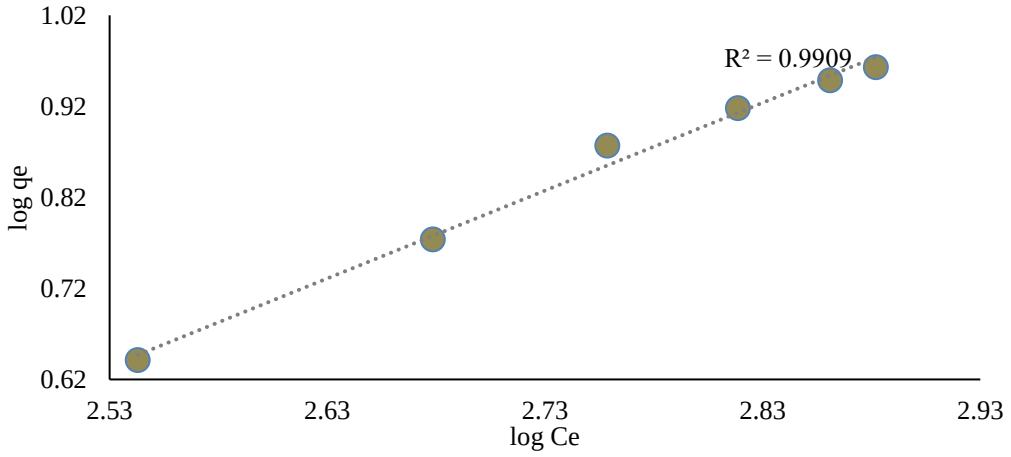

Figure 4.27. Freundlich isotherm graph of COM-AC for formaldehyde at 1220 µg/m³.

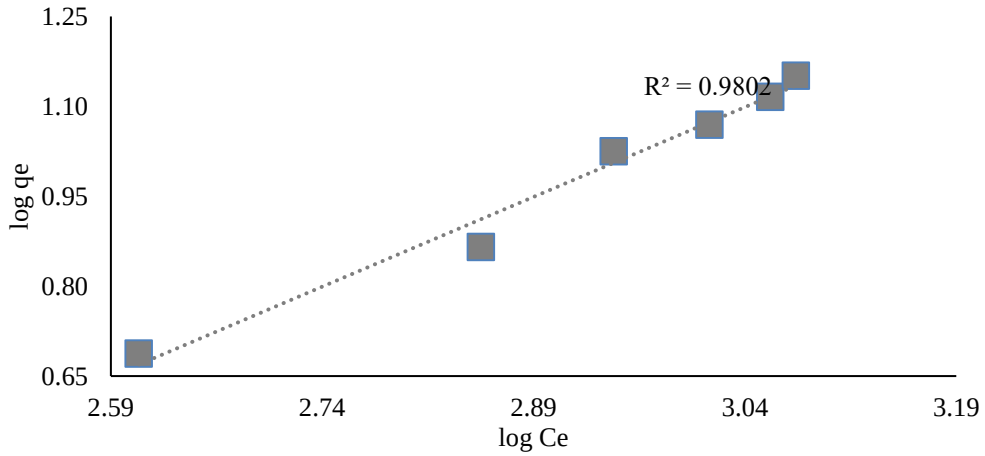

Figure 4.28. Freundlich isotherm graph of COM-AC for formaldehyde at 1900 µg/m³.

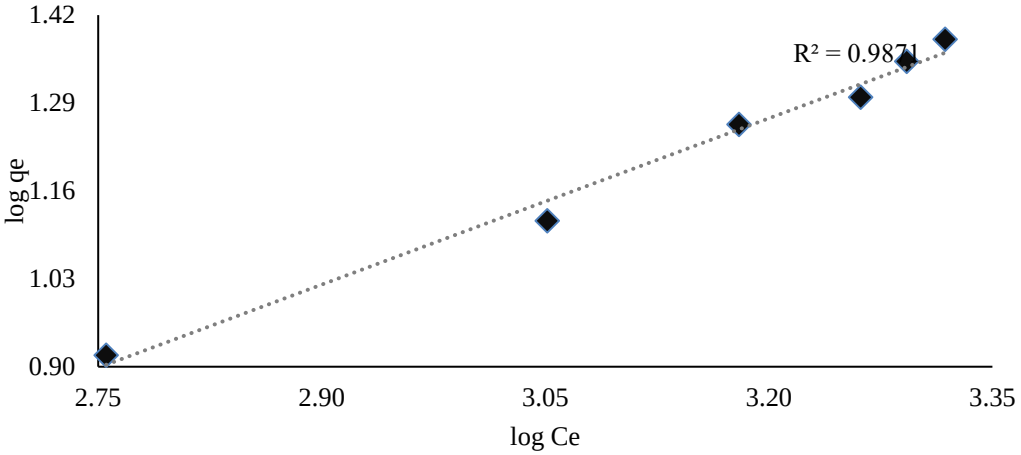

Figure 4.29. Freundlich isotherm graph of COM-AC for formaldehyde at 3290 µg/m³.

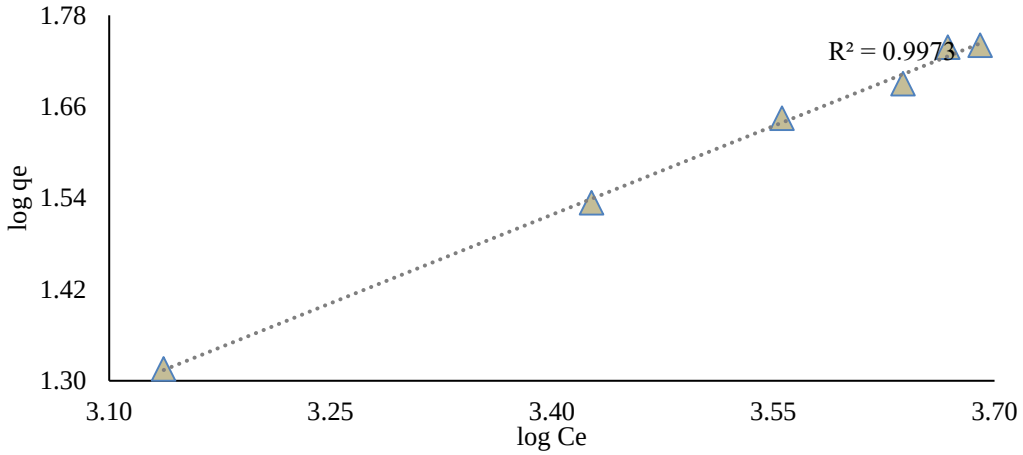

Figure 4.30. Freundlich isotherm graph of COM-AC for formaldehyde at 7650 µg/m³.

The linearized graphs of the data obtained from low concentration formaldehyde removal studies with the COM-AC were givenin Figure 4.23 and Figure 4.30.

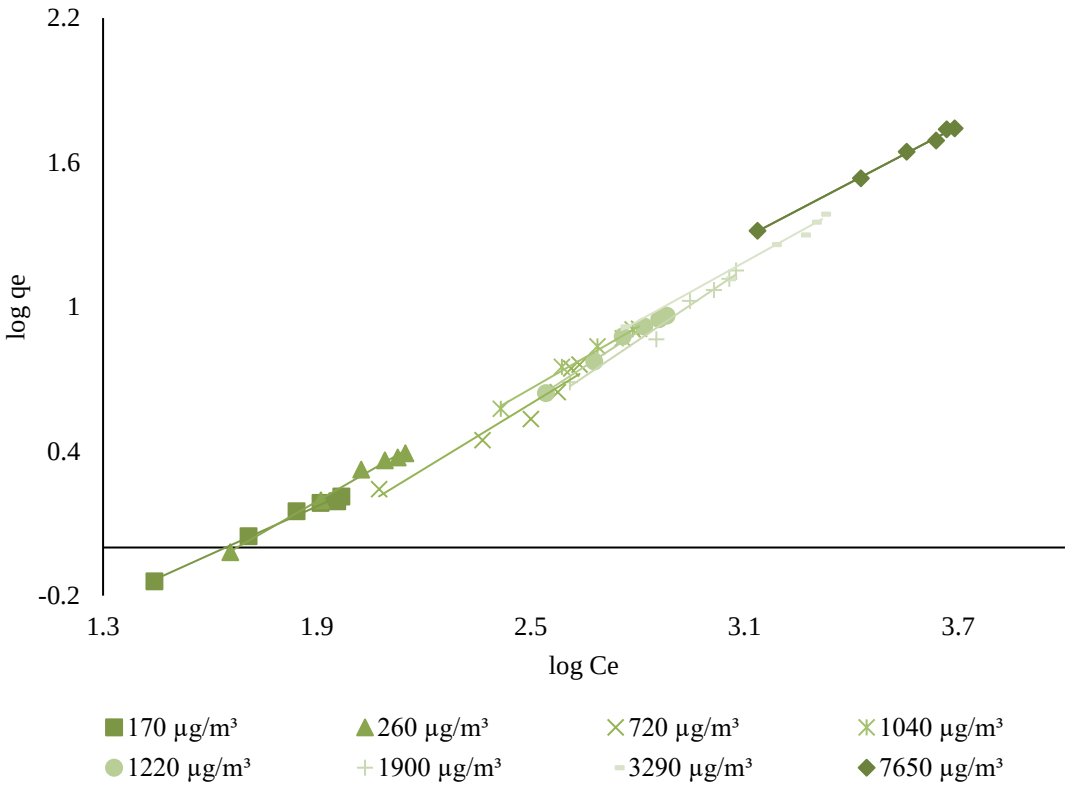

Figure 4.31. Freundlich isotherm graph for COM-AC for all low formaldehyde concentrations.

The studies carried out with COM-AC in terms of comparison as a linearized is given in a single graphic, which was suitable for the distribution at different concentrations from 170±14.92 µg/m^3 to 7650±111.18 µg/m^3.

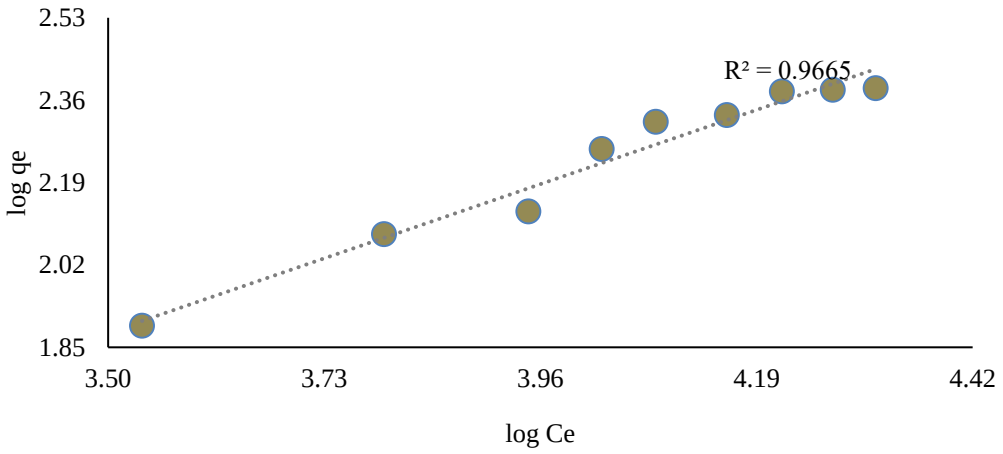

Figure 4.32. Freundlich isotherm graph of COM-AC for formaldehyde at 30,000 µg/m³.

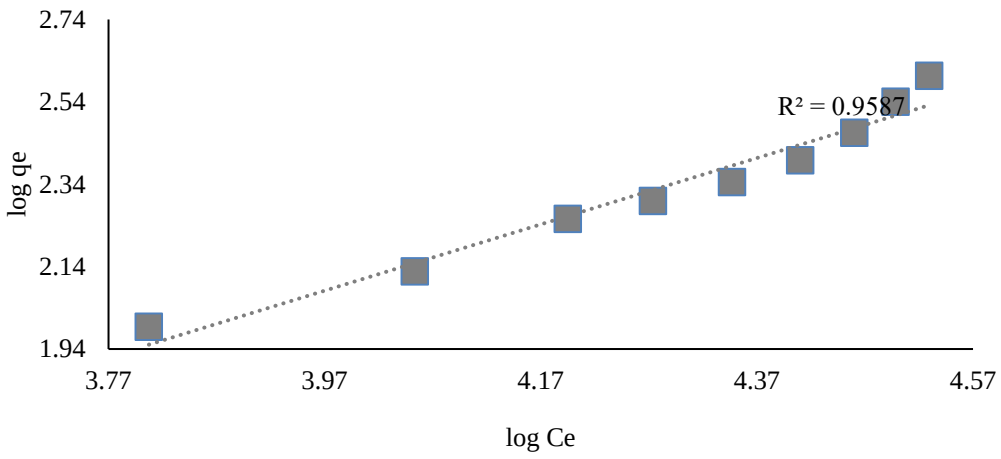

Figure 4.33. Freundlich isotherm graph of COM-AC for formaldehyde at 50,000 µg/m³.

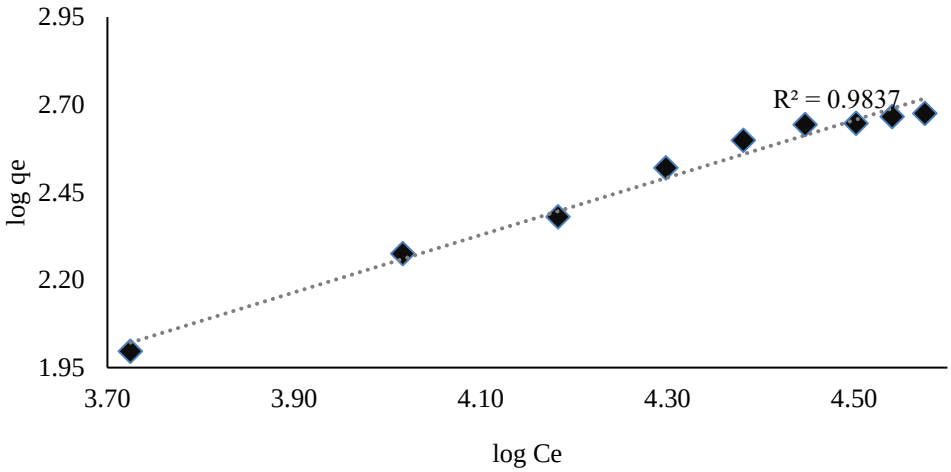

Figure 4.34. Freundlich isotherm graph of COM-AC for formaldehyde at 60,000 µg/m³.

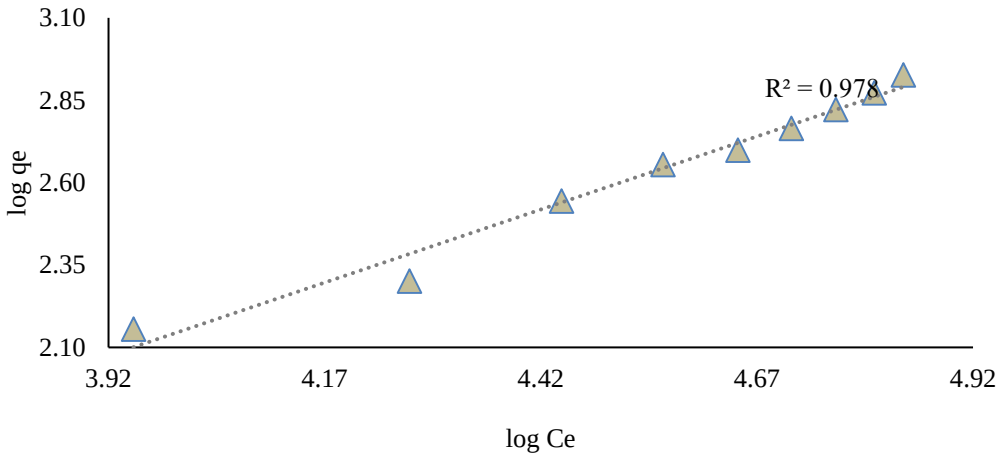

Figure 4.35. Freundlich isotherm graph of COM-AC for formaldehyde at 110,000 µg/m³.

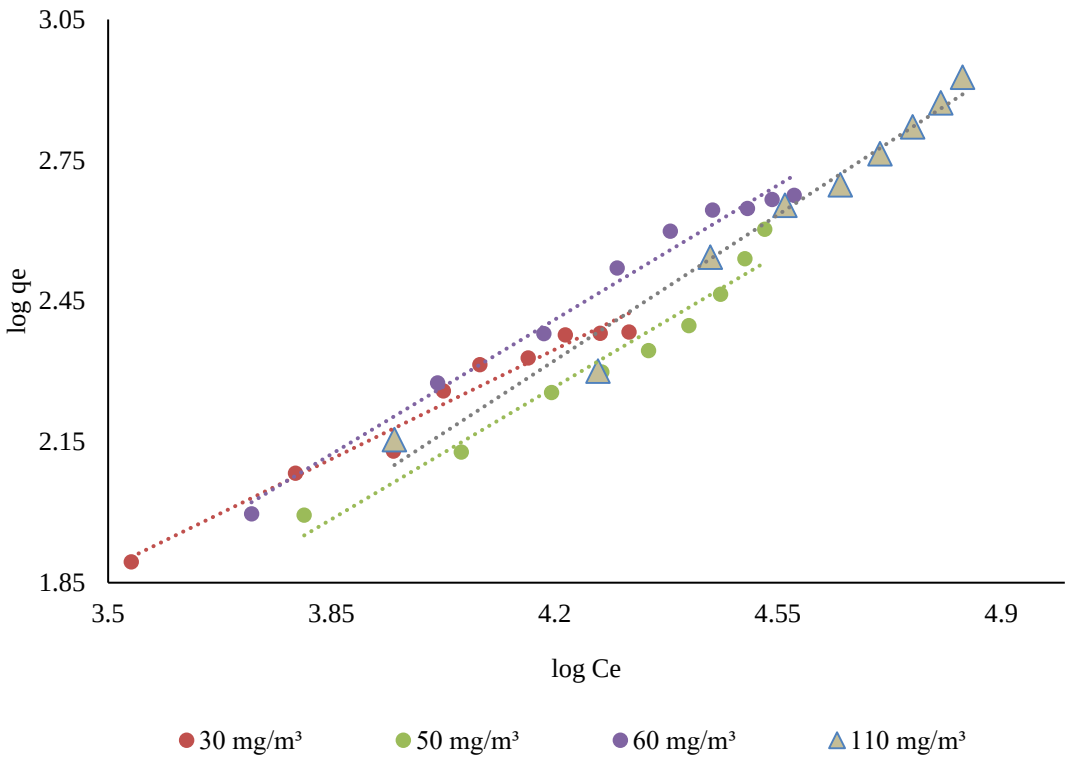

Figure 4.36. Freundlich isotherm graph of COM-AC of all high formaldehyde concentrations.

The isotherm studies performed a high concentration of formaldehyde with the COM-AC between Figure 4.32 and Figure 4.35. These high concentrations as a linearized were givenon the same graph, which was suitable for the distribution from 30,000 µg/m³ to 110,000 µg/m^3 in Figure 4.36.

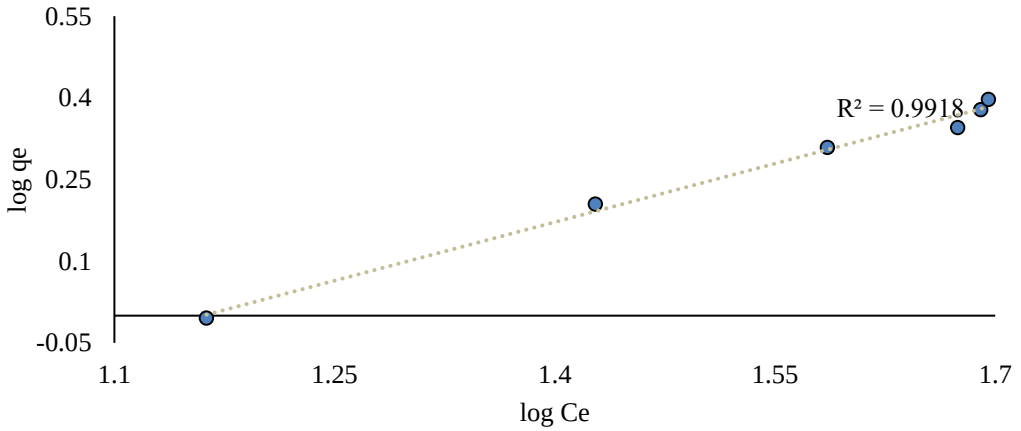

Figure 4.37. Freundlich isotherm graph of KN-AC for formaldehyde at 170 µg/m³.

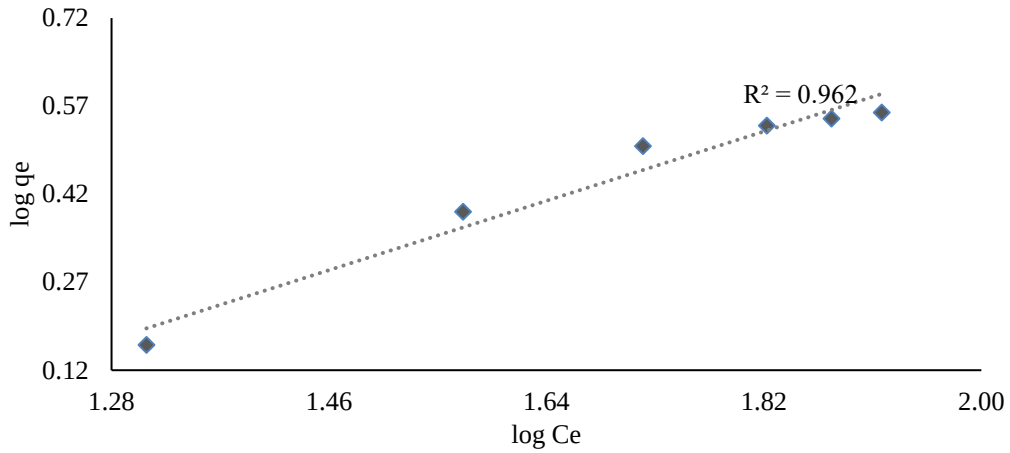

Figure 4.38. Freundlich isotherm graph of KN-AC for formaldehyde at 260 µg/m³.

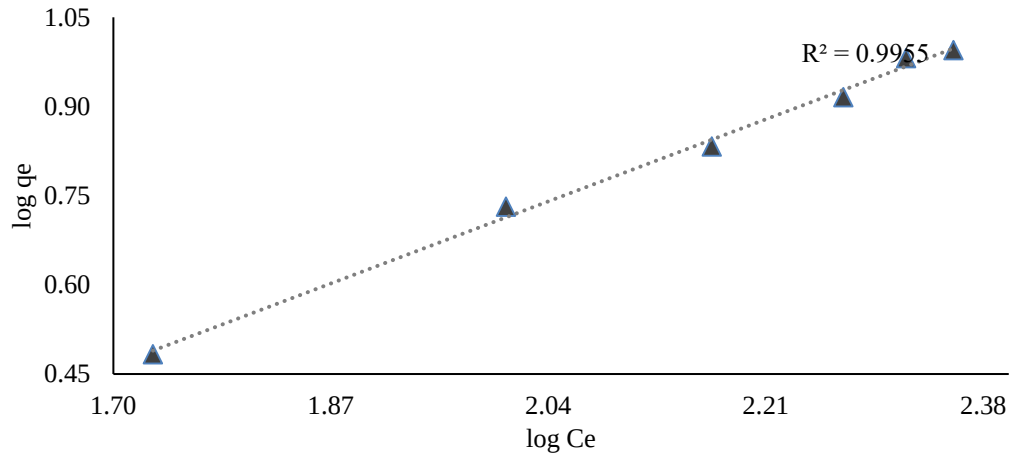

Figure 4.39. Freundlich isotherm graph of KN-AC for formaldehyde at 720 µg/m³.

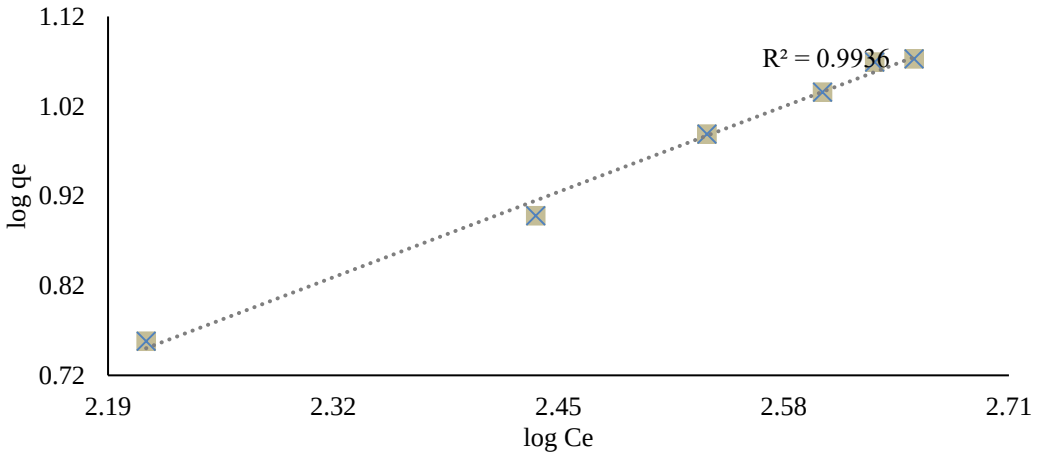

Figure 4.40. Freundlich isotherm graph of KN-AC for formaldehyde at 1040 µg/m³.

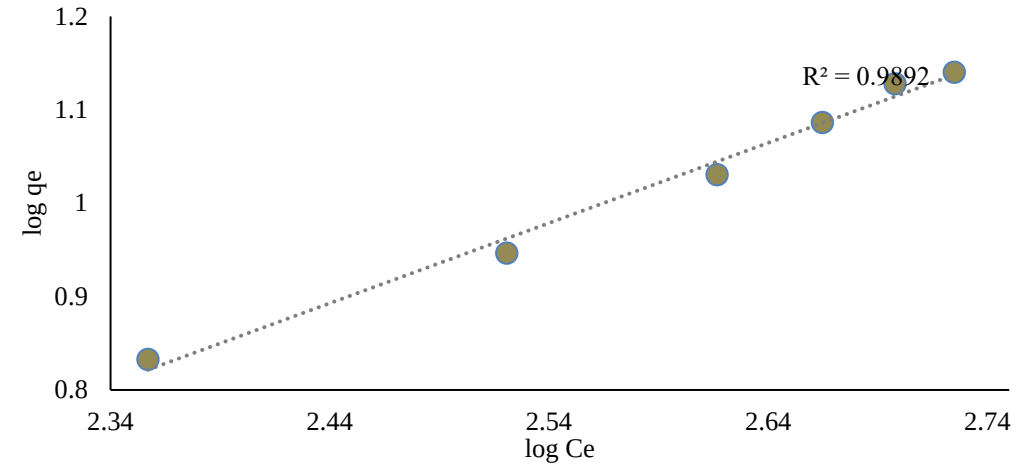

Figure 4.41. Freundlich isotherm graph of KN-AC for formaldehyde at 1220 µg/m³.

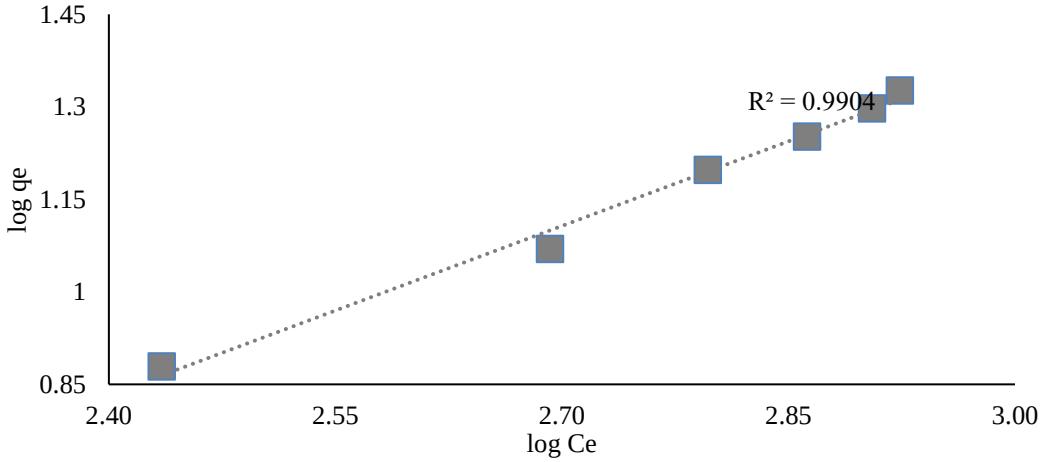

Figure 4.42. Freundlich isotherm graph of KN-AC for formaldehyde at 1900 µg/m³.

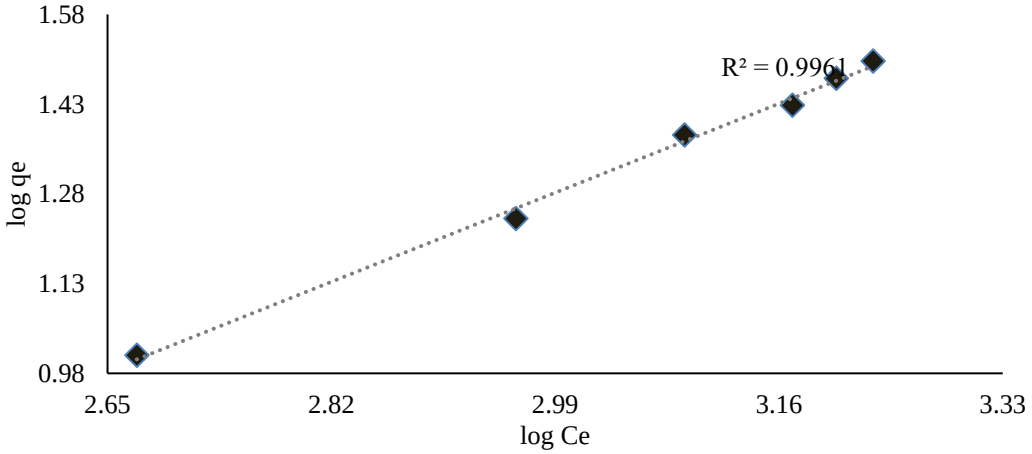

Figure 4.43. Freundlich isotherm graph of KN-AC for formaldehyde at 3290 µg/m³.

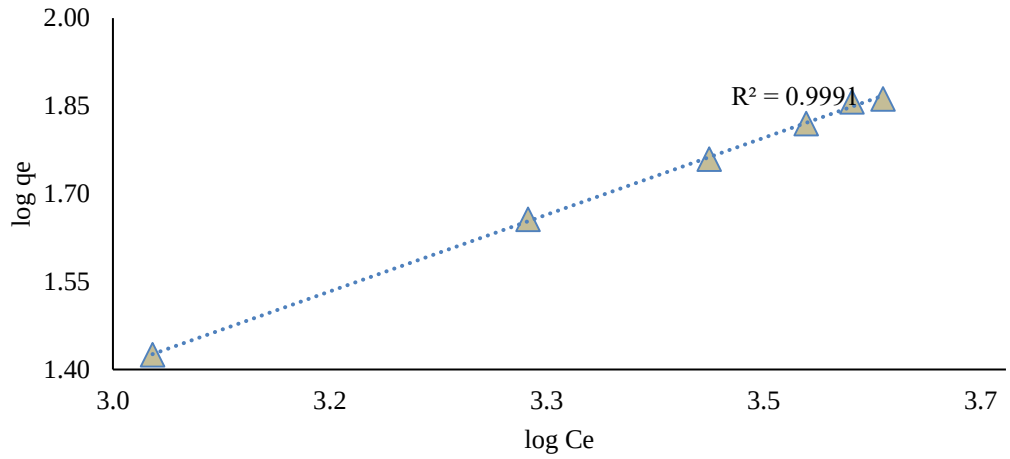

Figure 4.44. Freundlich isotherm graph of KN-AC for formaldehyde at 7650 µg/m³.

The linearized graphs of the data acquired from low concentration formaldehyde removal studies with the KN-AC were givenin between Figure 4.37 and Figure 4.44. These low concentrations as a linearized were expensed on the same graph, which was suitable for the distribution from 170±14.92 µg/m^3 to 7650±111.18 µg/m^3 in Figure 5.45.

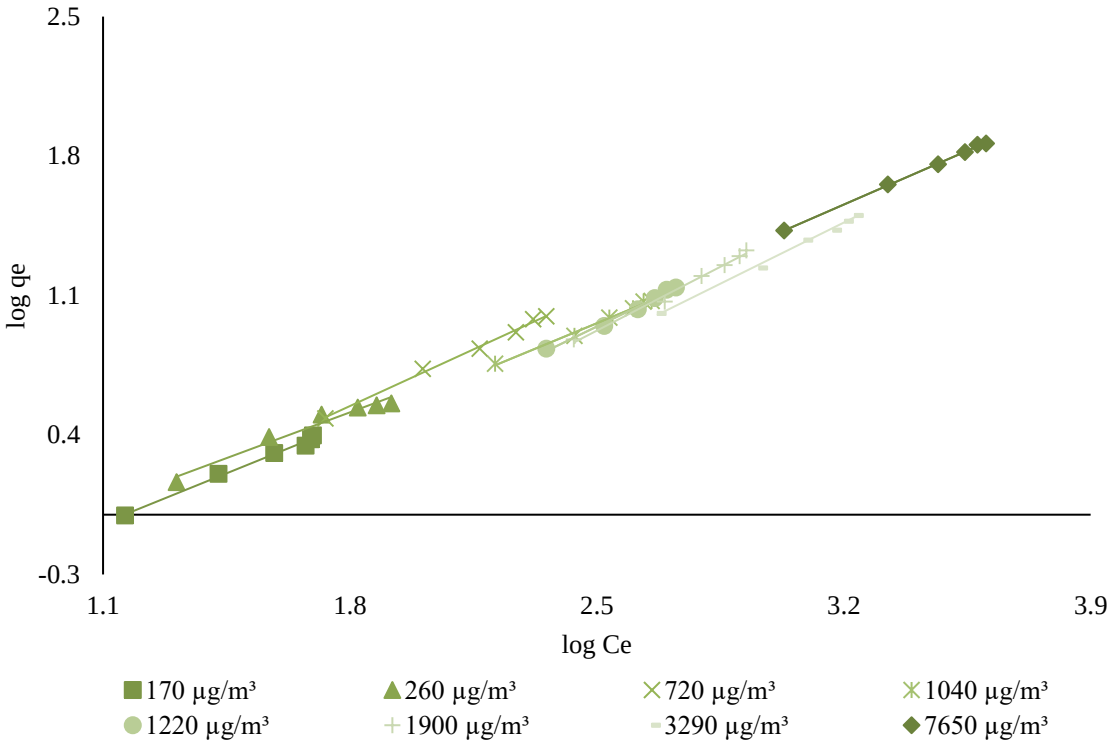

Figure 4.45. Freundlich isotherm graph for KN-AC for all low formaldehyde concentrations.

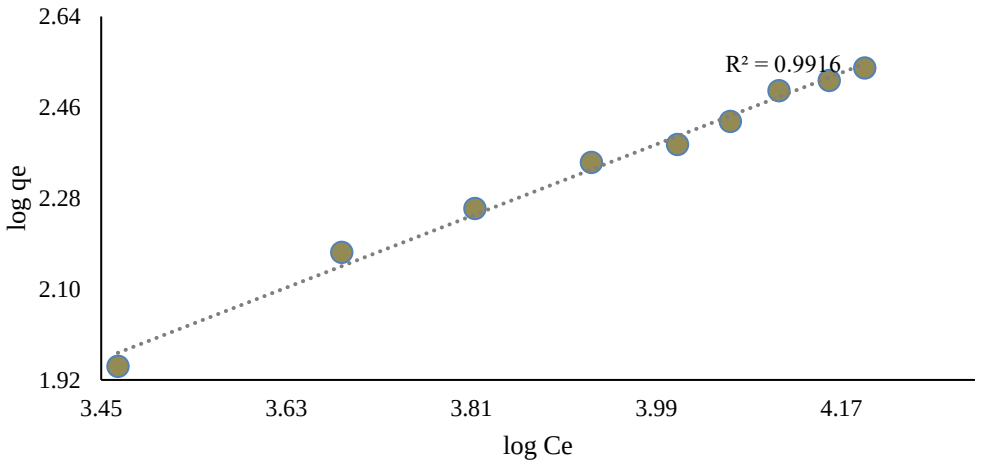

Figure 4.46. Freundlich isotherm graph of KN-AC for formaldehyde at 30,000 µg/m³.

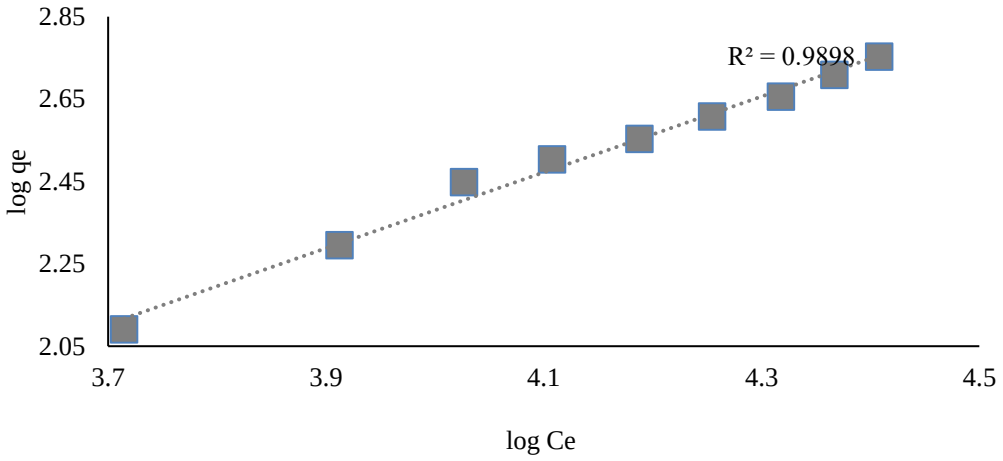

Figure 4.47. Freundlich isotherm graph of KN-AC for formaldehyde at 50,000 µg/m³.

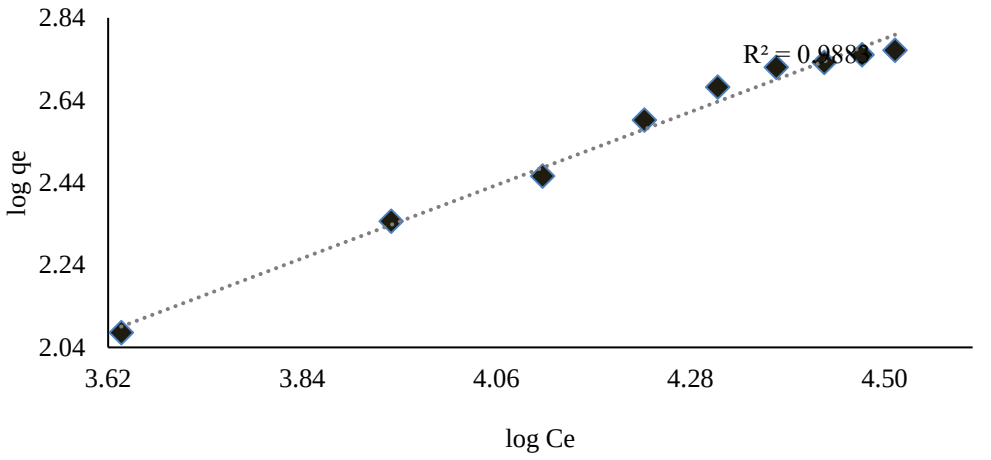

Figure 4.48. Freundlich isotherm graph of KN-AC for formaldehyde at 60,000 µg/m³.

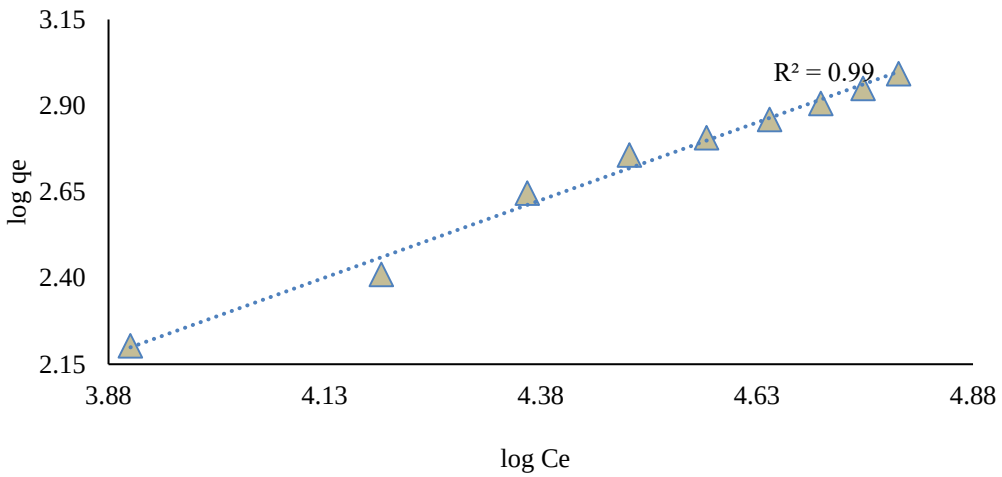

Figure 4.49. Freundlich isotherm graph of KN-AC for formaldehyde at 110,000 µg/m³.

After isotherm studies with COM-AC, studies with KN-AC in Freundlich isotherm as a linearized is given in a single graphic, which was found to be suitable the distribution at different concentrations from 30,000 µg/m³ to 110,000 µg/m^3 in Figure 4.50.

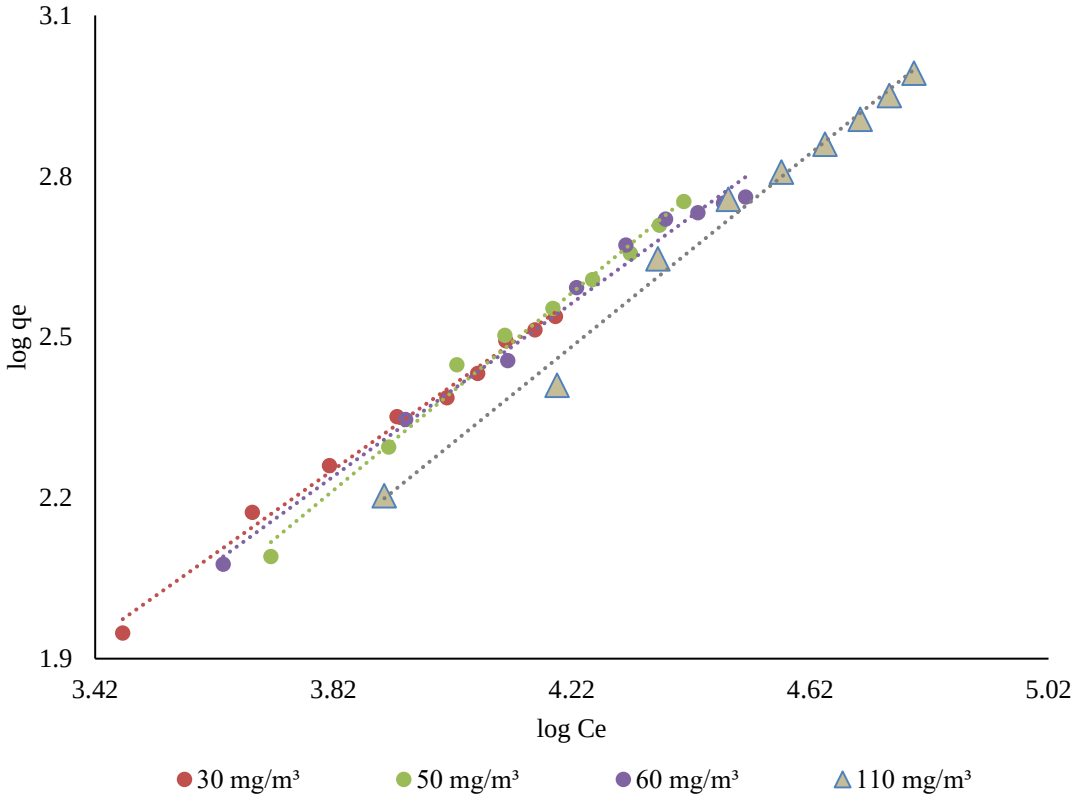

Figure 4.50. Freundlich isotherm graph of KN-AC of all high formaldehyde concentrations.

Freundlich parameters of the COM-AC is given in Table 4.7. The data obtained as a result of the studies conducted according to the particular concentration. The investigations were first started with 170±14.92 μg/m³, which is the commonly measured quantity in IAQ, and ended with 110,000±497.21 μg/m³, a very high concentration of formaldehyde. According to R^2, values was investigated in all concentrations in Table 4.7.

Table 4.7. Parameters of Freundlich isotherm for formaldehyde of COM-AC.

Average±SD of C_0 (μg/m³)	K_F	n	R^2	q_{max} (μg/g)
170±14.92	0.08	1.50	0.9919	0.04
260±23.76	0.04	1.18	0.9917	0.03
720±47.61	0.03	1.11	0.9515	0.02
1040±68.47	0.04	1.18	0.9893	0.02
1220±72.14	0.02	1.04	0.9909	0.02
1900±83.37	0.02	1.01	0.9802	0.02
3290±95.44	0.05	1.15	0.9961	0.03
7650±111.18	0.07	1.29	0.9973	0.07
30,000±207.44	0.04	1.51	0.9665	0.36
50,000±338.61	0.08	1.25	0.9587	0.08
60,000±376.89	0.12	1.23	0.9837	0.11
110,000±497.21	0.04	1.13	0.9780	0.04

Although the highest value is obtained at 7650±111.18 μg/m³ with 0.9973, the smallest amount is the concentration value of 720±47.61 μg/m³ with 0.9515. It is concluded that formaldehyde removal studies with COM-AC were suitable because it is more significant than one according to n value, which is an essential indicator of Freundlich parameter.

Freundlich parameters of the KN-AC show that the studies conducted according to the significant concentration obtained the data. The investigations were first started with 170±14.92 µg/m³, which is the commonly measured quantity in IAQ, and ended with 110,000 µg/m³, which is a very high concentration of formaldehyde in Table 4.8.

Table 4.8. Parameters of Freundlich isotherm for formaldehyde of KN-AC.

Average±SD of C_0 (µg/m³)	K_F	n	R^2	q_{max} (µg/g)
170±14.92	0.15	1.40	0.9918	0.09
260±23.76	0.22	1.53	0.9620	0.09
720±47.61	0.13	1.24	0.9955	0.07
1040±68.47	0.14	1.37	0.9936	0.05
1220±72.14	0.07	1.17	0.9892	0.04
1900±83.37	0.05	1.10	0.9904	0.03
3290±95.44	0.05	1.15	0.9961	0.03
7650±111.18	0.12	1.30	0.9991	0.12
30,000±207.44	0.18	1.27	0.9916	0.18
50,000±338.61	0.05	1.09	0.9898	0.05
60,000±376.89	0.15	1.24	0.9883	0.15
110,000±497.21	0.05	1.12	0.9900	0.05

According to R^2, values was observed in all concentrations. Although the highest value is obtained at 7650 µg/m³ with 0.9991, the smallest amount is the concentration value of 260 µg/m³ with 0.9620. It is concluded that formaldehyde removal studies with KN-AC were suitable because it is more significant than one according to n value, which is an essential indicator of the Freundlich parameter. The highest R^2 value was obtained in 7650±111.18 µg/m³ as standard value in Table 4.7 and Table 4.8.

4.2.1.2. Langmuir Isotherm Modelling of Formaldehyde

Langmuir isotherm model for formaldehyde, COM-AC and KN-AC was made and its suitability was examined. For this purpose, Langmuir isotherm model Eq. (2) is drawn using the CH_2O of the COM-AC and KN-AC isotherm lines of these adsorbents were givenin between Figure 4.51 and Figure 4.78.

The isotherm constants such as a line which this slope of the graph is $1/n$ were determined from the slope and shear values of the lines obtained from the graph in these Figures, and the results were presented in Table 4.2 with the R^2. According to Langmuir Isotherm, if separation factor (R_L) value >1: it indicates that the adsorption process is unfavorable, if R_L value is $0 < R_L < 1$: it is favorable, if $R_L = 0$: process is irreversible and finally if $R_L = 1$, it is linear R_L value being obtained lower than 1 proposed that formaldehyde adsorption process onto KN-AC surface was a favorable and R_L values gained closer to zero value mean it was more appropriate for favorable formaldehyde adsorption in Eq. (3) [312].

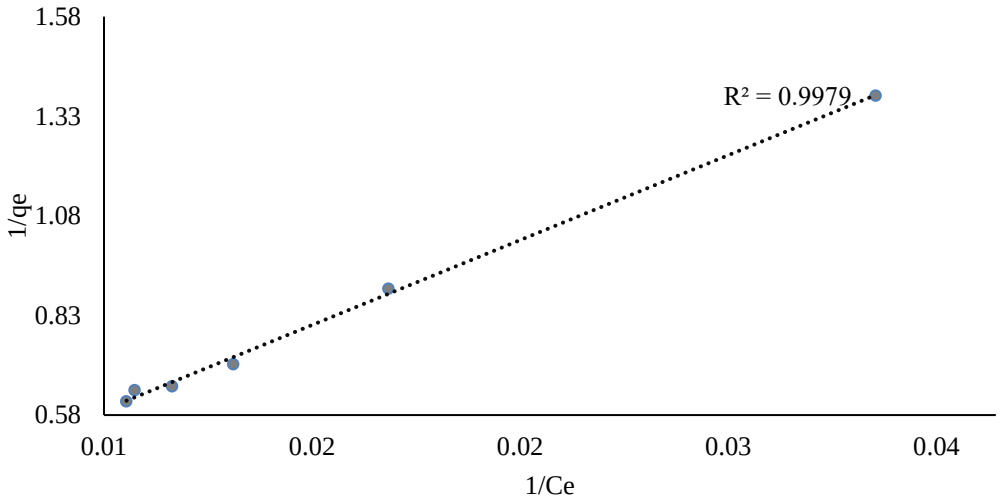

Figure 4.51. Langmuir isotherm graph of COM-AC for formaldehyde at 170 µg/m³.

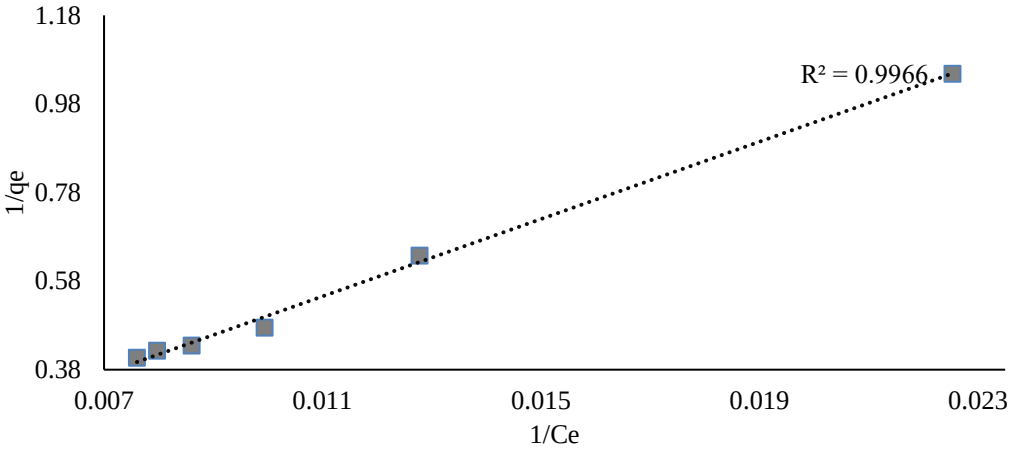

Figure 4.52. Langmuir isotherm graph of COM-AC for formaldehyde at 260 µg/m³.

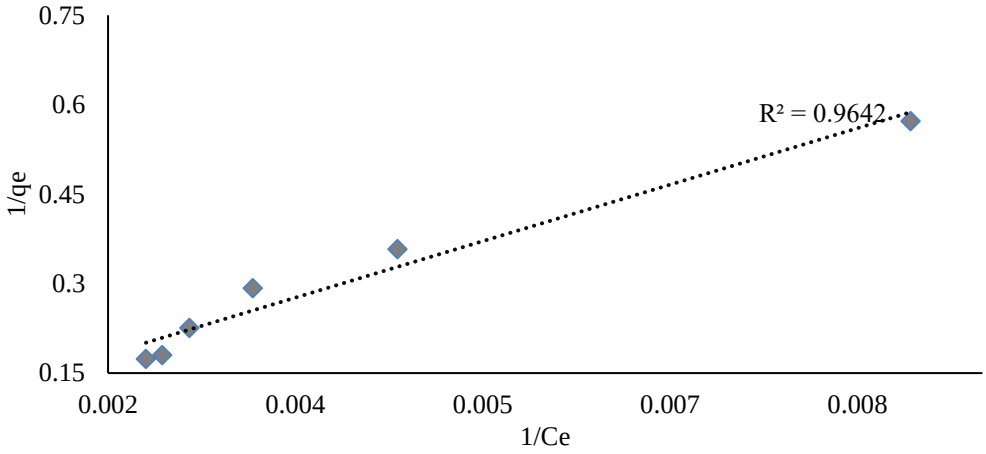

Figure 4.53. Langmuir isotherm graph of COM-AC for formaldehyde at 720 µg/m³.

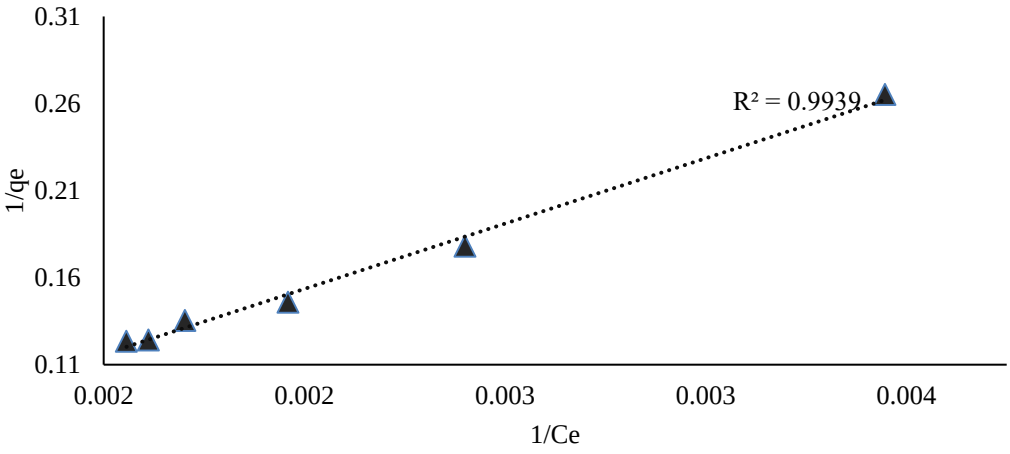

Figure 4.54. Langmuir isotherm graph of COM-AC for formaldehyde at 1040 µg/m³.

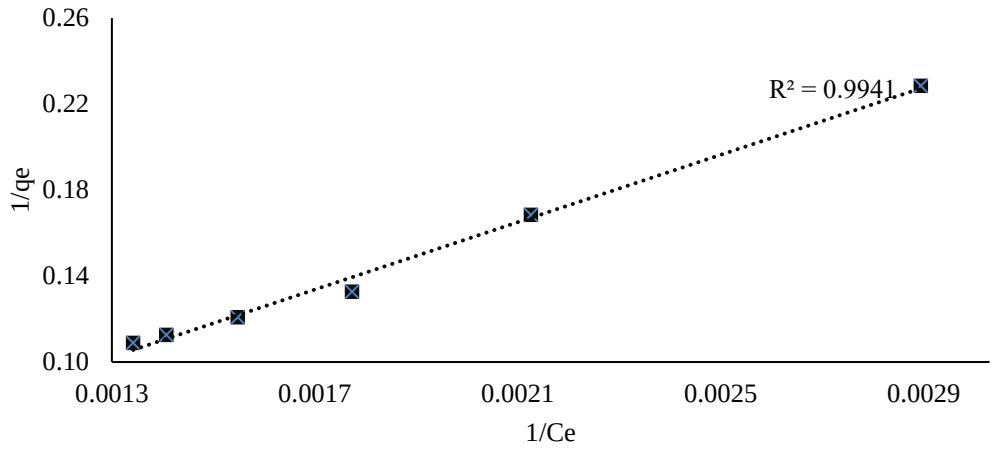

Figure 4.55. Langmuir isotherm graph of COM-AC for formaldehyde at 1220 µg/m³.

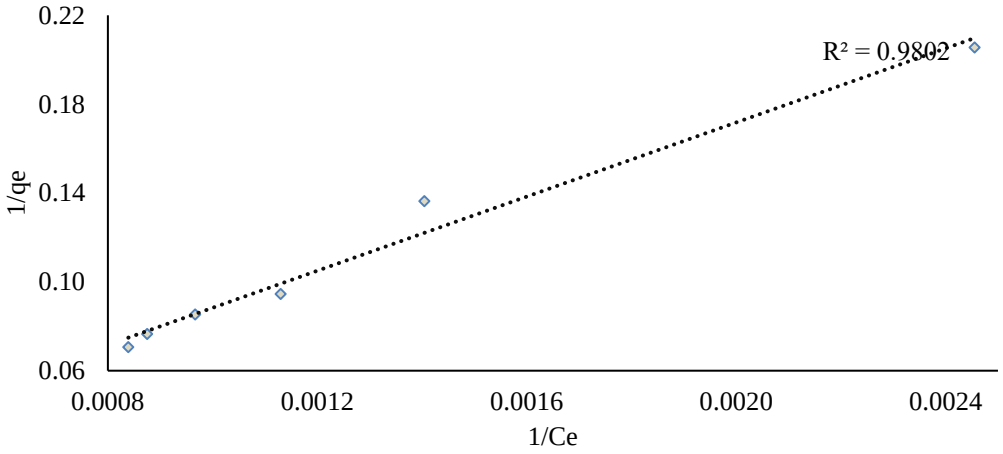

Figure 4.56. Langmuir isotherm graph of COM-AC for formaldehyde at 1900 µg/m³.

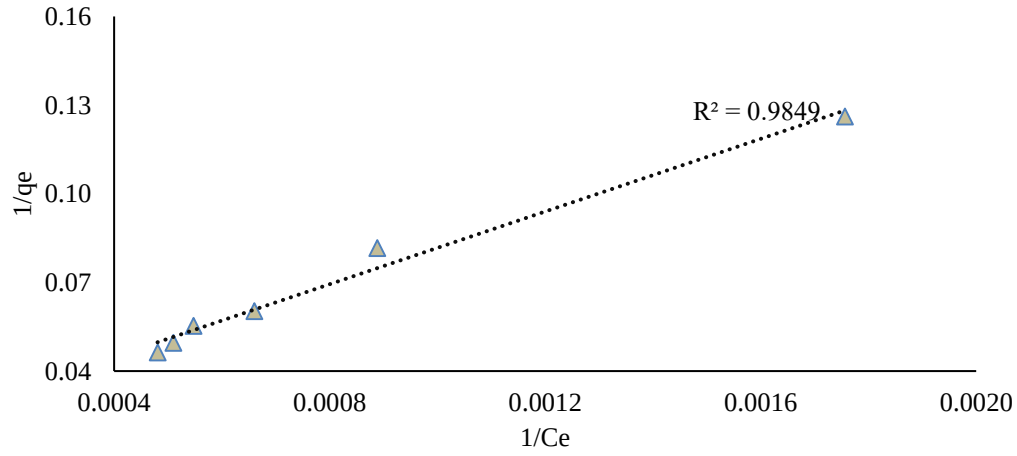

Figure 4.57. Langmuir isotherm graph of COM-AC for formaldehyde at 3290 µg/m³.

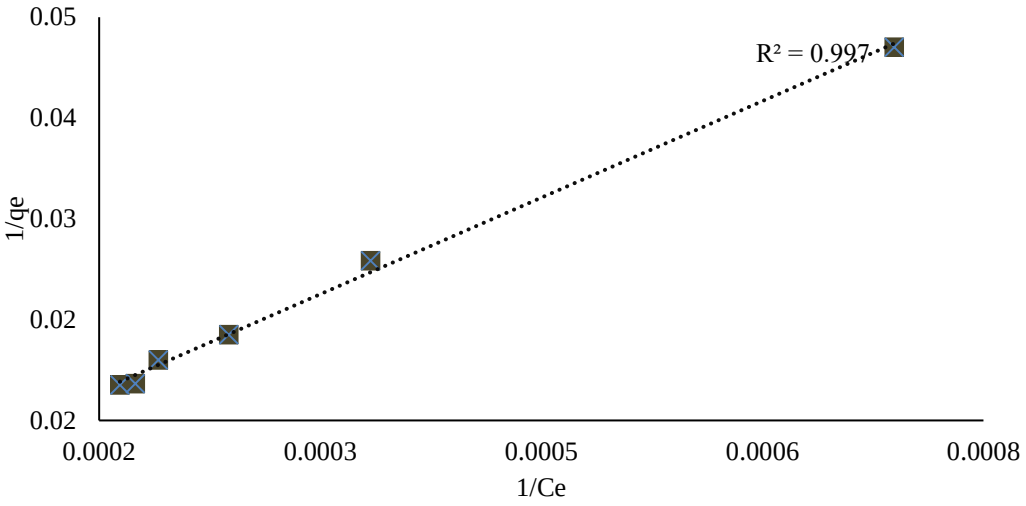

Figure 4.58. Langmuir isotherm graph of COM-AC for formaldehyde at 7650 µg/m³.

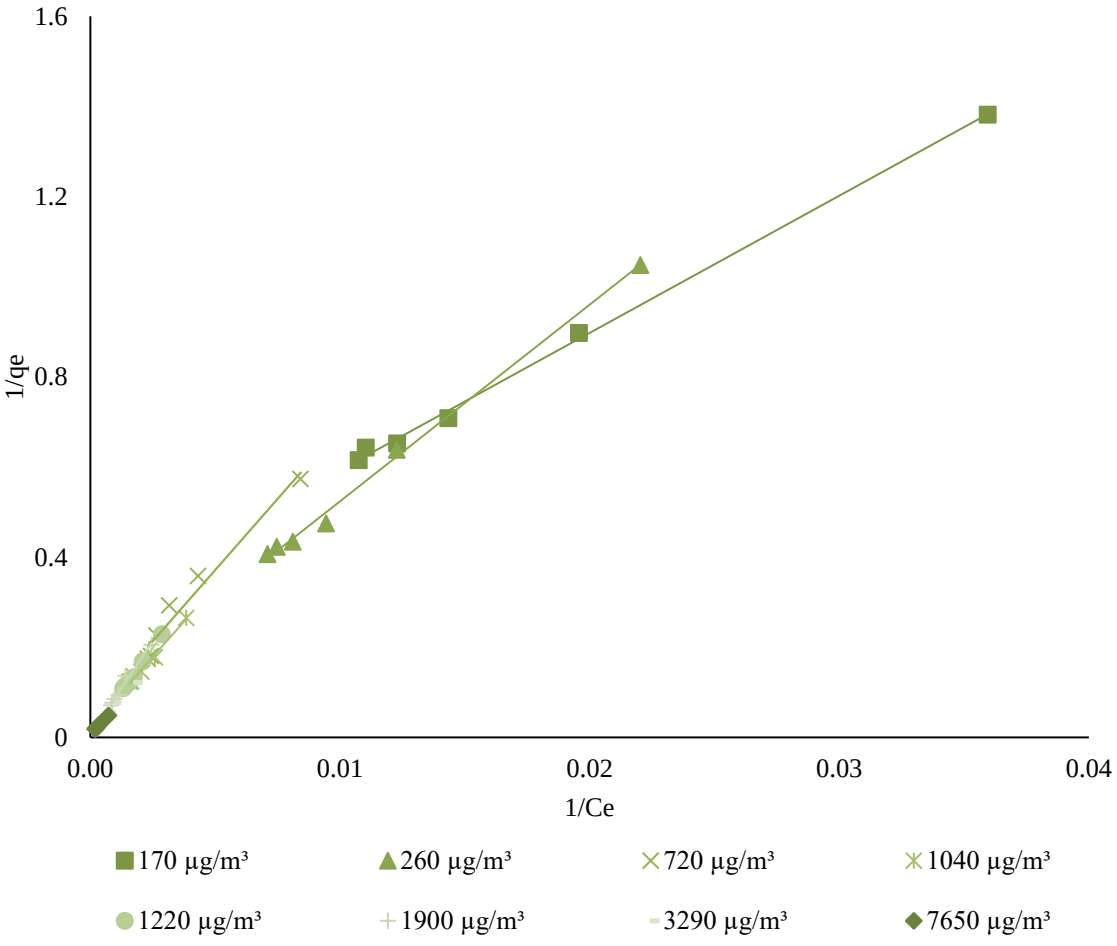

Figure 4.59. Langmuir isotherm graph for COM-AC for all low formaldehyde concentrations.

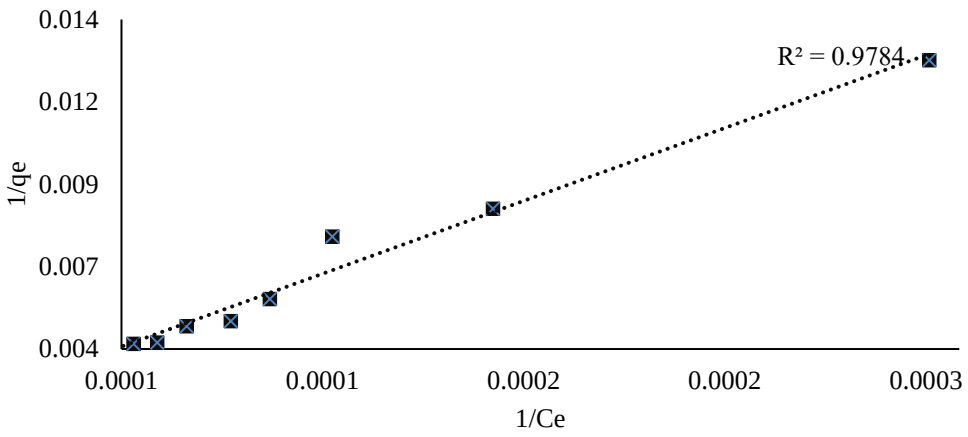

Figure 4.60. Langmuir isotherm graph of COM-AC for formaldehyde at 30,000 µg/m³.

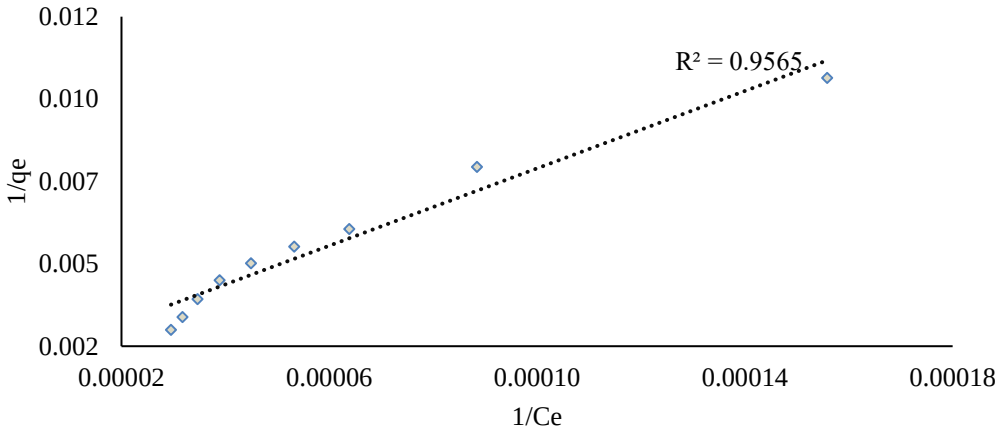

Figure 4.61. Langmuir isotherm graph of COM-AC for formaldehyde at 50,000 µg/m³.

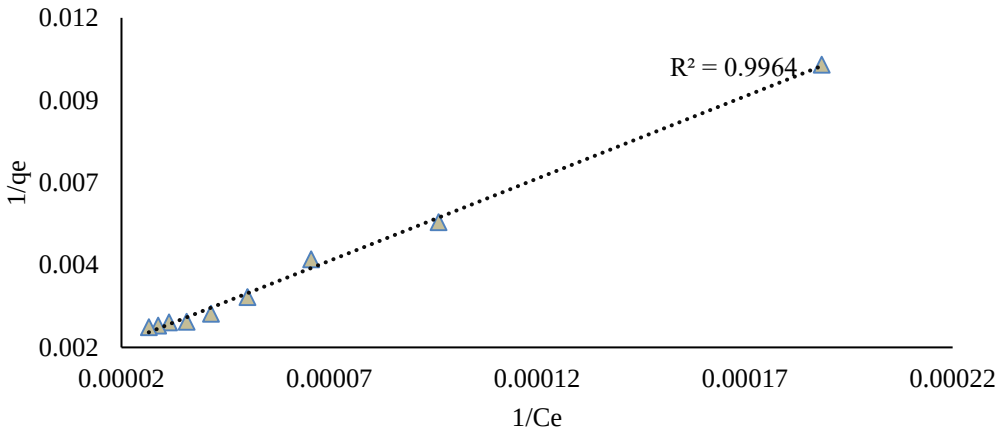

Figure 4.62. Langmuir isotherm graph of COM-AC for formaldehyde at 60,000 µg/m³.

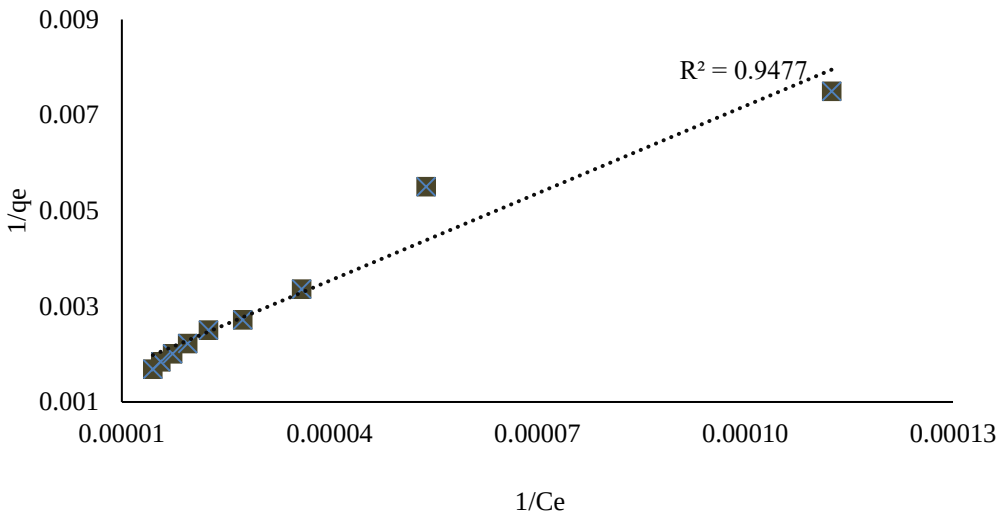

Figure 4.63. Langmuir isotherm graph of COM-AC for formaldehyde at 110,000 µg/m³.

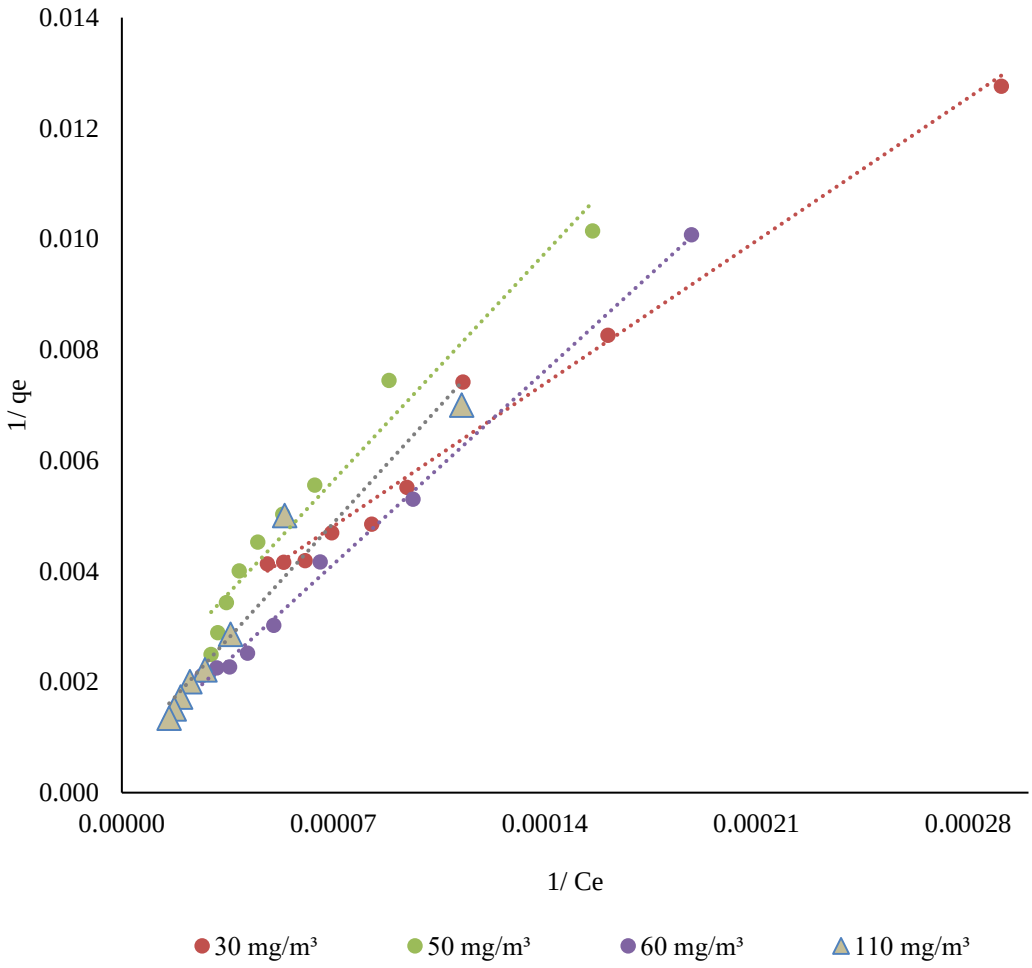

Figure 4.64. Langmuir isotherm graph of COM-AC of all high formaldehyde concentrations.

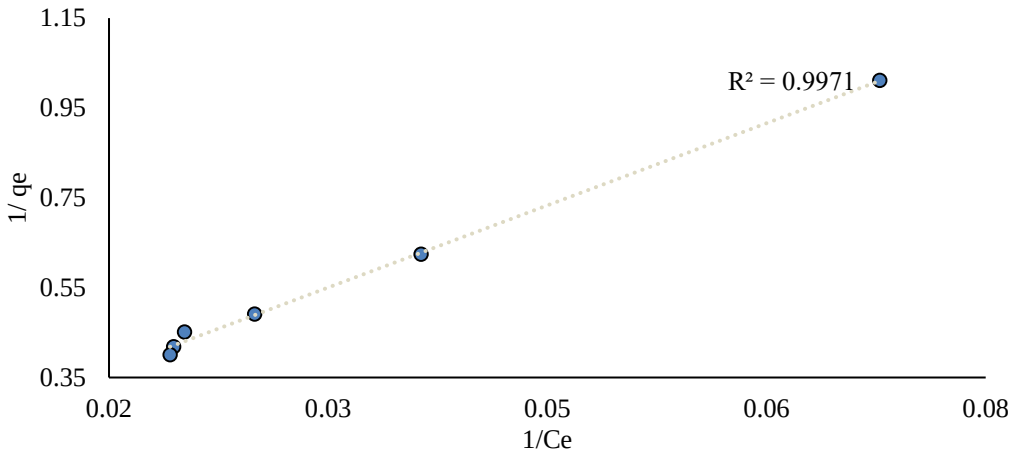

Figure 4.65. Langmuir isotherm graph of KN-AC for formaldehyde at 170 µg/m³.

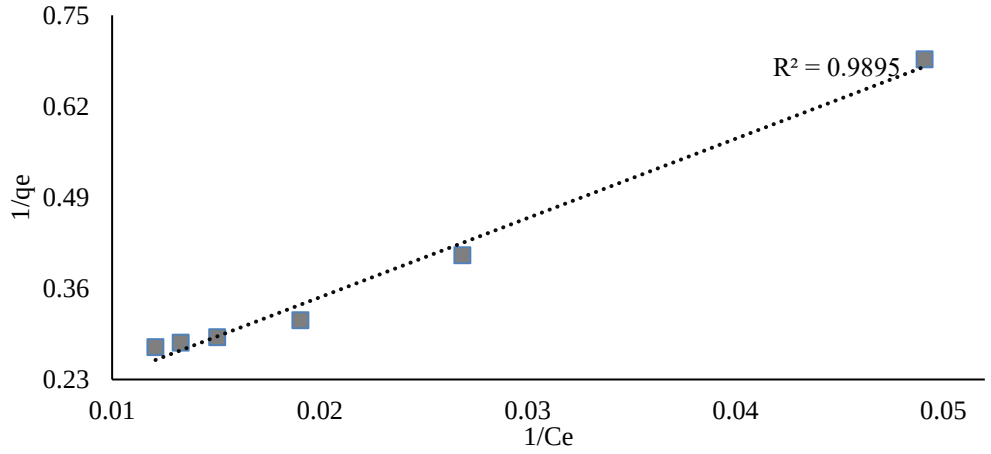

Figure 4.66. Langmuir isotherm graph of KN-AC for formaldehyde at 260 µg/m³.

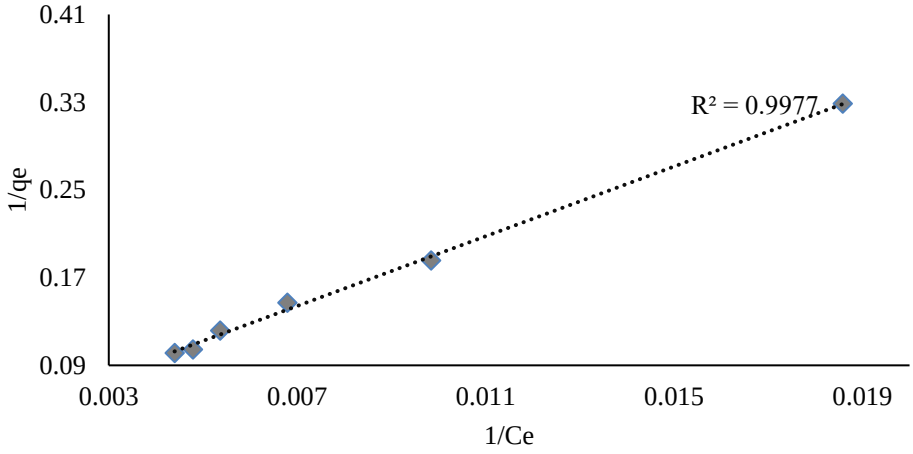

Figure 4.67. Langmuir isotherm graph of KN-AC for formaldehyde at 720 µg/m³.

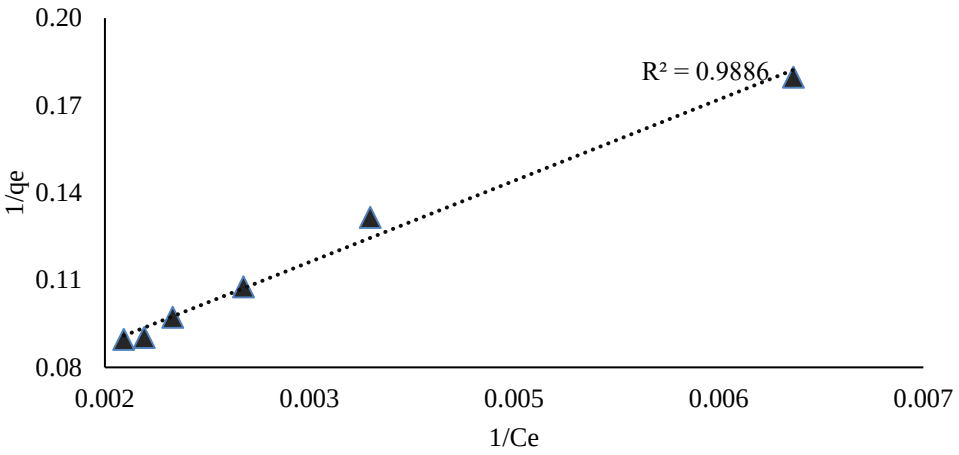

Figure 4.68. Langmuir isotherm graph of KN-AC for formaldehyde at 1040 µg/m³.

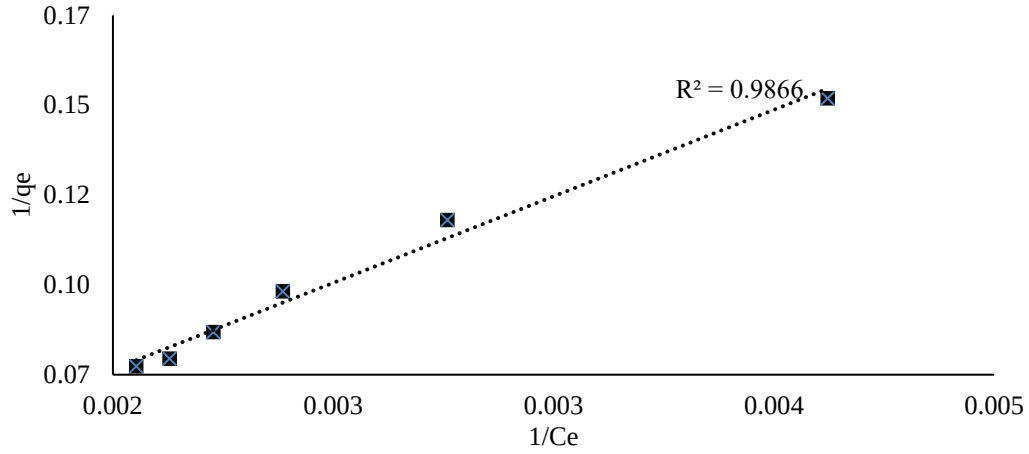

Figure 4.69. Langmuir isotherm graph of KN-AC for formaldehyde at 1220 µg/m³.

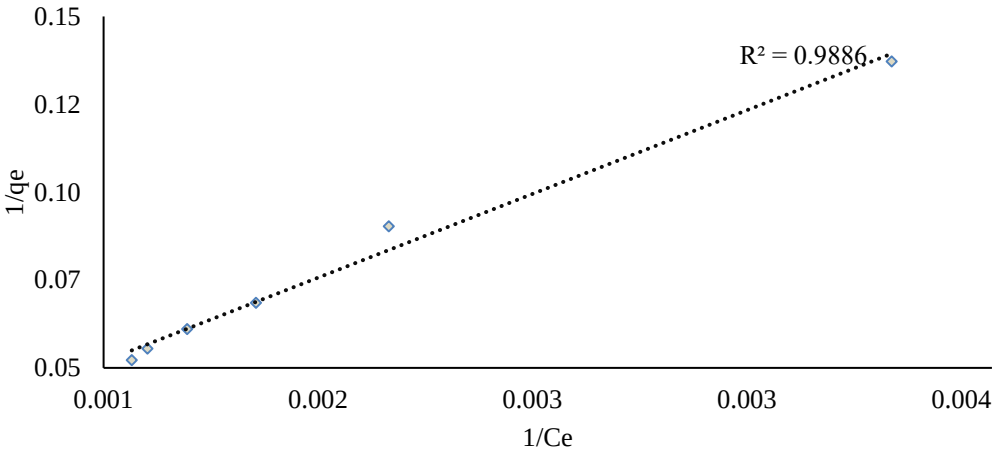

Figure 4.70. Langmuir isotherm graph of KN-AC for formaldehyde at 1900 µg/m³.

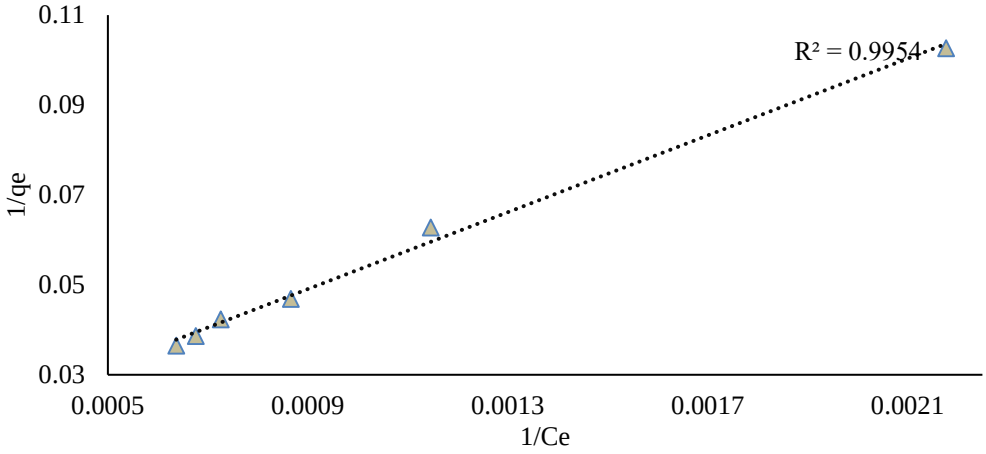

Figure 4.71. Langmuir isotherm graph of KN-AC for formaldehyde at 3290 µg/m³.

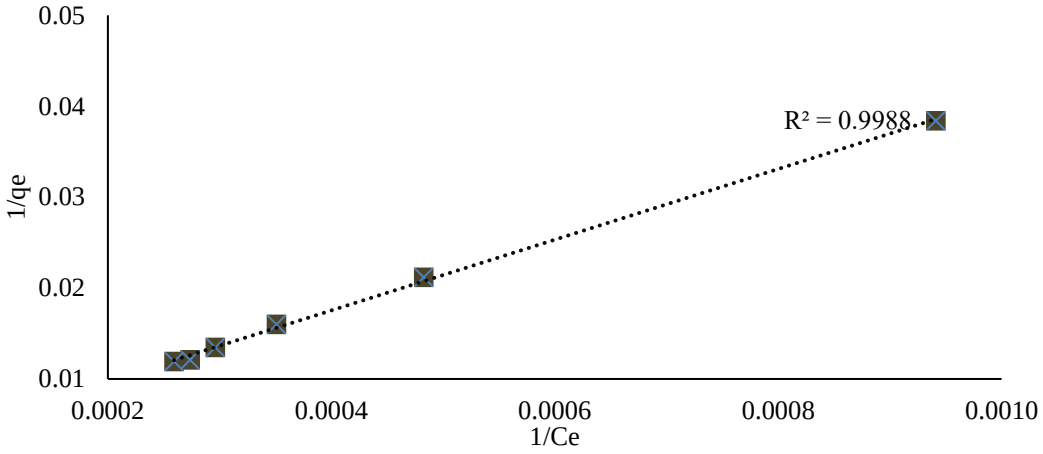

Figure 4.72. Langmuir isotherm graph of KN-AC for formaldehyde at 7650 µg/m³.

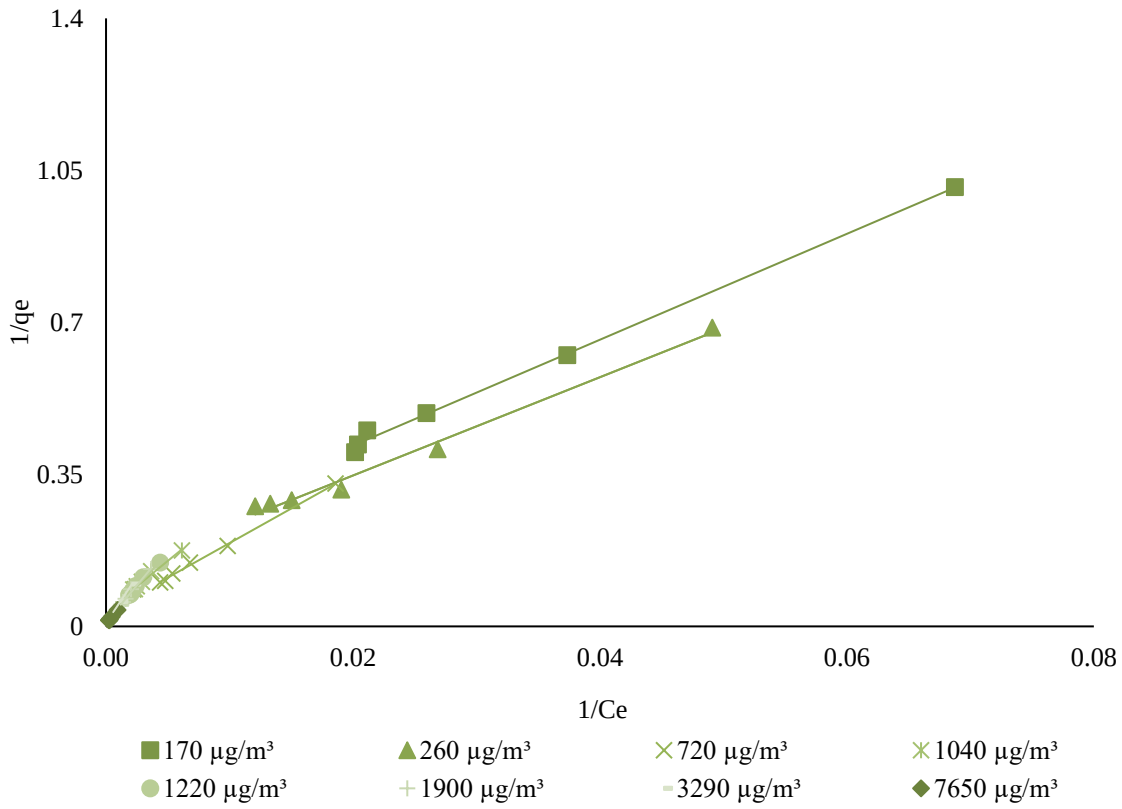

Figure 4.73. Langmuir isotherm graph of KN-AC of all low concentrations of formaldehyde.

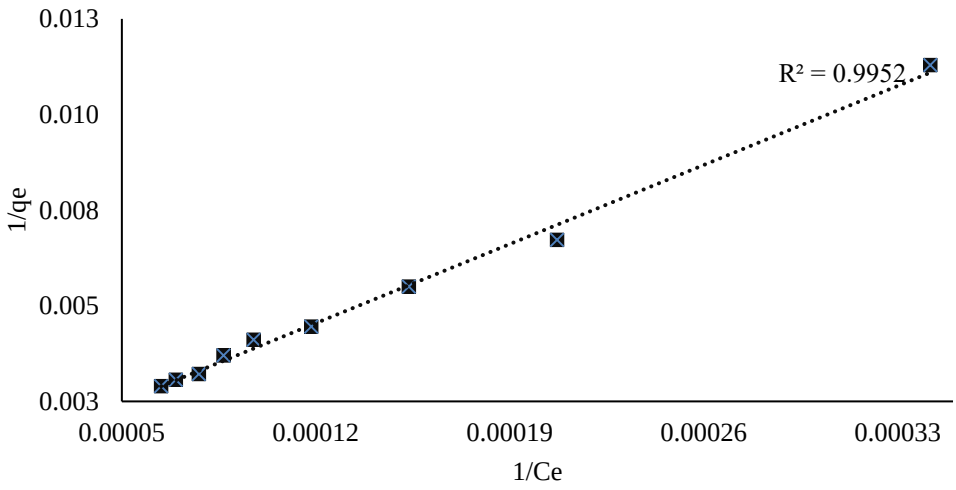

Figure 4.74. Langmuir isotherm graph of KN-AC for formaldehyde at 30,000 µg/m³.

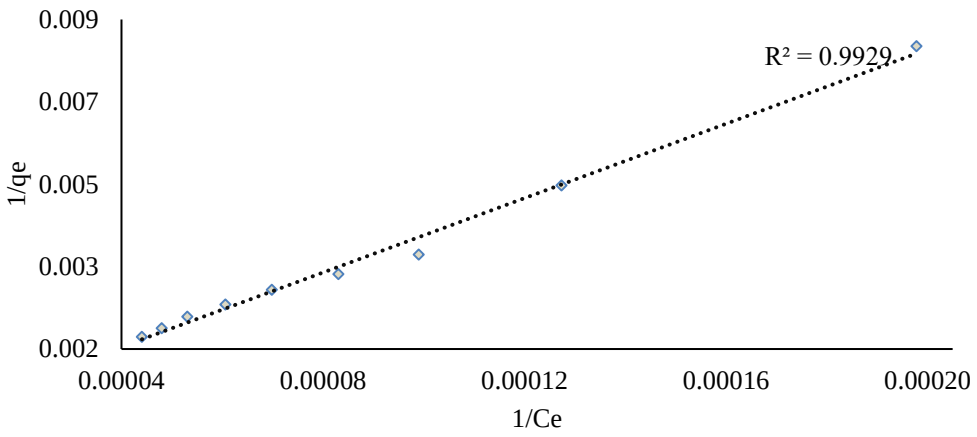

Figure 4.75. Langmuir isotherm graph of KN-AC for formaldehyde at 50,000 µg/m³.

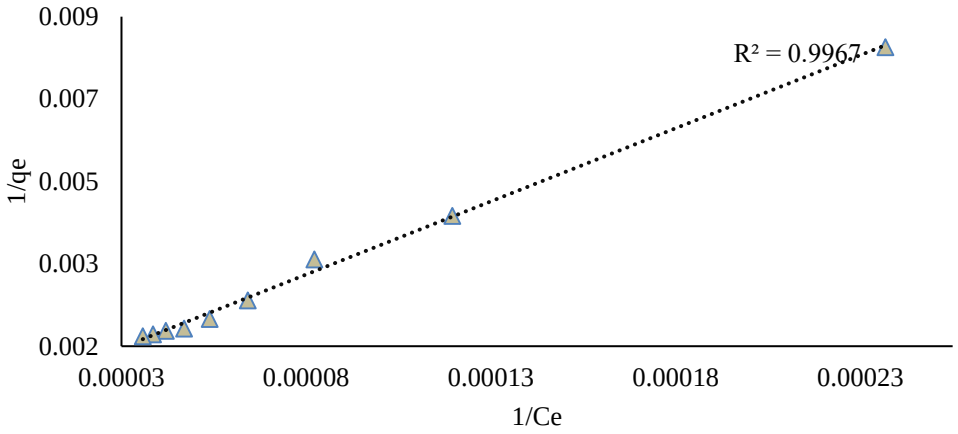

Figure 4.76. Langmuir isotherm graph of KN-AC for formaldehyde at 60,000 µg/m³.

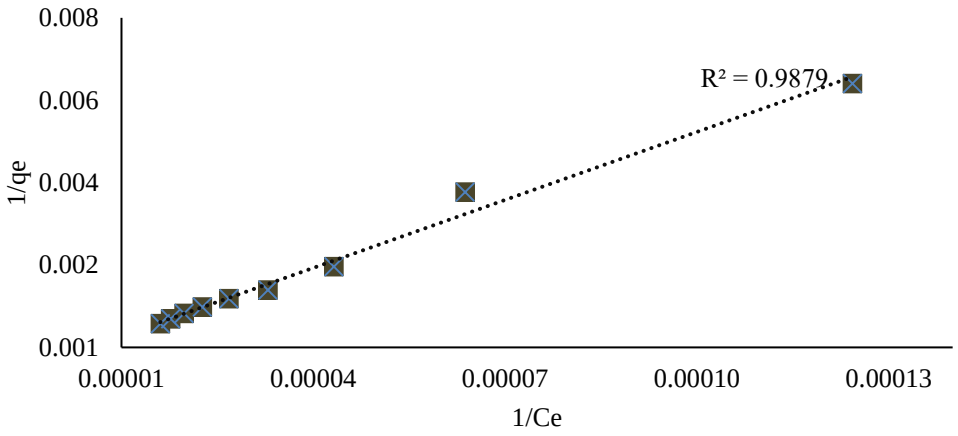

Figure 4.77. Langmuir isotherm graph of KN-AC for formaldehyde at 110,000 µg/m³.

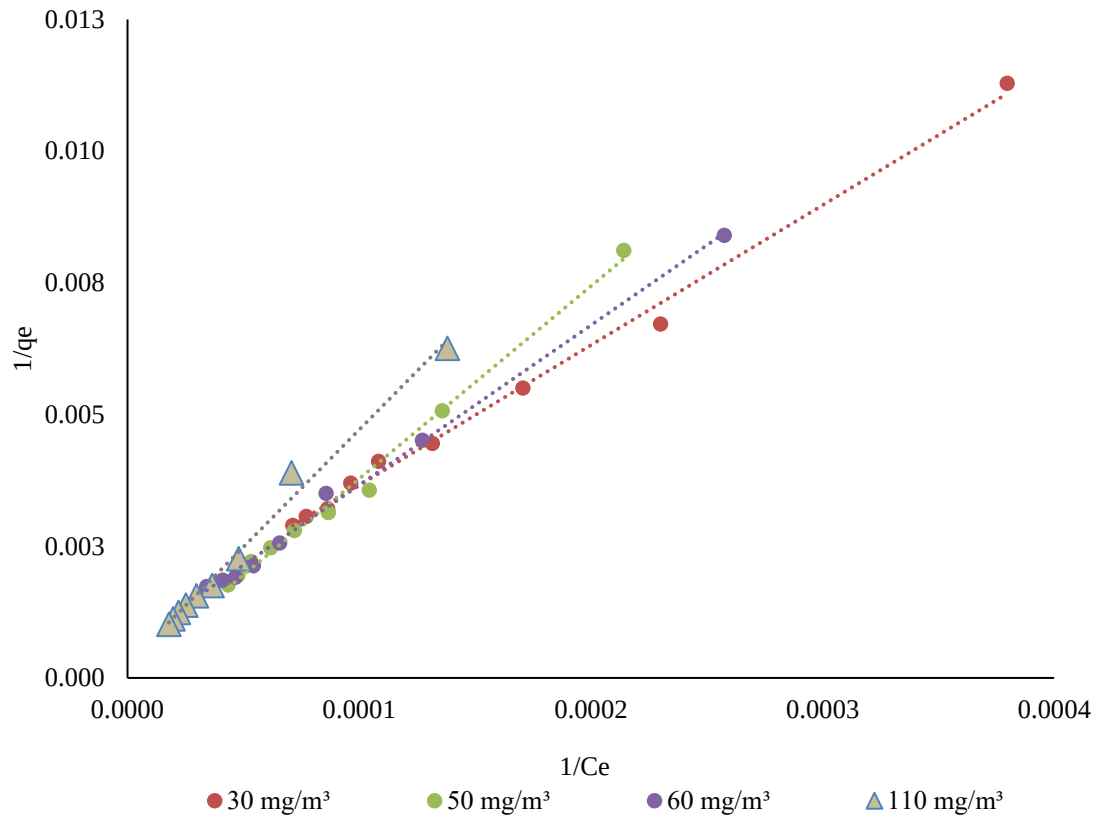

Figure 4.78. Langmuir isotherm graph of KN-AC of all high concentrations of formaldehyde.

When the R^2 (Correlation Coefficient) values were considered, it was found that Langmuir isotherm is more compatible at low concentration values and Freundlich isotherm is more compatible at high concentration on values for both KN-AC and COM-AC. However, the Correlation Coefficients ($R^2 \approx 0.95$ to 0.99) were fairly close together. On the other hand, If the parameter n is greater than 1 (n>1), it indicates that the values were following the Freundlich isotherm [108].

According to Table 4.9 and Table 4.10, Langmuir parameters were giventhat considered to be greater than R^2 value 0.9477 and it means that the adsorption process is suitable for the monolayer adsorption principle. Simultaneously, when the q_{max} value is observed, the COM-AC's q_{max} value is as low as KN-AC. Both of COM-AC adsorbent was found to be suitable for formaldehyde removal in the Langmuir study.

Langmuir parameters of the COM-AC were givenin Table 4.9. The data obtained as a result of the studies conducted according to the particular concentration. The investigations were first started with 170±14.92 μg/m³, which is the commonly measured quantity in IAQ, and ended with 110,000±497.21 μg/m³, a very high concentration of formaldehyde in Table 4.9.

Table 4.9. Parameters of Langmuir isotherm for formaldehyde of COM-AC.

Average±SD of C_0 (μg/m³)	K_L (L/μg)	R^2	q_{max} (μg/g)
170±14.92	105.46	0.9979	32.85
260±23.76	498.77	0.9966	22.92
720±47.61	1137.80	0.9642	15.84
1040±68.47	2816.97	0.9939	15.99
1220±72.14	27700.73	0.9941	12.76
1900±83.37	17191.59	0.9802	11.98
3290±95.44	4048.63	0.9849	16.26
7650±111.18	8544.00	0.9970	17.40
30,000±207.44	16507.73	0.9784	27.14
50,000±338.61	38385.54	0.9565	17.04
60,000±376.89	79127.55	0.9964	20.03
110,000±497.21	101620.31	0.9477	16.42

According to R^2, values was investigated in all concentrations. Although the highest value is obtained at 170±14.92 μg/m³ with R^2 value 0.9979, the smallest value is the concentration value of 110,000±497.21 μg/m³ with 0.9477.

The Langmuir parameters of the KN-AC were expensed in Table 4.10. The data were attained as a result of the studies conducted according to the unlike concentration. The investigations were first started with 170±14.92 μg/m³, which is the commonly measured quantity in IAQ, and ended with 110,000±497.21 μg/m³, a very high concentration of formaldehyde in Table 4.10.

Table 4.10. Parameters of Langmuir isotherm for formaldehyde of KN-AC.

Average±SD of C_0 (μg/m³)	K_L (L/μg)	R^2	q_{max} (μg/g)
170±14.92	70.69	0.9971	82.04
260±23.76	93.43	0.9895	88.38
720±47.61	485.60	0.9977	62.87
1040±68.47	675.78	0.9886	42.99
1220±72.14	1736.33	0.9866	33.24
1900±83.37	3617.11	0.9886	29.38
3290±95.44	5509.45	0.9954	23.41
7650±111.18	6822.36	0.9988	28.57
30,000±207.44	29533.50	0.9952	33.86
50,000±338.61	322418.91	0.9929	24.62
60,000±376.89	54007.98	0.9967	29.65
110,000±497.21	193869.74	0.9879	20.20

According to R^2, values was investigated in all concentrations. Although the highest value is obtained at 7650±111.18 μg/m³ with 0.9988, the smallest amount is the concentration value of 1220±72.14 μg/m³ with R^2 value 0.9866. It is concluded that formaldehyde removal studies with KN-AC were suitable at low concentrations.

4.2.1.3. Dubinin-Radushkevich Isotherm Modelling of Formaldehyde

Dubinin-Radushkevich was another isotherm by using well-known adsorption isotherm equations at various concentrations in the study. These graphs were plotted as a linear form between Figure 4.79 and Figure 4.102.

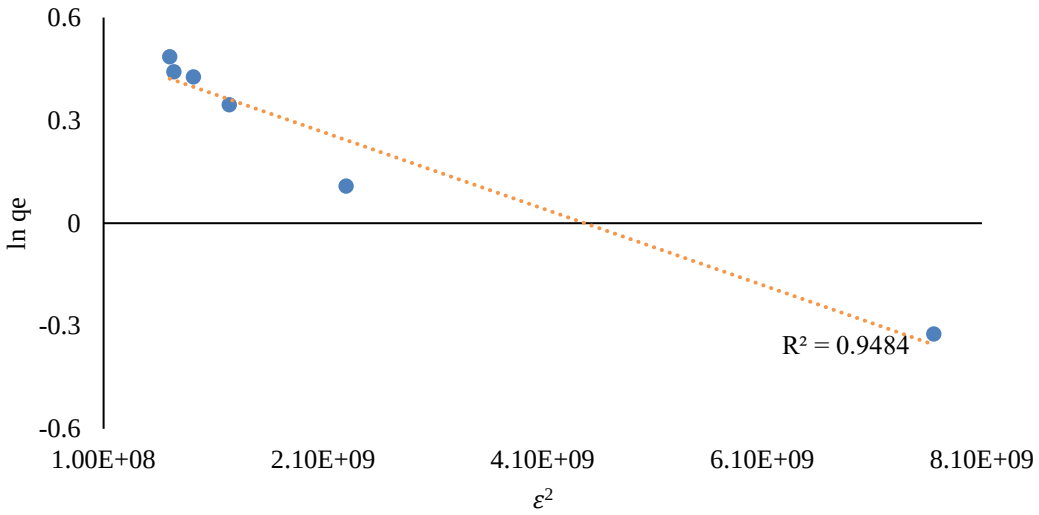

Figure 4.79. D-R isotherm graph of COM-AC for formaldehyde at 170 µg/m³.

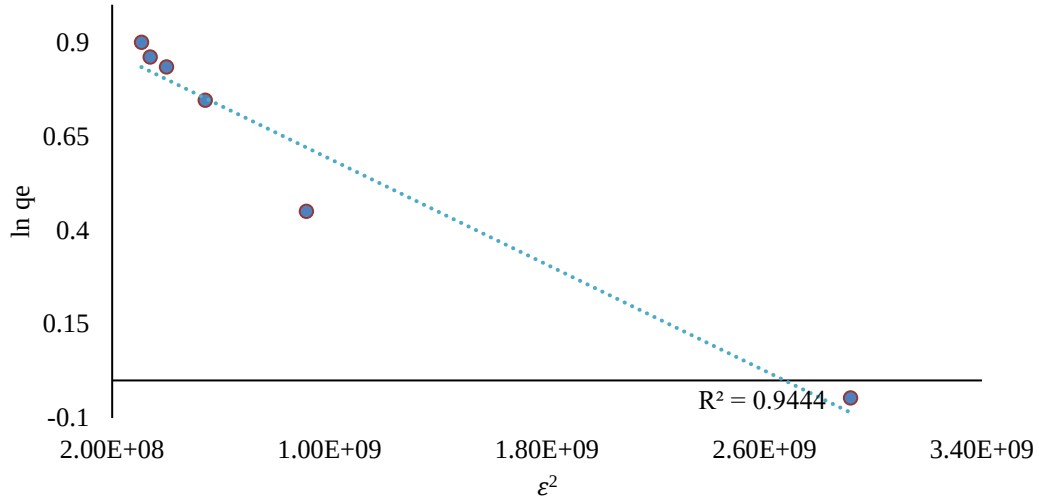

Figure 4.80. D-R isotherm graph of COM-AC for formaldehyde at 260 µg/m³.

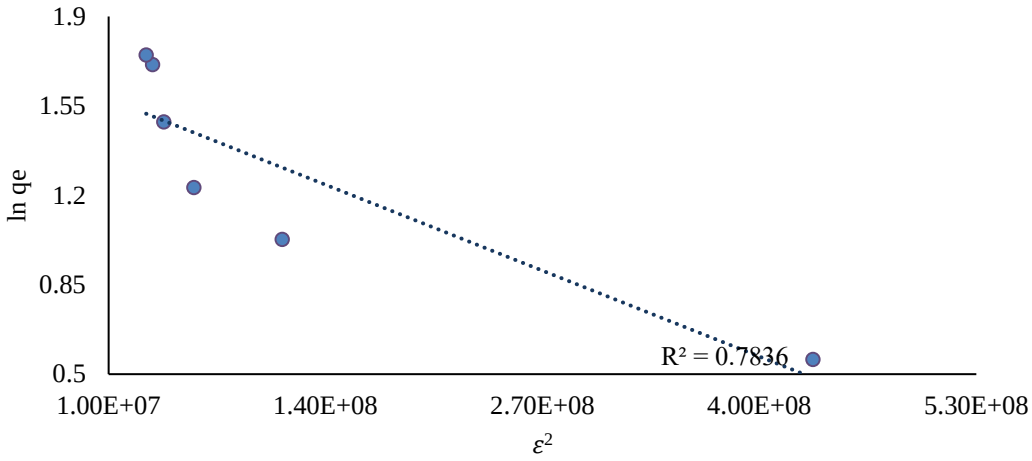

Figure 4.81. D-R isotherm graph of COM-AC for formaldehyde at 720 µg/m³.

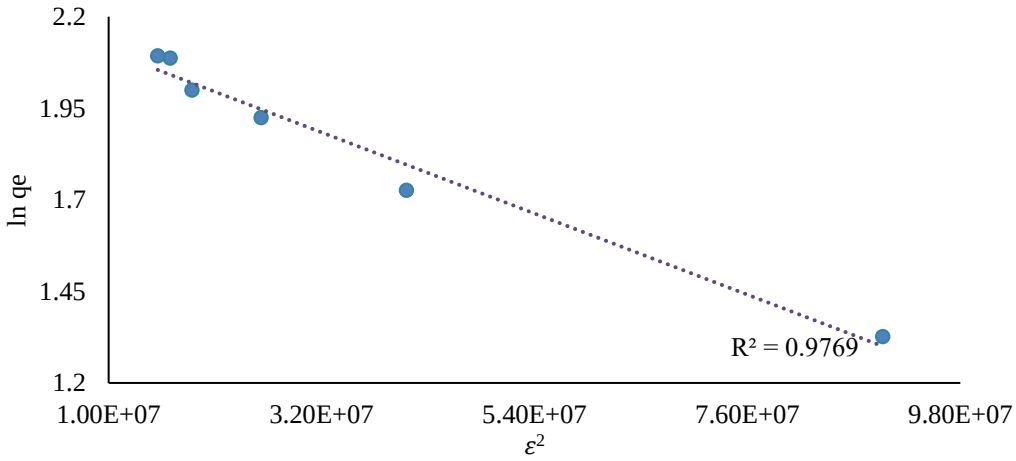

Figure 4.82. D-R isotherm graph of COM-AC for formaldehyde at 1040 µg/m³.

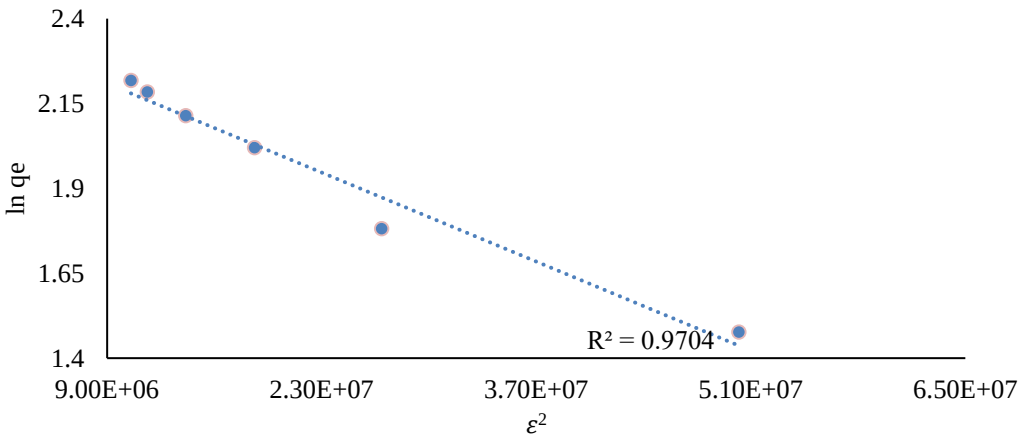

Figure 4.83. D-R isotherm graph of COM-AC for formaldehyde at 1220 µg/m³.

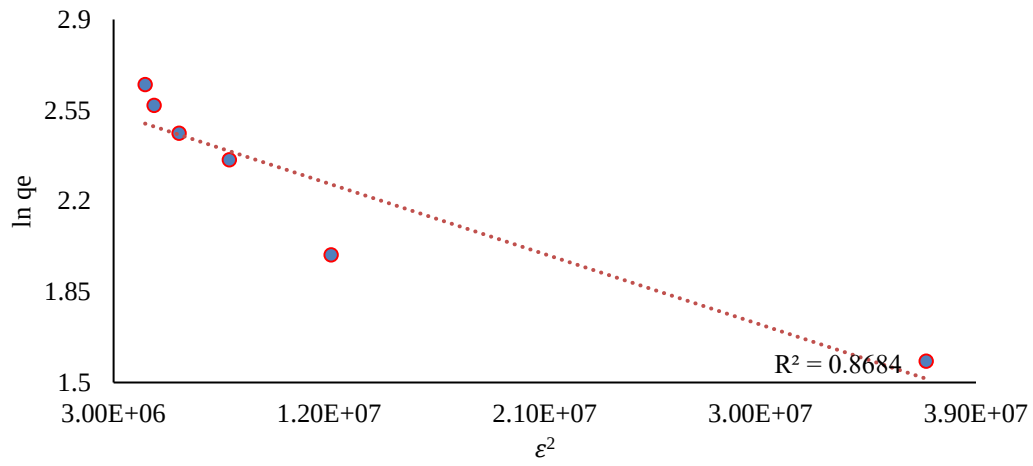

Figure 4.84. D-R isotherm graph of COM-AC for formaldehyde at 1900 µg/m³.

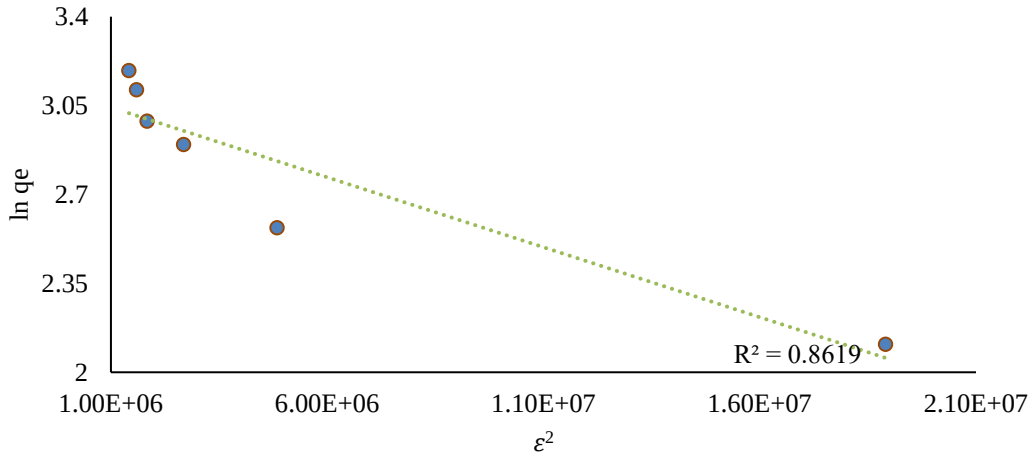

Figure 4.85. D-R isotherm graph of COM-AC for formaldehyde at 3290 µg/m³.

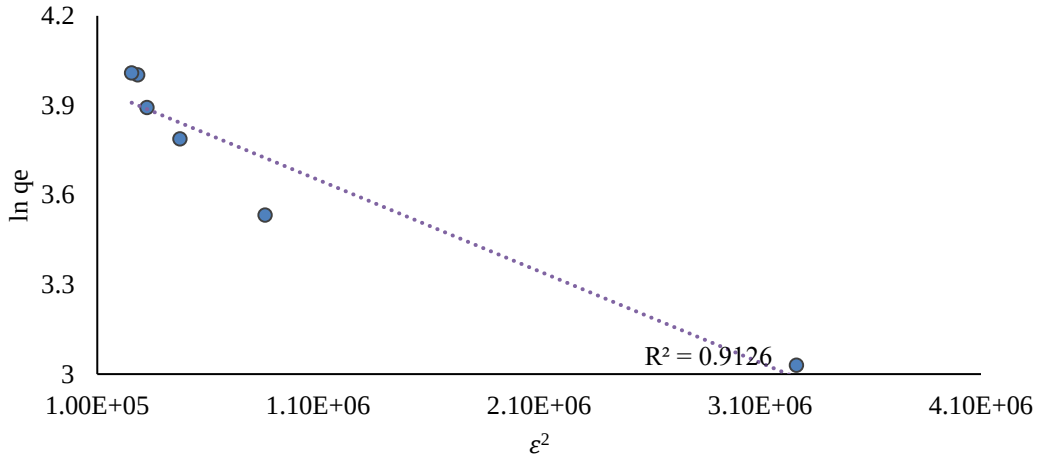

Figure 4.86. D-R isotherm graph of COM-AC for formaldehyde at 7650 µg/m³.

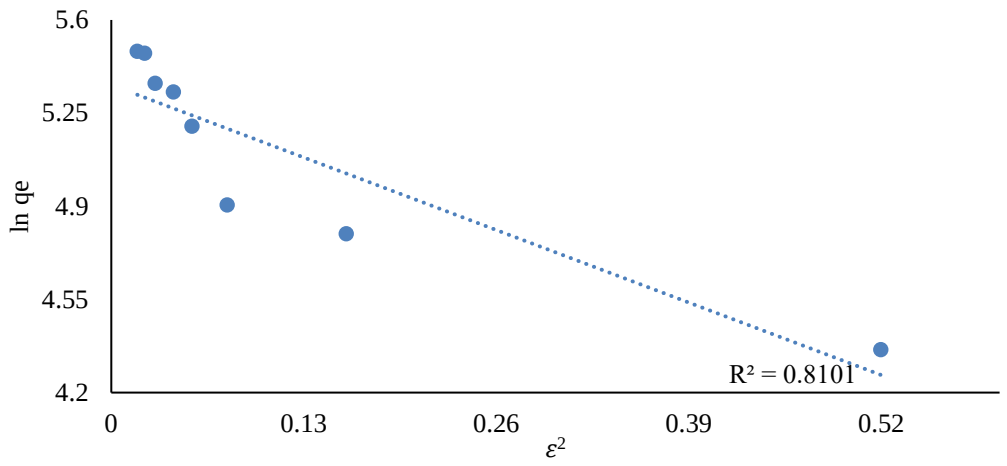

Figure 4.87. D-R isotherm graph of COM-AC for formaldehyde at 30,000 µg/m³.

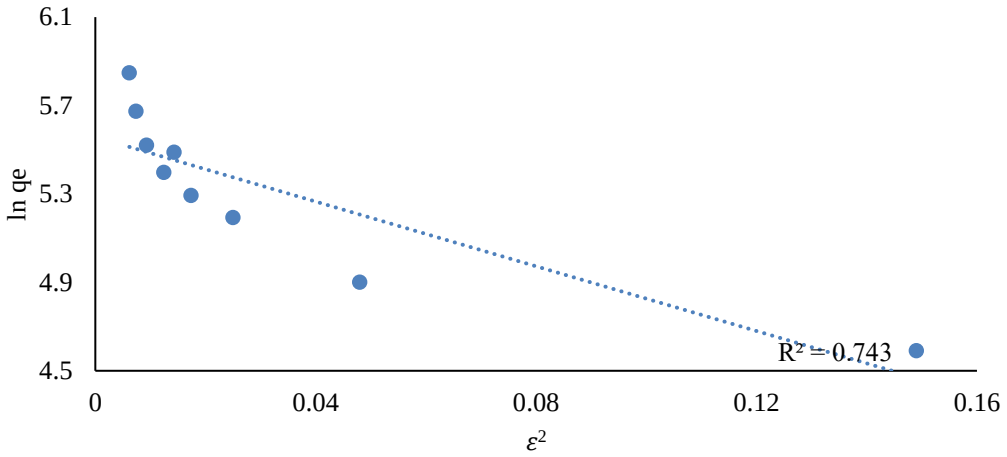

Figure 4.88. D-R isotherm graph of COM-AC for formaldehyde at 50,000 µg/m³.

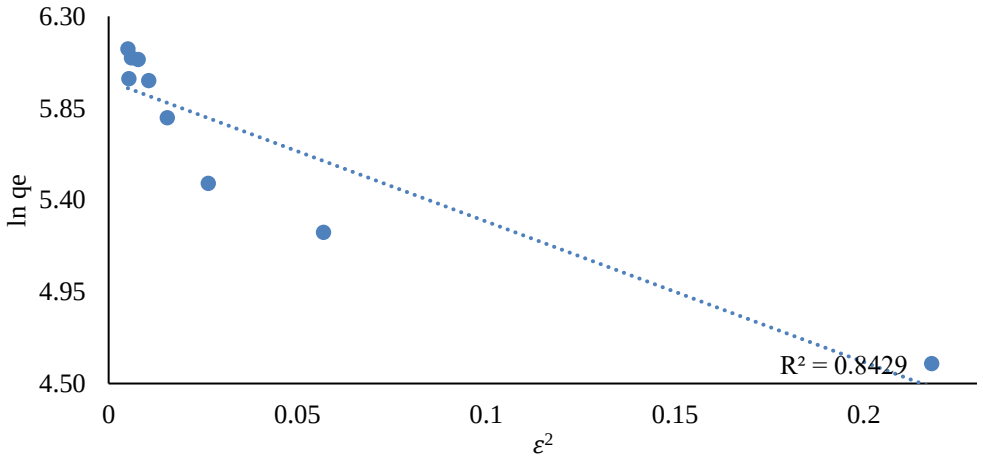

Figure 4.89. D-R isotherm graph of COM-AC for formaldehyde at 60,000 µg/m³.

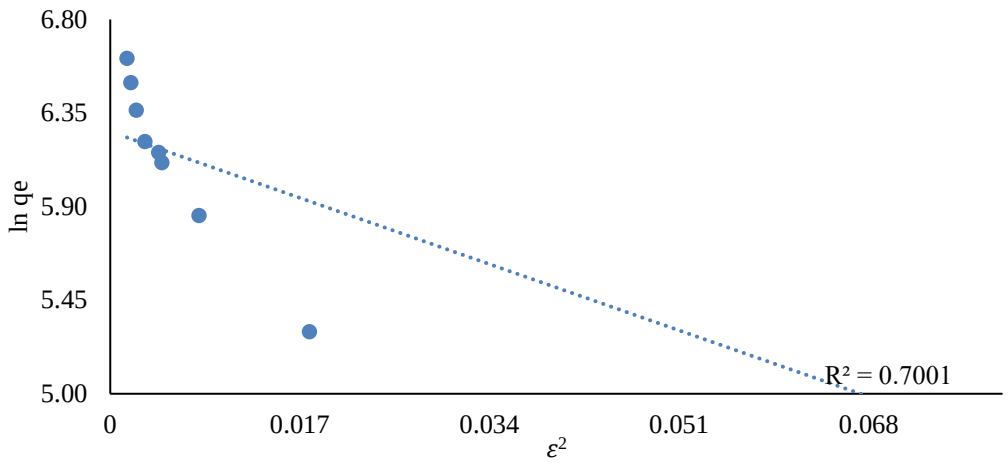

Figure 4.90. D-R isotherm graph of COM-AC for formaldehyde at 110,000 µg/m³.

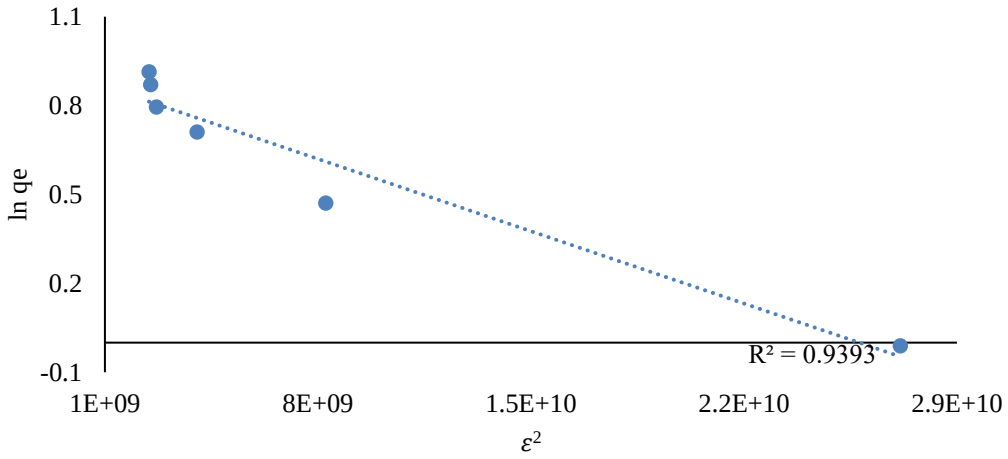

Figure 4.91. D-R isotherm graph of KN-AC for formaldehyde at 170 µg/m³.

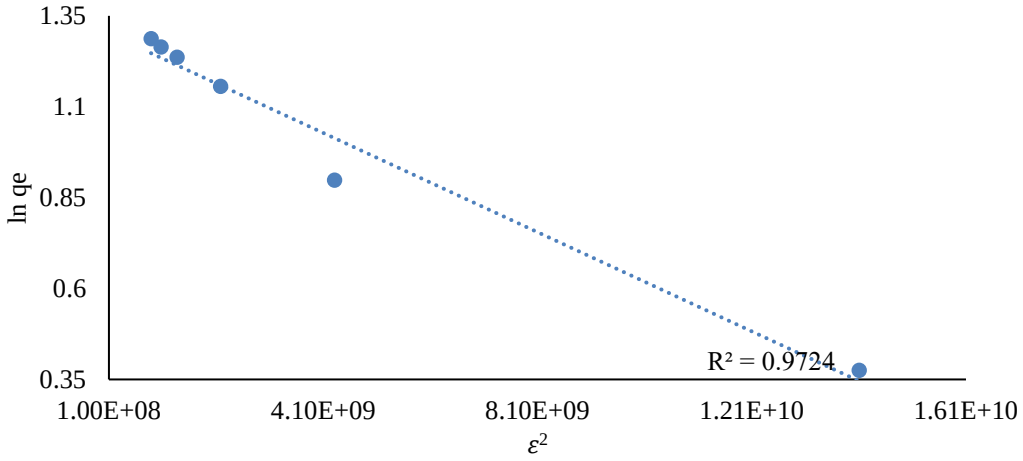

Figure 4.92. D-R isotherm graph of KN-AC for formaldehyde at 260 µg/m³.

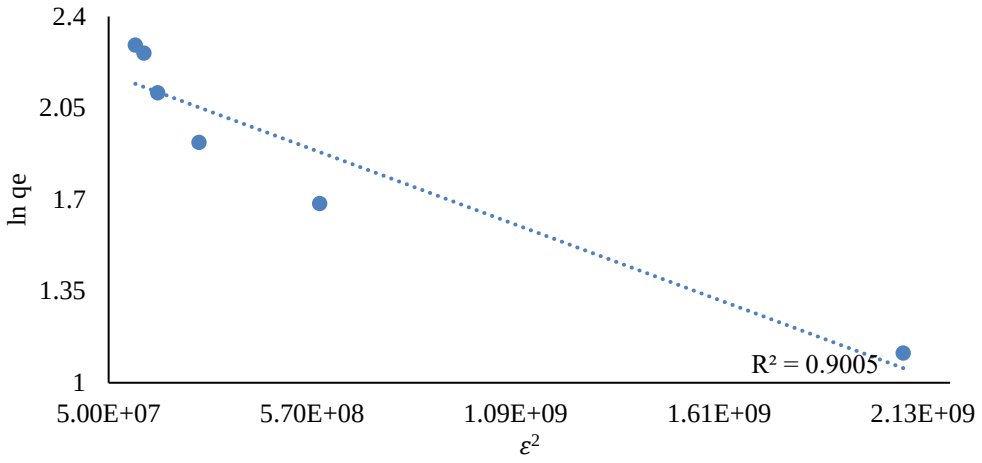

Figure 4.93. D-R isotherm graph of KN-AC for formaldehyde at 720 µg/m³.

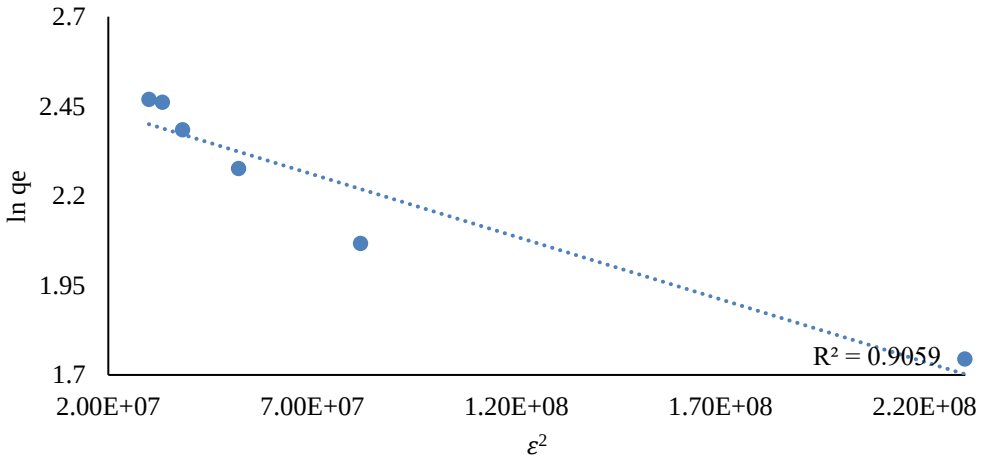

Figure 4.94. D-R isotherm graph of KN-AC for formaldehyde at 1040 µg/m³.

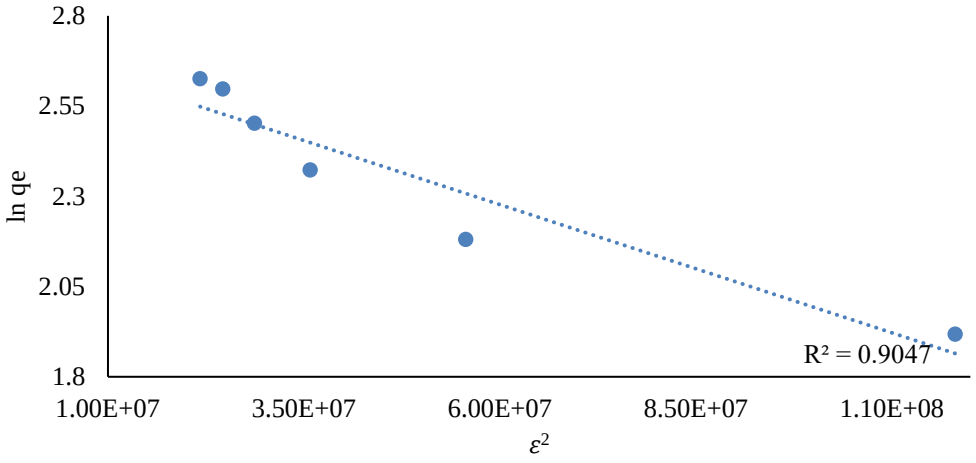

Figure 4.95. D-R isotherm graph of KN-AC for formaldehyde at 1220 µg/m³.

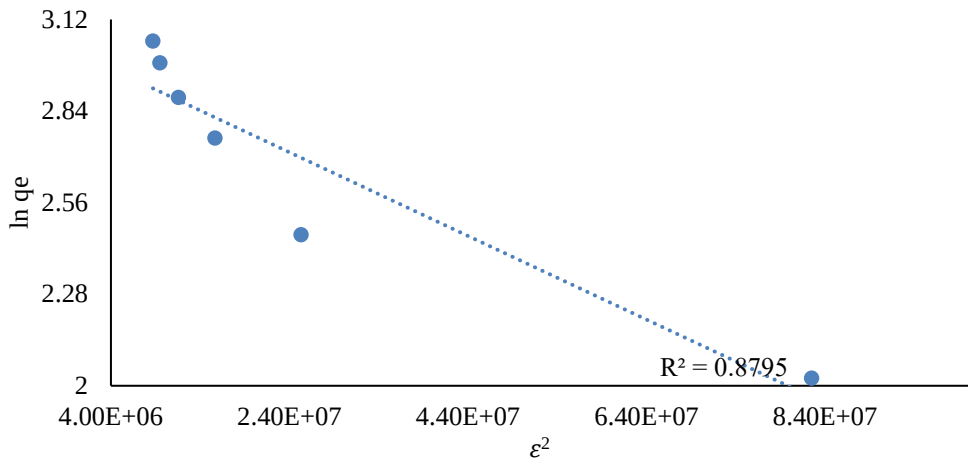

Figure 4.96. D-R isotherm graph of KN-AC for formaldehyde at 1900 µg/m³.

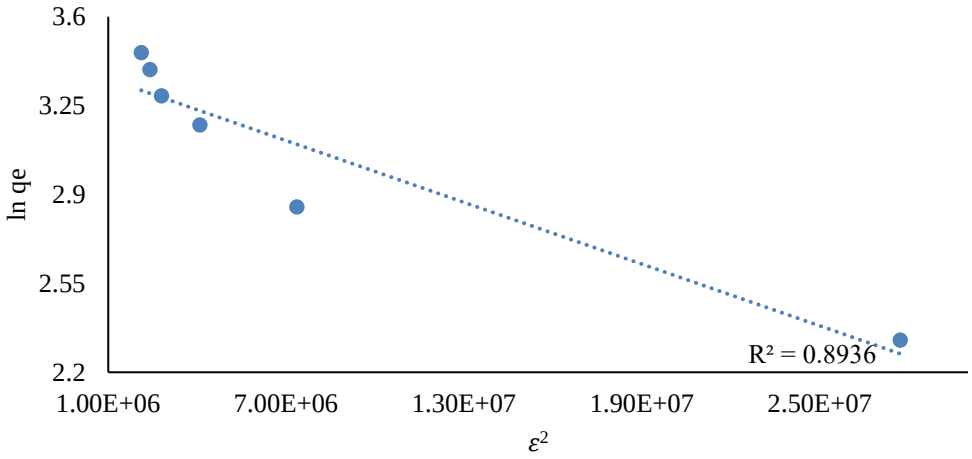

Figure 4.97. D-R isotherm graph of KN-AC for formaldehyde at 3290 µg/m³.

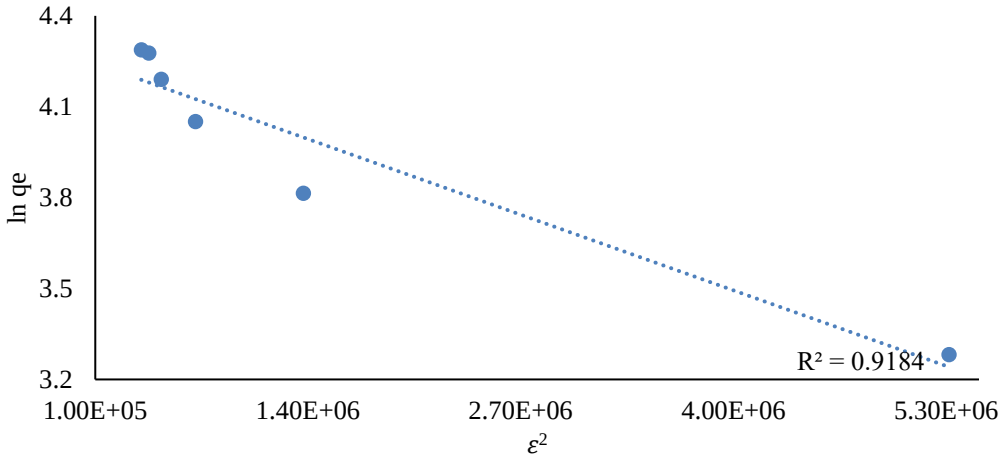

Figure 4.98. D-R isotherm graph of KN-AC for formaldehyde at 7650 µg/m³.

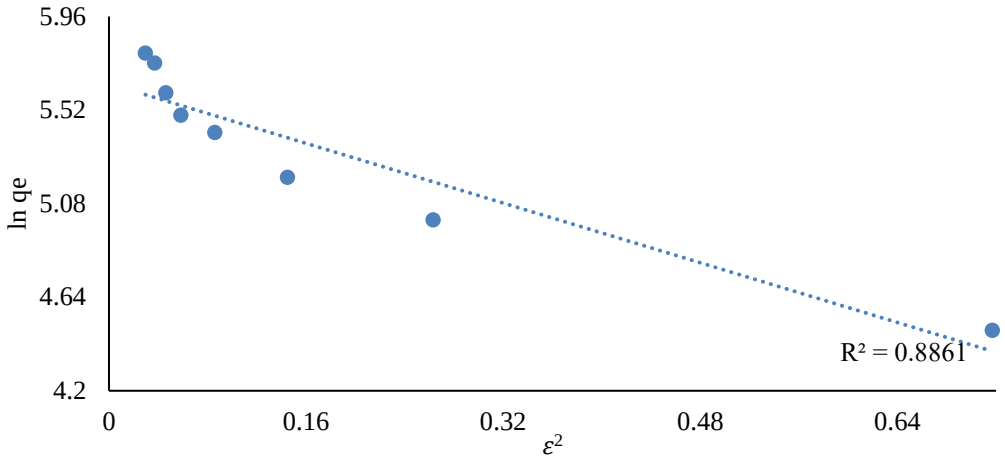

Figure 4.99. D-R isotherm graph of KN-AC for formaldehyde at 30,000 µg/m³.

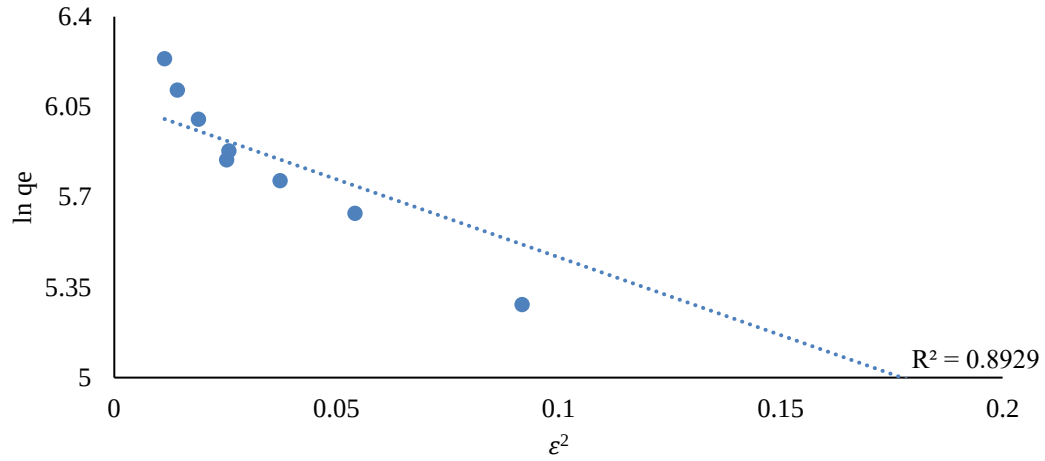

Figure 4.100. D-R isotherm graph of KN-AC for formaldehyde at 50,000 µg/m³.

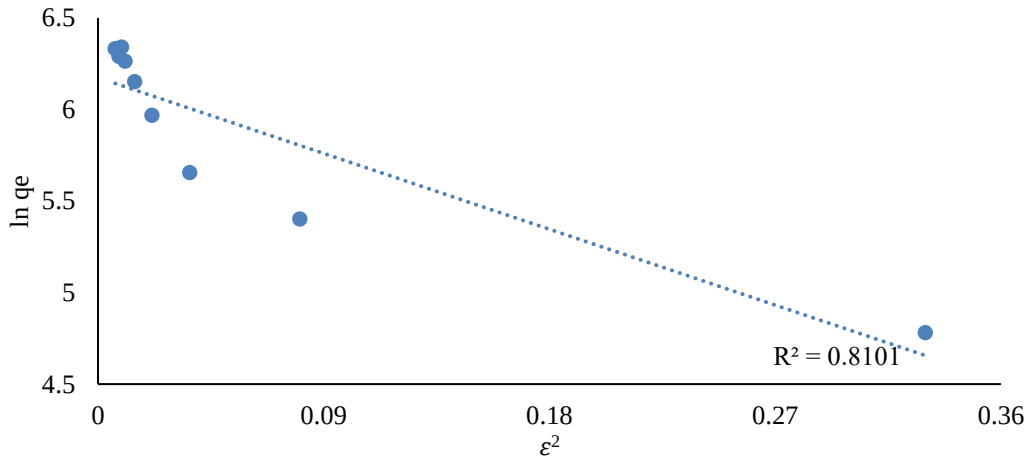

Figure 4.101. D-R isotherm graph of KN-AC for formaldehyde at 60,000 µg/m³.

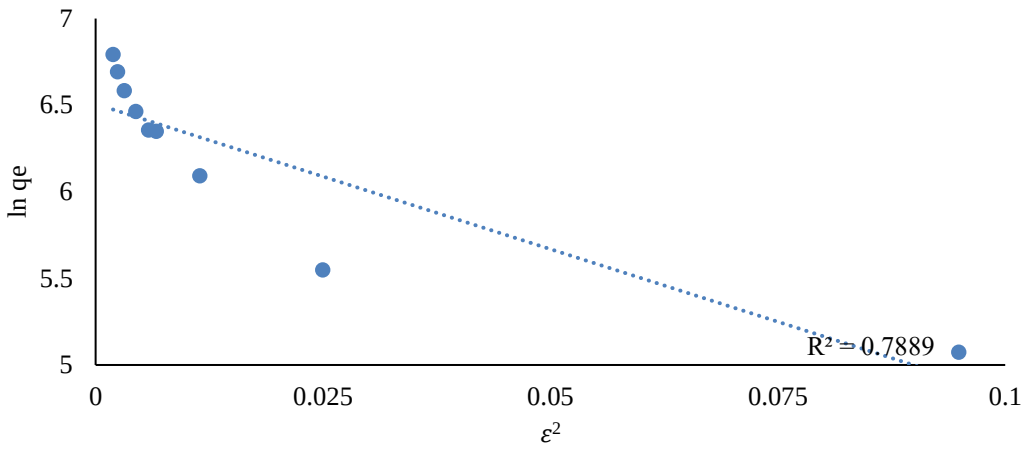

Figure 4.102. D-R isotherm graph of KN-AC for formaldehyde at 110,000 µg/m³.

The graphs of formaldehyde removal studies adapted to Dubinin-Radushkevich isotherm and parameter values were givenin Table 4.11 and Table 4.12.

Table 4.11. Parameters of D-R isotherm for formaldehyde of COM-AC.

Average±SD of C_0 (µg/m³)	*K*	*E*	R^2	q_m (µg/g)
170±14.92	-1.12E-10	66.95	0.948	0.50
260±23.76	-3.52E-10	37.66	0.944	0.94
720±47.61	-2.59E-09	13.90	0.784	1.60
1040±68.47	-1.01E-08	7.05	0.977	2.21
1220±72.14	-1.87E-08	5.17	0.970	2.38
1900±83.37	-3.02E-08	4.07	0.868	2.63
3290±95.44	-5.51E-08	3.01	0.862	3.10
7650±111.18	-3.06E-07	1.28	0.913	3.99
30,000±207.44	-1.85936E-06	0.52	0.831	5.27
50,000±338.61	-7.99878E-06	0.25	0.847	5.41
60,000±376.89	-7.03267E-06	0.27	0.847	5.88
110,000±497.21	-1.99921E-05	0.16	0.731	6.11

Dubinin-Radushkevich parameters of the COM-AC were givenin Table 4.11. The data were obtained as a result of the studies conducted according to the particular concentration. The investigations were first started with 170±14.92 μg/m³, which was the commonly measured quantity in IAQ, and ended with 110,000±497.21 μg/m³, a very high concentration of formaldehyde. According to R^2, values was investigated in all engagements. Although the highest value was obtained at 1040±68.47 μg/m³ with R^2 value 0.977, the smallest value was the concentration value of 110,000±497.21 μg/m³ with 0.731. It was concluded that formaldehyde removal studies with COM-AC were chemical holding at low concentrations, it becomes physical holding as it increases in concentration. This supports the Freundlich isotherm.

Table 4.12. Parameters of D-R isotherm for formaldehyde of KN-AC.

Average±SD of C_0 (μg/m³)	*K*	*E*	R^2	q_{max} (μg/g)
170±14.92	-3.48E-11	119.79	0.939	0.90
260±23.76	-6.82E-11	85.61	0.972	1.31
720±47.61	-5.54E-10	30.05	0.901	2.21
1040±68.47	-3.49E-09	11.97	0.906	2.50
1220±72.14	-7.10E-09	8.39	0.905	2.70
1900±83.37	-1.28E-08	6.25	0.879	3.02
3290±95.44	-4.05E-08	3.51	0.894	3.40
7650±111.18	-1.92E-07	1.61	0.918	4.26
30,000±207.44	-1.8E-06	0.52	0.939	5.54
50,000±338.61	-6.5E-06	0.28	0.934	5.98
60,000±376.89	-4.6E-06	0.33	0.830	6.04
110,000±497.21	-1.8E-05	0.17	0.813	6.38

The Dubinin-Radushkevich parameters of the KN-AC were derived in Table 4.12. According to R^2 values was investigated in all concentrations. Although the highest value was obtained at 260±23.76 μg/m³ with 0.972, the smallest value was the concentration

value of 110,000±497.21 μg/m³ with 0.813 of R^2 value. It was concluded that formaldehyde removal studies with COM-AC were chemical holding at low concentrations, it becomes physical holding as it increases in concentration.

4.2.2. Formaldehyde Removal Efficiency of ACs

KN-AC produced within the thesis's scope aimed to examine adsorption capacities and commercially available COM-AC in Table 4.13. The removal efficiency (RE) was calculated according to time and drawn by the formula given in Eq. (11). Here C_e and C_o was defined as the initial adsorbate concentration (μg/m³) and adsorbate concentration in equilibrium (μg/m³).

$$Removal\ \% = \frac{C_o - C_e}{C_o} x100 \qquad \text{Eq. (11)}$$

Table 4.13. Removal efficiency of COM-AC and KN-AC in formaldehyde.

C_0 (μg/m³)	Time (min)	COM-AC	KN-AC	C_0 (μg/m³)	Time (min)	COM-AC	KN-AC
170±14.92	0	0	0	1220±72.14	0	0	0
	10	21.29	29.09		10	17.93	27.90
	20	32.79	47.09		20	24.34	36.26
	30	41.55	59.89		30	30.87	43.98
	40	45.10	65.15		40	33.92	50.04
	50	45.78	70.29		50	36.40	55.05
	60	47.83	73.37		60	37.64	56.62
260±23.76	0	0.00	0.00	1900±83.37	0	0.00	0.00
	10	18.35	27.97		10	12.80	19.90
	20	30.17	47.17		20	19.29	30.87
	30	40.53	61.07		30	27.84	41.46

	40	44.30	66.18		40	30.85	46.98
	50	45.50	68.06		50	34.34	52.18
	60	47.29	69.63		60	37.22	55.79
	0	0.00	0.00		0	0.00	0.00
	10	12.12	21.13		10	12.55	15.56
	20	19.39	37.45		20	19.84	26.32
720±47.61	30	23.76	47.27	3290±95.44	30	27.54	36.31
	40	30.71	57.17		40	30.21	40.74
	50	38.47	66.52		50	34.14	45.18
	60	39.92	68.61		60	36.83	48.27
	0	0.00	0.00		0	0.00	0.00
	10	18.13	27.53		10	13.52	17.40
	20	27.02	37.99		20	22.35	29.63
1040±68.47	30	32.95	46.83	7650±111.18	30	28.86	37.53
	40	35.50	52.17		40	32.04	43.16
	50	38.76	56.35		50	35.76	47.04
	60	38.98	56.82		60	35.99	47.58
	0	0	0		0	0	0
	10	13.06	14.77		10	8.27	9.92
	20	20.18	24.81		20	15.72	18.48
30,000±207.44	30	22.48	30.31	60,000±376.89	30	20.00	23.80
	40	30.23	37.42		40	27.60	32.56
	50	34.40	40.58		50	33.10	39.10
	60	35.52	45.09		60	36.70	43.69
50,000±338.61	0	0	0	110,000±497.21	0	0	0

	10	9.86	12.32	10	6.49	7.26
	20	13.44	19.71	20	9.09	11.68
	30	18.00	28.06	30	15.89	20.11
	40	19.90	31.85	40	20.50	25.98
	50	22.11	35.75	50	22.67	29.17
	60	24.98	40.47	60	26.39	32.89

The different initial concentrations given in 10-minute sampling in total one-hour COM-AC and the capacity of KN-AC yields were examined in Table 4.13. While the highest efficiency capacities were at KN-AC, the highest efficiency results were found in low concentrations.

Adsorption efficiency time graphs were givenin between Figure 4.103 and Figure 4.110. Accordingly, against the lowest concentration value (170±14.92 μg/m³), both KN-AC and COM-AC reached the highest efficiency holding capacity and the highest concentration (7650±111.18 μg/m³) reached the lowest efficiency holding capacity. This is because the high concentration of activated carbon has high fill in the pores. Approximately most of the formaldehyde has been trapped in the middle of the test period.

Compared to the COM-AC performance at the 60th minute of the experiment, the removal efficiency of the COM-AC remains constant after the first 30 minutes and the holding capacity was lower compared to the KN-AC. When the experiment was completed, the efficiency of COM-AC remained at 47.83% and the efficiency of KN-AC reached 73.37%. Generally, yield increases in the first 40 minutes. It depends on removing the yields after minutes were almost fixed at the end of the study.

The COM-AC purchased from the market when we first look at the concentration of 170 μg/m³, 21.29% yield obtained at the end of 10 minutes, 32.79% at the end of 20 minutes, 41.55% at the end of 30 minutes and after there is no significant increase in value up to

60 minutes reached the highest value in itself together with 47.83%. Although the performance of KN-AC increases up to 73.37% in Figure 4.103.

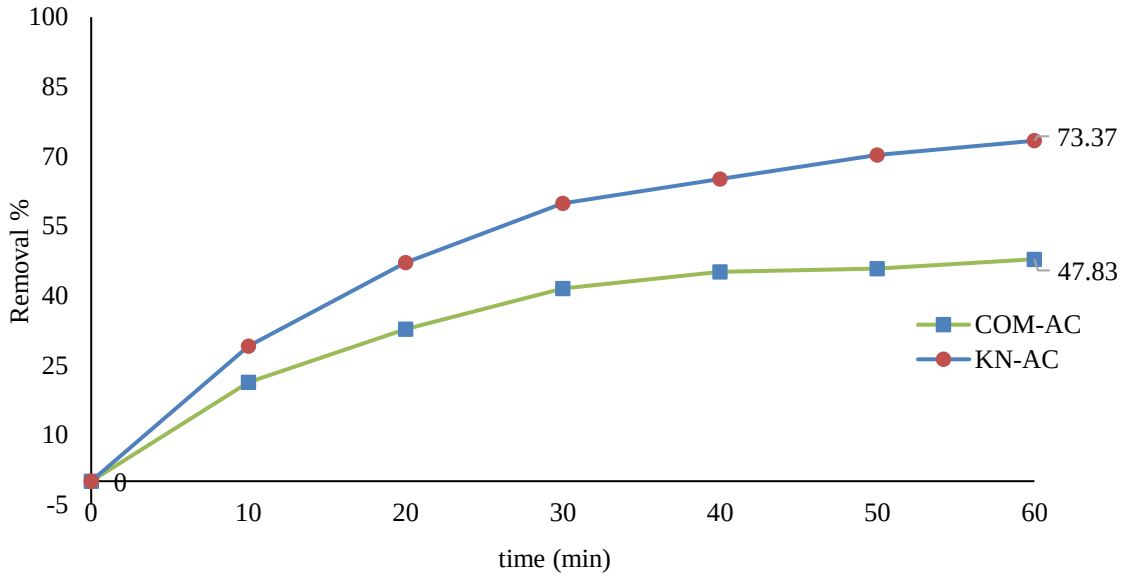

Figure 4.103. Removal efficiency of formaldehyde at 170 µg/m³ for ACs.

The second concentration value 260±23.76 µg/m³ subject to the study, 18.35% yield obtained at the end of 10 minutes, 30.17% at the end of 20 minutes, 40.53% at the end of 30 minutes and after there is no significant increase in value up to 60 minutes reached the highest value with 39.92%. As the concentration increases in KN-AC, the decreasing trend is also seen the maximum efficiency increases up to 69.63% in Figure 4.104.

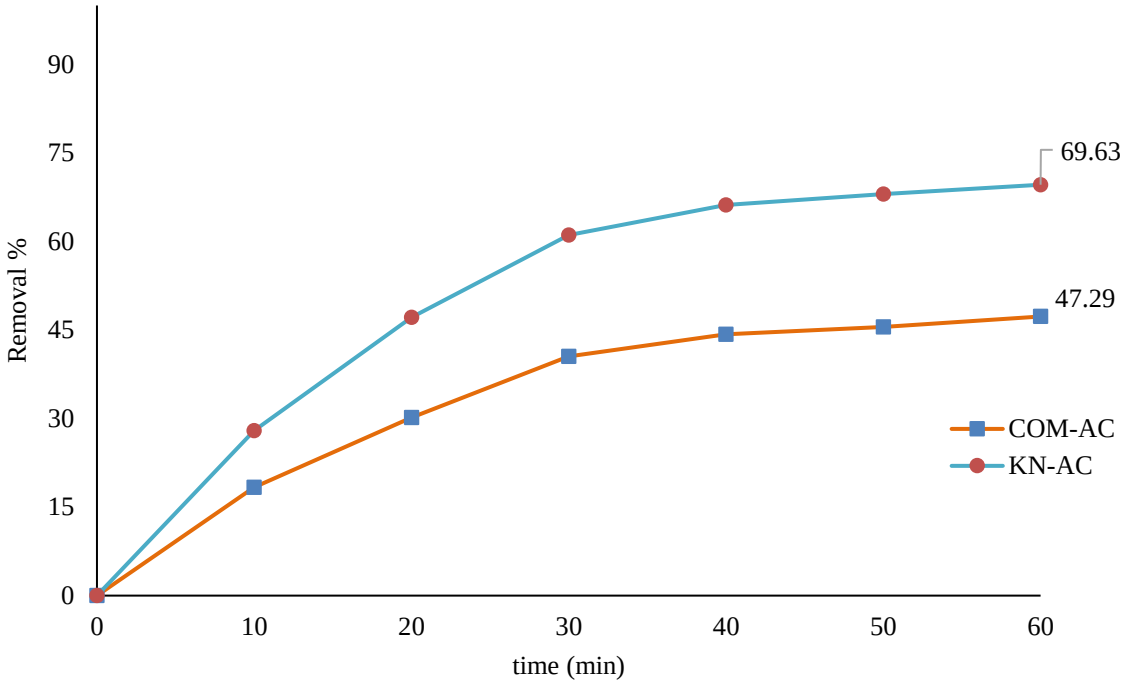

Figure 4.104. Removal efficiency of formaldehyde at 260 µg/m³ for ACs.

The other concentration value 720±47.61 µg/m³ subject to the study, 12.12% yield obtained at the end of 10 minutes, 19.39% at the end of 20 minutes, 23.76% at the end of 30 minutes, 30.17% at the end of 40 minutes, 38.47% at the end of 50 minutes and after there is no significant increase in value up to 60 minutes reached the highest value with 38.92%. Unlike COM-AC, the yield obtained as 68.61% after 60 minutes for KN-AC in Figure 4.105.

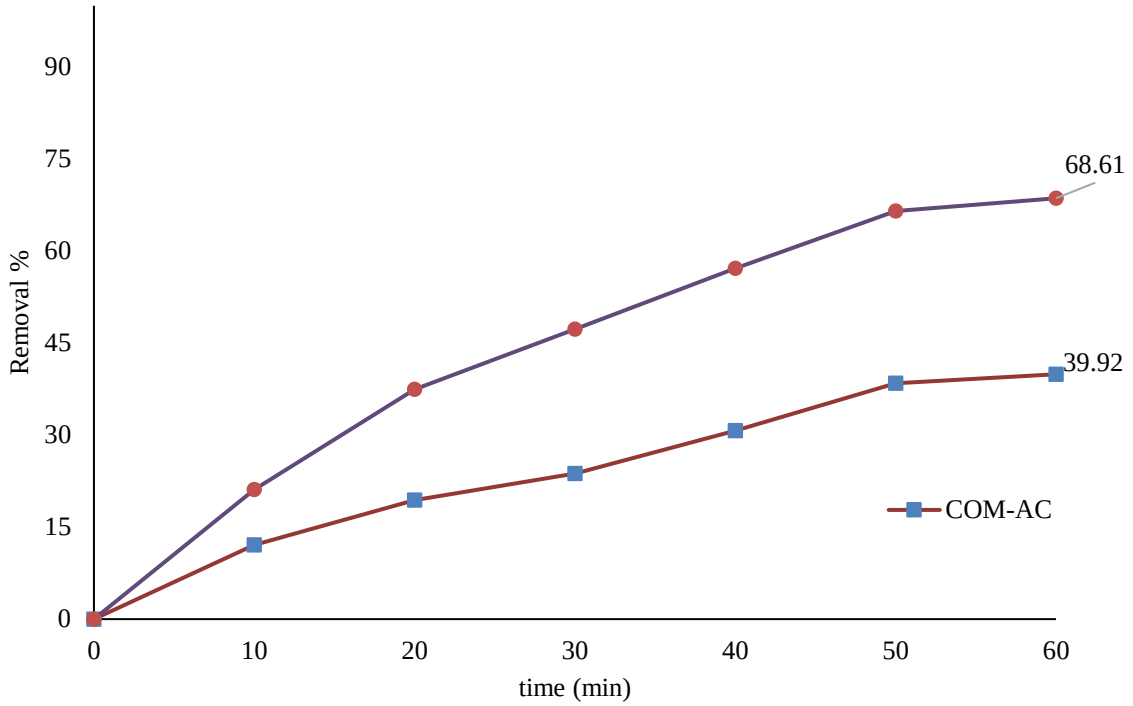

Figure 4.105. Removal efficiency of formaldehyde at 720 µg/m³ for ACs.

In the first 10 minutes of the experiment, initial removal efficiencies were 18.13% for COM-AC and 27.53% for KN-AC. At the 50th minute, there is a decrease in the increasing tendency of the yields and it is seen that it reaches the saturation with 38.76% for COM-AC and 56.35% for KN-AC. Another concentration studied was 1040±68.47 µg/m³ that here, the max data obtained were 38.98% for COM-AC and 56.82% for KN-AC, respectively in Figure 4.106.

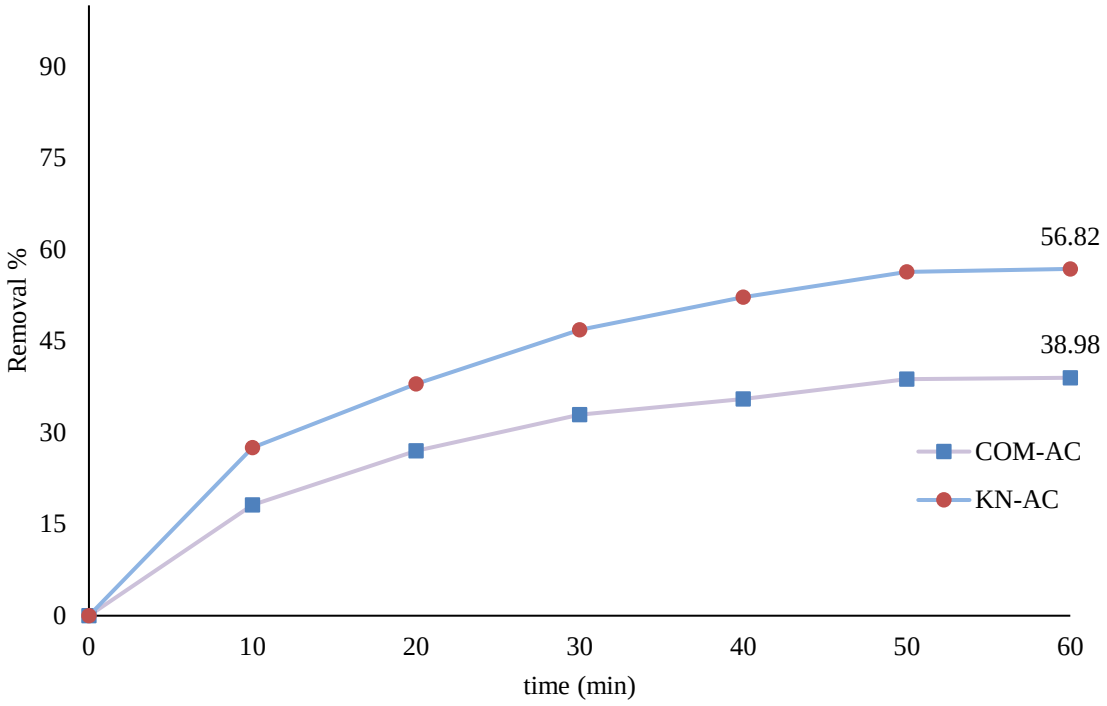

Figure 4.106. Removal efficiency of formaldehyde at 1040 µg/m³ for ACs.

The concentration of 1220±72.14 µg/m³ subject to the study, 17.93% yield obtained at the end of 10 minutes in COM-AC while this value was 27.90% in KN-AC. Next 10 minutes, 24.34%, 30.87% at the end of 30 minutes, 33.92% at the end of 40 minutes, 36.40% at the end of 50 minutes, and no significant increase in value up to 60 minutes reached the highest value with 37.64% for COM-AC. However, after the 40th minute, COM-AC's pores filled faster than KN-AC and its efficiency decreased. KN-AC reached the maximum value with 56.62% in Figure 4.107.

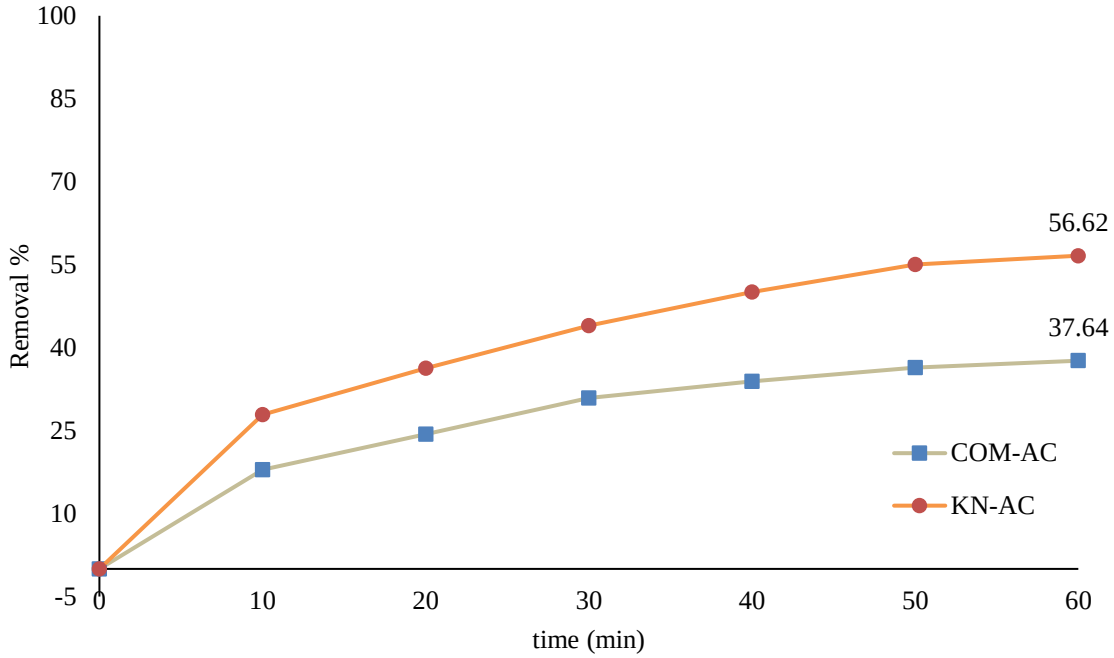

Figure 4.107. Removal efficiency of formaldehyde at 1220 µg/m³ for ACs.

The concentration of 1900±83.37 µg/m³ subject to the study, 12.80% yield obtained at the end of 10 minutes. After ten minutes, 19.29%, 27.84% at the end of 30 minutes, 30.84% at the end of 40 minutes, 34.84% at the end of 50 minutes, and no significant increase in value up to 60 minutes reached the highest value with 37.22% for COM-AC. However, an increase in yield was observed in KN-AC due to the fact that the gicerim yield pores were not easily filled, and this value was 55.79% in Figure 4.108.

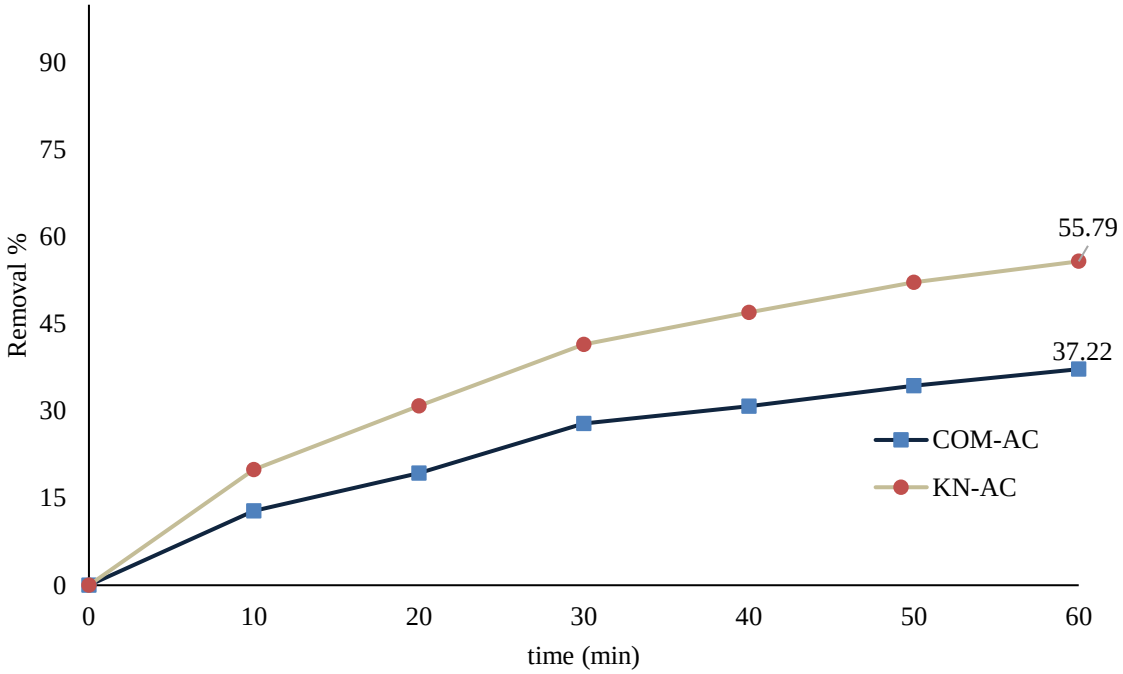

Figure 4.108. Removal efficiency of formaldehyde at 1900 µg/m³ for ACs.

The concentration of 3290±95.44 µg/m³ subject to the study, according to COM-AC, 12.55% yield obtained at the end of 10 minutes. Second ten minutes 19.84%, 27.54% at the end of 30 minutes, 30.21% at the end of 40 minutes, 34.14% at the end of 50 minutes, and no significant increase in value up to 60 minutes reached the highest value with 36.83%. In KN-AC, although the formaldehyde retention rate decreased after the 40th minute, it was higher than COM-AC and reached its maximum value with 48.27% in Figure 4.109.

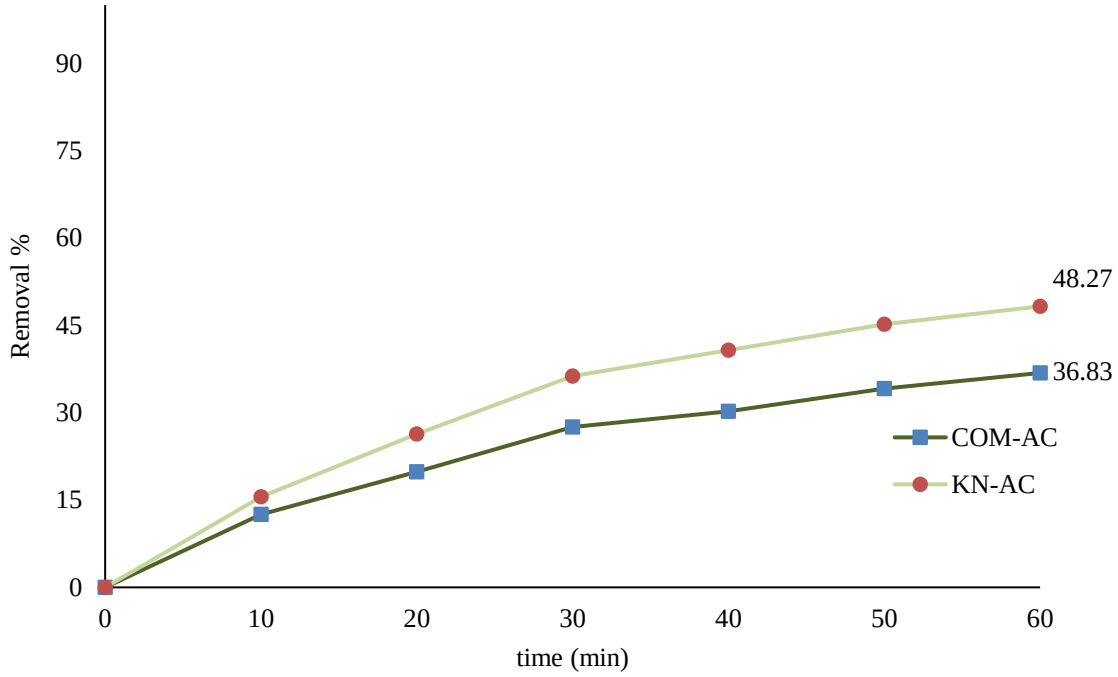

Figure 4.109. Removal efficiency of formaldehyde at 3290 µg/m³ for ACs.

The concentration of 7650±111.18 µg/m³ subject to the study, 13.52% yield obtained at the end of 10 minutes. Other ten minutes 22.35%, 28.86% at the end of 30 minutes, 32.04% at the end of 40 minutes, 35.76% at the end of 50 minutes, and no significant increase in value up to 60 minutes reached the highest value with 35.99% by COM-AC. Although KN-AC give of the removal efficiency as 47.58% at the end of the experiment in Figure 4.110.

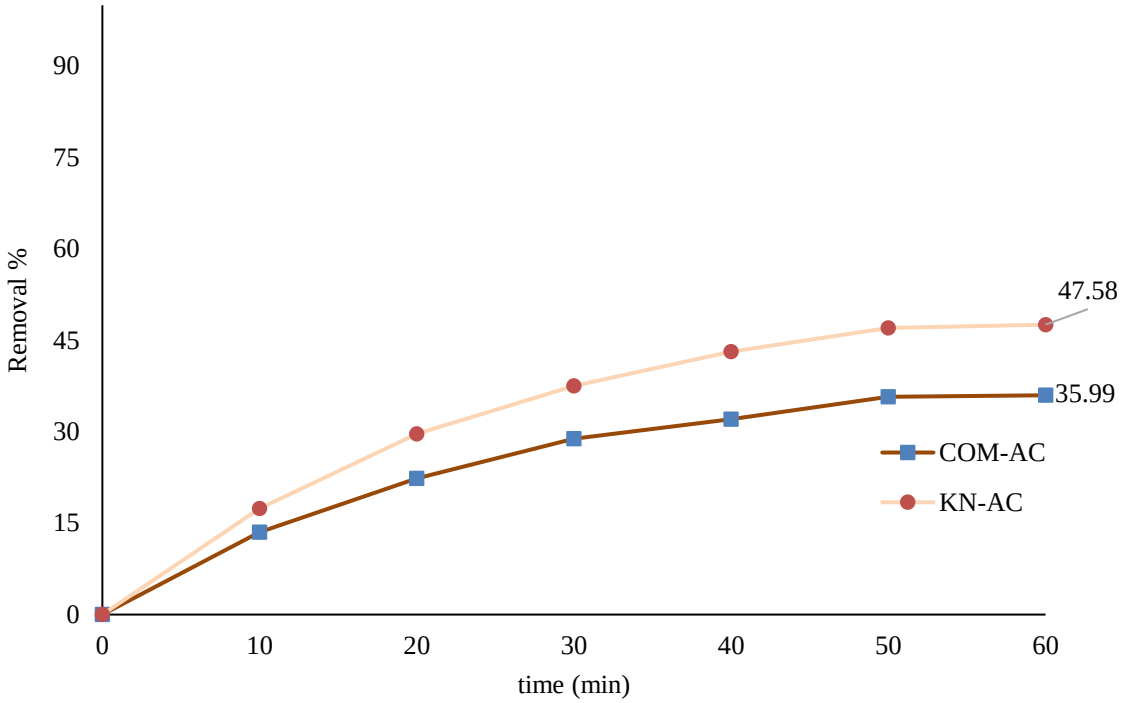

Figure 4.110. Removal efficiency of formaldehyde at 7650 µg/m³ for ACs.

Formaldehyde adsorption experiments were successfully performed with eight different initial concentrations. These values were chosen as values of 170±14.92 µg/m³, 260±23.76 µg/m³, 720±47.61 µg/m³, 1040±68.47 µg/m³, 1220±72.14 µg/m³, 1900±83.37 µg/m³, 3290±95.44 µg/m³, 7650±111.18 µg/m³, which were frequently encountered in the indoor air It gives removal of initial values, with COM-AC and with KN-AC in Figure 4.111.

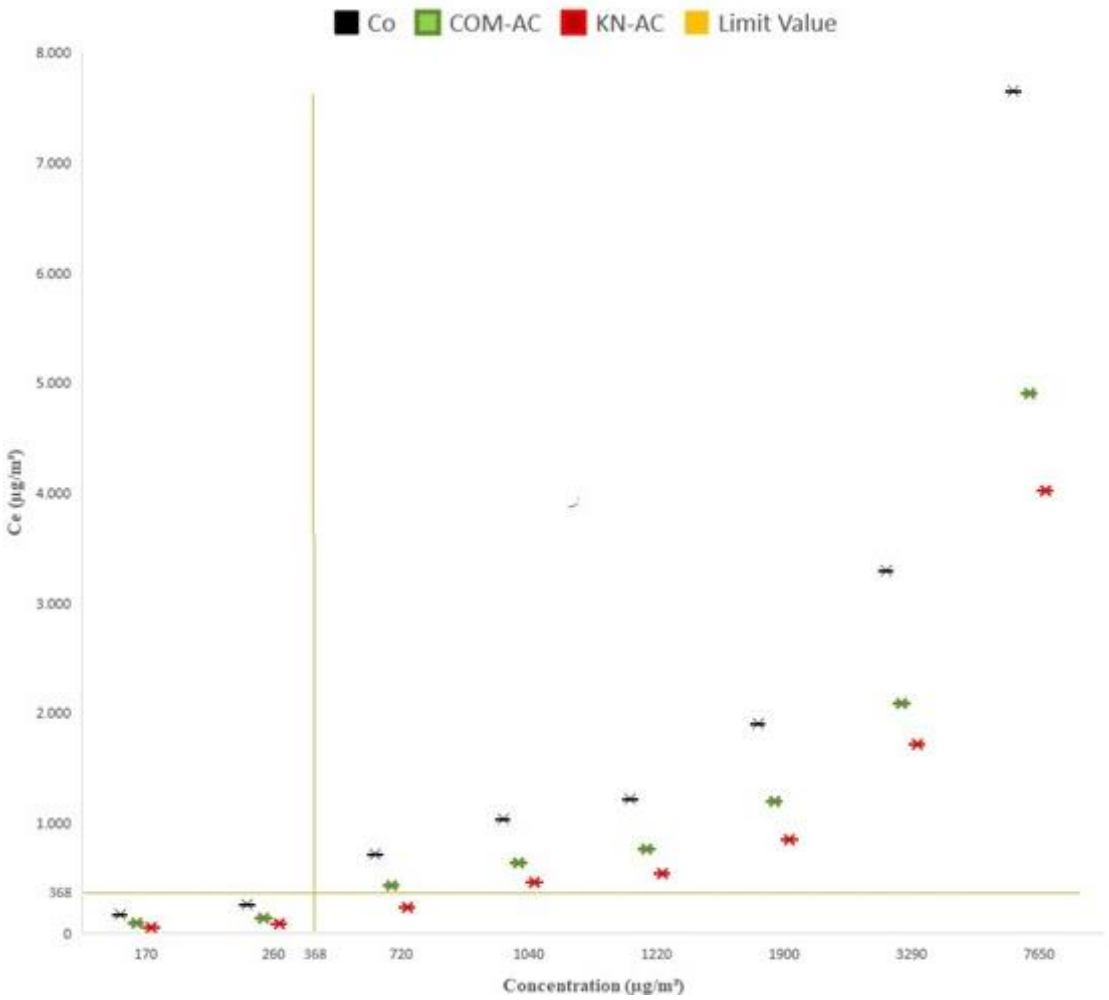

Figure 4.111. Concentrations of substances remaining in air after formaldehyde adsorption.

The differences of the used adsorbent can also be analyzed after certain time values to perform system held stationary conditions was provided immediately before starting the experiment. It demonstrated that drawn horizontally and vertically were shown as generally the limit value in indoor air quality. The points were determined below and above of value.

Initial values decreased from 170±14.92 µg/m³ to 50±7.22 µg/m³, from 260±23.76 µg/m³ to 82±16.38 µg/m³, from 720±47.61 µg/m³ to 227±28.58 µg/m³, from 1040±68.47 µg/m³ to 452±37.61 µg/m³, from 1220±72.14 µg/m³ to 530±39.93 µg/m³, from 1900±83.37 µg/m³ to 839±43.79 µg/m³, from 3290±95.44 µg/m³ to 1704±51.64 µg/m³, from 7650±111.18 µg/m³ to 4013±52.88 µg/m³ respectively for KN-AC.

While the removal efficiency was very close in the first 10 minutes, there is a differentiation in efficiency with increasing time. Especially in the 30th minute, COM-AC was found to retain the pollutant at a rather slow rate than KN-AC. Removal efficiencies of KN-AC and COM-AC were 45.09% and 35.52%, respectively, at the indicated concentration in Figure 4.112.

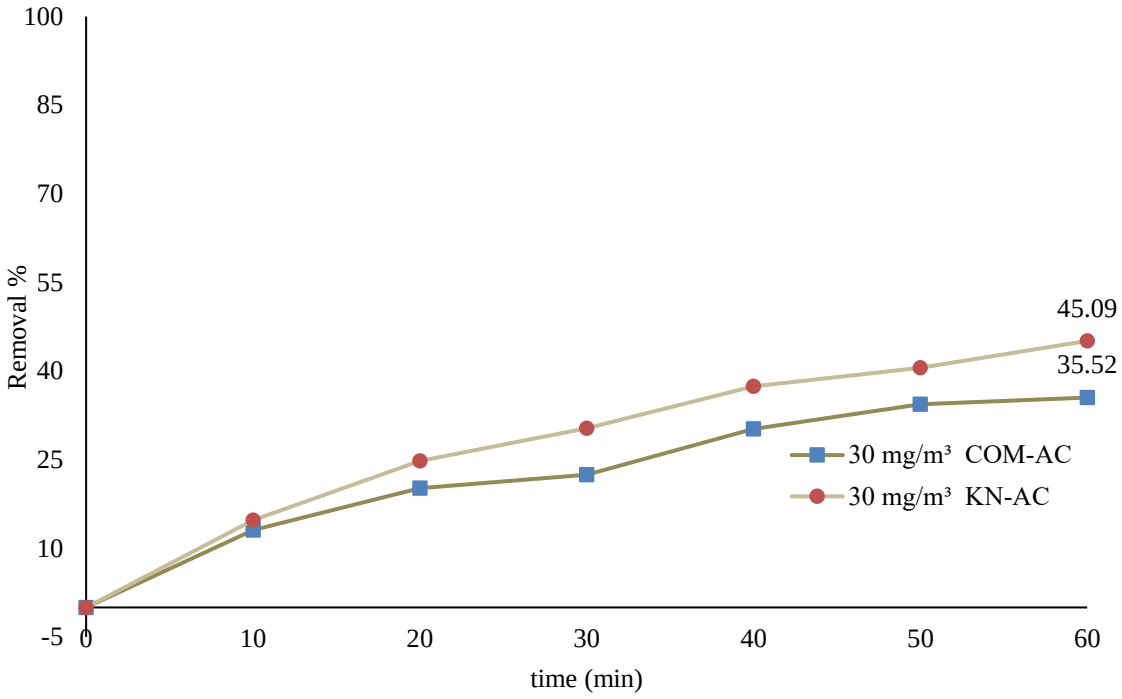

Figure 4.112. Removal efficiency of formaldehyde at 30,000 µg/m³ for ACs.

At the 10th minute of the experiment, removal efficiencies were 9.86% for COM-AC, while this value was 12.32% for KN-AC. However, the difference was increased in the 40th minute and it was 19.90% in COM-AC and 31.85% in KN-AC. As seen in Figure 5.91, while the efficiency obtained at the end of the test period was 40.47% in KN-AC, this value decreased to 24.98% in COM-AC in Figure 4.113.

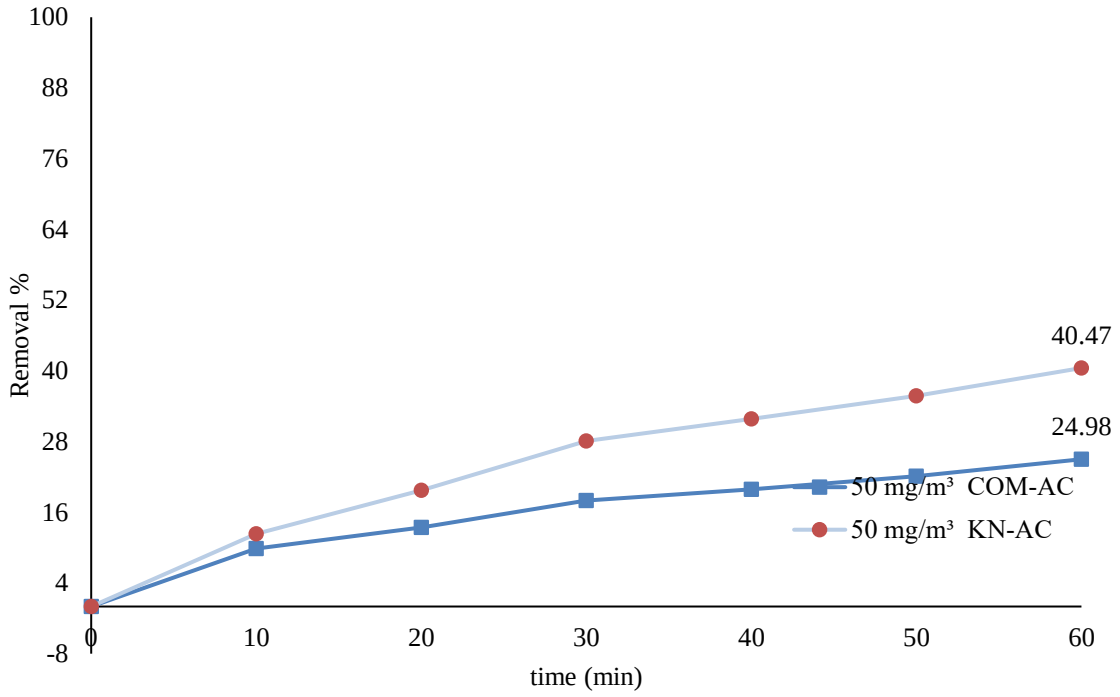

Figure 4.113. Removal efficiency of formaldehyde at 50,000 µg/m³ for ACs.

Although the COM-AC and KN-AC removal efficiencies appear to be close at the 10th minute, this rate can easily be seen in the following minutes with the rapid filling of the pores of COM-AC and the retention efficiency. In line with the data obtained in Figure 5.92, while the efficiency obtained at the end of the test period was 43.69% in KN-AC, this value decreased to 36.70% in COM-AC in Figure 4.114.

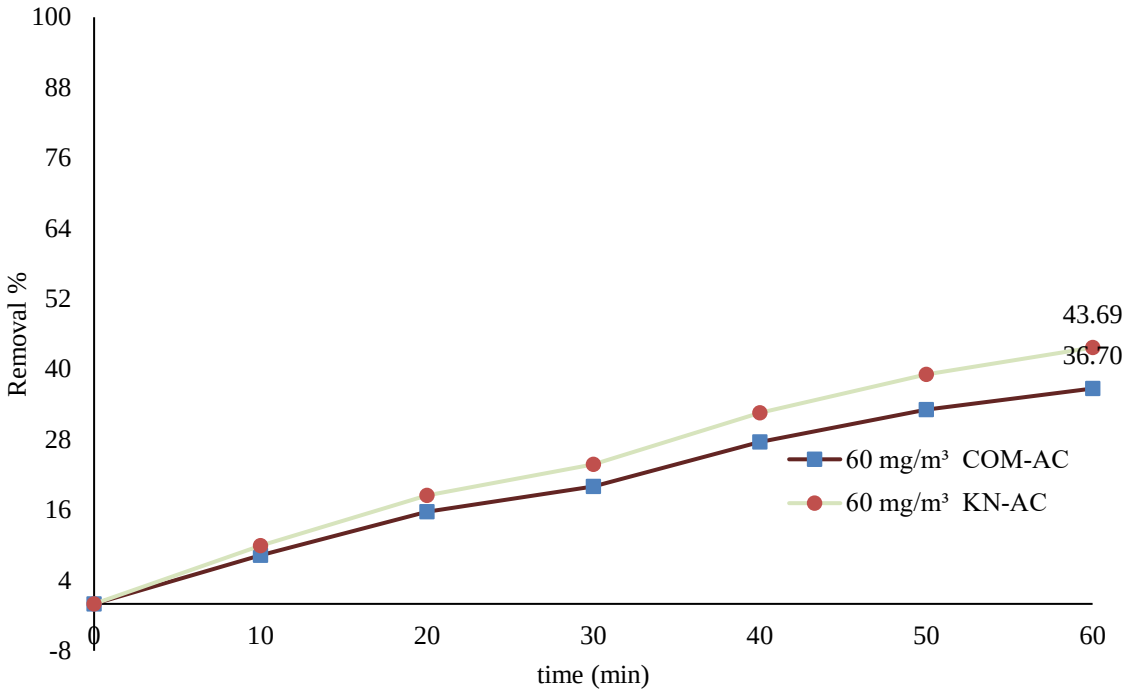

Figure 4.114. Removal efficiency of formaldehyde at 60,000 µg/m³ for ACs.

Formaldehyde adsorption experiments were successfully performed with high concentrations. In the experiment performed at the maximum concentration, it was observed that KN-AC retains 32.89% more formaldehyde than COM-AC. These values were chosen as values of 30,000±207.44 µg/m³, 50,000±338.61 µg/m³, 60,000±376.89 µg/m³, 110,000±497.21 µg/m³, which were rarely presented as appalling conditions like in industry. It gives removal of initial values, with COM-AC and with KN-AC in Figure 4.115.

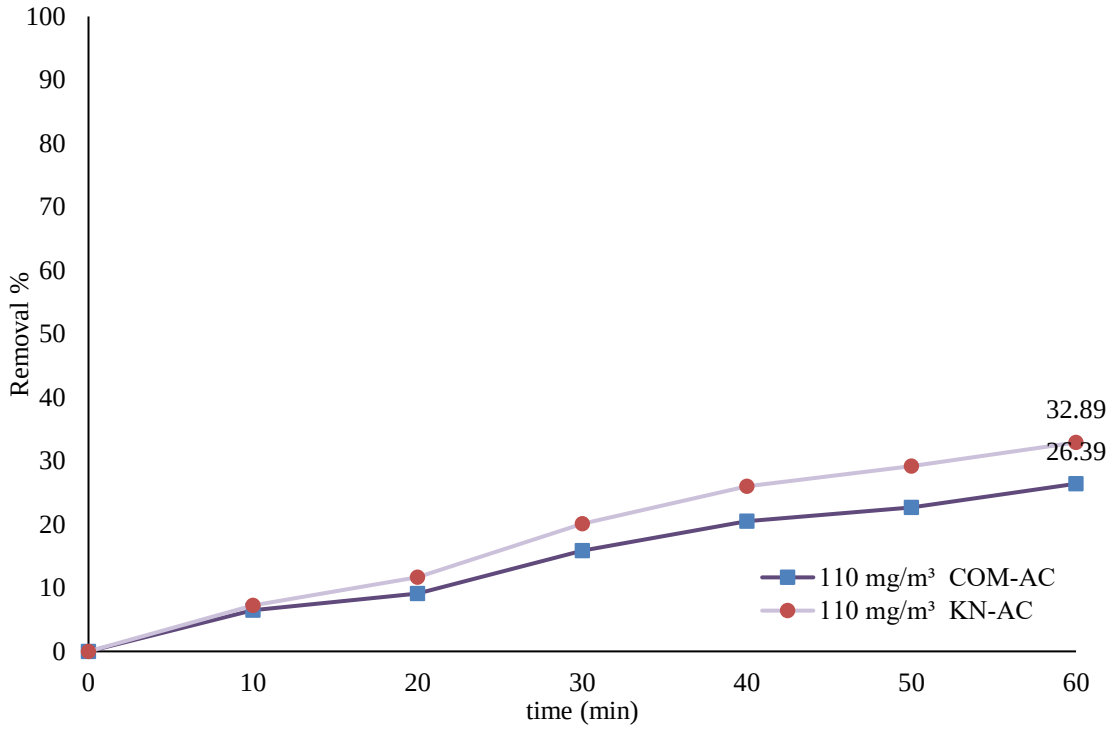

Figure 4.115. Removal efficiency of formaldehyde at 110,000 µg/m³ for ACs.

Formaldehyde removal studies with activated carbon have been studied with low and high concentrations and with different amounts of activated carbons. ACs from coconut husk associated with zeolite (ZSM-5) were researched for formaldehyde removal as almost 1240 µg/m^3. It used both activated carbon and zeolite as adsorbent. After the adsorption process, it was subjected to a desorption process at 120°C. However, with activated carbon, the removal efficiency has increased to 90% by Shiraishi et al. [313]. In our study, only active carbon removal was tested. Removal of not only low concentrations but also high concentrations was achieved. The removal efficiency was 73.37%. This is because the experimental setup used in that study is the cylindrical ceramic-paper honeycomb rotor, and we have the batch reactor.

Boonamnuayvitaya et al. [314] researched removing formaldehyde vapors on coffee residue-derived carbons activated with $ZnCl_2$. The concentrations fixed as 13 767, 30 431, 50 899, and 74 216 ppm. The CZn-N2 sample presented a moderate pore size and surface area 470±12 m^2/g). The formaldehyde removal efficiency was obtained 25% after the experiment. The efficiency was further reduced due to the lower surface area activated

carbon used in the investigation. The maximum adsorption capacity for HCHO measured at a concentration of 20 ppm was almost 400, 350, and 250 mg/g on ACF, GAC1 and GACF, respectively. In this study, Due to the differences in the surface area of the different 1 M, 3 M and 5 M $ZnCl_2$ activated carbons we produced, the highest efficiency was found at 3 M. Even though their highest yield was 37% in KN-AC.

In another study investigated formaldehyde adsorption with APETW, APETOX and APAN. Their surface areas were 1440, 1509 and 356 m^2/g, respectively. The oxygen content was 4.3%, 10% and 5.4%, respectively, Initial formaldehyde concentration was 2852 $\mu g/m^3$ and removal efficiency was found 14 $\mu L/g$ of carbon by Laszlo [315]. In the thesis, Elemental contents obtained of HCS, 1 M KN-AC, 3 M KN-AC, 5 M KN-AC was 40.79%, 10.17%, 8.83%, 25.09%, respectively and the surface area of 3 M KN-AC was 1858 m^2/g.

Another experiment of formaldehyde removal investigated activated carbon from rice husks and commercial coconut shell -based activated carbon. The surface area of the produced activated carbon from rice husk based is 466.9 m^2/g and the total pore volume is 0.35 cm^3/g. The initial concentration of gas was 1245 $\mu g/m^3$ [316]. In this study BET surface areas of the activated carbons synthesized at 1 M $ZnCl_2$, 3 M $ZnCl_2$ and 5 M $ZnCl_2$ concentrations were determined as 795, 1858 and 1600 m^2/g at 600°C carbonization temperature also micro, meso and total pore size results of activated carbons were 0.47, 0.14 and 0.33 cm^3/g; 0.49, 0.24 and 0.73 cm^3/g, and 0.34, 0.07 and 0.41 cm^3/g, respectively.

Rong et al. used rayon-based ACFs for formaldehyde adsorption from vapor. The highest surface area among the samples was obtained with 1635 m^2/g. The gas used in the study was obtained from a solution of formaldehyde in water as air-oxidized between 350 and 450 C for 1-3 h [317]. Within the thesis's scope, the gas aimed to be removed was adjusted in the determined concentration ranges and removal from the steam was made at 25 C.

Some study worked by considering different moisture levels. Besides pore sizes as in other studies, it found the amount of formaldehyde adsorbed depends not only on pore the size and the amount of nitrogen in the carbon matrix. It has been determined that N-oxide, pyridonic, and oxadiazoles, which are present in active carbon, reduce the formaldehyde removal in a humid environment [318]. In our study, the humidity was kept constant. It was not found other compounds in the structure of KN-AC.

Formaldehyde Removal studies have also been carried out with other materials preferred as adsorbates such as natural graphite, expanded graphite, hammer mill type graphite and fluid mill-type graphite. The initial formaldehyde concentration almost 380 $\mu g/m^3$. They calculated 1 day and after 7 days for the total adsorption capacities were between 5.41 $\mu g/m^3$ and 28.35 $\mu g/m^3$ on natural graphite. When expanded graphite was used as adsorbate from 4.81 $\mu g/m^3$ to 24.55 $\mu g/m^3$ also maximum adsorption rate of fluid type graphite was 36 $\mu g/m^3$ after 3 days [319]. In our study, samples were taken in periods of 15 minutes each and at the end of a total of 60 minutes, approximately 93 $\mu g/m^3$ were collected at the lowest concentration.

Table 4.14. Comparison with other studies of KN-AC removal efficiency for formaldehyde.

Adsorbent	Surface area m^2/g	Amounts $\mu g/m^3$	Adsorption efficiencies %	Ref.
TiO_2-ACFs	1020.6	988	14.6	[320]
TiO_2/AC	-	1228	26-80	[321]
CZn-N_2	470	92027	24.5	[314]
BC	105.24	248000	27.5	[322]
$AC_{0.1}$	-	2775	8	[323]
A-420-1h	1635	-	58.3	[317]
RHs	1119.7	1250	10	[316]

4.3. Removal of BTEX

The time of arrival of the standards prepared for each BTEX calibration, the R^2 values of the calibration curves and the mean and accuracy value for the 100 ng/µL standard. The retention time, correlation coefficient, average and accuracy of the gases was given in Table 4.15, respectively.

Table 4.15. GC-MS calibration parameters were performed with BTEX standard.

VOCs	Retention Time(min)	R^2	Average	Accuracy
Benzene	4.882	0.997	97.36	-2.64
Toluene	6.858	0.996	100.78	0.78
Ethylbenzene	9.331	0.999	98.89	-1.11
M, p-xylene	9.584	0.990	101.01	1.01
O-xylene	10.288	0.995	99.54	0.46

To determine whether the thermally cleaned tubes used in the VOC sampling were exposed to contamination from the laboratory environment, laboratory blind samples were tried to be determined. The chromatogram of one of the blind models was given in Figure 4.116.

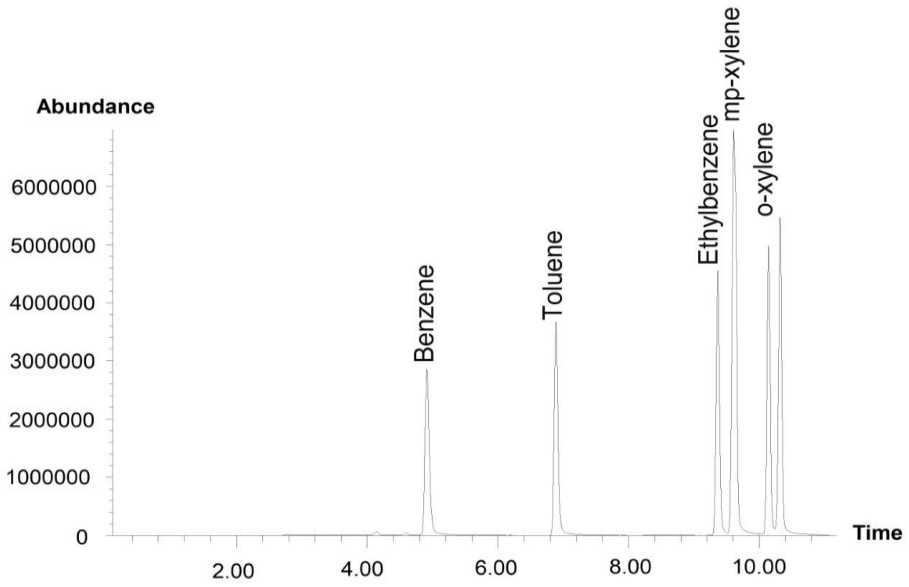

Figure 4.116. The chromatogram of blind samples.

4.3.1. Sorption Equilibrium Modeling of BTEX

The linearity of kinetic models was essential for deciding the model's suitability for the adsorption system. The graphs were plotted to determine which isotherm were more suitable for BTEX removal in between Figure 4.117 and Figure 4.185.

4.3.1.1. Freundlich Isotherm Modelling of BTEX

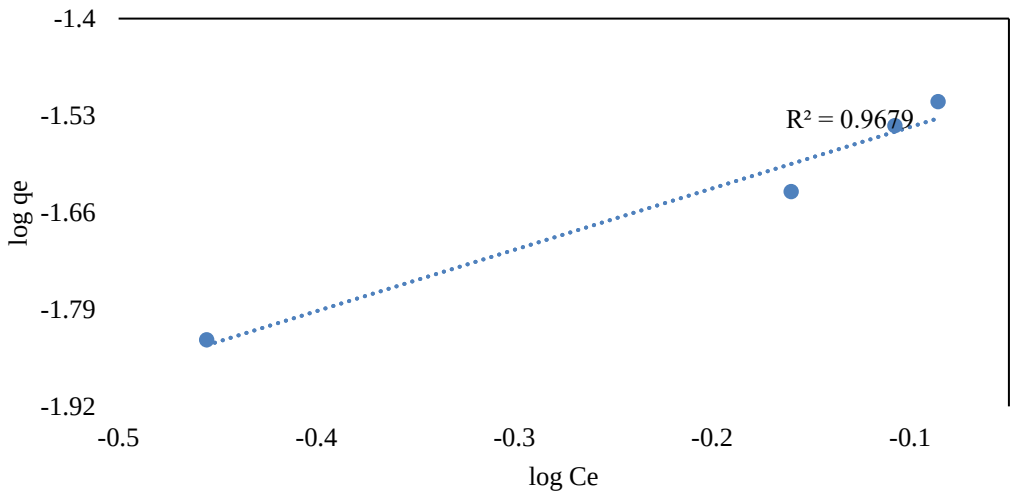

Figure 4.117. Freundlich isotherm graph of COM-AC for benzene at 2.4 µg/m³.

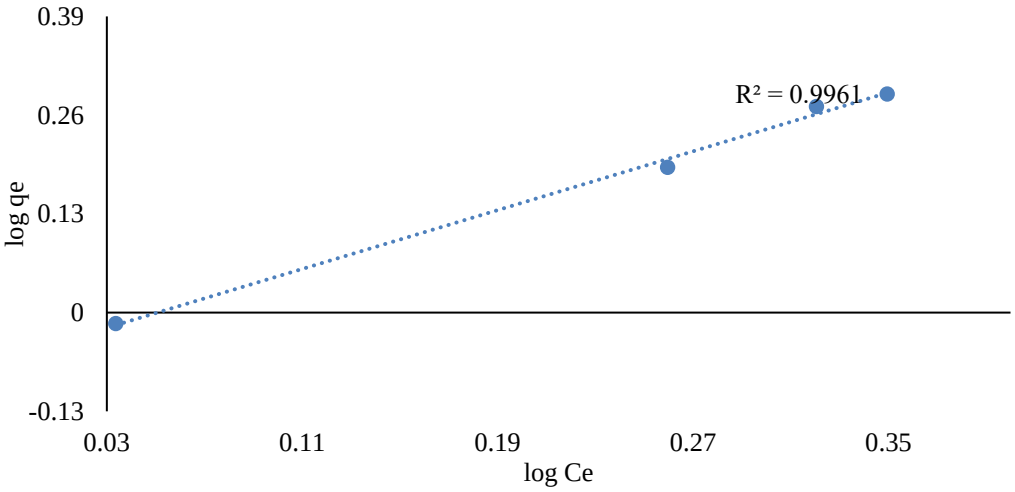

Figure 4.118. Freundlich isotherm graph of COM-AC for benzene at 5.5 µg/m³.

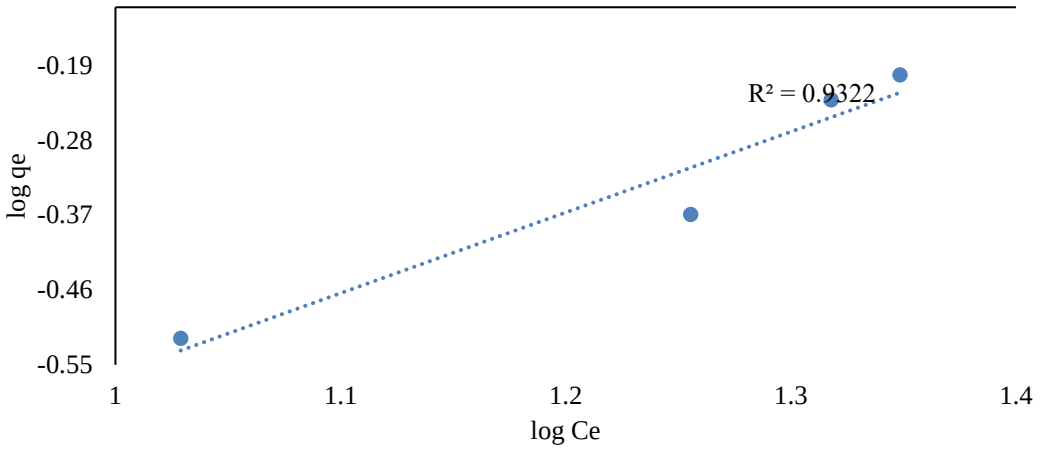

Figure 4.119. Freundlich isotherm graph of COM-AC for benzene at 54 µg/m³.

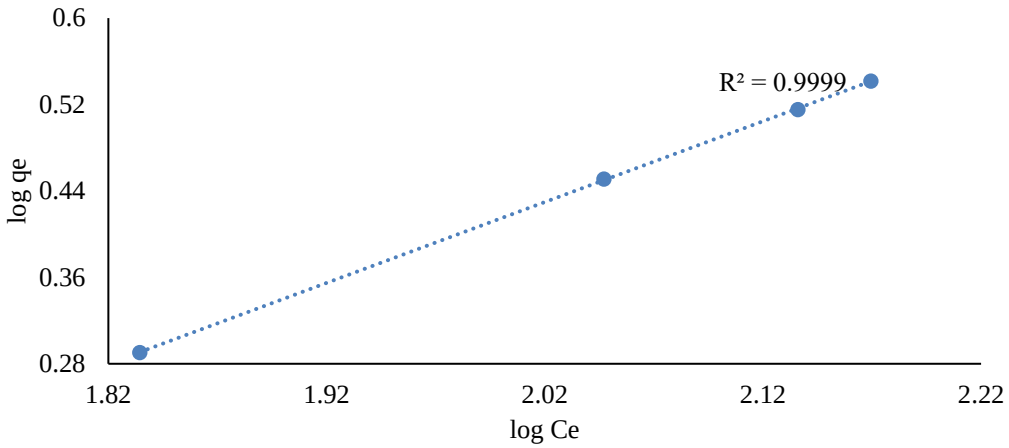

Figure 4.120. Freundlich isotherm graph of COM-AC for benzene at 322 µg/m³.

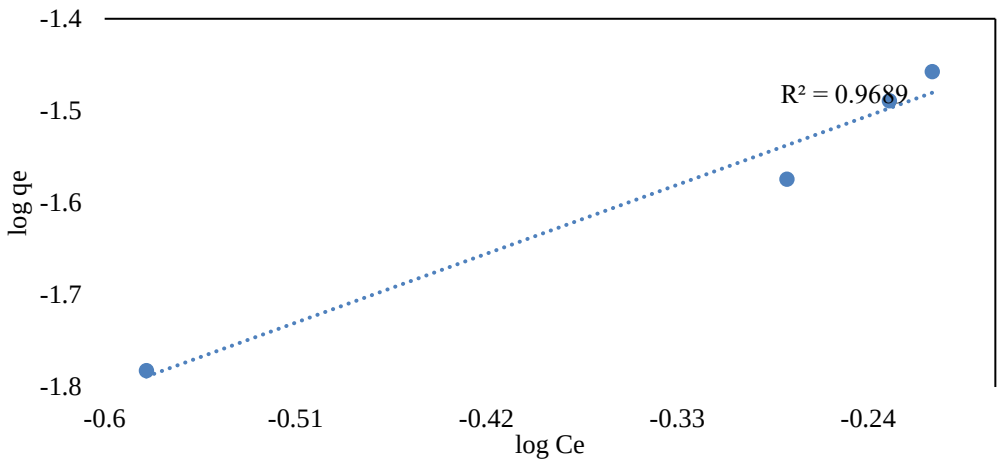

Figure 4.121. Freundlich isotherm graph of KN-AC for benzene at 2.4 µg/m³.

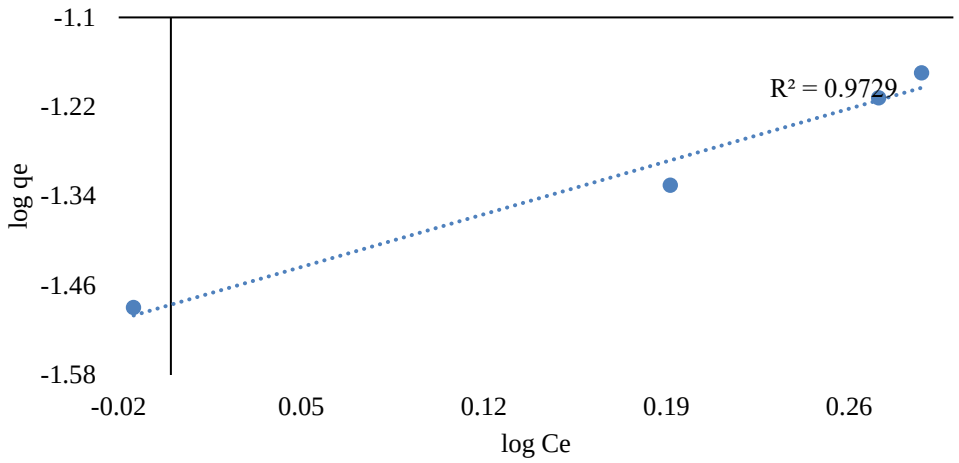

Figure 4.122. Freundlich isotherm graph of KN-AC for benzene at 5.5 µg/m³.

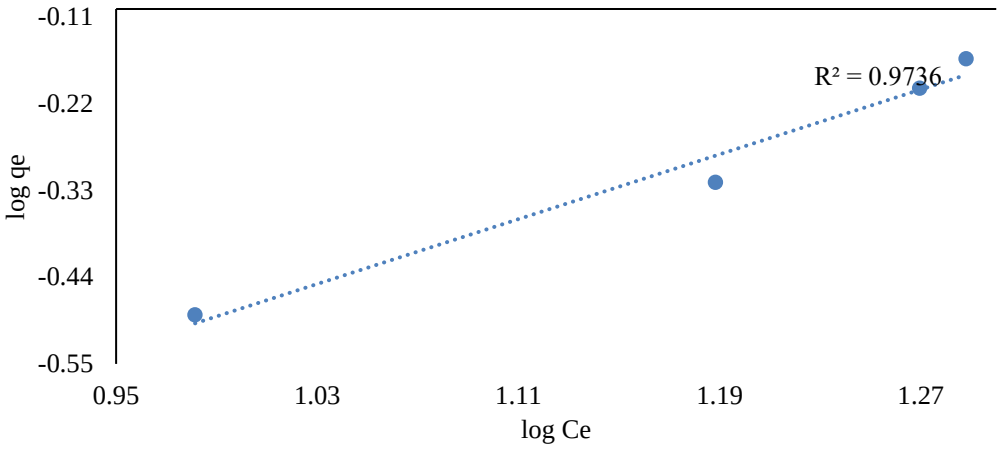

Figure 4.123. Freundlich isotherm graph of KN-AC for benzene at 54 µg/m³.

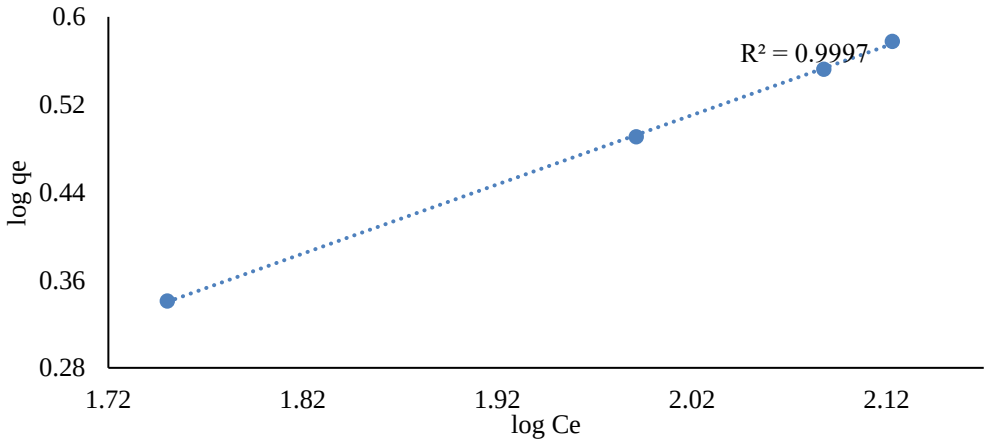

Figure 4.124. Freundlich isotherm graph of KN-AC for benzene at 322 µg/m³.

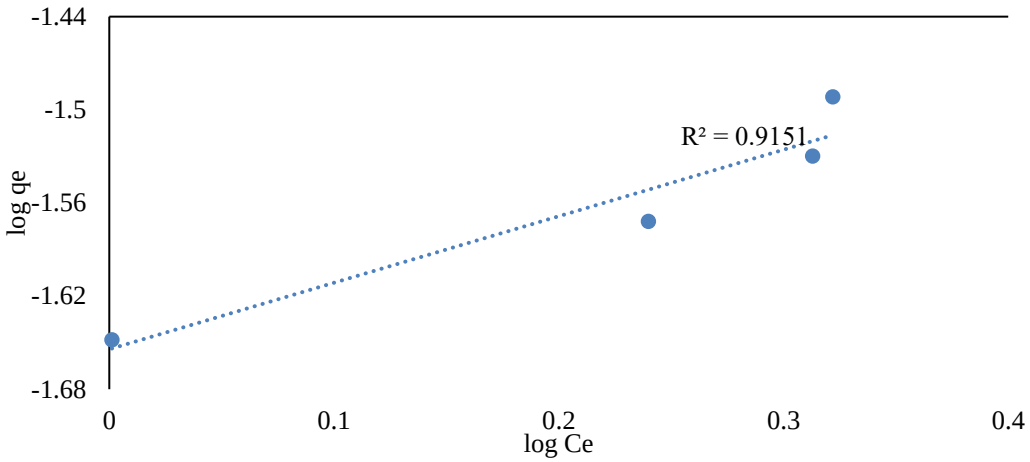

Figure 4.125. Freundlich isotherm graph of COM-AC for toluene at 3.7 µg/m³.

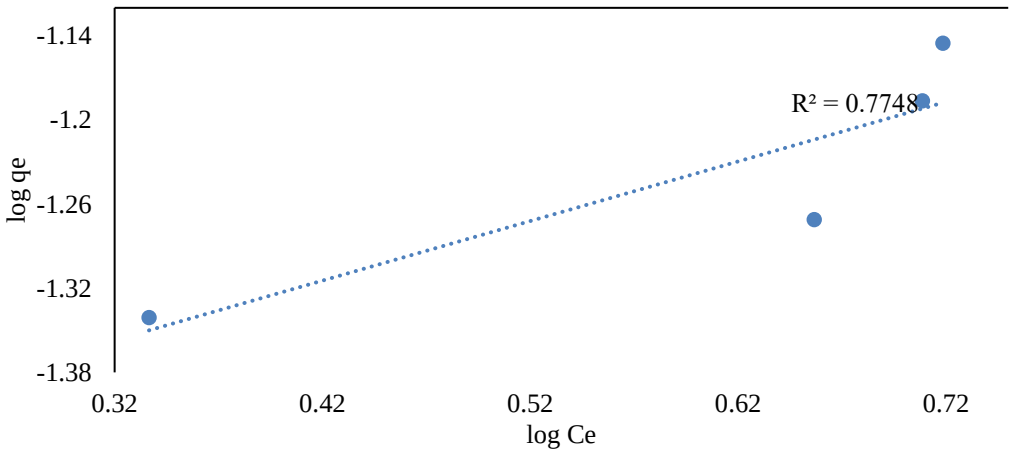

Figure 4.126. Freundlich isotherm graph of COM-AC for toluene at 9 µg/m³.

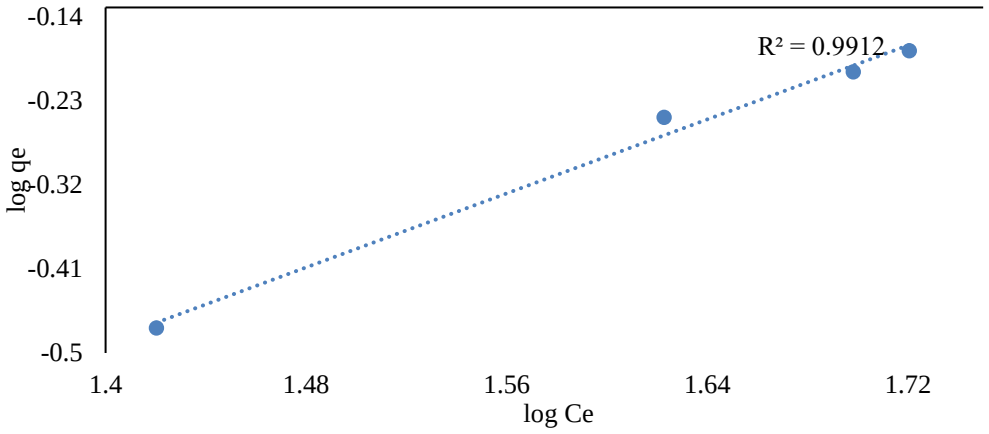

Figure 4.127. Freundlich isotherm graph of COM-AC for toluene at 86 µg/m³.

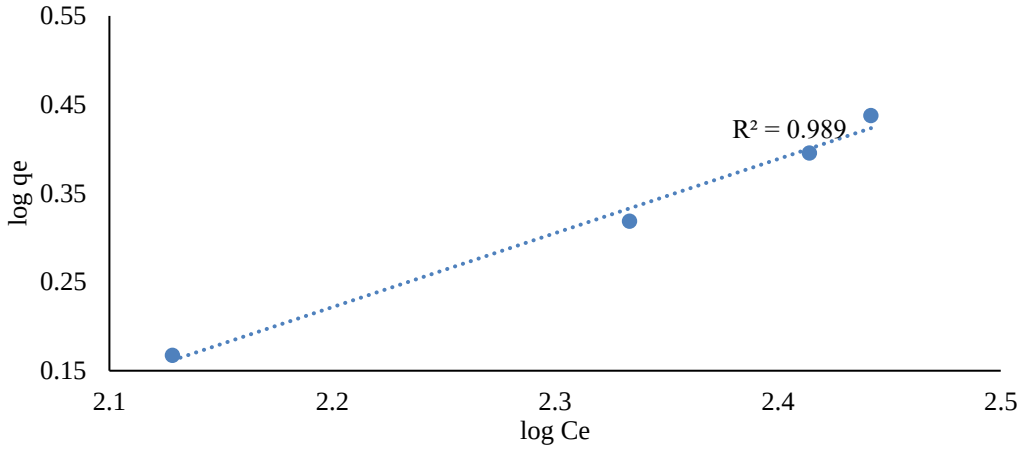

Figure 4.128. Freundlich isotherm graph of COM-AC for toluene at 414 µg/m³.

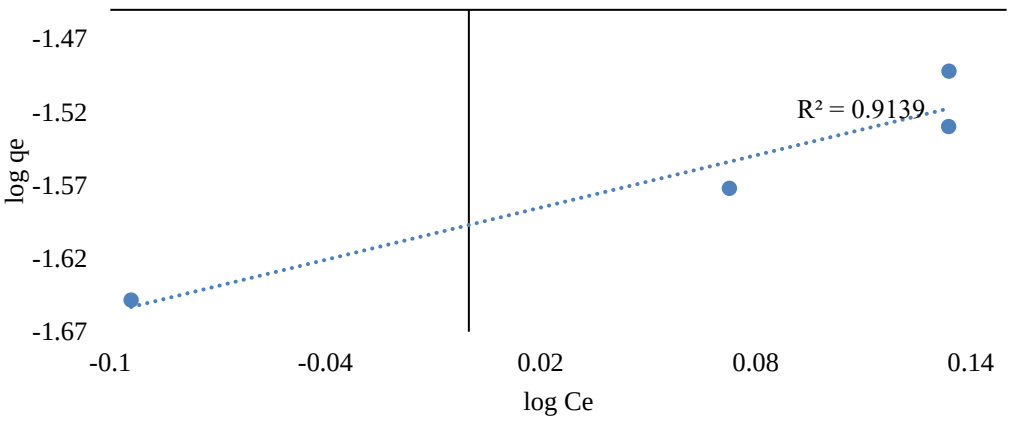

Figure 4.129. Freundlich isotherm graph of KN-AC for toluene at 3.7 µg/m³.

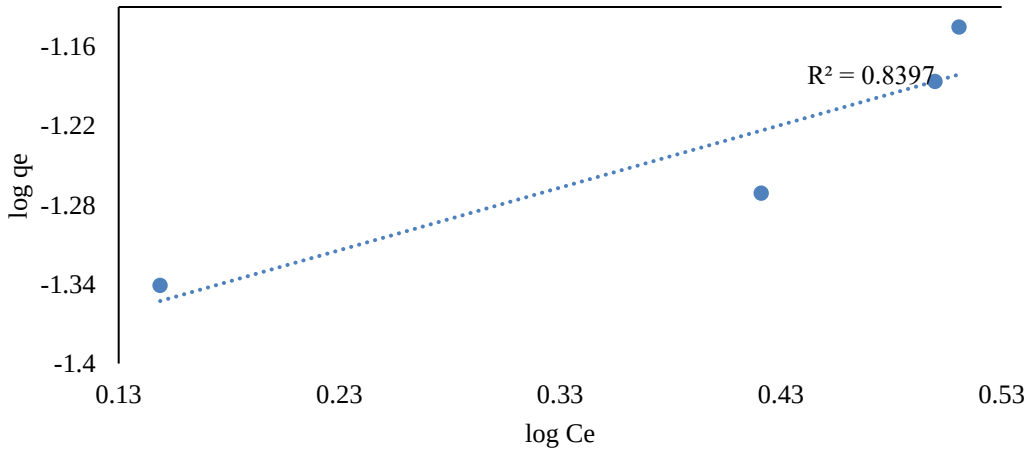

Figure 4.130. Freundlich isotherm graph of KN-AC for toluene at 9 µg/m³.

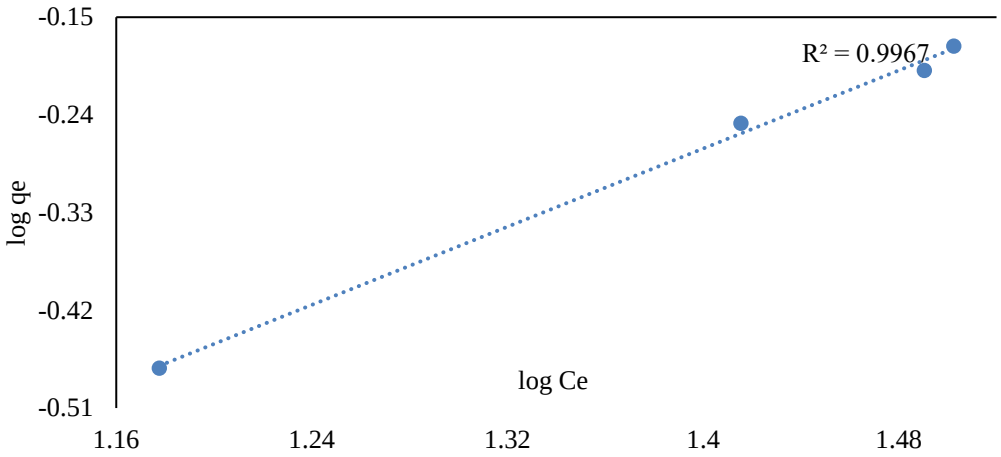

Figure 4.131. Freundlich isotherm graph of KN-AC for toluene at 86 µg/m³.

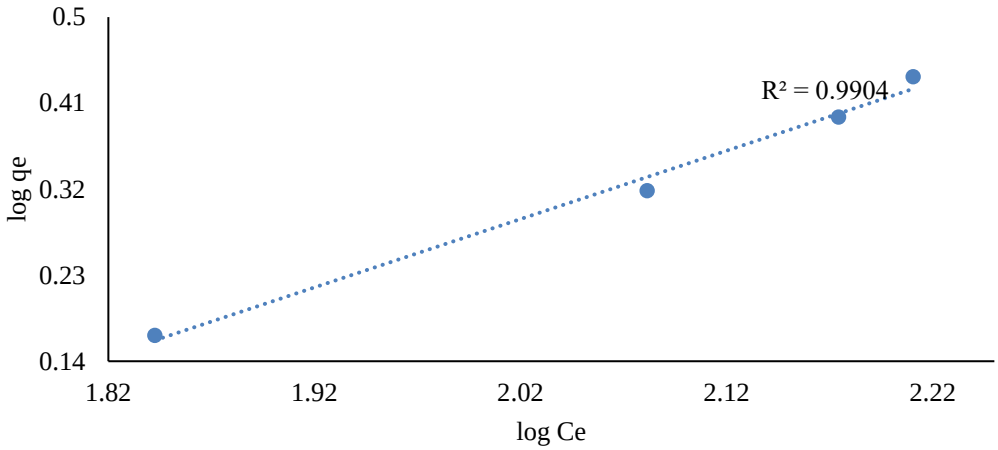

Figure 4.132. Freundlich isotherm graph of KN-AC for toluene at 414 µg/m³.

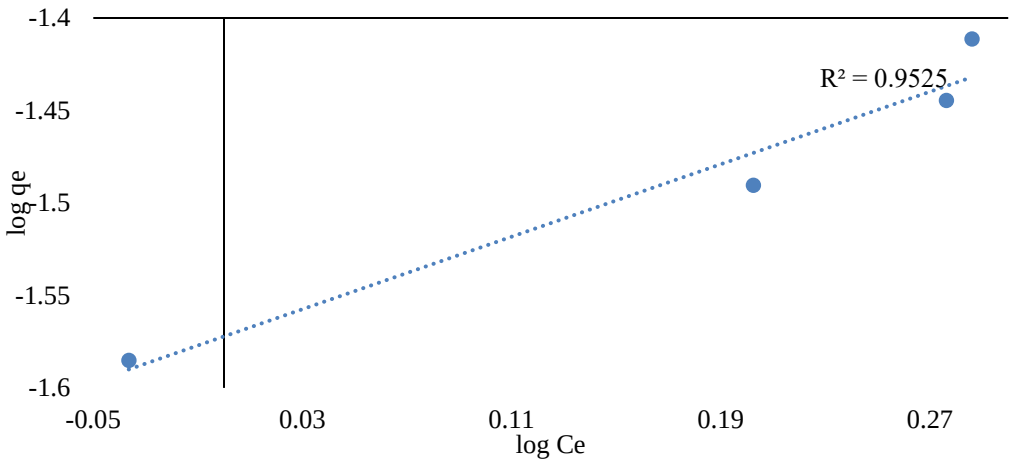

Figure 4.133. Freundlich isotherm graph of COM-AC for ethylbenzene at 3.9 µg/m³.

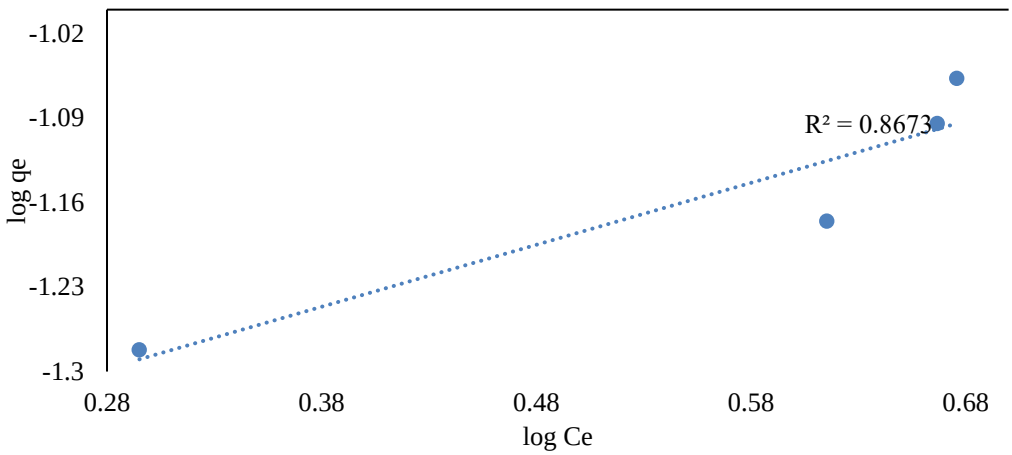

Figure 4.134. Freundlich isotherm graph of COM-AC for ethylbenzene at 9.2 µg/m³.

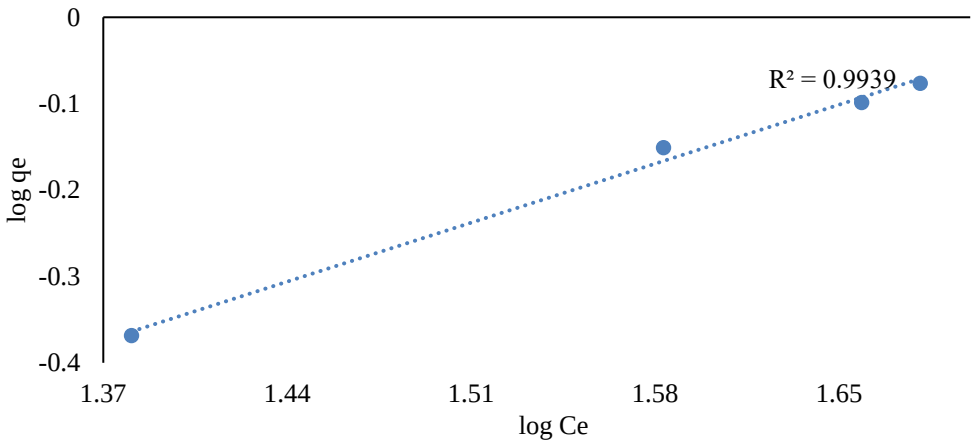

Figure 4.135. Freundlich isotherm graph of COM-AC for ethylbenzene at 90 µg/m³.

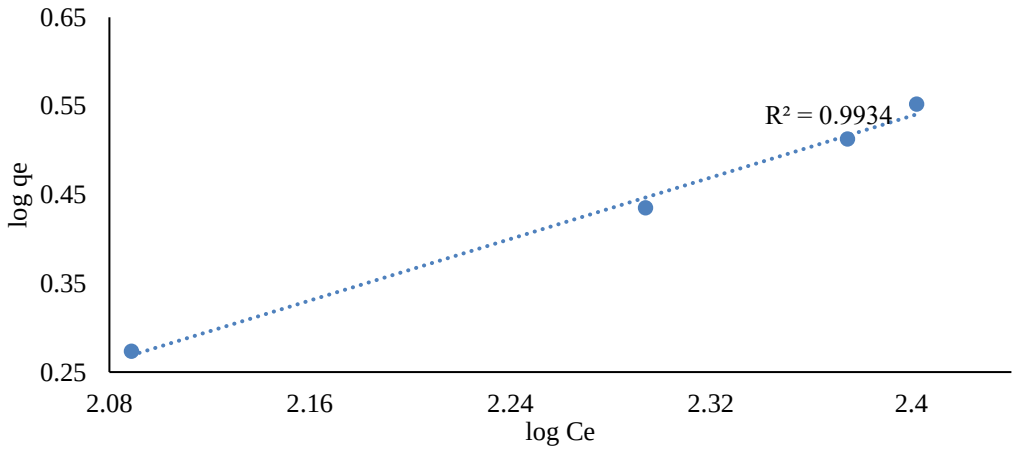

Figure 4.136. Freundlich isotherm graph of COM-AC for ethylbenzene at 430 µg/m³.

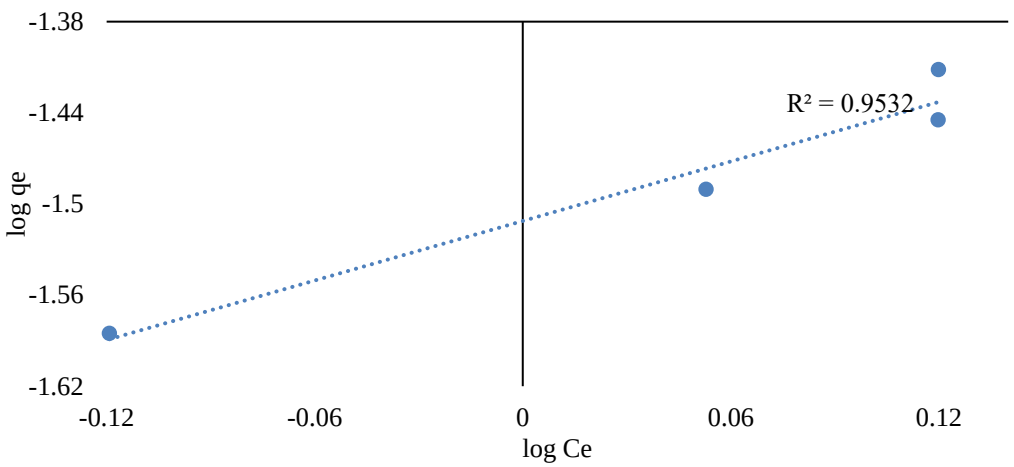

Figure 4.137. Freundlich isotherm graph of KN-AC for ethylbenzene at 3.9 µg/m³.

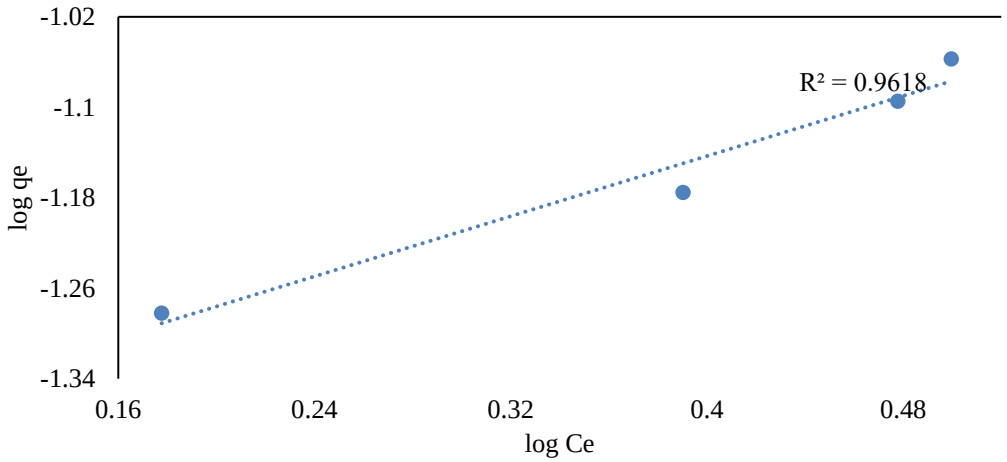

Figure 4.138. Freundlich isotherm graph of KN-AC for ethylbenzene at 9.2 µg/m³.

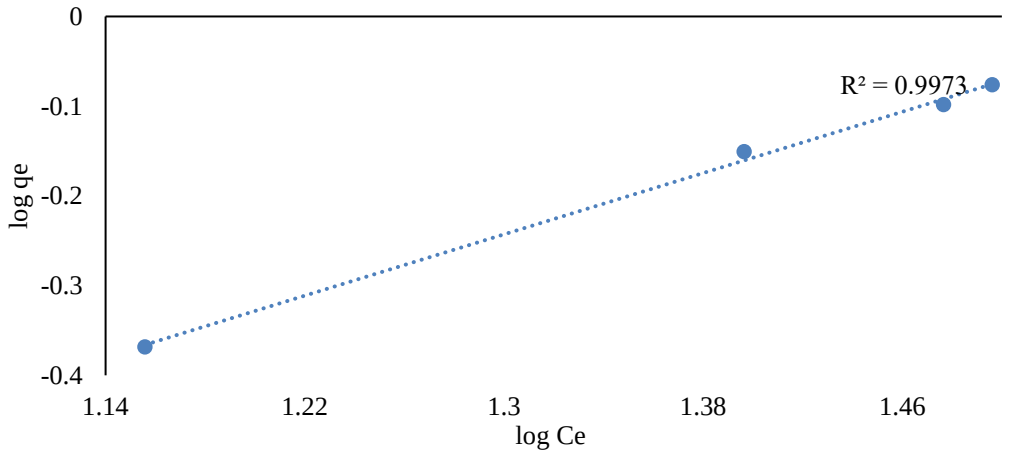

Figure 4.139. Freundlich isotherm graph of KN-AC for ethylbenzene at 90 µg/m³.

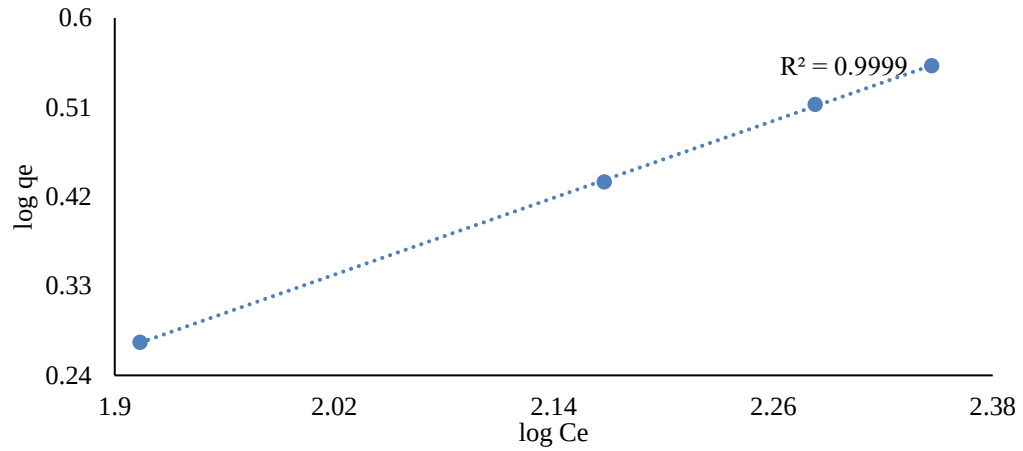

Figure 4.140. Freundlich isotherm graph of KN-AC for ethylbenzene at 430 µg/m³.

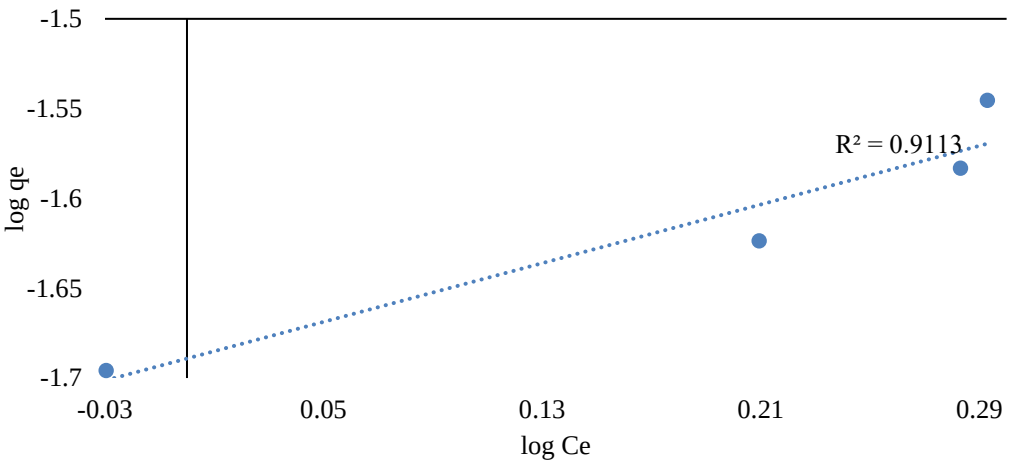

Figure 4.141. Freundlich isotherm graph of COM-AC for m, p-xylene at 3.4 µg/m³.

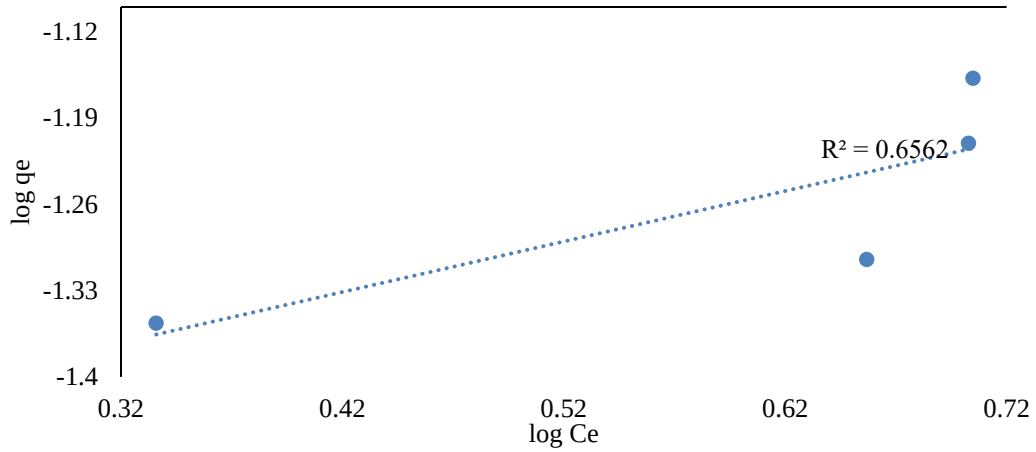

Figure 4.142 Freundlich isotherm graph of COM-AC for m, p-xylene at 8.5 µg/m³.

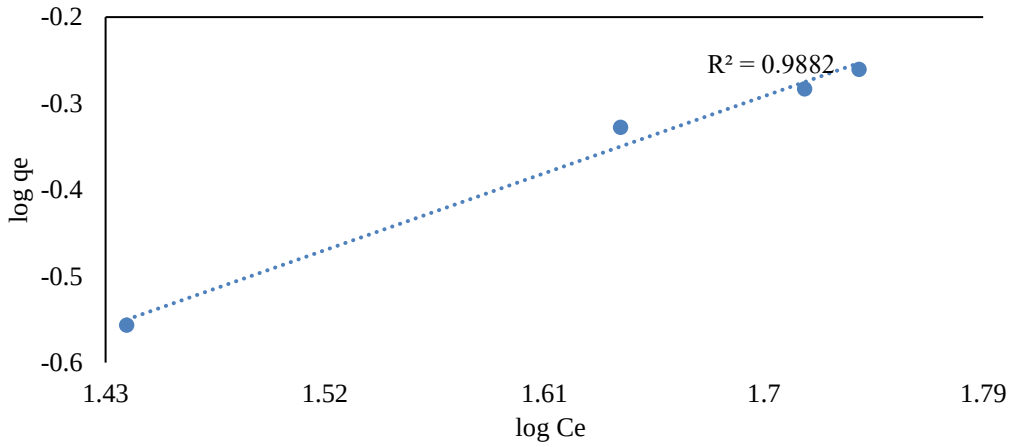

Figure 4.143. Freundlich isotherm graph of COM-AC for m, p-xylene at 83 µg/m³.

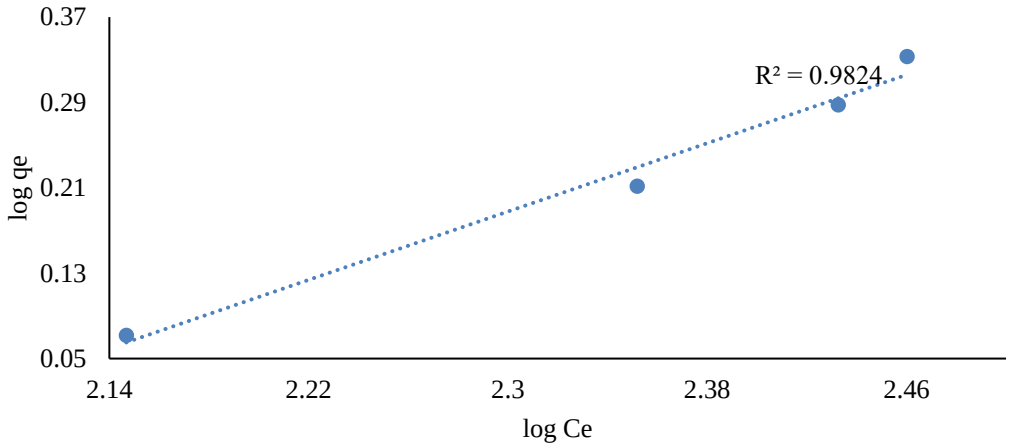

Figure 4.144. Freundlich isotherm graph of COM-AC for m, p-xylene at 397 µg/m³.

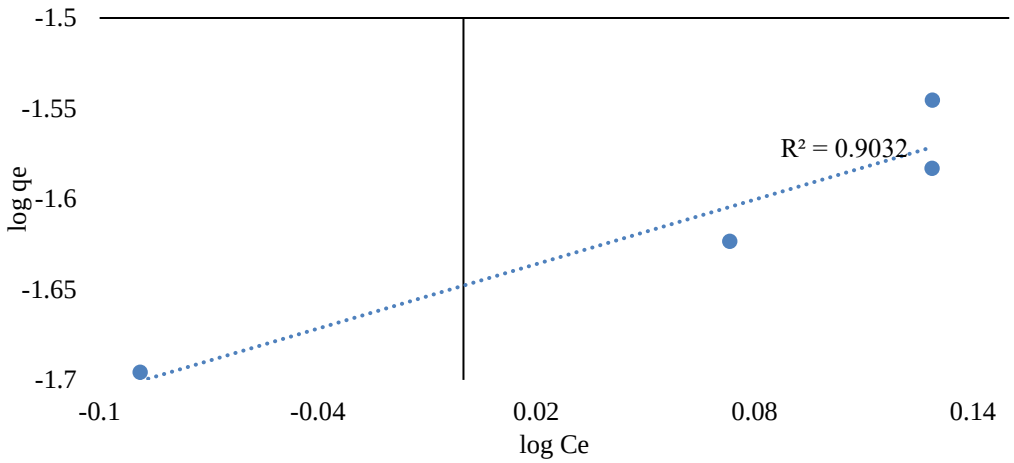

Figure 4.145. Freundlich isotherm graph of KN-AC for m, p-xylene at 3.4 µg/m³.

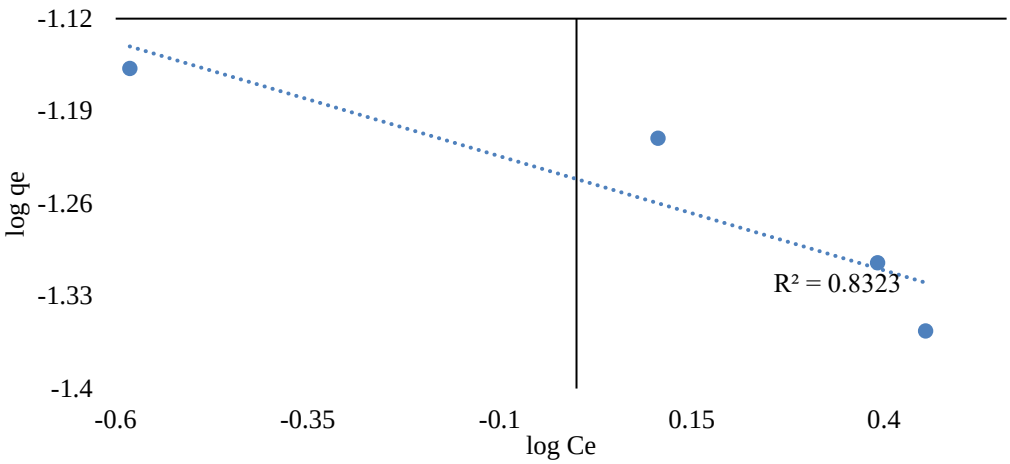

Figure 4.146. Freundlich isotherm graph of KN-AC for m, p-xylene at 8.5 µg/m³.

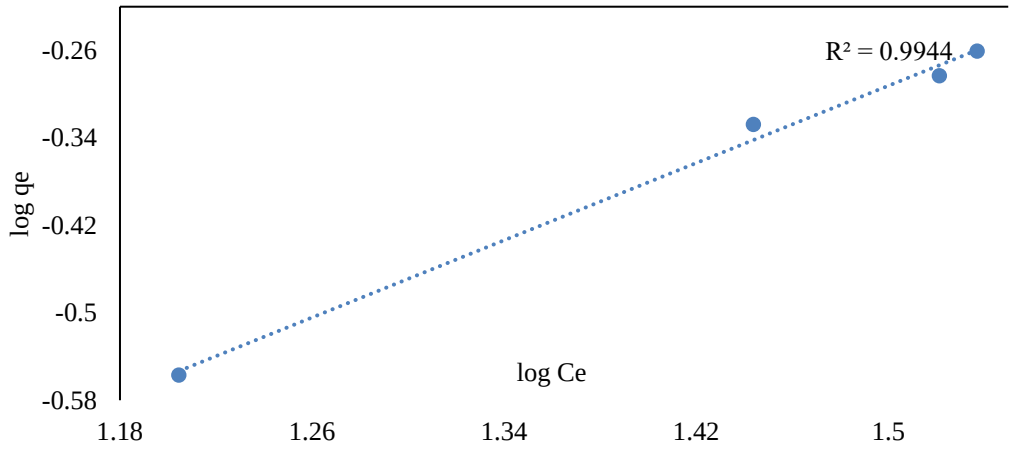

Figure 4.147. Freundlich isotherm graph of KN-AC for m, p-xylene at 83 µg/m³.

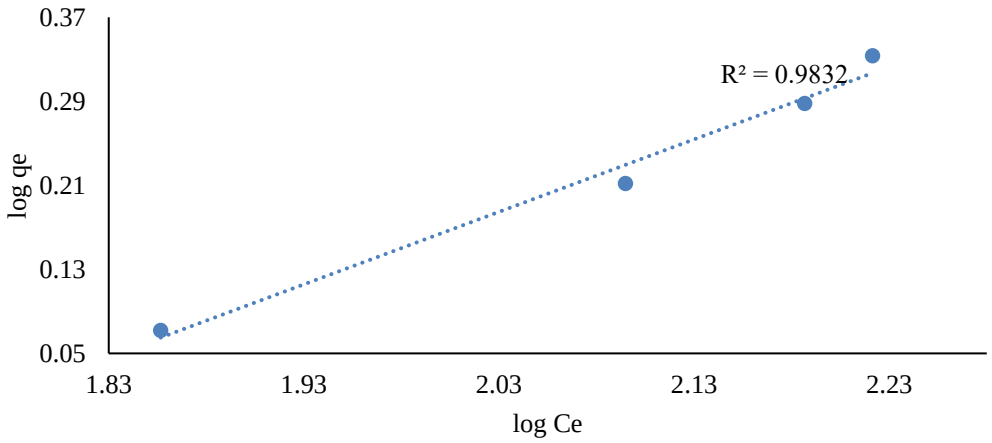

Figure 4.148. Freundlich isotherm graph of KN-AC for m, p-xylene at 397 µg/m³.

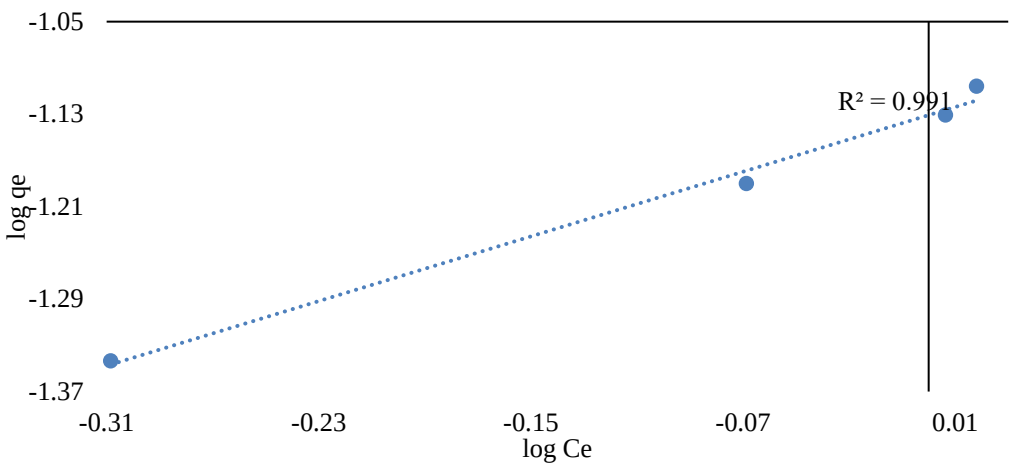

Figure 4.149. Freundlich isotherm graph of COM-AC for o-xylene at 5.2 µg/m³.

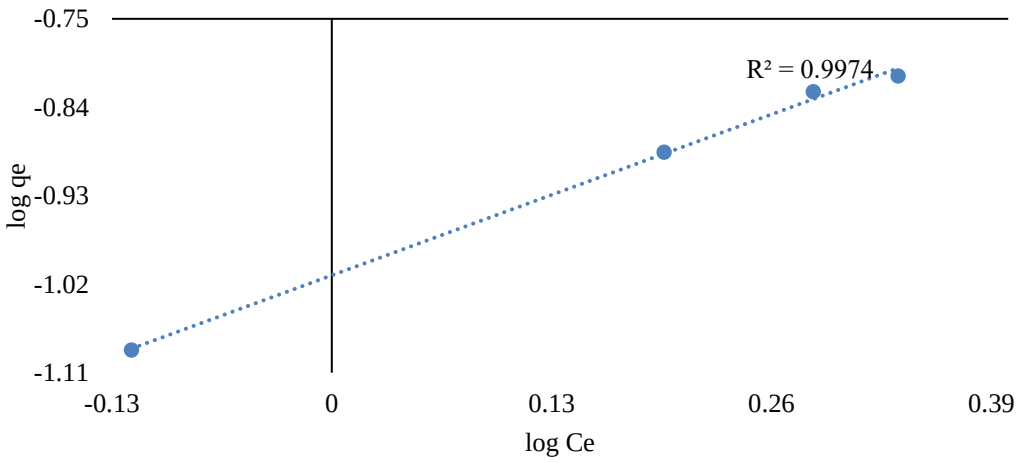

Figure 4.150. Freundlich isotherm graph of COM-AC for o-xylene at 10 µg/m³.

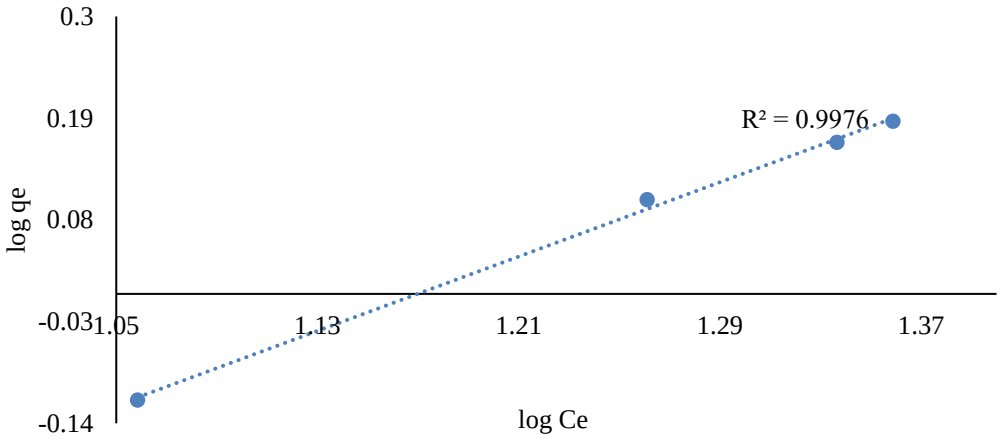

Figure 4.151. Freundlich isotherm graph of COM-AC for o-xylene at 100 µg/m³.

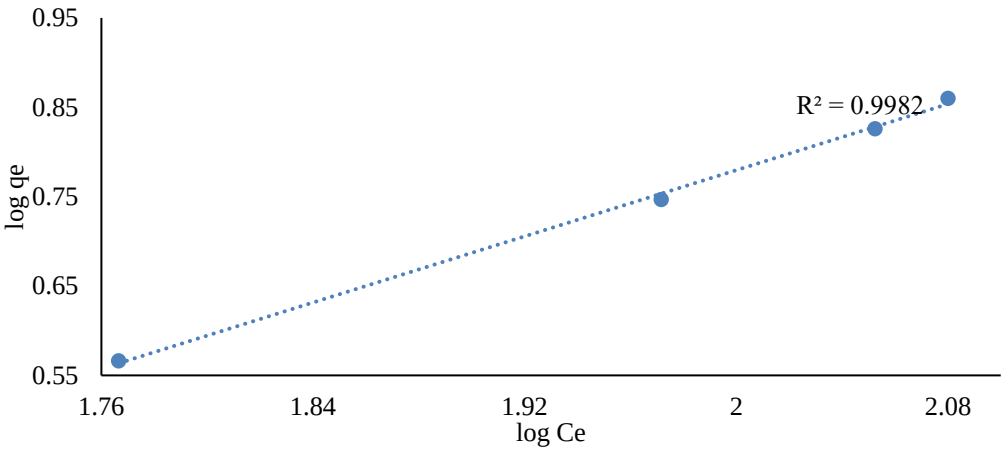

Figure 4.152. Freundlich isotherm graph of COM-AC for o-xylene at 483 µg/m³.

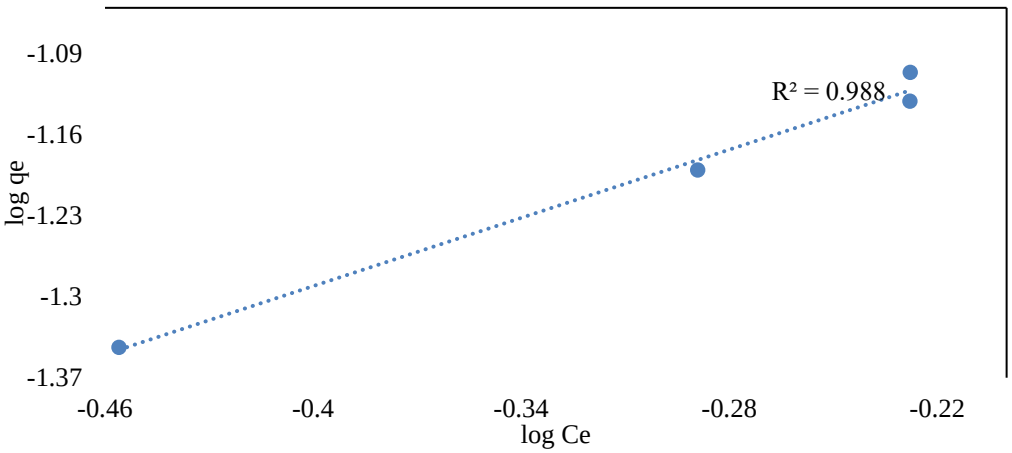

Figure 4.153. Freundlich isotherm graph of KN-AC for o-xylene at 5.2 µg/m³.

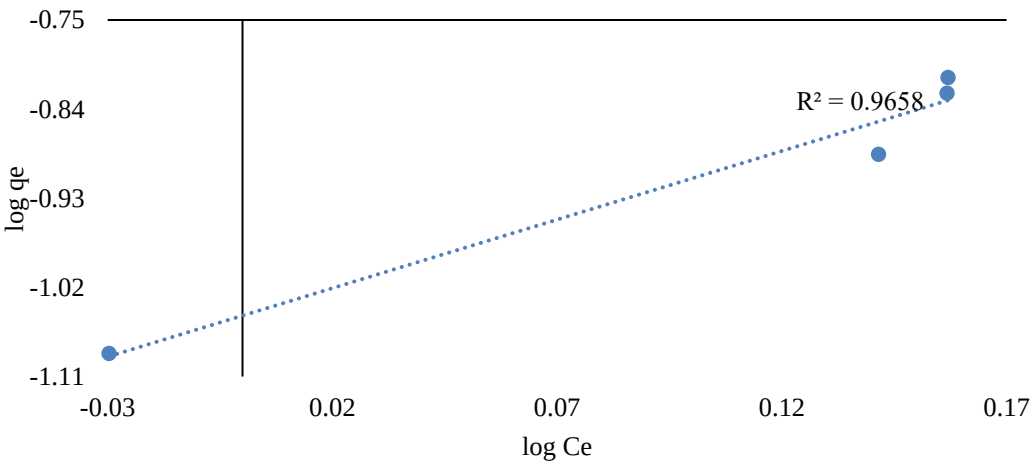

Figure 4.154. Freundlich isotherm graph of KN-AC for o-xylene at 10 µg/m³.

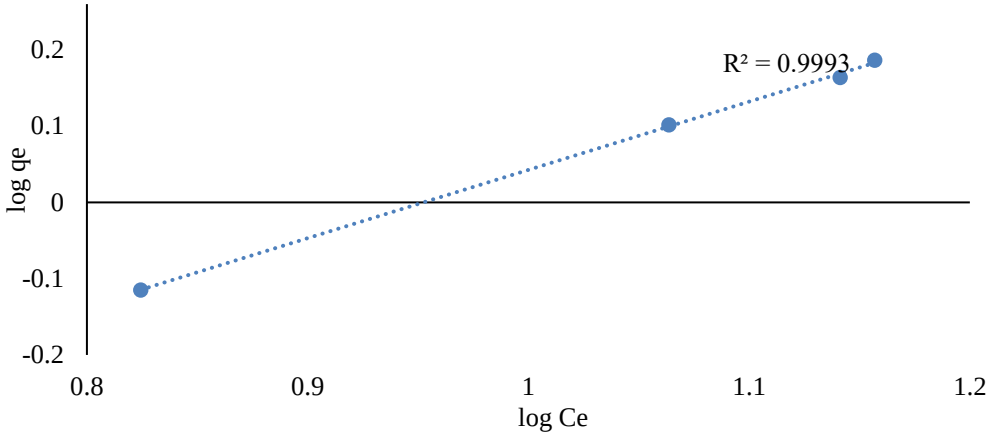

Figure 4.155. Freundlich isotherm graph of KN-AC for o-xylene at 100 µg/m³.

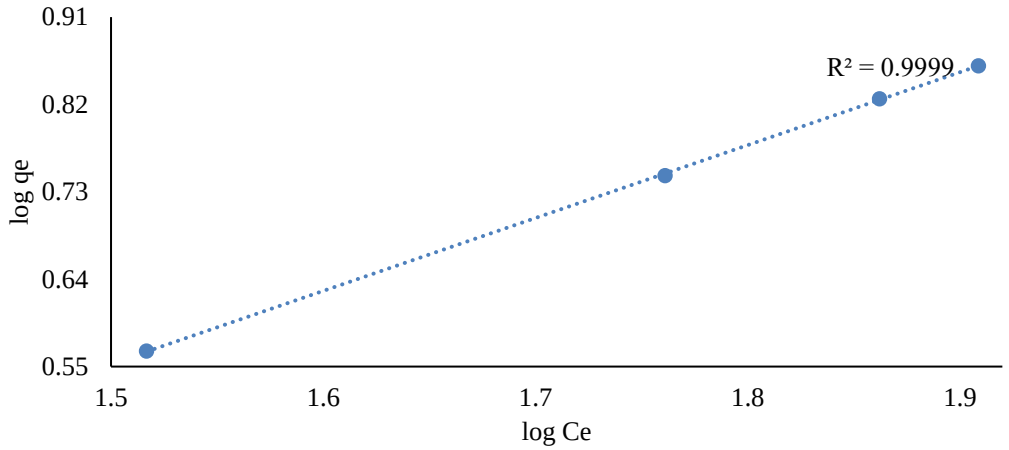

Figure 4.156. Freundlich isotherm graph of KN-AC for o-xylene at 483 µg/m³.

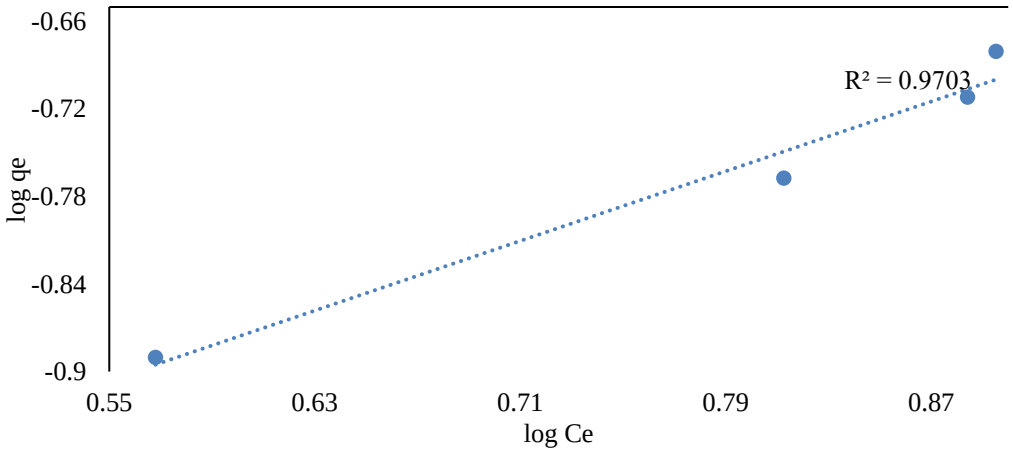

Figure 4.157. Freundlich isotherm graph of COM-AC for BTEX at 18.5 µg/m³.

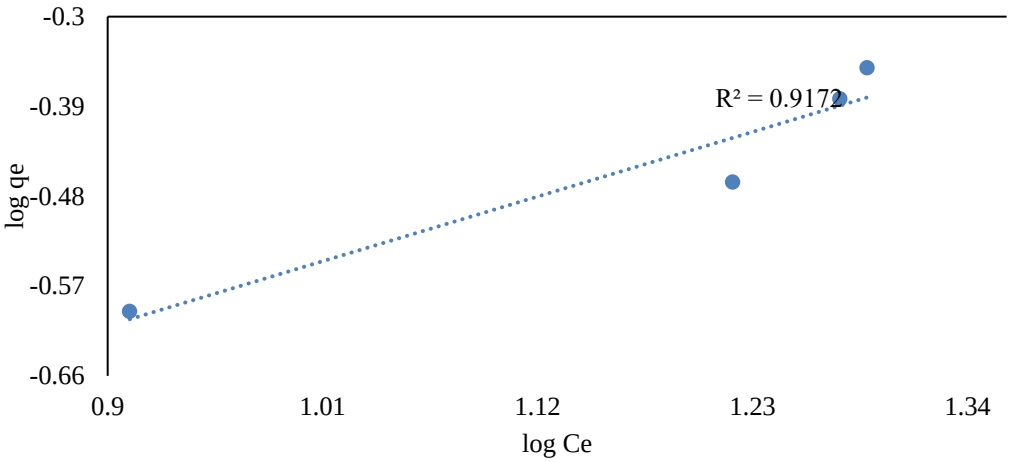

Figure 4.158. Freundlich isotherm graph of COM-AC for BTEX at 42 µg/m³.

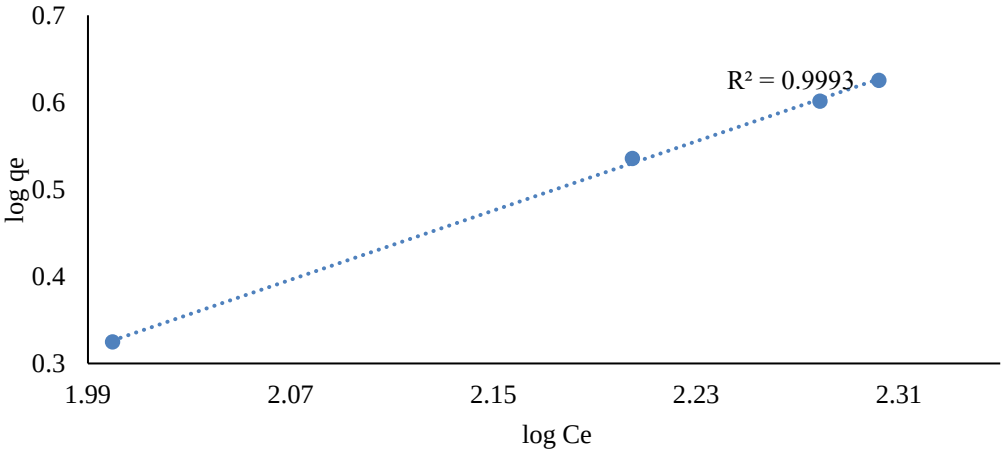

Figure 4.159. Freundlich isotherm graph of COM-AC for BTEX at 412 µg/m³.

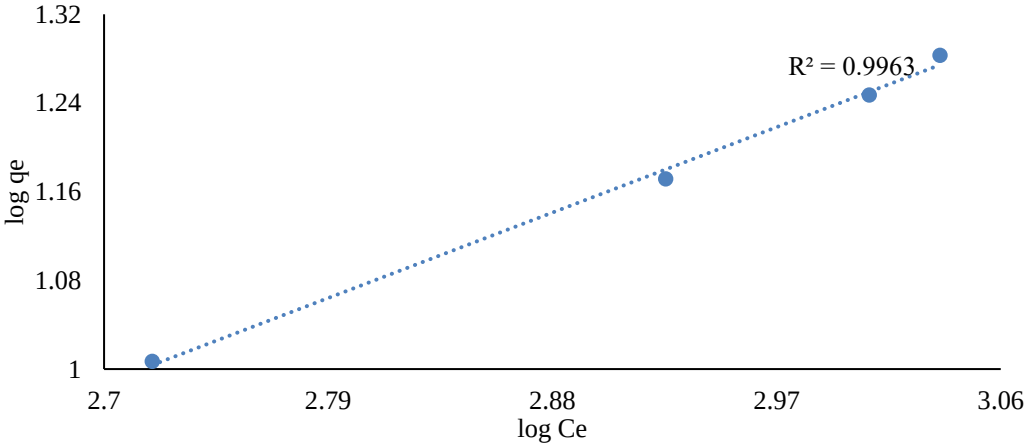

Figure 4.160. Freundlich isotherm graph of COM-AC for BTEX at 2045 µg/m³.

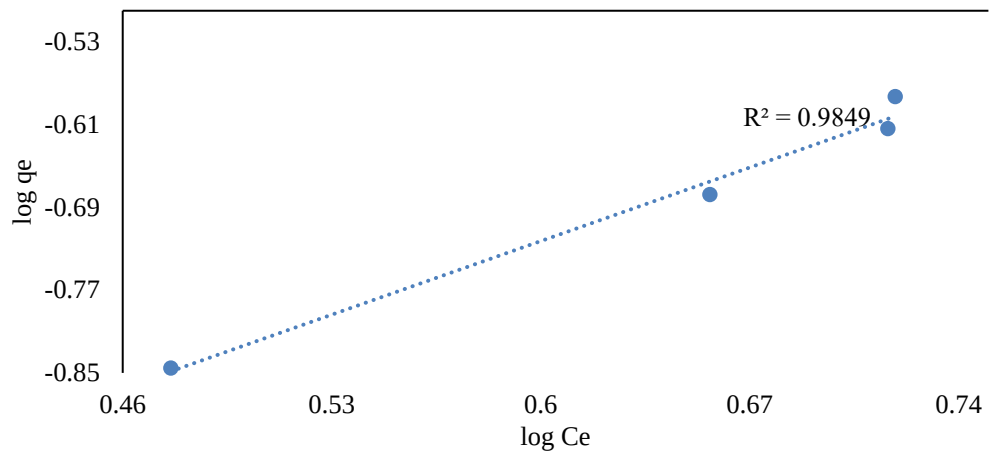

Figure 4.161. Freundlich isotherm graph of KN-AC for BTEX at 18.5 µg/m³.

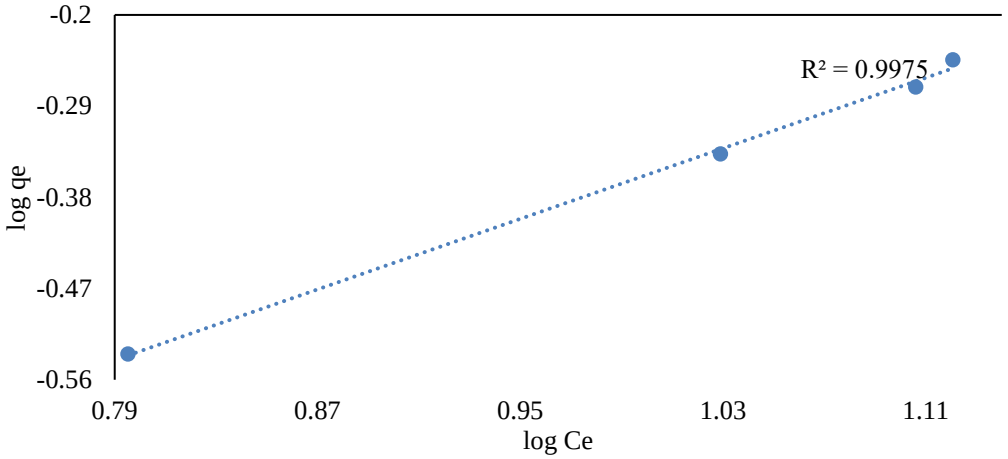

Figure 4.162. Freundlich isotherm graph of KN-AC for BTEX at 42 µg/m³.

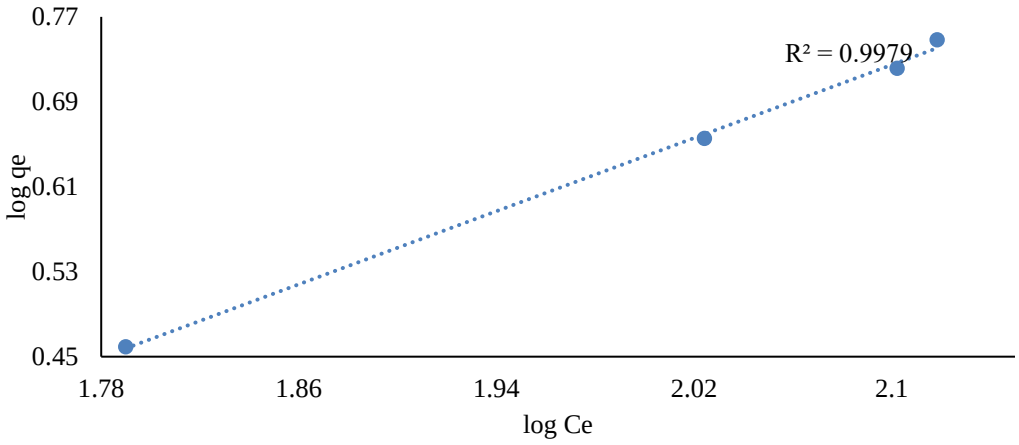

Figure 4.163. Freundlich isotherm graph of KN-AC for BTEX at 412 µg/m³.

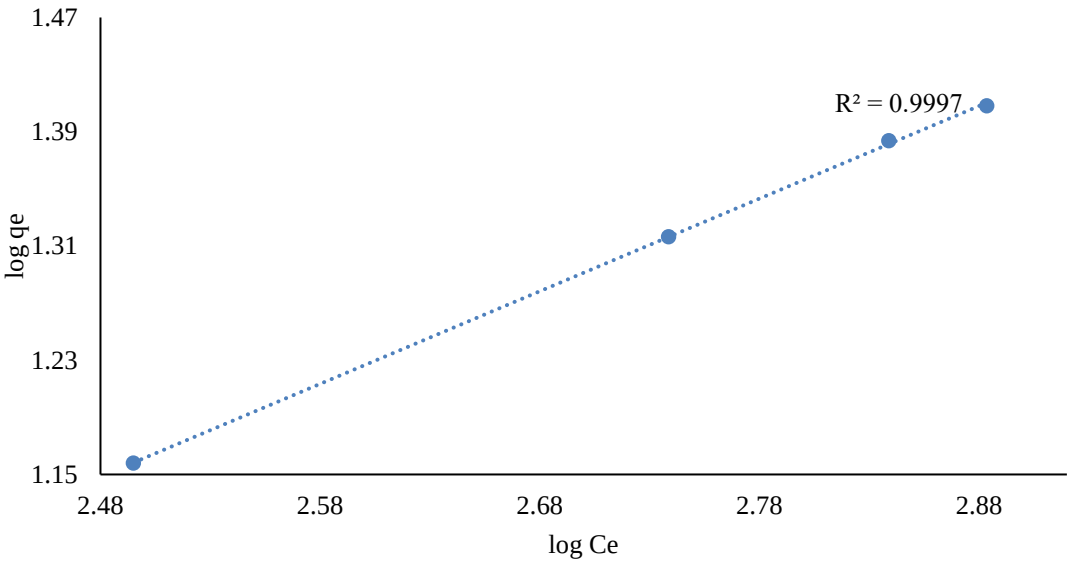

Figure 4.164. Freundlich isotherm graph of KN-AC for BTEX at 2045 µg/m³.

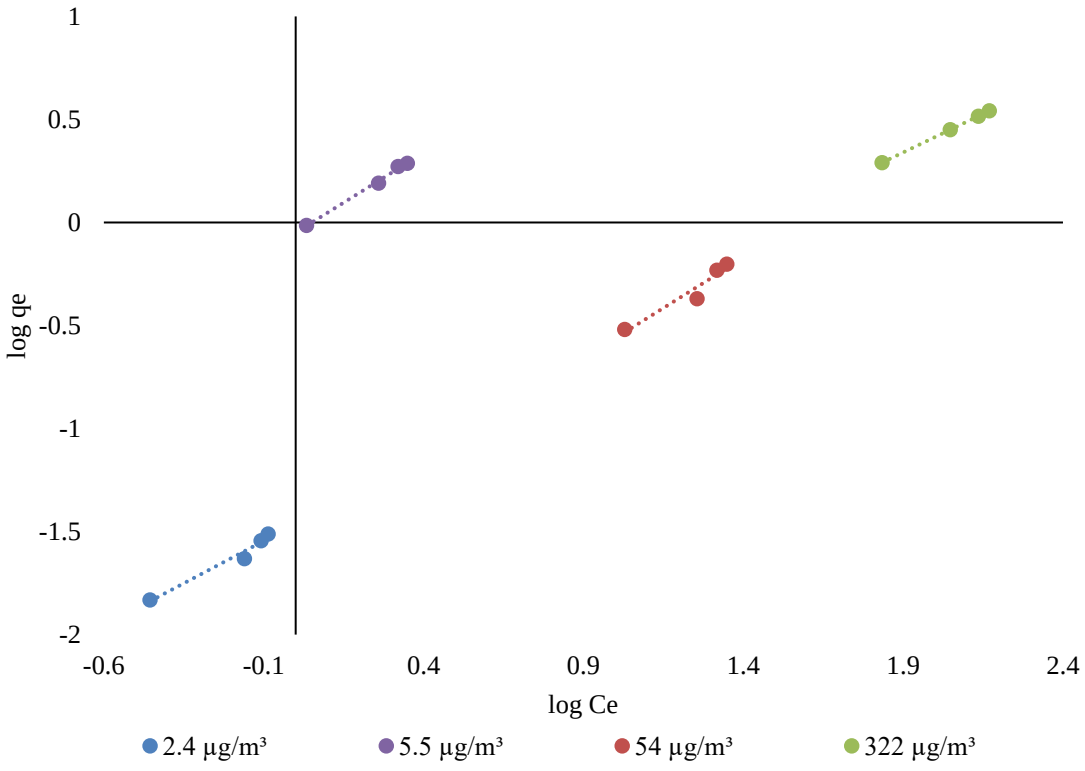

Figure 4.165. Freundlich isotherm graph of COM-AC for all benzene concentrations.

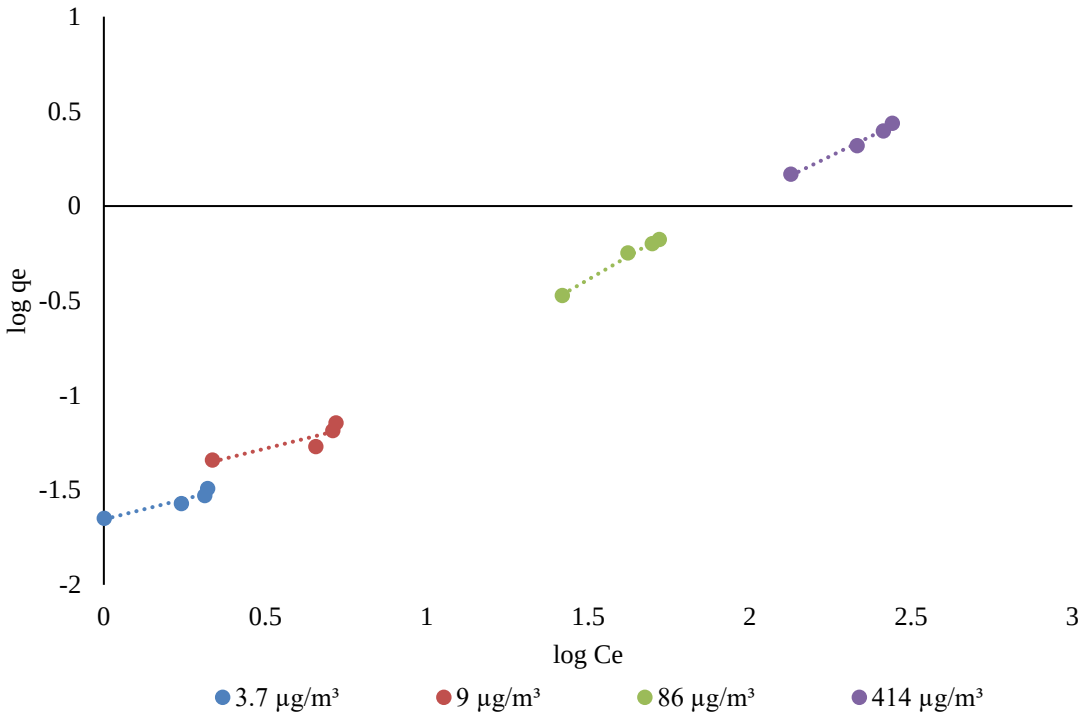

Figure 4.166. Freundlich isotherm graph of COM-AC for all toluene concentrations.

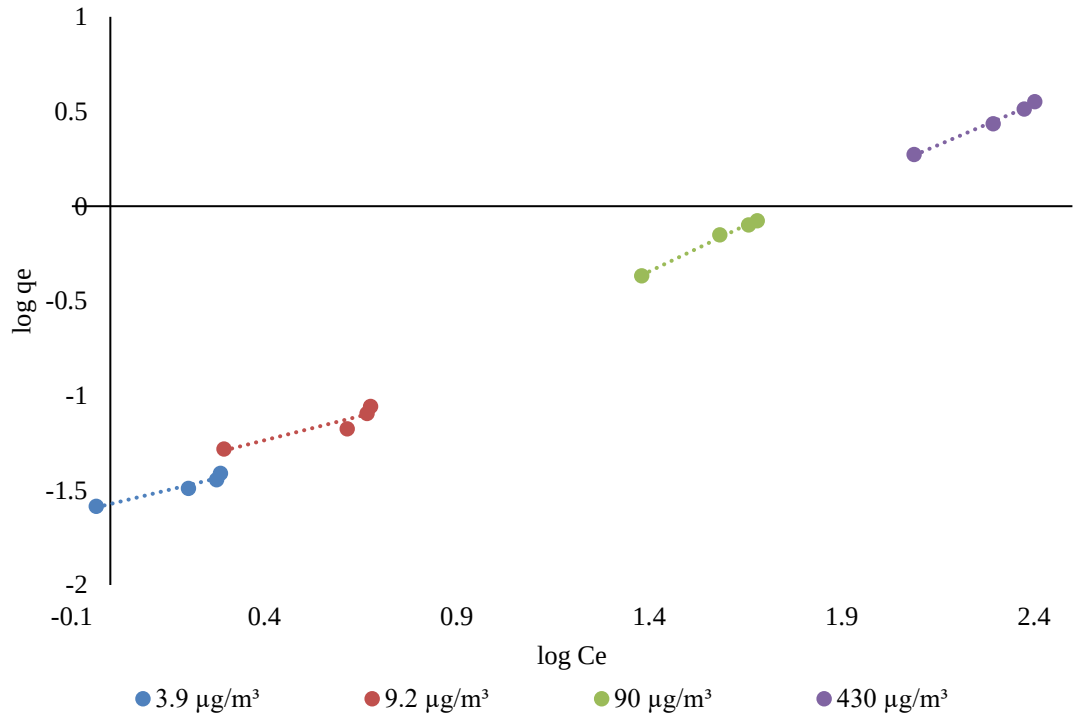

Figure 4.167. Freundlich isotherm graph of COM-AC for all ethylbenzene concentrations.

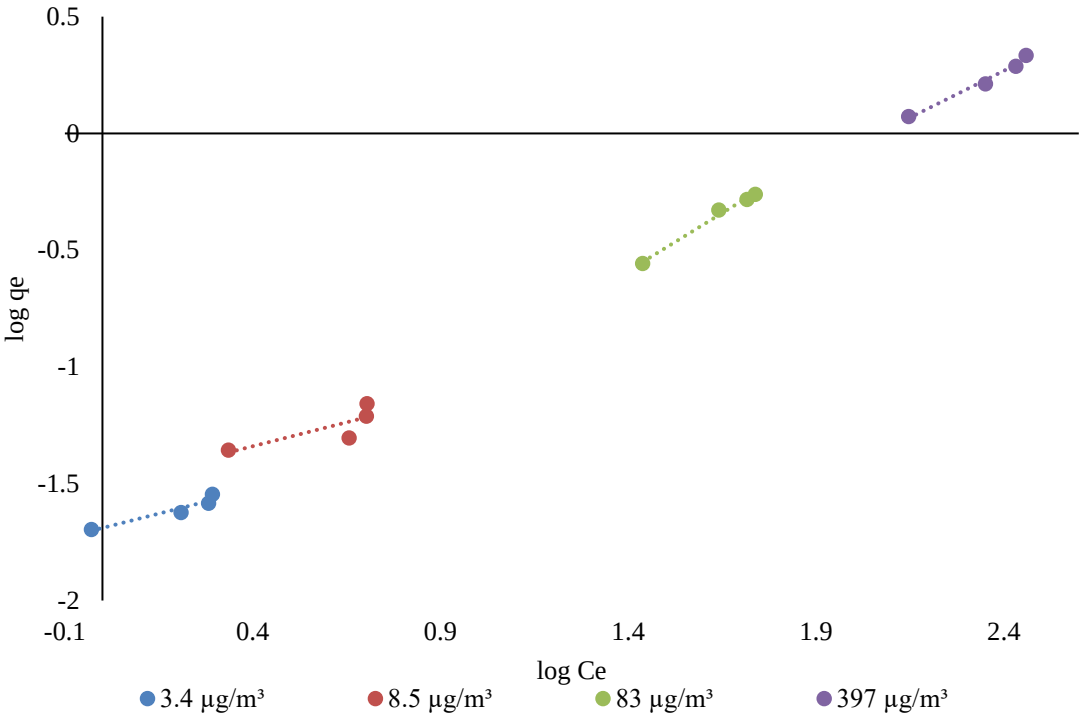

Figure 4.168. Freundlich isotherm graph of COM-AC for all m, p-xylene concentrations.

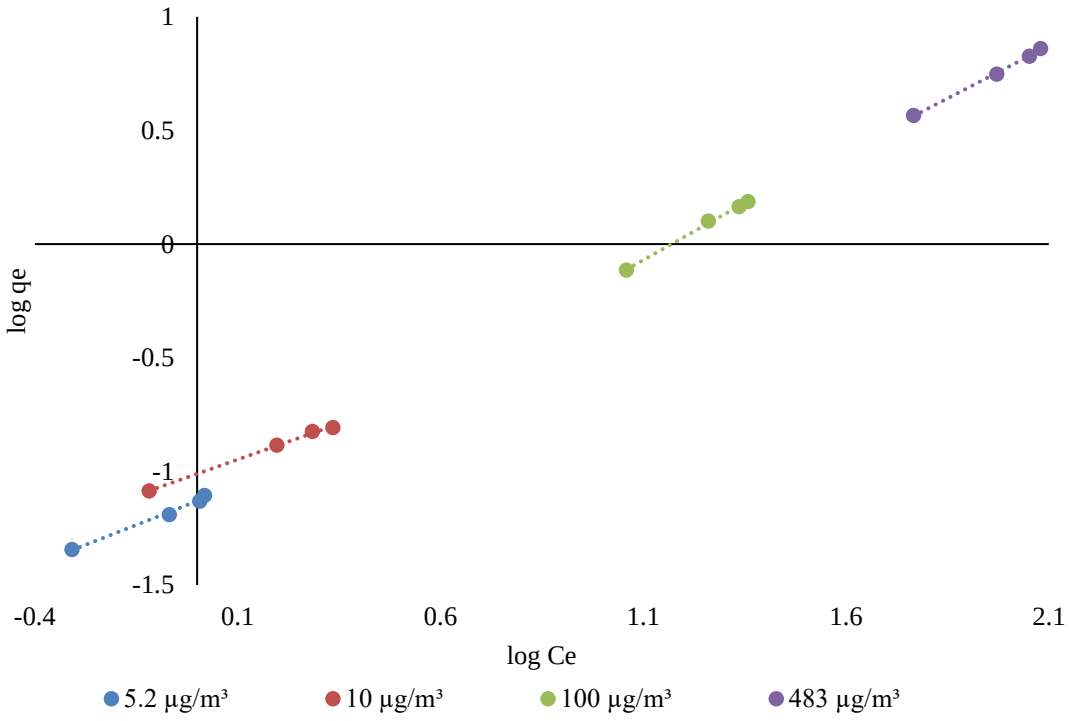

Figure 4.169. Freundlich isotherm graph of COM-AC for all o-xylene concentrations.

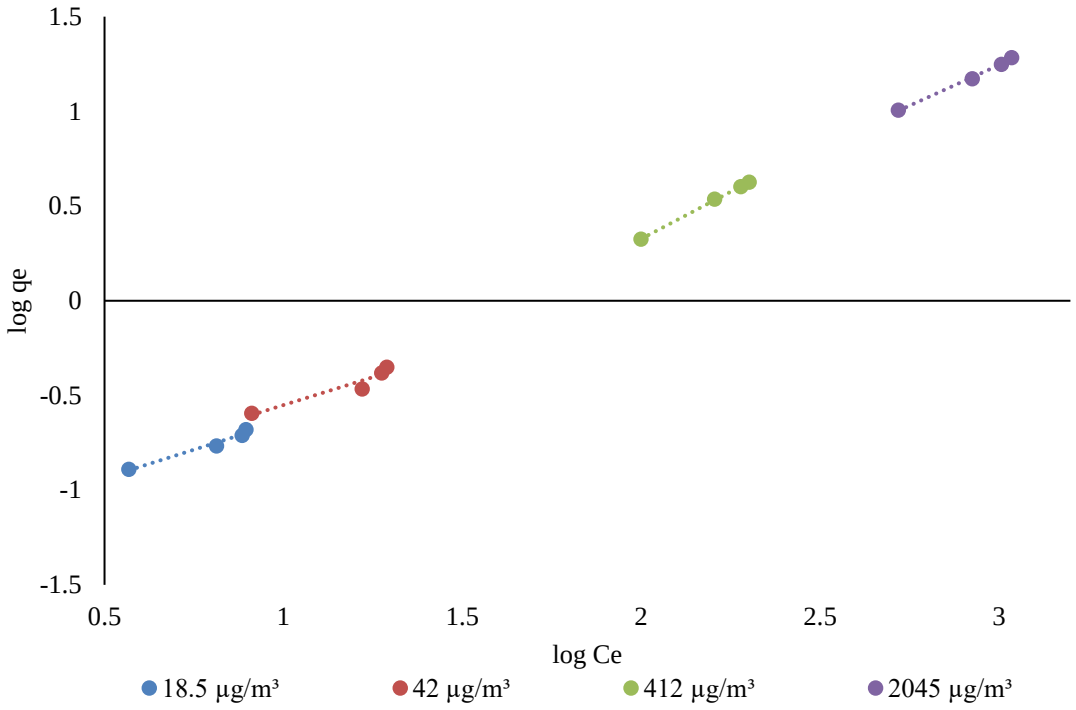

Figure 4.170. Freundlich isotherm graph of COM-AC for all BTEX concentrations.

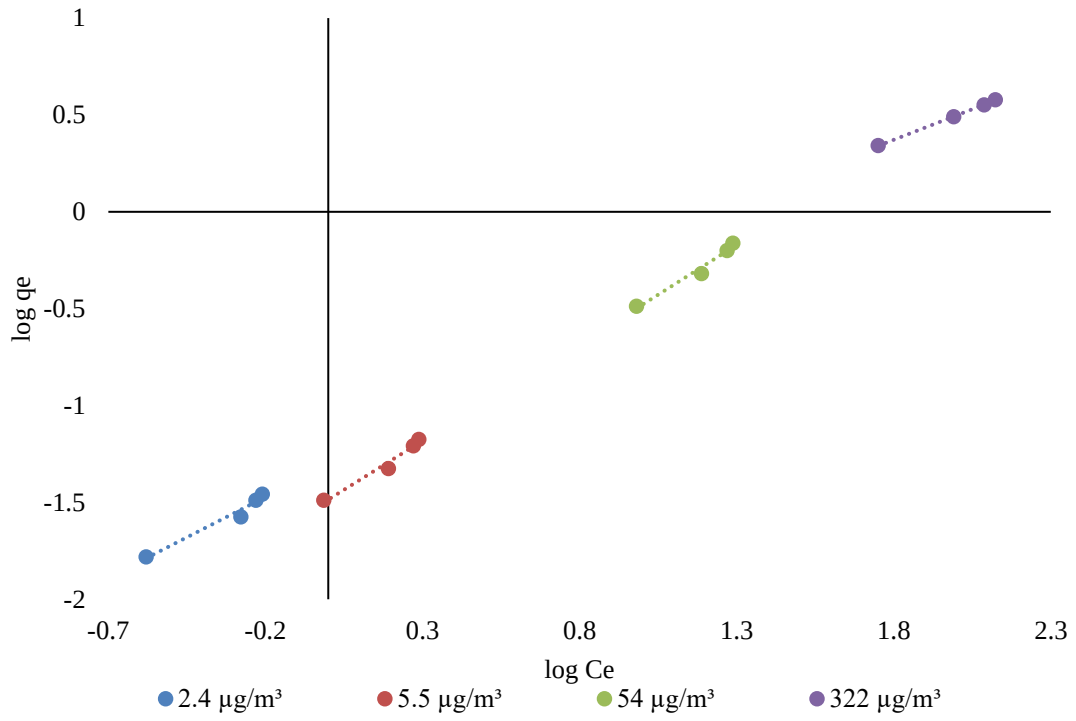

Figure 4.171. Freundlich isotherm graph of KN-AC for all benzene concentrations.

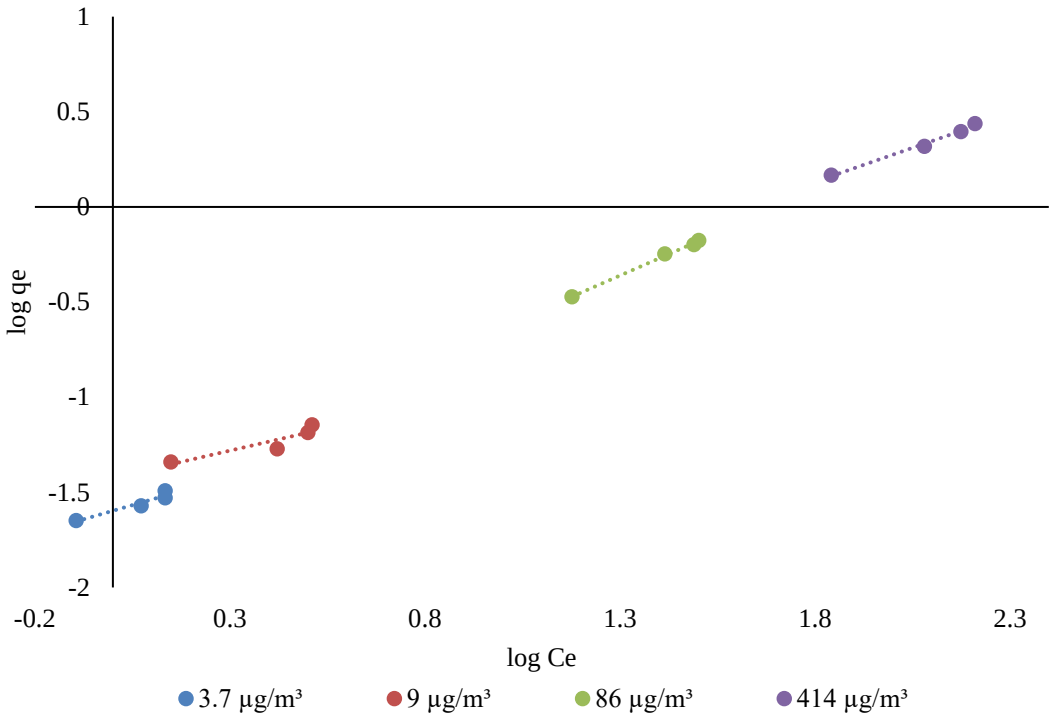

Figure 4.172. Freundlich isotherm graph of KN-AC for all toluene concentrations.

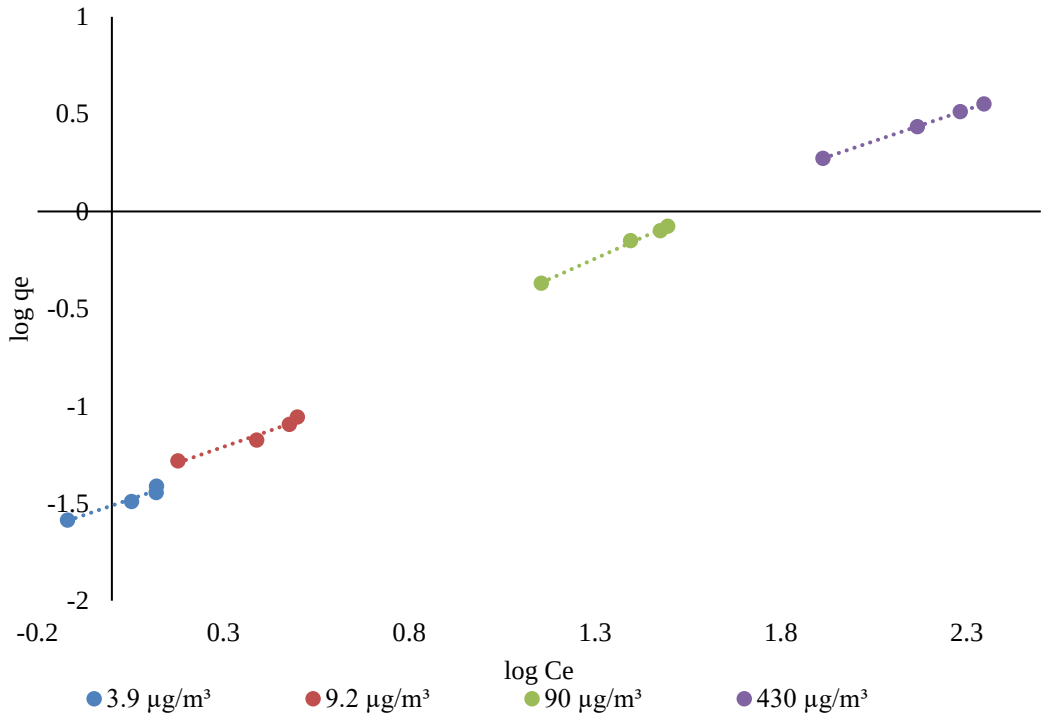

Figure 4.173. Freundlich isotherm graph of KN-AC for all ethylbenzene concentrations.

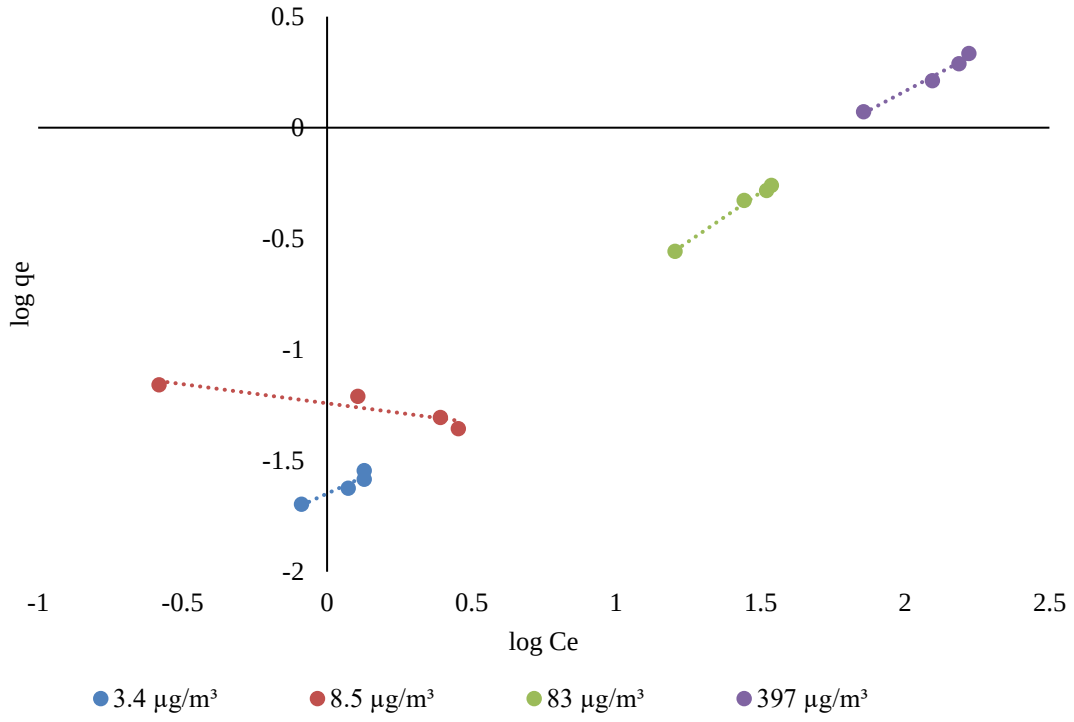

Figure 4.174. Freundlich isotherm graph of KN-AC for all m, p-xylene concentrations.

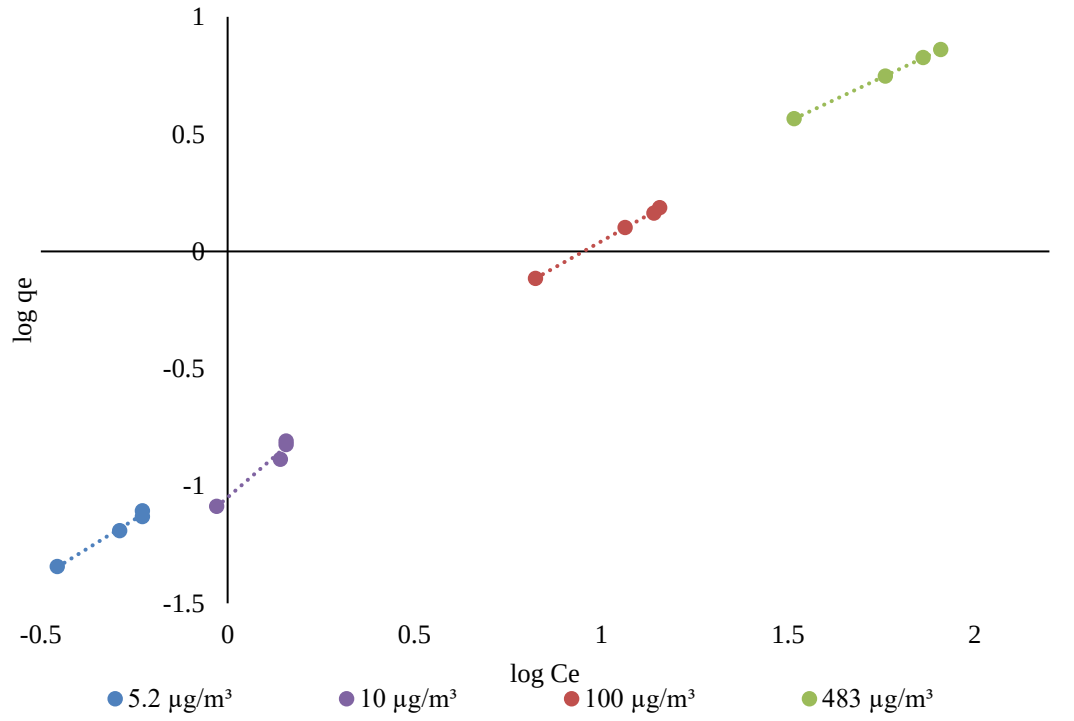

Figure 4.175. Freundlich isotherm graph of KN-AC for all o-xylene concentrations.

According to Freundlich's charts isotherm was plotted for COM-AC and KN-AC, the linearized graph shows its suitability for all concentrations between Figure 4.166 and Figure 4.185.

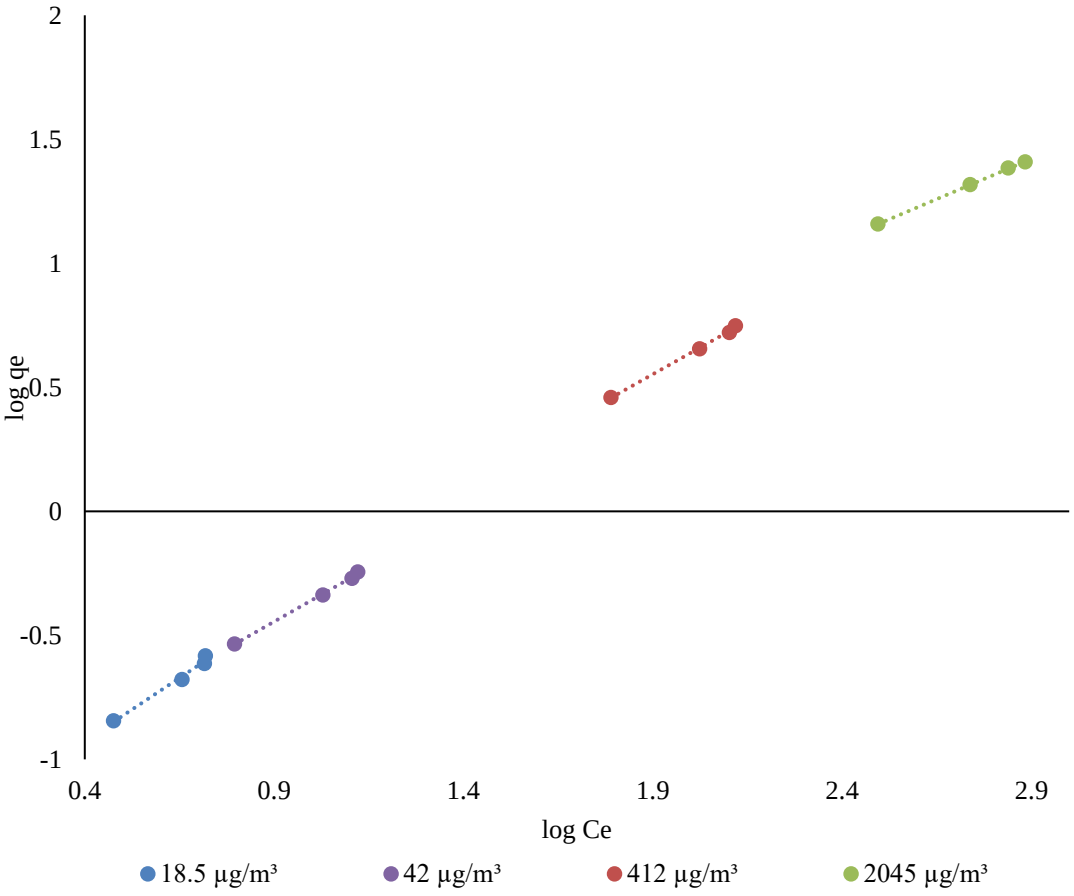

Figure 4.176. Freundlich isotherm graph of KN-AC for all BTEX concentrations.

The Freundlich parameters obtained from the Freundlich graph plotted for COM-AC were givenin Table 4.16. Accordingly, when the R^2 values for benzene were compared between their concentration values, the highest value for R^2 values is 0.9999 at 322±47.80 µg/m^3. These values 0.9912 in toluene at 86 µg/m^3, R^2 value is 0.9939 with 90±15.55 µg/m^3 in ethylbenzene, it is 0.9882 at 83±12.95 µg/m^3 with m, p xylene, it is 0.9982 at 483±102.67 µg/m^3 with o-xylene, and with BTEX 0.9993 was found with 412 µg/m^3.

Table 4.16. Parameters of Freundlich isotherm for BTEX of COM-AC.

Gases	Average and SD of C_0 (μg/m³)	K_F	n	R^2	q_{max} (μg/g)
Benzene	2.4±0.45	0.04	1.22	0.9679	0.10
	5.5±1.09	0.90	1.04	0.9961	6.33
	54±10.73	0.03	1.04	0.9322	1.95
	322±47.80	0.09	1.34	0.9999	11.54
Toluene	3.7±0.58	0.03	2.34	0.9151	0.11
	9±2.62	0.04	2.36	0.7748	0.24
	86±15.83	0.02	1.01	0.9912	2.20
	414±47.26	0.03	1.20	0.9890	8.78
Ethylbenzene	3.9±0.66	0.03	2.05	0.9525	0.13
	9.2±1.59	0.04	1.95	0.8673	0.29
	90±15.55	0.02	1.03	0.9939	2.77
	430±46.64	0.03	1.16	0.9934	11.42
M.p-xylene	3.4±0.72	0.02	2.45	0.9113	0.10
	8.5±1.32	0.04	2.45	0.6562	0.22
	83±12.95	0.02	1.02	0.9882	1.82
	397±82.10	0.03	1.25	0.9824	6.90
O-xylene	5.2±0.82	0.08	1.43	0.9910	0.26
	10±2.49	0.10	1.59	0.9974	0.52
	100±24.38	0.07	1.01	0.9976	5.03
	483±102.67	0.09	1.09	0.9982	23.21
BTEX	18.5±1.89	0.06	1.68	0.9703	0.70
	42±4.97	0.08	1.70	0.9172	1.46
	412±48.74	0.03	1.08	0.9993	13.76

	2045±203.37	0.05	1.17	0.9963	61.84

The Freundlich parameters obtained from the Freundlich graph plotted for KN-AC were givenin Table 4.17. Accordingly, when the R^2 values for benzene were compared between their concentration values, the highest value for R^2 values is 0.9997 at 322±47.80 μg/m^3. These values 0.9967 in toluene at 86±15.83 μg/m^3, R^2 value is 0.9999 with 430±46.64 μg/m^3 in ethylbenzene, it is 0.9944 at 83±12.95 μg/m^3 with m, p-xylene, it is 0.9999 at 483±102.67 μg/m^3 with o-xylene, and with BTEX 0.9997 was found with 2045±203.37 μg/m^3.

Table 4.17. Parameters of Freundlich isotherm for BTEX of KN-AC.

Gases	Average and SD of C_0 (μg/m³)	K_F	n	R^2	q_{max} (μg/g)
Benzene	2.4±0.45	0.05	1.21	0.9689	0.11
	5.5±1.09	0.04	0.99	0.9729	0.21
	54±10.73	0.04	0.98	0.9736	2.12
	322±47.80	0.18	1.59	0.9997	12.63
Toluene	3.7±0.58	0.03	1.69	0.9139	0.11
	9±2.62	0.04	2.11	0.8397	0.24
	86±15.83	0.03	1.12	0.9967	2.20
	414±47.26	0.08	1.40	0.9904	8.78
Ethylbenzene	3.9±0.66	0.04	1.54	0.9532	0.13
	9.2±1.59	0.04	1.51	0.9618	0.29
	90±15.55	0.05	1.18	0.9973	2.77
	430±46.64	0.12	1.55	0.9999	11.42
M, p-xylene	3.4±0.72	0.03	1.69	0.9032	0.10
	8.5±1.32	0.06	1.24	0.8323	0.22

	83±12.95	0.03	1.14	0.9944	1.82
	397±82.10	0.07	1.45	0.9832	6.90
O-xylene	5.2±0.82	0.13	1.02	0.9880	0.26
	10±2.49	0.09	1.64	0.9658	0.52
	100±24.38	0.15	1.12	0.9993	5.03
	483±102.67	0.27	1.34	0.9999	23.21
BTEX	18.5±1.89	0.05	0.98	0.9849	0.86
	42±4.97	0.06	1.15	0.9975	1.86
	412±48.74	0.09	1.16	0.9979	18.27
	2045±203.37	0.35	1.54	0.9997	84.90

4.3.1.2. Langmuir Isotherm Modelling of BTEX

The graph were created to determine Langmuir isotherm for BTEX removal in between Figure 4.177 and Figure 4.236.

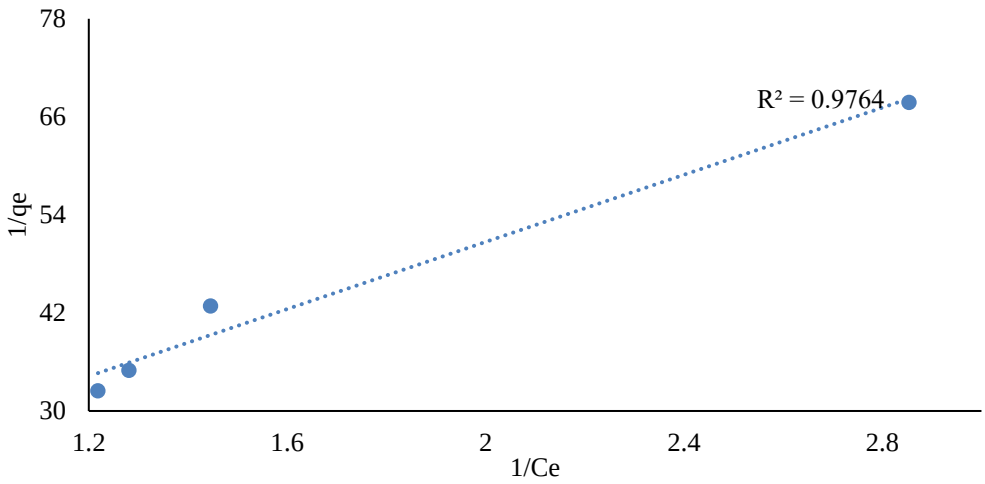

Figure 4.177. Langmuir isotherm graph of COM-AC for benzene at 2.4 µg/m³.

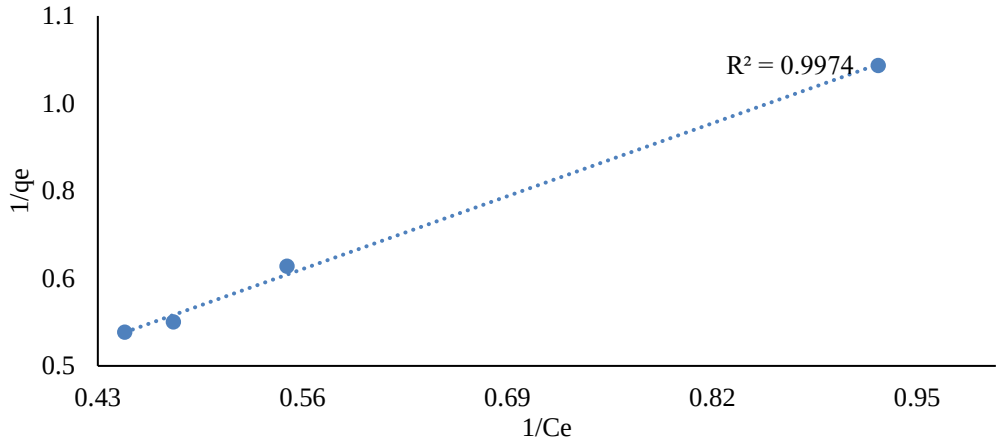

Figure 4.178. Langmuir isotherm graph of COM-AC for benzene at 5.5 µg/m³.

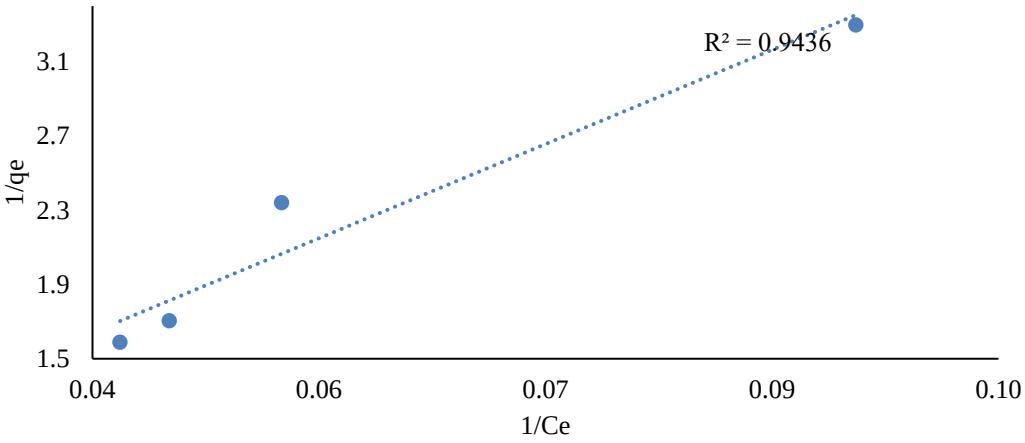

Figure 4.179. Langmuir isotherm graph of COM-AC for benzene at 54 µg/m³.

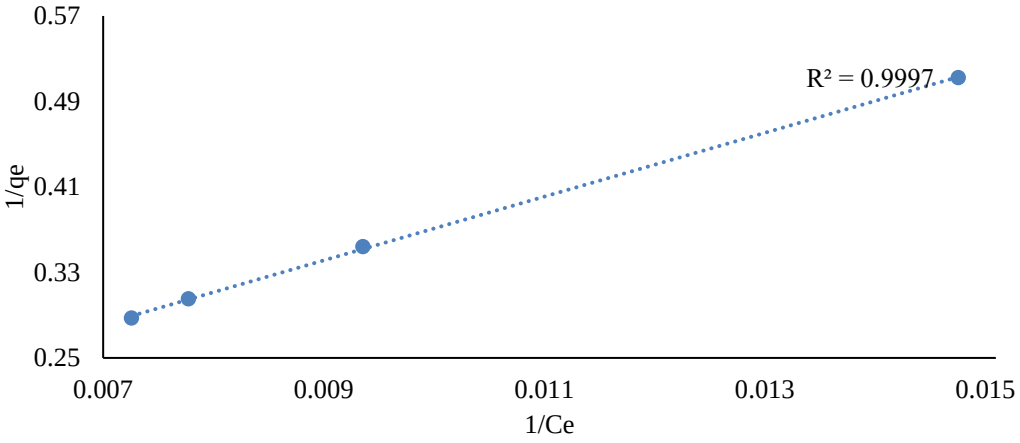

Figure 4.180. Langmuir isotherm graph of COM-AC for benzene at 322 µg/m³.

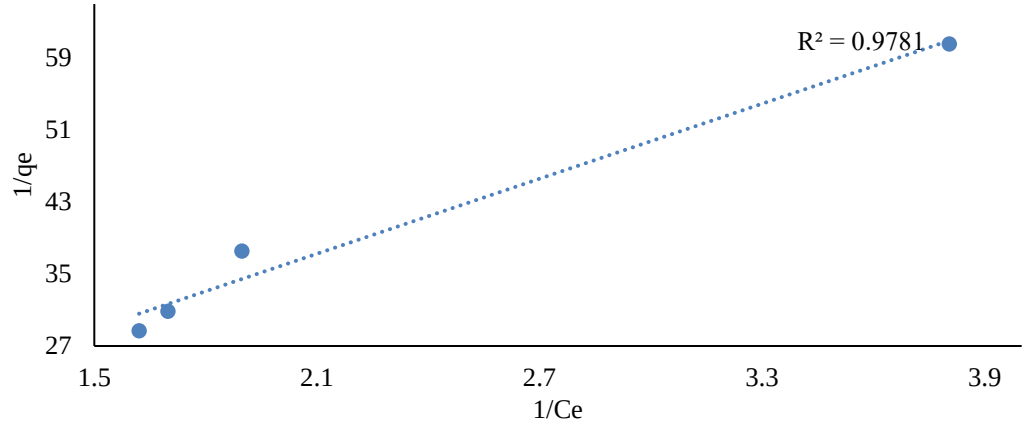

Figure 4.181. Langmuir isotherm graph of KN-AC for benzene at 2.4 µg/m³.

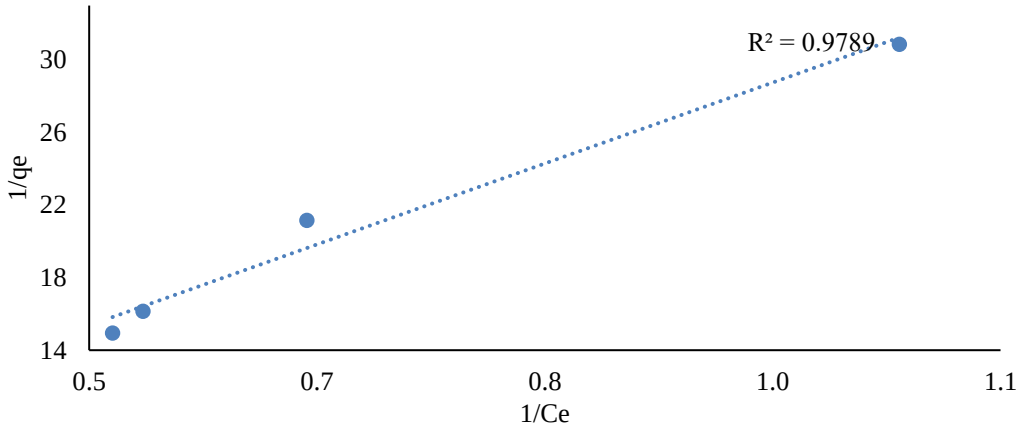

Figure 4.182. Langmuir isotherm graph of KN-AC for benzene at 5.5 µg/m³.

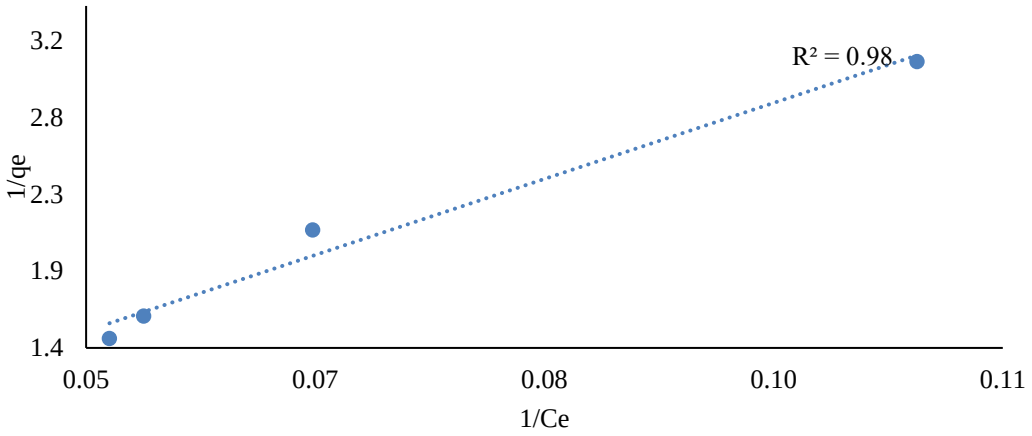

Figure 4.183. Langmuir isotherm graph of KN-AC for benzene at 54 µg/m³.

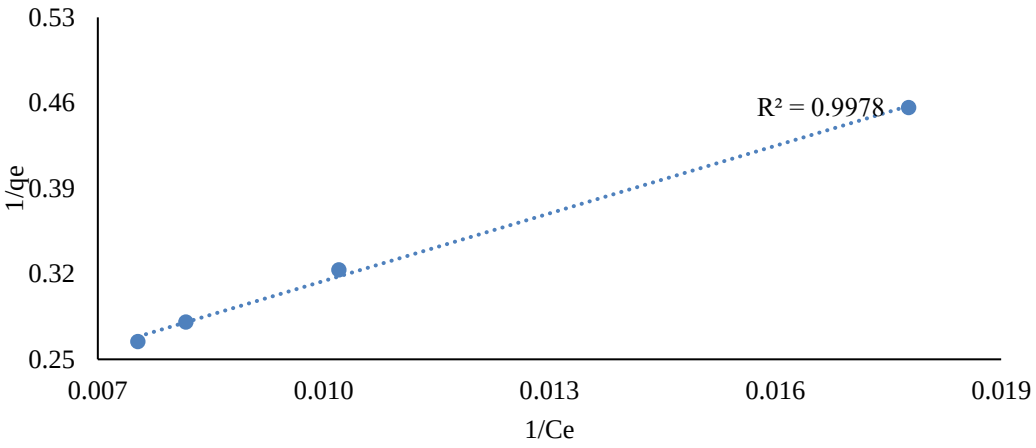

Figure 4.184. Langmuir isotherm graph of KN-AC for benzene at 322 µg/m³.

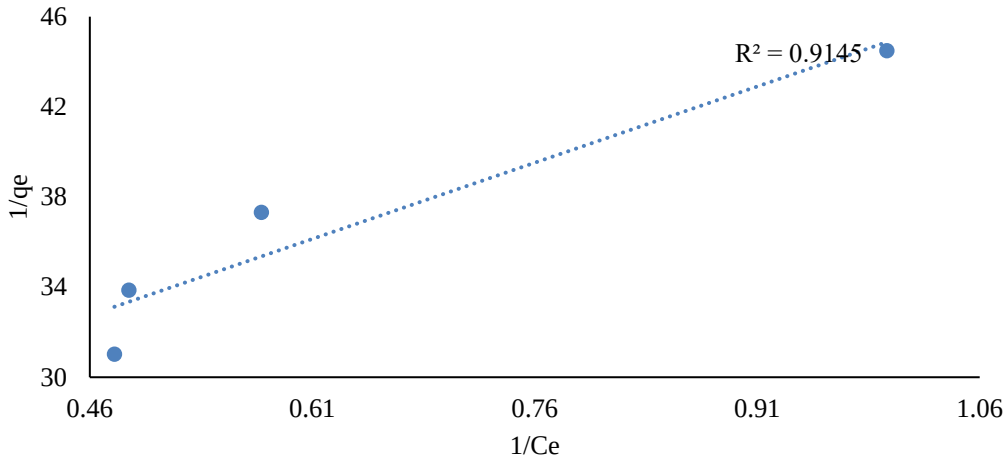

Figure 4.185. Langmuir isotherm graph of COM-AC for toluene at 3.7 µg/m³.

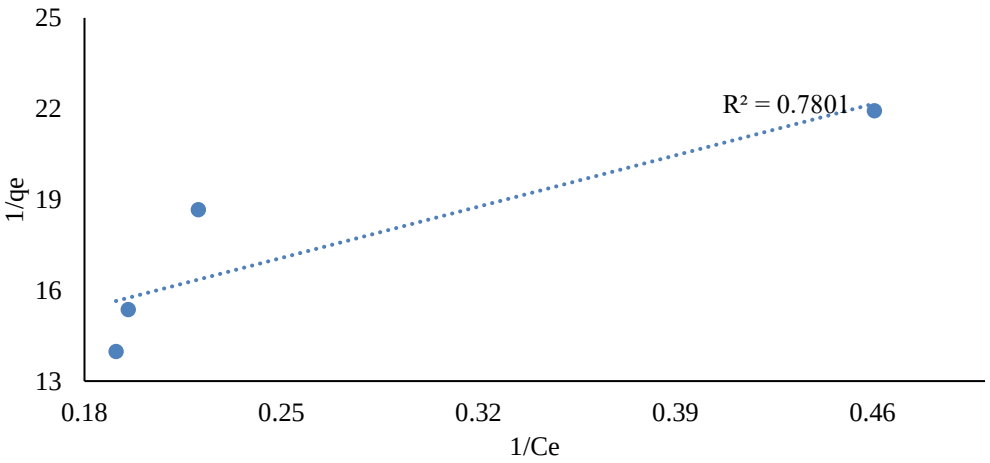

Figure 4.186. Langmuir isotherm graph of COM-AC for toluene at 9 µg/m³.

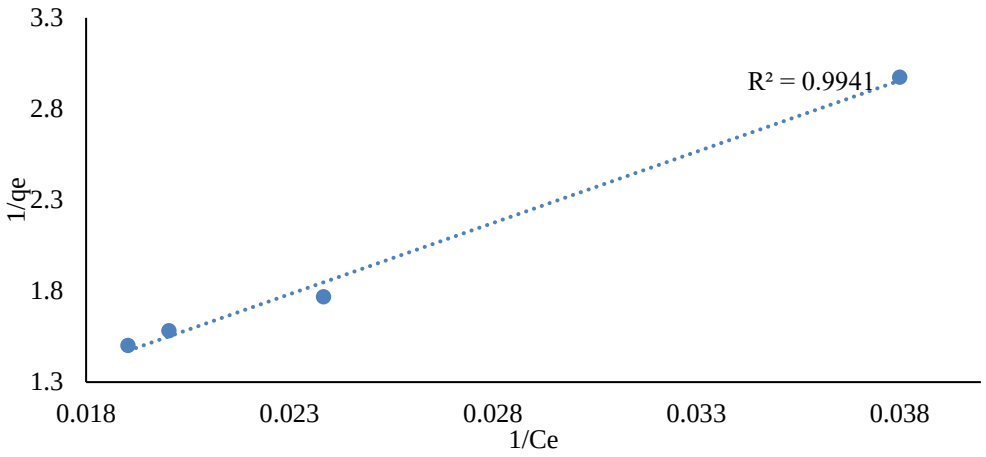

Figure 4.187. Langmuir isotherm graph of COM-AC for toluene at 86 µg/m³.

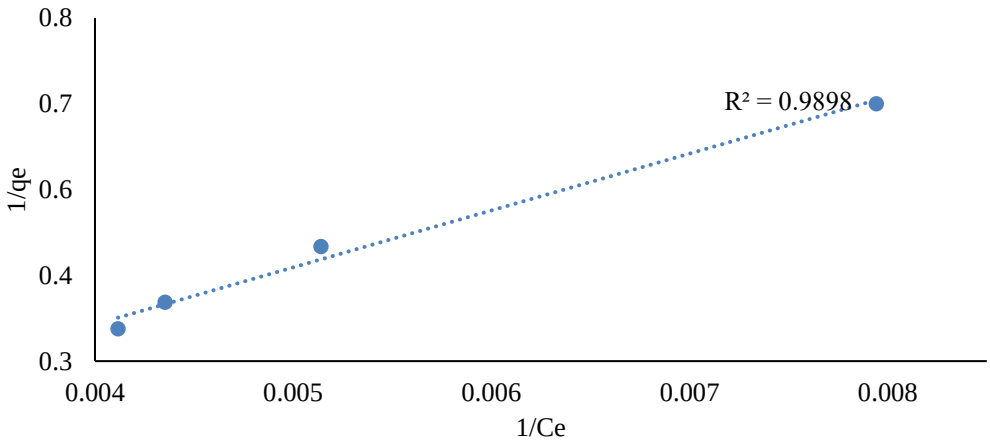

Figure 4.188. Langmuir isotherm graph of COM-AC for toluene at 414 µg/m³.

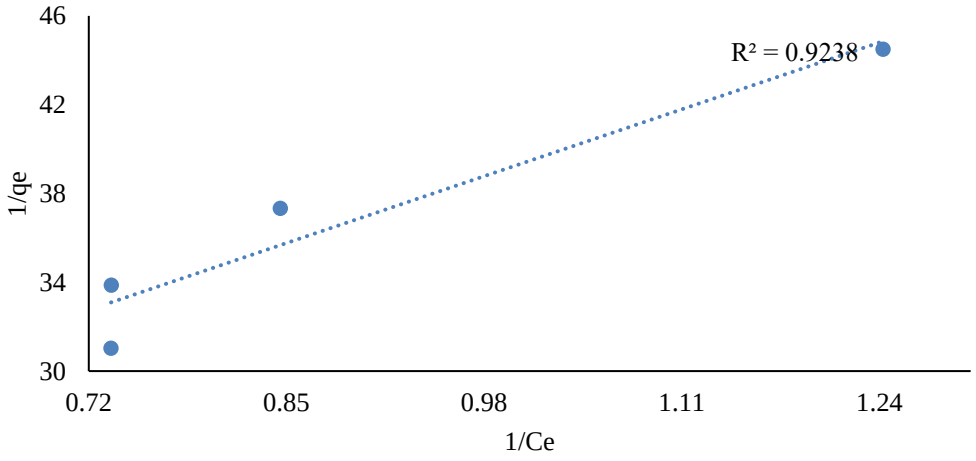

Figure 4.189. Langmuir isotherm graph of KN-AC for toluene at 3.7 µg/m³.

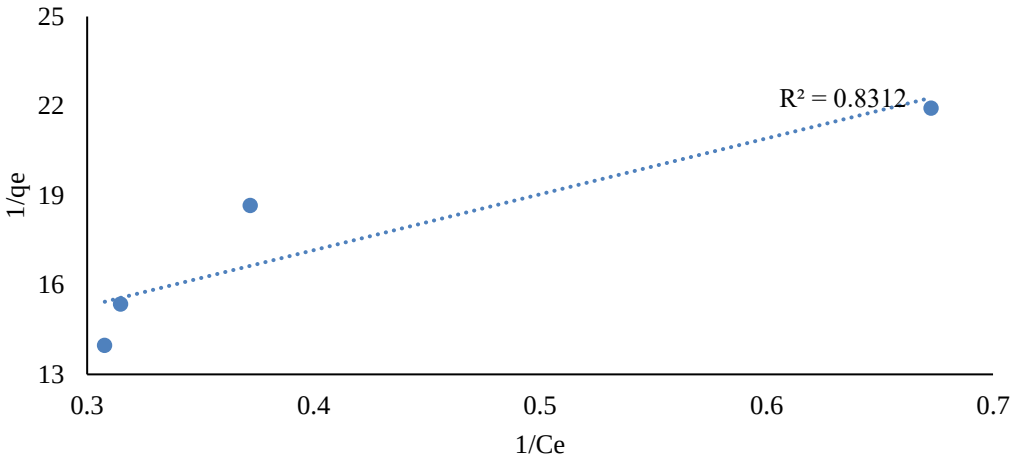

Figure 4.190. Langmuir isotherm graph of KN-AC for toluene at 9 µg/m³.

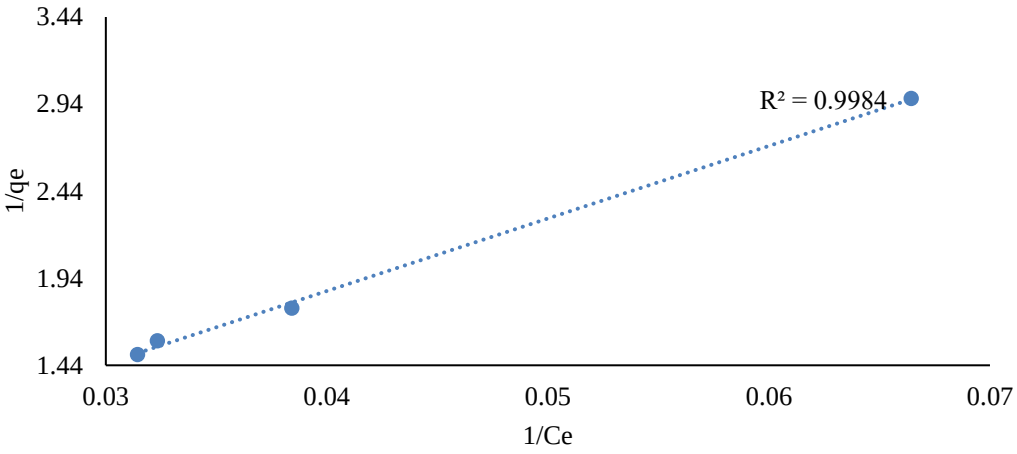

Figure 4.191. Langmuir isotherm graph of KN-AC for toluene at 86 µg/m³.

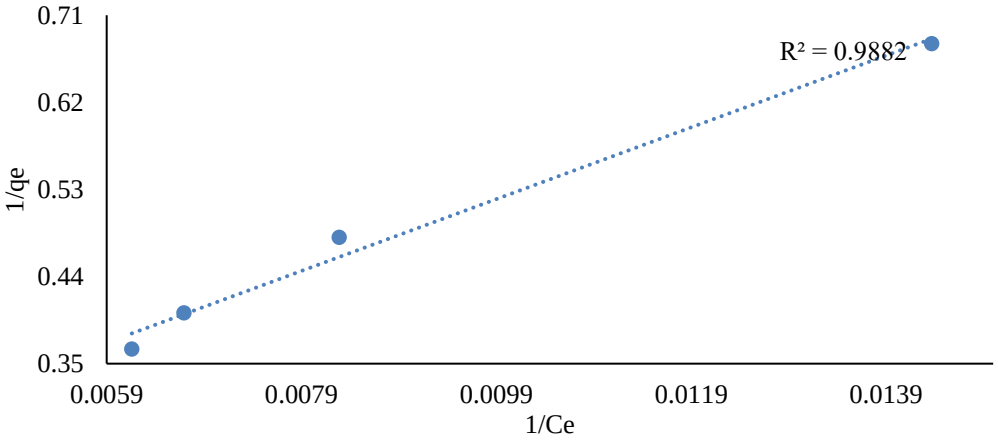

Figure 4.192. Langmuir isotherm graph of KN-AC for toluene at 414 µg/m³.

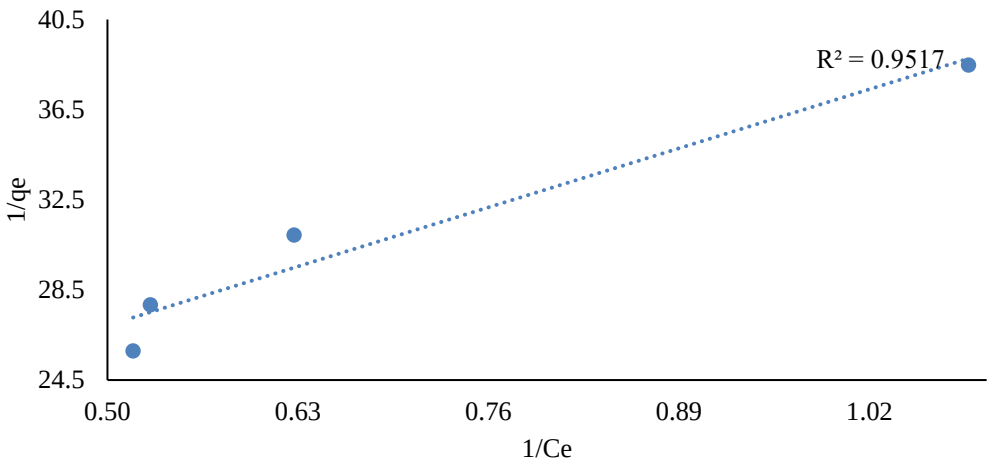

Figure 4.193. Langmuir isotherm graph of COM-AC for ethylbenzene at 3.9 µg/m³.

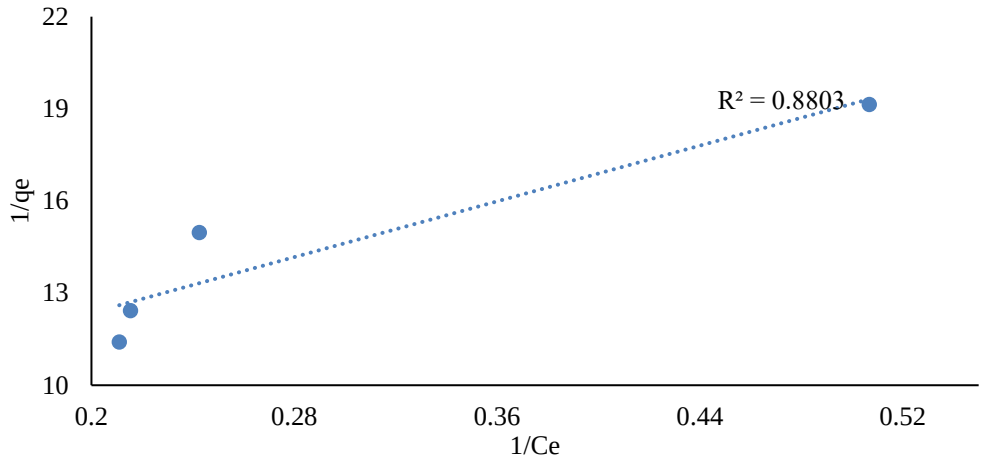

Figure 4.194. Langmuir isotherm graph of COM-AC for ethylbenzene at 9.2 µg/m³.

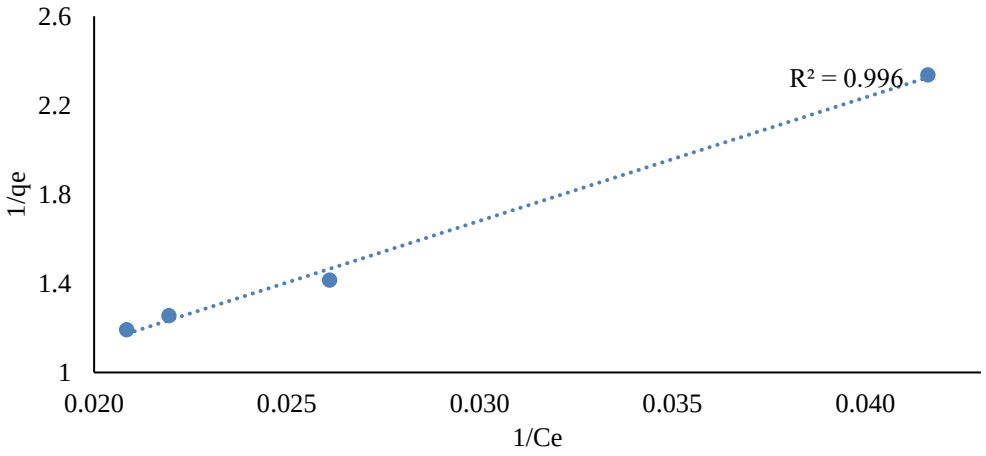

Figure 4.195. Langmuir isotherm graph of COM-AC for ethylbenzene at 90 µg/m³.

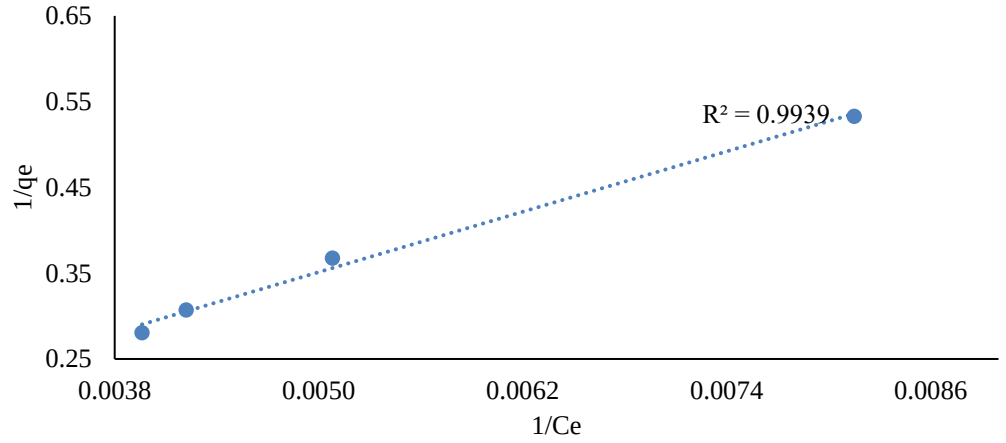

Figure 4.196. Langmuir isotherm graph of COM-AC for ethylbenzene at 430 µg/m³.

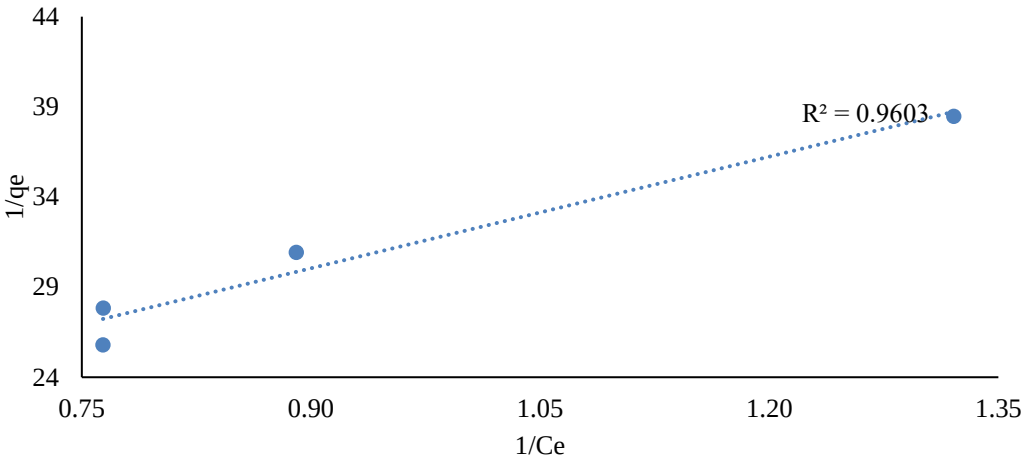

Figure 4.197. Langmuir isotherm graph of KN-AC for ethylbenzene at 3.9 µg/m³.

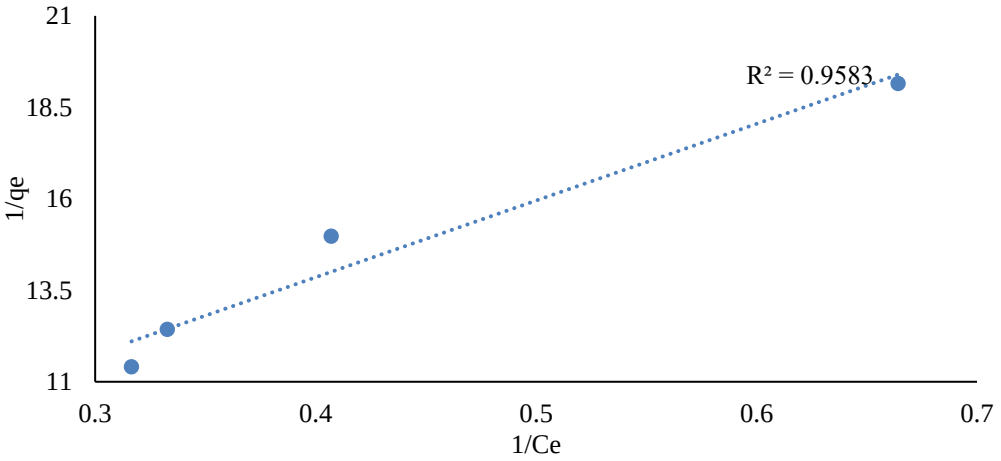

Figure 4.198. Langmuir isotherm graph of KN-AC for ethylbenzene at 9.2 µg/m³.

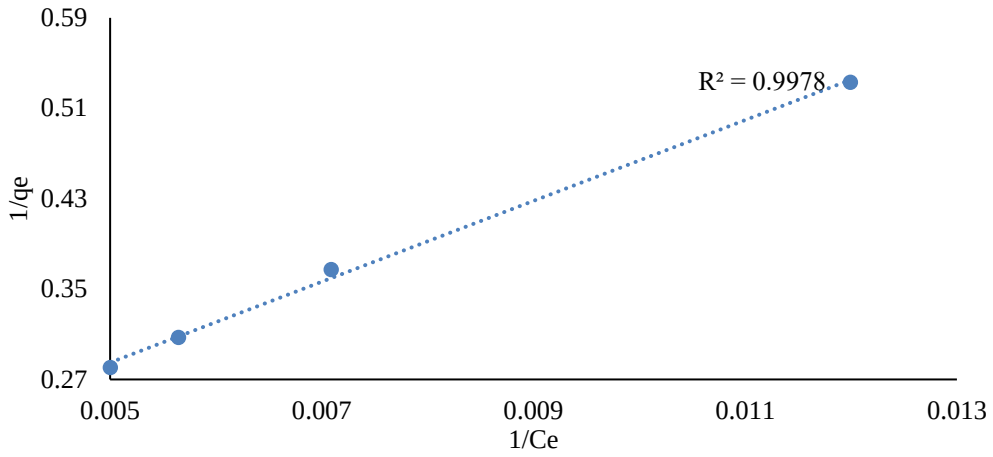

Figure 4.199. Langmuir isotherm graph of KN-AC for ethylbenzene at 90 µg/m³.

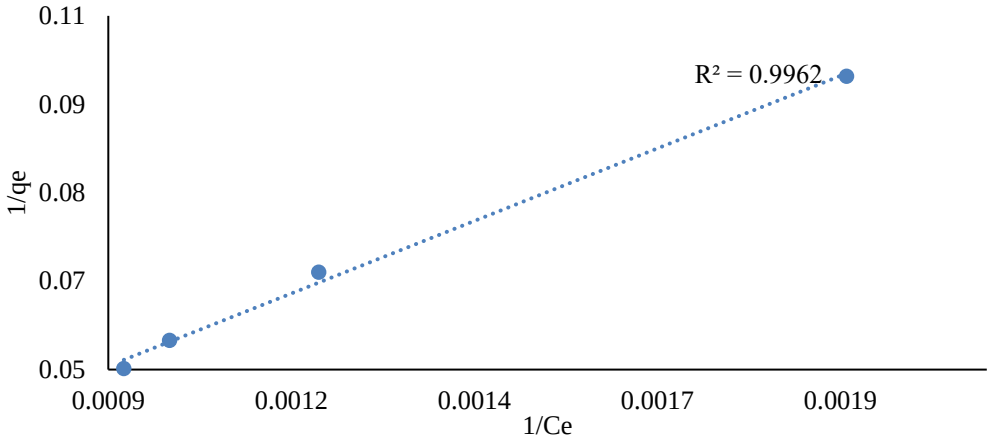

Figure 4.200. Langmuir isotherm graph of KN-AC for ethylbenzene at 430 µg/m³.

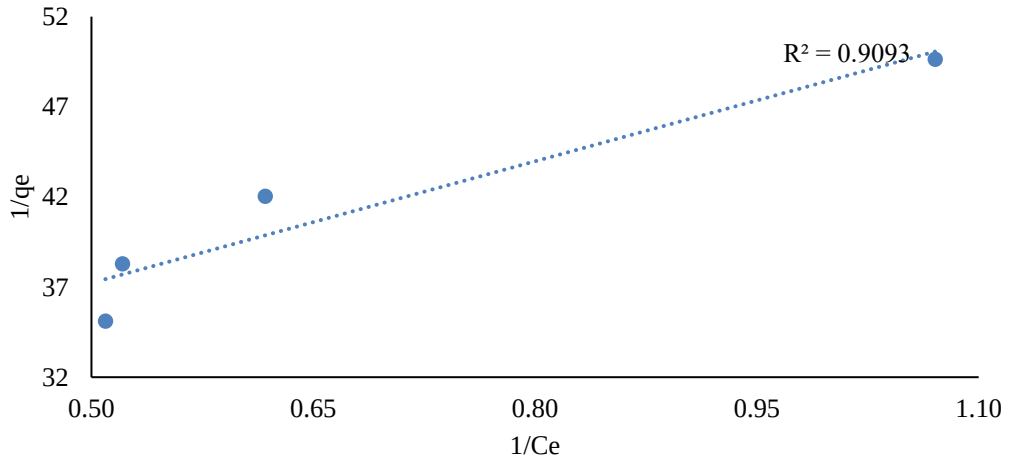

Figure 4.201. Langmuir isotherm graph of COM-AC for m, p-xylene at 3.4 µg/m³.

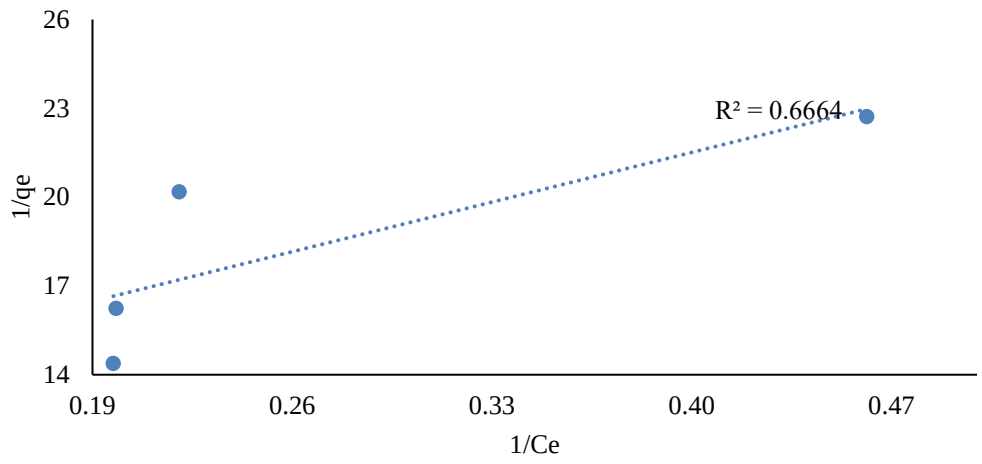

Figure 4.202. Langmuir isotherm graph of COM-AC for m, p-xylene at 8.5 µg/m³.

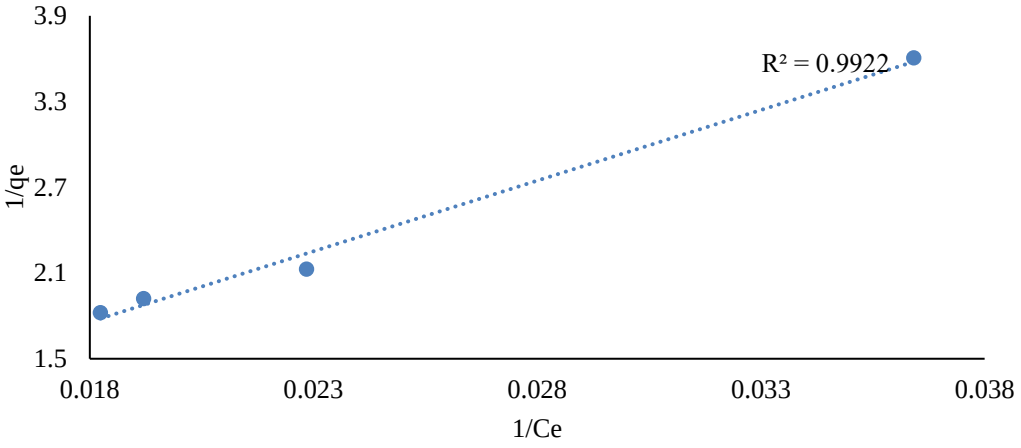

Figure 4.203. Langmuir isotherm graph of COM-AC for m, p-xylene at 83 µg/m³.

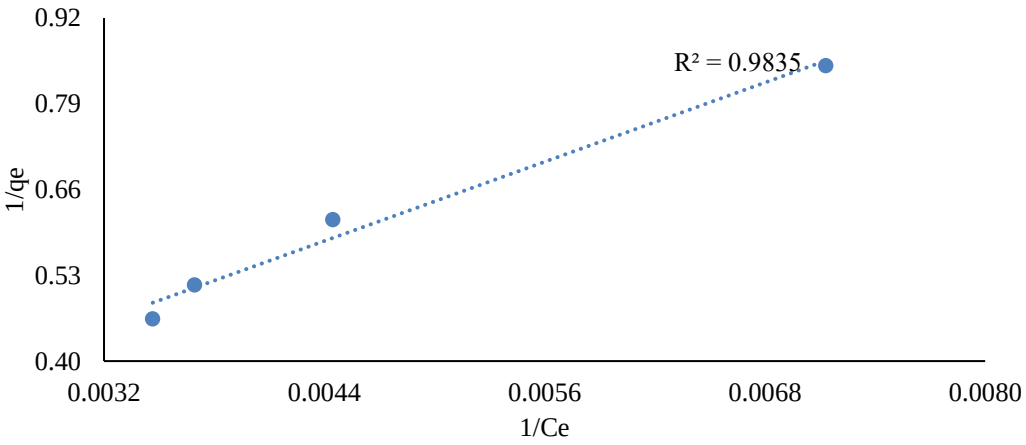

Figure 4.204. Langmuir isotherm graph of COM-AC for m, p-xylene at 397 µg/m³.

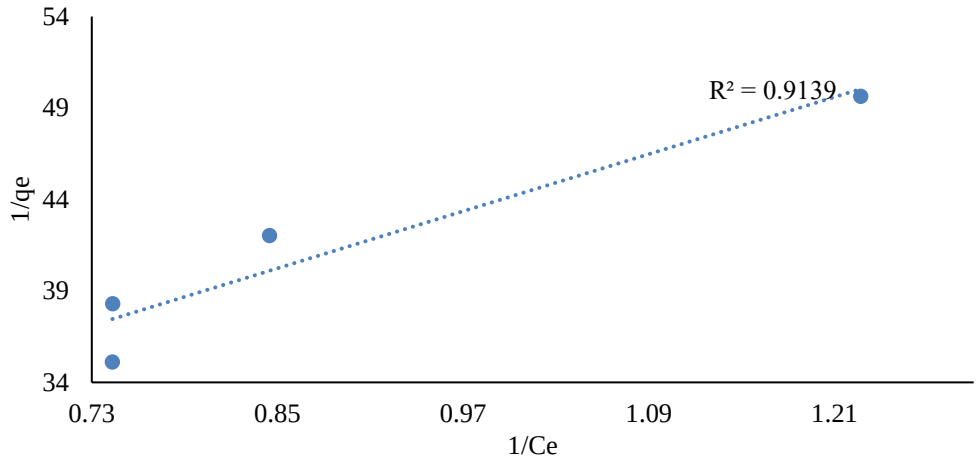

Figure 4.205. Langmuir isotherm graph of KN-AC for m, p-xylene at 3.4 µg/m³.

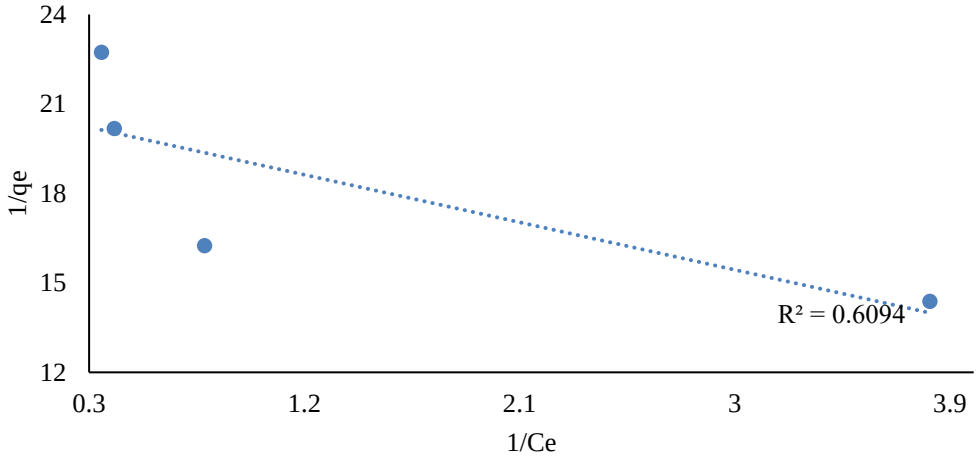

Figure 4.206. Langmuir isotherm graph of KN-AC for m, p-xylene at 8.5 µg/m³.

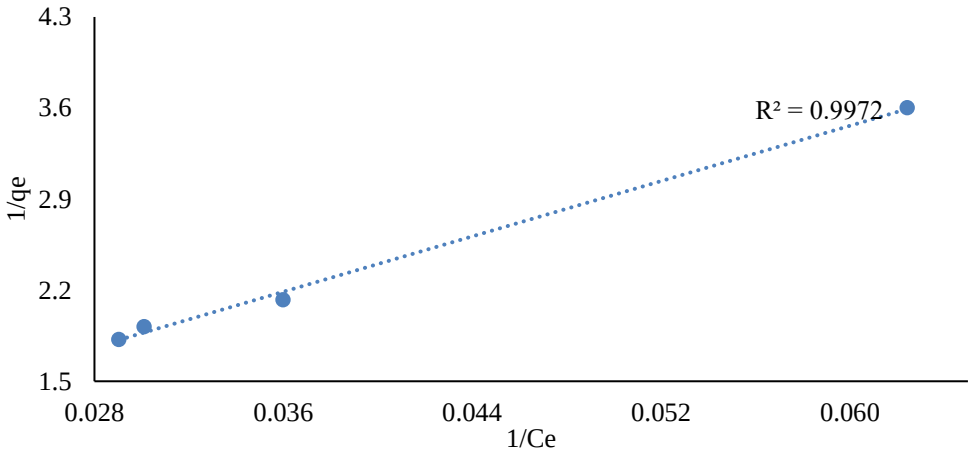

Figure 4.207. Langmuir isotherm graph of KN-AC for m, p-xylene at 83 µg/m³.

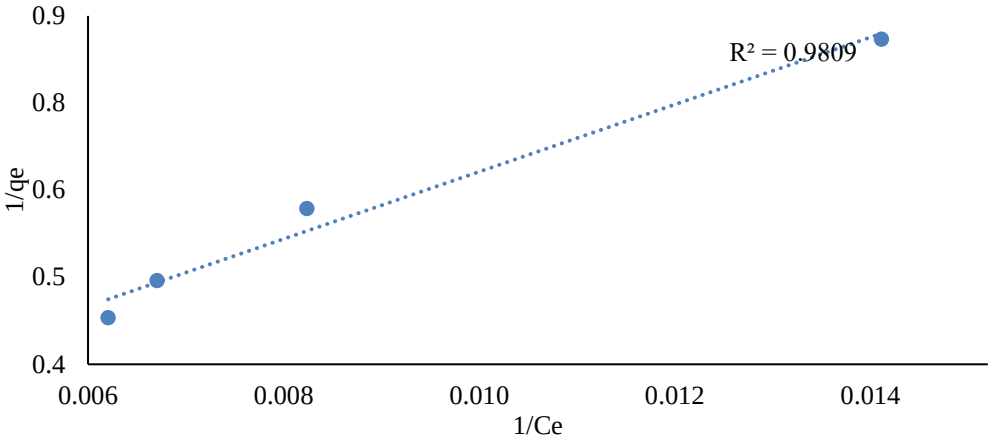

Figure 4.208. Langmuir isotherm graph of KN-AC for m, p-xylene at 397 µg/m³.

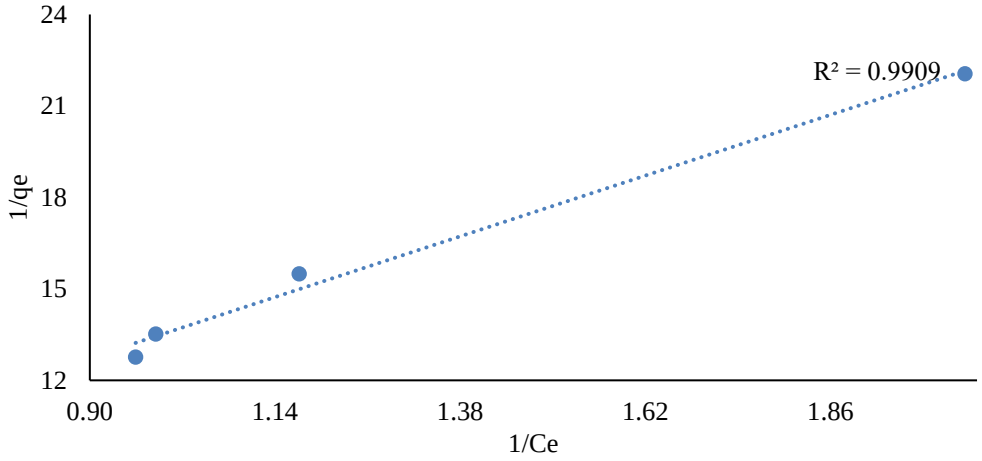

Figure 4.209. Langmuir isotherm graph of COM-AC for o-xylene at 5.2 µg/m³.

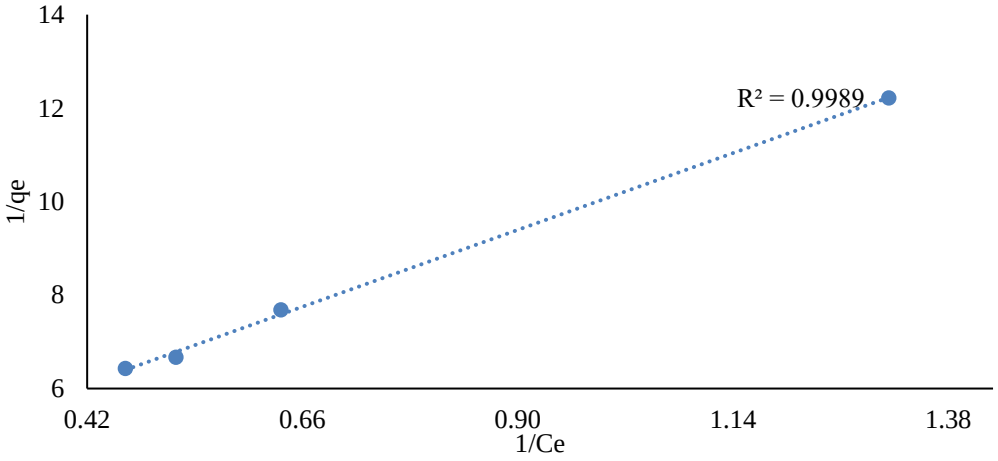

Figure 4.210. Langmuir isotherm graph of COM-AC for o-xylene at 10 µg/m³.

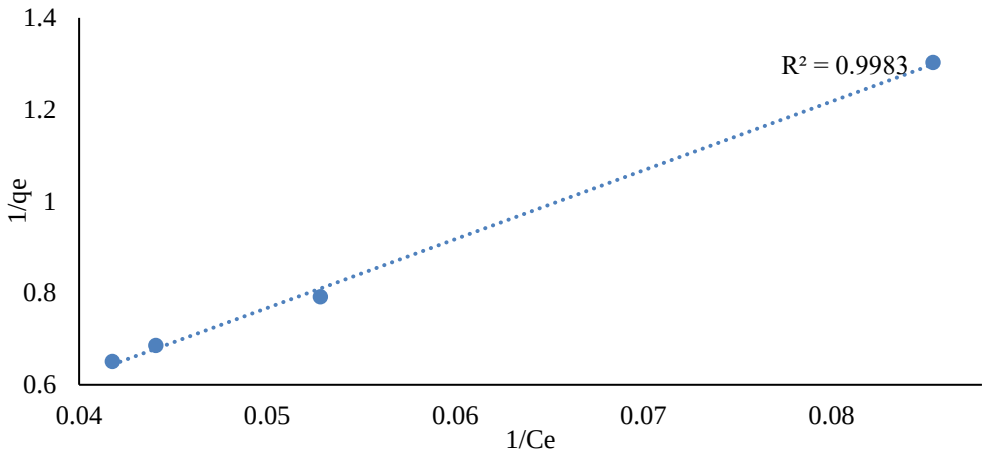

Figure 4.211. Langmuir isotherm graph of COM-AC for o-xylene at 100 µg/m³.

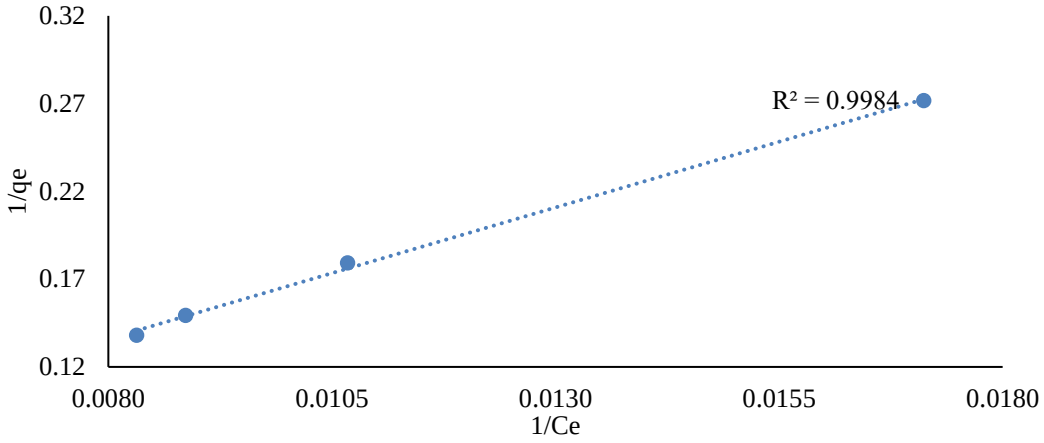

Figure 4.212. Langmuir isotherm graph of COM-AC for o-xylene at 483 µg/m³.

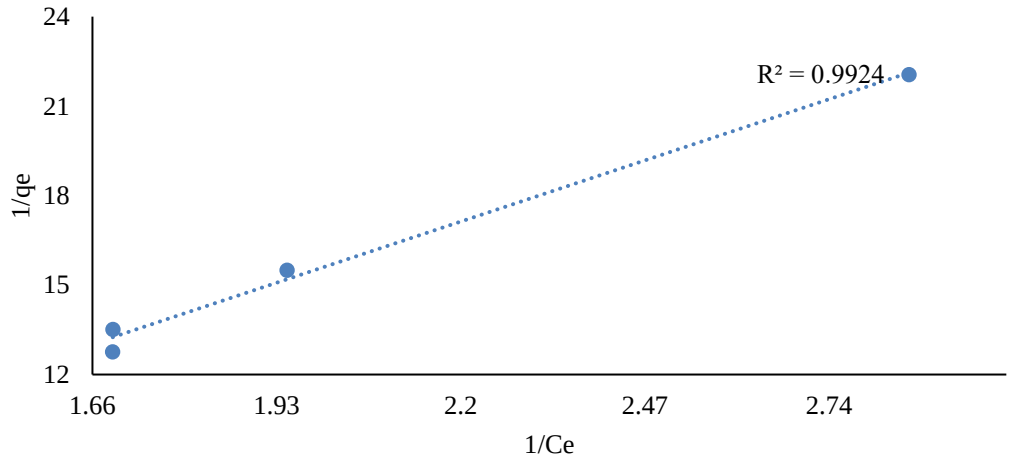

Figure 4.213. Langmuir isotherm graph of KN-AC for o-xylene at 5.2 µg/m³.

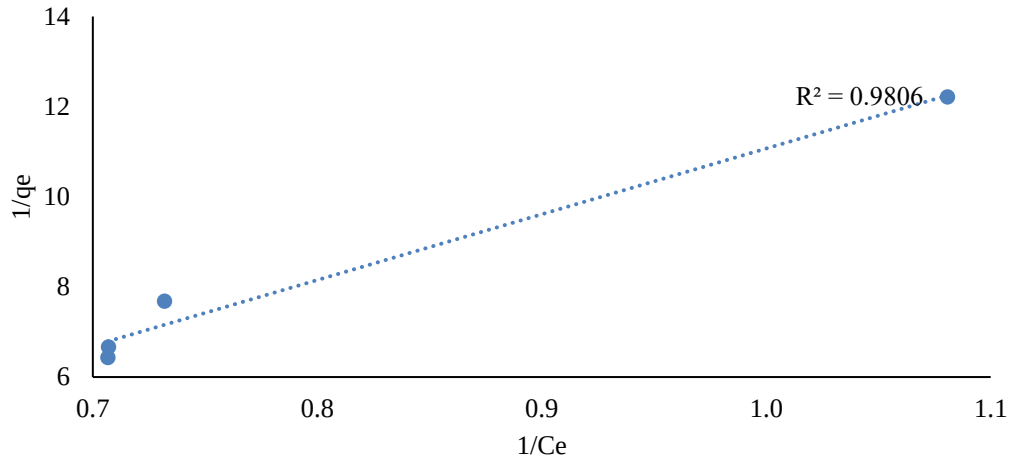

Figure 4.214. Langmuir isotherm graph of KN-AC for o-xylene at 10 µg/m³.

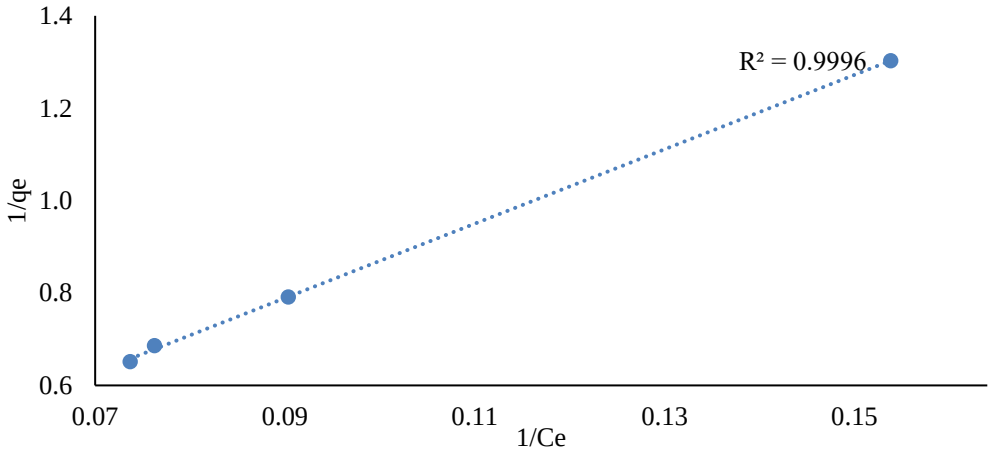

Figure 4.215. Langmuir isotherm graph of KN-AC for o-xylene at 100 µg/m³.

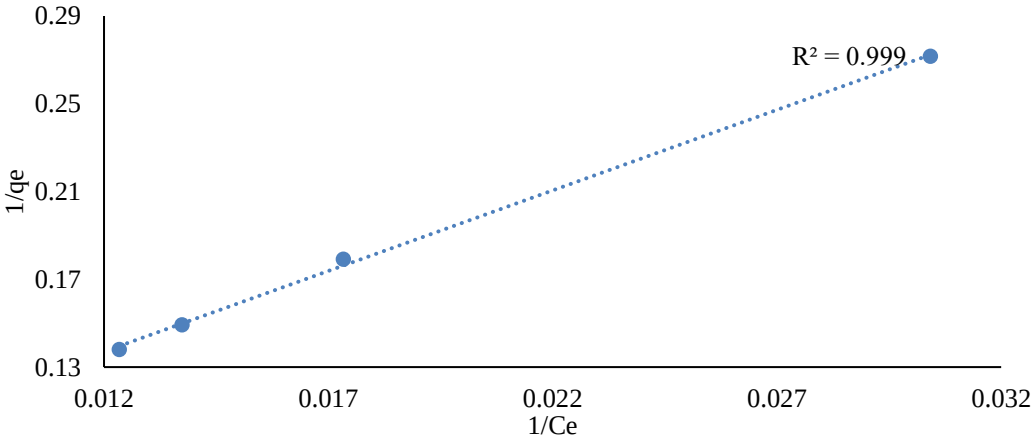

Figure 4.216. Langmuir isotherm graph of KN-AC for o-xylene at 483 µg/m³.

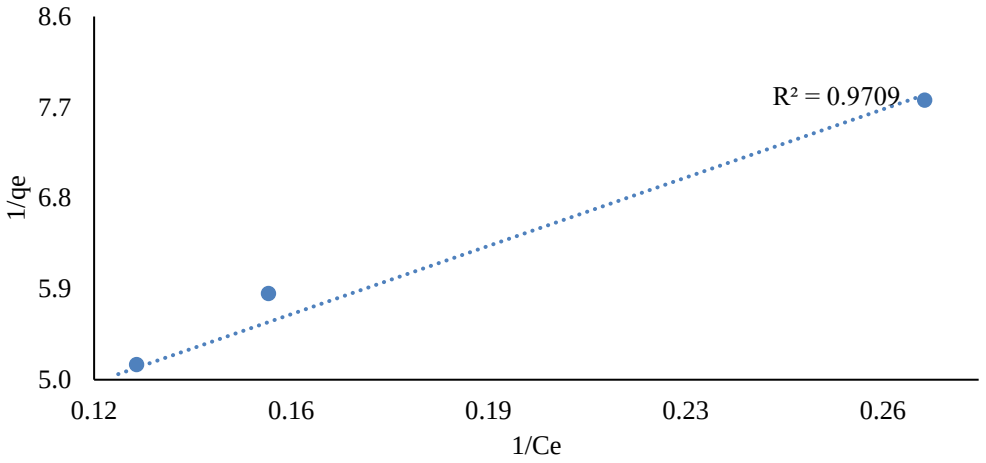

Figure 4.217. Langmuir isotherm graph of COM-AC for BTEX at 18.5 µg/m³.

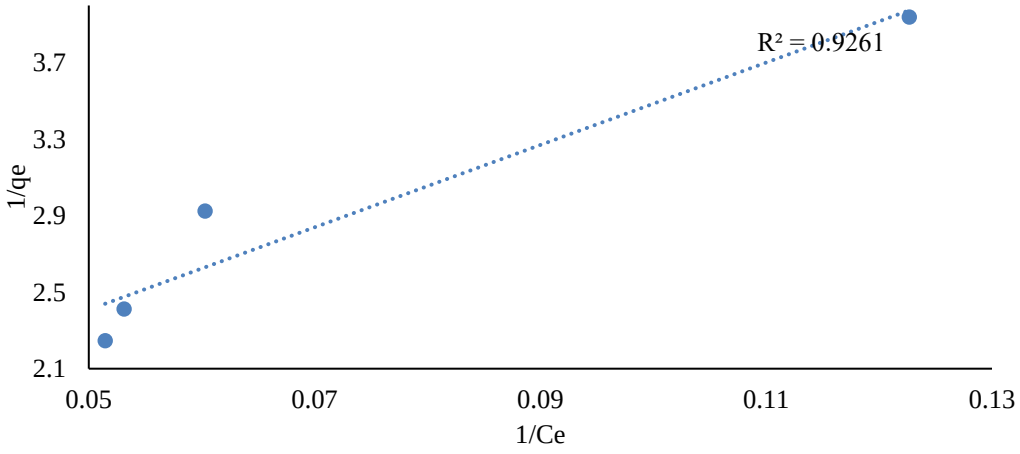

Figure 4.218. Langmuir isotherm graph of COM-AC for BTEX at 42 µg/m³.

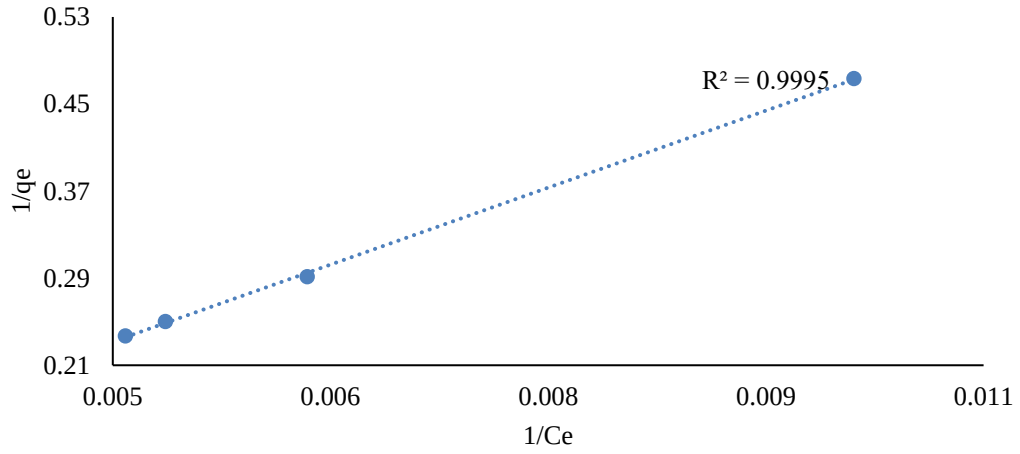

Figure 4.219. Langmuir isotherm graph of COM-AC for BTEX at 412 µg/m³.

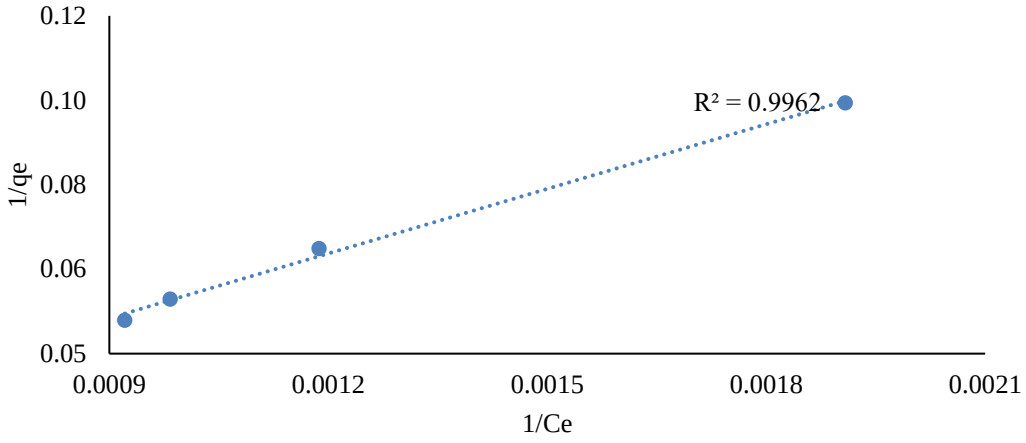

Figure 4.220. Langmuir isotherm graph of COM-AC for BTEX at 2045 µg/m³.

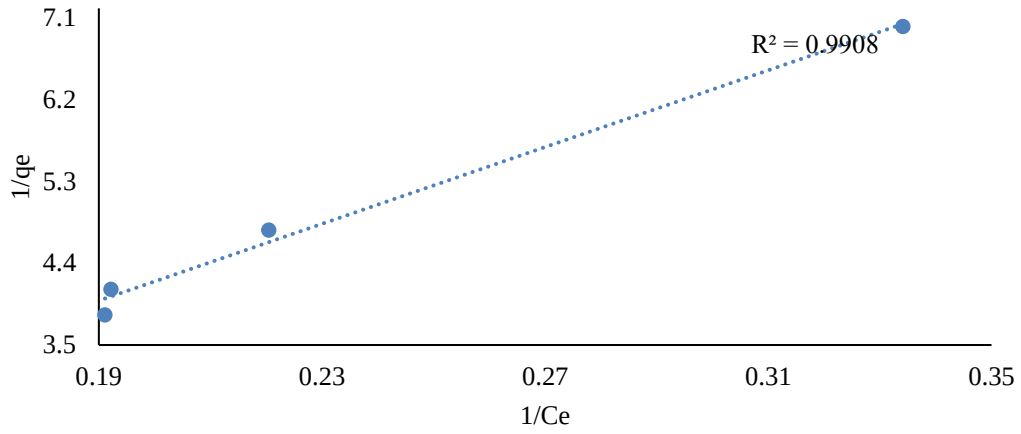

Figure 4.221. Langmuir isotherm graph of KN-AC for BTEX at 18.5 µg/m³.

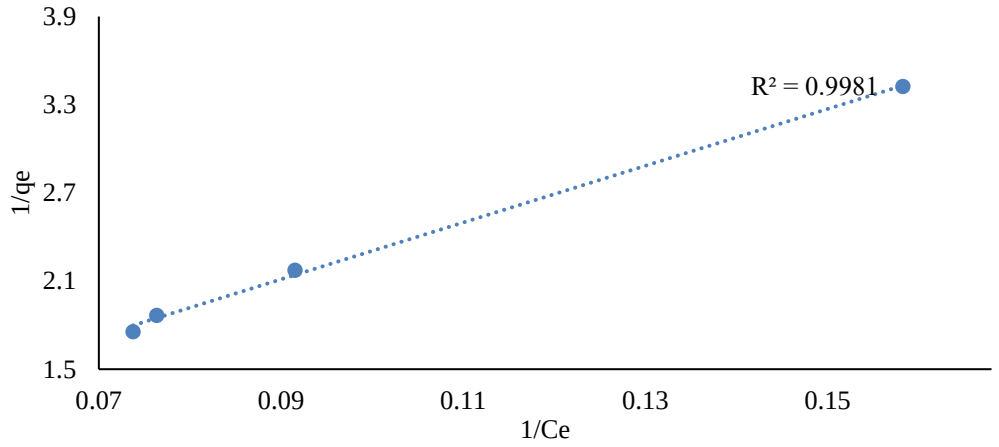

Figure 4.222. Langmuir isotherm graph of KN-AC for BTEX at 42 µg/m³.

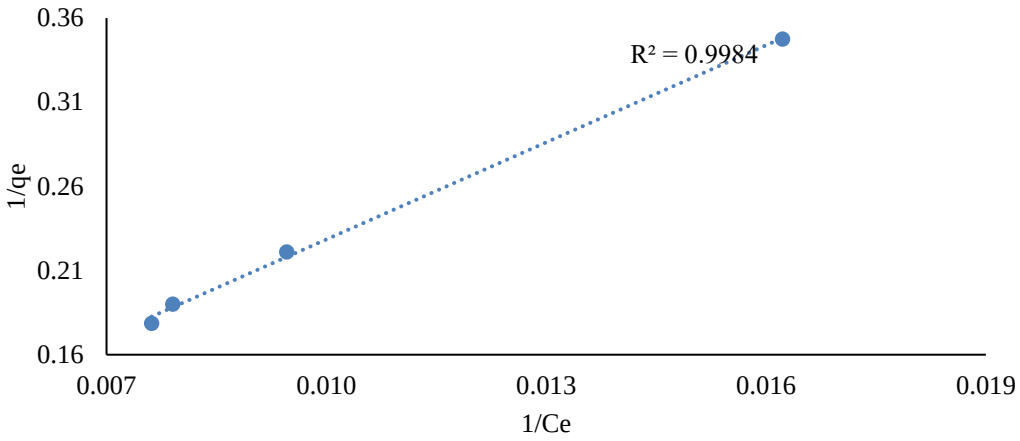

Figure 4.223. Langmuir isotherm graph of KN-AC for BTEX at 412 µg/m³.

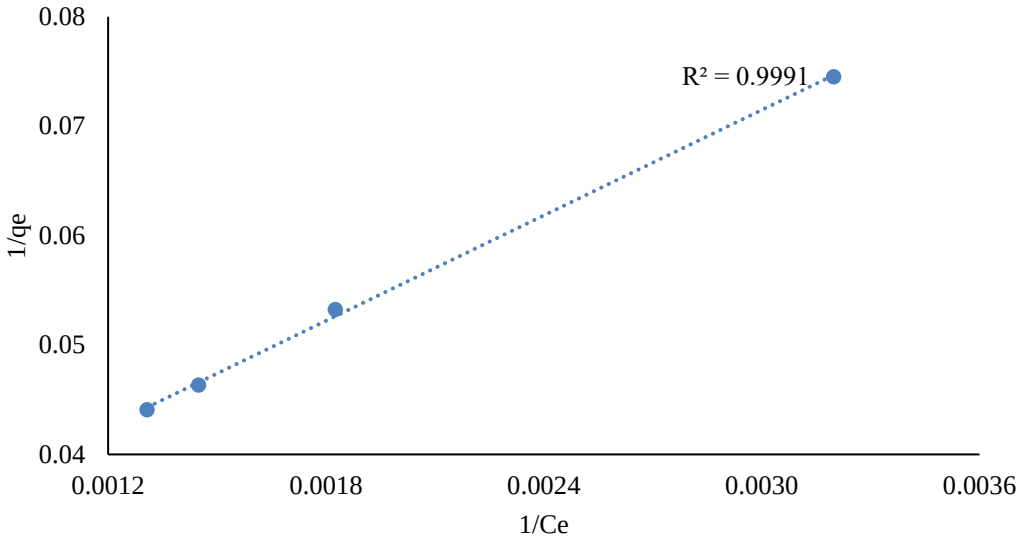

Figure 4.224. Langmuir isotherm graph of KN-AC for BTEX at 2045 µg/m³.

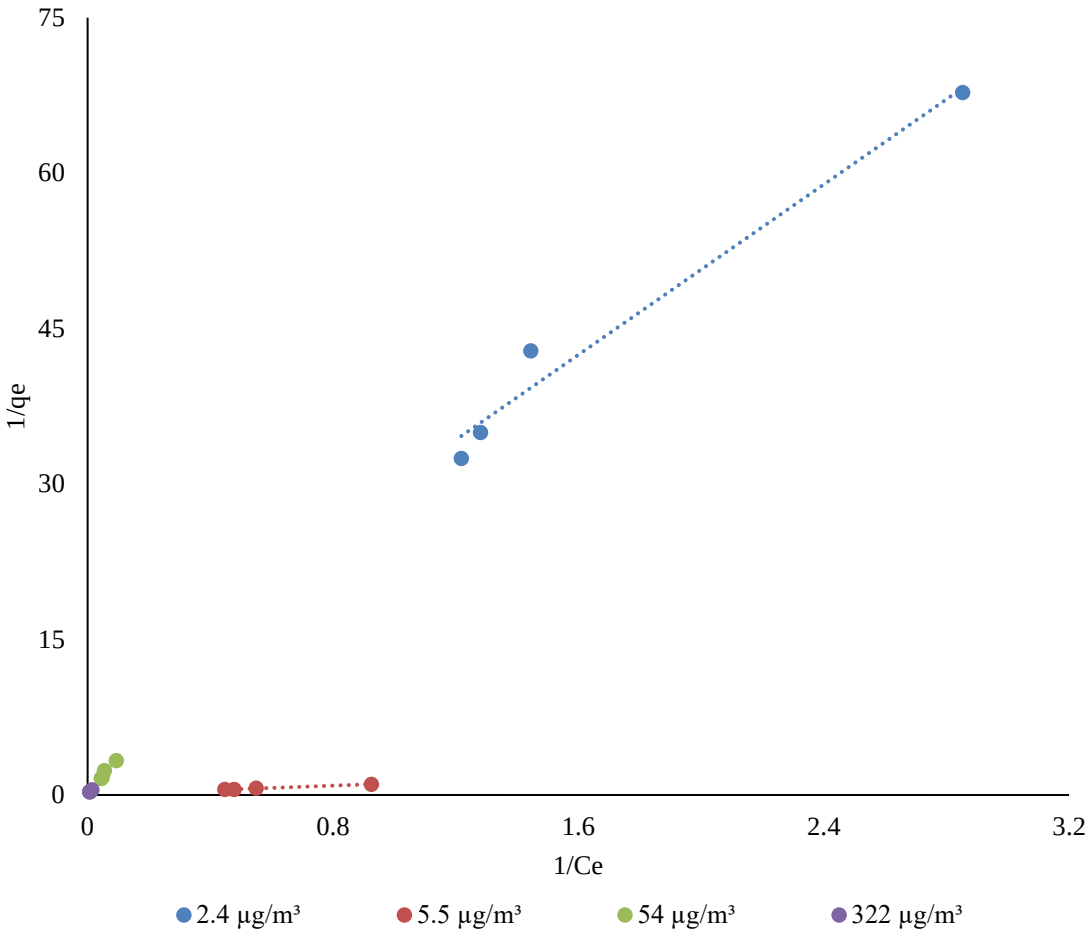

Figure 4.225. Langmuir isotherm graph of COM-AC for all benzene concentrations.

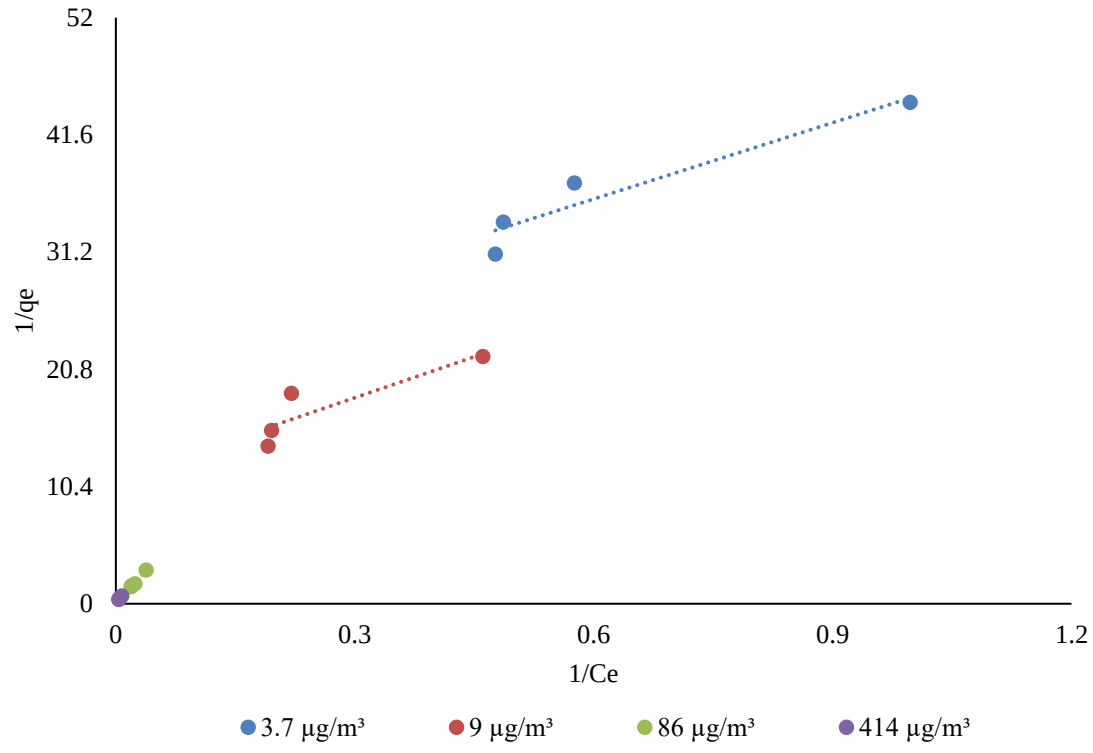

Figure 4.226. Langmuir isotherm graph of COM-AC for all toluene concentrations.

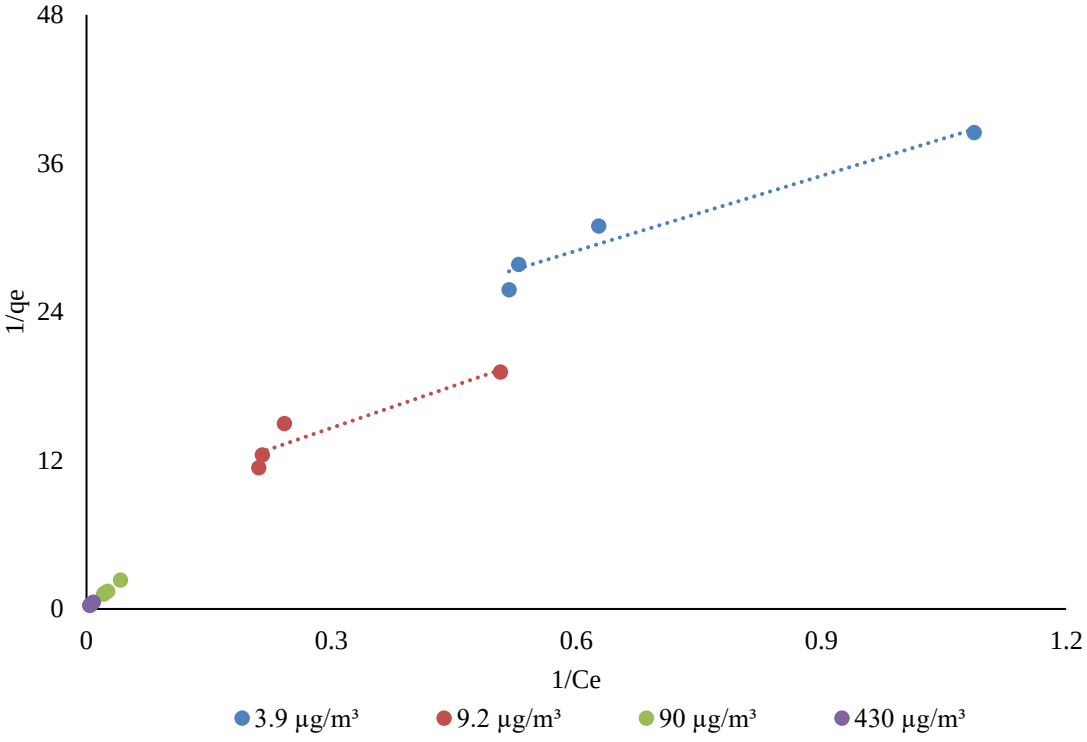

Figure 4.227. Langmuir isotherm graph of COM-AC for all ethylbenzene concentrations.

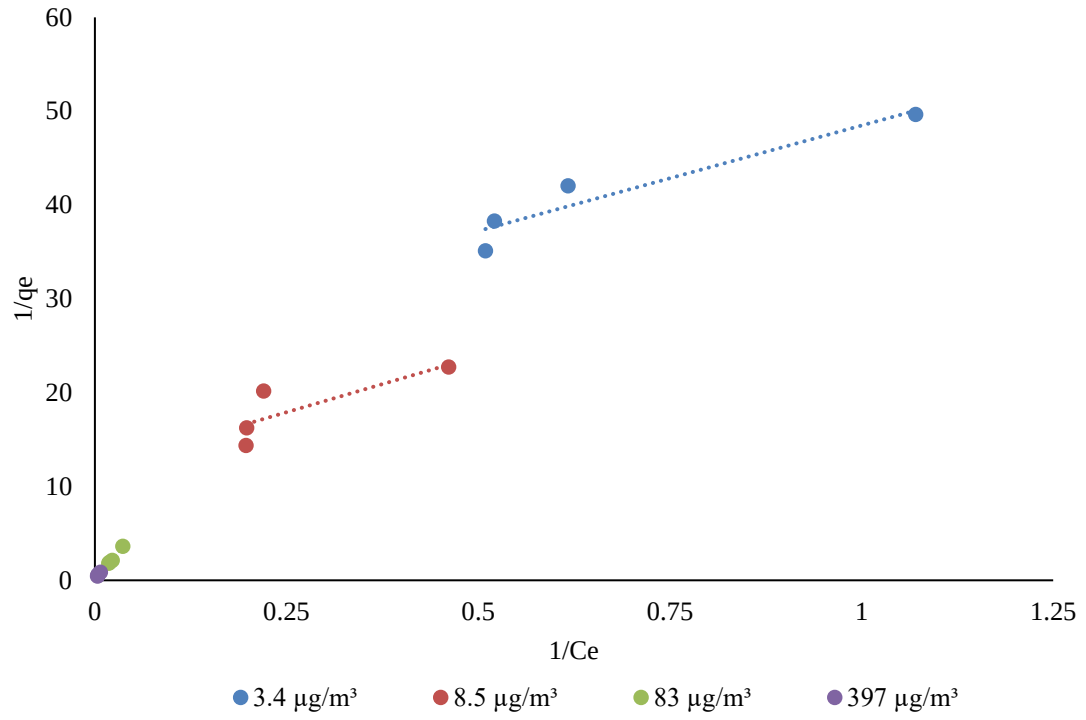

Figure 4.228. Langmuir isotherm graph of COM-AC for all m, p-xylene concentrations.

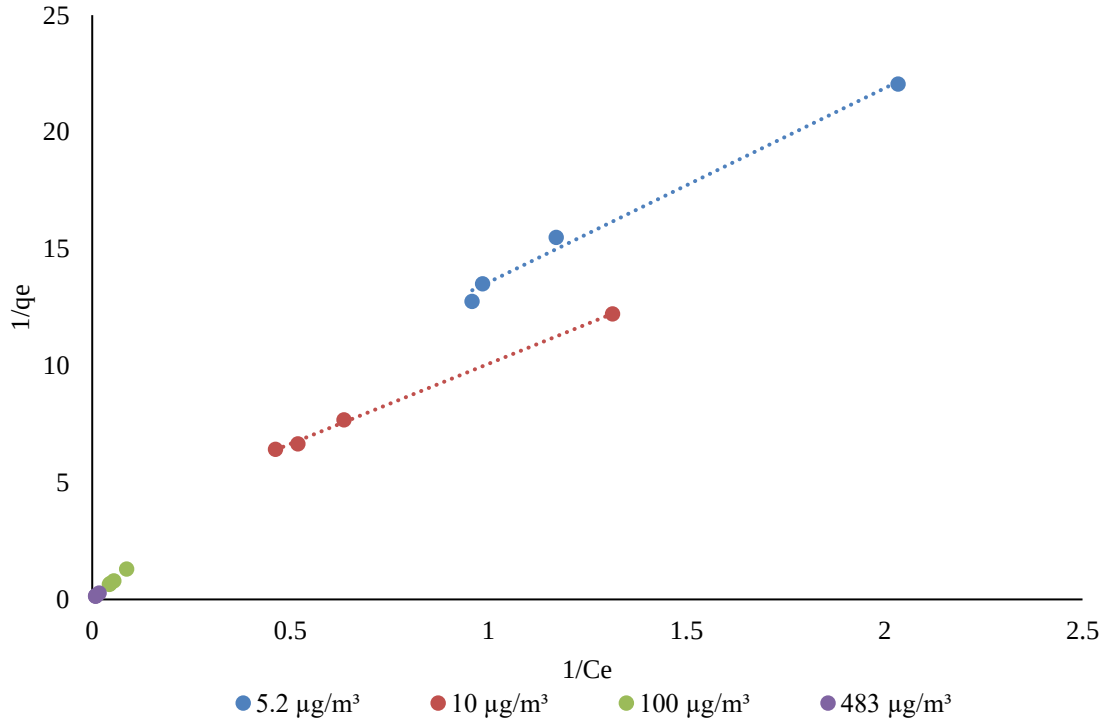

Figure 4.229. Langmuir isotherm graph of COM-AC for all o-xylene concentrations.

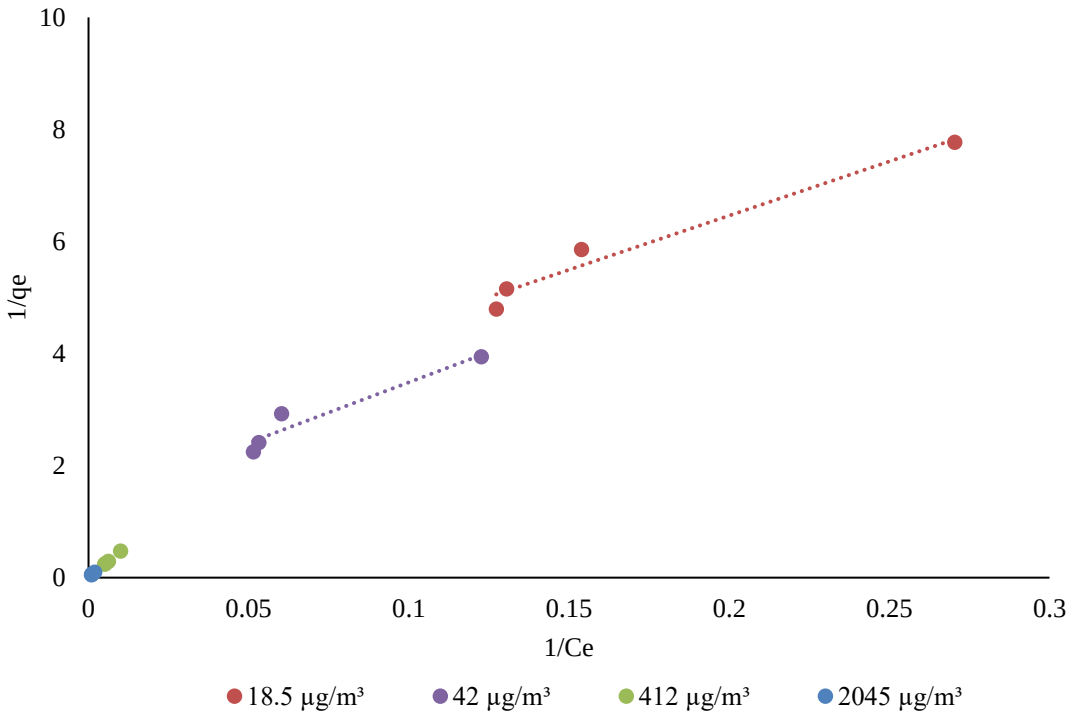

Figure 4.230. Langmuir isotherm graph of COM-AC for all BTEX concentrations.

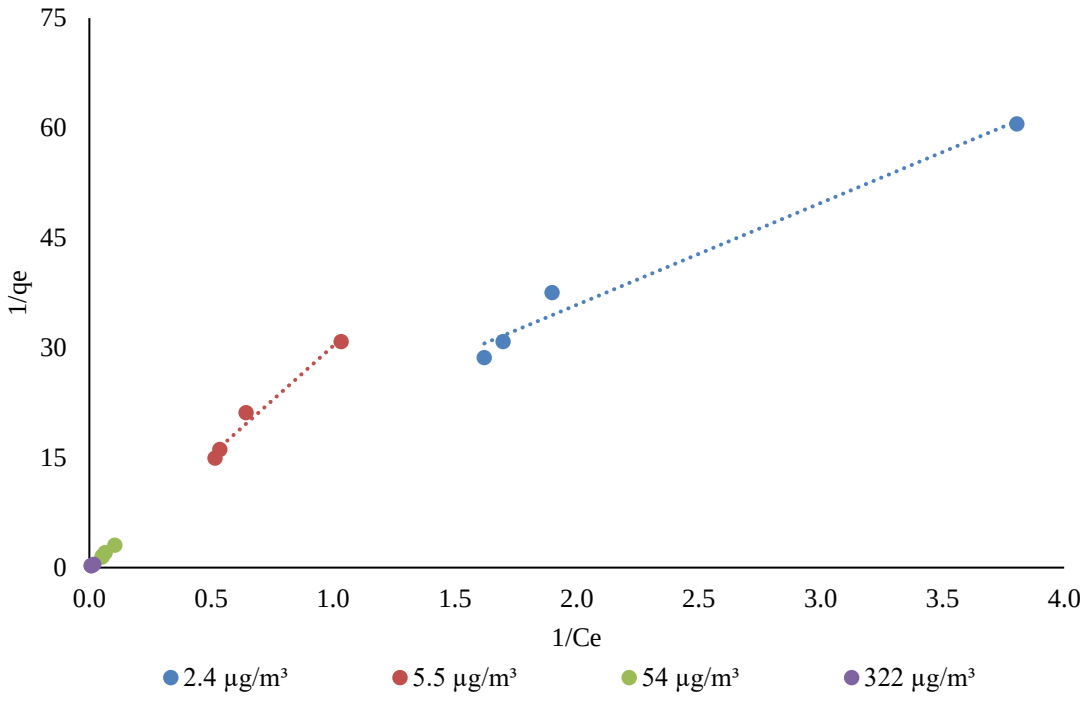

Figure 4.231. Langmuir isotherm graph of KN-AC for all benzene concentrations.

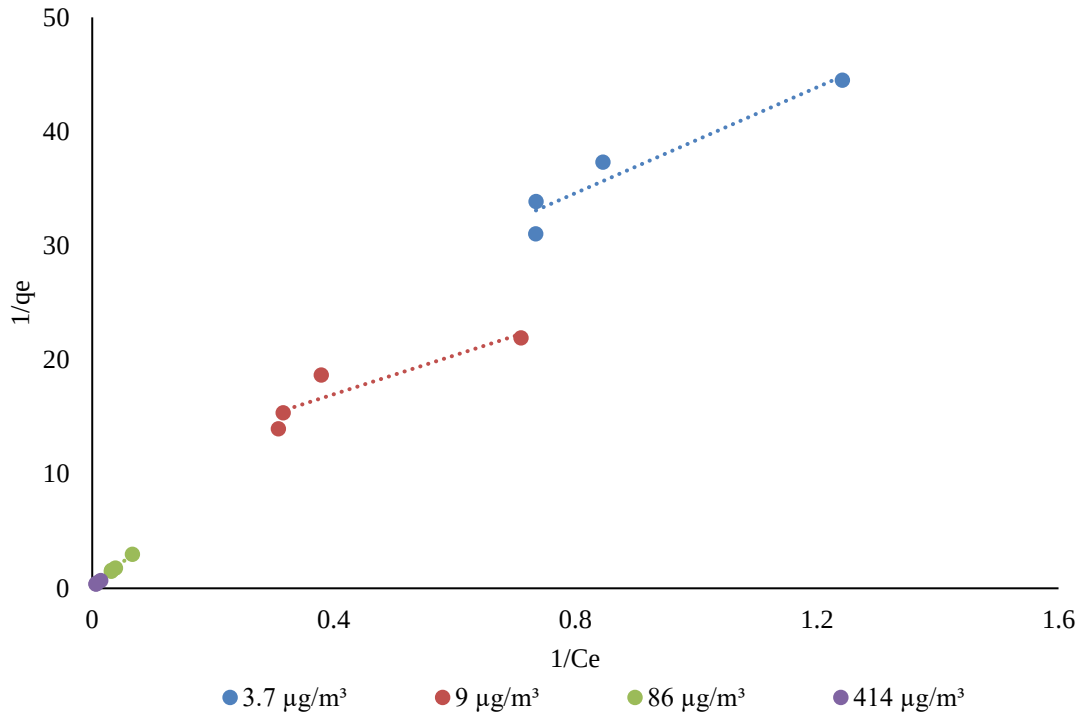

Figure 4.232. Langmuir isotherm graph of KN-AC for all toluene concentrations.

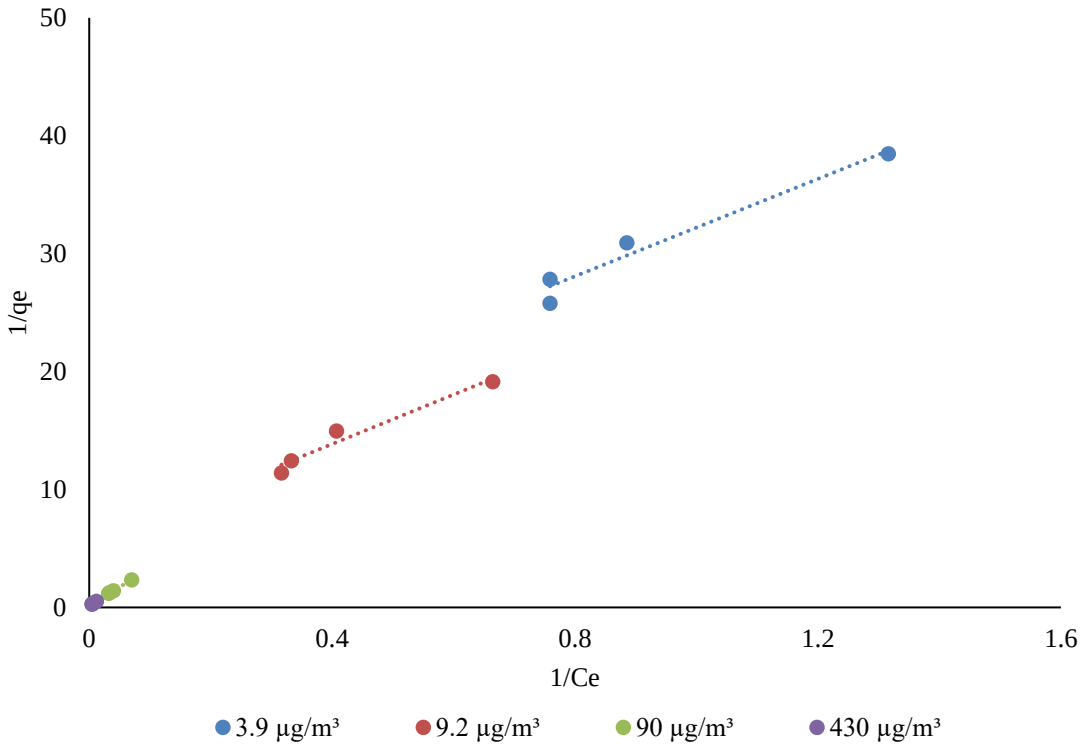

Figure 4.233. Langmuir isotherm graph of KN-AC for all ethylbenzene concentrations.

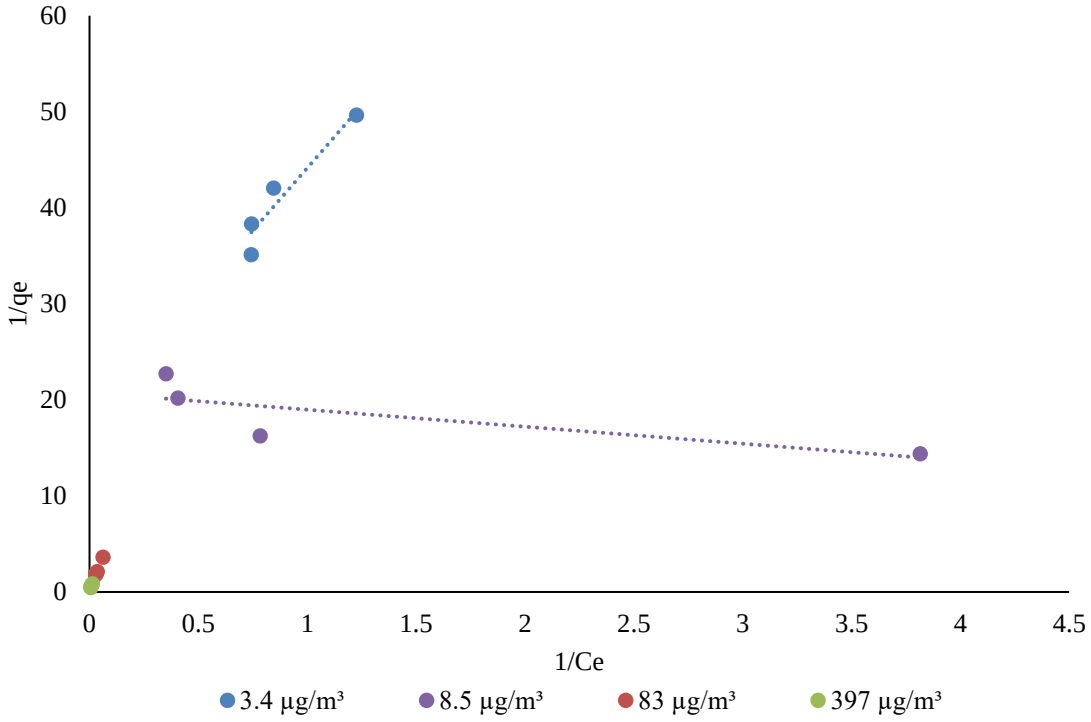

Figure 4.234. Langmuir isotherm graph of KN-AC for all m, p-xylene concentrations.

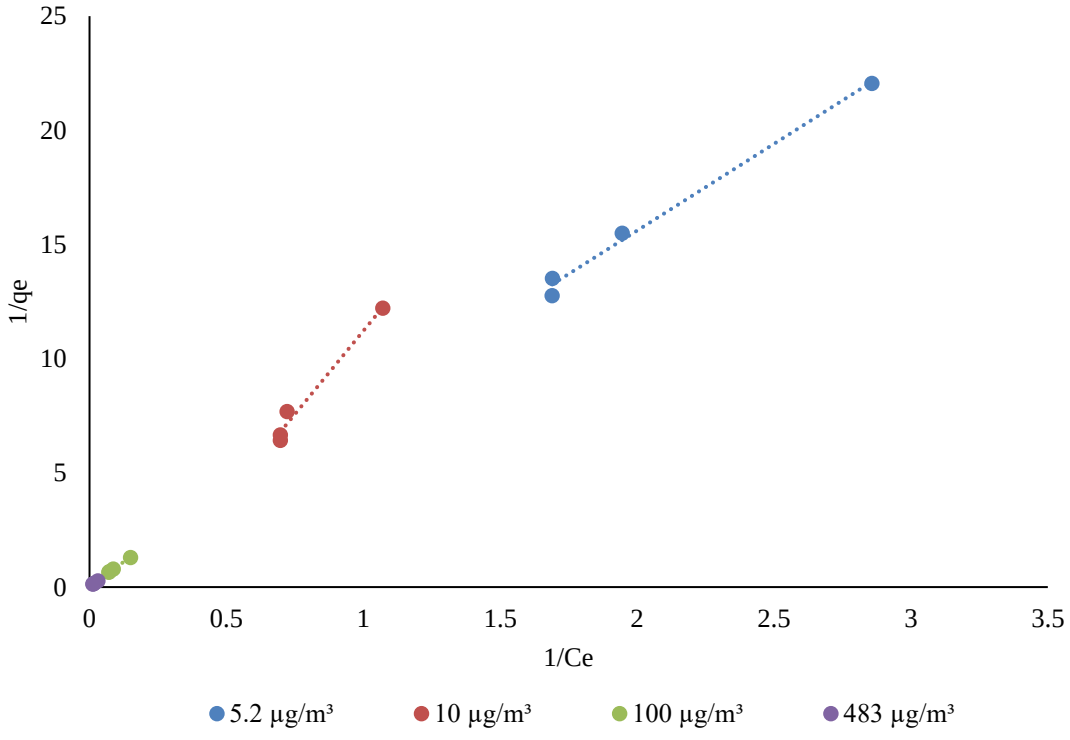

Figure 4.235. Langmuir isotherm graph of KN-AC for all o-xylene concentrations.

According to the charts of Langmuir isotherm was plotted for COM-AC and KN-AC for all concentrations between Figure 4.186 and Figure 4.245.

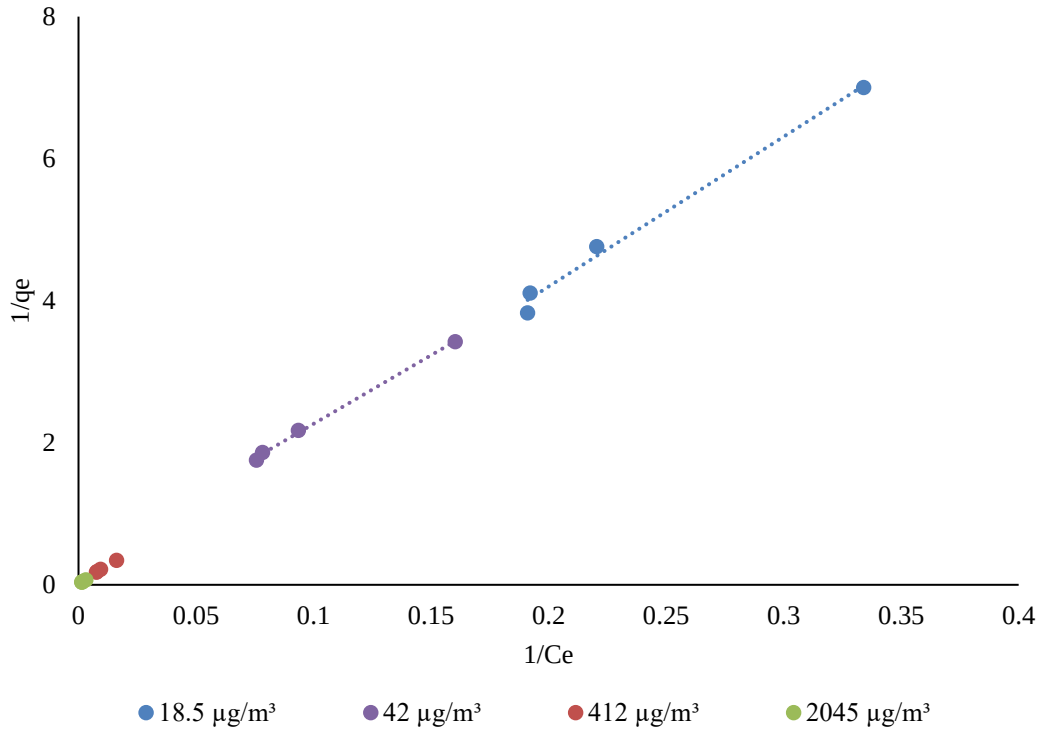

Figure 4.236. Langmuir isotherm graph of KN-AC for all BTEX concentrations.

The Langmuir parameters obtained from the Langmuir graph plotted for COM-AC were givenin Table 4.18. Accordingly, when the R^2 values for benzene were compared between their concentration values, the highest value for R^2 is 0.9997 at 322±47.80 µg/m^3. These values 0.9941 in toluene at 86±15.83 µg/m^3, R^2 value is 0.9960 with 90 µg/m^3 in ethylbenzene, it is 0.9922 at 83±12.95 µg/m^3 with m, p-xylene, it is 0.9989 at 10±2.49 µg/m^3 with o-xylene, and with BTEX 0.9995 was found with 412 µg/m^3.

Table 4.18. Parameters of Langmuir isotherm for BTEX of COM-AC.

Gases	Average and SD of C_0 (µg/m³)	q_{max} (µg/g)	K_L	R^2

Benzene	2.4±0.45	0.05	2.14	0.9764
	5.5±1.09	0.92	38.41	0.9974
	54±10.73	0.03	181.29	0.9436
	322±47.80	0.04	293.05	0.9997
Toluene	3.7±0.58	0.05	1.09	0.9145
	9±2.62	0.02	2.20	0.7801
	86±15.83	0.02	432.77	0.9941
	414±47.26	0.02	856.33	0.9898
Ethylbenzene	3.9±0.66	0.05	1.20	0.9517
	9.2±1.59	0.02	2.90	0.8803
	90±15.55	0.02	295.25	0.9960
	430±46.64	0.02	1010.30	0.9939
M, p-xylene	3.4±0.72	0.05	0.87	0.9093
	8.5±1.32	0.01	2.01	0.6664
	83±12.95	0.01	543.77	0.9922
	397±82.10	0.01	705.71	0.9835
O-xylene	5.2±0.82	0.12	1.58	0.9909
	10±2.49	0.15	2.12	0.9989
	100±24.38	0.07	568.35	0.9983
	483±102.67	0.07	924.95	0.9984
BTEX	18.5±1.89	0.06	7.46	0.9709
	42±4.97	0.03	16.19	0.9261
	412±48.74	0.03	801.22	0.9995
	2045±203.37	0.03	4087.38	0.9962

The Langmuir parameters obtained from the Langmuir graph plotted for KN-AC were givenin Table 4.19. Accordingly, when the R^2 values for benzene were compared between their concentration values, the highest value was R^2 values is 0.9978 at 322±47.80 μg/m^3.

These values 0.9984 in toluene at 86±15.83 µg/m^3, R^2 value is 0.9989 with 90 µg/m3 in ethylbenzene, it is 0.9972 at 83±12.95 µg/m^3 with m, p-xylene, it is 0.9996 at 10±2.49 µg/m^3 with o-xylene, and with BTEX 0.9991 was found with 2045±203.37 µg/m^3.

Table 4.19. Parameters of Langmuir isotherm for BTEX of KN-AC.

Gases	Average and SD of C_0 (µg/m³)	q_{max} (µg/g)	K_L	R^2
Benzene	2.4±0.45	0.08	1.72	0.9781
	5.5±1.09	0.04	59.87	0.9789
	54±10.73	0.04	1773.35	0.9800
	322±47.80	0.06	142.34	0.9978
Toluene	3.7±0.58	0.05	1.44	0.9238
	9±2.62	0.03	1.68	0.8312
	86±15.83	0.03	207.84	0.9984
	414±47.26	0.03	242.49	0.9882
Ethylbenzene	3.9±0.66	0.05	1.79	0.9603
	9.2±1.59	0.03	3.84	0.9583
	90±15.55	0.03	129.15	0.9989
	430±46.64	0.03	234.53	0.9978
M, p-xylene	3.4±0.72	0.04	1.44	0.9139
	8.5±1.32	0.03	6.09	0.6094
	83±12.95	0.02	193.50	0.9972
	397±82.10	0.02	219.01	0.9809
O-xylene	5.2±0.82	0.14	18.26	0.9924
	10±2.49	0.14	24.33	0.9806
	100±24.38	0.13	83.26	0.9996

	483±102.67	0.14	149.82	0.9990
BTEX	18.5±1.89	0.05	10.75	0.9908
	42±4.97	0.05	57.76	0.9981
	412±48.74	0.05	530.58	0.9984
	2045±203.37	0.06	876.34	0.9991

4.3.1.3. Dubinin-Radushkevich Isotherm Modelling of BTEX

The graphs were created to determine Dubinin-Radushkevich isotherm for BTEX removal in between Figure 4.237 and Figure 4.283.

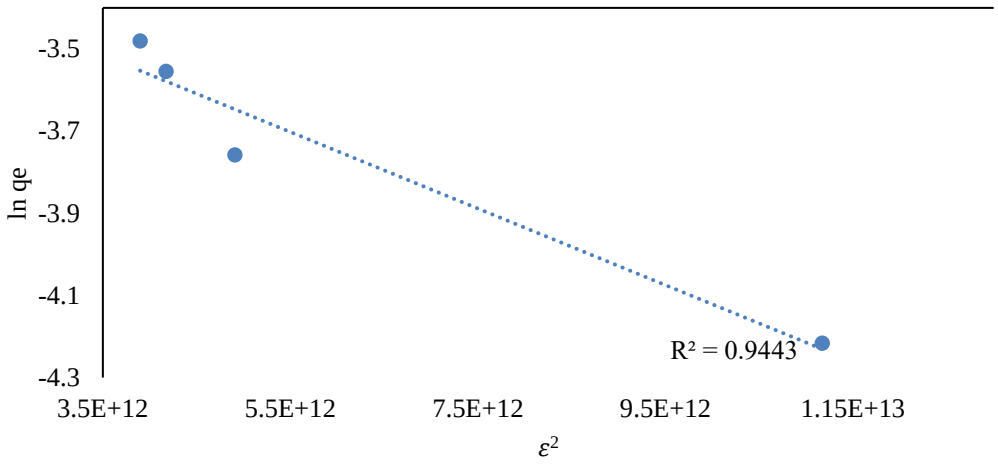

Figure 4.237. D-R isotherm graph of COM-AC for benzene at 2.4 µg/m³.

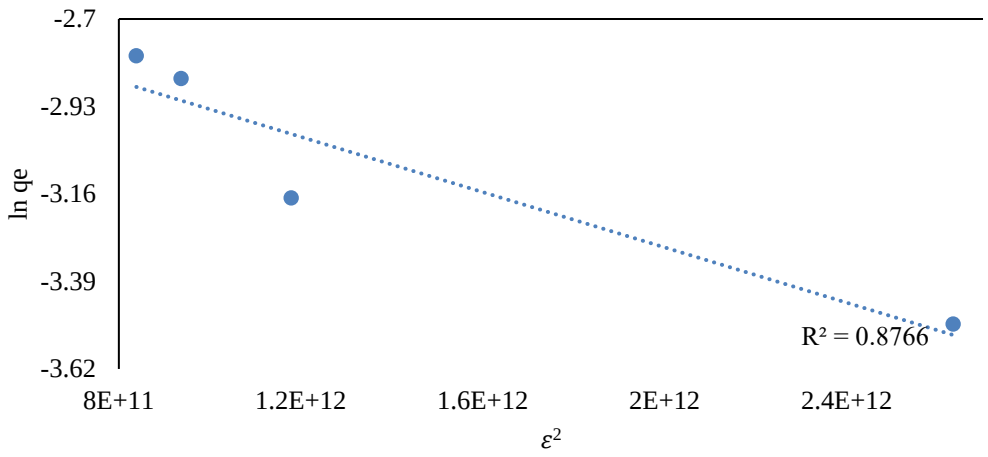

Figure 4.238. D-R isotherm graph of COM-AC for benzene at 5.5 µg/m³.

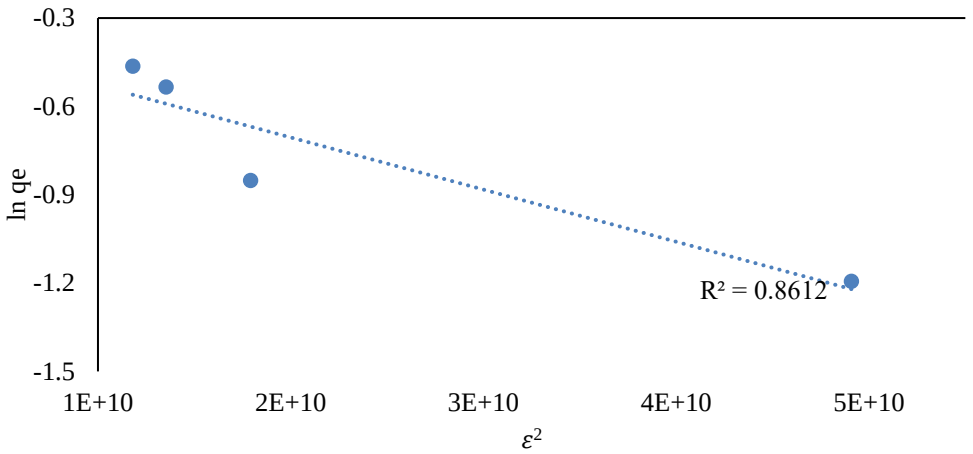

Figure 4.239. D-R isotherm graph of COM-AC for benzene at 54 µg/m³.

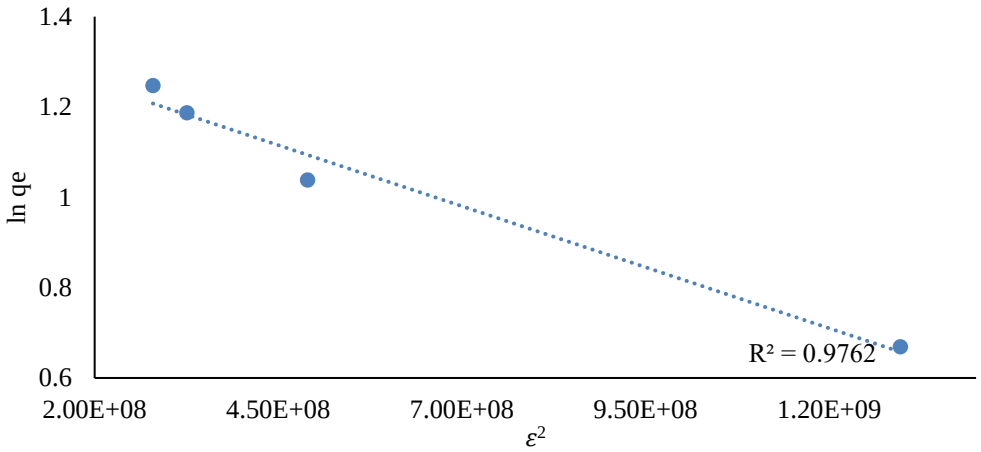

Figure 4.240. D-R isotherm graph of COM-AC for benzene at 322 µg/m³.

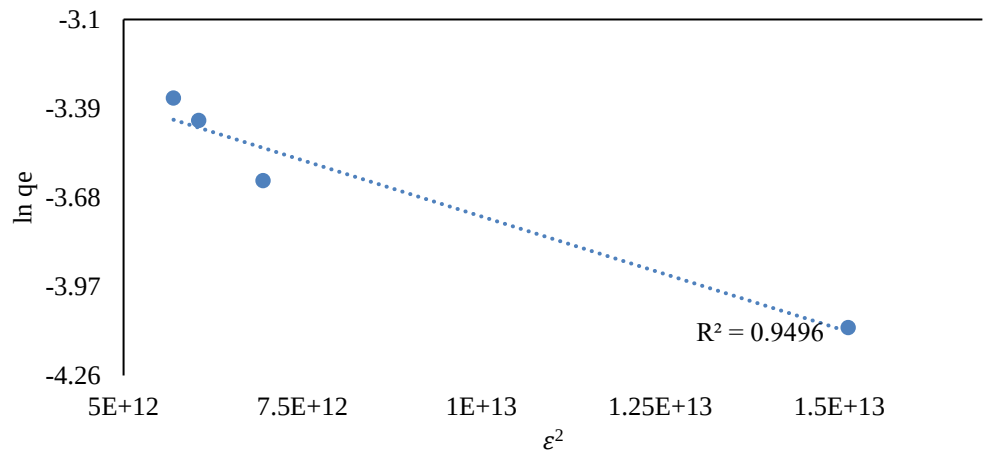

Figure 4.241. D-R isotherm graph of KN-AC for benzene at 2.4 µg/m³.

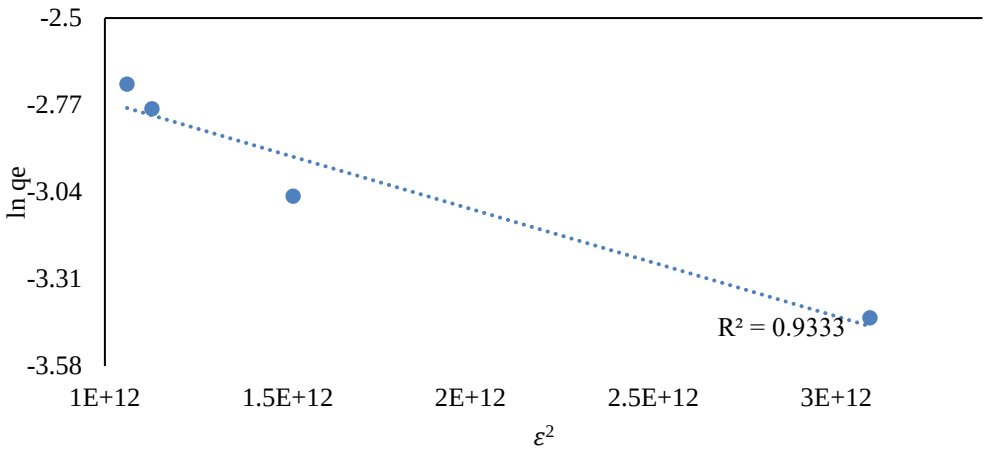

Figure 4.242. D-R isotherm graph of KN-AC for benzene at 5.5 µg/m³.

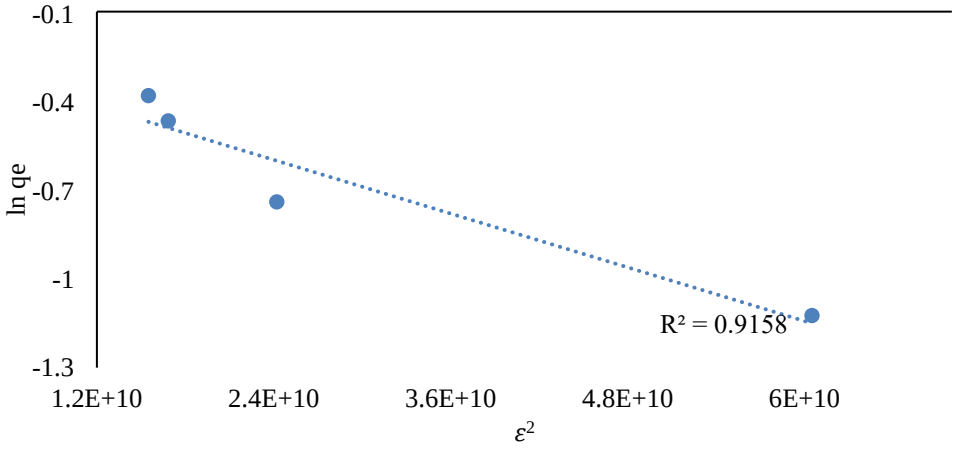

Figure 4.243. D-R isotherm graph of KN-AC for benzene at 54 µg/m³.

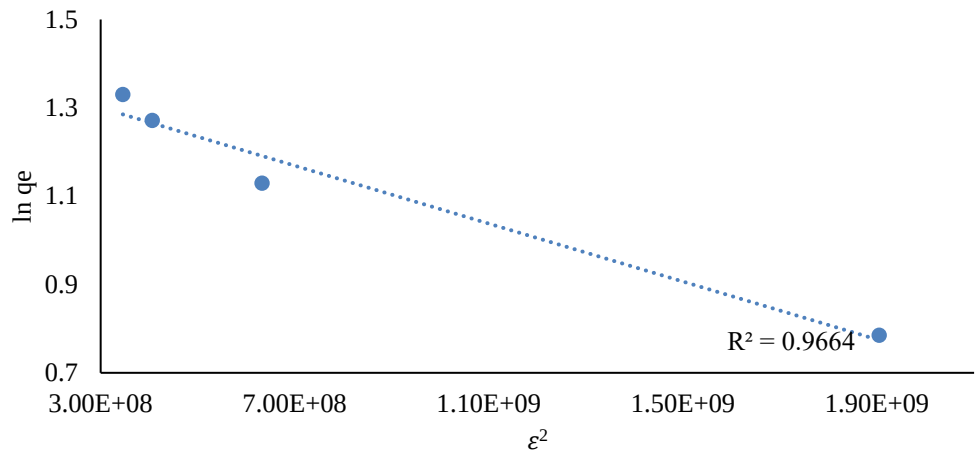

Figure 4.244. D-R isotherm graph of KN-AC for benzene at 322 µg/m³.

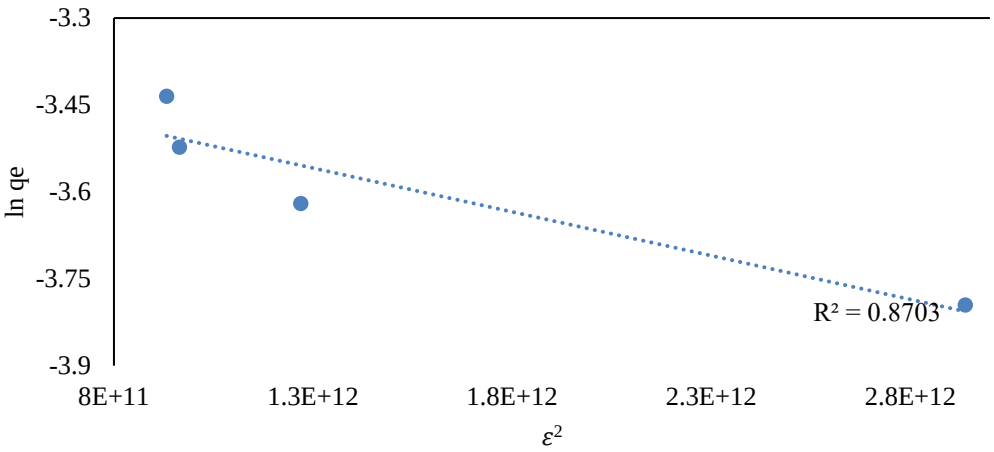

Figure 4.245. D-R isotherm graph of COM-AC for toluene at 3.7 µg/m³.

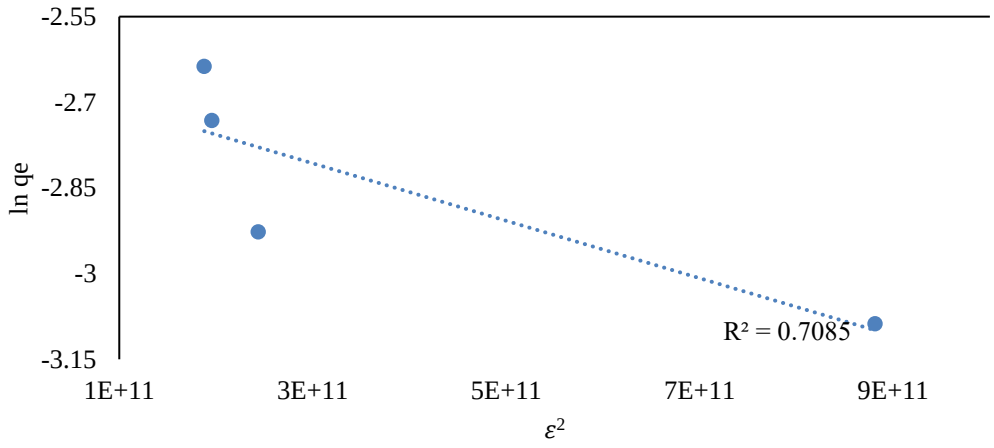

Figure 4.246. D-R isotherm graph of COM-AC for toluene at 9 µg/m³.

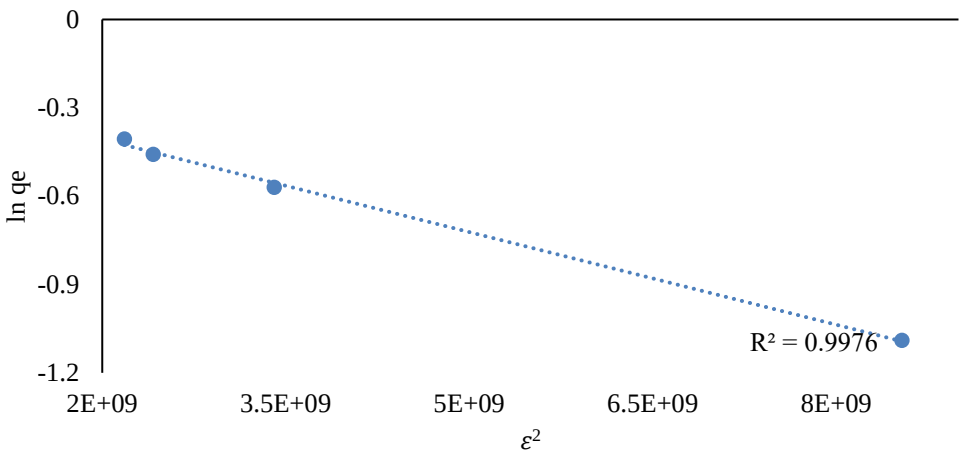

Figure 4.247. D-R isotherm graph of COM-AC for toluene at 86 µg/m³.

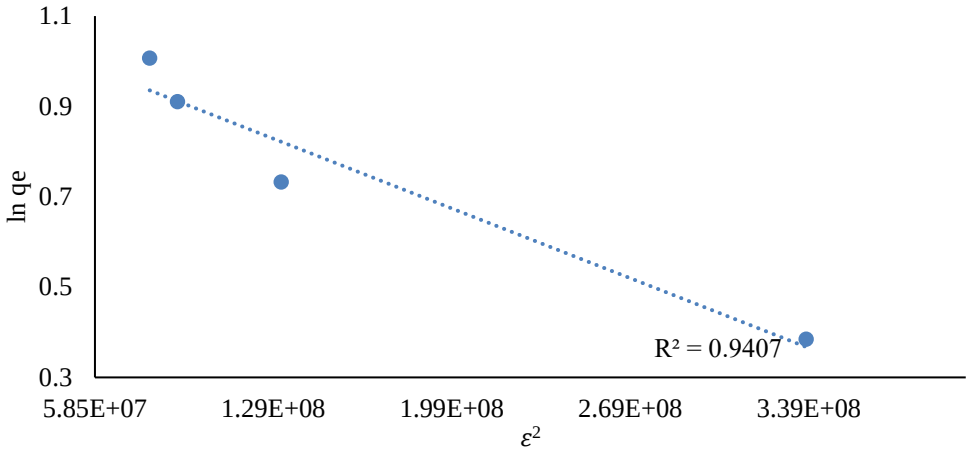

Figure 4.248. D-R isotherm graph of COM-AC for toluene at 414 µg/m³.

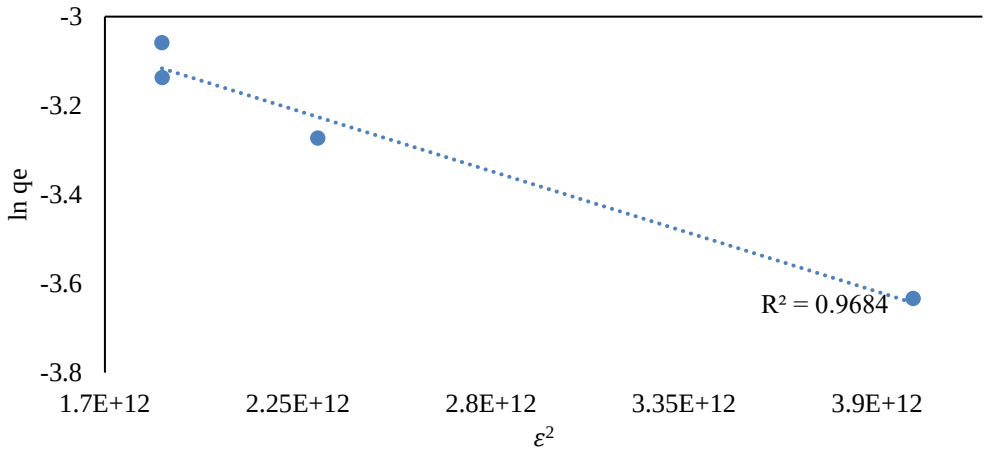

Figure 4.249. D-R isotherm graph of KN-AC for toluene at 3.7 µg/m³.

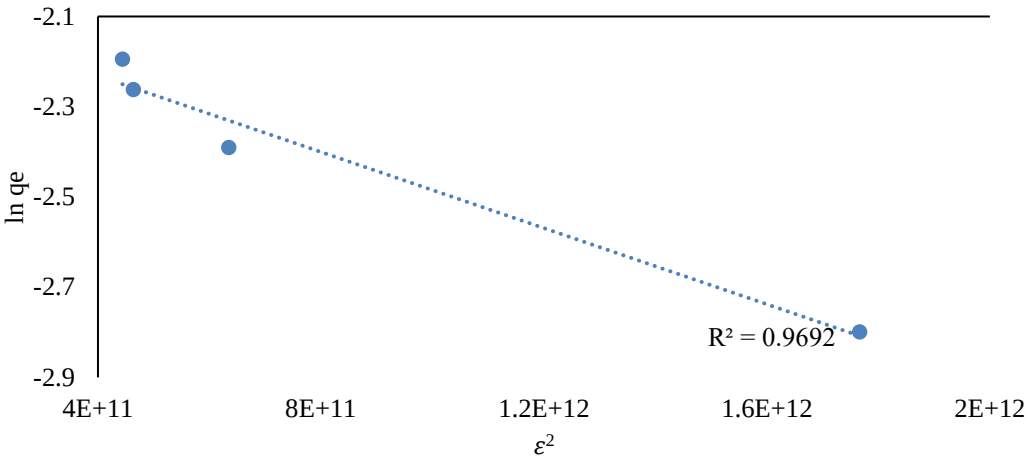

Figure 4.250. D-R isotherm graph of KN-AC for toluene at 9 µg/m³.

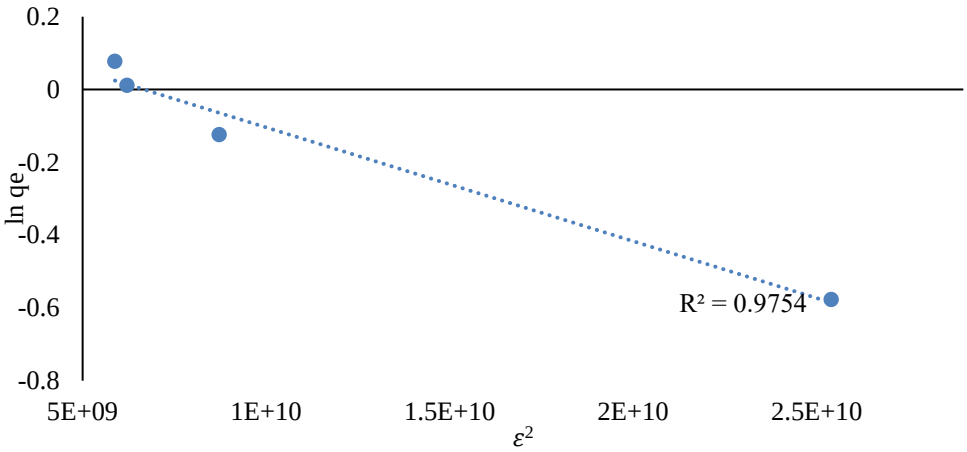

Figure 4.251. D-R isotherm graph of KN-AC for toluene at 86 µg/m³.

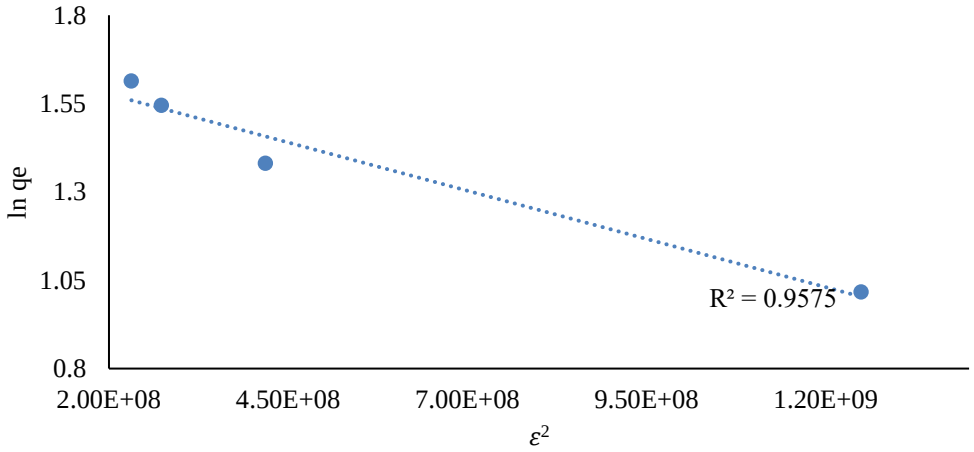

Figure 4.252. D-R isotherm graph of KN-AC for toluene at 414 µg/m³.

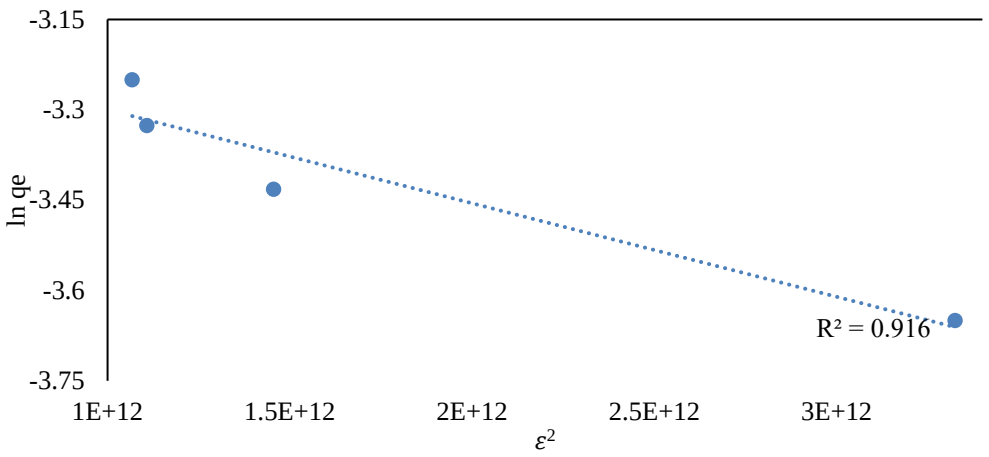

Figure 4.253. D-R isotherm graph of COM-AC for ethylbenzene at 3.9 µg/m³.

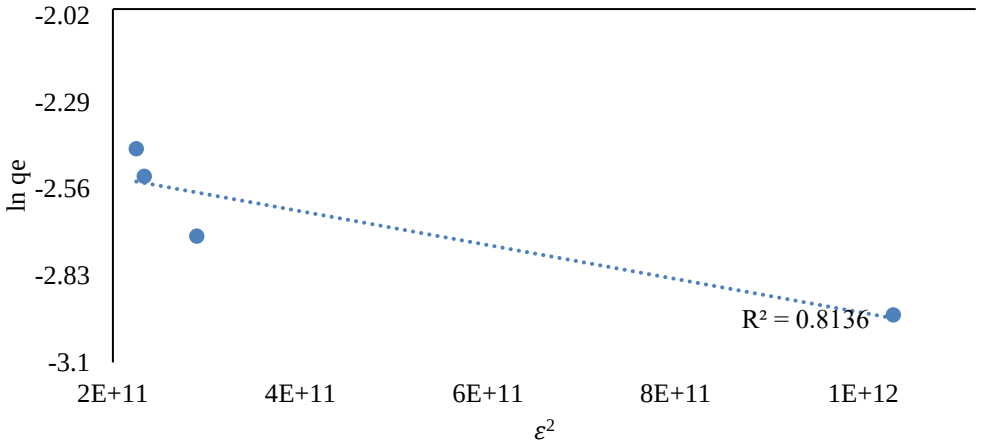

Figure 4.254. D-R isotherm graph of COM-AC for ethylbenzene at 9.2 µg/m³.

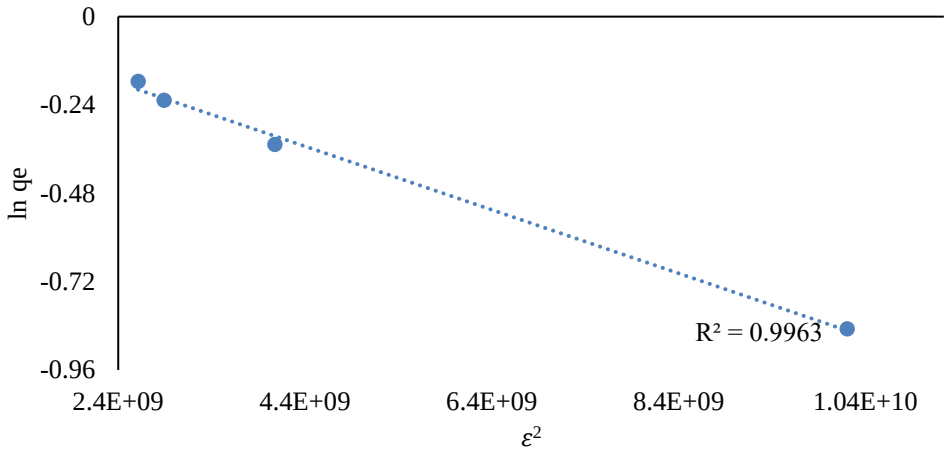

Figure 4.255. D-R isotherm graph of COM-AC for ethylbenzene at 90 µg/m³.

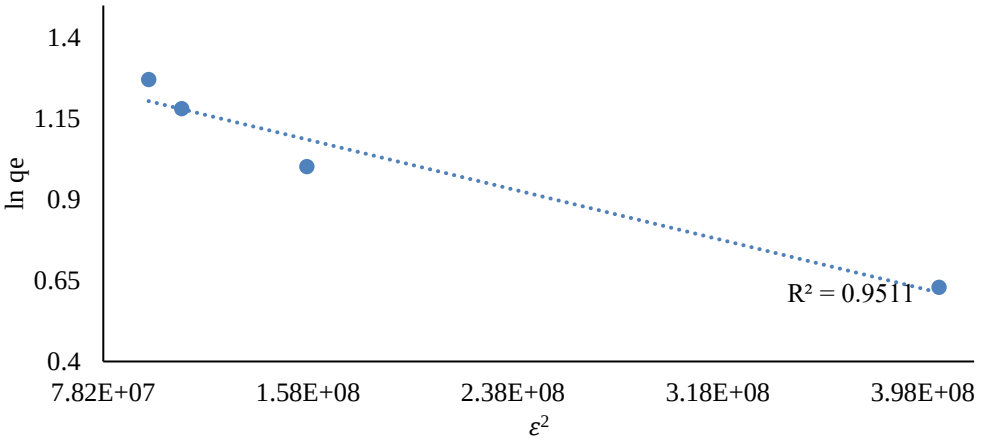

Figure 4.256. D-R isotherm graph of COM-AC for ethylbenzene at 430 µg/m³.

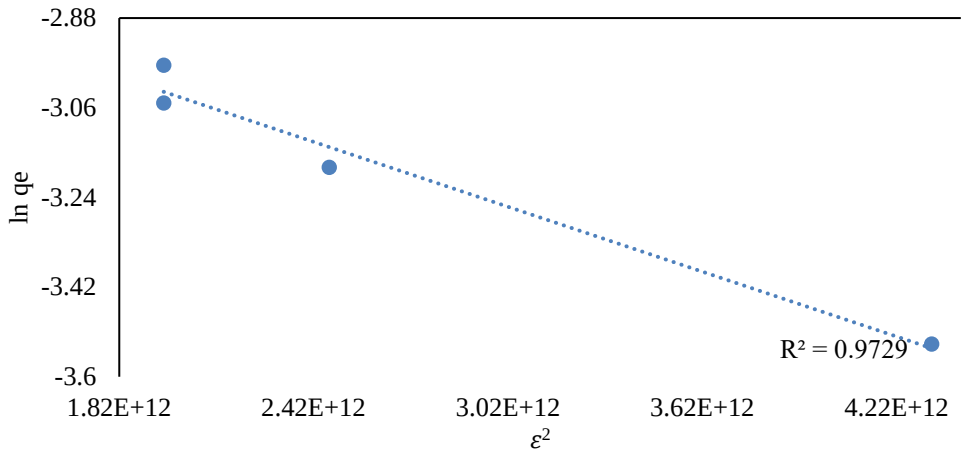

Figure 4.257. D-R isotherm graph of KN-AC for ethylbenzene at 3.9 µg/m³.

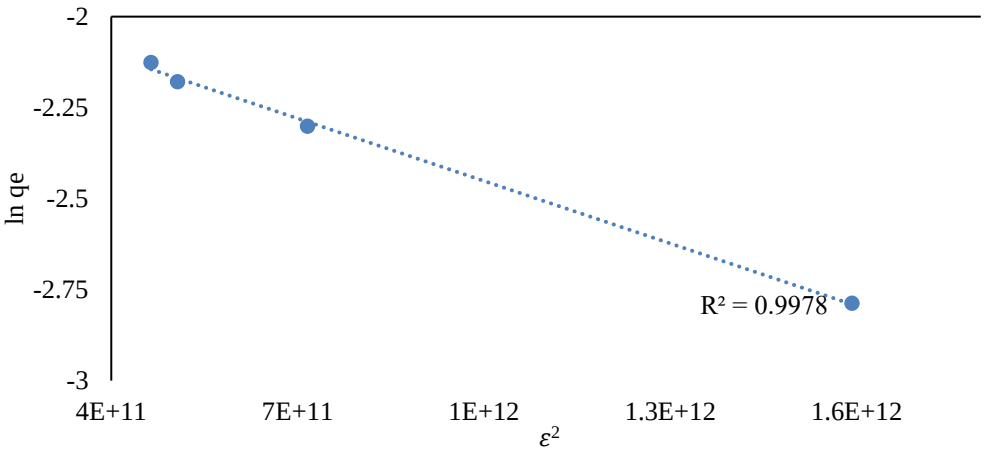

Figure 4.258. D-R isotherm graph of KN-AC for ethylbenzene at 9.2 µg/m³.

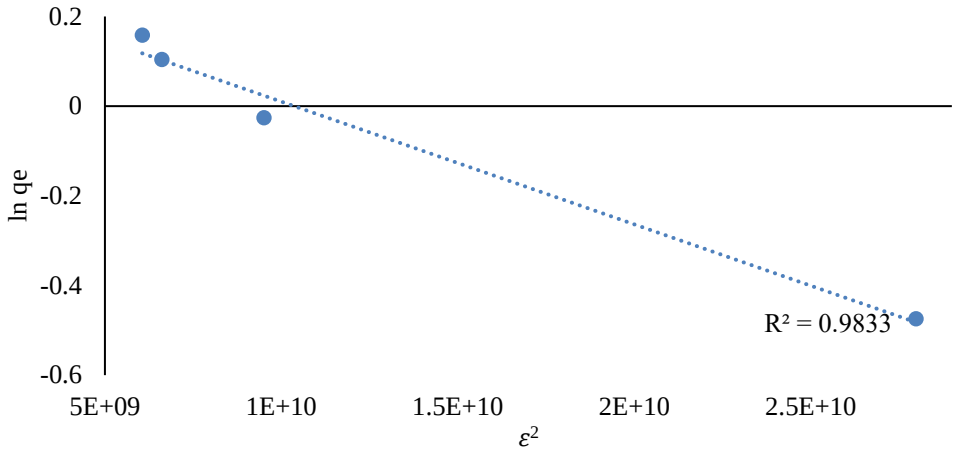

Figure 4.259. D-R isotherm graph of KN-AC for ethylbenzene at 90 µg/m³.

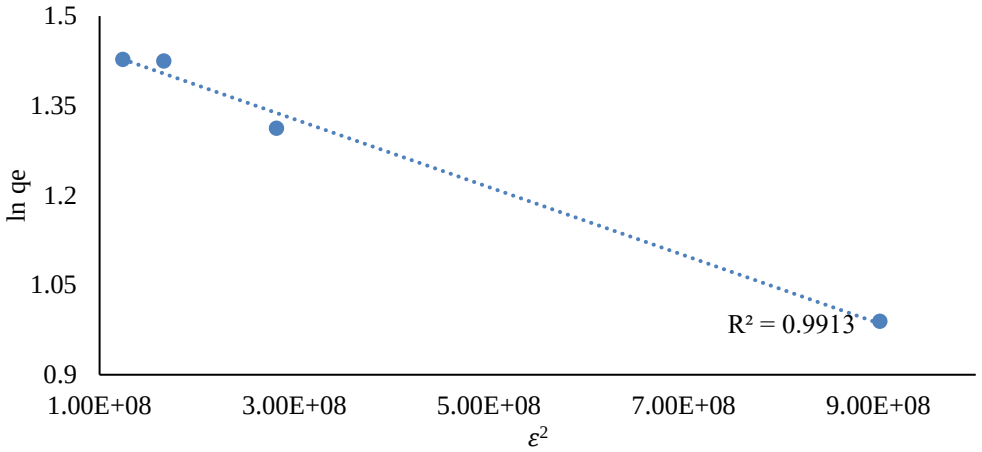

Figure 4.260. D-R isotherm graph of KN-AC for ethylbenzene at 430 µg/m³.

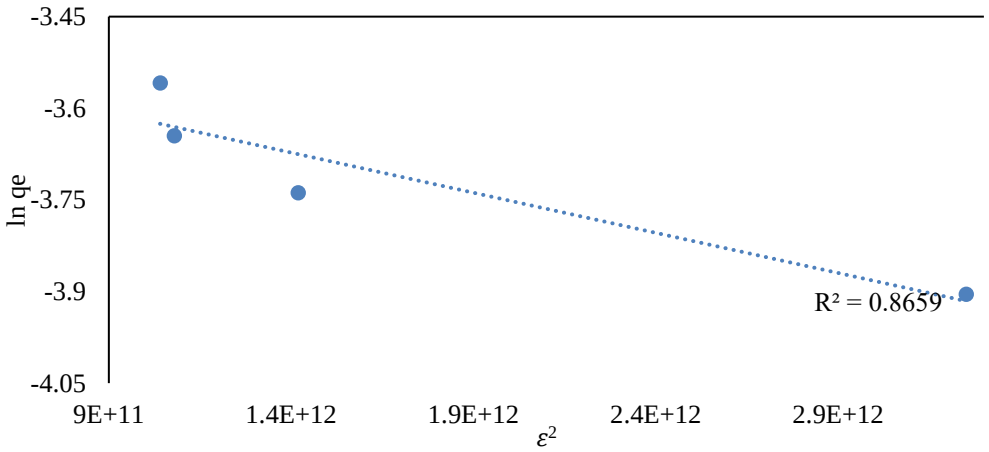

Figure 4.261. D-R isotherm graph of COM-AC for m, p-xylene at 3.4 µg/m³.

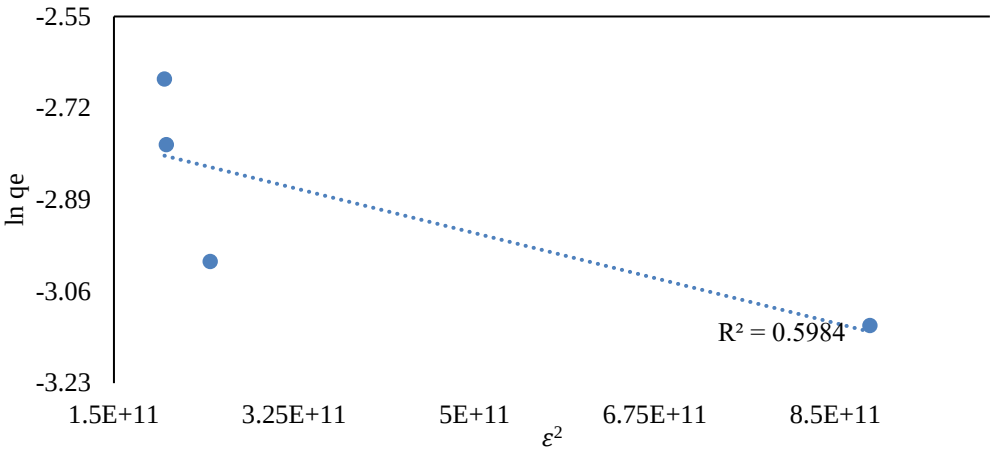

Figure 4.262. D-R isotherm graph of COM-AC for m, p-xylene at 8.5 µg/m³.

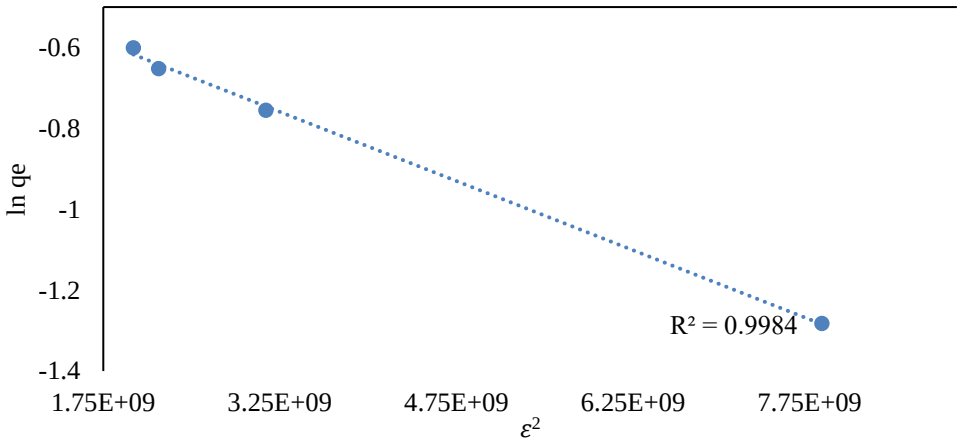

Figure 4.263. D-R isotherm graph of COM-AC for m, p-xylene at 83 µg/m³.

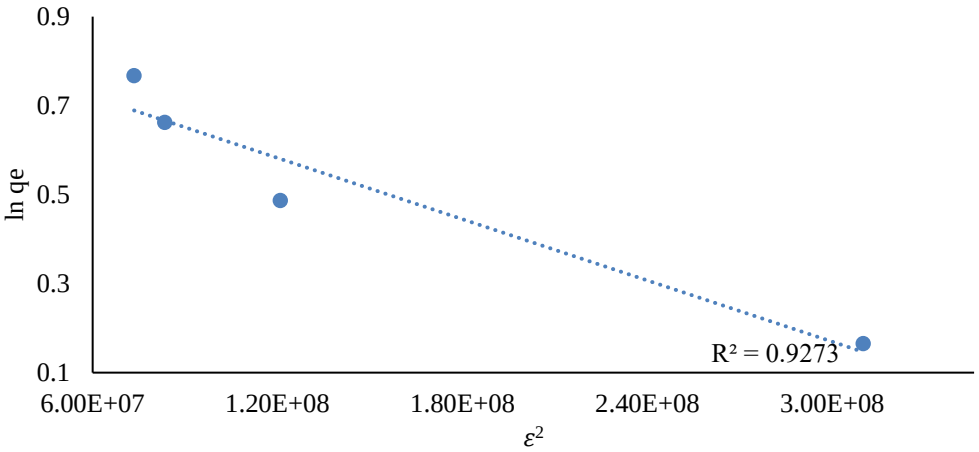

Figure 4.264. D-R isotherm graph of COM-AC for m, p-xylene at 397 µg/m³.

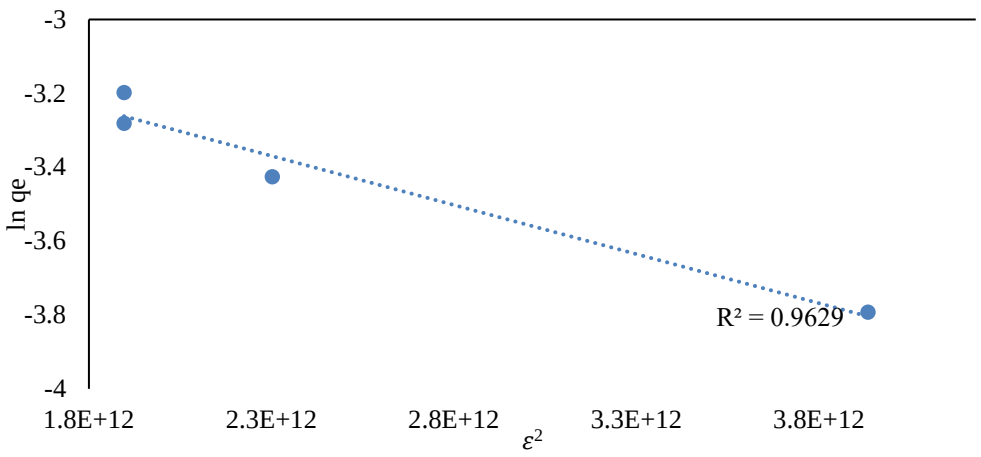

Figure 4.265. D-R isotherm graph of KN-AC for m, p-xylene at 3.4 µg/m³.

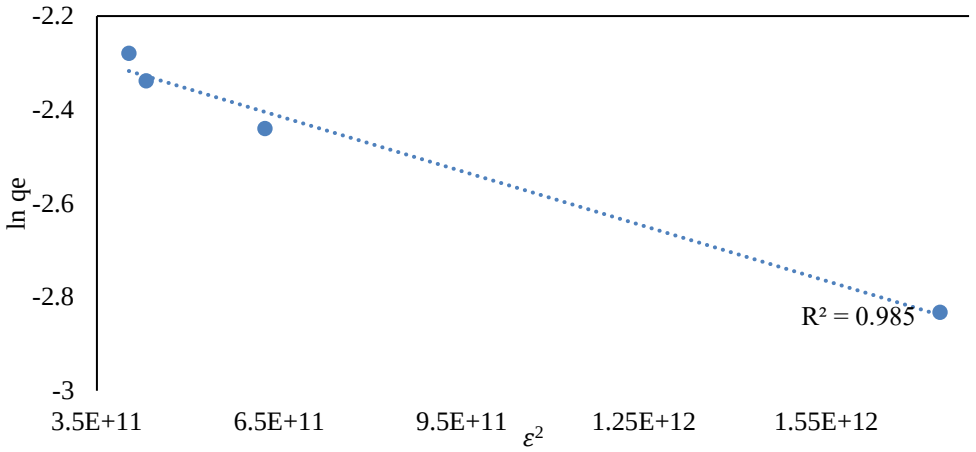

Figure 4.266. D-R isotherm graph of KN-AC for m, p-xylene at 8.5 µg/m³.

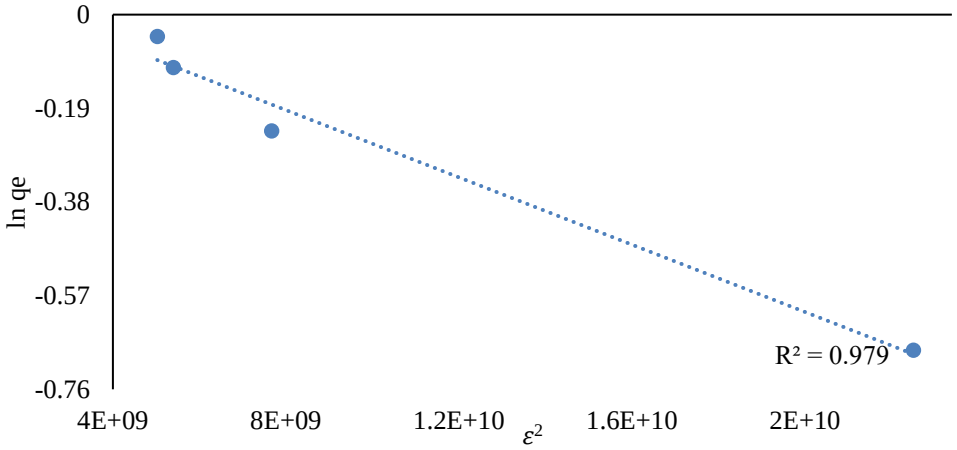

Figure 4.267. D-R isotherm graph of KN-AC for m, p-xylene at 83 µg/m³.

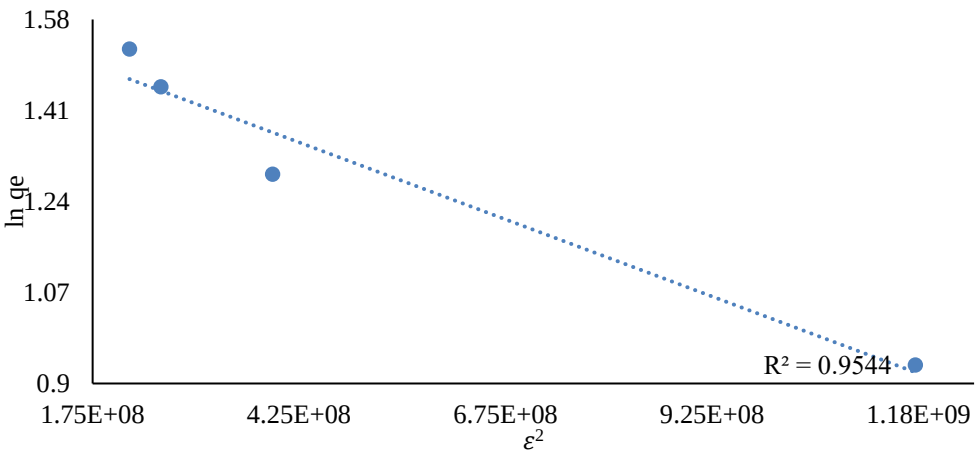

Figure 4.268. D-R isotherm graph of KN-AC for m, p-xylene at 397 µg/m³.

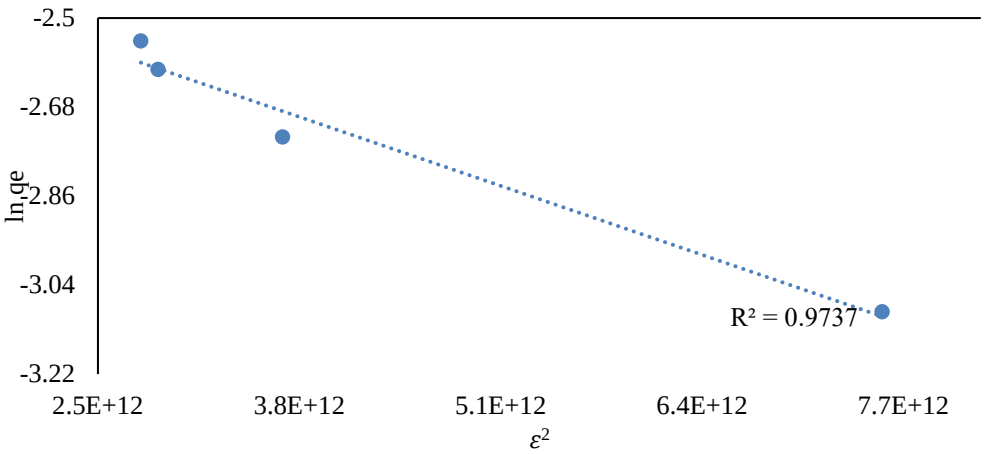

Figure 4.269. D-R isotherm graph of COM-AC for o-xylene at 5.2 µg/m³.

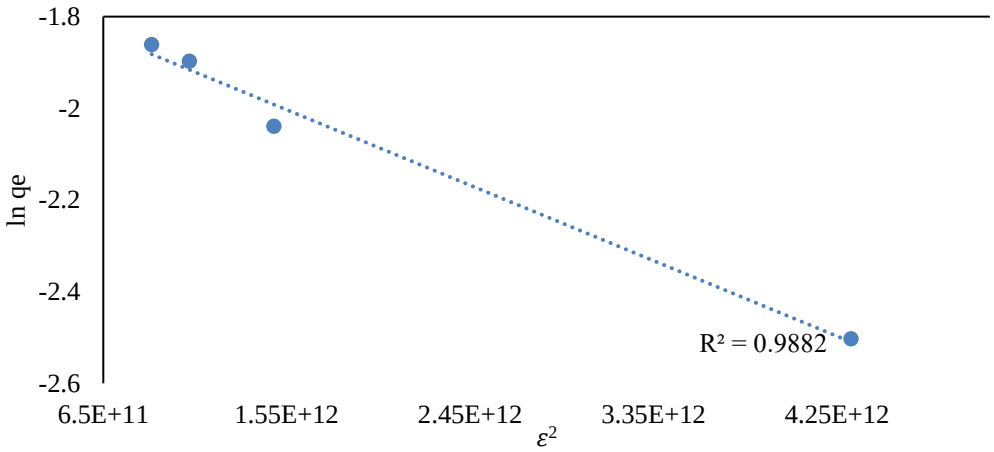

Figure 4.270. D-R isotherm graph of COM-AC for o-xylene at 10 µg/m³.

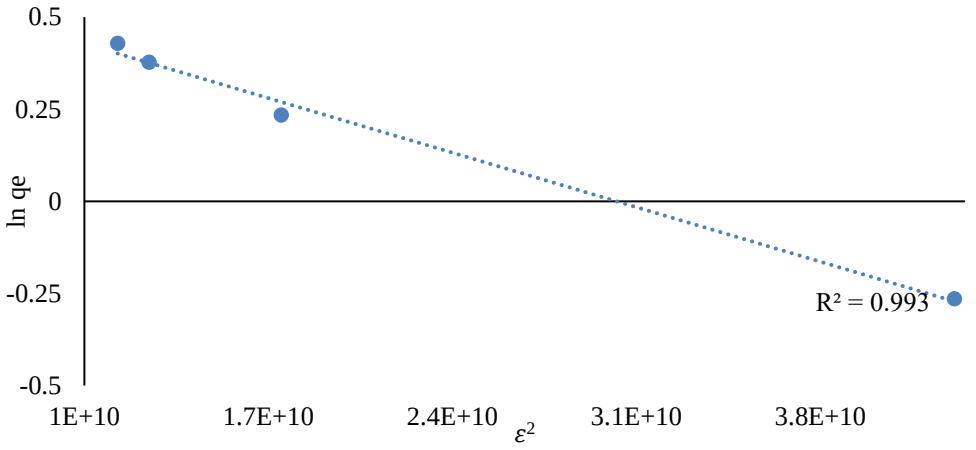

Figure 4.271. D-R isotherm graph of COM-AC for o-xylene at 100 µg/m³.

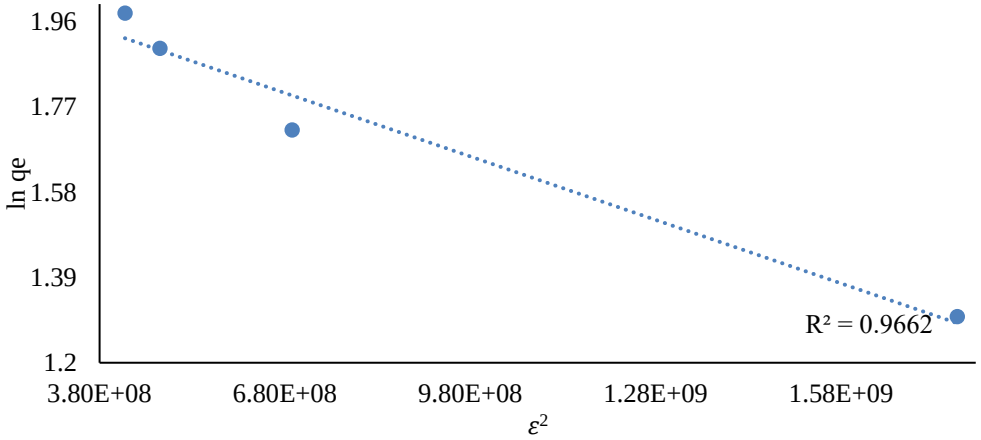

Figure 4.272. D-R isotherm graph of COM-AC for o-xylene at 483 µg/m³.

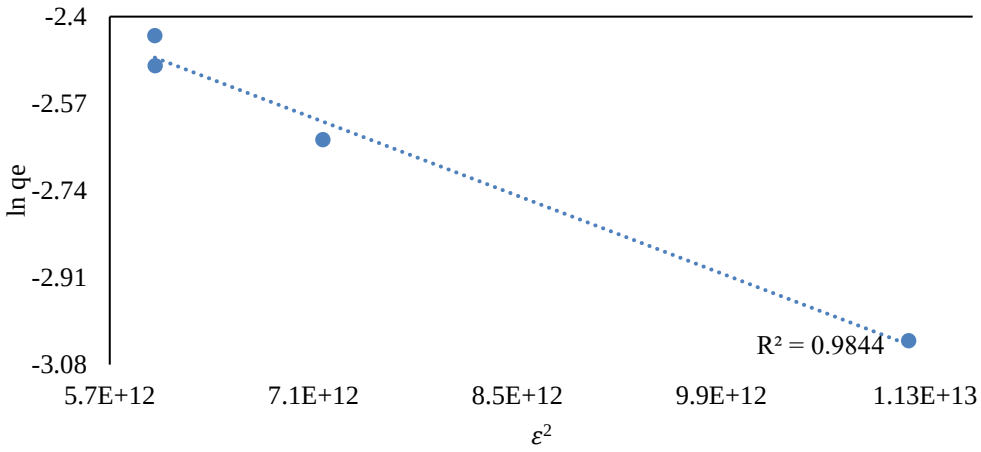

Figure 4.273. D-R isotherm graph of KN-AC for o-xylene at 5.2 µg/m³.

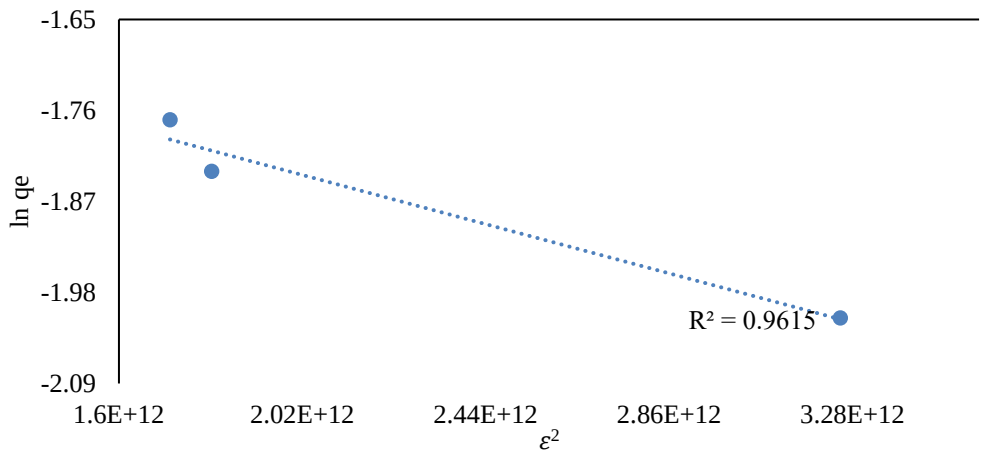

Figure 4.274. D-R isotherm graph of KN-AC for o-xylene at 10 µg/m³.

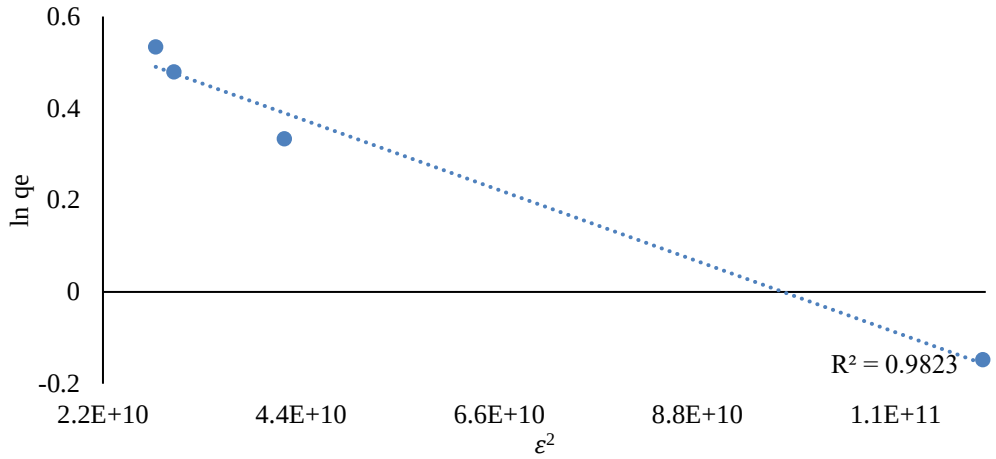

Figure 4.275. D-R isotherm graph of KN-AC for o-xylene at 100 µg/m³.

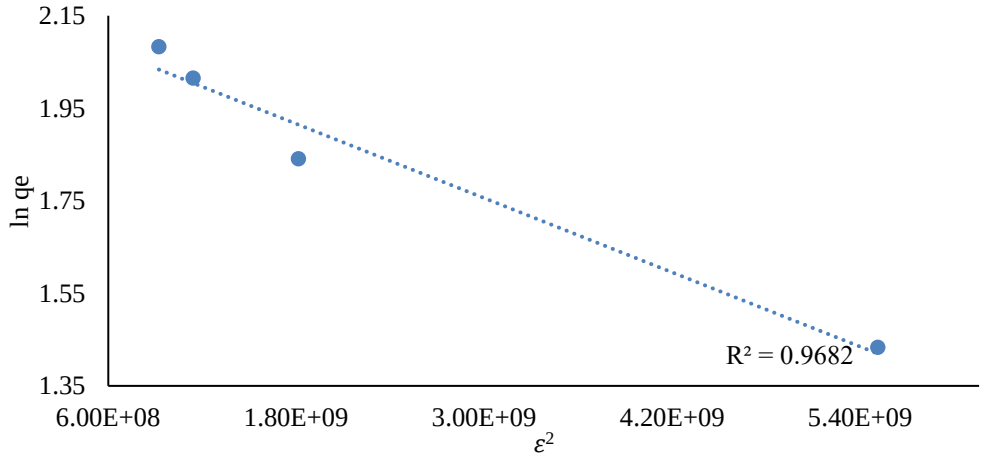

Figure 4.276. D-R isotherm graph of KN-AC for o-xylene at 483 µg/m³.

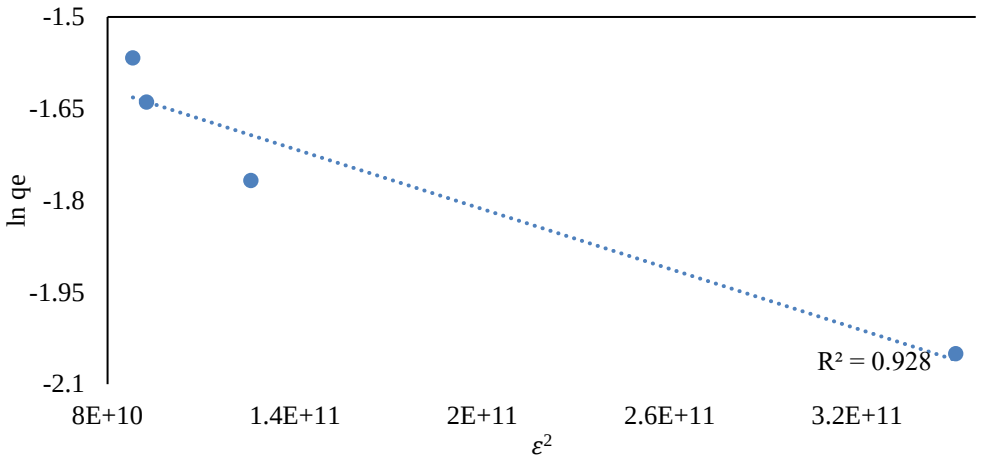

Figure 4.277. D-R isotherm graph of COM-AC for BTEX at 18.5 µg/m³.

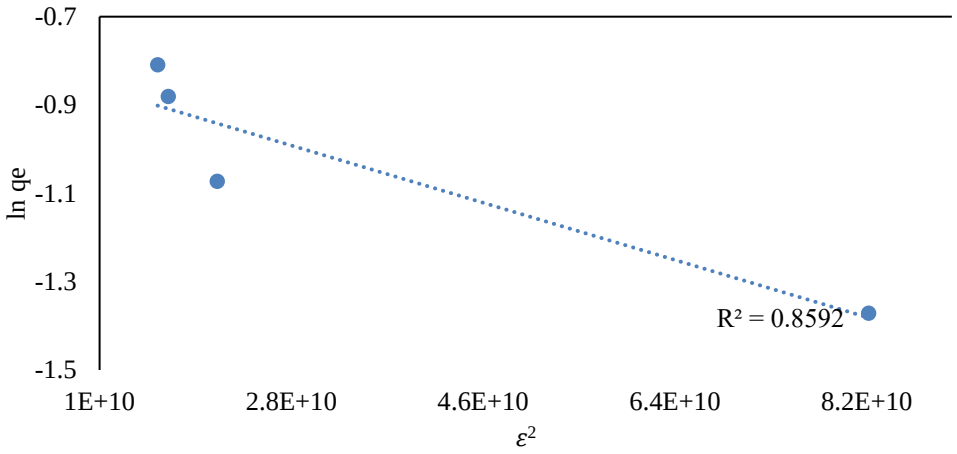

Figure 4.278. D-R isotherm graph of COM-AC for BTEX at 42 µg/m³.

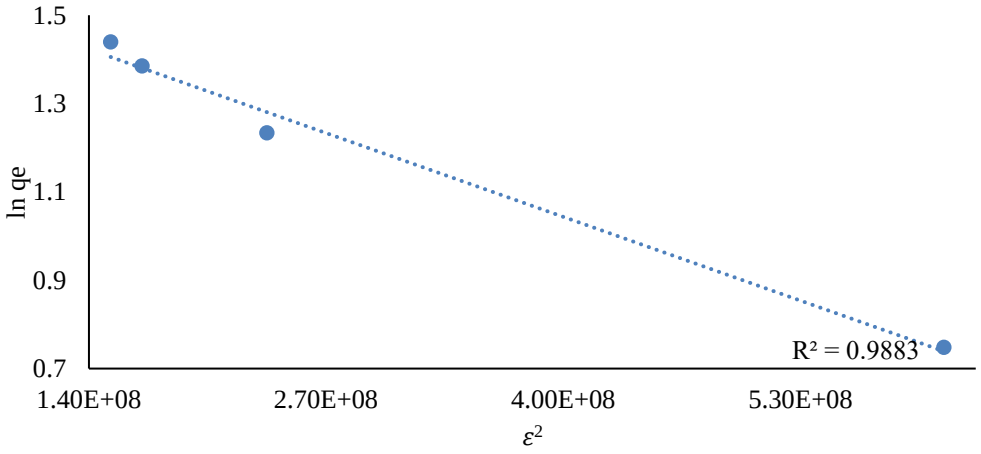

Figure 4.279. D-R isotherm graph of COM-AC for BTEX at 412 µg/m³.

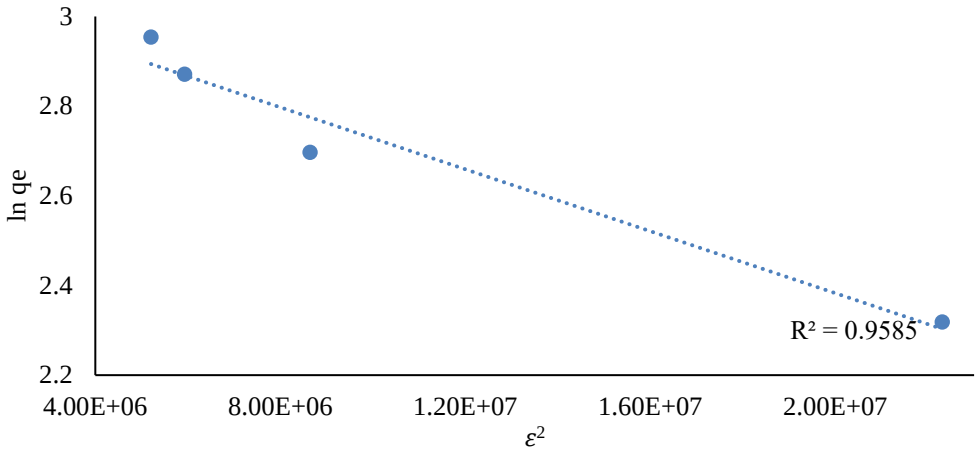

Figure 4.280. D-R isotherm graph of COM-AC for BTEX at 2045 µg/m³.

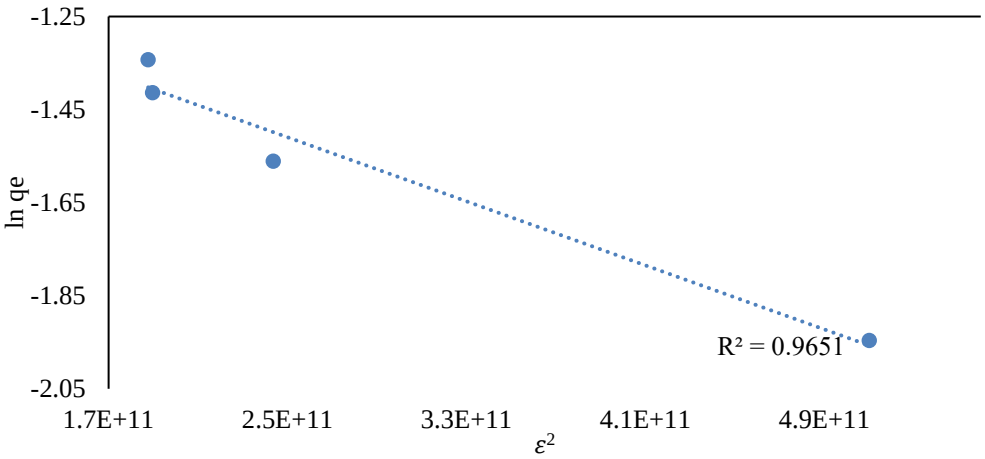

Figure 4.281. D-R isotherm graph of KN-AC for BTEX at 18.5 µg/m³.

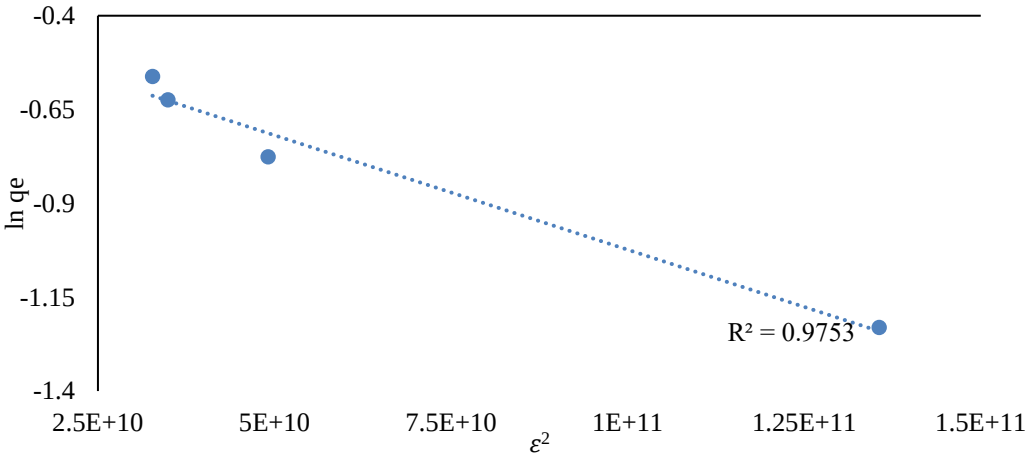

Figure 4.282. D-R isotherm graph of KN-AC for BTEX at 42 µg/m³.

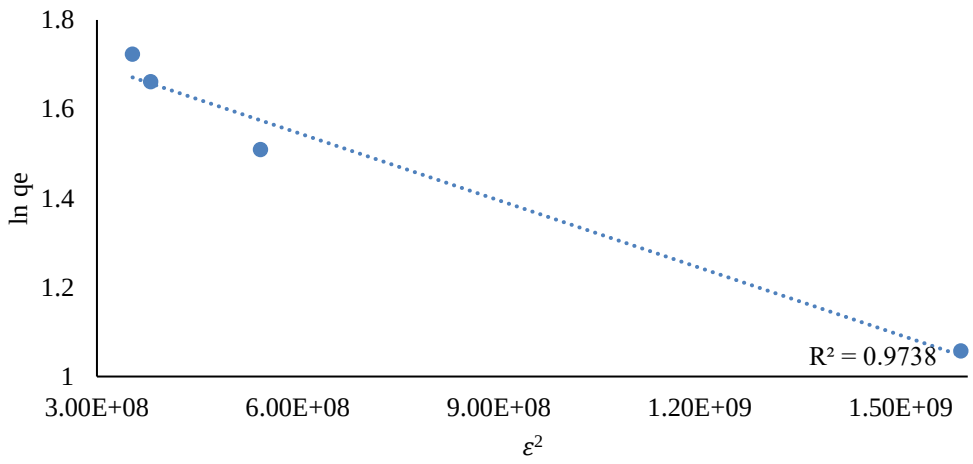

Figure 4.283. D-R isotherm graph of KN-AC for BTEX at 412 µg/m³.

In the given between Figure 4.236 and Figure 4.283 showed that it is compatible with Dubinin-Radushkevich models in line with the parameters obtained from the linear lnqe-ε^2 curves created.

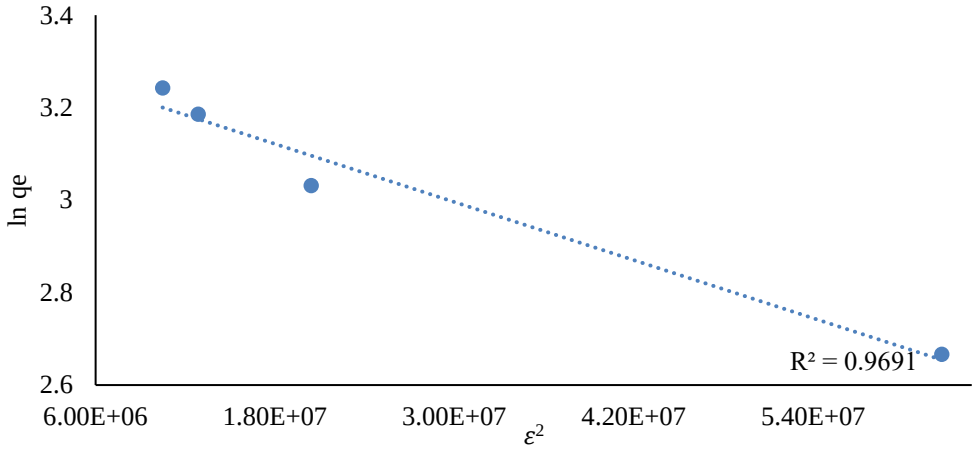

Figure 4.284. D-R isotherm graph of KN-AC for BTEX at 2045 µg/m³.

The D-R parameters obtained from the graph plotted of COM-AC for BTEX were givenin Table 4.20. Accordingly, when the R^2 values for benzene were compared between their concentration values, the highest value was R^2 values was 0.905 at 322±47.80 µg/m^3. These values 0.905 in toluene at 9 µg/m^3, R^2 value was 0.561 with 3.9±0.66 µg/m^3 in

ethylbenzene, it was 0.949 at 397±82.10 µg/m^3 with m, p-xylene, it was 0.949 at 10±2.49 µg/m^3 with o-xylene, and with BTEX 0.893 was found with 42±4.97 µg/m^3.

Table 4.20. Parameters of D-R isotherm for BTEX of COM-AC.

Gases	Average and SD of C_0 (µg/m³)	*K*	q_{max}	*E*	R^2
Benzene	2.4±0.45	-9.32E-14	-3.19	2316.62	0.688
	5.5±1.09	-7.33E-14	-3.01	2612.58	0.802
	54±10.73	-1.51E-13	-3.36	1818.98	0.571
	322±47.80	-2.46E-13	-2.66	1425.09	0.905
Toluene	3.7±0.58	-1.51E-13	-3.36	1818.98	0.571
	9±2.62	-2.46E-13	-2.66	1425.09	0.905
	86±15.83	-1.55E-13	-3.14	1794.46	0.561
	414±47.26	-2.17E-13	-2.60	1517.44	0.712
Ethylbenzene	3.9±0.66	-1.55E-13	-3.14	1794.46	0.561
	9.2±1.59	-2.17E-13	-2.60	1517.44	0.712
	90±15.55	-1.31E-13	-3.49	1951.27	0.305
	430±46.64	-2.66E-13	-2.76	1371.37	0.259
M, p-xylene	3.4±0.72	-1.31E-13	-3.49	1951.27	0.305
	8.5±1.32	-2.66E-13	-2.76	1371.37	0.259
	83±12.95	-1.07E-13	-2.29	2159.05	0.889
	397±82.10	-1.08E-13	-1.83	2148.45	0.949
O-xylene	5.2±0.82	-1.07E-13	-2.29	2159.05	0.889
	10±2.49	-1.08E-13	-1.83	2148.45	0.949
	100±24.38	-1.63E-12	-1.49	553.91	0.877
	483±102.67	-1.72E-12	-1.08	539.09	0.893
BTEX	18.5±1.89	-1.63E-12	-1.49	553.91	0.877
	42±4.97	-1.72E-12	-1.08	539.09	0.893

	412±48.74	-3.63E-13	-2.57	1173.27	0.740
	2045±203.37	-3.33E-13	-2.43	1224.74	0.862

The D-R parameters obtained from the graph plotted of KN-AC for BTEX were givenin Table 4.21. Accordingly, when the R^2 values for benzene were compared between their concentration values, the highest value was R^2 values was 0.905 at 54±10.73 μg/m^3. These values 0.905 in toluene at 3.7±0.58 μg/m^3, R^2 value was 0.889 with 430±46.64 μg/m^3 in ethylbenzene, it was 0.949 at 83±12.95 μg/m^3 with m, p-xylene, it was 0.949 at 5.2 μg/m^3 with o-xylene, and with BTEX 0.893 was found with 18.5±1.89 μg/m^3.

Table 4.21. Parameters of D-R isotherm for BTEX of KN-AC.

Gases	Average and SD of C_0 (μg/m³)	*K*	q_{max}	*E*	R²
Benzene	2.4±0.45	-7.33E-14	-3.01	2612.58	0.802
	5.5±1.09	-1.51E-13	-3.36	1818.98	0.571
	54±10.73	-2.46E-13	-2.66	1425.09	0.905
	322±47.80	-1.55E-13	-3.14	1794.46	0.561
Toluene	3.7±0.58	-2.46E-13	-2.66	1425.09	0.905
	9±2.62	-1.55E-13	-3.14	1794.46	0.561
	86±15.83	-2.17E-13	-2.60	1517.44	0.712
	414±47.26	-1.31E-13	-3.49	1951.27	0.305
Ethylbenzene	3.9±0.66	-2.17E-13	-2.60	1517.44	0.712
	9.2±1.59	-1.31E-13	-3.49	1951.27	0.305
	90±15.55	-2.66E-13	-2.76	1371.37	0.259
	430±46.64	-1.07E-13	-2.29	2159.05	0.889
M, p-xylene	3.4±0.72	-2.66E-13	-2.76	1371.37	0.259
	8.5±1.32	-1.07E-13	-2.29	2159.05	0.889
	83±12.95	-1.08E-13	-1.83	2148.45	0.949

	397±82.10	-1.63E-12	-1.49	553.91	0.877
O-xylene	5.2±0.82	-1.08E-13	-1.83	2148.45	0.949
	10±2.49	-1.63E-12	-1.49	553.91	0.877
	100±24.38	-1.72E-12	-1.08	539.09	0.893
	483±102.67	-3.63E-13	-2.57	1173.27	0.740
BTEX	18.5±1.89	-1.72E-12	-1.08	539.09	0.893
	42±4.97	-3.63E-13	-2.57	1173.27	0.740
	412±48.74	-3.33E-13	-2.43	1224.74	0.862
	2045±203.37	-5.03E-13	-2.66	997.25	0.597

The adsorption studies were performed separately for benzene and BTEX as two groups. Freundlich, Langmuir and Dubinin-Radushkevich isotherm models were applied to determine the isotherm model of adsorption on KN-AC. Also, log qe versus log ce were plotted linearly, which the coefficient values of the isotherm 1/n, KF and R^2 were found to be valued for Langmuir isotherm. By applying linear benzene and BTEX gases to Langmuir isotherm, respectively, the fixed values of 1/qe versus 1/Ce were determined Q_e, K_L, Q_m values.

In Table 4.16, linearized equations and isotherm constants of both isotherms were givenfor adsorption of benzene. In parallel, Freundlich and Langmuir parameters of BTEX were givenin Table 4.17.

According to Table 4.16, when the R^2 values were considered, it was found that values Langmuir isotherm was more compatible at various concentrations for both KN-AC and COM-AC. However, the correlation coefficients ($R^2 \approx 0.95$ to 0.99) were relatively close together. On the other hand, If the parameter n is greater than 1 (n>1), it indicates that the values were following the Langmuir isotherm [137]. In general, it was suitable for the monolayer and multilayer adsorption principle, so Langmuir was more appropriate. When the values in Table 6.2 were examined, n values obtained by calculating the measurements

made in all concentrations prove that the study was compatible with Langmuir isotherm [108].

According to R^2 values in Table 4.17, Langmuir was considered to be greater than 0.96 and the adsorption process was suitable for the monolayer adsorption principle. Simultaneously, when the R_L value is close to 0, it is between 0 and 1, which is called favorable. Both of COM-AC and KN-AC adsorbents were found to be suitable for formaldehyde removal in the Langmuir study.

Another value of Langmuir isotherm is "maximum adsorption capacity" (qmax) of the COM-AC and KN-AC were compared with each other and the capacity of KN-AC was found higher than COM-AC. At the lowest concentration of 2.4±0.45 μg/m³, maximum adsorption capacities of KN-AC and COM-AC were found respectively 0.08 μg/g and 0.05 μg/g. At the highest concentration of 322±47.80 μg/m³, maximum adsorption capacities of KN-AC and COM-AC were found respectively 0.05 μg/g and 0.04 μg/g. It was seen that the maximum adsorption capacity decreases as the concentration increases.

The profile obtained from Table 4.2 at various concentrations was used to obtain Langmuir and Langmuir adsorption isotherm by using well-known adsorption isotherm equations for benzene. In both the cases, linear plots were obtained, which reveal the applicability of these isotherms on the ongoing adsorption process. According to average, positive adsorption tends to remain constant n between 1 and 10 of Langmuir at the same time for Langmuir. There was a small deviation of the Langmuir from the data. However, the Langmuir equation seemed to fit the data better over the entire range of initial concentration. It means that the surfaces of ACs were mainly made up of heterogeneous adsorption.

Linearized equations and isotherm constants of both isotherm models for benzene were givenin Table 4.16 and Table 4.17. The linear correlation coefficient of linearized Langmuir isotherm applied for benzene adsorption was calculated as R^2 value 0.9997

with a value of 322±47.80 µg/m³ and linearized correlation coefficient Langmuir isotherm was calculated as R^2 value 0.9999 with the same concentration.

The lowest linear correlation coefficient of linearized Langmuir isotherm applied for benzene adsorption was R^2 values 0.9436 with 54±10.73 µg/m³, and the correlation coefficient of linearized Langmuir isotherm was calculated as 0.9322. When Langmuir isotherm was compared separately for COM-AC and KN-AC, the highest R^2 values were found to be 0.9999 at the 322±47.80 µg/m³.

In BTEX adsorption parameters, linearized equations and isotherm constants of both isotherm models were givenin between Table 4.16 and Table 4.17. The linear correlation coefficient of linearized langmuir isotherm applied for BTEX adsorption was calculated as 0.9606 lowest value of R^2 value with 18.5±1.89 µg/m³ and the correlation coefficient of linearized Langmuir isotherm was calculated as R^2 value 0.9605 with the same concentration. The highest value of linear correlation coefficient of linearized Langmuir isotherm applied for BTEX adsorption was R^2 values 0.9921 with 412±48.74 µg/m³ and 2045±203.37 µg/m³, and the correlation coefficient of linearized Langmuir isotherm was calculated as 0.9992 and 0.9997

4.3.2. BTEX Removal Efficiency of ACs

The removal efficiency (RE) graphs for KN-AC and COM-AC for BTEX were givenin between Table 4.22 and Table 4.27. According to the RE, the formula given in Eq. (11) in time was calculated and drawn. Here C_0 was defined as the adsorbate concentration in equilibrium (µg/m³). The removal efficiencies of benzene, toluene, ethylbenzene, m, p-xylene, o-xylene and the total BTEX gases, respectively, with COM-AC and KN-AC in the batch reactor. The number of samples from the batch reactor was 4 in total and taken at 15-minute intervals.

Accordingly, KN-AC and COM-AC have the highest efficiency holding capacity against all BTEX gases' lowest concentration value. However, the highest concentration reached the lowest efficient holding capacity. This is because the high concentration of activated

carbon has a high fill in the pores and approximately most of the BTEX have been trapped in the middle of the experiment. The removal study of benzene with COM-AC and KN-AC was given in Table 6.7. When the second concentration value of 5.5±1.09 μg/m³ was analyzed in itself, the data obtained at the end of the experiment showed COM-AC removal with 57.69% efficiency. At the same time, KN-AC was more successful, with 63.29%. In another concentration 54±10.73 μg/m³, the removal efficiency was the highest 58.51% for COM-AC and this value was 63.90% for KN-AC. The lowest RE was 322±47.80 μg/m³ with 54.09%. Despite this, the highest yield was 2.4±0.45 μg/m³ with 65.23% in a batch reactor with the COM-AC. However, the lowest efficiency was at 322±47.80 μg/m³ with 58.75%, while the highest efficiency was at 2.4±0.45 μg/m³ with 73.86 % in KN-AC.

Table 4.22. Removal efficiency of COM-AC and KN-AC for benzene.

	Benzene					
Time (min)	C_0 (μg/m³)	COM-AC %	KN-AC %	C_0 (μg/m³)	COM-AC %	KN-AC %
0	2.4±0.45	0	0	54±10.73	0	0
15		31.26	34.97		28.19	30.25
30		49.44	56.43		39.73	44.53
45		60.57	68.69		54.56	58.65
60		65.23	73.86		58.51	63.90
0	5.5±1.09	0	0	322±47.80	0	0
15		28.50	30.64		30.33	34.06
30		39.72	44.70		43.88	48.06
45		54.36	58.59		50.91	55.39
60		57.69	63.29		54.09	58.75

The studies having different concentration values of benzene, toluene, ethylbenzene, m, p-xylene, o-xylene and total BTEX gases were examined with specific amounts COM-AC and KN-AC of removal efficiency of them in Figure 4.285 and Figure 4.296.

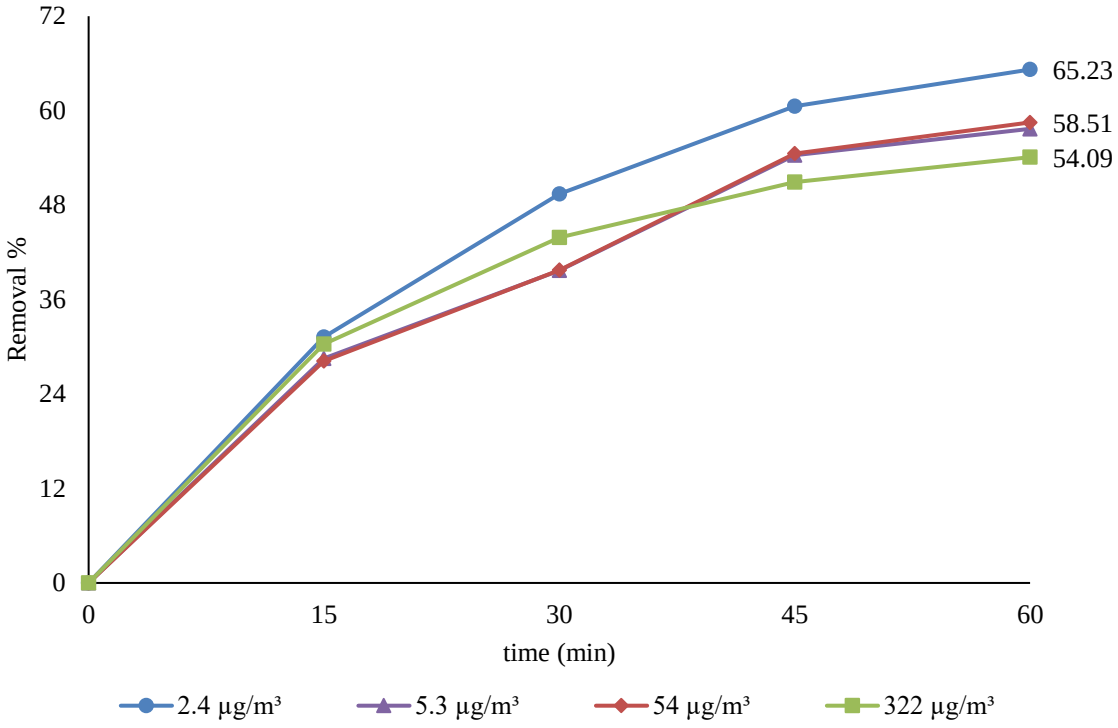

Figure 4.285. Removal efficiency of benzene for COM-AC.

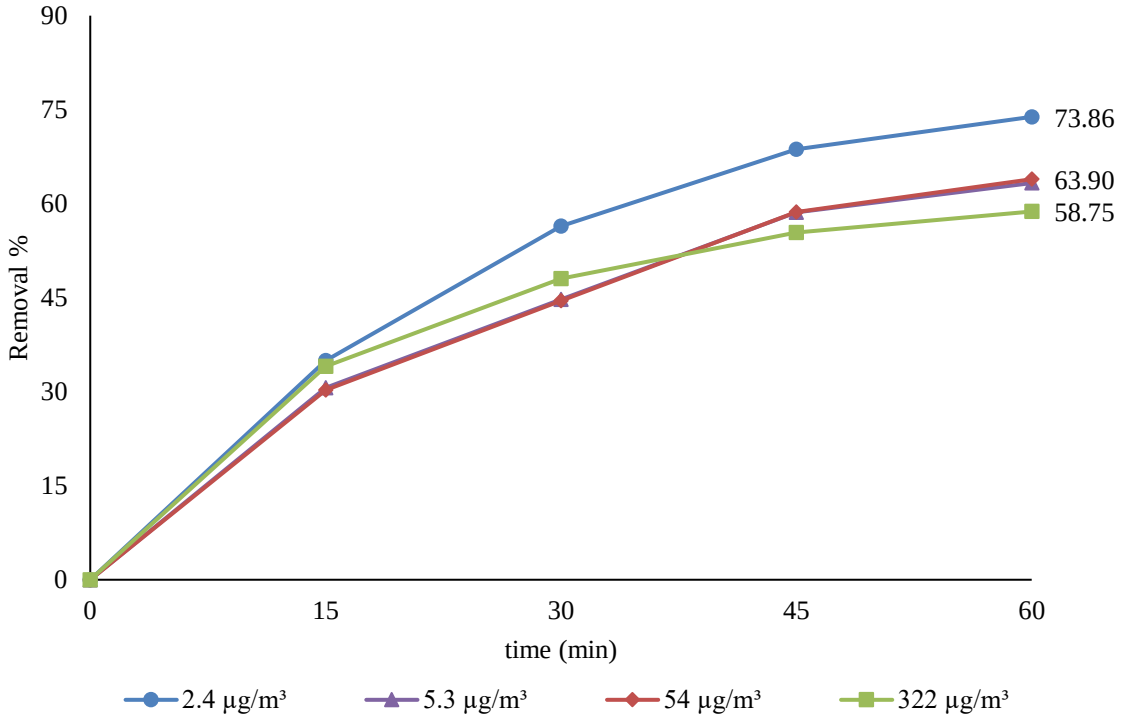

Figure 4.286. Removal efficiency of benzene for KN-AC.

The removal study of toluene with COM-AC and KN-AC was given in Table 4.23. When the second concentration value of 9±2.62 was analyzed in itself, the data obtained at the end of the experiment showed COM-AC removal with 40.63% efficiency, while KN-AC was more successful with 63.21%. In another concentration, 86±15.83 µg/m³, the RE was the highest 38.79% for COM-AC and this value was 62.95% for KN-AC. The lowest RE was 414±47.26 µg/m³, with 33.12%. Despite this, the highest yield was 3.7±0.58 µg/m³with 63.31% in a batch reactor with the COM-AC. However, when the KN-AC was placed in the batch reactor and the work started, the lowest efficiency was 414±47.26 µg/m³ with 60.72%, while the highest efficiency was at 3.7±0.58 µg/m³ with 63.31%.

Table 4.23. Removal efficiency of COM-AC and KN-AC for toluene.

Time (min)	Toluene					
	C_0 (μg/m³)	COM-AC %	KN-AC %	C_0 (μg/m³)	COM-AC %	KN-AC %
0		0	0		0	0
15		30.29	35.62		19.59	32.71
30	3.7±0.58	36.11	51.07	86±15.83[3]	32.92	51.47
45		39.80	58.52		36.83	58.94
60		43.44	63.31		38.79	62.95
0		0	0		0	0
15		25.89	34.54		17.77	33.44
30	9±2.62[3]	30.41	51.96	414±47.26	25.17	48.11
45		36.95	59.11		30.06	56.68
60		40.63	63.21		33.12	60.72

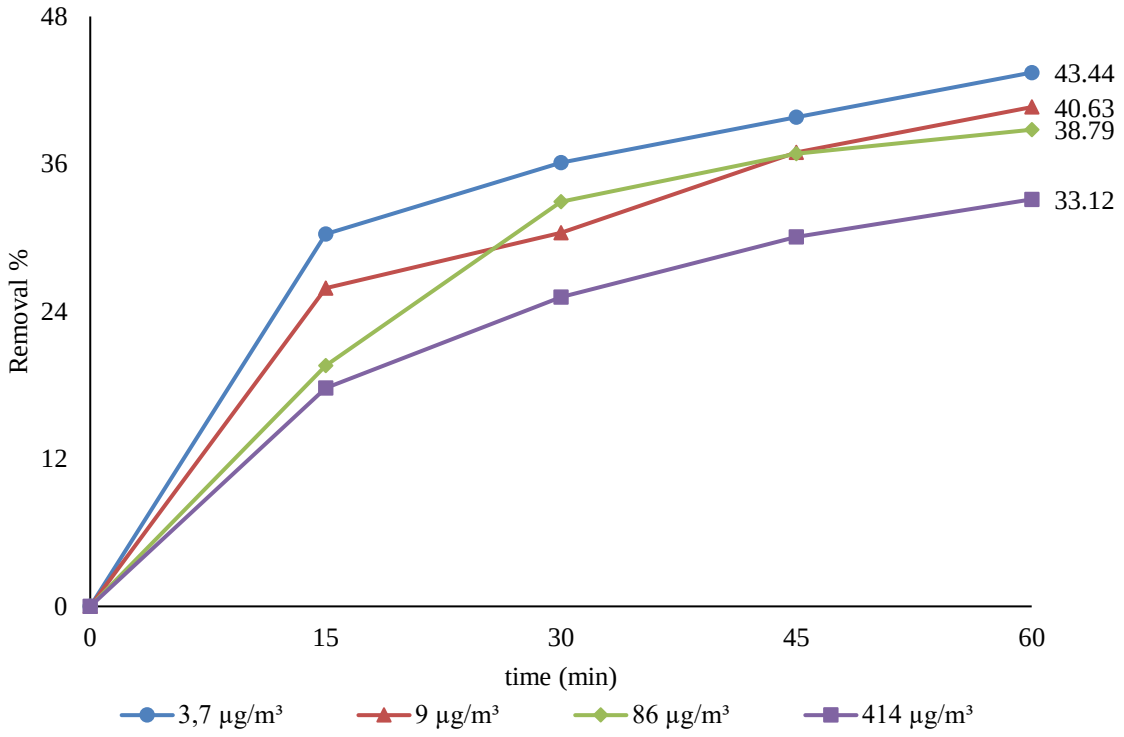

Figure 4.287. Removal efficiency of toluene for COM-AC.

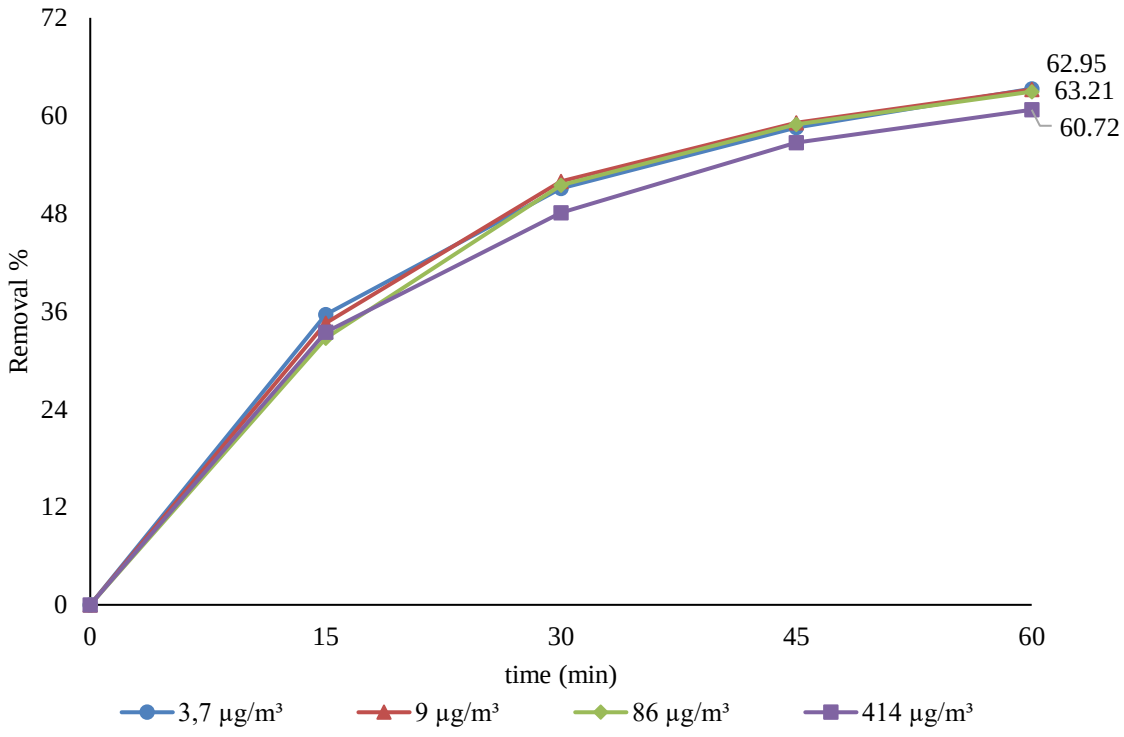

Figure 4.288. Removal efficiency of toluene for KN-AC.

Another contaminant, ethylbenzene study with COM-AC and KN-AC, was given in Table 4.24. When the second concentration value of 9.2±1.59 μg/m³ was analyzed in itself, the data obtained at the end of the experiment showed COM-AC removal with 48.05% efficiency, while KN-AC was more successful with 65.37%. In another concentration 90±15.55 μg/m³, the RE was the highest 46.64% for COM-AC and this value was 65.15% for KN-AC. The lowest RE was 430±46.64 μg/m³, with 41.38%. Despite this, the highest yield was 3.9±0.66 μg/m³ with 50.08% in a batch reactor with the COM-AC. However, when the KN-AC was placed in the batch reactor and the work started, the lowest efficiency was 430±46.64 μg/m³ with 48.41%, while the highest efficiency was at 3.7±0.58 μg/m³ with 65.96%.

Table 4.24. Removal efficiency of COM-AC and KN-AC for ethylbenzene.

Time (min)	Ethylbenzene					
	C_0 (μg/m³)	COM-AC %	KN-AC %	C_0 (μg/m³)	COM-AC %	KN-AC %
0	3.9±0.66	0	0	90±15.5³	0	0
15		33.57	37.69		23.80	23.80
30		41.75	53.76		39.30	39.30
45		46.40	61.17		44.32	44.32
60		50.08	65.96		46.64	65.15
0	9.2±1.59	0	0	430±46.6	0	0
15		28.62	28.62		21.79	31.23
30		36.60	36.60		31.60	43.13
45		44.09	44.09		37.81	48.27
60		48.05	65.37		41.38	48.41

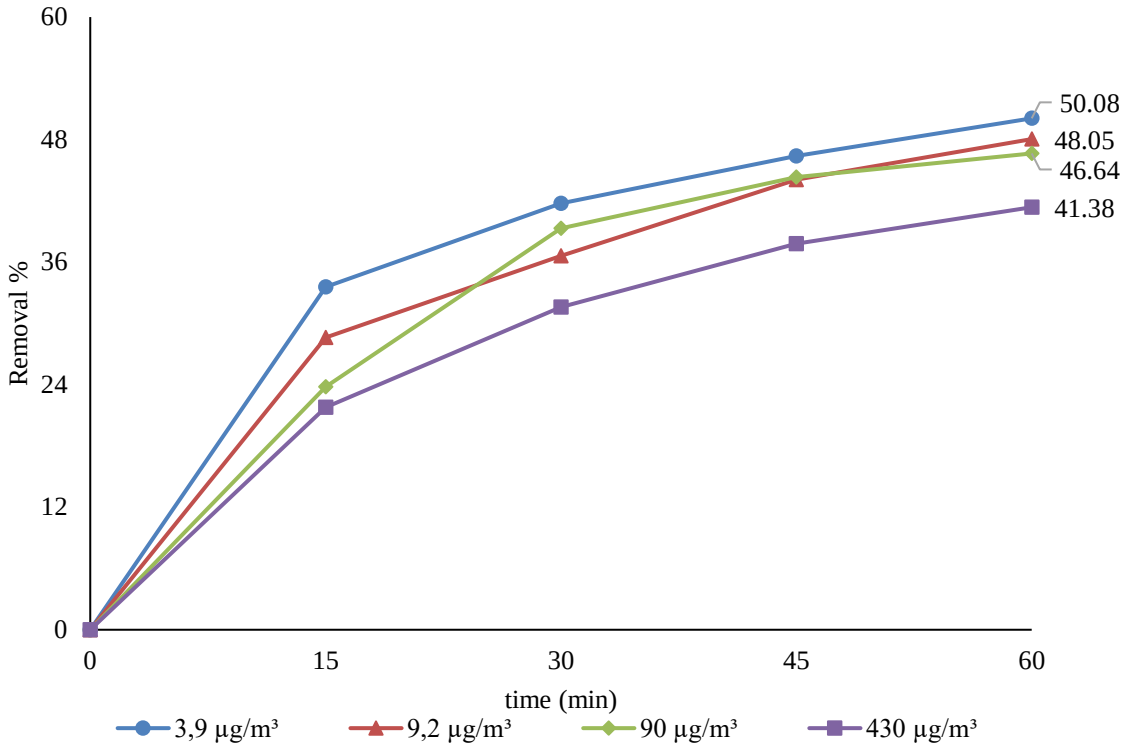

Figure 4.289. Removal efficiency of ethylbenzene for COM-AC.

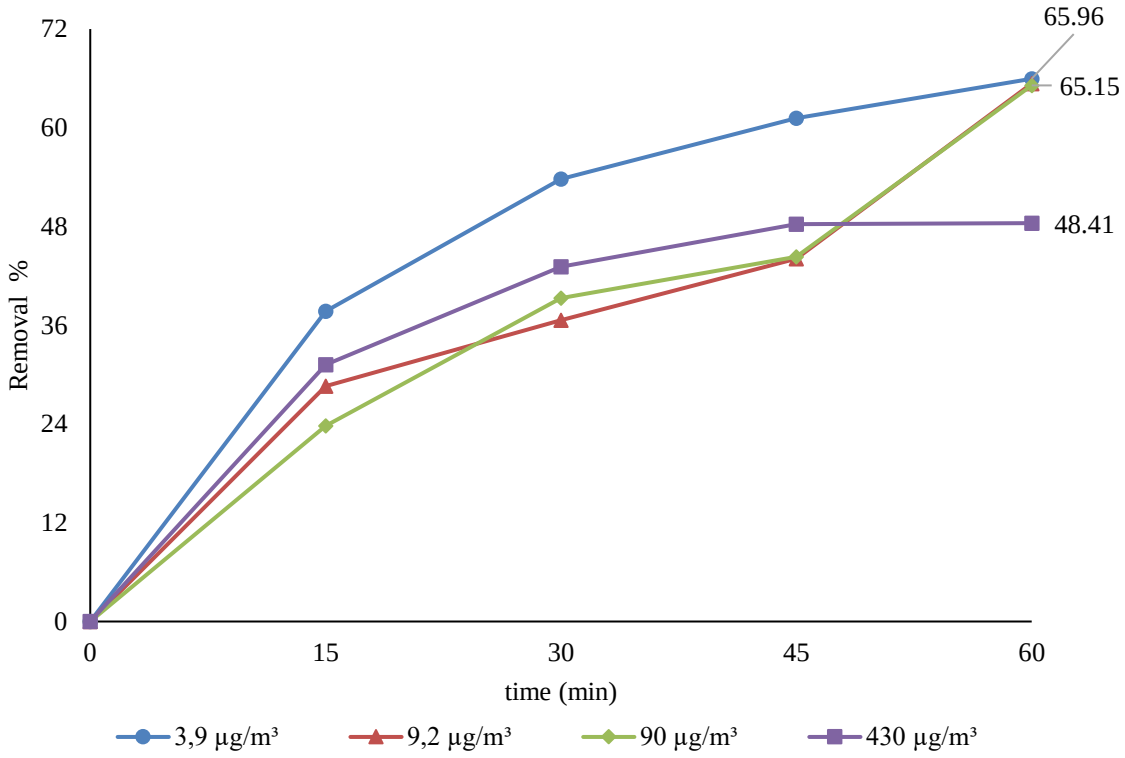

Figure 4.290. Removal efficiency of ethylbenzene for KN-AC.

The different polluter was m, p-xylene removal study with COM-AC and KN-AC was given in Table 4.25. When the second concentration value of 8.5±1.32 μg/m³ was analyzed in itself, the data achieved at the end of the experiment showed COM-AC removal with 40.69% efficiency. At the same time, KN-AC was more successful, with 59.90%. In another concentration 83±12.95 μg/m³, the RE was the highest 33.35% for COM-AC and this value was 58.13% for KN-AC. The lowest RE was 397±82.10 μg/m³ with 27.18%. Despite this, the highest yield was 3.4±0.72 μg/m³ with 42.04% in a batch reactor with the COM-AC. However, when the KN-AC was placed in the batch reactor and the work started, the lowest efficiency was at 397±82.10 μg/m³ with 57.98%, while the highest efficiency was at 3.4±0.72 μg/m³ with 60.28%.

Table 4.25. Removal efficiency of COM-AC and KN-AC for m, p-xylene.

Time (min)	m, p-xylene					
	C_0 (μg/m³)	COM-AC %	KN-AC %	C_0 (μg/m³)	COM-AC %	KN-AC %
0	3.4±0.72	0	0	83±12.95	0	0
15		29.74	33.26		16.86	30.77
30		35.12	47.99		28.58	48.02
45		38.55	55.50		31.66	54.60
60		42.04	60.28		33.35	58.13
0	8.5±1.32	0	0	397±82	0	0
15		25.75	34.45		14.89	32.13
30		29.01	51.02		20.54	45.89
45		36.03	56.50		24.48	54.03
60		40.69	59.90		27.18	57.98

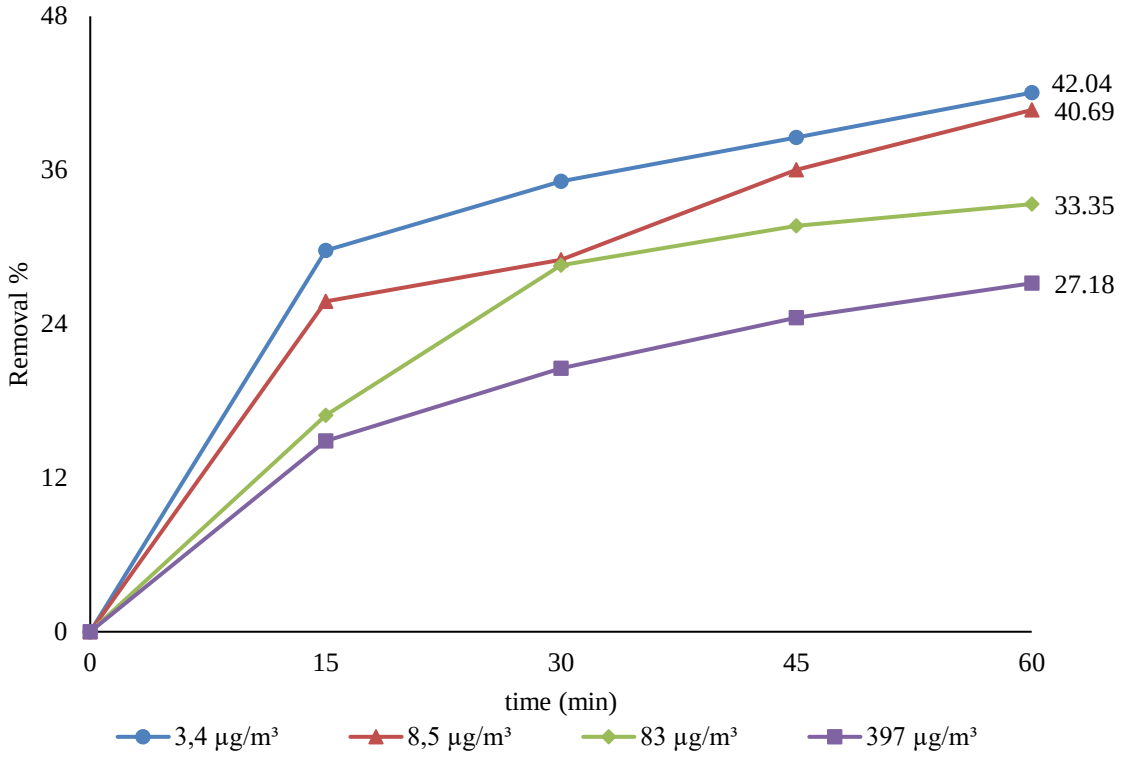

Figure 4.291. Removal efficiency of m, p-xylene for COM-AC.

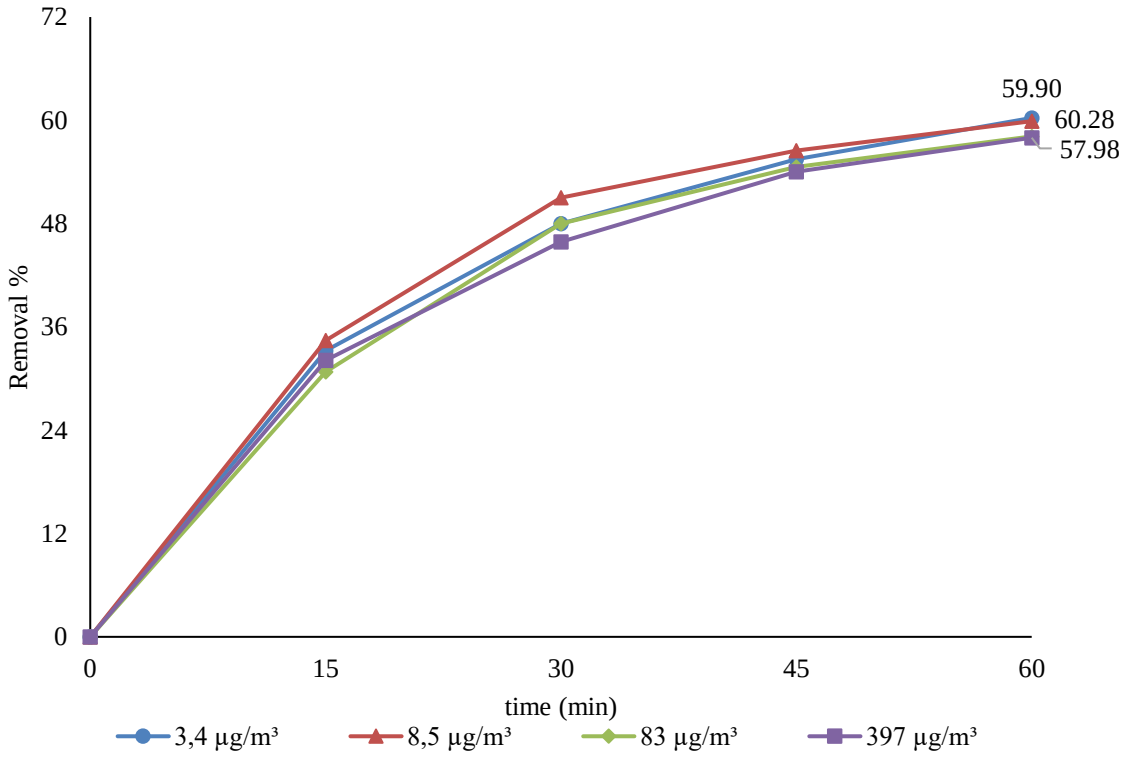

Figure 4.292. Removal efficiency of m, p-xylene for KN-AC.

The following pollutant was an o-xylene removal study with COM-AC and KN-AC was given in Table 4.26. When the second concentration value of 10±2.49 μg/m³ was analyzed in itself, the data was procured at the end of the experiment showed COM-AC removal with 78.25% efficiency, while KN-AC was more successful with 85.56%. In another concentration 100±24.38 μg/m³, the RE was the highest 77.07% for COM-AC and this value was 85.60% for KN-AC. The lowest RE was 483±102.67 μg/m³ with 75.08%. Despite this, the highest yield was 5.2±0.82 μg/m³ with 78.99% in batch reactor with the COM-AC. However, when the KN-AC was placed in the batch reactor and the work started, the lowest efficiency was 483±102.67 μg/m³ with 83.20%, while the highest efficiency was 5.2±0.82 μg/m³ with 88.07%.

Table 4.26. Removal efficiency of COM-AC and KN-AC for o-xylene.

Time (min)	o-xylene					
	C_0 (μg/m³)	COM-AC %	KN-AC %	C_0 (μg/m³)	COM-AC %	KN-AC %
0	5.2±0.82	0	0	100±24.38	0	0
15		45.69	48.55		38.51	43.30
30		65.04	71.89		63.40	70.08
45		74.57	83.09		73.17	81.06
60		78.99	88.07		77.07	85.60
0	10±2.49	0	0	483±102.67	0	0
15		41.18	39.45		38.16	43.46
30		65.46	67.34		57.86	65.33
45		75.45	80.40		69.43	77.73
60		78.25	85.56		75.08	83.20

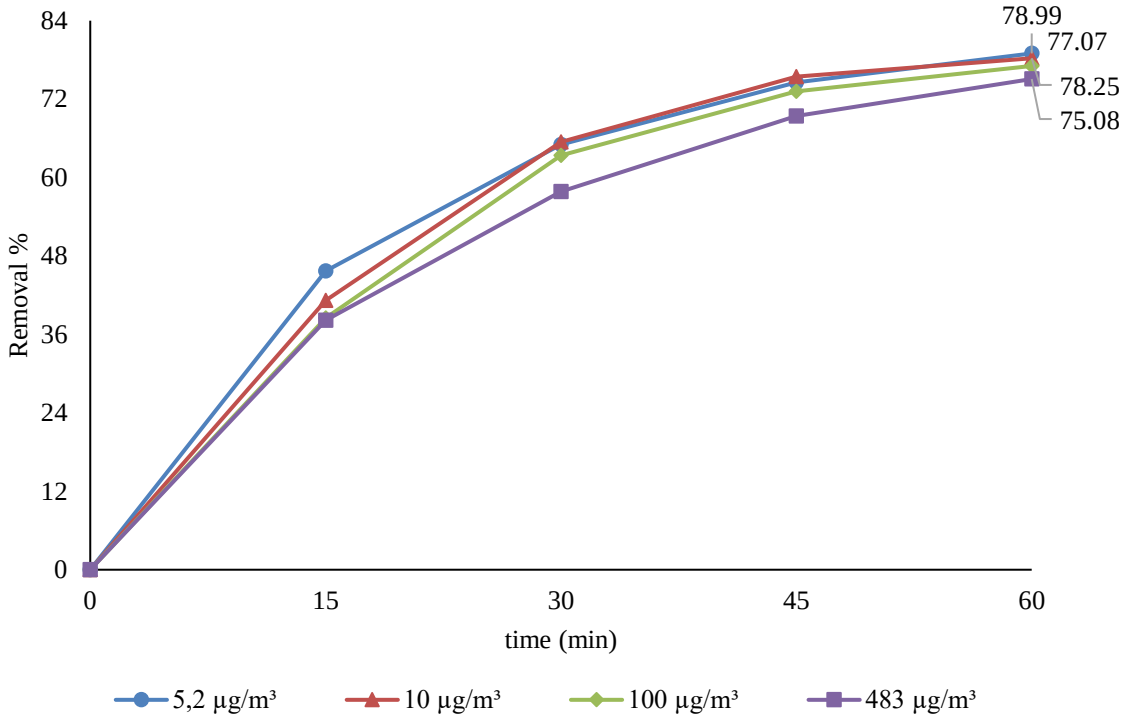

Figure 4.293. Removal efficiency of o-xylene for COM-AC.

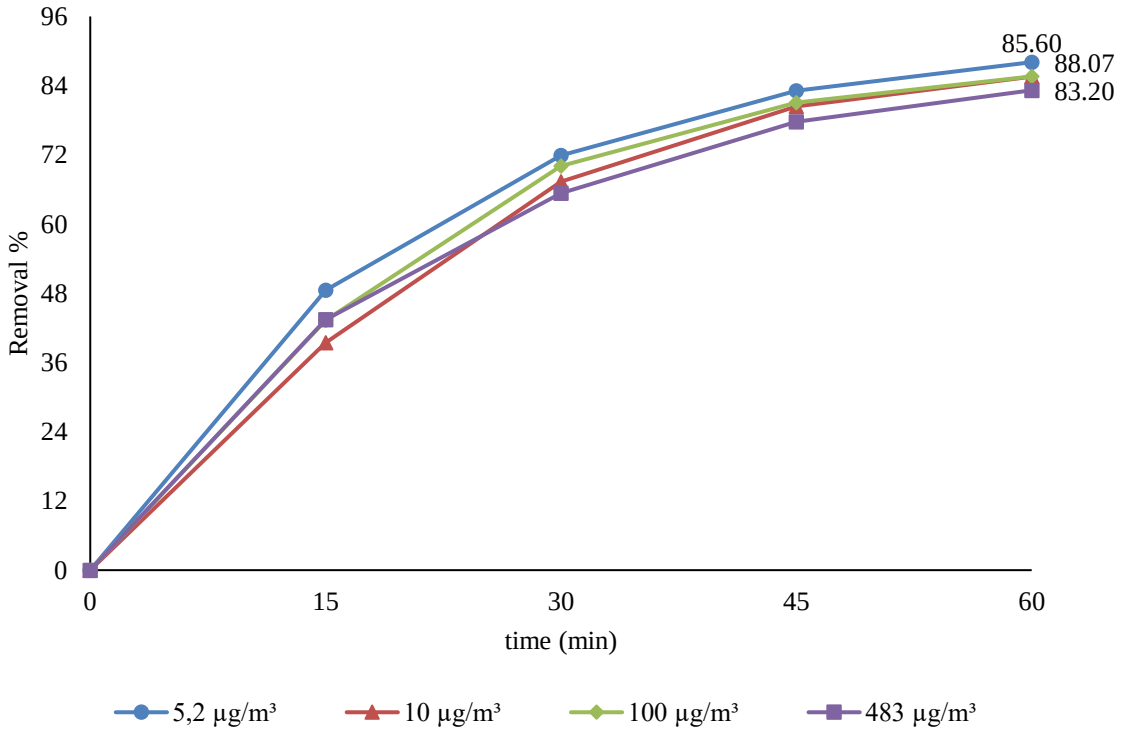

Figure 4.294. Removal efficiency of o-xylene for KN-AC.

At the last point discussed, the study data applied to all BTEX gases were given for COM-AC and KN-AC in Table 4.27. When the second concentration value of 42±4.97 μg/m³ was analyzed in itself, the data was procured at the end of the experiment showed COM-AC removal with 53.39% efficiency. At the same time, KN-AC was more successful 68.34%. In another concentration 412±48.74 μg/m³, the RE was the highest 51.27% for COM-AC and this value was 68.08% for KN-AC. The lowest RE was 2045±203.37 μg/m³ with 46.91%. Despite this, the highest yield was 18.5±1.89 μg/m³ with 57.04% in the batch reactor with the COM-AC. However, when the KN-AC was placed in the batch reactor and the work started, the lowest efficiency was at 2045±203.37 μg/m³, with 62.59%, while the highest efficiency was at 18.5±1.89 μg/m³ with 71.39%. The BTEX removal efficiency of COM-AC and KN-AC studies of the capacity was examined at different initial concentrations found at the concentration of 2.4±0.45 μg/m³ both COM-AC and KN-AC for benzene, which values was 73.86% and 65.23%, respectively.

Table 4.27. Removal efficiency of COM-AC and KN-AC for BTEX.

Time (min)	BTEX					
	C_0 (μg/m³)	COM-AC %	KN-AC %	C_0 (μg/m³)	COM-AC %	KN-AC %
0	18.5±1.89	0	0	412±48.74	0	0
15		35.19	39.04		25.67	34.98
30		46.69	57.41		41.72	54.97
45		53.08	66.50		48.55	63.99
60		57.04	71.39		51.27	68.08
0	42±4.97	0	0	2045±203.37	0	0
15		30.43	35.02		24.84	35.18
30		41.01	55.15		36.29	50.68
45		49.71	64.23		43.18	59.16
60		53.39	68.34		46.91	62.59

The several concentrations of BTEX were flyspecked of gas removal efficiencies by COM-AC in Figure 4.295. The removal efficiency of COM-AC of 18.5±1.89, 42±4.97, 412±48.74, 2045±203.37 µg/m³ was investigated concerning time for BTEX concentrations that 6 samples were taken in 60-minute cycles. In terms of concentration, removal of efficiency as a percentage, the highest yield which was the lowest concentration 2.4±0.45 µg/m³ and the lowest output, which was 322±47.80 µg/m³ with the highest concentration.

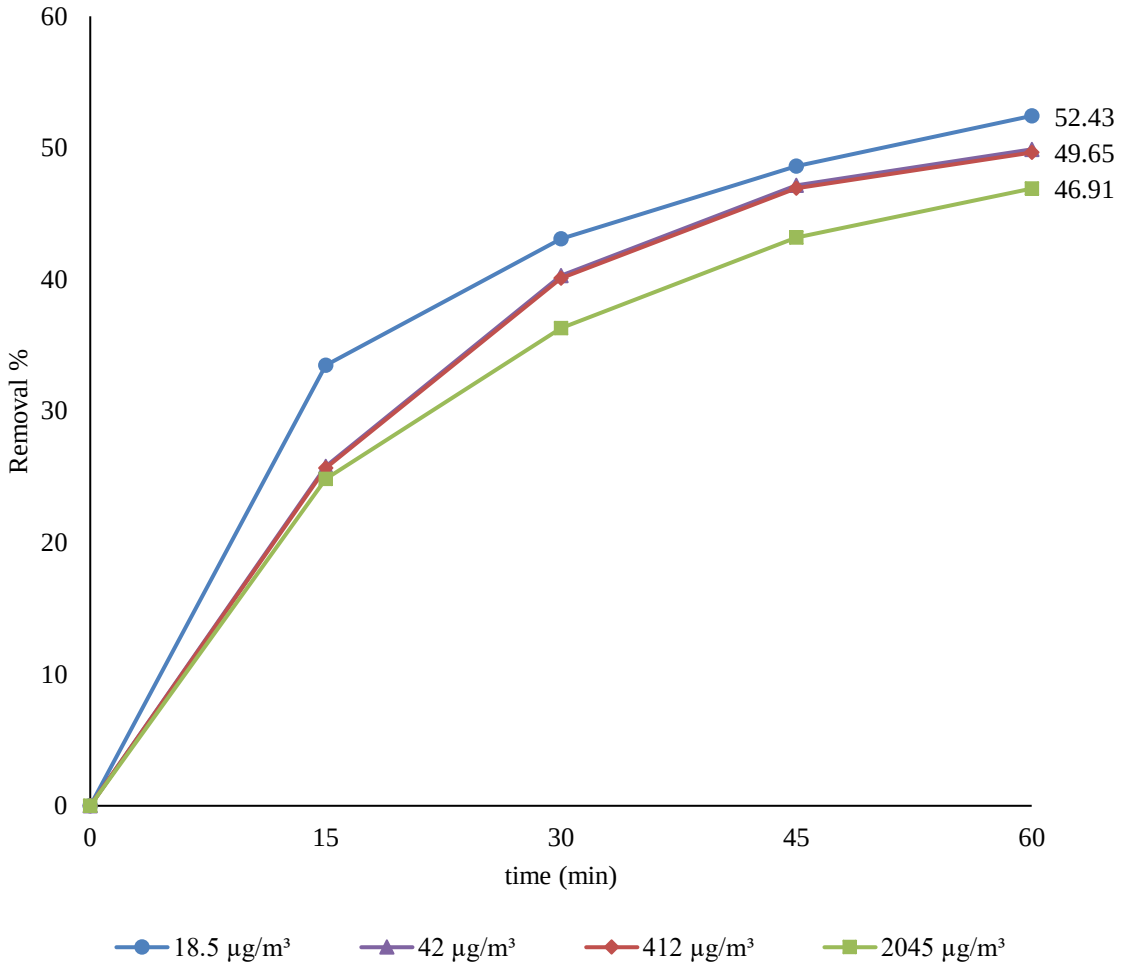

Figure 4.295. Removal efficiency of BTEX for COM-AC.

When the benzene removal sequence was performed, these values were the highest value 2.4 µg/m³ with 52.43%, with the concentration of 5.5 µg/m³ having the highest value of

50.43%, the concentration of 54±10.73 µg/m³ having the highest value of 49.65% and the value of 322±47.80 µg/m³ having the lowest value of 46.91%.

An experimental study was conducted to eliminate BTEX with KN-AC, which with concentration of 2.4±0.45, 5.5±1.09, 54±10.73, 322±47.80 µg/m³. In terms of concentration, removal of efficiency as a percentage, the highest yield which was the lowest concentration 2.4±0.45 µg/m³ and the lowest yield which was 322±47.80 µg/m³ with the highest concentration. When the BTEX removal was carried out, these values were the highest value 2.4µg/m³ with 71.70%, with the concentration of 5.3 µg/m³ having the highest value of 68.90%, the concentration of 54±10.73 µg/m³ having the highest value of 68.08% and the value of 322±47.80 µg/m³ having the lowest value of 62.59%.

The studies with different concentration values of BTEX were examined with COM-AC and KN-AC. It was shown that KN-AC had superior removal efficiency against to COM-AC. It was seen that the efficiency expressed as a percentage at the removal of BTEX gas from the indoor air. This study has achieved a more successful reduction in KN-AC compared to COM-AC.

Accordingly, against the lowest concentration value (2.4±0.45 µg/m³), both KN-AC and COM-AC reached the highest efficiency holding capacity, altough the highest concentration (322±47.80 µg/m³) reached the lowest efficiency holding capacity. This is because the high concentration of activated carbon has a high fill in the pores. When COM-AC and KN-AC were compared to the removal benzene's performance, there was no significant increase after 40th minute of the experiment. The lowest removal efficiency results were obtained at data in which these values were found to be 54.09 µg/m³ for COM-AC and 58.75 µg/m³ for KN-AC at the last and highest concentration of 322±47.80 µg/m³ in between Figure 4.284 and Figure 4.296.

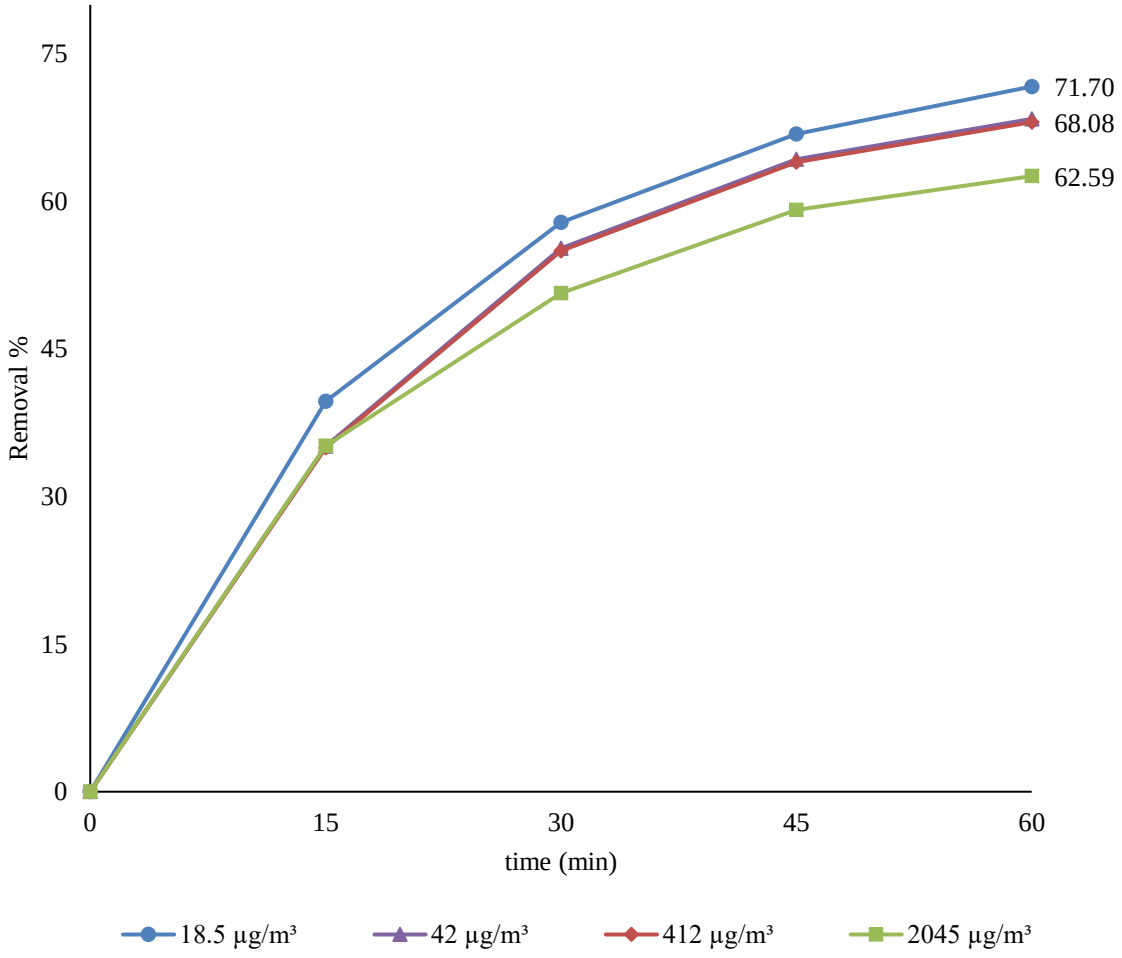

Figure 4.296. Removal efficiency of BTEX for KN-AC.

Benzene adsorption experiments were successfully performed with four different initial concentrations. These values were chosen as values of 5 µg/m³, 10±2.49 µg/m³, 50 µg/m³, 300 µg/m³, which were frequently encountered in the indoor air It gives removal of initial values, with COM-AC and with KN-AC in Figure 4.294. The differences of the used adsorbent can also be analyzed after certain time values to perform system held stationary conditions was provided immediately before starting the experiment. Figure 4.306 demonstrated that five dissimilar values, drawn horizontally and vertically, was shown to limit indoor air quality. The points were determined below and above of value.

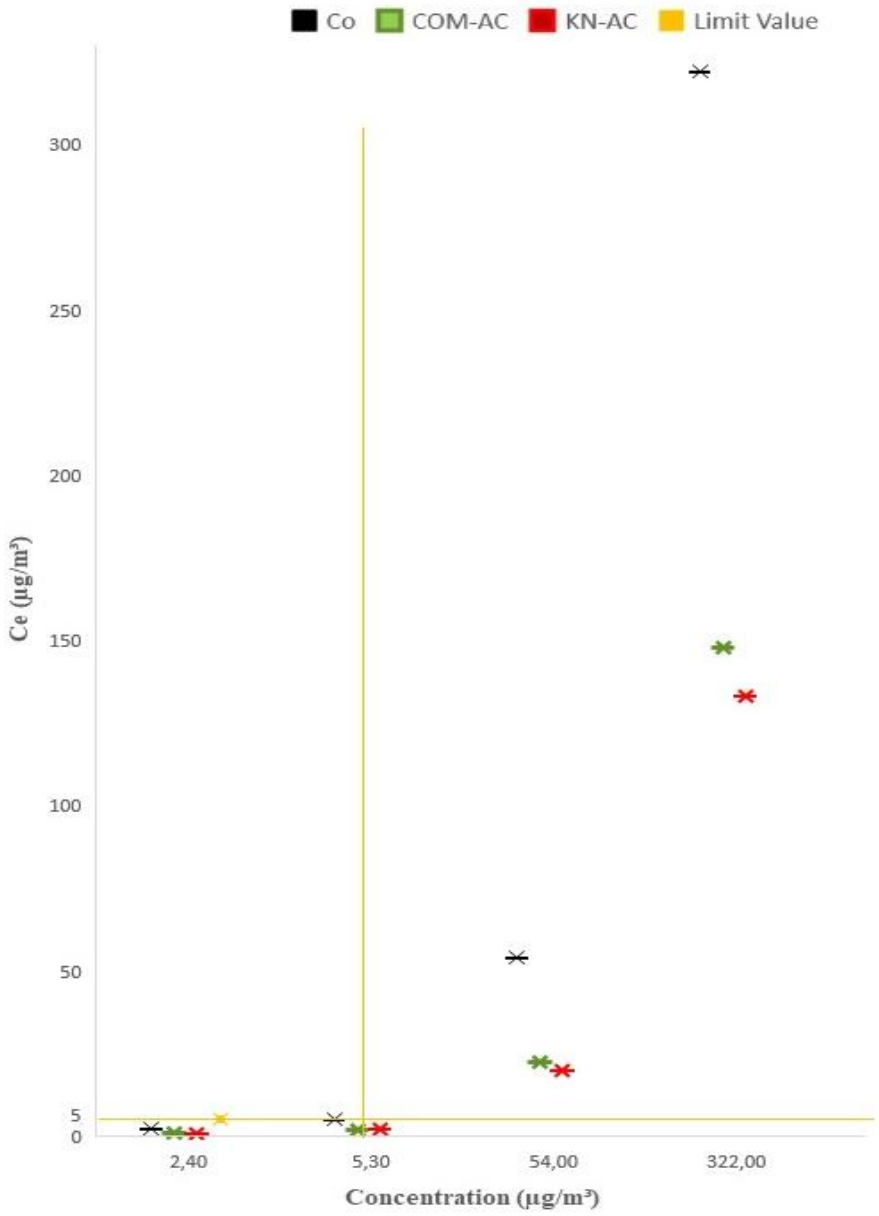

Figure 4.297. Concentrations of substances remaining in air after benzene adsorption.

The initial values for each concentration were black, green in COM-AC, red in KN-AC in color. Initial values decreased from 2.4±0.45 µg/m³ to 0.82 µg/m³, from 5.5 µg/m³ to 2.01 µg/m³, from 54±10.73 µg/m³ to 22.31 µg/m³, from 322±47.80 µg/m³ to 147.74 µg/m³ respectively for COM-AC. Initial values decreased from 2.4±0.45 µg/m³ to 0.62 µg/m³, from 5.5 µg/m³ to 1.81 µg/m³, from 54±10.73 µg/m³ to 19.41 µg/m³, from 322±47.80 µg/m³ to 132.75 µg/m³ respectively for KN-AC.

Another work for BTEX adsorption were successfully accomplished with four different initial concentrations. These values were chosen as values of 18.50 μg/m³, 42±4.97 μg/m³, 412±48.74 μg/m³, 2045±203.37 μg/m³, which were frequently encountered in the indoor air and it gives removal of initial values, with COM-AC and with KN-AC in Figure 4.307. It demonstrated that five different values were shown as the typical concentration of indoor air quality.

The initial values for each concentration were black, green in COM-AC, red in KN-AC in color. Initial values decreased from 18.5±1.89 μg/m³ to 8.80±0.67 μg/m³, from 42±4.97 μg/m³ to 20.71±2.41 μg/m³, from 412±48.74 μg/m³ to 207.18±12.94 μg/m³, from 2045±203.37 μg/m³ to 1085.58±62.96 μg/m³ respectively for COM-AC. Initial values decreased from 18.5±1.89 μg/m³ to 5.23±0.53 μg/m³, from 42±4.97 μg/m³ to 13±2.27 μg/m³, from 412±48.74 μg/m³ to 131.34± 25.96 μg/m³, from 2045±203.37 μg/m³ to 764.90±76.44 μg/m³ respectively for KN-AC.

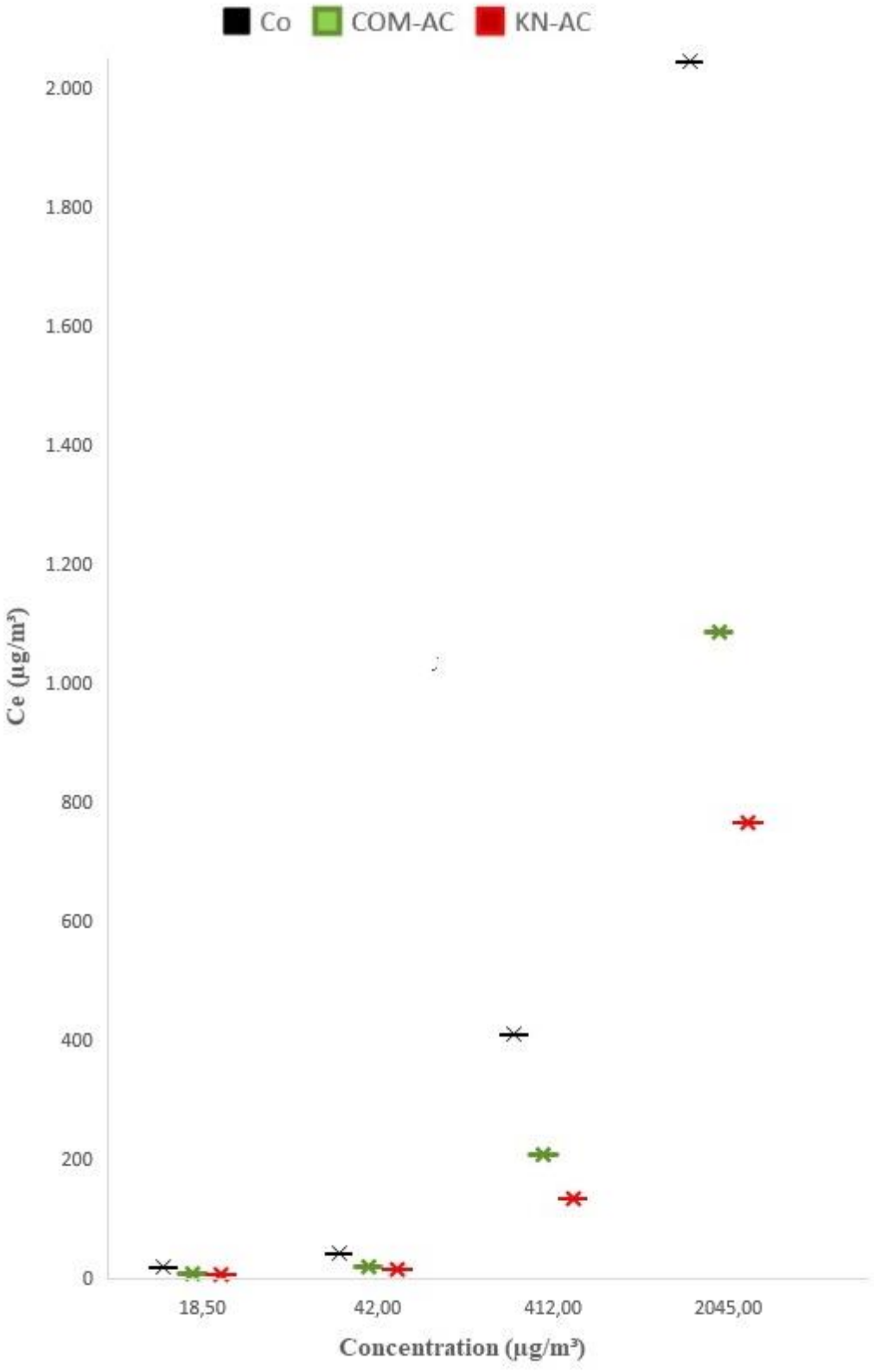

Figure 4.298. Concentrations of substances remaining in air after BTEX adsorption.

To compare the adsorption capacity of activated carbons for various species of BTEX. The adsorbed amount of BTEX on ACs was obtained by listing as follows. Benzene, toluene, m-xylene, p-xylene and o-xylene were removed with domestically granular activated carbon (GAC). The adsorbed amounts studied under the conditions of 6000 ppm and using 2 g of GAC during almost 17 h at 20°C in fixed bed reactor. The removal efficiency of benzene, toluene and o-xylene were 27.50, 29.40 and 90.40%, respectively. [324]. In this study, the initial concentrations for benzene, toluene, o-xylene were 322, 414, 483 $\mu g/m^3$, respectively. The removal efficiencies were 58.75, 56.65 and 83.20% at 25°C using 0.1 g of KN-AC.

Commericial activated carbon purchased and washed with de-ionised water 4−5 times to eliminate their surface impurities. Particle diameter of AC-1 was 4 mm and desiccated in vacuum at 150°C for 12 h. Surface areas were determined as 951.50 m^2/g. The inlet flow rate of 0.8 m^3/h and adsorbed amount was 36.49 mg/g [325]. In this study, KN-AC produced and COM-AC purchased activated carbon commercially. They tested the difference between each other comparatively for removal of BTEX. The initial concentration of each BTEX were given differently.

In another study used activated carbon (AC), silica gel (SG), and type-13X synthetic zeolite (T-13X). They were used with gravimetric adsorption method for benzene, toluene, o-xylene, p-xylene, and m-xylene. The obtained data fitted to Freundlich isotherm. Also the standard deviations for the predicted adsorption isotherms in the activated carbon bed were from 0.44 to 0.92, and the standard deviations were from 0.25 to 4.79 in the silica gel bed and were from 0.12 to 0.87 in the zeolite bed. Results obtained with adsorption experiments of benzene, toluen, m-xylene and o-xylene were 61.42, 10.94, 31.49 and 11.47 %, respectively [326]. In this study other adsorbent was not use from KN-AC and the obtained data were applied to Langmuir, Freundlich and Dubinin Radushkevich isotherm. The standard deviations obtained vary according to the concentrations. The adsorption experiments of benzene, toluen, m-xylene and o-xylene were 58.75, 56.68, 57.98 and 83.20%, respectively.

Activated carbon monolith used as an adsorbent for toluene, 1-butanol, and ethyl acetate at 20, 60, 100, and 140°C using a microbalance. The experimental data were arranged with Langmuir, Freundlich, Langmuir−Freundlich, and Toth isotherms. The Langmuir−Freundlich and Toth equations best fits to the experimental data [327]. In this study, multiple degassing were carried out simultaneously, these were benzene, toluene, ethylbenzene, m, p-xylene and o-xylene at only room temperature. Also experimental data best fits to Freundlich.

Another experimental study was made to guess mass-transfer rate during adsorption of VOCs in an activated carbon bed with a linear driving force (LDF) model. The model was validated for an adsorption of seven kinds of VOC [328]. In this study it was adapted to isotherm models.

Activated carbons from cork powder used in the control of VOCs. It was obtained by chemical activation as a KOH and surface areas higher than 1300 m^2/g [329]. In this study the choice of activating agent favored $ZnCl_2$ because of it is to more open the structure.

Activated carbon from coconut shell based carbons (CS-GAC) used chemical activation by ammonia, sodium hydroxide, nitric acid, sulphuric acid, and phosphoric acid for VOCs. Both SEM/EDAX and BET were used to identify the structural characteristics of the tested AC, while IR spectroscopy and Boehm's titration were applied to analysis the surface functional groups. Relationships between physicochemical characteristics of CS-GAC and their adsorption performances demonstrated that o-xylene adsorption capacity was related to surface area, pore volume, and functional groups of the CS-GAC surface. Removing surface oxygen groups, which constitute the source of surface acidity, and reducing hydrophilic carbon surface favors adsorption capacity of hydrophobic VOCs on carbons [330]. In this study The KN-ACs samples were synthesized from HSC by chemical activation using $ZnCl_2$ and carbonization process; characterized by BET, XRD, FTIR-ATR, DTA/TG and SEM/EDX; and used for hydrogen storage at 25°C and -169°C.

Table 4.28. Comparison with other studies of KN-AC for removal efficiency of for BTEX.

Adsorbent	Surface area m^2/g	Adsorbate	Adsorption efficiencies %	Conditions	Ref.
GAC	804.6	benzene	27.50	29.85ºC, 6000 ppm and fixed bed	[324]
AC, SG, T-13X	-	benzene	61.42	0.680 P_0	[326]
KN-AC	1858	benzene	58.75	25°C, 322 $\mu g/m^3$-1 h	In this study
AC-1	951.5	toluene	36.49	25°C, 0.8 $m^3\ h^{-1}$	[325]
GAC	804.6	toluene	29.4	20°C, 6000 ppm, almost 17 h and fixed bed	[324]
AC, SG, T-13X	-	toluene	10.94	0.818 P_0	[326]
AC Monolith	-	toluene	366.72	20°C, 2910 Pa	[327]
AC	-	toluene	424.40	20°C, 5 L h^{-1} , 50 g m^{-3}	[328]
KN-AC	1858	toluene	56.68	25°C, 414 $\mu g/m^3$,1 h	In this study
AC, SG, T-13X	-	m-xylene	31.09	0.606 P_0	[326]
AC from Cork Powder	1300	m-xylene	292.40	25°C, <0.2 P_0	[329]
AC, SG, T-13X	-	p-xylene	29.46	0.556 P0	[326]
KN-AC	1858	m, p - xylene	57.98	25°C, 397 $\mu g/m^3$,1 h	In this study
CS-GAC	-	o-xylene	305.70	22–27°C, 45 mL min^{-1} , 2176–2239 mg m^{-3}	[330]

GAC	804.6	o-xylene	90.40	29.85°C, 6000 ppm and fixed bed	[324]
AC, SG, T-13X	-	o-xylene	11.47	0.741 P_0	[326]
KN-AC	1858	o-xylene	83.20	25°C, 483 $\mu g/m^3$,1 h	In this study

4.4. Cost-Benefit Analysis

The cost-benefit analysis (CBA) that a particular investment will provide over the lifetime is found in monetary terms. The welfare economy's foundation, which has spanned many years, is based on a planned cost-benefit analysis. The benefits and costs arising in different periods were discounted with an ordinary discount rate. The present value of the benefit was compared with the present value of the cost. It is generally used in irrigation, dam, transportation and hydroelectric power plant investments. As a result of the different social and economic conditions, the analysis used in these countries is more diverse than the developed countries [331].

4.4.1. Energy Consumptions

Turkey is rapidly growing need for electricity and natural gas imports to meet due to its energy demands [332]. Both the surplus of energy demand to have favorable conditions for the production of both electricity in Turkey has become an attractive country for many investors. The study's electricity consumption sums up the electricity consumption of various laboratory kinds of electricity consumption sources. The hourly basis and the data consumed in Turkey are increasing along with the report's yearly economic growth percentages. The production of activated carbon in laboratory usage term includes in the base of electricity utilization. The current price of electricity used in Turkey was given in Table 4.29.

Table 4.29. Current price of electricity in Turkey.

Commercial electricity kWh price (including all taxes)			
Commercial Class	Daytime (06:00 - 17:00)	Peak (17:00 - 22:00)	Night (22:00 - 06:00)
One Time		0.16 ¢	
Three Timed	0.15 ¢	0.23 ¢	0.099 ¢
kWh prices for three-time residential tariff			
Residential Class	Daytime (06:00 - 17:00)	Peak (17:00 - 22:00)	Night (22:00 - 06:00)
One Time		0.13 ¢	
Three Timed	0.12 ¢	0.17 ¢	0.074 ¢

* It was created on the based on EMRA Tariff Tables of January 2020.

4.4.2. Potential of Purewater Consumptions

The main area of increased membrane uses with developing technological materials is water purification, even ultra-purification processes. It has been an invention that opens up new horizons used in many different fields from laboratory studies to industrial processes. Membrane applications used as filters in pure and laboratory applications of pure water have also varied. Water quality; The correct excerpting design and effectiveness of the technologies used to purify water depend on the accuracy and sensitivity of the devices used to monitor water contaminant levels. Strict Quality Assurance (Certification, Calibration, Qualification and Validation) is imperative to ensure that water purification and monitoring techniques are applied correctly in manufactured products to give the foregone conclusion. Purification of water also costs money. While maintaining adequate technical standards, it was considered to use the right water quality for each application to minimize operating costs for a laboratory. Devices that consider the enterprises' resources and the correct water quality for various applications were designed in Table 4.30.

Table 4.30. Ultra pure water device cost.

Scope of application	Use of filter type	Pure Water Quality	Price
Chromatography, elemental analysis, tissue culture, molecular biology and biochemistry, preparation of histology dyes, dishwashers, autoclave.	Membrane or ultrafiltration cartridge	Ion Waste:> 96% Organic Waste (Molecular Weight> 200KDa)> 99% Bacteria and Particles:> 99%	1000 $ - 6500 $ depending on the make of the device

4.4.3. Investment Costs

In the thesis, first, one owning cost components of decorative products such as investment costs and running costs was weighed. Then, the calculated cost Figures were introduced. Furthermore, in this thesis, cost data for the alternative options was originated from published information such as reports, journals, websites, and conference proceedings. Fundamentally, investment costs and operating costs were determined for each of the alternatives. According to the cost information gathered, to manipulate them, some financial concepts were evaluated for economic analysis in decorative products for VOC removal studies was given in Table 4.31.

Table 4.31. Initial investment cost [333].

Incubator	Furnace	Ball grinder	Sieve	Mold press
2300 $	1450 $	3270 $	1700 $	6480 $

4.4.4. Production of KN-AC

The main reason for this part of the study is that the product, which is likely to be realized in the future, will be offered to the market to meet the real sector's needs, not only in the literature. Physical infrastructure investments used, such as energy projects, development

of water resources and irrigation projects, transportation projects. Also, social infrastructure projects were used such as preventive healthcare and education services projects, and cost-effectiveness analysis in housing and urban and environmental management. Such services were both private and social benefits services. It is possible to calculate the benefits of the projects prepared for these services' production by using CBA.

Today, in the activated carbon usage sector, a wide variety of activated carbon is produced and sold at different prices depending on their quality, raw material, and surface area. This preference's main reason is its low investment and operating costs compared to the other treatment methods such as active or passive removal in indoor environments. These costs can be easily reduced in large-scale facilities and mass production facilities. However, a cost analysis was aimed at the KN-AC used in the study. The main target in doing this is that the expenditure's efficiency is higher than that of commercially purchased activated carbons. In general, the price of materials from abroad is relatively high. The raw horse chestnut's necessary operations, KN-AC was produced with a 65% loss, which was achieved in our net hands. The KN-AC price per 1 kg obtained at the end of all expenditures was found to be 356.79 $ in Table 4.32.

Table 4.32. Cost analysis of KN-AC.

Operation	Type	Cost per unit	Processing fee 1 kg HCS	Fee of 1 kg KN-AC
Collecting raw materials	Day laborer	8 $/h	8 $	22.88 $
Washing the raw material	Device and care	0.75 ¢/L	3.75 $	10.73 $
Drying of the raw material	Device and care	1250 watt/h	7.2 $	20.59 $

Grinding of raw materials	Device and care	1250 watt/h	0.45 ¢	1.29 $
Using $ZnCl_2$	Activation	75 $/1 kg	52 $	148.72 $
Burning of raw materials	Device and care	3000 watt/h	1.08 $	3.09 $
	Using N_2 for prolysis	17 $/tube (6 m^3 size)	5.67 $	16.22 $
	Day laborer	8 $/h	32 $	91.52 $
Washing with HCl	After prolysis	36 $/2.5 L	11 $	31.46 $
Final drying	Device and care	1250 watt/h	3.6 $	10.29 $
Total Price			124.75 $	356.79 $

4.4.5. Product Suggestion

The final step was decorative products until processes. The ashtray, which was initially designed, was set out with cigarette smoke in mind. Due to the superior VOCs capture efficiency of KN-AC produced within the thesis's scope, price analysis varies depending on the gram of KN-AC used. Later, ornamental material was considered to remove the VOCs that were pollutants in the interior. The remaining activated carbon used varies according to the size of the objects. As an example to these have been included candlestick, vase and medium-scaled sculpture in Table 4.33.

Table 4.33. Cost analysis of decorative products for passive VOCs removal with KN-AC.

Mold for decorative purposes	Price spent/per mold ($)	Day laborer	Clay and ceramic mortar	KN-AC content	KN-AC Price ($)	Optional organic paint ($)	Product Price ($)
Ashtray	2.30	8 $/h	25 $/ton	7 g	2.50	1.8	14.63
Candlestick	3.2			10 g	3.56	2.3	17.09

Vase	3.5		15 g	5.35	2.9	19.83
Medium Scaled Sculpture	4.5		20 g	7.14	3.4	23.27

Consequently, the price found a comparison between the investment costs of the decoratives with KN-AC. This passive removal of VOCs that it can be concluded from investment needs to be cheaper because processes were nearly troublesome than commercial activated carbon.

5. CONCLUSION AND FURTHER SUGGESTION

Specific methods can remove VOCs that we encounter in every area. It is accepted that activated carbons can be widely used to remove VOCs by the adsorption method as a control strategy. However, this is costly because the activated carbons, which are subject to cost, are usually imported from abroad. For this reason, the companies prefer low cost ways of removing VOCs resulting from the process. Within the research scope, VOCs' removal by the adsorption method was investigated using activated carbon obtained from the horse chestnut shell, which is organic waste, without using any commercial product from but rather collected from nature in its original form. In this context, the determination of optimum conditions in which activated carbon can be produced was first investigated. The maximum surface area was obtained as 600ºC and 3 M $ZnCl_2$. The result of studies was to reach optimum carbonization of activated carbon by using $ZnCl_2$ at different temperature values and different molarities (1 M, 3 M and 5 M) at 400, 500, 550, 600, 700, 800 and 900ºC respectively.

Based on the produced activated carbon samples' analysis, especially surface area and SEM image, the hydrogen storage capacity of the produced activated carbon was measured and the activated carbon character was determined. The surface area of KN-AC was higher than that of COM-AC. In SEM images, it was observed that commercially activated carbon was homogeneous and KN-AC was inhomogeneous. However, when the raw horse chestnut shell images and the images obtained after the carbonization process were taken into consideration, it was seen that the structure of the activated carbon becomes highly porous.

Another topic investigated in this thesis was determination of the hydrogen storage capacity of the produced activated carbon. The hydrogen storage capacity of the activated carbons varies depending on the temperature. Therefore, hydrogen storage capacity measurements were performed first at room temperature (25ºC) and then at low temperature (cryogenic temperature -169ºC). The effect of the concentration of chemical activating agents on hydrogen storage capacity was tested using 1 M $ZnCl_2$, 3 M $ZnCl_2$,

and 5 M $ZnCl_2$. The highest capacity was obtained by using 3 M $ZnCl_2$ and -169ºC. The KN-ACs samples were synthesized from HSC by chemical activation using $ZnCl_2$ and a carbonization process; characterized by BET, XRD, FTIR-ATR, DTA/TG and SEM/EDX; and used for hydrogen storage at 25ºC and -169ºC. The BET surface areas of the activated carbons synthesized at 1 M $ZnCl_2$, 3 M $ZnCl_2$ and 5 M $ZnCl_2$ concentrations were determined as 795, 1858 and 1600 m^2/g at 600ºC carbonization temperature, respectively. FTIR-ATR and XRD analysis confirmed that activated carbon was synthesized from HCS. DTA/TG analysis showed no significant mass loss in the thermogram of HSC. The values wereT_{max1} 321.7°C and ΔY 49.4% for HCS, T_{max1} 634.7°C and ΔY 19.78% for 1 M $ZnCl_2$, T_{max1} 958.4°C and ΔY 3% for 3 M $ZnCl_2$, T_{max1} 619.5°C and ΔY 9.7% for 5 M $ZnCl_2$ This result was in agreement with the experimental results in which the effect of carbonization temperature on activated carbon synthesis was investigated. The mass losses in DTA/TG thermograms of the activated carbons were relatively low compared to HCS. The SEM images showed that a porous structure was formed and EDX analysis showed that carbon contents of activated carbons increased and oxygen contents decreased. The hydrogen storage capacities of activated carbon samples were higher at -169ºC and increased with increase in surface area and micropore volume. 1 M $ZnCl_2$ were 2.20 wt%, 3 M $ZnCl_2$ was 3.18 wt%, and 5 M $ZnCl_2$ was as 1.94 wt% at max mbar. Storage pressure increases with increasing pressure in both molarities. As a result, the KN-AC (3 M $ZnCl_2$) sample synthesized in this study, and whose storage capacity is similar to the literature results can be used as an adsorbent for hydrogen storage.

In the next stage of the study, the activated carbons' adsorption levels were determined for the VOC groups, which are abundant in indoor air. A batch reactor with a volume of 0.002 m^3 specially produced for working from sealed glass material was used to be used in the formaldehyde and BTEX adsorption experiments. In the experimental studies of formaldehyde removal, its concentration collected in pure water in certain periods was measured in the experimental apparatus where nitrogen (N_2) was bound as the pump provided the propellant and gas movement. Taking the limit values into consideration, samples of different concentrations were prepared for the compounds to cover these values. Firstly, the apparatus was run until as stable as possible without activated carbon, and pure water concentrations were measured. In this study, the data obtained from

experiments with COM-AC and KN-AC were used as to compare reparations success. In so doing, 0.5 g of COM-AC and KN-AC were placed in the reactor and 3 replicates measured at all concentrations with the mean values were calculated respectively. A spectrophotometer was used to measure concentration in formaldehyde removal experiments. While selecting the batch reactor's internal environment concentration, it was studied together with the most common levels scanned in the literature, which are values essentially divided into two groups.

Firstly, formaldehyde values were measured in homes, offices, hospitals, libraries, places where people often live in the indoor air, then the other groups where higher values are common such as in some factories and in location producing materials etc. Twelve different values of initial concentrations of formaldehyde were determined, those being 170±14.92, 260±23.76, 720±47.61, 1040±68.47, 1,220±72.14, 1,900±83.37, 3290±95.44 and 7650±111.18 $\mu g/m^3$ for low concentration, as well as 30,000±207.44, 50,000±338.61, 60,000±376.89, 110,000±497.21 $\mu g/m^3$ for high concentrations. In all experiments, the adsorption efficiency of KN-AC was higher than that of COM-AC. In the first stage of the experiment, in the 10th minute, although there is a close ratio in removal efficiency, this rate could easily be seen in the following minutes with the rapid filling of the pores of COM-AC and the retention efficiency. However, in experiments, the removal efficiency decreased as concentration increased, with the lowest concentration being the highest. In the formaldehyde test at 170±14.92 $\mu g/m^3$ concentration, COM-AC yielded 47.83% and KN-AC yielded 73.37%. At a concentration of 7650±111.18 $\mu g/m^3$, COM-AC reached 35.99% and KN-AC 47.58% removal efficiency. Subsequently, the data obtained was adapted on the adsorption parameters, which was more suitable.

The GC-MS was used for measurement of concentration in BTEX removal experiments. Based on the data obtained, that are quite frequent in indoor air, the initial concentrations for benzene were 2.4±0.45; 5.3; 54±10.73 and 322±47.80 $\mu g/m^3$; for toluene were 3.7±0.58±0.58, 9, 86±15.83 and 414±47.26 $\mu g/m^3$, for ethylbenzene were 3.9±0.66, 9.2±1.59, 90±15.55 and 430±46.64 $\mu g/m^3$, for m, p-xylene were 3.4±0.72, 8.5±1.32, 83±12.95 and 397±82.10 $\mu g/m^3$, for o-xylene were 5.2±0.82, 10±2.49, 100±24.38 and 483±102.67 $\mu g/m^3$, and for BTEX were 18.5±1.89, 42±4.97, 412±48.74 and 2045±203.37

μg/m^3. In the studies, the process was not performed until the batch reactor volume's indoor concentration level was fixed in the experiment.

As a result of the experiments, the adsorption efficiency of KN-AC was higher than COM-AC. In the first stage of the experiment although there is a close ratio in removal efficiency in the 10th minute, this rate can easily be seen in the following minutes with the rapid filling of the pores of COM-AC and the retention efficiency. However, in experiments the removal efficiency decreases as concentration increases, with the lowest concentration being the highest. In the benzene removal test at 2.4±0.45 μg/m^3 concentration, COM-AC reached 65.23% and KN-AC reached 73.86%. At the 322±47.80 μg/m^3, COM-AC reached 43.88% and KN-AC removal efficiency reached 48.06%. In the BTEX removal test at 18.5±1.89 μg/m^3 concentration, COM-AC yielded 52.43% and KN-AC yielded 71.7%. At the concentration of 2045±203.37 μg/m^3, COM-AC reached 36.29% and KN-AC 50.68% removal efficiency. In formaldehyde and BTEX removal experiments, the decrease in yield as concentration increases is explained by the decrease in adsorption capacity due to the saturation of the activated carbon pores.

Adsorption data were applied to the Langmuir, Freundlich and Dubinin-Radushkevich isotherm and the status of the isotherm representing the equilibrium data were investigated. In the Freundlich isotherm, the log qe graph against log Ce and the Langmuir isotherm 1/Ce versus 1/qe graph and D-R isotherm graph parameters were obtained from experimental studies. In formaldehyde and BTEX experiments, it was found that the correlation coefficient was $R^2 \approx 0.95$ to 0.99 and it represented both isotherms well in isotherm. Langmuir isotherm was found to be more appropriate at low concentrations and Freundlich at higher concentrations which are supported by Dubinin-Radushkevich.

The studies' main purpose is to remove the volatile organic compounds in the indoor air without any energy. Since KN-AC produced for this purpose gives better results than COM-AC, it is thought that using this decorative material will give good results. To obtain the KN-AC, a calculation of money spent until a final product is obtained was attempted. This showed us that as a result of the cost-benefit analysis, the product's price is quite low compared to other passive samplers

If a summary is made considering the experimental results, KN-AC obtained from raw materials collected from nature in the thesis and obtained yield values obtained from the commercial product are higher compared to COM-AC at high cost, which is valid for all compounds and concentrations. Adsorption experiments support analyses to determine the character of activated carbon.

The KN-AC's pore structure, high surface area, and adsorption capacity prove that horse chestnut husk is a potential raw material for activated carbon production. All the findings show that the KN-AC produced within the study's scope is highly effective and gives high performance. It is thought that it can be used as a practical, economical and environmentally friendly formaldehyde and BTEX adsorbent to improve indoor air quality.

This thesis requires the use of a wide variety of chemicals and devices. It is the basis of the study. Unfortunately, the fact that the materials used are quite expensive requires a strong financial support. Lignocellulosic based wastes that are abundant in nature and have not been made into activated carbon before and could be offered as an alternative to horse chestnut selected as raw material in the study. It could be possible that the activated carbon has a larger surface area and becomes microporous by changing certain conditions during the active carbon production phase. During the production phase, another activation agent was tried other than $ZnCl_2$. The results can be given comparatively using different activation agents. It is known that the removal efficiency increases after the modification process for Formaldehyde and BTEX gases that are desired to be removed. The extent the efficiency would increase could be tested with regards analyzing the modified activated carbons.

Within the scope of the study, a batch reactor was used in the removal of Formaldehyde and BTEXs. Repeating the experiments by changing the reactor type could enrich the study. Different results could be achieved in different working environments by diversifying the concentrations of gases aimed to be removed. However, multiple analyses can be performed at the same time with the currently-developed versions of the

devices used for reading the analysis. More precise results could be obtained with these devices.

After the removal with activated carbons, the desorption process of the pollutant gases adsorbed on the solid surface can be performed. Desorption of activated carbons for physically adsorbed substances rather than chemically adsorbed substances increases recovery. In this context, the results within the scope of the study have shown that physical adsorption takes place and can be easily applied to the desorption process. Thus, the contaminants on the surface are removed and the activated carbon can be reused. This also ensures that gases with economic value are recovered.

Activated carbons produced within the scope of the thesis have been tested to remove gases with a batch reactor in indoor air. The efficiency of activated carbons could be tested with measurements on volatile organic compounds that were released heavily in different-scale spaces. Volatile organic compounds from fuel stations, chimney emissions in industrial facilities, emissions from heating, etc. sources differ. Filter production potential could be investigated by determining the efficiency on these compounds.

Materials for the production of decorative products are presented within the scope of the thesis. How much VOC it can hold and how far it can retain its adsorption ability could also be demonstrated by experiments. Likewise, the desorption studies of decorative materials could be given in detail. Studies on the possibility of desorption occurring simultaneously with the adsorption process could be developed when the produced activated carbon is used indoors for decorative material and filter.

REFERENCES

[1] G. McInnes, Joint Emep/Corinair Atmospheric Emission Inventory Guidebook, European Environment Agency, Copenhagen, **1996**.

[2] L.J. Adgate, L.E. Eberly, C. Stroebel, D.E. Pellizzari and K. Sexton, Personal, Indoor, and Outdoor VOC Exposures in a Probability Sample of Children, Journal of Exposure Science and Environmental Epidemiology, 14 (**2004**) 4.

[3] J. Fenger, Air Pollution in the Last 50 Years–From Local to Global, Atmospheric Environment, 43 (**2009**) 13.

[4] J.C. Weschler, Changes in Indoor Pollutants since the 1950s, Atmospheric Environment, 43 (**2009**) 153.

[5] H. Akimoto, Global Air Quality and Pollution, Science 302 (**2003**) 1716.

[6] D. Pradhan, Waste Management, Bibechana, 7 **(2011)** 65.

[7] R.K. Ibrahim, M. Hayyan, M.A. AlSaadi, A. Hayyan and S. Ibrahim, Environmental Application of Nanotechnology: Air, Soil, and Water, Environmental Science and Pollution Research, 23 (**2016**) 13754.

[8] M. Krzyzanowski, WHO Air Quality Guidelines for Europe, Journal of Toxicology and Environmental Health, Part A 71 (**2008**) 47.

[9] R. Atkinson, Gas-Phase Tropospheric Chemistry of Volatile Organic Compounds: 1. Alkanes and Alkenes, Journal of Physical and Chemical Reference Data, 26 (**1997**) 215.

[10] R. Atkinson and J. Arey, Atmospheric Degradation of Volatile Organic Compounds, Chemical Reviews, 103 (**2003**) 4605.

[11] P.J. Franklin, Indoor Air Quality and Respiratory Health of Children, Paediatric Respiratory Reviews, 8 (**2007**) 281).

[12] D.J. Clements-Croome, Work Performance, Productivity and Indoor Air, Scandinavian Journal of Work Environment and Health, (**2008**) 69.

[13] S.C. Lee, M.Y. Chiu, K.F. Ho, S.C. Zou and X. Wang, Volatile Organic Compounds (VOCs) in Urban Atmosphere of Hong Kong, Chemosphere, 48 (**2002**) 375.

[14] M. Prager, E. Stephens and W. Scott, Aerosol Formation from Gaseous Air Pollutants, Industrial and Engineering Chemistry, 52 (**1960**) 521.

[15] National Research Council, Rethinking the Ozone Problem in Urban and Regional Air Pollution, National Academy Press, Washington DC, **1991**.

[16] M.R. Azari, M. Masoudınezhad and S. Motesadi, A New Sampler and Analysis Method for BTEX in Ambient Air, National Research Institute of Tuberculosis and Lung Disease, Iran, **2008**.

[17] K. Badjagbo, S. Loranger, S. Moore, R. Tardif and S. Sauve, BTEX Exposures Among Automobile Mechanics and Painters and Their Associated Health Risks, Human and Ecological Risk Assessment: An International Journal, 16 (**2010**) 301.

[18] M.A. Bari, W.B. Kindzierski, A.J. Wheeler, M.E. Héroux and L.A. Wallace, Source Apportionment of Indoor and Outdoor Volatile Organic Compounds at Homes in Edmonton, Canada, Building and Environment, 90 (**2015**)114.

[19] J.H. Seinfeld, Urban Air Pollution: State of the Science, Science, 243 (**1989**) 745.

[20] S. Solomon, M. Manning, M. Marquis and D. Qin, Climate Change 2007-The Physical Science Basis: Working Group I Contribution to the Fourth Assessment Report of the IPCC, Cambridge University Press, 4 **(2007)**.

[21] R. Torres-Jardon, J.A. García-Reynoso, A. Jazcilevich, L.G. Ruiz-Suárez and T.C. Keener, Assessment of the Ozone-Nitrogen Oxide-Volatile Organic Compound Sensitivity of Mexico City Through an Indicator-Based Approach: Measurements and Numerical Simulations Comparison, Journal of the Air and Waste Management Association, 59 (**2009**) 1155.

[22] S. Madronich, M. Shao, S.R. Wilson, K.R. Solomon, J.D. Longstreth and X.Y. Tang, Changes in Air Quality and Tropospheric Composition due to Depletion of Stratospheric Ozone and Interactions with Changing Climate: Implications

for Human and Environmental Health, Photochemical and Photobiological Sciences, 14 **(2015)** 149.

[23] J.H. Seinfeld, ES Books: Atmospheric Chemistry and Physics of Air Pollution, Environmental Science and Technology, 20 (**1986**) 863.

[24] S. Batterman, C. Jia and G. Hatzivasilis, Migration of Volatile Organic Compounds from Attached Garages to Residences: A Major Exposure Source, Environmental Research, 104 (**2007**) 224.

[25] M.G. Baumann, S.A. Batterman and G.Z. Zhang, Terpene Emissions from Particleboard and Medium-Density Fiberboard Products, Forest Products Journal, 49 (**1999**) 49.

[26] A. Bazan, P. Nowicki, P. Półrolniczak and R. Pietrzak, Thermal Analysis of Activated Carbon Obtained from Residue After Supercritical Extraction of Hops, Journal of Thermal Analysis and Calorimetry, 125 (**2016**) 1199.

[27] A. Berenjian, N. Chan and H.J. Malmiri, Volatile Organic Compounds Removal Methods: A review, American Journal of Biochemistry and Biotechnology, 8 (**2012**) 220.

[28] G. Güllü, G. Doğan and G. Tuncel, Atmospheric Trace Element and Major Ion Concentrations over the Eastern Mediterranean Sea: Identification of Anthropogenic Source Regions. Atmospheric Environment, 39 (**2005**) 6376.

[29] B. Metz, O. Davidson, P. Bosch, R. Dave and L. Meyer, Climate Change 2007: Mitigation of Climate Change, Cambridge University Press **2007**.

[30] P. Brimblecombe, Air Pollution and Architecture: Past, Present and Future, Journal of Architectural Conservation, 6 (**2000**) 30.

[31] E. Rehfuess and WHO, Fuel for Life: Household Energy and Health, World Health Organization, **2006**.

[32] J.O.M. Bockris, The Hydrogen Economy: Its History, International Journal of Hydrogen Energy, 38 (**2013**) 2579.

[33] M. Böhm, M.Z. Salem and J. Srba, Formaldehyde Emission Monitoring from a Variety of Solid Wood, Plywood, Blockboard and Flooring Products

Manufactured for Building and Furnishing Materials, Journal of Hazardous Materials, 221 (**2012**) 68.

[34] A.L. Bolden, C.F. Kwiatkowski and T. Colborn, New Look at BTEX: Are Ambient Levels a Problem?, Environmental Science and Technology, 49 (**2015**) 5261.

[35] G. Bond, E.A. McLaren, C.L. Baldwin and R.R. Cook, An Update of Mortality Among Chemical Workers Exposed to Benzene, Occupational and Environmental Medicine, 43 (**1986**) 685.

[36] L.P. Brown, Do Rats Comply with EPA Policy on Cancer Risk Assessment for Formaldehyde?, Regulatory Toxicology and Pharmacology, 10 (**1989**) 196.

[37] S. Bianchi, W. Plastino, A.G. di Sarra, S. Piacentino and D. Sferlazzo, Carbon Dioxide Time Series Analysis: A New Methodological Approach for Event Screening Categorisation. In Mathematical Approach to Climate Change and its Impacts, Springer, **(2020)** 201.

[38] Global Monitoring Laboratory, Monthly Average Mauna Loa CO2, https://www.esrl.noaa.gov/gmd/webdata/ccgg/trends/co2_data_mlo.pdf (Accessed: **September 10 2020**).

[39] F. Chouza, T. Leblanc, J. Barnes, M. Brewer, P. Wang and D. Koon, Long-Term (1999–2019) Variability of Stratospheric Aerosol Over Mauna Loa, Hawaii, As Seen By Two Co-Located Lidars and Satellite Measurements, Atmospheric Chemistry and Physics, 20 (**2020**) 6821.

[40] K.S. Brown, Volatile Organic Pollutants in New and Established Buildings in Melbourne, Australia, Indoor Air, 12 (**2002**) 55.

[41] S. Brunauer, P.H. Emmett and E. Teller, Adsorption of Gases in Multimolecular Layers, Journal of the American Chemical Society, 60 (**1938**) 309.

[42] O. Isinkaralar, K. Isinkaralar, A. Ekizler and C. Ilkdogan, Changes in the Amounts of CO2 and Particulate Matter in Kastamonu Province Depending on Weather Conditions and Locations, Journal of Chemical, Biological and Physical Sciences, 7 (**2017**) 643.

[43] M. Cetin, H. Sevik and K. Isinkaralar, Changes in the Particulate Matter and CO2 Concentrations Based on the Time and Weather Conditions: The Case of Kastamonu, Oxidation Communications, 40 (**2017**) 477.

[44] M. Swash and A. Eisen, Hypothesis: Amyotrophic Lateral Sclerosis and Environmental Pollutants, Muscle and Nerve, **2020**.

[45] G. Wielgosiński and J. Czerwińska, Smog Episodes in Poland, Atmosphere, 11 (**2020**) 277.

[46] T.T. Chau and K.Y. Wang, An Association Between Air Pollution and Daily Most Frequently Visits of Eighteen Outpatient Diseases in an Industrial City, Scientific Reports, 10 (**2020**) 1.

[47] I.R. Burling, R.J. Yokelson, S.K. Akagi, S. Urbanski, C.Wold, D.W. Griffith and D.R. Weise, Airborne and Ground-Based Measurements of the Trace Gases and Particles Emitted by Prescribed Fires in the United States, Atmospheric Chemistry and Physics, 11 (**2011**) 12197.

[48] L. Calvo, M. Sánchez, A. Morán and A. García, TG-MS as a Technique for A Better Monitoring of the Pyrolysis, Gasification and Combustion of Two Kinds of Sewage Sludge, Journal of thermal Analysis and Calorimetry, 78 (**2004**) 587.

[49] M.A. Campesi, C.D. Luzi, G.F. Barreto and O.M. Martínez, Evaluation of an Adsorption System to Concentrate VOC in Air Streams Prior to Catalytic Incineration, Journal of Environmental Management, 154 (**2015**) 216.

[50] O. Ramírez, A.M.S. de la Campa, D. Sánchez-Rodas and D. Jesús, Hazardous Trace Elements in Thoracic Fraction of Airborne Particulate Matter: Assessment of Temporal Variations, Sources, and Health Risks in a Megacity, Science of the Total Environment, 710 (**2020**) 136344.

[51] D. Mage, G. Ozolins, P. Peterson, A. Webster, R. Orthofer, V. Vandeweerd and M. Gwynne, Urban Air Pollution in Megacities of the World, Atmospheric Environment, 30 (**1996**) 681.

[52] T.F. Bidleman, Atmospheric Processes, Environmental Science and Technology, 22 **(1988)** 361.

[53] J.F. Pankow, Review and Comparative Analysis of the Theories on Partitioning Between the Gas and Aerosol Particulate Phases in the Atmosphere, Atmospheric Environment, 21 **(1987)** 2275.

[54] J.R. Odum, T.P.W. Jungkamp, R.J. Griffin, R.C. Flagan and J.H. Seinfeld, The Atmospheric Aerosol-Forming Potential of Whole Gasoline Vapor, Science 276 **(1997)** 96.

[55] J. Kesselmeier and M. Staudt, Biogenic Volatile Organic Compounds (VOC): An Overview on Emission, Physiology and Ecology, Journal of Atmospheric Chemistry, 33 (**1999**) 23.

[56] J. Biswas and K. John, Climate Change Impacts on Regional and Urban Air Quality in South Texas, The Changing Climate of South Texas, 2100 (**1900**) 91.

[57] F.I. Khan and A.K. Ghoshal, Removal of Volatile Organic Compounds from Polluted Air, Journal of Loss Prevention in the Process Industries, 13 (**2000**) 527.

[58] S.S. Kety, M.H. Harmel, H.T. Broomell and C.B. Rhode, The Solubility of Nitrous Oxide in Blood and Brain, Journal of Biological Chemistry, 173 (**1948**) 487.

[59] H.J. Schumacher, The Mechanism of the Photochemical Decomposition of Ozone, Journal of the American Chemical Society, 52 (**1930**) 2377.

[60] A.C. Byrns and G.K. Rollefson, The Photochemistry of Mixtures of Chlorine and Ozone, Journal of the American Chemical Society, 56 (**1934**) 2245.

[61] B. Brunekreef and S.T. Holgate, Air Pollution and Health, Lancet, 360 (**2002**) 1233.

[62] R.S. Chandra, A Survey of Formaldehyde in Shampoos and Skin Creams on the Danish Market, Contact Dermatitis, 27 (**1992**) 235.

[63] H. Tesarek, Investigations Concerning the Employment Possibilities of the Diesel-Gas Process for Reducing Exhaust Emissions, Especially Soot (Particulate Matters), SAE Technical Paper, (**1975**) 750158.

[64] J.D. Spengler and K. Sexton, Indoor Air Pollution: A Public Health Perspective, Science, 221 (**1983**) 9.

[65] A. Turkyilmaz, H. Sevik, K. Isinkaralar and M. Cetin, Use of Tree Rings as a Bioindicator to Observe Atmospheric Heavy Metal Deposition, Environmental Science and Pollution Research, 26 (**2019**) 5122.

[66] A. Turkyilmaz, H. Sevik, K. Isinkaralar and M. Cetin, Using Acer Platanoides Annual Rings to Monitor the Amount of Heavy Metals Accumulated in Air, Environmental Monitoring and Assessment, 190 (**2018**) 578.

[67] K.H. Rasmussen, M. Taheri and R.L. Kabel, Global Emissions and Natural Processes for Removal of Gaseous Pollutants, Water, Air, and Soil Pollution, 4 (**1975**) 33.

[68] K.W. Ragland, Multiple Box Model for Dispersion of Air Pollutants from Area Sources, Atmospheric Environment, 7 (**1973**) 1017.

[69] C. Accinelli, M.L. Saccà, I. Batisson, J. Fick, M. Mencarelli and R. Grabic, Removal of Oseltamivir (Tamiflu) and Other Selected Pharmaceuticals from Wastewater Using a Granular Bioplastic Formulation Entrapping Propagules of Phanerochaete Chrysosporium, Chemosphere, 81 (**2010**) 436.

[70] A. Gajewicz, M. Haranczyk and T. Puzyn, Predicting Logarithmic Values of the Subcooled Liquid Vapor Pressure of Halogenated Persistent Organic Pollutants with QSPR: How Different are Chlorinated and Brominated Congeners?, Atmospheric Environment, 44 (**2010**) 1428.

[71] B. Weinhold, Pollution Portrait: The Fourth National-Scale Air Toxics Assessment, **2011**.

[72] D. Cheddie, Ammonia as a Hydrogen Source for Fuel Cells: A Review, Intech, **2012**.

[73] X. Chen, G. Zhang, Q. Zhang and H. Chen, Mass Concentrations of BTEX inside Air Environment of Buses in Changsha, China, Building and Environment, 46 (**2011**) 421.

[74] H.M. Cheng, Q.H. Yang and C. Liu, Hydrogen Storage in Carbon Nanotubes, Carbon, 39 (**2001**) 1447.

[75] K.C. Huang, Z. Zhao, G.E. Hoag, A. Dahmani and P.A. Block, Degradation of Volatile Organic Compounds with Thermally Activated Persulfate Oxidation, Chemosphere, 61 (**2005**) 551.

[76] R.G. Prinn, J. Huang, R.F. Weiss, D.M. Cunnold, P.J. Fraser, P.G. Simmonds and S. O'Doherty, Evidence for Variability of Atmospheric Hydroxyl Radicals over the Past Quarter Century, Geophysical Research Letters, 32 (**2005**).

[77] P.L. Tanaka, D.D. Riemer, S. Chang, G. Yarwood, E.C. McDonald-Buller, E.C. Apel and J.D. Neece, Direct Evidence for Chlorine-Enhanced Urban Ozone Formation in Houston, Texas, Atmospheric Environment, 37 (**2003**) 1393.

[78] W.P.L.J. Carter, Development of Ozone Reactivity Scales for Volatile Organic Compounds, Journal of the Air and Waste Management Association, 44 (**1994**) 881.

[79] C. Prado, J. Garrido and J.F. Periago, Urinary Benzene Determination by SPME/GC–MS: A Study of Variables by Fractional Factorial Design and Response Surface Methodology, Journal of Chromatography B, 804 (**2004**) 255.

[80] A.J. Cohen and C.A. Pope 3rd Lung Cancer and Air Pollution, Environ Health Perspect, 103 (**1995**) 219.

[81] B. Ireland, J.J. Collins, C.F. Buckley and D. Shepperly, Lymphohaematopoeitic Cancer Mortality Among Workers with Benzene Exposure, Occupational and Environmental Medicine, 60 (**2003**) 676.

[82] R.G. Derwent and M.E. Jenkin, Hydrocarbons and the Long-Range Transport of Ozone and PAN Across Europe, Atmospheric Environment, Part A. General Topics, 25 (**1991**) 1661.

[83] W. Wu, B. Zhao, S. Wang and J. Hao, Ozone and Secondary Organic Aerosol Formation Potential from Anthropogenic Volatile Organic Compounds Emissions in China, Journal of Environmental Sciences, 53 (**2017**) 224.

[84] W.P. Carter, Computer Modeling of Environmental Chamber Measurements of Maximum Incremental Reactivities of Volatile Organic Compounds, Atmospheric Environment, 29 (**1995**) 2513.

[85] Y. Liu, Q. Li, G. Su, D. Wei, M. Zheng, L. Gao and G. Liu, Photochemical Conversion of Toluene in Simulated Atmospheric Matrix and Characterization of Large Molecular Weight Products by+ APPI FT-ICR MS, Science of the Total Environment, 649 (**2019**) 111.

[86] Z. Jiang, B. Grosselin, V. Daële, A. Mellouki and Y. Mu, Seasonal and Diurnal Variations of BTEX Compounds in the Semi-Urban Environment of Orleans, France, Science of The Total Environment, 574 (**2017**) 1659.

[87] National Health and Medical Research Council, Ambient Air Quality Goals and Interim National Indoor Air Quality Goals, Caberra, **1996**.

[88] J. Tuff and H.S.C. O'Neill, The Effect of Sulfur on the Partitioning of Ni and Other First-Row Transition Elements Between Olivine and Silicate Melt, Geochimica et Cosmochimica Acta, 74 (**2010**) 6180.

[89] J.F. Müller, Geographical Distribution and Seasonal Variation of Surface Emissions and Deposition Velocities of Atmospheric Trace Gases, Journal of Geophysical Research: Atmospheres, 97 (**1992**) 3787.

[90] US Environmental Protection Agency, National Air Quality and Emissions Trends Report, 1999, Office of Air Quality Planning and Standards Emissions Monitoring and Analysis, **2001**.

[91] A. Guenther, C.N. Hewitt, D. Erickson, R. Fall, C. Geron, T. Graedel and T. Pierce, A Global Model of Natural Volatile Organic Compound Emissions, Journal of Geophysical Research Atmospheres, 100 (**1995**) 8873.

[92] F.D. Russell, W. Henrik and R.O. Michael, Process Integration Design Methods for Water Conservation and Wastewater Reduction in Industry, Waste Management, 14 (**2001**) 103.

[93] S. Donatello, H. Moons and O.W. JRC, Revision of EU Ecolabel Criteria for Furniture Products, European Commission, **2017**.

[94] L.W. Hu, N. Gurram, M.S. Bloom, Z. Qian, S.W. Howard, J. Iwelunmor and K.K. Liu, Impact on Lung Function Among Children Exposed to Home New Surface Materials: The Seven Northeastern Cities Study in China, Indoor Air, 29 (**2019**) 477.

[95] J. Williams and R. Koppmann, Volatile Organic Compounds in the Atmosphere: an Overview, Volatile Organic Compounds in the Atmosphere, (**2007**) 1.

[96] J.I. Kroschwitz, Polymers: Biomaterials and Medical Applications, Wiley-Interscience, **1989**.

[97] P. Kruger, J. Blakeley and J. Leaver, Potential in New Zealand for Use of Hydrogen as a Transportation Fuel, International Journal of Hydrogen Energy, 28 (**2003**) 795.

[98] M.A. Kolade, A. Kogelbauer and E. Alpay, Adsorptive Reactor Technology for VOC Abatement, Chemical Engineering Science, 64 (**2009**) 1167.

[99] B. Kolarik, L. Gunnarsen, A. Logadottir and L.W. Funch, Concentrations of Formaldehyde in New Danish Residential Buildings in Relation to WHO Recommendations and CEN Requirements, Indoor and Built Environment, 21 (**2012**) 552.

[100] J.T. Knudsen, R. Eriksson, J. Gershenzon and B. Ståhl, Diversity and Distribution of Floral Scent, The Botanical Review, 72 (**2006**) 1.

[101] R. Ewald, Requirements for Advanced Mobile Storage Systems, International Journal of Hydrogen Energy, 23 (**1998**) 803.

[102] K.L. Feilberg, M.S. Johnson and C.J. Nielsen, Relative Reaction Rates of HCHO, HCDO, DCDO, H13CHO, and HCH18O with OH, Cl, Br, and NO_3 radicals, The Journal of Physical Chemistry A, 108 (**2004**) 7393.

[103] P.H. Fischer, G. Hoek, H.D.J.B. van Reeuwijk, D.J. Briggs, E. Lebret, J.H.Van Wijnen and P.E. Elliott, Traffic-Related Differences in Outdoor and Indoor Concentrations of Particles and Volatile Organic Compounds in Amsterdam, Atmospheric Environment, 34 (**2000**) 3713.

[104] J. Zhu, P. Zhang, Y. Wang, K. Wen, X. Su, R. Zhu and Y. Xi, Effect of Acid Activation of Palygorskite on Their Toluene Adsorption Behaviors, Applied Clay Science, 159 (**2018**) 60.

[105] J. Williams and R. Koppmann, An Overview, In Volatile Organic Compounds in the Atmosphere, R. Koppmann, **2007**.

[106] J. Madrazo, A. Clappier, L.C. Belalcazar, O. Cuesta, H. Contreras and F. Golay, Screening Differences Between a Local Inventory and the Emissions Database for Global Atmospheric Research (EDGAR), Science of the Total Environment, 631 (**2018**) 934.

[107] H. Shen, Y. Huang, R. Wang, D. Zhu, W. Li, G. Shen and H. Chen, Global Atmospheric Emissions of Polycyclic Aromatic Hydrocarbons from 1960 to 2008 and Future Predictions, Environmental Science and Technology, 47 (**2013**) 6415.

[108] A.P. Jones, Indoor Air Quality and Health, Atmospheric Environment, 33 (**1999**) 4535.

[109] G.S. Tonnesen and R.L. Dennis, Analysis of Radical Propagation Efficiency to Assess Ozone Sensitivity to Hydrocarbons and NO x: 1. Local Indicators of Instantaneous Odd Oxygen Production Sensitivity, Journal of Geophysical Research: Atmospheres, 105 (**2000**) 9213.

[110] World Health Organization, Air Quality Guidelines for Europe, **2000**.

[111] L.I. Kleinman, The Dependence of Tropospheric Ozone Production Rate on Ozone Precursors, Atmospheric Environment, 39 (**2005**) 575.

[112] Z. Mo, M. Shao and S. Lu, Compilation of a Source Profile Database for Hydrocarbon and OVOC Emissions in China, Atmospheric Environment, 143 (**2016**) 209.

[113] G.S. Tonnesen and R.L. Dennis, Analysis of Radical Propagation Efficiency to Assess Ozone Sensitivity to Hydrocarbons and NO x: 2. Long-Lived Species as Indicators of Ozone Concentration Sensitivity, Journal of Geophysical Research: Atmospheres, 105 (**2000**) 9227.

[114] F.S. Rowland, Stratospheric Ozone Depletion, In Twenty Years of Ozone Decline, Springer, Dordrecht, **(2009)** 23.

[115] J.S. Garcia and R.D. Harbison, Aldehydes and Ketones, In Hamilton and Hardy's Industrial Toxicology, Hoboken, New Jersey: John Wiley and Sons, Inc., **(2015)** 445.

[116] R.A. García, V. Morales, S. Martín, E. Vilches and A. Toledano, Volatile Organic Compounds Analysis in Breath Air in Healthy Volunteers and Patients

Suffering Epidermoid Laryngeal Carcinomas, Chromatographia, 77 (**2014**) 501.

[117] I.J. George, R.R. Black, C.D. Geron, J.Aurell, M.D. Hays, W.T. Preston and B.K. Gullett, Volatile and Semivolatile Organic Compounds in Laboratory Peat Fire Emissions, Atmospheric Environment, 132 (**2016**) 163.

[118] Y. Morinaka, T. Sakamoto, Y. Inukai, M. Agetsuma, H. Kitano, M. Ashikari and M. Matsuoka, Morphological Alteration Caused by Brassinosteroid Insensitivity Increases the Biomass and Grain Production of Rice, Plant Physiology, 141 (**2006**) 924.

[119] J.N. Cape, Effects of Airborne Volatile Organic Compounds on Plants, Environmental Pollution, 122 (**2003**) 145.

[120] M.D. Cruz, J.H. Christensen, J.D. Thomsen and R. Müller, Can Ornamental Potted Plants Remove Volatile Organic Compounds from Indoor Air?—A review, Environmental Science and Pollution Research, 21 (**2014**) 13909.

[121] O. Wild, A.M. Fiore, D.T. Shindell, R.M. Doherty, W.J. Collins, F.J. Dentener and P. Hess, Modelling Future Changes in Surface Ozone: A Parameterized Approach, **2012**.

[122] L. Zhang, B.K. Miller and P.A. Crozier, Atomic Level in situ Observation of Surface Amorphization in Anatase Nanocrystals during Light İrradiation in Water Vapor, Nano Letters, 13 (**2013**) 679.

[123] C. Guizard, B. Boutevin, F. Guida, A. Ratsimihety, P. Amblard, J.C. Lasserre and S. Naiglin, VOC Vapour Transport Properties of New Membranes Based on Cross-Linked Fluorinated Elastomers, Separation and Purification Technology, 22 (**2001**) 23.

[124] G.R. Parmar and N.N. Rao, Emerging Control Technologies for Volatile Organic Compounds, Critical Reviews in Environmental Science and Technology, 39 (**2008**) 41.

[125] J.C. William and P.E. Lead, VOC Control Strategies in Plant Design. Chemical Processing: Project Engineering Annual, **(1997)** 44.

[126] D.M. Ruthven, Principles of Adsorption Processes, New York: John Wiley, **1984**.

[127] R.W. Baker, Future Directions of Membrane Gas Separation Technology. Industrial and Engineering Chemistry Research, 41 **(2002)** 1393.

[128] N.J.R. Kraakman, R.W. Melse, B.B. Koers and J. Van Dijk, Biological Treatment of Waste Gases Containing H2S in Combination with Either Odor or CS2, in Proc USC-TRG Conf Biofiltration, **(1998)** 22.

[129] Z. Cai and G.A. Sorial, Treatment of Dynamic VOC Mixture in a Trickling-Bed Air Biofilter Integrated with Cyclic Adsorption/Desorption Beds, Chemical Engineering Journal, 151 (**2009**) 105.

[130] US Environmental Protection Agency, Policy Assessment for the Review of the Ozone National Ambient Air Quality Standards, Washington, DC: U.S. Environmental Protection Agency [Accessed: **6 May 2019**].

[131] N.O. Sonntag, The Reactions of Aliphatic Acid Chlorides, Chemical Reviews, 52 (**1953**) 237.

[132] R. Atkinson, Atmospheric Chemistry of VOCs and NOx, Atmospheric Environment, 34 **(2000)** 2063.

[133] E.P. Leimkuehler, G.J. Suppes and T. Supervisor, Production, Characterization, and Applications of Activated Carbon, Article, **2010**.

[134] R. Atkinson, Gas-Phase Tropospheric Chemistry of Organic Compounds: A Review, Atmospheric Environment, Part A. General Topics, 24 **(1990)** 1.

[135] H. Hajimiragha, U. Ewers, A. Brockhaus and A. Boettger, Levels of Benzene and Other Volatile Aromatic Compounds in the Blood of Non-Smokers and Smokers, International Archives of Occupational and Environmental Health, 61 **(1989)** 513.

[136] S. Kim, S.Y. Kim, M. Lee, H. Shim, G.M. Wolfe, A.B. Guenther and J. Han, Impact of Isoprene and HONO Chemistry on Ozone and OVOC Formation in a Semirural South Korean Forest, Atmospheric Chemistry and Physics (Online), **(2015)** 15.

[137] R.S. Gohlke and F.W. McLafferty, Early Gas Chromatography/Mass Spectrometry, Journal of the American Society for Mass Spectrometry, 4 (**1993**) 367.

[138] T. Godish, Formaldehyde Exposures from Tobacco Smoke: A Review, American Journal of Public Health, 79 (**1989**) 1044.

[139] R. Golden, Identifying an Indoor Air Exposure Limit for Formaldehyde Considering Both Irritation and Cancer Hazards, Critical Reviews in Toxicology, 41 (**2011**) 672.

[140] A.J. Rocke, Kekulé, Butlerov and the Historiography of the Theory of Chemical Structure, The British Journal for the History of Science, (**1981**) 27.

[141] S. Kim, K. Jo, K.B. Hong, S.H. Han and H.J. Suh, GABA and L-Theanine Mixture Decreases Sleep Latency and Improves NREM Sleep, Pharmaceutical Biology, 57 (**2019**) 64.

[142] F.A. Esteve-Turrillas, A. Pastor and M. de la Guardia, Assessing Air Quality Inside Vehicles and at Filling Stations by Monitoring Benzene, Toluene, Ethylbenzene and Xylenes with the Use of Semipermeable Devices, Analytica Chimica Acta, 593 (**2007**) 108.

[143] T.J. Kelly, D.L. Smith and J. Satola, Emission Rates of Formaldehyde from Materials and Consumer Products Found in California Homes, Environmental Science and Technology, 33 (**1999**) 81.

[144] S. Halvarsson, H. Edlund and M. Norgren, Properties of Medium-Density Fibreboard (MDF) Based on Wheat Straw and Melamine Modified Urea Formaldehyde (UMF) Resin. Industrial Crops and Products, 28 (**2008**) 37.

[145] J.P. DiGangi, E.S. Boyle, T. Karl, P. Harley, A. Turnipseed, S. Kim and S.R. Hall, First Direct Measurements of Formaldehyde Flux viaEddy Covariance: Implications for Missing in-Canopy Formaldehyde Sources, Atmospheric Chemistry and Physics, 11 (**2011**) 10565.

[146] G. Poulhet, S. Dusanter, S. Crunaire, N. Locoge, V. Gaudion, C. Merlen and P. Coddeville, Investigation of Formaldehyde Sources in French Schools Using a Passive Flux Sampler, Building and Environment, 71 (**2014**) 111.

[147] S.K. Brown, Chamber Assessment of Formaldehyde and VOC Emissions from Wood-Based Panels, Indoor Air, 9 (**1999**) 209.

[148] N.L. Gilbert, M. Guay, D. Gauvin, R.N. Dietz, C.C. Chan and B. Lévesque, Air Change Rate and Concentration of Formaldehyde in Residential Indoor Air, Atmospheric Environment, 42 (**2008**) 2424.

[149] E. Gorham, C. Lehman and J. Kelly, Relationships of the Environmental Performance Index to Six Interrelated Variables in Nations Around the World, Bulletin of the Ecological Society of America, 100 (**2019**) 1.

[150] A. Grant, A.T. Archibald, M.C. Cooke and D.E. Shallcross, Modelling the Oxidation of Seventeen Volatile Organic Compounds to Track Yields of CO and CO2, Atmospheric Environment, 44 (**2010**) 3797.

[151] A.C. De Groot, M.A. Flyvholm, G. Lensen, T. Menné and P.J. Coenraads, Formaldehyde-Releasers: Relationship to Formaldehyde Contact Allergy, Contact Allergy to Formaldehyde and Inventory of Formaldehyde-Releasers, Contact Dermatitis, 61 (**2009**) 63.

[152] D. Grosjean, E.L. Williams, E. Grosjean, J.M. Andino and J.H. Seinfeld, Atmospheric Oxidation of Biogenic Hydrocarbons: Reaction of Ozone with. Beta.-Pinene, D-Limonene and Trans-Caryophyllene, Environmental Science and Technology, 27 (**1993**) 2754.

[153] B. Kolarik, L. Gunnarsen, A. Logadottir and L.W. Funch, Concentrations of Formaldehyde in New Danish Residential Buildings in Relation to WHO Recommendations and CEN Requirements, Indoor and Built Environment, 21 (**2012**) 552.

[154] WHO, World Health Organization Guidelines for Indoor Air Quality: Selected Pollutants, **2010**.

[155] T.K. Bastia, S. Lenka and P.L. Nayak, Synthetic Resins: XX. Chelation Ion Exchange Properties of Resins Derived from Semicarbazone of 2-Hydroxy Acetophenone-Substituted Benzoic Acid–Formaldehyde, Journal of Applied Polymer Science, 46 (**1992**) 739.

[156] A.P. Das, S. Lenka and P.L. Nayak, Synthetic Resins: I. Preparation and Characterization of Resins from Substituted Benzoic Acid–Formaldehyde, Journal of Applied Polymer Science, 30 (**1985**) 4619.

[157] Y. Liu, X. Zhao and L. Ye, A Novel Elastic Urea–Melamine–Formaldehyde Foam: Structure and Properties, Industrial and Engineering Chemistry Research, 55 (**2016**) 8743.

[158] A. Pizzi, Melamine-Formaldehyde Adhesives, Handbook of Adhesive Technology, **2003**.

[159] M. Dunky, Urea–Formaldehyde (UF) Adhesive Resins for Wood, International Journal of Adhesion and Adhesives, 18 (**1998**) 95.

[160] M. Kujawa, Some Naturally Occurring Substances: Food Items and Constituents, Heterocyclic Aromatic Amines and Mycotoxins, IARC Monographs on the Evaluation of Carcinogenic Risks to Humans, Herausgegeben von der International Agency for Research on Cancer, World Health Organization, 56 **(1994)**.

[161] K. Kadirvelu and C. Namasivayam, Activated Carbon from Coconut Coirpith as Metal Adsorbent: Adsorption of Cd (II) from Aqueous Solution, Advances in Environmental Research, 7 (**2003**) 471.

[162] S. Hazrati, R. Rostami, M. Farjaminezhad and M. Fazlzadeh, Preliminary Assessment of BTEX Concentrations in Indoor Air of Residential Buildings and Atmospheric Ambient Air in Ardabil, Iran, Atmospheric Environment, 132 (**2016**) 91.

[163] R.E. Hester and R.M. Harrison, Volatile Organic Compounds in the Atmosphere (No. 4), Royal Society of Chemistry, **1995**.

[164] Merchant Research and Consulting Ltd., World Benzene Production to Exceed 50.95 Mln Tonnes in 2017, https://mcgroup.co.uk/news/20140502/benzene-production-exceed-5095-mln-tonnes.html, (Accessed: **1 May 2020**).

[165] H. Reingruber and L.B. Pontel, Formaldehyde Metabolism and Its Impact on Human Health, Current Opinion in Toxicology, 9 (**2018**) 28.

[166] R.R. Hoque, P.S. Khillare, T. Agarwal, V. Shridhar and S. Balachandran, Spatial and Temporal Variation of BTEX in the Urban Atmosphere of Delhi, India, Science of the Total Environment, 392 (**2008**) 30.

[167] L.W. Hu, N. Gurram, M.S. Bloom, Z. Qian, S.W. Howard, J. Iwelunmor and K.K. Liu, Impact on Lung Function Among Children Exposed to Home New

Surface Materials: The Seven Northeastern Cities Study in China, Indoor Air, 29 (**2019**) 477.

[168] D.J. Mason, M.D. Sykes, S.W. Panton and E.H. Rippon, Determination of Naturally-Occurring Formaldehyde in Raw and Cooked Shiitake Mushrooms by Spectrophotometry and Liquid Chromatography-Mass Spectrometry, Food Additives and Contaminants, 21 (**2004**) 1071.

[169] WHO, World Health Organization Guidelines for Drinking-Water Quality: First Addendum to the Fourth Edition, **2017**.

[170] D.E. Hun, R.L. Corsi, M.T. Morandi and J.A. Siegel, Formaldehyde in Residences: Long-Term Indoor Concentrations and Influencing Factors, Indoor Air, 20 (**2010**) 196.

[171] E.L. Hult, H. Willem, P.N. Price, T. Hotchi, M.L. Russell and B.C. Singer, Formaldehyde and Acetaldehyde Exposure Mitigation in US Residences: In-Home Measurements of Ventilation Control and Source Control, Indoor Air, 25 (**2015**) 523.

[172] T. Malaka and A.M. Kodama, Respiratory Health of Plywood Workers Occupationally Exposed to Formaldehyde, Archives of Environmental Health: An International Journal, 45 (**1990**) 288.

[173] P.C. Wu, Y.Y. Li, C.C. Lee, C.M. Chiang and H.J. Su, Risk Assessment of Formaldehyde in Typical Office Buildings in Taiwan, Indoor Air, 13 (**2003**) 359.

[174] C.B. Keil, F. Akbar-Khanzadeh and K.A. Konecny, Characterizing Formaldehyde Emission Rates in a Gross Anatomy Laboratory, Applied Occupational and Environmental Hygiene, 16 (**2001**) 967.

[175] R. Pitchai and K. Klier, Partial Oxidation of Methane, Catalysis Reviews, 28 (**1986**) 13.

[176] S.G.B. Amyes and J.T. Smith, Trimethoprim Action and Its Analogy with Thymine Starvation, Antimicrobial Agents and Chemotherapy, 5 (**1974**) 169.

[177] S.K. Brown, Air Toxics in a New Australian Dwelling over an 8-Month Period, Indoor and Built Environment, 10 (**2001**) 160.

[178] F. Akbar-Khanzadeh and J.S. Mlynek, Changes in Respiratory Function After One and Three Hours of Exposure to Formaldehyde in Non-Smoking Subjects, Occupational and Environmental Medicine, 54 (**1997**) 296.

[179] K.B. Rumchev, J.T. Spickett, M.K. Bulsara, M.R. Phillips and S.M. Stick, Domestic Exposure to Formaldehyde Significantly Increases the Risk of Asthma in Young Children, European Respiratory Journal, 20 (**2002**) 403.

[180] L.W. Stanek, J.S. Brown, J. Stanek, Gift and D.L. Costa, Air Pollution Toxicology—A Brief Review of the Role of the Science in Shaping the Current Understanding of Air Pollution Health Risks, Toxicological Sciences, 120 (**2011**) 8.

[181] R. Duarte-Davidson, C. Courage, L. Rushton and L. Levy, Benzene in the Environment: An Assessment of the Potential Risks to The Health of the Population, Occupational and Environmental Medicine, 58 (**2001**) 2.

[182] O. Vandenplas, P. Fievez, J.P. Delwiche, J. Boulanger and J. Thimpont, Persistent Asthma Following Accidental Exposure to Formaldehyde, Allergy: European Journal of Allergy and Clinical Immunology, 59 (**2004**) 115.

[183] T.J. Kulle, Acute Odor and Irritation Response in Healthy Nonsmokers with Formaldehyde Exposure, Inhalation Toxicology, 5 (**1993**) 323.

[184] D.P.Y.A.T. Kulle, N.S.R.S.J. Swenberg and H.W.S.B. Horowitz, A Recommended Occupational Exposure Limit for Formaldehyde Based on Irritation, Journal of Toxicology and Environmental Health Part A, 50 (**1997**) 217.

[185] R. Gomes and M.E Meek, Acrolein, World Health Organization, **2002**.

[186] B. Pavoni, D. Drusian, A. Giacometti and M. Zanette, Assessment of Organic Chlorinated Compound Removal from Aqueous Matrices by Adsorption on Activated Carbon, Water Research, 40 (**2006**) 3571.

[187] W. Xiaoyan, W. Huixiang and W. Shaoli, Ambient Formaldehyde and Its Contributing Factor to Ozone and $^{\bullet}OH$ Radical in a Rural Area, Atmospheric Environment, 44 (**2010**) 2074.

[188] M.Z.M. Salem and M. Böhm, Understanding of Formaldehyde Emissions from Solid Wood: An Overview, BioResources, 8 (**2013**) 4775.

[189] L. Tubbs, B.A. Wybourne and J.S. Lumsden, Nodular Gill Disease Causing Proliferative Branchitis and Mortality in Chinook Salmon (Oncorhynchus Tshawytscha), New Zealand Veterinary Journal, 58 (**2010**) 59.

[190] B.C. Wolverton and J.D. Wolverton, Plants and Soil Microorganisms: Removal of Formaldehyde, Xylene, and Ammonia from the Indoor Environment, Journal of the Mississippi Academy of Sciences, 38 (**1993**) 11.

[191] WHO, Formaldehyde, World Health Organization, **1989**.

[192] WHO, Environmental Health Criteria 89, Formaldehyde, Royal Society for the Promotion of Health, 111 (**1991**) 38.

[193] B.C. Wolverton, R.C. McDonald and E. Watkins, Foliage Plants for Removing Indoor Air Pollutants from Energy-Efficient Homes, Economic Botany, 38 (**1984**) 224.

[194] S.M. Correa, G. Arbilla, M.R. Marques and K.M. Oliveira, The impact of BTEX Emissions from Gas Stations into the Atmosphere, Atmospheric Pollution Research, 3 (**2012**) 163.

[195] K.A. Daily, L.P. Hanrahan, M.A. Woodbury and M.S. Kanarek, Formaldehyde Exposure in Nonoccupational Environments, Archives of Environmental Health: An International Journal, 36 (**1981**) 277.

[196] Chemical Abstracts Service, Naming and Indexing of Chemical Substances for Chemical Abstracts 2007 Edition, the American Chemical Society, **2008.**

[197] Y. Kerchich and R. Kerbachi, Measurement of BTEX (Benzene, Toluene, Ethybenzene, and Xylene) Levels at Urban and Semirural Areas of Algiers City Using Passive Air Samplers, Journal of the Air and Waste Management Association, 62 (**2012**) 1370.

[198] C.L. Myung, A. Ko, Y. Lim, S. Kim, J. Lee, K. Choi and S. Park, Mobile Source Air Toxic Emissions from Direct Injection Spark Ignition Gasoline and LPG Passenger Car Under Various in-Use Vehicle Driving Modes in Korea, Fuel Processing Technology, 119 (**2014**) 19.

[199] P. Rattanajongjitrakorn and T. Prueksasit, Temporal Variation of BTEX at the Area of Petrol Station in Bangkok, Thailand, APCBEE Procedia, 10 (**2014**) 37.

[200] K.S. Suslick, Kirk-Othmer Encyclopedia of Chemical Technology, J. Wiley and Sons: New York, 26 (**1998**) 517.

[201] G. Huang, R. Brook, M. Crippa, G. Janssens-Maenhout, C. Schieberle, C. Dore and R. Friedrich, Speciation of Anthropogenic Emissions of Non-Methane Volatile Organic Compounds: A Global Gridded Data Set for 1970–2012, Atmospheric Chemistry and Physics, 17 (**2017**) 7683.

[202] J. Kaźmierczak, S. Biniak, A. Swiatkowski and K.H. Radeke, Interdependence of Different Parameters Characterizing the Chemistry of an Activated Carbon Surface, Journal of the Chemical Society, Faraday Transactions, 87 (**1991**) 3557.

[203] J.E. Kelsall, J.M. Samet, S.L. Zeger and J. Xu, Air Pollution and Mortality in Philadelphia, 1974–1988, American Journal of Epidemiology, 146 (**1997**) 750.

[204] J.J. Collins, R.Ness, R.W. Tyl, N. Krivanek, N.A. Esmen and T.A. Hall, A review of Adverse Pregnancy Outcomes and Formaldehyde Exposure in Human and Animal Studies, Regulatory Toxicology and Pharmacology, 34 (1) (**2001**) 17.

[205] J.V.H. Constable, A.B. Guenther, D.S. Schimel and R.K. Monson, Modelling Changes in VOC Emission in Response to Climate Change in the Continental United States, Global Change Biology, 5 (**1999**) 791.

[206] C.D. Cooper and F.C. Alley, Air Pollution Control: A Design Approach, Waveland Press, **2010**.

[207] O.R. Cooper, A. Stohl, M. Trainer, A. M. Thompson, J.C. Witte, S.J. Oltmans and R.C. Cohen, Large Upper Tropospheric Ozone Enhancements Above Midlatitude North America During Summer: In Situ Evidence from the IONS and MOZAIC Ozone Measurement Network, Journal of Geophysical Research: Atmospheres, 111 (**2006**).

[208] F. Nowshad, M.N. Islam and M.S. Khan, Concentration and Formation Behavior of Naturally Occurring Formaldehyde in Foods, Agriculture and Food Security, 7 (**2018**) 17.

[209] R.G. Nuzzo, F.A. Fusco and D.L. Allara, Spontaneously Organized Molecular Assemblies, 3. Preparation and Properties of Solution Adsorbed Monolayers

of Organic Disulfides on Gold Surfaces, Journal of the American Chemical Society, 109 (**1987**) 2358.

[210] M. Dehghani, M. Fazlzadeh, A. Sorooshian, H.R. Tabatabaee, M. Miri, A.N. Baghani and M. Rashidi, Characteristics and Health Effects of BTEX in a Hot Spot for Urban Pollution, Ecotoxicology and Environmental Safety, 155 (**2018**) 133.

[211] F. Golkhorshidi, A. Sorooshian, A.J. Jafari, A. M. A.N. Baghani, M. Kermani, R.R. Kalantary and M. Delikhoon, On the Nature snd Health Impacts of BTEX in A Populated Middle Eastern City: Tehran, Iran, Atmospheric Pollution Research, 10 (**2019**) 921.

[212] A. Srivastava, A.E. Joseph and S. Nair, Ambient Levels of Benzene in Mumbai City, International Journal of Environmental Health Research, 14 (**2004**) 215.

[213] F. Esmaelnejad, Y. Hajizadeh, H. Pourzamani and M.M. Amin, Monitoring of Benzene, Toluene, Ethyl Benzene, and Xylene Isomers Emission from Shahreza Gas Stations in 2013, International Journal of Environmental Health Engineering, 4 (**2015**) 17.

[214] M. Weiss, P. Bonnel, J. Kühlwein, A. Provenza, U. Lambrecht, S. Alessandrini and P. Le Lijour, Will Euro 6 Reduce the NOx Emissions of New Diesel Cars?–Insights From on-Road Tests with Portable Emissions Measurement Systems (PEMS), Atmospheric Environment, 62 (**2012**) 657.

[215] S.N. Sax, D.H. Bennett, S.N. Chillrud, J. Ross, P.L. Kinney and J.D. Spengler, A Cancer Risk Assessment of Inner-City Teenagers Living in New York City and Los Angeles, Environmental Health Perspectives, 114 (**2006**) 1558.

[216] E. Ilgen, K. Levsen, J. Angerer, P. Schneider, J. Heinrich and H.E. Wichmann, Aromatic Hydrocarbons in the Atmospheric Environment–Part II: Univariate and Multivariate Analysis and Case Studies of Indoor Concentrations, Atmospheric Environment, 35 (**2001**) 1253.

[217] P. Schneider, I. Gebefugi and K. Richter, INGA Study Group, Indoor Exposure and Genetics in Asthma, Indoor and Outdoor BTX Levels in German Cities Sci Total Environ, 267 (**2001**) 41.

[218] G.G. Pandit, P.K. Srivastava and A.M. Rao, Monitoring of Indoor Volatile Organic Compounds and Polycyclic Aromatic Hydrocarbons Arising from Kerosene Cooking Fuel, Science of the Total Environment, 279 (**2001**) 159.

[219] T. Amagai, T. Ohura, T. Sugiyama, M. Fusaya and H. Matsushita, Gas Chromatographic/Mass Spectrometric Determination of Benzene and Its Alkyl Derivatives in Indoor and Outdoor Air in Fuji, Japan, Journal of AOAC International, 85 (**2002**) 203.

[220] E.S. Alves, B.B. Moura and M. Domingos, Structural Analysis of Tillandsia Usneoides L. Exposed to Air Pollutants in São Paulo City–Brazil, Water, Air, and Soil Pollution, 189 (**2008**) 61.

[221] C.J. Smith, S.D. Livingston and D.J. Doolittle, An International Literature Survey of "IARC Group I Carcinogens" Reported in Mainstream Cigarette Smoke, Food and Chemical Toxicology, 35 (**1997**) 1107.

[222] S. Fustinoni, M. Buratti, L. Campo, A. Colombi, D. Consonni, A.C. Pesatori and D.F. Merlo, Urinary T, T-Muconic Acid, S-Phenylmercapturic Acid and Benzene as Biomarkers of Low Benzene Exposure, Chemico-Biological Interactions, 153 (**2005**)

[223] M. Helmut, Air Pollution in Cities, Atmospheric Environment, 33 (**1999**) 4029.

[224] G.J. McDougall, The Physical Nature and Manufacture of Activated Carbon, Journal of the Southern African Institute of Mining and Metallurgy, 91 (**1991**) 109.

[225] M.W. Ackley, S.U. Rege and H. Saxena, Application of Natural Zeolites in the Purification and Separation of Gases, Microporous and Mesoporous Materials, 61 (**2003**) 25.

[226] M.D. Donohue and G.L. Aranovich, Classification of Gibbs Adsorption Isotherms, Advances in Colloid and Interface Science, 76 (**1998**) 137.

[227] C.H. Yun, Y.H. Park and C.R. Park, Effects of Pre-Carbonization on Porosity Development of Activated Carbons from Rice Straw, Carbon, 39 (**2001**).

[228] C. Sangwichien, G.L. Aranovich and M.D. Donohue, Density Functional Theory Predictions of Adsorption Isotherms with Hysteresis Loops, Colloids and Surfaces A: Physicochemical and Engineering Aspects, 206 (**2002**) 313.

[229] W.T. Tsai, C.Y. Chang, M.C. Lin, S.F. Chien, H.F. Sun and M.F. Hsieh, Adsorption of Acid Dye onto Activated Carbons Prepared from Agricultural Waste Bagasse by ZnCl2 Activation, Chemosphere, 45 (**2001**) 51.

[230] Y.S. Ho, Pseudo-Isotherms Using a Second Order Kinetic Expression Constant, Adsorption, 10 (**2004**) 151.

[231] S.U. Rege, R.T. Yang and M.A. Buzanowski, Sorbents for Air Prepurification in Air Separation, Chemical Engineering Science, 55 (**2000**) 4827.

[232] A. Mittal, L. Kurup and J. Mittal, Freundlich and Langmuir Adsorption Isotherms and Kinetics for the Removal of Tartrazine from Aqueous Solutions Using Hen Feathers, Journal of Hazardous Materials, 146 (**2007**) 243.

[233] S. Dubey, D. Gusain and Y.C. Sharma, Kinetic and Isotherm Parameter Determination for the Removal of Chromium from Aqueous Solutions by Nanoalumina, a Nanoadsorbent, Journal of Molecular Liquids, 219 (**2016**) 1.

[234] I.A.W. Tan, A.L. Ahmad and B.H. Hameed, Adsorption of Basic Dye on High-Surface-Area Activated Carbon Prepared from Coconut Husk: Equilibrium, Kinetic And Thermodynamic Studies, Journal of Hazardous Materials, 154 (**2008**) 337.

[235] M.O.M.R. Gouamid, M.R. Ouahrani and M.B. Bensaci, Adsorption Equilibrium, Kinetics and Thermodynamics of Methylene Blue from Aqueous Solutions Using Date Palm Leaves, Energy Procedia, 36 (**2013**) 898.

[236] D.G. Kinniburg, Multipurpose Sorption Isotherms, Environmental Science and Technology, 20 (**1986**) 895.

[237] A.A.M Daifullah, S.M. Yakout and S.A. Elreefy, Adsorption of Fluoride in Aqueous Solutions Using KMNO4-Modified Activated Carbon Derived from Steam Pyrolysis of Rice Straw, Journal of Hazardous Materials, 147 (**2007**) 633.

[238] T. Fan, Y. Liu, B. Feng, G. Zeng, C. Yang, M. Zhou and X. Wang, Biosorption of Cadmium (II), Zinc (II) and Lead (II) by Penicillium Simplicissimum: Isotherms, Kinetics and Thermodynamics, Journal of Hazardous Materials, 160 (**2008**) 655.

[239] K.D. Henning and H. von Kienle, Carbon, 5. Activated Carbon, Ullmann's Encyclopedia of Industrial Chemistry, **2000**.

[240] O. Ioannidou and A. Zabaniotou, Agricultural Residues as Precursors for Activated Carbon Production—A Review, Renewable and Sustainable Energy Reviews, 11 (**2007**) 1966.

[241] M.L. Martinez, M.M. Torres, C.A. Guzman and D.M. Maestri, Preparation and Characteristics of Activated Carbon from Olive Stones and Walnut Shells, Industrial Crops and Products, 23 (**2006**) 23.

[242] J. Kesselmeier and M. Staudt, Biogenic Volatile Organic Compounds (VOC): An Overview on Emission, Physiology and Ecology, Journal of Atmospheric Chemistry, 33 (**1999**) 23.

[243] H. Fuchs, F. Holland and A. Hofzumahaus, Measurement of Tropospheric RO 2 and HO 2 Radicals by a Laser-Induced Fluorescence Instrument, Review of Scientific Instruments, 79 (**2008**) 084104.

[244] S.M.M. Gahyva and J.F. Siqueira Junior, Direct Genotoxicity and Mutagenicity of Endodontic Substances and Materials as Evaluated by Two Prokaryotic Test Systems, Journal of Applied Oral Science, 13 (**2005**) 387.

[245] S.S. Stavitskaya, Catalytıcal Properties of Active Carbons and the Main Factors Determining Them, **1999**.

[246] J. Kesselmeier, U. Kuhn, A. Wolf, M.O. Andreae, P. Ciccioli, E. Brancaleoni and T. de Oliva, Atmospheric Volatile Organic Compounds (VOC) at a Remote Tropical Forest Site in Central Amazonia, Atmospheric Environment, 34 (**2000**) 4063.

[247] M.G. Lussier, J.C. Shull and D.J. Miller, Activated Carbon from Cherry Stones, Carbon, 32 (**1994**) 1493.

[248] L.R. Snyder, Active Carbon, Manufacture, Properties and Applications: M. Smišek and S. Černy, Elsevier, Amsterdam, **1971**.

[249] X. Zhou, Y. Liu, C. Song, X. Wang, F. Wang and J. Liu, Modelling and Testing of VOC Source Suppression Effect of Building Materials Modified with Adsorbents, Building and Environment, 154 (**2019**) 122.

[250] S.H. Hansen and L.K Sydnes, Photochemical Oxidation of Benzyl Alcohol, Acta Chemical Scand, 43 (**1989**) 395.

[251] J.C. Clinger and P.T. O'Shaughnessy, Breakthrough Analysis for Filtering Facepiece Respirators Impregnated with Activated Carbon, Journal of Occupational and Environmental Hygiene, 16 (**2019**) 423.

[252] S. Sircar and T.C. Golden, Purification of Hydrogen by Pressure Swing Adsorption, Separation Science and Technology, 35 (**2000**) 667.

[253] J. Jänchen, D.L. Bish, D.T. Möhlmann and H. Stach, Investigation of the Water Sorption Properties of Mars-Relevant Micro-and Mesoporous Minerals, Icarus, 180 (**2006**) 353.

[254] F.J. Weber and S. Hartmans, Use of Activated Carbon as a Buffer in Biofiltration of Waste Gases with Fluctuating Concentrations of Toluene, Applied Microbiology and Biotechnology, 43 (**1995**) 365.

[255] K. Inomata, K. Kanazawa, Y. Urabe, H. Hosono and T. Araki, Natural Gas Storage in Activated Carbon Pellets Without a Binder, Carbon, 40 (**2002**) 87.

[256] M.A. De la Casa-Lillo, F. Lamari-Darkrim, D. Cazorla-Amoros and A. Linares-Solano, Hydrogen Storage in Activated Carbons and Activated Carbon Fibers, The Journal of Physical Chemistry B, 106 (**2002**) 10930.

[257] E. Auer, A. Freund, J. Pietsch and T. Tacke, Carbons As Supports for Industrial Precious Metal Catalysts, Applied Catalysis A: General, 173 (**1998**) 259.

[258] C. Ng, J.N. Losso, W.E. Marshall and R.M. Rao, Freundlich Adsorption Isotherms of Agricultural by-Product-Based Powdered Activated Carbons in a Geosmin–Water System, Bioresource Technology, 85 (**2002**) 131.

[259] Y.S. Ko, Y.J. Lee and S.H. Nam, Evaluation of a Pilot Scale Dual Media Biological Activated Carbon Process for Drinking Water, Korean Journal of Chemical Engineering, 24 (**2007**) 253.

[260] A.M. Pintor, C.I. Ferreira, J.C. Pereira, P. Correia, S.P. Silva, V.J. Vilar and R.A. Boaventura, Use of Cork Powder and Granules for the Adsorption of Pollutants: A Review, Water Research, 46 (**2012**) 3152.

[261] R.G. Rice, The Use of Ozone to Control Trihalomethanes in Drinking Water Treatment, (**1980**) 75.

[262] M.F. Rahman, E.K. Yanful and S.Y. Jasim, Endocrine Disrupting Compounds (EDCS) and Pharmaceuticals and Personal Care Products (PPCPS) in the Aquatic Environment: Implications for the Drinking Water Industry and Global Environmental Health, Journal of Water And Health, 7 (**2009**) 224.

[263] S.M. Gates, J.N. Jr Russell and J.T.Jr. Yates Bond Activation Sequence Observed in the Chemisorption and Surface Reaction of Ethanol on Ni (111), Surface Science, 171 (**1986**) 111.

[264] V.L. Snoeyink and W.J. Weber, The Surface Chemistry of Active Carbon; A Discussion of Structure and Surface Functional Groups, Environmental Science and Technology, 1 (**1967**) 228.

[265] A. Kalijadis, M.M. Vukcevic, Z.M. Jovanović, Z. Laušević and M.D. Lausevic, Characterisation of Surface Oxygen Groups on Different Carbon Materials by The Boehm Method and Temperature-Programmed Desorption, Journal of the Serbian Chemical Society, 76 (**2011**) 757.

[266] W. Buser and P. Graf, Differenzierung von Mangan (II)-manganit und δ-MnO2 durch Oberflächenmessung nach Brunauer-Emmet-Teller, Helvetica Chimica Acta, 38 (**1955**) 830.

[267] L. Meyer, First Adsorbed Layer of Helium, Physical Review, 103 (**1956**) 1593.

[268] D. Dollimore, P. Spooner and A. Turner, The BET Method of Analysis of Gas Adsorption Data and Its Relevance to the Calculation of Surface Areas, Surface Technology, 4 (**1976**) 121.

[269] C.J. Radke and J.M. Prausnitz, Adsorption of Organic Solutes from Dilute Aqueous Solution of Activated Carbon, Industrial and Engineering Chemistry Fundamentals, 11 (**1972**) 445.

[270] W.A. Patterson III, K.J. Edwards and D.J. Maguire, Microscopic Charcoal as a Fossil Indicator of Fire, Quaternary Science Reviews, 6 (**1987**) 3.

[271] H. Jüntgen, New Applications for Carbonaceous Adsorbents, Carbon, 15 (**1977**) 273.

[272] C. Srinivasakannan and M.Z.A. Bakar, Production of Activated Carbon from Rubber Wood Sawdust, Biomass and Bioenergy, 27 (**2004**) 89.

[273] W.K. Lafi, Production of Activated Carbon from Acorns and Olive Seeds, Biomass and Bioenergy, 20 (**2001**) 57.

[274] P. Behrens, Mesoporous Inorganic Solids, Advanced Materials, 5 (**1993**) 127.

[275] R. Seshadri and F.C. Meldrum, Bioskeletons as Templates for Ordered, Macroporous Structures, Advanced Materials, 12 (**2000**) 1149.

[276] R.C. Bansal and M. Goyal, Activated Carbon Adsorption, CRC Press, **2005**.

[277] K. Tsuchiya, Y. Hayashi, M. Onodera and T. Hasegawa, Toxicity of Formaldehyde in Experimental Animals, The Keio Journal of Medicine, 24 (**1975**) 19.

[278] G. Tzvetkov, N. Kaneva and T. Spassov, Room-Temperature Fabrication of Core-Shell Nano-Zno/Pollen Grain Biocomposite for Adsorptive Removal of Organic Dye From Water, Applied Surface Science, 400 (**2017**) 481.

[279] C. Selomulya, V. Meeyoo and R. Amal, Mechanisms of Cr (VI) Removal from Water by Various Types of Activated Carbons, Journal of Chemical Technology and Biotechnology, 74 (**1999**) 111.

[280] Y. Al-Degs, M.A.M. Khraisheh, S.J. Allen and M.N.A. Ahmad, Sorption Behavior of Cationic and Anionic Dyes from Aqueous Solution on Different Types of Activated Carbons, Separation Science and Technology, 36 (**2001**) 91.

[281] S.H. Jensen, P.H. Larsen and M. Mogensen, Hydrogen and Synthetic Fuel Production from Renewable Energy Sources, International Journal of Hydrogen Energy, 32 (**2007**) 3253.

[282] T. Valdés-Solıs, M.J.G. Linders, Kapteijn, F., Marban, G. B. F. A. and A. B. Fuertes, Adsorption and Breakthrough Performance of Carbon-Coated Ceramic Monoliths at Low Concentration of N-Butane, Chemical Engineering Science, 59 (**2004**) 2791.

[283] B.E. Rittmann, Opportunities for Renewable Bioenergy Using Microorganisms, Biotechnology and Bioengineering, 100 (**2008**) 203.

[284] M.I. Khan, A.B. Chhetri and M.R. Islam, Community-Based Energy Model: A Novel Approach to Developing Sustainable Energy, Energy Sources, Part B, 2 (**2007**) 353.

[285] L. Schlapbach and A. Züttel, Hydrogen-Storage Materials for Mobile Applications, In Materials for Sustainable Energy: A Collection of Peer-Reviewed Research and Review Articles from Nature Publishing Group, **(2011)** 265.

[286] H. Barthelemy, M. Weber and F. Barbier, Hydrogen Storage: Recent Improvements and Industrial Perspectives, International Journal of Hydrogen Energy, 42 (**2017**) 7254.

[287] D.A. Crowl and Y.D. Jo, The Hazards and Risks of Hydrogen, Journal of Loss Prevention in the Process Industries, 20 (**2007**) 158.

[288] F. Schüth, B. Bogdanović and M. Felderhoff, Light Metal Hydrides And Complex Hydrides for Hydrogen Storage, Chemical Communications, 20 (**2004**) 2249.

[289] H. Wu, Z. Li, D. Ji, Y. Liu, L. Li, D. Yuan and S. Licht, One-Pot Synthesis of Nanostructured Carbon Materials from Carbon Dioxide via Electrolysis in Molten Carbonate Salts, Carbon, 106 (**2016**) 208.

[290] J. Zheng, X. Liu, P. Xu, P. Liu, Y. Zhao and J. Yang, Development of High Pressure Gaseous Hydrogen Storage Technologies, International Journal of Hydrogen Energy, 37 (**2012**) 1048.

[291] Y. Bai, C. Wu, F. Wu, J.H. Yang, L.L. Zhao, F. Long and B.L. Yi, Thermal Decomposition Kinetics of Light-Weight Composite NANH2–NABH4 Hydrogen Storage Materials for Fuel Cells, International Journal of Hydrogen Energy, 37 (**2012)** 12973.

[292] C. Chilev and F.D. Lamari, Hydrogen Storage at Low Temperature and High Pressure for Application in Automobile Manufacturing, International Journal of Hydrogen Energy, 41 (**2016**) 1744.

[293] T. Riis, G. Sandrock, Ø. Ulleberg and P.J. Vie, Hydrogen Storage–Gaps and Priorities, HIA HCG Storage, 11 (**2005**) 1.

[294] H. Barthélémy, Hydrogen Storage–Industrial Prospectives, International Journal of Hydrogen Energy, 37 (**2012**) 17364.

[295] H. Ibrahim, A. Ilinca and J. Perron, Energy Storage Systems—Characteristics and Comparisons, Renewable and Sustainable Energy Reviews, 12 (**2008**) 1221.

[296] J. Germain, J.M. Fréchet and F. Svec, Nanoporous Polymers for Hydrogen Storage, Small, 5 (**2009**) 1098.

[297] M.D. Mat, K. Aldas and O.J. Ilegbusi, A Two-Phase Flow Model for Hydrogen Evolution in an Electrochemical Cell, International Journal of Hydrogen Energy, 29 (**2004**) 1015.

[298] K.H.C. Baser, Atkestanesi, Bagbahce, 47 **(2013)** 32.

[299] U.S. Environmental Protection Agency, https://www.epa.gov/sites/production /files/2019-8/documents/method_323_0.pdf (Accessed: **October 9 2018**).

[300] E. Woolfenden, Monitoring VOCs in Air Using Sorbent Tubes Followed by Thermal Desorption-Capillary GC Analysis: Summary of Data and Practical Guidelines, Journal of the Air and Waste Management Association, 47 (**1997**) 20.

[301] L. Mølhave, G. Clausen, B. Berglund, J. De Ceaurriz, A. Kettrup, T. Lindvall and B. Seifert, Total Volatile Organic Compounds (TVOC) in Indoor Air Quality Investigations, Indoor Air, 7 (**1997**) 225.

[302] D. Iso, 16000-6: Innenraumluftverunreinigungen–Teil 6: Bestimmung von VOC in der Innenraumluft und in Prüfkammern, Probenahme auf TENAX TA®, Thermische Desorption und Gaschromatographie mit MS/FID, Berlin: Beuth, **2004**.

[303] E.A. Woolfenden and W.A. McClenny, Method TO-17: Determination of Volatile Organic Compounds in Ambient Air Using Active Sampling onto Sorbent Tubes, Compendium of Methods for the Determination of Toxic Organic Compounds in Ambient Air, **1999**.

[304] E. De Hoffmann, Mass Spectrometry, Kirk-Othmer Encyclopedia of Chemical Technology, **2000**.

[305] Z. Xie, W. Guan, F. Ji, Z. Song and Y. Zhao, Production of Biologically Activated Carbon from Orange Peel and Landfill Leachate Subsequent Treatment Technology. Journal of Chemistry, **2014**.

[306] S. Kadi, S. Lellou, K. Marouf-Khelifa, J. Schott, I. Gener-Batonneau and A. Khelifa, Preparation, Characterisation and Application of Thermally Treated Algerian Halloysite, Microporous and Mesoporous Materials, 158 (**2012**) 47.

[307] S.J. Yang, H. Jung, T. Kim and C.R. Park, Recent Advances in Hydrogen Storage Technologies Based on Nanoporous Carbon Materials, Progress in Natural Science: Materials International, 22 (**2012**) 631.

[308] M. Molina-Sabio and F. Rodrıguez-Reinoso, Role of Chemical Activation in the Development of Carbon Porosity, Colloids and Surfaces A: Physicochemical and Engineering Aspects, 241 (**2004**) 15.

[309] I. Wróbel-Iwaniec, N. Díez and G. Gryglewicz, Chitosan-Based Highly Activated Carbons for Hydrogen Storage, International Journal of Hydrogen Energy, 40 (**2015**) 5788.

[310] S.S. Samantaray, S.R. Mangisett and S. Ramaprabhu, Investigation of Room Temperature Hydrogen Storage in Biomass Derived Activated Carbon, Journal of Alloys and Compounds, 789 (**2019**) 800.

[311] H. Wang, Q. Gao and J. Hu, High Hydrogen Storage Capacity of Porous Carbons Prepared by Using Activated Carbon, Journal of the American Chemical Society, 131 (**2009**) 7016.

[312] H.S. Blair and J.R. Gardner, Adsorption of Dye on Chitin, Journal of Applied Polymer Science, 27 (**1982**) 3043.

[313] F. Shiraishi, S. Yamaguchi and Y. Ohbuchi, A Rapid Treatment of Formaldehyde in a Highly Tight Room Using a Photocatalytic Reactor Combined with a Continuous Adsorption and Desorption Apparatus, Chemical Engineering Science 58 **(2003)** 929.

[314] V. Boonamnuayvitaya, S. Saeung and W. Tanthapanichakoon, Preparation of Activated Carbons from Coffee Residue for the Adsorption of Formaldehyde, Separation and Purification Technology, 42 **(2005)** 159.

[315] K. Laszlo, Characterization and Adsorption Properties of Polymer-based Microporous Carbons with Different Surface Chemistry, Microporous Mesoporous Mater, 80 **(2005)** 205.

[316] S. Kumagai, K. Sasaki, Y. Shimizu and K. Takeda, Formaldehyde and Acetaldehyde Adsorption Properties of Heat-treated Rice Husks, Separation and Purification Technology, 61 **(2008)** 398.

[317] H. Rong, Z. Ryu, J. Zheng and Y. Zhang, Effect of Oxidation of Rayon Based Activated Carbon Fibers on the Adsorption Behavior for Formaldehyde, Carbon 40 **(2002)** 2291.

[318] K.J. Lee, J. Miyawaki, N. Shiratori, S.-H. Yoon and J. Jang, Toward an Effective Adsorbent for Polar Pollutants: Formaldehyde Adsorption by Activated Carbon, Journal of Hazardous Material, 260 **(2013)** 82.

[319] J.H. Lee and S. Kim, The Determination of the Adsorption Performance of Graphite for VOCs and Formaldehyde, Energy Building, 46 **(2012)** 56.

[320] R.F. Liu, W.B. Li, A.Y. Peng, A facile Preparation of TiO2/ACF with C-Ti Bond and Abundant Hydroxyls and Its Enhanced Photocatalytic Activity for Formaldehyde Removal, Applied Surface Science 427 **(2018)** 608.

[321] Y. Lu, D. Wang, C. Ma and H. Yang, The Effect of Activated Carbon Adsorption on the Photocatalytic Removal of Formaldehyde, Building and Environment, 45 **(2010)** 615.

[322] A. Rezaee, H. Rangkooy, A. Jonidi-Jafari and A. Khavanin, Surface Modification of Bone Char for Removal of Formaldehyde from Air, Applied Surface Science, 286 **(2013)** 235.

[323] C. Ma, X. Li and T. Zhu, Removal of Low-Concentration Formaldehyde in Air by Adsorption on Activated Carbon Modified by Hexamethylene Diamine, Carbon, 49 **(2011)** 2873.

[324] K.J. Oh, D.W. Park, S.S. Kim and S.W. Park, Breakthrough Data Analysis of Adsorption of Volatile Organic Compounds on Granular Activated Carbon, Korean Journal, Chemical Engineering, 27 **(2010)** 632.

[325] L.Q. Li, J.F. Song, X.L. Yao, G.J. Huang, Z. Liu and L. Tang, Adsorption of Volatile Organic Compounds on Three Activated Carbon Samples: Effect of Pore Structure, Journal of Central South University, 19 **(2012)** 3530.

[326] C.M. Wang, K.S. Chang, T.W. Chung and H. Wu, Adsorption Equilibria of Aromatic Compounds on Activated Carbon, Silica Gel, and 13x Zeolite, Journal of Chemical and Engineering Data, 49 **(2004)** 527.

[327] F.D. Yu, L.A. Luo and G. Grevillot, Adsorption Isotherms of VOCs onto an Activated Carbon Monolith: Experimental Measurement and Correlation with Different Models, Journal of Chemical and Engineering Data, 47 **(2002)** 467.

[328] F. Delage, P. Pré and P. Le Cloirec, Mass Transfer and Warming during Adsorption of High Concentrations of VOCs on an Activated Carbon Bed: Experimental and Theoretical Analysis, Environmental Science and Technology, 34 **(2000)** 4816.

[329] B. Cardoso, A.S. Mestre, A.P. Carvalho and J. Pires, Activated Carbon Derived from Cork Powder Waste by Koh Activation: Preparation, Characterization, and VOCs Adsorption, Industrial and Engineering Chemistry Research, 47 **(2008)** 5841.

[330] L. Li, S. Liu and J. Liu, Surface Modification of Coconut Shell Based Activated Carbon the Improvement of Hydrophobic VOC Removal, Journal of Hazardous Materials, 192 **(2011).**

[331] D. Pearce, G. Atkinson and S. Mourato, Cost-Benefit Analysis and the Environment: Recent Developments, Organisation for Economic Co-Operation and Development, **2006**.

[332] U. Shahzad, B. Doğan, A. Sinha and Z. Fareed, Does Export Product Diversification Help to Reduce Energy Demand: Exploring the Contextual Evidences from the Newly Industrialized Countries, Energy, 214 (**2020**) 118881.

[333] Initial Investment Cost, Terra Universal, https://www.laboratory-equipment.com/ (Accessed: **June 10 2019**).

APPENDIX

HACETTEPE UNIVERSITY
GRADUATE SCHOOL OF SCIENCE AND ENGINEERING
THESIS/DISSERTATION ORIGINALITY REPORT

HACETTEPE UNIVERSITY
GRADUATE SCHOOL OF SCIENCE AND ENGINEERING
TO THE DEPARTMENT OF ENVIRONMENTAL ENGINEERING

Date: 01/12/2020

Thesis Title / Topic: REMOVAL OF FORMALDEHYDE AND BTEX IN INDOOR AIR USING ACTIVATED CARBON PRODUCED FROM HORSE CHESTNUT (Aesculus hippocastanum L.) SHELL
According to the originality report obtained by ~~myself~~/my thesis advisor by using the *Turnitin* plagiarism detection software and by applying the filtering options stated below on 01/12/2020 for the total of 298 pages including the a) Title Page, b) Introduction, c) Main Chapters, d) Conclusion sections of my thesis entitled as above, the similarity index of my thesis is 10%.

Filtering options applied:

1. Bibliography/Works Cited excluded
2. Quotes ~~excluded~~ / included
3. Match size up to 5 words excluded

I declare that I have carefully read Hacettepe University Graduate School of Sciene and Engineering Guidelines for Obtaining and Using Thesis Originality Reports; that according to the maximum similarity index values specified in the Guidelines, my thesis does not include any form of plagiarism; that in any future detection of possible infringement of the regulations I accept all legal responsibility; and that all the information I have provided is correct to the best of my knowledge.

I respectfully submit this for approval.

01/12/2020

Name Surname:	KAAN IŞINKARALAR
Student No:	N14241781
Department:	ENVIRONMENTAL ENGINEERING
Program:	PHD
Status:	☐ Masters ☒ Ph.D. ☐ Integrated Ph.D.

ADVISOR APPROVAL

APPROVED.

Prof. Dr. Gülen GÜLLÜ